water

Adsorbents for Water and Wastewater Treatment and Resource Recovery

Edited by

Sílvia Santos, Cidália Botelho and Ariana Pintor

Printed Edition of the Special Issue Published in *Water*

www.mdpi.com/journal/water

MDPI

Adsorbents for Water and Wastewater Treatment and Resource Recovery

Adsorbents for Water and Wastewater Treatment and Resource Recovery

Editors

Sílvia Santos
Cidália Botelho
Ariana Pintor

MDPI • Basel • Beijing • Wuhan • Barcelona • Belgrade • Manchester • Tokyo • Cluj • Tianjin

Editors

Sílvia Santos	Cidália Botelho	Ariana Pintor
Faculty of Engineering	Faculty of Engineering	Faculty of Engineering
University of Porto	University of Porto	University of Porto
Porto	Porto	Porto
Portugal	Portugal	Portugal

Editorial Office
MDPI
St. Alban-Anlage 66
4052 Basel, Switzerland

This is a reprint of articles from the Special Issue published online in the open access journal *Water* (ISSN 2073-4441) (available at: www.mdpi.com/journal/water/special_issues/adsorbents_water_wastewater_treatment_resource_recovery).

For citation purposes, cite each article independently as indicated on the article page online and as indicated below:

LastName, A.A.; LastName, B.B.; LastName, C.C. Article Title. *Journal Name* **Year**, *Volume Number*, Page Range.

ISBN 978-3-0365-4722-0 (Hbk)
ISBN 978-3-0365-4721-3 (PDF)

Contents

About the Editors

Sílvia Santos

Sílvia C. Santos is a Postdoctoral Researcher at LSRE-LCM (Laboratory of Separation and Reaction Engineering –Laboratory of Catalysis and Materials) and ALiCE (Associate Laboratory in Chemical Engineering), at the Faculty of Engineering of the University of Porto (FEUP). She obtained a PhD in Chemical and Biological Engineering in 2009 from FEUP. Her research interests include alternative adsorbents, plant-based coagulants, water decontamination, arsenic and antimony removal, textile wastewater treatment, and the recovery of precious metals. She has taught Bachelor's and Master's programmes of Environmental and Chemical Engineering, covering analytical methods, water quality and water treatment. S. Santos has been working on international projects related to surface water quality and modeling and sustainable processes for critical metals recovery from mining waste. S. Santos has published 28 papers and 3 chapters in international books (citations in 1649 documents; H-index of 18). Since 2018, she has been financed by the Portuguese national funding agency for science, research and technology (FCT), with a postdoctoral fellowship (SFRH/BPD/117387/2016).

Cidália Botelho

Cidália M. S. Botelho is an Assistant Professor at Faculdade de Engenharia—University of Porto (FEUP). She obtained her PhD (1998) in Chemical Engineering from FEUP, and Master's in Applied Chemistry from Instituto Superior Técnico—University of Lisbon. She teaches Environmental Chemistry, the Characterization and Monitoring of Water and Wastewater, Technologies and Systems of Water and Wastewater Treatment.

She is member of the research lab LSRE-LCM and of the associate lab ALiCE. Her main research interests are water chemistry; water quality and monitoring; water and wastewater treatment; and adsorption. In these areas, she has supervised 7 PhD theses (5 concluded), 35 master students and 5 postdoctoral researchers, and published 96 scientific papers, with 4061 citations and an H-index of 35 (Scopus, 6/2022), and 5 book chapters.

Ariana Pintor

Ariana Pintor is a junior researcher at the Laboratory of Separation and Reaction Engineering—Laboratory of Catalysis and Materials (LSRE-LCM) and the Associate Laboratory in Chemical Engineering (ALiCE) at the Faculty of Engineering of the University of Porto. She completed her PhD in Environmental Engineering at this institution in 2014. Since then, she has continued to pursue postdoctoral research on the development of natural adsorbents, especially cork-based materials, to remove various pollutants from water and wastewater. She has published 21 international peer-reviewed papers (H-index=14) and has supervised several undergraduate and graduate students on the topic of adsorption for environmental remediation.

Preface to ″Adsorbents for Water and Wastewater Treatment and Resource Recovery″

Adsorption is a well-established operation used for water decontamination and the remediation of industrial effluents. It is also recognized as a key technology for recovering substances of economic interest or at risk of scarcity. Adsorption from aqueous solution has aroused great interest in the scientific community in recent decades. This interest has been driven by: (i) the increasing demanding standards of drinking water, irrigation water and discharge limits imposed by legislation; (ii) the recognition of new and emerging contaminants and their possible deleterious effects on human health and ecosystems; and (iii) the need to refine wastewater treatment to a level that allows its reuse in multiple applications. The new sustainability paradigm of the circular economy and the current context of promoting the efficient use of natural resources and energy are additional motivations for research on this topic. This Special Issue was open for submissions from January to November 2020. Submissions covering the latest findings and progress on the use of adsorbents for water and wastewater treatment and recovering substances were encouraged. In it are 21 papers (17 research articles and 4 reviews), published by researchers of 18 countries.

The removal of heavy metals from water has been addressed in several articles; some use biochars (Wang et al.; Guo et al.; Kim et al.; Zhu et al.), other bio-derived materials (Vázquez-Guerrero et al.; Hamoud et al., Zhang et al.) and industrially derived adsorbents (Kobayashi et al.; Liu et al.). Interesting contributions were also received on the removal of organoselenium compounds (Okonji et al.) by granular activated carbon and nano zerovalent iron, and on arsenic uptake (Ogata et al.) using complex metal hydroxides. Torrinha et al. presented a study on the uptake of gold from strong acidic solutions, aiming to recover the metal from secondary sources, such as hydrometallurgical liquors of e-waste. This Special Issue also contains several works addressing the removal of organic contaminants from water. Studies conducted by Angosto et al. showed the effective removal of diclofenac from water using agro-food waste and compared it with advanced oxidation techniques. Martín-Lara et al. presented a study on removing bisphenol A using commercial activated carbon and evaluated the effect of coexisting metal cations in solution. Turco et al. studied the removal of phenolics from olive mill wastewater by oxidized multiwalled carbon nanotubes entrapped in a microporous polymeric matrix of polydimethylsiloxane. Adewuyi reviewed the literature on biosorbent use for the removal of emerging pharmaceutical compounds from water. Zango et al. provided a state-of-the-art perspective on removing PAHs (polycyclic aromatic hydrocarbons) and phenolic compounds by carbon porous materials, porous polymers, mesoporous silica, and metal–organic frameworks. The research articles of Yu et al. and Kuang et al. cover the surfactant modifications of sepiolite and activated carbon to decolorize effluents containing mixed and cationic dyes, respectively. Srivatsav et al. presented a comprehensive review paper covering the decolorization of dye-containing wastewater using biochars. Frišták et al. introduced an additional adsorption application to this Special Issue, by presenting an interesting review on the use of biochars to remove microcystins and improve water quality.

This Special Issue expects to be a good reference material in the field of water decontamination and effluent treatment by adsorption. The guest editors would like to thank those who contributed with their research work or reviewed the manuscripts.

Sílvia Santos, Cidália Botelho, and Ariana Pintor
Editors

water

MDPI

Review

The Use of Biochar and Pyrolysed Materials to Improve Water Quality through Microcystin Sorption Separation

Vladimír Frišták [1,*], H. Dail Laughinghouse IV [2] and Stephen M. Bell [3]

[1] Department of Chemistry, Trnava University in Trnava, 91843 Trnava, Slovakia
[2] Fort Lauderdale Research and Education Center, Agronomy Department, University of Florida/IFAS, Davie, FL 33314, USA; hlaughinghouse@ufl.edu
[3] Institute of Environmental Science and Technology (ICTA-UAB), Universitat Autónoma de Barcelona, 08193 Barcelona, Spain; Stephen.Bell@uab.cat
* Correspondence: fristak.vladimir.jr@gmail.com; Tel.: +421-33-592-1459

Received: 27 August 2020; Accepted: 13 October 2020; Published: 15 October 2020

Abstract: Harmful algal blooms have increased globally with warming of aquatic environments and increased eutrophication. Proliferation of cyanobacteria (blue-green algae) and the subsequent flux of toxic extracellular microcystins present threats to public and ecosystem health and challenges for remediation and management. Although methods exist, there is currently a need for more environmentally friendly and economically and technologically feasible sorbents. Biochar has been proposed in this regard because of its high porosity, chemical stability, and notable sorption efficiency for removing of cyanotoxins. In light of worsening cyanobacterial blooms and recent research advances, this review provides a timely assessment of microcystin removal strategies focusing on the most pertinent chemical and physical sorbent properties responsible for effective removal of various pollutants from wastewater, liquid wastes, and aqueous solutions. The pyrolysis process is then evaluated for the first time as a method for sorbent production for microcystin removal, considering the suitability and sorption efficiencies of pyrolysed materials and biochar. Inefficiencies and high costs of conventional methods can be avoided through the use of pyrolysis. The significant potential of biochar for microcystin removal is determined by feedstock type, pyrolysis conditions, and the physiochemical properties produced. This review informs future research and development of pyrolysed materials for the treatment of microcystin contaminated aquatic environments.

Keywords: biochar; microcystin; separation; water quality; cyanobacteria; algal bloom

---

1. Introduction

Recent studies indicate that cyanobacterial harmful algal blooms (cyanoHABs) are occurring more frequently in inland fresh waters (i.e., ponds, lakes, streams, and rivers) and estuaries worldwide [1–4]. Higher temperatures linked to global climate change and increased eutrophication have intensified cyanoHABs, posing significant environmental, social, and economic impacts partly due to the effects of toxins produced by several taxa [5–8]. Monitoring toxicity following such events in waterbodies can be complicated as cyanobacterial blooms contain complex mixtures of different classes of toxins [9–11]. Nevertheless, increased research efforts on the toxic impacts of these blooms under a changing climate and practical tools and methods for their management and remediation are clearly needed [4–14].

Microcystins (MCs) are a group of naturally occurring toxic secondary metabolites (cyanotoxins) produced by various genera of cyanobacteria [9–15]. They can be fatal to freshwater organisms even at very low concentrations [5–16] and have been classified by the International Agency for Research on Cancer (IARC) as possible human carcinogens [17]. To meet World Health Organization

(WHO) guidelines for maximum allowed surface water concentrations [18], there are several processes available for the removal of extracellular MCs. Powdered and granular activated carbon are commonly applied to adsorb MCs during treatment processes of drinking water because of their unique sorbent characteristics [19–21]. However, production costs for activated carbon and other materials (e.g., carbon nanotubes) have limited their potential for widespread application [19–22].

There is a current demand for more environmentally friendly and economically and technologically feasible sorbents for water quality remediation to be used in tandem with bloom prevention and risk reduction [23]. Pyrolysis, the thermochemical conversion of organic matter into char under anoxic or low-oxygen conditions, is a cheap and attractive method for the production of new sorption materials for water treatment purposes [24,25]. As a product of pyrolysis, biochar is of interest in this regard owing to the possibility of specifically designing, through feedstock and production process manipulation, more efficient sorption properties [26]. The high porosity, chemical stability, and significant sorption efficiency for removing cyanotoxins are among the central advantages of biochar [25]. In aqueous solutions, biochar and modified charcoal have provided promising results as sorbents [27–29], however, existing knowledge gaps have hindered widespread application in water treatment processes.

To address the need for an updated review of microcystin removal strategies, this paper first provides an overview of microcystin toxicity in natural water bodies followed by a discussion on conventional and alternative sorbents for microcystin separation. Here, this review focuses on the most pertinent chemical and physical sorbent properties responsible for effective removal of various pollutants from wastewater, liquid wastes, and aqueous solutions. Furthermore, an in-depth assessment of the pyrolysis process for sorbent production is given, providing the first comprehensive evaluation of biochar as a sorbent for microcystin removal. This review informs future research and development of pyrolysed materials for the treatment of microcystin in aquatic environments.

2. Microcystin Origin and Toxicity in Natural Water Bodies

Cyanobacteria are oxygenic photosynthetic bacteria that are prevalent in nutrient rich, warm, low turbulent freshwater bodies. When cyanobacteria die, their cell walls degrade, releasing intracellular toxins into the surrounding aquatic environment. MCs are a group of these naturally occurring toxins produced by various genera of cyanobacteria (e.g., *Anabaena*, *Anabaenopsis*, *Aphanocapsa*, *Cyanobium*, *Dolichospermum*, *Hapalosiphon*, *Limnothrix*, *Microcoleus*, *Microcystis*, *Nostoc*, *Oscillatoria*, *Phormidium*, *Planktothrix*, *Pseudanabaena*, *Sphaerospermopsis*, and *Synechocystis*). Their structures are extremely stable in water and can withstand chemical breakdown such as hydrolysis or oxidation. From a chemical point of view, MCs represent cyclic peptides composed of five common amino acids and pairs of L-amino acids as variants [30]. The common ones are D-erythro-β-methylaspartic acid, alanine, *N*-methyldehydroalanine, glutamic acid, and a unique amino acid called Adda (3-amino-9-methoxy-2,6,8-trimethyl-10-phenyldeca-4,6-diene acid). There have been more than 240 variants of MCs reported [31,32].

The main structural differences between microcystin variants arise from the substitution of single amino acids (Figure 1). In MC-LR, the most toxic and abundant microcystin, the two variable L-amino acids are L-arginine and L-leucine [33]. Trinchet et al. [34] and Roegner et al. [23] highlighted preferential organ uptake, and thus the importance of other congeners such as MC-RR (arginine at positions 2 and 4), MC-LA (leucine and alanine), MC-YR (tyrosine and arginine), MC-LF (leucine and phenylalanine), and MC-LW (leucine and tryptophan). The WHO established the guideline of a maximum recommended concentration of 1 μg/L for MC-LR in surface water. However, there remains a lack of data with respect to other structures and metabolites. According to the IARC, MCs are placed into group 2B as possible human carcinogens [17]. They are classified as tumour initiators with DNA-damaging effects [35]. These heptapeptides are produced via a nonribosomal biosynthesis pathway by large multienzyme complexes that include peptide synthetases, polyketide synthases, and tailoring enzymes [36].

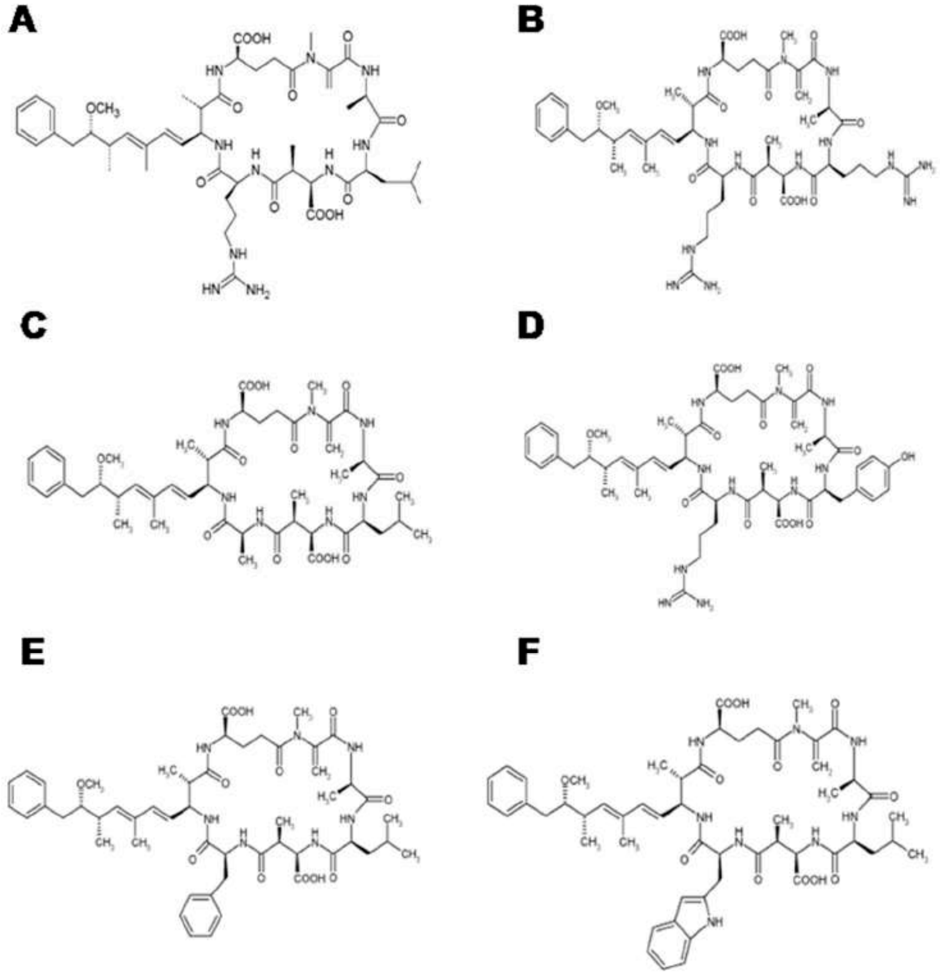

Figure 1. (**A**) Chemical structure of microcystin (MC)-LR, (**B**) microcystin-RR, (**C**) microcystin-LA, (**D**) microcystin-YR, (**E**) microcystin-LF, and (**F**) microcystin-LW.

In active and growing cyanobacteria, most MCs are cell-bound with intracellular concentrations of MCs several orders higher than concentrations of dissolved MCs in water. However, bloom senescence and cell lysis can cause the release of high quantities of MCs into the water. Mazur-Marzec et al. [37] and Jones et al. [38] reported that MC-LR can persist in aquatic for 1–3 months, but this is dependent on limnological and environmental parameters [39]. Based on acute toxicity, MC-LR is considered one of the most significant cyanobacterial toxins. As hepatotoxins, MCs mainly affect liver functioning, and can cause mortality and morbidity through necrosis and haemorrhage [40]. The hydrophilic characteristic of most MCs facilitates its uptake in vertebrates via active transport compared with cell membranes [41]. Membrane transport occurs mainly via organic anion transporting polypeptides [42].

Inside the hepatocytes, MCs inhibit eukaryotic protein serine/threonine phosphatases 1 and 2A [41], resulting in cytoskeletal disruption, rearrangement of associated filamentous actin, and morphological changes [23]. Frangez et al. [43] confirmed covalent binding of microcystin structure to protein phosphatases, leading to hyperphosphorylation of cytoskeletal proteins and the disruption of many cellular processes. Davis et al. [44] showed the effect of MC-LR on activation of the mitogen-activated protein kinase pathway. MCs induce apoptosis through free radical formation and mitochondrial alternations [23–45]. Human health problems are mostly related to chronic exposure to MCs via food and water consumption. As tumor-promoting toxins, MCs alter the regulation of phosphorylation and induce DNA damage in hepatocytes [46].

3. Conventional Strategies of Microcystin Removal

The removal or inactivation of MCs from water can be affected by several factors. The most crucial among these is if MCs are concentrated extracellularly or intracellularly. As mentioned, the majority (>95%) of MCs are found intracellularly during the growth stage of the bloom. However, when blooms collapse as a result of nutrient depletion, high temperatures, viral attack, and/or through the effect of chemical agents, intracellular MCs are released into the water as extracellular, increasing dissolved microcystin concentrations. The most common processes of extracellular MCs removal from drinking water are divided into three general steps: physical removal, biological inactivation, and chemical inactivation. Very often, these steps are cross-linked and supplied by processes such as sedimentation and flocculation. Physical removal includes the adsorption by effective sorbents (usually activated carbon) and the application of several filtration techniques [47,48]. Conventional sand filtration may be sufficient, but could also enhance the release of high concentrations of MCs into treated water [49,50]. Suboptimal set-up of filtration parameters, such as flow rate, can very often lead to enormous leaching of MCs from lysed microbial cells.

The main objective of the traditional sequence of coagulation–sedimentation–flocculation processes is to remove live algae, their residues, and organic and inorganic matter. A potential side-effect is cell lysis and subsequent increases in dissolved cyanotoxins' (e.g., MC) concentrations. The character and properties of cyanobacterial organic matter and toxic compounds decrease the efficacy of the conventional process for inorganic substances. Roegner et al. [23] described in detail the main disadvantages and pitfalls of the coagulation–sedimentation system when applied for MCs removal. Teixeira and Rosa [51] highlighted the significant effect of local water quality on MCs removal by this conventional method. Additionally, the quantity and quality of the chemical coagulant represents an important factor in the removal process. The application of flotation, a process whereby solids in suspension are recovered by their attachment to gas (usually air) bubbles, in combination with coagulation and flocculation, shows positive results in MCs separation [52]. The particles most effectively removed are in the size range of 10–200 µm. The particle-bubble aggregates that are formed have a density less than the suspension itself and they rise to the surface to be removed. Despite the high efficiency of this technology for algal residues removal, the question of extracellular toxins removal is still quite open. Therefore, the application of other methods is still needed.

From a treatment standpoint, MCs have three general areas subject to oxidation: the conjugated double bond in the Adda moiety; the single double bond in the Mdha moiety; and the side chain of amino acids [47]. Laszakovits and MacKay [53] described in detail the removal of cyanotoxins by potassium permanganate. However, this method represents a pH dependent and chemically demanding process. Several studies exist on verifying the efficiency of registered chemical algaecides and herbicides (especially copper-based and peroxide-based products) for bloom treatment and MC removal [54–56]. These compounds have been used successfully for decades, but initial cyanobacterial cell and toxin concentrations, algal species, and limnological characteristics can affect efficacy. Further, usage of waters (e.g., recreation vs. drinking water) and local regulations must be considered before application. Brooke et al. [57] showed reduced concentrations of MC-LR in water after ozone application. However, this pH dependent process is less effective under alkaline conditions. Chlorination can be viewed as another potential method to remove cyanotoxins from aqueous solutions [58]. Oxidation, chlorination, and ozonization can bring new risk such as secondary pollution from their by-products. Lawton et al. [59] showed the application of ultraviolet radiation as an effective, but expensive method to remove MCs from water.

Activated carbon produced from different precursor feedstocks such as coal or coconut represents the main sorption material used in separation processes of MCs from aqueous solutions [20–60]. The surface characteristics and pore structure of activated carbon determine its range of applicability in purification technologies of polluted water [61]. The activation process affects the adsorptive capacity, which can vary and only be effective for a specific group of contaminants. Activated carbon removes

MCs mainly via mechanisms of adsorption and intraparticular diffusion [62,63]. MCs primarily interact with carbon surfaces by hydrophobic forces and electrostatic interactions [64].

Generally, two basic types of activated carbon, powdered activated carbon and granular activated carbon, are applied in treatment processes for drinking water. The main difference in use is based on type and character of the contaminant (synthetic/natural, inorganic/organic). Porosity (total pore volume), porous character, and surface characteristics are crucial for efficiency of MCs sorption. Activated carbon provides a system of micropores with diameters of <2 nm, mesopores with diameters from 2 to 50 nm, and macropores at >50 nm. Microporous filtration materials restrict water flow and reduce contact between MCs and active surface sites, and thus can be considered as less effective in the removal process. On the other hand, MCs can be easily separated by activated carbon with high concentrations of mesopore structures [64].

Researchers have confirmed the different sorption efficiencies of activated carbons for MC-LR compared with MC-RR, MC-YR, and MC-LA. Mesoporous carbon materials with targeted functional groups represent an option in MCs separation from aqueous solutions [65]. Granular activated carbon is very often used in fixed beds as a filtration medium or adsorbent to remove fragile particles and chemicals under continual flow conditions [47]. However, Newcombie et al. [66] showed the inefficiency of granular activated carbon-based filters for microcystin separation compared with granular activated carbon-based adsorbents with proper regeneration or replacement, which can be potentially used as auxiliary barriers. Ho and Newcombie [67] found that powdered activated carbon can be easily bound up in the floc structure during the coagulation process, and thus can reduce the efficiency of MCs removal. Roegner et al. [23] showed the importance of the activated carbon's feedstock on the removal efficiency of MCs from potable water. The authors summarized that activated carbon produced from wood contains a system of mesopores and micropores, while coconut-based activated carbon contains just micropores, which can limit its MCs sorption application. Hena et al. [63] described the sorption process of MC-LR by activated carbon prepared from rubber wood sawdust as pH dependent with a maximal sorption capacity of 296 mg/g.

The effect of feedstock pH and the value of the point of zero charge (pHzpc) can significantly affect the adsorption efficiency of MCs [68]. Huang et al. [69] showed the relation between the pHzpc of activated carbon and sorption process of cyanotoxins. The higher pHzpc of the feedstock results in a neutral or positive charge of the produced activated carbon and higher adsorption potential for MCs [23]. The efficiency of activated carbon and activated carbon-based filters in separation of MCs from drinking water is considered sufficient (>99%) [70]. However, concentrations of cyanotoxins in water are potentially low and filters are not typically challenged with higher doses or the competitive effect of other toxic agents. Chlorine pre-treatment of potable water presents a problem for MCs sorption separation efficiency related to the reaction between residual chlorine and active carbon sites. Another problematic issue of causing a decrease in sorption separation with activated carbon application in water can be high concentrations of organic matter. Natural organic matter competes simultaneously with MCs for active sorption sites on surfaces of activated carbon.

Granular activated carbon can additionally be used as an ideal habitat for microbial growth thanks to its large surface area [47]. The growth of different microorganisms on activated carbon-based filters and biofilm formation can enhance the MCs removal owing to the combined effect of MCs biological degradation and sorption separation [69]. On the other hand, biofilm formation can decrease pore availability and thus reduce separation efficiency [23]. Drogui et al. [71] showed the lower efficiency of activated carbon-based filters after colonization by microbial communities compared with sterile filters during separation of MC-LR from water. The concerning literature discrepancies in the assessment of microbial colonization on MCs separation by activated carbon require additional and more detailed studies.

Numerous research studies refer to the decrease in accessibility and increase in mass production costs of activated carbon derived from typical feedstocks such as coal, coconut, or wood [19–22]. Zhi et al. [72] reported a price of 1650–9900 USD/t for activated carbon for pollutant removal, while Lou et al. [73] determined a range of 20,000–80,000 USD/t for carbon nanotubes. Based on these assessments, more economical and environmentally friendly sorbents are needed for water quality control.

4. Alternative Microcystin Separation Sorbents

Conventional technologies of MCs removal from water can be expensive and very often simply insufficient. More affordable methods with low technological requirements in water treatment are needed according to Gurbuz and Codd [50]. The authors highlighted a number of natural and artificial materials with extensive internal porosity for application in water purification. Despite possessing a lipophilic side chain of ADDA residue, molecules of microcystins are quite hydrophilic because of two carboxylic groups on its aspartic/glutamic acid side and one guanidine group on its arginine acid side [74]. Kim et al. [75] applied industrial waste biomass of *Escherichia coli* to develop biosorbents for MC-LR immobilization. The authors created biomass stabilization with polysulfone, coating the polysulfone-biomass composite with polyethylenimine, and subsequent decarboxylation of coated material. Such prepared materials can be recommended as highly efficient sorbents for MC-LR removal from aquatic environments with maximum sorption capacities of 1.2–1.9 mg/g at approximately pH 5. MC-LR can be effectively removed from aqueous solutions by sorbents prepared from *Moringa oleifera* Lam. seeds, as shown by Yasmin et al. [76]. The authors applied an acid pre-treatment of seed powder to increase pore size and volume. The sorption capacity of modified biosorbent for MC-LR was >92 mg/g. Sathya et al. [77] applied an exocellular polymer from *Enterobacter ludwigii* to remove microcystin-RR extracted from *Microcystis aeruginosa* (Kützing) Kützing. The maximum removal of MC-RR by the studied polymer was optimized by response surface methodology and achieved at a contact time of 5 h, pH 10, temperature of 30 °C, agitation speed of 150 rpm, and polymer dose of 4 mg/mL. This study confirmed the removal efficiency of MC-RR by exocellular polymer with a maximum sorption capacity of 23.76 ng/mg. Additionally, the authors showed a positive effect of Cu^{2+} ions on the MC-RR removal process by microbial polymeric material.

Application of native or dried biomass to separate MCs from aqueous solutions can cause secondary contamination by releasing other polymeric substances of heterogeneous composition into purified solution. The instability of biomass-derived sorbents represents a hazardous point that has to be mentioned [78]. Therefore, inorganic and thermochemically transformed materials are a more promising choice [79]. Morris et al. [80] showed high efficiency (>80%) of MC-LR separation from water by naturally-occurring clay particles. Laughinghouse et al. [81] found that lanthanum modified bentonite clay was able to sediment MC-LR at higher concentrations (around 500 µg/L) when compared with lower concentrations (50 and 100 µg/L). Adsorption of MC-LR onto nano-sized montmorillonite was investigated and optimized by Wang et al. [82]. Their work indicated a pH dependent process with the maximum of 0.186 mg/g reached at pH 2.96. Removal of MC-LR from model aqueous solutions by nano-sized montmorillonite represents a rapid process with several kinetic stages. Desorption efficiency of sorbed MC-LR (>75%) can be reached using 0.1 mol/L NaOH as the eluting media. Superabsorbent polymer composites appear to be a cost-effective solution for MC-LR adsorptive removal [83]. The porous network structure and the ionic functional groups of superabsorbent polymers ensure diffusion and binding of microcystin molecules. Wang et al. [83] showed the effective application of polyacrylamide/sodium alginate-modified montmorillonite to remove MC-LR from aqueous solution. Their study described sorption as a fast process, reaching equilibrium within 80 min of contact time. The maximum adsorption capacity of polyacrylamide/sodium alginate-modified montmorillonite for MC-LR was 32.66 mg/g. The authors also discovered that over 85% adsorption and 80% desorption could be achieved after five regeneration cycles. Recovery of studied microcystin reached more than 92% without ionic effect.

The sorption potential of pumice for MCs has also been described by Gurbuz and Codd [50]. Pumice is a porous material with high numbers of active sites that can be used as effective filtration material. The application of pumice in slow filtration processes to remove pathogens from irrigation water is a well-known method in horticulture [84]. Gurbuz and Codd [50] showed MC-LR adsorption on a pumice-based sorbent as a pH dependent process with maximal efficiency at pH 4. Experimental studies on the removal of MC-LR by peat showed the important role of this biomaterial in separation processes of cyanotoxins [85]. The maximum adsorption capacity of peat for MC-LR was found to be 0.26 mg/g at pH 3. Regeneration of peat-based sorbent using 2 mol/L NaOH showed a 94% efficiency in MC-LR desorption.

Iron oxides and hydroxides influence the mobility of organic and inorganic compounds in soils, sediments, and surface water. Therefore, Lee and Walker [86] studied the potential of maghemite nanoparticles to adsorb MC-LR from model solutions and confirmed a strong effect of pH with maximum removal efficiency at pH 3. They described the electrostatic interactions and hydrophobic forces as being crucial MC-LR sorption mechanisms. The adsorption process of microcystin onto maghemite nanoparticles is not significantly affected by the presence of river fulvic acid at lower concentrations (<2.5 mg/L). At higher concentrations of fulvic acid, the adsorption process of MC-LR by iron oxide nanoparticles decreased as a result of competition for limited active sorption sites. Along similar lines, Okupnik et al. [87] investigated the use of titanium dioxide nanoparticles for removal of MC-LR in environmental relevant concentrations from water samples. The authors tested different crystalline phases of nano-TiO_2 such as anatase, rutile, and an anatase–rutile mixture in comparison with a bulk TiO_2 counterpart. Sorption separation of MC-LR by titanium dioxide nanoparticles represents a complex mechanism, with chemisorption and sorbent particle size as the most influencing factors. Kinetic and equilibrium results of microcystin-LR and microcystin-RR removal by graphene oxide from water polluted by other environmental co-pollutants were described in a study by Pavagadhi et al. [61]. The tested graphene oxide showed significant adsorption capacity at 1.70 mg/g for MC-LR and 1.88 mg/g for MC-RR even in the presence of Mg^{2+}, Ca^{2+}, K^+, and Na^+ cations and NO^{2-}, NO^{3-}, Cl^-, $SO_4{}^{2-}$, and $PO_4{}^{3-}$ anions. The sorption kinetic experiments revealed that more than 90% removal of both microcystin variants is achieved within the first 5 min. New sorbents based on N-doped carbon xerogel for MC-LR adsorption were synthesized by Wu et al. [88]. Their results indicate fast microcystin uptake within 10 min and an adsorption capacity of 1.92 mg/g. The authors highlighted the efficiency of sorbent regeneration using 1 mol/L NaOH applied as the desorption agent.

5. New Sorption Materials Produced with Pyrolysis

Various feedstocks can be thermochemically converted into char using carbonization processes such as torrefaction, pyrolysis, hydrothermal carbonization, or gasification. Pyrolysis proceeds under strict anoxic or low oxygen conditions at temperatures from 350 to 1000 °C, and it is the main carbonization technique to produce conventional biochar with required characteristics [89]. During the pyrolysis process, solid (char), liquid (condensable crude oil), and gaseous (non-condensable syngas) products are formed. The solid products of hydrothermal carbonization, torrefaction, or gasification do not fulfil the main definition of biochar. According to Shaheen et al. [90], pyrolysis represents a less expensive and more robust technology involving thermochemical decomposition of organic matter compared with the other methods mentioned.

The physical and chemical characteristics of biochar are fully dependent on the feedstock properties and production system (Figure 2) [91]. The European Biochar Certificate outlines a wide range of biomass feedstocks approved for use in biochar production [89]. Biomass can be sourced through local waste collection services following waste separation (biodegradable wastes), garden waste (leaves, flowers, roots, hay, grass, prunings from trees, vines, bushes), agriculture and forestry (harvest leftovers, straw, husks and grain dust, seeds, plants, bark and chippings, sawdust, wood, wool), animal by-products (bones, manure, skins, hairs, feathers), material from food and confectionary production (leftovers from the production of canned food; residues from potato, rice, or corn starch production; residues from dairy processing; tobacco dust; slacks; ribs; tea; and coffee grounds), textiles (cellulose, cotton fibres, wool leftovers, hemp), or biogas plants (fermentation residues). Additionally, there exist several approved mineral-organic additives such as lime, bentonite, clay, loam, rock flour, or lignite to improve pyrolysis conditions and, subsequently, the quality of the produced biochar.

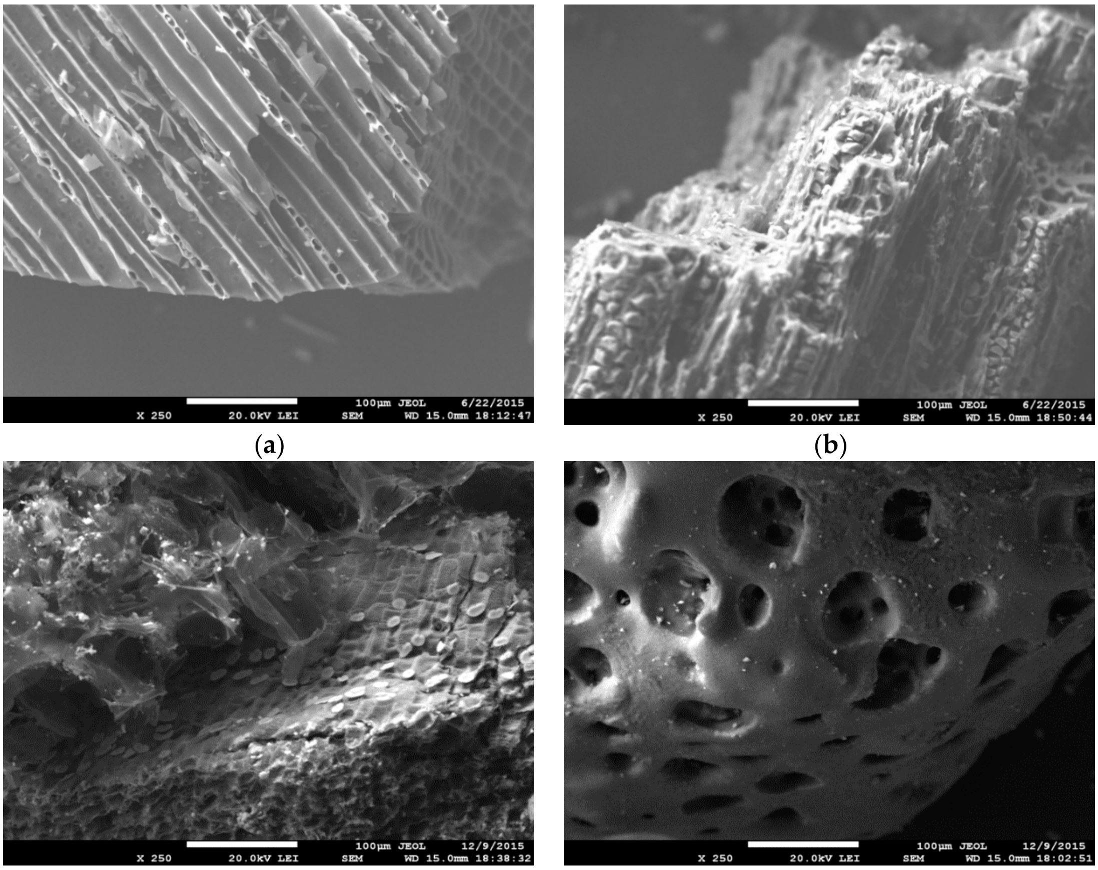

(**a**) (**b**)

(**c**) (**d**)

Figure 2. Scanning electron microscopy (SEM)—images of biochar derived from wood chips (**a**), garden green waste (**b**), corn cobs (**c**), and sewage sludge (**d**) at magnification 250× (with permission of authors—Micháleková-Richveisová et al. [91]).

Pyrolysis usually includes slow, fast, and flash processes [25]. Slow pyrolysis (conventional carbonization) is characterized by feedstock placement into a reactor and then initiating heating at a rate of about 0.1–1 °C/s until achieving a residence time from 20 min to several hours at temperatures of 400–700 °C. This process produces a solid char product rather that crude oil and syngas. While for fast and flash pyrolysis, addition of feedstock into the reactor occurs after pyrolysis temperature has been reached, with a significantly reduced residence time of several seconds to a few minutes at temperatures from 500 to 800 °C [92]. Fast pyrolysis produces a major bio-oil fraction and minor biochar and syngas by-products [93].

The fibrous biomass consists of cellulose, hemicelluloses, and lignin with smaller quantities of organic extractives and inorganic minerals. These constituents vary among different kinds of biomass. Cellulose as a linear condensation polymer of β-(1–4)-ᴅ-glucopyranose creates sheets of glucopyranose rings lying in a plane with successive sheets stacked on top of each other to form three-dimensional particles that aggregate into an elementary crystalline micro-fibril arrangement. This makes cellulose more thermal and chemically resistant compared with hemicellulose. Hardwood materials are rich in xylans and poor in glucomannans, while softwood feedstock contains more glucomannans compared with xylans [94]. Cellulose, hemicelluloses, and lignin have distinctive thermal decomposition behaviours that depend upon heating rates. Hemicellulose is the first to decompose, beginning at 220 °C and completed at 315 °C [94]. Cellulose does not start to decompose until about 315 °C.

Although lignin begins to decompose at 160 °C, it is a slow process extending to 850–900 °C. Pyrolysis of hemicellulose produces mainly no-condensable gases (CO, CO_2, H_2, and CH_4) and low molecular weight organic compounds such as carboxylic acids, alkanes, esters, and aldehydes [95]. Cellulose is a main source of considerable biochar product and the product of cellulose decomposition can vary depending on reaction conditions. The process of decomposition includes an exothermic and endothermic pathway. The exothermic pathway via anhydrocellulose yields char and non-condensable gases, while the endothermic pathway via levoglucosan is a devolatization process leading to tarry vapours or char. Mohan et al. [96] described the extent of secondary reactions affected by temperature, residence time, and catalysts occurring in feedstock. They yield a wide range of organic compounds such as carboxylic acids, ketones, aldehydes, and alcohols. The pyrolysis products of cellulose are mainly in the form of solid C, CO_2, and H_2O [97].

Many scientific studies focus on the utilisation of biochar and pyrolysis carbonaceous materials as effective sorbents in processes of organic and inorganic pollutant removal from aqueous solutions (Table 1). Several authors have confirmed different effects of physical and chemical properties on sorption efficiency. Therefore, the major material properties responsible for effective removal of various pollutants from wastewater, liquid wastes, and aqueous solutions are reviewed below.

Table 1. Removal of inorganic and organic pollutants from aqueous solutions by biochar.

Pollutant	Feedstock	Pyrolysis Temperature (°C)	Initial Concentration (mg/L)	Removal Efficiency (%)	Reference
copper	macroalga	500	10	80	[98]
cadmium	rape straw	600	20	100	[99]
lead	celery	500	400	98	[99]
zinc	wheat straw	650–700	100	100	[100]
chromium	rice husk	450–500	100	100	[101]
arsenic	sewage sludge	300	0.09	53	[102]
nickel	sewage sludge	600	30	26	[103]
tetracycline	sewage sludge	800	200	60	[104]
methylene blue	mangosteen peel	800	50	80	[105]
ibuprofen	wood chips	550	2	6	[106]
atrazine	cornstraw	500	30	100	[107]
sulfamethazine	cucumber	700	50	95	[108]

The area of internal and external surfaces, commonly called specific surface area (SSA), represents a crucial physical characteristic of pyrogenic carbonaceous material. Its value is the result of feedstock quality and production conditions (i.e., pyrolysis temperature, residence time, presence of catalysts, pre-treatment of feedstock or post-treatment of biochar). SSA determination for carbon-based sorbents involves mainly N_2 or CO_2 adsorptions followed by the Brunauer–Emmett–Teller (BET) equation application.

The method of SSA determination by liquid N_2 adsorption on biochar surface at a lower temperature (77 K) indicates the total specific surface area [109]. The method of CO_2 adsorption at a relatively high temperature (273 K) reflects the surface area of pores < 1.5 nm [110]. Micháleková-Richveisová et al. [91] and Dieguez-Alonso et al. [110] discussed the effect of pyrolysis temperature on porous structure formation and thus surface area development. Zama et al. [111] produced biochar from *Morus alba* at temperatures of 350 °C and 550 °C and confirmed more than 3.5 times higher SSA at the higher temperature. The effect of feedstock on SSA of biochar is also worth addressing. Jiang et al. [112] discussed the differences in surface areas of biochars prepared from pine wood and jarrah wood. Micháleková-Richveisová et al. [91] compared three biochars from different woody and agricultural wastes and found SSA values in the range of 16–26 m^2/g for the biochars with particle sizes of 0.5–1 mm. The effect of biochar post-treatment and feedstock pre-treatment can also significantly change SSA values of the resulting products [90].

Biochar pH ranges from 5 to 11 based on the feedstock and pyrolysis temperature [97]. There is a linear correlation between pH and pyrolysis temperature. Biochar produced at temperatures between 300 and 400 °C has a lower pH compared with biochar produced from the same feedstock at temperatures of 400–700 °C. Zhang et al. [29] explained the more alkaline pH of biochars produced at higher temperatures as a result of volatile organic compound losses and increases in basic cations. The lower pH values can be attributed to insufficient pyrolysis of material, biomass residues, and thus content with higher concentrations of phenolic and carboxylic functional groups. Elemental composition can be responsible for hydrophobicity and polarity of biochar, which can affect the contact of the material with the aqueous solution. The O/C molar ratio is used to estimate the hydrophilic nature of biochar and denote polar group concentrations in pyrogenic materials derived from carbohydrates in feedstock. The molar ratio of H/C can describe the degree of biochar carbonisation. Low values of H/C indicate a lower amount of non-carbonized biomass and thus a higher degree of carbonization [113].

The increased total content of elements such as K, Fe, Ca, Mg, and Mn can be attributed to higher concentrations of responding minerals, oxides, or oxohydroxides, which represent potential active sorption sites for pollutants removal [114]. Additionally, concentrations of surface functional groups such as carboxylic, hydroxyl, amino, phenolic, and lactic can be crucial for biochar assessment as effective sorption material. During pyrolysis under increasing temperature, most functional groups of feedstocks are lost. Kloss et al. [113] compared FT-IR spectra of biochars produced at different temperatures and found a decreased intensity of peaks corresponding to carboxylic and hydroxyl groups in samples produced at a higher temperature. Li et al. [115] applied ^{13}C NMR to investigate functional groups of rice straw and bran derived biochars produced at 100–800 °C. The authors confirmed the decreased content of aliphatic O-alkylated carbons and dominant aromatic structures in materials produced at temperatures > 300 °C.

Based on the type of contaminants, different mechanisms of sorption interactions can be proposed [116,117]. Sorption mechanisms of metals by biochar are fully dependent on the pH of the reaction solution, DOC, and competing elements concentrations [30]. Generally, complexation, cation exchange, precipitation, electrostatic interactions, and chemical reduction represent the main metal sorption mechanisms. However, the role of each mechanism is variable for each metal. Li et al. [115] described the target mechanisms of As, Cr, Pb, Cd, and Hg in detail. On the other hand, sorption of ionisable and ionic organic compounds such as pharmaceuticals and pesticides on biochar-based sorbents is a more complex process and the relative contribution of each sub-mechanism is dependent on the type of sorbate, pH, and sorbent properties [116]. These authors suggested and characterized the main active processes in sorption of organic molecules from liquid media as nonspecific van der Waals force (exactly London dispersion force), solvophobic effect, H-bond, charge assisted H-bond, electron donor-acceptor interactions, electrostatic (coulombic) interactions, ligand exchange, Lewis acid–base reactions, covalent bond, and oxidative coupling.

6. Biochar for Microcystin Sorption Separation

The study of biochar application in the removal of various organic structures has illustrated the potential of this pyrogenic material in separation processes. The biochar boom in environmental technologies and agronomy raised the question of potential risk evaluation for MCs interaction with this pyrogenic carbonaceous material present in sediment/water environments [74]. While at the same time, Zhang et al. [29], Li et al. [27], and Liu et al. [28] revealed the efficiency of modified charcoal and biochar utilization as potential sorbents of MC-LR from aqueous solutions. In each case, existing knowledge gaps on sorption behaviour of cyanotoxins in contact with biochar limit widespread usage of this engineered waste-derived sorbent in water purification processes. Sorbents derived from biochar exhibit different structure and properties compared with activated carbon. Incomplete carbonization at low temperatures in the range of 300–700 °C and the absence of activation processes can bring new challenges in the characterization and subsequent application of biochar sorbents. The effect of feedstock and mineral composition can be crucial for sorption properties of pyrogenic carbonaceous material [27].

The mechanisms of sorption interactions between microcystin and biochar can be characterized by several potential processes such as electrostatic and hydrogen bonding, ion exchange, complexation, mesopore filling, hydrophobic interactions, and interactions with aromatic carbon (such as $\pi \pm \pi$ EDA and $\pi - \pi$ stacking) (Figure 3). $\Pi \pm \pi$ EDA represents $\pi \pm \pi$ electron donor–acceptor interactions between protonated guanidine groups of MCs and π-electron rich graphene surfaces of biochar [28]. $\Pi - \pi$ stacking is the main interaction between the benzene ring of MCs and aromatic units on biochar surfaces [74]. As mentioned previously, molecules of MCs have a more hydrophilic character with reactive carboxyl or guanidine functional groups. Therefore, the dominant mechanism of MCs sorption can be often attributed to hydrophobic interactions [74]. Liu et al. [28] reported that the hydrophobic leucine unit in a MC-LR molecule tends to be attracted to hydrophobic surfaces of giant reed-derived biochar via a hydrophobic interaction. The authors showed that the positive correlation between pyrolysis temperature and hydrophobic interactions, thus hydrophobicity, is a driving force in the sorption of MC-LR. Teixidó et al. [118] described sorption removal of hydrophilic sulfamethazine by biochar with electron donor–acceptor interaction between protonated aniline ring and on π-electrons rich carbon surface as the predominant driving force. However, this kind of interaction is not a major force during MCs interactions with biochar-based sorbents. Isolated π electron systems in the Adda side chain represent small fractions of the hydrophilic macromolecule.

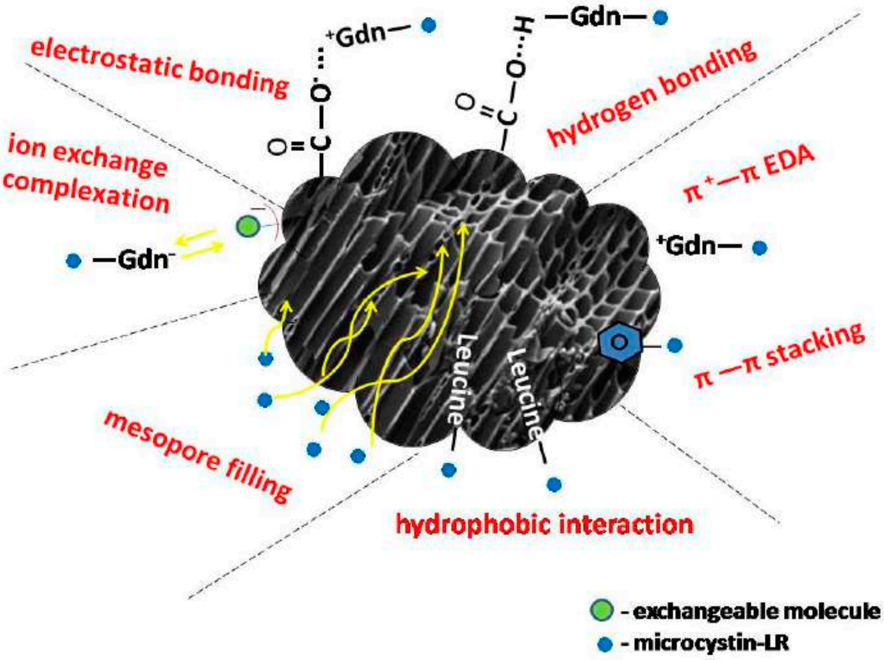

Figure 3. Suggested model of MC-LR sorption interactions with biochar-based sorbents.

On the other hand, Li et al. [74] showed how chemisorptions are the main force responsible for sorption of MC-LR molecules on wood-based biochar produced at 300 °C. Additionally, the authors confirmed physisorption and hydrogen bonding as the primary forces in sorption of MC-LR by the same biochar produced at 700 °C. One adsorbed MC-LR molecule can displace a considerable number of water molecules at the solid/liquid interface [119]. Thermodynamic calculations by Li et al. [74] demonstrated the ability of the MC-LR molecule to replace more water molecules on the biochar produced at lower temperatures. Li et al. [27] reported $\pi \pm \pi$ EDA interactions as the major driving forces of MC-LR sorption by biochars produced at 600 °C compared with biochars produced from the same feedstocks at 300 °C. Biochar produced at higher temperatures consists of highly aromatic structures providing larger π-electron-rich graphene sheets as electron donors.

The effect of porosity, as mentioned in Section 3, is crucial for sorption efficiency. According to Li et al. [27] and Zhang et al. [29], the three-dimensional size of the MC-LR molecule was determined to be 1.9 nm × 1.5 nm × 1.1 nm, with a maximum length of 2.94 nm and width of 2.55 nm. Therefore, micropores represent inaccessible spaces for MC-LR molecules [27]. Biochars with lower surface area and lower concentration of mesopores can be less effective in sorption removal of MC-LR [74]. Liu et al. [28] showed that giant reed derived biochars produced at higher temperatures (>500 °C) have predominantly mesoporous structures and are thus more suited and effective in the removal of MC-LR from aqueous solutions.

The pH values of biochar and surface point of zero charge are further driving forces in the sorption mechanism of MCs. Biochars with lower pH, or under lower pH environmental conditions, can still contain minor surfaces with positive charges, thus columbic attraction between anionic microcystin molecules and sorbent can still be considered. The pH of the aquatic environment can severely influence the sorption efficiency of MCs. Generally speaking, sorption of these microbial toxins decreases with increasing pH of the environment. Sorption processes of MCs are inhibited by electrostatic repulsion between their mono oxoanionic species induced by increasing pH (2–4) and higher negative charge of biochar surfaces at pH 3–8 [28].

Additionally, molecules of MCs tend to coil under more acidic conditions, and thus sorption can be more effective. Higher pH provides higher concentrations of hydrophilic microcystin molecules and thus a higher tendency of MCs to remain in the aqueous environment rather than to interact with hydrophobic biochar-based sorbents. Wu et al. [120] confirmed this trend in MC-LR sorption by natural sediments, and Sathishkumar et al. [85] for MC-LR sorption by peats-derived sorbents. Ionisable functional groups of MCs and biochar surfaces can be easily protonated or deprotonated at different pH values. According to Li et al. [74], adsorption of MC-LR on biochars is attributed to the binding of MC-LR- anions to biochars with pH-dependent charges in aquatic systems. Liu et al. [28] found the highest sorption efficiency of MC-LR removal by giant reed-derived biochars at pH 3.5.

The sorption separation of MCs by biochar can also be influenced by competitive substances such as phosphates, citric acid, oxalic acid, and tannic acid, but with negligible effects from gallic acid, nitrates, and chlorides [74]. These authors suggested anion exchange as a possible contributing factor to MC-LR adsorption. Liu et al. [28] investigated the contribution of mineral composition to the overall sorption of MC-LR by giant reed-derived biochar. Their reported results revealed that mineral removal by deashing treatment barely impacts the adsorption of MC-LR by biochars produced at temperatures < 400 °C, whereas it significantly reduces sorption of MCs by biochars produced at temperatures > 400 °C.

Li et al. [74] showed adsorption irreversibility of MC-LR sorbed to wood-derived biochar and increased accumulation of MC-LR in biochar-amended sediments. The authors confirmed the associated risk of the undetermined prolonged fate of MC-LR in sediments and thus in aquatic environments. However, the benefits of high porosity, chemical stability, and significant sorption efficiency for removal processes of cyanotoxins can help guide the optimization of pyrolysis processes and the creation of a new class of so-called engineered or designed sorbents for water purification.

7. Conclusions

Elevated cyanotoxin concentrations in freshwater systems and drinking water sources following toxic cyanobacterial blooms require remediation to reduce risks to human and ecosystem health. Conventional methods for microcystin removal are insufficient or, as in the case of activated carbon, too expensive for widespread adoption. Alternative methods exist and have shown interesting results, but require continued research efforts. This review illustrates the potential of the pyrolysis process to inexpensively transform organic materials into efficient sorbents. In particular, biochar has proven effective as a sorbent for MCs in water thanks to its high porosity, chemical stability, and notable sorption efficiency. The physiochemical properties of a specifically engineered biochar for MCs remediation can be optimized through manipulating feedstock and pyrolysis conditions. Future research and product development for MCs sorption separation from contaminated aquatic environments can consider pyrolysed materials as attractive candidates. This work supports the continued exploration of inexpensive and feasible water remediation sorbents produced through pyrolysis, but also demonstrates the need for further studies evaluating their effectiveness in the field under diverse conditions following harmful algal blooms worldwide.

Author Contributions: Conceptualization, V.F., H.D.L.IV, and S.M.B.; methodology, V.F. and H.D.L.IV; formal analysis, V.F. and S.M.B.; investigation, V.F., H.D.L.IV, and S.M.B.; writing—original draft preparation, V.F. and S.M.B.; writing—review and editing, V.F., H.D.L.IV, and S.M.B.; visualization, V.F.; supervision, V.F. and H.D.L.IV; project administration, V.F.; funding acquisition, V.F. All authors have read and agreed to the published version of the manuscript.

Funding: This research was funded by Scientific Grant Agency of the Ministry of Education, Science, Research, and Sport of the Slovak Republic, project number VEGA1/0178/20; and Trnava University in Trnava, project number 2/TU/2019 and 4/TU/2020.

Acknowledgments: Authors are thankful to David Erwin Berthold for technical support.

Conflicts of Interest: The authors declare no conflict of interest. The funders had no role in the design of the study; in the collection, analyses, or interpretation of data; in the writing of the manuscript; or in the decision to publish the results.

References

1. Griffith, A.W.; Gobler, C.J. Harmful algal blooms: A climate change co-stressor in marine and freshwater ecosystems. *Harmful Algae* **2020**, *91*, 101590. [CrossRef]
2. Hoagland, P.; Anderson, D.M.; Kaoru, Y.; White, A.W. The economic effects of harmful algal blooms in the United States: Estimates, assessment issues, and information needs. *Estuaries* **2002**, *25*, 819–837. [CrossRef]
3. Harke, M.J.; Steffen, M.M.; Gobler, C.J.; Otten, T.G.; Wilhelm, S.W.; Wood, S.A.; Paerl, H.W. A review of the global ecology, genomics, and biogeography of the toxic cyanobacterium, *Microcystis* spp. *Harmful Algae* **2016**, *54*, 4–20. [CrossRef]
4. Wood, S.A.; Kelly, L.; Bouma-Gregson, K.; Humbert, J.F.; Laughinghouse IV, H.D.; Lazorchak, J.; McAllister, T.; McQueen, A.; Pokrzywinski, K.; Puddick, J.; et al. Toxic benthic freshwater cyanobacterial proliferations: Challenges and solutions for enhancing knowledge and improving monitoring and mitigation. *Freshw. Biol.* **2020**, *65*, 1824–1842. [CrossRef]
5. Codd, G.A.; Morrison, L.F.; Metcalf, J.S. Cyanobacterial toxins: Risk management for health protection. *Toxicol. Appl. Pharmacol.* **2005**, *203*, 264–272. [CrossRef] [PubMed]
6. Dodds, W.K.; Bouska, W.W.; Eitzmann, J.L.; Pilger, T.J.; Pitts, K.L.; Riley, A.J.; Schloesser, J.T.; Thornbrugh, D.J. Eutrophication of U. S. freshwaters: Analysis of potential economic damages. *Environ. Sci. Technol.* **2009**, *43*, 12–19. [CrossRef] [PubMed]
7. Paerl, H.W.; Huisman, J. Climate change: A catalyst for global expansion of harmful cyanobacterial blooms. *Environ. Microbiol. Rep.* **2009**, *1*, 27–37. [CrossRef] [PubMed]
8. Almanza, V.; Pedreros, P.; Laughinghouse IV, H.D.; Félez, J.; Parra, O.; Azocar, M.; Urrutia, R. Association between trophic state, watershed use and blooms of cyanobacteria in south-central Chile. *Limnologica* **2019**, *75*, 30–41. [CrossRef]
9. Huisman, J.; Codd, G.A.; Paerl, H.W.; Ibelings, B.W.; Verspagen, J.M.H.; Visser, P.M. Cyanobacterial blooms. *Nat. Rev. Microbiol.* **2018**, *16*, 471–483. [CrossRef]
10. Kust, A.; Řeháková, K.; Vrba, J.; Maicher, V.; Mareš, J.; Hrouzek, P.; Chiriac, M.C.; Benedová, Z.; Tesařová, B.; Saurav, K. Insight into Unprecedented Diversity of Cyanopeptides in Eutrophic Ponds Using an MS/MS Networking Approach. *Toxins* **2020**, *12*, 561. [CrossRef]
11. Carvalho, L.R.; Pipole, F.; Werner, V.R.; Laughinghouse IV, H.D.; Rangel, M.; Konno, K.; Camargo, A.C.M.; Sant'Anna, C.L. A Toxic Cyanobacterial Bloom in an Urban Coastal Lake, Rio Grande do Sul, Southern Brazil. *Braz. J. Microbiol.* **2008**, *39*, 761–769. [CrossRef] [PubMed]
12. Burford, M.A.; Carey, C.C.; Hamilton, D.P.; Huisman, J.; Paerl, H.W.; Wood, S.A.; Wulff, A. Perspective: Advancing the research agenda for improving understanding of cyanobacteria in a future of global change. *Harmful Algae* **2020**, *91*, 101601. [CrossRef]
13. Wells, M.L.; Karlson, B.; Wulff, A.; Kudela, R.; Trick, C.; Asnaghi, V.; Berdalet, E.; Cochlan, W.; Davidson, K.; De Rijcke, M.; et al. Future HAB science: Directions and challenges in a changing climate. *Harmful Algae* **2020**, *91*, 101632. [CrossRef] [PubMed]

14. Paerl, H.W.; Gardner, W.S.; Havens, K.E.; Joyner, A.J.; McCarthy, M.J.; Newell, S.E.; Qin, B.; Scott, J.D. Mitigating cyanobacterial harmful algal blooms in aquatic ecosystems impacted by climate change and anthropogenic nutrients. *Harmful Algae* **2016**, *54*, 213–222. [CrossRef]
15. Dawson, R.M. The toxicology of microcystins. *Toxicon* **1998**, *36*, 953–962. [CrossRef]
16. Shahmohamadloo, R.S.; Poirier, D.G.; Ortiz Almirall, X.; Bhavsar, S.P.; Sibley, P.K. Assessing the toxicity of cell-bound microcystins on freshwater pelagic and benthic invertebrates. *Ecotoxicol. Environ. Saf.* **2020**, *188*, 109945. [CrossRef]
17. IARC. *Ingested Nitrate and Nitrite, and Cyanobacterial Peptide Toxins/IARC Monographs on the Evaluation of Carcinogenic Risks to Humans Volume 94*; IARC: Lyon, France, 2010.
18. WHO. *Guidelines for Drinking-Water Quality: Fourth Edition Incorporating the First Addendum*; WHO: Geneva, Switzerland, 2017.
19. Park, J.A.; Jung, S.M.; Choi, J.W.; Kim, J.H.; Hong, S.; Lee, S.H. Mesoporous carbon for efficient removal of microcystin-LR in drinking water sources, Nak-Dong River, South Korea: Application to a field-scale drinking water treatment plant. *Chemosphere* **2018**, *193*, 883–891. [CrossRef]
20. Ho, L.; Lambling, P.; Bustamante, H.; Duker, P.; Newcombe, G. Application of powdered activated carbon for adsorption of cylindrospermopsin and microcystin toxins from drinking water supplies. *Water Res.* **2011**, *45*, 2954–2964. [CrossRef]
21. Falconer, I.R.; Runnegar, M.T.C.; Buckley, T.; Huyn, L.; Bradshaw, P. Using activated carbon to remove toxicity from drinking water containing cyanobacterial blooms. *J. Am. Water Work. Assoc.* **1989**, *81*, 102–106. [CrossRef]
22. Mashile, P.P.; Mpupa, A.; Nomngongo, P.N. Adsorptive removal of microcystin-LR from surface and wastewater using tyre-based powdered activated carbon: Kinetics and isotherms. *Toxicon* **2018**, *145*, 25–31. [CrossRef]
23. Roegner, F.A.; Brena, B.; González-Sapienza, G.; Puschner, B. Microcystins in potable surface waters: Toxic effects and removal strategies. *J. Appl. Toxicol.* **2014**, *34*, 441–457. [CrossRef]
24. Basu, P. *Pyrolysis, in: Biomass Gasification, Pyrolysis and Torrefaction: Practical Design and Theory*; Elsevier: Amsterdam, The Netherlands, 2018; pp. 155–187.
25. Wang, J.; Wang, S. Preparation, modification and environmental application of biochar: A review. *J. Clean. Prod.* **2019**, *227*, 1002–1022. [CrossRef]
26. Ahmed, M.J.; Hameed, B.H. Insight into the co-pyrolysis of different blended feedstocks to biochar for the adsorption of organic and inorganic pollutants: A review. *J. Clean. Prod.* **2020**, *265*, 121762. [CrossRef]
27. Li, J.; Cao, L.; Yuan, Y.; Wang, R.; Wen, Y.; Man, J. Comparative studz for microcystin-LR sorption onto biochars produced from various plant-and animal-wastes at different pyrolysis temperatures: Influencing mechanisms of biochar properties. *Bioresour. Technol.* **2018**, *247*, 794–803. [CrossRef] [PubMed]
28. Liu, G.; Zheng, H.; Zhai, X.; Wang, Z. Characteristics and mechanisms of microcystin/LR adsorption by giant reed-derived biochars: Role of minerals, pores and functional groups. *J. Clean. Prod.* **2018**, *176*, 463–473. [CrossRef]
29. Zhang, H.; Zhu, G.; Jia, X.; Ding, Y.; Zhang, M.; Gao, Q.; Hu, C.; Xu, S. Removal of microcystin-LR from drinking water using a bamboo-based charcoal adsorbents modified with chitosan. *J. Environ. Sci.* **2011**, *23*, 1983–1988. [CrossRef]
30. Li, J.M.; Li, R.H.; Li, J. Current research scenario for microcystins biodegradation—A review on fundamental knowledge, application prospects and challenges. *Sci. Total Environ.* **2017**, *595*, 615–632. [CrossRef]
31. Spoof, L.; Catherine, A. Tables of microcystins and nodularins, Appendix 3. In *Handbook of Cyanobacterial Monitoring and Cyanotoxin Analysis*, 1st ed.; Meriluoto, J., Spoof, L., Cold, G.A., Eds.; John Wiley and Sons, Ltd.: Hoboken, NJ, USA, 2017.
32. Turner, A.D.; Dhanji-Rapkova, M.; OŃeill, A.; Coates, L.; Lewis, A.; Lewis, K. Analysis of microcystins in cyanobacterial blooms from freshwater bodies in England. *Toxins* **2018**, *10*, 39. [CrossRef] [PubMed]
33. Merel, S.; Clement, M.; Thomas, O. State of the art on cyanotoxins in water and their behaviour towards chlorine. *Toxicon* **2010**, *55*, 677–691. [CrossRef]
34. Trinchet, I.; Cadel-Six, S.; Djediat, C.; Marie, B.; Bernard, C.; Puiseux-Dao, S.; Krys, S.; Edery, M. Toxicity of harmful cyanobacterial blooms to bream and roach. *Toxicon* **2013**, *71*, 121–127. [CrossRef]

35. Humpage, R.; Hardy, S.J.; Moore, E.J.; Froscio, S.M.; Falconer, I.R. Microcystins (cyanobacterial toxins) in drinking water enhance the growth of aberrant cryptfoci in the mouse colon. *J. Toxicol. Environ. Health A* **2000**, *61*, 155–165. [PubMed]
36. Tillett, D.; Dittmann, E.; Erhard, M.; von Dohren, H.; Borner, T.; Neilan, B.A. Structural organization of microcystin biosynthesis in Microcystis aeruginosa PCC7806: An integrated peptide-polyketide synthetase systém. *Chem. Biol.* **2000**, *7*, 753–764. [CrossRef]
37. Mazur-Marzec, H.; Plinski, M. Do toxic cyanobacteria blooms pose a threat to the Baltic ecosystem? *Oceanologia* **2009**, *51*, 293–319. [CrossRef]
38. Jones, G.J.; Falconer, I.R.; Wilkins, R.M. Persistence of cyclic peptide toxins in dried Microcystis aeruginosa crusts from lake Mokoan, Australia. *Environ. Toxicol. Water Qual.* **1995**, *10*, 19–24. [CrossRef]
39. Schmidt, J.R.; Wilhelm, S.W.; Boyer, G.L. The Fate of Microcystins in the Environment and Challenges for Monitoring. *Toxins* **2014**, *6*, 3354–3387. [CrossRef]
40. Boopathi, T.; Ki, J.S. Impact of environmental factors on the regulation of cyanotoxin production. *Toxins* **2014**, *6*, 1951–1978. [CrossRef]
41. Žegura, B.; Štraser, A.; Filipič, M. Genotoxicity and potential carcinogenicity of cyanobacterial toxins–A review. *Mutat. Res. Rev. Mutat.* **2011**, *727*, 16–41. [CrossRef]
42. Fischer, A.; Hoeger, S.J.; Stemmer, K.; Feurstein, D.J.; Knobeloch, D.; Nussler, A.; Dietrich, D.R. The role of organic anion transporting polypeptides (OATPs/SLCOs) in the toxicity of different microcystin congeners in vitro: A comparison of primary human hepatocytes and OATP-transfected HEK293 cells. *Toxicol. Appl. Pharmacol.* **2010**, *245*, 9–20. [CrossRef]
43. Frangez, R.; Zuzek, M.C.; Mrkun, J.; Suput, D.; Sedmak, B.; Kosec, M. Microcystin-LR affects cytoskeleton and morphology of rabbit primary whole embryo cultured cells in vitro. *Toxicon* **2003**, *41*, 999–1005. [CrossRef]
44. Davis, M.A.; Chang, S.H.; Trump, B.F. Differential sensitivity of normal and H-ras Oncogene-transformed rat kidney epithelial cells to okadaic acid-induced apoptosis. *Toxicol. Appl. Pharmacol.* **1996**, *141*, 93–101. [CrossRef]
45. Ding, W.X.; Nam-Ong, C. Role of oxidative stress and mitochondrial changes in cyanobacteria-induced apoptosis and hepatotoxicity. *FEMS Microbiol. Lett.* **2003**, *220*, 1–7. [CrossRef]
46. Žegura, B.; Volcic, M.; Lah, T.T.; Filipic, M. Different sensitivities of human colon adenocarcinoma (CaCo-2), astrocytoma (IPDDC-A2) and lymphoblastoid (NCNC) cell lines to microcystin-LR induced reactive oxygen species and DNA damage. *Toxicon* **2008**, *52*, 518–525. [CrossRef] [PubMed]
47. Westrick, J.A.; Szlag, D.C.; Southwell, B.J.; Sinclair, J. A review of cyanobacteria and cyanotoxins removal/inactivation in drinking water treatment. *Anal. Bioanal. Chem.* **2010**, *397*, 1705–1714. [CrossRef] [PubMed]
48. Teixeira, M.R.; Rosa, M.J.; Sorlini, S.; Biasibetti, M.; Christophoridis, C. Removal of Cyanobacteria and Cyanotoxins by Conventional Physical-chemical Treatment. In *Water Treatment for Purification from Cyanobacteria and Cyanotoxins*; Hiskia, A.E., Triantis, T.M., Antoniou, M.G., Kaloudis, T., Dionysiou, D.D., Eds.; Wiley: Hoboken, NJ, USA, 2020; pp. 69–98.
49. Feitz, A.J.; Waite, T.D.; Jones, G.J.; Boyden, B.H.; Orr, P.T. Photocatalytic degradation of the blue green algal toxin microcystin-LR in a natural organic-aqueous matrix. *Environ. Sci. Technol.* **1999**, *33*, 243–249. [CrossRef]
50. Gurbuz, F.; Codd, G.A. Microcystin removal by a natural-occuring substance: Pumice. *Bull. Environ. Contam. Toxicol.* **2008**, *81*, 323–327. [CrossRef] [PubMed]
51. Teixeira, M.R.; Rosa, M.J. Comparing dissolved air flotation and conventional sedimentation to remove cyanobacterial cells of Microcystis aeruginosa Part II. The effect of water background organics. *Sep. Purif. Technol.* **2007**, *53*, 126–134. [CrossRef]
52. Crossley, I.A.; Valade, M.T. A review of the technological developments of dissolved air flotation. *J. Water Supply Res. Technol.* **2006**, *55*, 479–491. [CrossRef]
53. Laszakovits, J.; MacKay, A.A. Removal of cyanotoxins by potassium permanganate: Incorporating competition from natural water constituents. *Water Res.* **2019**, *155*, 86–95. [CrossRef]
54. Kinley-Baird, C.; Calomeni, A.; Berthold, D.E.; Lefler, F.W.; Barbosa, M.; Rodgers, J.H.; Laughinghouse, H.D., IV. Laboratory-scale evaluation of effectiveness for control of microcystin producing cyanobacteria from Lake Okeechobee, Florida (USA). *Ecotoxicol. Environ. Saf.* **2021**, *207*, 111233. [CrossRef]

55. Kinley, C.M.; Iwinski-Wood, K.J.; Geer, T.D.; Hendrikse, M.; McQueen, A.D.; Calomeni, A.J.; Liang, J.; Friesen, V.; Simair, M.C.; Rodgers, J.H. Microcystin-LR degradation following copper-based algaecide exposures. *Water Air Soil Pollut.* **2018**, *229*, 62. [CrossRef]
56. Jones, G.J.; Orr, P.T. Release and degradation of microcystin following algicide treatment of a *Microcystis aeruginosa* bloom in a recreational lake, as determined by HPLC and protein phosphatase inhibition assay. *Water Res.* **1994**, *28*, 871–876. [CrossRef]
57. Brooke, S.; Newcombe, G.; Nicholson, B.; Klass, G. Decrease in toxicity of microcystins LA and LR in drinking water by ozonation. *Toxicon* **2006**, *48*, 1054–1059. [CrossRef] [PubMed]
58. Ho, L.; Sawade, E.; Newcombe, G. Biological treatment options for cyanobacteria metabolite removal—A review. *Water Res.* **2012**, *46*, 1536–1548. [CrossRef] [PubMed]
59. Lawton, L.A.; Robertson, P.K.J. Physico-chemical treatment methods for the removal of microcystins (cyanobacterial hepatotoxins) from potable waters. *Chem. Soc. Rev.* **1999**, *28*, 217–224. [CrossRef]
60. Vlad, S.; Anderson, W.B.; Peldszus, S.; Huck, P.M. Removal of the cyanotoxin anatoxin-a by drinking water treatment processes: A review. *J. Water Health* **2014**, *12*, 601–617. [CrossRef] [PubMed]
61. Pavagadhi, S.; Tang, A.L.L.; Sathishkumar, M.; Loh, K.P.; Balasubramanian, R. Removal of microcystin-LR and microcystin-RR by graphene oxide: Adsorption and kinetic experiments. *Water Res.* **2013**, *47*, 4621–4629. [CrossRef] [PubMed]
62. Wang, X.L.; Xing, B.S. Sorption of organic contaminants by biopolymer-derived chars. *Environ. Sci. Technol.* **2007**, *41*, 8342–8348. [CrossRef]
63. Hena, S.; Ismail, N.; Isaam, A.M.; Ahmad, A.; Bhawani, S.A. Removal of microcystin-LR from agueous solutions using % burn-off activated carbon of waste wood material. *J. Water Supply Res. Technol.* **2014**, *63*, 332–341. [CrossRef]
64. Pendleton, P.; Schumann, R.; Wong, S.H. Microcystin adsorption by activated carbon. *J. Collod. Interf. Sci.* **2001**, *240*, 1–8. [CrossRef]
65. Teng, W.; Wu, Z.; Fan, J.; Zhang, W.X.; Zhao, D. Amino-functionalized ordered mesoporous carbon for the separation of toxic microcystin-LR. *J. Mat. Chem. A* **2015**, *3*, 19168. [CrossRef]
66. Newcombe, G.; Morrison, J.; Hepplewhite, C.; Knappe, D.R.U. Simultaneous adsorption of MIB and NOM onto activated carbon. II. Competitive effects. *Carbon* **2002**, *40*, 2147–2156. [CrossRef]
67. Ho, L.; Newcombe, G. Evaluating the adsorption of microcystin toxins using granular activated carbon (GAC). *J. Water Supply Res. Technol.* **2007**, *56*, 281–291. [CrossRef]
68. Hnatukova, P.; Kopecka, I.; Pivokonsky, M. Adsorption of cellular peptides of Microcystis aeruginosa and two herbicides onto activated carbon: Effect of surface charge and interactions. *Water Res.* **2011**, *45*, 3359–3368. [CrossRef] [PubMed]
69. Huang, W.J.; Cheng, B.L.; Cheng, Y.L. Adsorption of microcystin-LR by three types of activated carbon. *J. Hazard. Mater.* **2007**, *141*, 115–122. [CrossRef]
70. Campinas, M.; Rosa, M.J. Assessing PAC contribution to the NOM fouling control in PAC/UF systems. *Water Res.* **2010**, *44*, 1636–1644. [CrossRef] [PubMed]
71. Drogui, P.; Daghrir, R.; Simard, M.C.; Sauvageau, C.; Blais, J.F. Removal of microcystin-LR from spiked water using either activated carbon or anthracite as filter material. *Environ. Technol.* **2012**, *33*, 381–391. [CrossRef]
72. Zhi, M.; Yang, F.; Meng, F.; Li, M.; Manivannan, A.; Wu, N. Effects of pore structure on performance of an activated-carbon supercapacitor electrode recycled from scrap waste tires. *ACS Sustain. Chem. Eng.* **2014**, *2*, 1592–1598. [CrossRef]
73. Lou, F.; Zhou, H.; Tran, T.D.; Buan, M.E.M.; Vullum-Bruer, F.; Ronning, M.; Walmsley, J.C.; Chen, D. Coaxial carbon/metal oxide/aligned carbon nanotube arrays as high-performance anodes for lithium ion batteries. *ChemSusChem* **2014**, *7*, 1335–1346. [CrossRef]
74. Li, L.; Qiu, Y.; Huang, J.; Li, F.; Sheng, G.D. Mechanisms and factors influencing adsorption of microcystin-LR on biochars. *Water Air Soil Poll.* **2014**, *225*, 2220. [CrossRef]
75. Kim, S.; Yun, Y.S.; Choi, Y.E. Development of waste biomass based sorbent for removal of cyanotoxin microcystin-LR from aqueous phases. *Bioresource Technol.* **2018**, *247*, 690–696. [CrossRef]
76. Yasmin, R.; aftab, K.; Kashif, M. Removal of microcystin-LR from agueous solution using *Moringa oleifera* Lam. Seeds. *Water Sci. Technol.* **2019**, *79*, 104–113. [CrossRef] [PubMed]

77. Sathya, K.; Saranya, P.; Swarnalatha, S.; Mandal, A.; Sekaran, G. Removal of microcystin-RR, a membrane foulant using exocellular polymer from *Enterobacter ludwigii*: Kinetic and isotherm studies. *Desalination* **2015**, *369*, 175–187.
78. Park, J.H.; Wang, J.J.; Kim, S.H.; Kang, S.W.; Jeong, C.Y.; Jeon, J.R.; Park, H.P.; Cho, J.S.; Delaune, R.D.; Seo, D.C. Cadmium adsorption characteristics of biochars derived using various pine t tree residues and pyrolysis temperatures. *J. Colloid Interface Sci.* **2019**, *553*, 298–307. [CrossRef] [PubMed]
79. Frišták, V.; Pipíška, M.; Soja, G. Pyrolysis treatment of sewage sludge: A promising way to produce phosphorus fertilizer. *J. Clean. Prod.* **2018**, *172*, 1772–1778. [CrossRef]
80. Morris, R.J.; Williams, D.E.; Luu, H.A.; Holmes, C.F.; Andersen, R.J.; Calvert, S.E. The adsorption of microcystin-LR by natural clay particles. *Toxicon* **2000**, *38*, 303–308. [CrossRef]
81. Laughinghouse IV, H.D.; Lefler, F.W.; Berthold, D.E.; Bishop, W.M. Sorption of microcystin using lanthanum-modified bentonite clay. *J. Aquat. Plant Manag.* **2020**, *58*, 72–75.
82. Wang, Z.; Wang, C.; Wang, P.; Qian, J.; Hou, J.; Ao, Y. Process optimization for microcystin-LR adsorption onto nano-sized montmorillonite K10: Application of response surface methodology. *Water Air Soil Poll.* **2014**, *225*, 2124. [CrossRef]
83. Wang, Z.; Wang, C.; Wang, P.; Qian, J.; Hou, J.; Ao, Y. Response surface modelling and optimization of microcystin-LR remocal from agueous phase by polyacrylamide/sodium alginate-motmorillonite superabsorbent nanocomposite. *Desal. Eater Treat.* **2015**, *56*, 1121–1139. [CrossRef]
84. Akbal, F.O.; Akdemir, N.; Onar, A.N. FT-IR spectroscopic detection of pesticide after sorption onto modified pumice. *Talanta* **2000**, *53*, 131–135. [CrossRef]
85. Sathishkumar, M.; Pavagadhi, S.; Vijayaraghavan, K.; Balasubramanian, R.; Ong, S.L. Concomitant uptake of microcystin-LR and -RR by peat under various environmental conditions. *Chem. Eng. J.* **2011**, *172*, 754–762. [CrossRef]
86. Lee, J.; Walker, H.W. Adsorption of microczstin-LR onto iron oxide nanoparticles. *Colloid. Surface A* **2011**, *373*, 94–100. [CrossRef]
87. Okupnik, A.; Contardo-Jara, V.; Pflugmacher, S. Potential role of engineered nanoparticles as contaminant carriers in aquatic ecosystems: Estimating sorption processes of the cyanobacterial toxin microcystin-LR by TiO_2 nanoparticles. *Colloid. Surface A* **2015**, *481*, 460–467. [CrossRef]
88. Wu, L.; Lan, J.; Wang, S.; Zhu, J. Synthesis of N-doped carbon xerogel (N-CX) and its applications for adsorption removal of microcystin-LR. *Z. Phys. Chem.* **2017**, *231*, 1525–1541. [CrossRef]
89. EBC. *European Biochar Certificate-Guidelines for a Sustainable Production of Biochar*; EBC: Arbaz, Switzerland, 2015. [CrossRef]
90. Shaheen, S.M.; Niazi, N.K.; Hassan, N.E.E.; Bibi, I.; Wang, H.; Tsang, D.C.W.; Ok, Y.S.; Bolan, N.; Rinklebe, J. Wood-based biochar for the removal of potentially toxic elements in weter and wastewater: A critical review. *Int. Mater. Rev.* **2019**, *64*, 216–247. [CrossRef]
91. Micháleková-Richveisová, B.; Frišták, V.; Pipíška, M.; Ďuriška, L.; Moreno-Jimenez, E.; Soja, G. Iron-impregnated biochars as effective phosphate sorption materials. *Environ. Sci. Pollut. Res. Int.* **2017**, *24*, 463–475. [CrossRef]
92. Bridgwater, A.V. Review of fast pyrolysis of biomass and product upgrading. *Biomass Bioenergy* **2012**, *38*, 68–94. [CrossRef]
93. Kunhikrishnan, A.; Bibi, I.; Bolan, N.; Seshadri, B.; Choppala, G.; Niazi, N.K.; Kim, W.I.; Ok, Y.S.; Uchimiya, S.M.; Chang, S.; et al. Biochar for inorganic contaminant management in waste and wastewater. In *Biochar: Production, Characterization and Applications*; CRC Press: Boca Raton, FL, USA, 2015; pp. 167–219.
94. Brown, R.A.; Kercher, A.K.; Nguyen, T.H.; Nagle, D.C.; Ball, W.P. Production and characterization of synthetic wood chars for use as surrogates for natural sorbents. *Org. Geochem.* **2006**, *37*, 321–333. [CrossRef]
95. Rutherford, D.W.; Wershaw, R.L.; Cox, L.G. *Changes in Composition and Porosity Occurring during the Thermal Degradation of Wood and Wood Components*; US Geological Survey, Scientific Investigation Report 2004-5292; USGS: Reston, VA, USA, 2004.
96. Mohan, D.; Pittman, C.U.; Steele, P.H. Pyrolysis of wood/biomass for bio-oil: A critical review. *Energy Fuels* **2006**, *20*, 848–889. [CrossRef]
97. Lehmann, J.; Joseph, S. *Biochar for Environmental Management—Science, Technology and Implementation*, 2nd ed.; Routledge: London, UK; Sterling, VA, USA, 2015.
98. Park, S.H.; Cho, H.J.; Ryu, C.; Park, Y.K. Removal of copper (II) in aqueous solution using pyrolytic biochars derived from red macroalga *Porphyra tenera*. *J. Ind. Eng. Chem.* **2016**, *36*, 314–319. [CrossRef]

99. Zhang, R.H.; Li, Z.G.; Liu, X.D.; Wang, B.C.; Zhou, G.L.; Huang, X.X.; Lin, C.F.; Wang, A.H.; Brooks, M. Immobilization and bioavailability of heavy metals in greenhouse soils amended with rice straw-derived biochar. *Ecol. Eng.* **2017**, *98*, 183–188. [CrossRef]
100. Bogusz, A.; Oleszczuk, P.; Dobrowolski, R. Application of laboratory prepared and commercially available biochars to adsorption of cadmium, copper and zinc ions from water. *Bioresour. Technol.* **2015**, *196*, 540–549. [CrossRef] [PubMed]
101. Ma, Y.; Liu, W.J.; Zhang, N.; Li, Y.S.; Jiang, H.; Sheng, G.P. Polyethylenimine modified biochar adsorbent for hexavalent chromium removal from the aqueous solution. *Bioresour. Technol.* **2014**, *169*, 403–408. [CrossRef]
102. Agrafioti, E.; Kalderis, D.; Diamadopoulos, E. Ca and Fe modified biochars as adsorbents of arsenic and chromium in aqueous solutions. *J. Environ. Manag.* **2014**, *146*, 444–450. [CrossRef] [PubMed]
103. Inyang, M.; Gao, B.; Yao, Y.; Xue, Y.; Zimmerman, A.R.; Pullammanappallil, P.; Cao, X. Removal of heavy metals from aqueous solution by biochars derived from anaerobically digested biomass. *Bioresour. Technol.* **2012**, *110*, 50–56. [CrossRef]
104. Tang, L.; Yu, J.; Pang, Y.; Zeng, G.; Deng, Y.; Wang, J.; Ren, X.; Ye, S.; Peng, B.; Feng, H. Sustainable efficient adsorbent: Alkali-acid modified magnetic biochar derived from sewage sludge for aqueous organic contaminant removal. *Chem. Eng. J.* **2018**, *336*, 160–169. [CrossRef]
105. Ruthiraan, M.; Abdullah, E.C.; Mubarak, N.M.; Noraini, M.N. A promising route of magnetic based materials for removal of cadmium and methylene blue from waste water. *J. Environ. Chem. Eng.* **2017**, *5*, 1447–1455. [CrossRef]
106. Lin, L.; Jiang, W.; Xu, P. Comparative study on pharmaceuticals adsorption in reclaimed water desalination concentrate using biochar: Impact of salts and organic matter. *Sci. Total Environ.* **2017**, *601*, 857–864. [CrossRef]
107. Tan, X.; Liu, Y.; Gu, Y.; Xu, Y.; Zeng, G.M.; Hu, X.J.; Liu, S.B.; Wang, X.; Liu, S.M.; Li, J. Biochar-based nano-composites for the decontamination of wastewater: A review. *Bioresour. Technol.* **2016**, *212*, 318–333. [CrossRef] [PubMed]
108. Rajapaksha, A.U.; Chen, S.S.; Tsang, D.C.; Zhang, M.; Vithanage, M.; Mandal, S.; Gao, B.; Bolan, N.S.; Ok, Y.S. Engineered/designer biochar for contaminant removal/immobilization from soil and water: Potential and implication of biochar modification. *Chemosphere* **2016**, *148*, 276–291. [CrossRef]
109. Igalavithana, A.D.; Lee, S.E.; Lee, Y.H.; Tsang, D.C.W.; Rinklebe, J.; Kwon, E.E.; Ok, Y.S. Heavy metal immobilization and microbial community abundance by vegetable waste and pine cone biochar of agricultural soils. *Chemosphere* **2017**, *174*, 593–603. [CrossRef]
110. Dieguez-Alonso, A.; Anca-Couce, A.; Frišták, V.; Moreno-Jiménez, E.; Bacher, M.; Bucheli, T.D.; Cimò, G.; Conte, P.; Hagemann, N.; Haller, A.; et al. Designing biochar properties through the blending of biomass feedstock with metals: Impact on oxyanions adsorption behavior. *Chemosphere* **2019**, *214*, 743–753. [CrossRef] [PubMed]
111. Zama, E.F.; Zhu, Y.G.; Reid, B.J.; Sun, G.X. The role of biocharproperties in influencing the sorption and desorption of Pb(II), Cd(II) and As(III) in aqueous solution. *J. Clean Prod.* **2017**, *148*, 127–136. [CrossRef]
112. Jiang, J.; Pang, S.Y.; Ma, J. Comment on Adsorption of hydroxyl-and amino-substituted aromatics on carbon nanotubes. *Environ. Sci. Technol.* **2009**, *43*, 2–3. [CrossRef] [PubMed]
113. Kloss, S.; Zehetner, F.; Oburger, E.; Buecker, J.; Kitzler, B.; Wenzel, W.W.; Wimmer, B.; Soja, G. Trace element concentrations in leachates and mustard plant tissue (*Sinapis alba* L.) after biochar application to temperate soils. *Sci. Total Environ.* **2014**, *481*, 498–508. [CrossRef] [PubMed]
114. Frišták, V.; Micháleková-Richveisová, B.; Víglašová, E.; Ďuriška, L.; Galamboš, M.; Moreno-Jimenéz, E.; Pipíška, M.; Soja, G. Sorption separation of Eu and As from single-component systems by Fe-modified biochar: Kinetic and equilibrium study. *J. Iran. Chem. Soc.* **2017**, *14*, 521–530. [CrossRef]
115. Li, X.; Pignatello, J.J.; Wang, Y.; Xing, B. New insight into adsorption mechanism of ionizable compounds on carbon nanotubes. *Environ. Sci. Technol.* **2013**, *47*, 8334–8341. [CrossRef]
116. Kah, M.; Sigmund, G.; Xiao, F.; Hofmann, T. Sorption of ionizable and ionic organic compounds to biochar, activated carbon and other carbonaceous materials. *Water Res.* **2017**, *124*, 673–692. [CrossRef]
117. Sizmur, T.; Fresno, T.; Akgül, G.; Frost, H.; Moreno-Jiménez, E. Biochar modification to enhance sorption of inorganics from water- review. *Bioresour. Technol.* **2018**, *246*, 34–47. [CrossRef]
118. Teixidó, M.; Pignatello, J.J.; Beltrán, J.L.; Granados, M.; Peccia, J. Speciation of the ionizable antibiotic sulfamethazine on black carbon (biochar). *Environ. Sci. Technol.* **2011**, *45*, 10020–10027. [CrossRef]

119. Lin, Y.R.; Teng, H.S. Mesoporous carbons from waste tire char and their application in wastewater discoloration. *Micropor. Mesopor. Mat.* **2002**, *54*, 167–174. [CrossRef]
120. Wu, X.Q.; Xiao, B.D.; Li, R.H.; Wang, C.B.; Huang, J.T.; Wang, Z. Mechanisms and factors affecting sorption of microcystins onto natural sediments. *Environ. Sci. Technol.* **2011**, *45*, 2641–2647. [CrossRef]

water

MDPI

Review

Biochar as an Eco-Friendly and Economical Adsorbent for the Removal of Colorants (Dyes) from Aqueous Environment: A Review

Prithvi Srivatsav [1], Bhaskar Sriharsha Bhargav [1], Vignesh Shanmugasundaram [1], Jayaseelan Arun [2], Kannappan Panchamoorthy Gopinath [1,*] and Amit Bhatnagar [3,*]

[1] Department of Chemical Engineering, Sri Sivasubramaniya Nadar College of Engineering, Kalavakkam, Chennai 603110, Tamil Nadu, India; prithvi18043@chemical.ssn.edu.in (P.S.); sriharsha389@gmail.com (B.S.B.); vignesh18059@chemical.ssn.edu.in (V.S.)

[2] Centre for Waste Management, International Research Centre, Sathyabama Institute of Science and Technology, Jeppiaar Nagar, Chennai 600119, Tamil Nadu, India; arunjayaseelan93@gmail.com

[3] Department of Separation Science, LUT School of Engineering Science, LUT University, Sammonkatu 12, FI-50130 Mikkeli, Finland

* Correspondence: gopinathkp@ssn.edu.in (K.P.G.); Amit.Bhatnagar@lut.fi (A.B.)

Received: 15 November 2020; Accepted: 16 December 2020; Published: 18 December 2020

Abstract: Dyes (colorants) are used in many industrial applications, and effluents of several industries contain toxic dyes. Dyes exhibit toxicity to humans, aquatic organisms, and the environment. Therefore, dyes containing wastewater must be properly treated before discharging to the surrounding water bodies. Among several water treatment technologies, adsorption is the most preferred technique to sequester dyes from water bodies. Many studies have reported the removal of dyes from wastewater using biochar produced from different biomass, e.g., algae and plant biomass, forest, and domestic residues, animal waste, sewage sludge, etc. The aim of this review is to provide an overview of the application of biochar as an eco-friendly and economical adsorbent to remove toxic colorants (dyes) from the aqueous environment. This review highlights the routes of biochar production, such as hydrothermal carbonization, pyrolysis, and hydrothermal liquefaction. Biochar as an adsorbent possesses numerous advantages, such as being eco-friendly, low-cost, and easy to use; various precursors are available in abundance to be converted into biochar, it also has recyclability potential and higher adsorption capacity than other conventional adsorbents. From the literature review, it is clear that biochar is a vital candidate for removal of dyes from wastewater with adsorption capacity of above 80%.

Keywords: adsorption; biochar; dyes removal; wastewater treatment

1. Introduction

Water pollution has become a major environmental problem globally. Different types of contaminants, mainly discharged from the industrial and agricultural activities, significantly contribute to water pollution. One of the major contributors to water pollution is the release of untreated dye effluents. These dyes are not only harmful to the plants and aquatic life, but also to human beings. Cancer, allergies, skin diseases are some of the health complications that may arise due to the ingestion and absorption of dye-contaminated water by humans [1]. Biochar has been identified as a potential candidate for wastewater treatment. The use of biochar for wastewater treatment has an added advantage due to the availability of abundance of surface functional groups on biochar surface and having a large surface area. Biochar is produced by the decomposition of biomass by thermochemical methods in the absence or low amount of oxygen. Different biomass feedstocks could be utilized to synthesize biochar, which include algae, crop residues, forests biomass, and animal manures. Torrefaction, hydrothermal carbonization, microwave heating, and gasification are some of the methods available for thermal decomposition of biomass [2,3]. Before biochar can be used, it has to be subjected to pretreatment processes (e.g., sieving, washing, crushing, etc.), followed by pyrolysis.

Biochar is a heterogeneous, carbonaceous char obtained from thermally treating a large amount of organic waste/mixture that has been heated and decomposed completely. Biochar exhibit properties, such as catalytic activity, adsorption efficiency, high porosity, and high surface area, and has been found to enhance various processes, such as anaerobic digestion, soil retention, and adsorption [4]. As other methods of controlling pollution of water/air/soil, such as membrane separation, ion exchange filtration, etc., have exhibited significant economic demerits and low efficiencies, biochar has become an important material to remove the aquatic pollutants [5].

Environmentally friendly, economically feasible, and easily designable adsorbents for the treatment of water have gained popularity in the past few decades. In this regard, use of biochar, obtained from natural sources, such as forest and agricultural biomass, organic waste, and animal waste has become important [6,7]. This review focuses exclusively on how biochar works as an adsorbent for the removal of dyes, present in water ass pollutants. The inherent properties of biochar make it an ideal candidate for the adsorptive removal of dyes from water. Biochar has already been established as a viable non-toxic and environmentally-friendly adsorbent capable of adsorbing a large spectrum of compounds from wastewater [8,9]. The potential of biochar is influenced by a variety of factors starting from the source of biomass from which biochar is prepared along with the method of preparation, reaction conditions, nature of pollutants, and the mechanism of action, all of which have been examined extensively in this review. The use of biochar as being eco-friendly for the removal of dye from wastewater has been examined in the past by several researchers [10–13]. This review aims to summarize and provide a holistic view on the research on biochar as an adsorbent for the removal of dyes from wastewater.

2. Colorants in Water and Toxicity

2.1. Natural and Synthetic Dyes

Dyes can be defined as color-imparting organic compounds that are water or oil soluble; they are distinguished from pigments that are insoluble. Natural dyes are those that are derived or extracted from natural sources, such as animals, flowers, roots, mollusks, minerals, etc. Natural dyes are broadly classified into two types: adjective and substantive [14]. Adjective dyes give permanent color only when used along with a mordant to bind them to the fabric; meanwhile substantive dyes contain a natural mordant, called tannin, and can give fast color without the use of additional mordants [15]. Mordants are compounds that act as a bridge between the fabric molecules and the dye, holding it in place to promote fastness [16]. Weak acids, such as tannic acid and acetic acid, are some natural mordants [17,18], while metal salts, such as copper sulfate and ferrous sulfate, can also be utilized. The use of natural dyes is advantageous as these are relatively non-toxic and renewable in nature, but their use is not cost-effective in the industrial context, and they fail to give an even consistent hue when compared to the synthetic dyes. Natural dyes may still be used in domestic and small-scale operations.

Synthetic dyes are usually unsaturated organic molecules. The first synthetic dye prepared was Mauve, a reddish-purple dye, which quickly degraded under water or direct sunlight to form a pale purple color. The first synthetic dye was derived from coal tar, the product resulting from the carbonization of coal. In the current context, synthetic dyes are more economical and exhibit better color fastness in comparison to natural dyes; thus, they dominate the market. Though they are more economical, synthetic dyes are also decidedly more toxic and polluting than natural dyes, causing environmental pollution and adverse health effects on living organisms [15].

2.2. Classification of Dyes

2.2.1. Chromophores and Color Index (C.I.)

Atoms or groups of atoms are said to be chromogenic if they are able to impart colour to the dye, and different arrangements and numbers of these chromogenic groups in a molecule impart different colors to the dyes. The other atoms or groups of atoms in the molecule, which are bound to the chromophore, and influence or bring a change in the color of the dye, are called auxochromes [19]. Thus, different textile dyes have specific structures that contribute to their characteristic colors. Some examples of chromophores are carbonyl groups, nitro groups, azo groups, or a conjugated pi electron system. Groups such as hydroxyl, aniline, and sulfonic acid act as auxochromes [20]. Dyes are classified by their applications and are given a unique identifying name called the Color Index (CI). As dye structures can be very complex, referring to it by its chemical name can be impractical, and common names can change between regions; thus, the name of the dye is standardized by using its CI. Every dye is issued a generic name and a CI number; the generic name consists of the method of application of the dye (e.g., direct, reactive etc.), the hue, and an identification number. The dye is also given a CI number based on the functional group and configuration of the molecule. For example, the dye commonly known as Remazol Red B is referred to as CI Reactive Red 22 (CI number: 14,824) under CI classification rules [21].

2.2.2. Disperse Dyes

Disperse dyes are mostly non-ionic in nature and are insoluble or very sparingly soluble in water; they are named so because their application involves dispersing the dye into a very fine suspension in solvent [22]. The chromogenic groups in disperse dyes are azo, anthraquinone, or nitro groups. The non-ionic nature of disperse dyes make them an ideal choice for dying synthetic and hydrophobic fibers, such as acetate, polyester, and sometimes nylon and acrylic fibers [23]. This is because these fibers are negatively charged and so reactive or basic dyes cannot be used. Only the non-ionic disperse dyes, which are not affected by surface charge, are able to reliably dye these fabrics. Traditionally, a carrier is added to the dye to improve the dispersion action and to aid dyeing. Disperse dyes can be classified from class A to class D based on their sublimation temperature, with class A having the lowest and class D the highest [24]. Since sublimation temperature depends on the size of the molecule, class A dyes have lower relative molecular size compared to class D dyes. Due to its sparing solubility, non-ionic nature, and non-biodegradability, disperse dyes are particularly harmful when left untreated in wastewater [25].

2.2.3. Direct Dyes

Direct dyes are water-soluble, anionic dyes that, unlike reactive or vat dyes, can be applied directly onto substrates using a neutral or alkaline bath (using sodium chloride or sodium sulfate) [26]. These dyes have an affinity to cellulosic materials, such as paper, cardboard, cotton, etc., but can also be applied on fabrics, such as, rayon and silk, with the use of mordants. The chromogenic functional groups in direct dyes include stilbene, phthalocyanine, oxazine, thiazole, but mainly azo groups [27]. Direct dyes are advantageous compared to other dyes because they have superior lightfastness compared to most reactive dyed hues, even though they cost less and are, thus, more economical. They also require less water use and the salt concentrations of the effluent are much less, compared to most reactive dyes. Some direct dyes, such as, Congo red, are carcinogenic, and have been banned from use [28].

2.2.4. Reactive Dyes

Reactive dyes have become one of the most widely used synthetic dyes in the industrial context due to their excellent wash fastness and bright and varied types of hues [29]. The chromophores in reactive dyes are largely azo groups; blue and green colors are given due to the presence of anthraquinone and phthalocyanine structures [30]. Direct dyes are largely used to dye cellulosic substrates and fibers, although other substrates can be used too. Unlike direct dyes, however, reactive dyes form new covalent bonds with the nucleophilic sites in fabric molecules, thus leading to its remarkable wash fastness [21]. Some of the most commonly utilized groups in reactive dyes are trichloropyrimidine, sulphatoethylsulphone, dichloroquinoxaline, and dichlorotriazin [13]. The major disadvantage regarding reactive dyes is their environmental threat. Effluent from dyeing cotton, using reactive dyes, are extremely polluted, having very high chemical oxygen demand (COD), salt load, and visible color in water [31]. Both, the unfixed dye and its hydrolyzed form, are soluble in water, and thus their removal is particularly challenging [32]. Some reactive dyes are also associated with heavy metals, such as chromium, copper, or nickel, and these can later be released into aquatic ecosystems on degradation of the dye molecule.

2.3. Toxicity of Dyes

The global textile industry is estimated to be worth around $1 trillion USD and its contribution towards total world exports is around 7%, employing 35 million people worldwide [33]. Thus, this industry has a high impact on the environment and human health in general, due to the pollution it causes. The most prominent and destructive form of pollution, caused by the textile industry, is the water pollution due to manufacturing of dyes. Textile effluents are both aesthetically polluted, and have high salinity, chemical oxygen demand, and ecotoxicity [34], and due to their increasing ubiquity in surface water, can lead to adverse effects to human and wildlife health and to aquatic ecosystems in general. Most synthetic dyes are highly toxic to humans and aquatic beings, and have acute and chronic effects. For example, reactive dyes are notorious, causing health issues such as, dermatitis, occupational asthma, rhinitis, and other allergic reactions for the workers involved in these dyes manufacturing [32]. Dyes are also mutagenic and carcinogenic in nature [35,36], which leads to chronic effects, such as kidney, urinary bladder, and liver cancer in dye workers. A xanthene dye called erythrosine is carcinogenic, neurotoxic and DNA-damaging for humans and animals alike [30]. Metal complexed dyes, which are widely used for their resistance, have heavy metals, such as copper, nickel, and chromium. When discharged to aquatic environments, these metals can be taken up by fish gills and can be transferred to humans through the food chain [36]. Current treatment methods are inadequate to treat dye effluents effectively, because of their recalcitrant nature in aerobic environments [37], and thus, these substances can linger in soil and lead to bioaccumulation, leading to complications in organisms higher up the food chain [38]. Thus, current effluent treatment techniques are inadequate for the dyeing industry and to prevent the further insemination of surface water with such mutagenic and carcinogenic molecules, we must adopt novel and more effective treatment techniques, such as bioremediation or biochar adsorption.

3. Treatment Technologies for Dyes Removal from Water

3.1. Coagulation

Coagulation is one of the most popular wastewater treatment techniques used since the early 20th century. Coagulation is the process of adding chemical compounds to bind particles together until they acquire a large mass to ultimately settle down. These chemicals are known as coagulants and carry a positive charge, which are mixed rapidly in the wastewater for uniform distribution. Most of the dissolved/suspended particles encountered in wastewater carry a negative charge, which are neutralized by these coagulants, thus making these capable of sticking together. Coagulation process is usually employed as a preliminary step in wastewater treatment process. The most frequently used coagulants are iron or aluminum salts. However, wastewater (containing dyes) is rich in color, and have high COD levels. Hence, conventional methods, such as coagulation, prove inefficient and moreover cause the problem of sludge disposal [39]. A combination of the conventional coagulation technique with other treatment methods must be innovated to improve its efficiency. For example, combination of coagulation and adsorption techniques was a feasible way for the removal of reactive dyes from water [40]. The adsorbent used was activated carbon, derived from coconut shells, and the coagulation process was carried out using aluminum chloride as the coagulant. It was found that the removal efficiencies for Orange 16 and Black 5 reactive dyes were 84% and 90%, respectively [40].

3.2. Advanced Oxidation Processes (AOPs)

AOPs are chemical treatment methods used to remove the organic/inorganic contaminants present in wastewater by the oxidizing action caused due to the in-situ production of hydroxyl radicals ($^{\bullet}OH$) [41]. These radicals are produced by oxidizing agents (H_2O_2, O_3, $KMnO_4$), catalysts, or UV light. Some of the AOPs include photocatalysis, ozonation etc. [42]. The following sections briefly explain some of the AOPs used in dye removal from wastewater.

3.2.1. Ozonation

Most of the dyes, encountered in wastewater, have polycyclic aromatic structures containing elements, such as nitrogen, metals, and sulfur, which makes it difficult to treat the wastewater by physical, chemical, and biological methods. Conjugated chains present in the dye structures, responsible for imparting color, are actively destroyed by ozonation, which is an AOP method that involves the chemical treatment of wastewater by dissolving ozone in water [43]. Employing ozonation as a treatment technique is advantageous as zero sludge is generated. Degradation of the dye is achieved in a single step and furthermore, ozone decomposes into stable oxygen [44]. However, ozonation as a treatment process very rarely results in complete oxidation, so by-products are usually formed in the effluent stream [45].

3.2.2. Fenton's Reagent and Fenton-Like Processes

Fenton's reagent is a solution of ferrous iron along with hydrogen peroxide, which finds its use as a catalyst in oxidizing various contaminants present in wastewater. A composite of La-Fe-O [46] was used as a photo-Fenton catalyst in the presence of light irradiation and hydrogen peroxide, and it was found that rhodamine B dye was oxidized to 98% within 25 min.

3.3. Membrane Processes

Membranes have been in use for wastewater treatment as early as the 1960s. Since membrane processes were too expensive at that time, this process was only chosen for specialized applications. Since the 2000s, membranes have been made cost-effective and are being used with other conventional water treatment processes. A membrane is a thin, semi-permeable material that is attached to a porous support, and is used for the removal of dissolved substances, based on properties, such as, size or charge, when a driving force is applied on it. Membrane processes are used in reverse osmosis (RO), forward osmosis, nanofiltration, and ultrafiltration.

3.3.1. Nanofiltration

The membranes used for nanofiltration have pore size within the range of 0.1–10 nm. Nanofiltration membranes have the advantages of separating dyes with a high molecular weight and also have >90% rejection efficiency for dye removal, making it a promising approach towards dye removal [47]. For example, positively charged polyethylenimine-modified nanofiltration membrane showed semi-xylenol orange, Tropaeolin O, Victoria blue B dyes removal efficiency of 99%, 98.3%, and 99.2%, respectively [48].

3.3.2. Forward Osmosis (FO)

FO is a water treatment process that utilizes the osmotic pressure gradient to separate water from its dissolved solutes. Since FO process is completely devoid for the requirement of a driving force, it is more energy efficient compared to reverse osmosis and other membrane separation processes [49]. A thin-film composite membrane was used under forward osmosis by [50], and it was found that it had a dye rejection rate of ≥96% for commonly used dyes in the textile industries.

3.4. Biological Process

Biological process involves the usage of bacteria, microbes, and other microorganisms to treat wastewater. These biological processes are environmentally friendly, energy saving, generate low sludge, and require zero to minimal amount of chemicals to be used. The efficiency of biological processes could further be increased by varying the environmental conditions to favor the growth of the microorganisms. Algae is widely used by researchers as a potential option for the purpose of biosorption, as algae contains proteins, lipids and functional groups such as amino, carboxylate, sulfate, etc., in its structure [51]. Since algae possesses a wide surface area and excellent binding affinity in its cell structure, it results in high biosorption capabilities [52]. As algae is easily accessible (highly abundant in saltwater oceans and freshwater lakes), the use of algae could subsequently be extended for the dye removal from textile wastewater. For example, chemically (sulfuric acid) modified defatted Laminaria japonica biomass (renewable brown algae) showed methylene blue adsorption capacity of 549.45 mg/g, and quasi-equilibrium was achieved within 60 min under optimal conditions with a biosorbent dose of 0.6 g/L, pH 6 and temperature of 308 K [53].

Bioreactors are also becoming increasingly popular for dyes removal. Usually, a combination of both aerobic and anaerobic processes is used for the treatment of azo dyes. For example, the removal of Alizarin Yellow R dye was studied by the combined process of up-flow bio-electrocatalyzed electrolysis reactor and aerobic bio-contact oxidation reactor in just 6 h of hydraulic retention time [54]. Moreover, the COD removal efficiency and decolorization efficiency was found to be 93.0 ± 0.5% and 93.8 ± 0.7%, respectively, in the process.

3.5. Adsorption Process

As far as dye removal from water is concerned, adsorption has been found as one of the best treatment processes among other conventional water treatment methods due to its low-cost, affordability, greater efficiency, and the fact that it requires minimum maintenance [55]. Adsorption also has the added advantage of producing no detrimental residues and having the capacity to treat a large volumes of water [56]. An adsorbent could also be recycled multiple times for its usage in subsequent treatment processes [57]. Common materials, such as activated carbon, zeolites, activated alumina, silica gel and polymeric adsorbents have been widely used for water treatment. The use of biomaterials for adsorption processes instead of conventional materials is now being the subject of interest by many researchers as the commercial value of biomaterials is low, and also they are available in abundance [58]. Naturally-derived biopolymers, which are hyperreactive, chemically stable, possess good physicochemical properties have garnered significant attention that is worth looking into for employing these biopolymers for the role of green adsorbents [59]. Table 1 highlights the major advantages and disadvantages of treatment techniques, available for dye removal from water.

Table 1. The advantages and disadvantages of various treatment technologies for dyes removal from water.

Treatment Technology for Dyes Removal	Advantages	Disadvantages
Coagulation	• Reduced time for settling of suspended solids • Easy removal of fine particles • Effective in removing bacteria, protozoa, and virus	• High cost to spend for frequent monitoring and accurate dosing • Huge volume of sludge generation
Advanced Oxidation Processes (AOP)	• •OH radicals can treat a wide range of organic material • Zero sludge production	• Fenton's reagent AOP results in iron sludge generation • High capital and maintenance costs are expected

Table 1. *Cont.*

Treatment Technology for Dyes Removal	**Advantages**	**Disadvantages**
Membrane Processes	• Minor, valuable products can be recovered from the feed stream • Process can be easily "scaled-up" • No-phase changes involve between the feed and product stream • Eco-friendly as simple and non-toxic materials are used	• High flow rate has the potential to damage the membrane • This process results in membrane fouling effects. Regeneration and extensive cleaning are required. • High equipment cost
Biological Processes	• Almost all biodegradable organic matter is effectively removed • Efficient attenuation of color • Eco-friendly and a common wastewater treatment mechanism	• Slow process • An optimal favorable environment is crucial • Biological sludge generation • Remediation of dye molecules is tough
Adsorption Processes	• Highly efficient process • Applicable for a wide variety of target contaminants • Treatment technology is easy to employ	• Deterioration of adsorbent performance when subjected to multiple operational cycles • Spent adsorbent is likely to be a hazardous waste • Regeneration of adsorbent material is expensive

4. Biochar

4.1. Biochar Synthesis by Various Methods

Biochar is essentially a by-product formed when a large amount of organic matter (biomass) is heated at high temperatures in the absence or low amount of oxygen. Therefore, depending on the source and nature of the raw material, the process to prepare biochar also varies. In the industries however, there are mainly three processes, which dominate when it comes to the preparation of biochar. These are pyrolysis, hydrothermal liquefaction, and hydrothermal carbonization [60,61]. The three processes mentioned are used, depending on the raw material, hence the nature of biochar prepared by these three processes vary from one another.

4.1.1. Hydrothermal Carbonization

Hydrothermal carbonization in simple words is a method used to produce "structured" carbon such as charcoal, biochar, etc., from organic matter [62,63]. The main concept behind hydrothermal carbonization is to replicate natural carbon formation (when bioorganic compounds are exposed to extreme pressures and temperatures over thousands of years), but accomplish the same result in a shorter duration. In essence, hydrothermal carbonization is done by taking a mixture of biomass (animal wastes, plants etc.) and water in a pressure vessel, which is then heated to high temperatures (180–250) °C and extremely high pressures of 10 bars or more [62–66]. At such high temperatures and pressure, the pH of the solution decreases due to the increase in production of oxonium ion. At these specific conditions, more and more organic matter releases into the water due to the low pH conditions, which causes the formation of a sludge-like compound that is predominantly made of carbon. The sludge obtain can be separated and dried. Various compounds such as bio-oil, hydrochar, biochar, carboxylic acids, ketones, aromatics, etc., can then be used for various purposes [64,67]. Depending on the required product, the reaction can be stopped at multiple stages to obtain a variety of products. The biochar produced from regular pyrolysis varies in many aspects from the biochar produced by hydrothermal carbonization; hence, the product obtained from hydrothermal carbonization is called as hydrochar rather than biochar. Hydrochar and biochar vary in properties and conditions in which they are prepared [68], but they are essentially composed of the same chemical constituents and are prepared from the same raw material [64,65].

Hydrochar produced as a result of hydrothermal carbonization has shown to have large amount of polyfuran and N-heterocyclic aromatics, which have a tendency to reduce the mobility of nitrogen thereby, preventing its quick release into the soil [69]. Unlike many types of biochars, it has been seen that hydrochar produced as a result of hydrothermal carbonization has low organic content and reduced mobility of heavy metals, which makes it ideal for soil amendment. Addition of hydrochar to soil has shown to improve water retention capacity, microbial community, nutrient holding capacity, and much more [69,70]. Since the use of hydrochar has grown considerably only during the last decade, research on different aspects of hydrochar is still yet to be studied thoroughly. The extreme conditions of hydrothermal carbonization not only lead to the decomposition and dissolution of organic matter, but also makes heavy metals "bio-available". Therefore, detailed research is needed in order to ascertain the total capacity and effect of hydrochar, especially its use as a soil amendment, and how different hydrochar produced from different raw materials behave.

4.1.2. Hydrothermal Liquefaction

Hydrothermal liquefaction is essentially a decomposition process in which wet biomass is converted into a variety of products including bio-oil (liquid), biochar (solid) by means of thermal depolymerization. Wet biomass is exposed to extreme temperatures (250–550 °C) and pressures of (5–25) MPa. During hydrothermal liquefaction, a variety of chemical processes take place on biomass including hydrolysis, fragmentation, dehydration, aromatization and repolymerization, which results in the formation of biochar along with other compounds [71–74]. As stated before, the nature of the biochar obtained depends on different factors, such as, temperature, pressure, nature of raw material, residence time, etc. [75]. Extensive research into composition of biomass, and hence the properties of biochar, suggests that the main constituents of biomass (lignin, cellulose, and hemi-cellulose) play a key role in influencing the formation, as well as properties of biochar, especially lignin [76–79]. When biomass is heated at 220 °C, lignin gets dissolved very easily into water by hydrolysis leading to the formation of many phenolic compounds. Similarly, cellulose and hemicellulose, which are present in the biomass, also undergo various reaction leading to the formation of char [71]. Rice husks/pinewood was used as feedstock into a 100 mL autoclave along with deionized water. The autoclave was operated for 20 min at 573 K and the products that were formed (bio-oil and biochar) were removed using acetone, and the biochar was subsequently dried in a hot-air oven [71]. At very high temperatures, all of the biomolecules present in biomass, such as lignin, completely degraded and, therefore, the conversion needed to form biochar ceased to occur [71]. Very fast heating and sudden rises in temperatures inhibit biochar formation and slower and steadier processes are preferred [71]. Many studies show that physical properties, such as surface area and volume of biochar, is much lower while producing biochar from hydrothermal liquefaction (HTL) than from pyrolysis, however, recent studies suggest that biochar produced using HTL seems to be effective in adsorbing heavy metals and acting as biological catalysts [80].

Even though water is an abundant resource and is easy to use, it has been seen that use of different types of alcohols (butanol, methanol, etc.) improves the properties of biochar, as well as the amount of biochar that will be produced by HTL [81]. However, it was observed that water does not support polymerization reactions and, hence, production of bio-oil is more preferential as compared to biochar when water is used as a solvent [71]. Chemically prepared biochar as a result of hydrothermal liquefaction, has been found to have very high oxygen content in the form of hydroxyl, carboxyl, cyclic oxygenates, such as phenyls, glycerol, etc., and particularly phenol and lactone hydroxyls in biochar formation from rice husks/pinewood [71,75,81]. The functional groups in each biochar vary significantly and temperature plays a key role in determining the functional group. For example, if biochar is prepared at 280 °C and 360 °C, the functional groups were significantly less in the biochar prepared at higher temperatures [71].

Alcohol as solvent has significant advantages over the use of water, some of which include better reaction conditions, ability to release hydrogen for stabilization, higher reactivity with acid-components to form esters compared to water [81]. Apart from increase in biochar production, bio-oil production is also significantly increased, when alcohol is used as a solvent. Usage of glycerol as co-solvent acts as a high lipid additive and helps in converting low-lipid algae into bio-oil and biochar, which would usually be difficult and would require extreme conditions, which are not economical [81]. In conclusion, hydrothermal liquefaction is a process, which is still improving, and certain characteristics can be helpful under certain specific conditions when necessary.

4.1.3. Pyrolysis

Pyrolysis is mainly used to produce many forms of carbons from biomasses under high temperature and inert conditions. However, as engineering advances, the use of pyrolysis for converting biomass to syngas and biochar has grown significantly. As the other processes described earlier, the products that are formed as a result of pyrolysis significantly depend on the biomass, reaction conditions, and feedstocks used. Bio-oil, which is formed as a pyrolysis result, can easily be upgraded into higher grade fuel and can be used for various applications [82]. Biochar is a valuable product formed from pyrolysis and has seen growth in applications such as improving soil retention, soil amendment, catalyst, carbon sequestration [82] and, hence, learning and gaining knowledge of production of biochar is of great interest. Use of biochar as soil amendment has shown promising results in the agricultural field and, hence, different types of biochars and different type of preparation techniques are studied in order to obtain the most effective biochar, which is capable of increasing soil nutrient availability, porosity, fertility, etc. [82]. Biomass with higher calcium oxide (lime) content when heated at temperature above 450 °C results in biochar with low amounts of oxygen functional groups and increased stability [82]. Further use of additives, such as phosphorus, zinc, iron, etc., during pyrolysis also modify biochar and, hence, expands its applications in various fields [83–85].

In the past few years, there has been extensive research on different methods of pyrolysis, which can affect the conversion of biomass to biochar. Optimization of pyrolysis methods makes it economic and advantageous over other processes. Figure 1 highlights the most preferred techniques for biochar production from various biomasses. The nature of biochar produced, as a result of pyrolysis, depends on many factors, some of which are biomass pre-treatment, reactor type, and dimensions, pressure, residence time in the reactor [86]. Compared to other processes, such as hydrothermal carbonization or hydrothermal liquefaction, pyrolysis has an advantage because of the fact that it can be used for a wide range of biomass and waste materials [87].

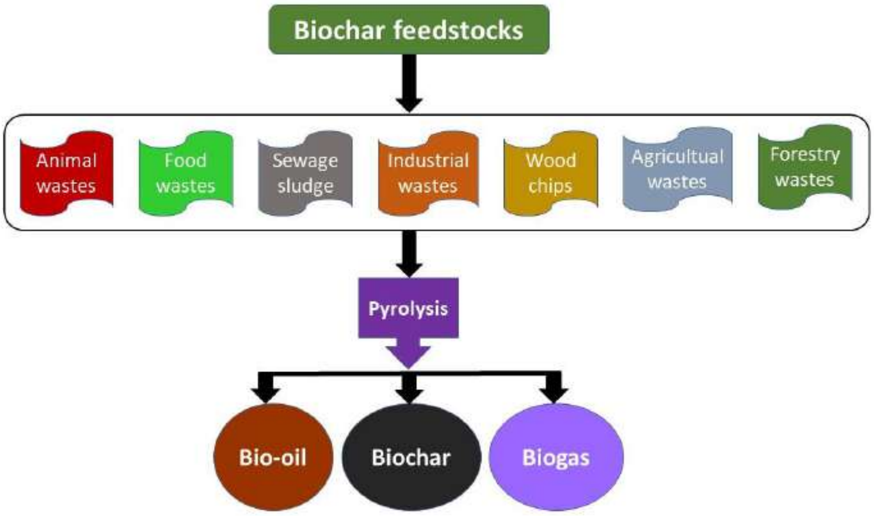

Figure 1. Schematic diagram showing biochar formation routes from different feedstocks.

Reactor designs and reactor types also have an important role to play and information regarding their influence on the type of pyrolysis has been studied [87]. In general, reactors such as auger reactors, rotary and drum Kilns are commonly used for pyrolysis. When the operating temperatures in these reactors are extremely high in the range of 800 °C to 1300 °C, the pyrolysis is referred to as fast pyrolysis [87]. The concept behind fast pyrolysis is that when the temperature is very high and residence time is low, char formation is prevented and the biomass undergoes thermal cracking. Slow pyrolysis, such as the name suggests, involves very slow rise in temperatures and very high residence time, thereby getting maximum exposure of biomass to heat [88]. Contrary to fast pyrolysis, in slow pyrolysis, liquified products are kept to a minimum and solid carbonaceous char is preferentially produced. Finally, pyrolysis is flexible in the sense that it can operate at varying reaction conditions and with different types of feedstocks, hence, resulting in a large variety of products. The biochar obtained as result of pyrolysis of sludge (wastewater sludge) has seen to have many properties, such as nutrient recyclability, heavy metal immobilization, good pore structure, and alkaline nature [89].

Due to its versatility and flexibility and its ability to operate on a wide range of raw feedstock, it is the ideal process to choose. Further, biochar formed because of pyrolysis is extremely valuable, and can be modified in a multitude of ways for various purposes. In recent times, pyrolytic biochar has been used in soil remediation, wastewater treatment, catalytic enhancer, and much more. Since research on this particular subject is still ongoing and different strides are being done on a consistent basis, one can only assume that this process is going to be more efficient and more economical in the future. Supplementary Table S1 depicts different methods of biochar synthesis, based on their sources, methods of preparation, and preparation conditions.

5. Biochar as an Adsorbent

Biochar, being environmentally friendly and extremely versatile, has been seen as a novel material for treating wastewater. Due to biochar adsorption properties, it has been a viable method to adsorb colorants that are potentially toxic and harmful to the environment.

5.1. Effect of Operational Parameters on the Adsorption of Dyes by Biochar

Biochar as an adsorbent works under extremely specific conditions. Concentration of dye/biochar, temperature and solution pH play important roles in determining the efficiency of biochar [90–95]. Nickel modified biochar was capable of adsorbing methylene blue with an adsorption capacity of 479.49 mg/g at 20 °C from wastewater [96]. Initially when the concentration of methylene blue was low, the adsorption by biochar was high due to the large number of active sites still available on the biochar for adsorption. Competitive adsorption was found to hinder the efficiency of adsorption of methylene blue by the biochar [96]. Research on the adsorption and degradation of acid red dye revealed that increase in temperature of the solution increased the rate of decolorization [97]. In this particular study, the temperature was maintained between 30 to 50 degree Celsius and it was observed that increase in temperature increased the rate of molecular collisions and, hence, the rate of the reaction resulting in the rapid increase of adsorption and decolorization of the solution.

One major factor that has constantly been seen to affect the way biochar behaves as an adsorbent is pH. In most studies, we see that the variation in pH causes major effects on the adsorption process using biochar. In study [91], on the investigation of the adsorption of methylene blue from wastewater, authors noted that the pH had a great influence on the degradation process of the dye. They observed that the efficiency of removal of the dye increased from a pH of 2 to 7 and then decreased from a pH of 7 to 11, which was due to the fact that the active sites on the surface of the biochar combined with the abundantly present hydroxyl groups, which caused a decrease in efficiency. A similar study was conducted by other researchers [92] on the adsorption of Congo red dye using biochar, made from organic peel waste, and the effect of different operational parameters on its adsorption was examined. It was observed that when the pH was kept between the range of 2–3, acidic conditions prevailed and the presence of H^+ ions aided the adsorption of Congo red dye onto the active sites present on the biochar. At the same time, however, for a pH of higher than 7, alkali conditions prevailed and the presence of OH^- ions hindered the adsorption of dye onto the biochar by competing for the active sites on the biochar. The results obtained in this study [92] were similar to that of other study [91], as both studies concluded that higher levels of pH are not ideal for the adsorption of dye using biochar due to undesirable electro-static conditions that were developed. The adsorption of organic dyes using food waste biochar was conducted and the effect of different parameters were examined [93]. As far as the effect of pH is concerned [93], authors observed that the removal efficiency of dye decreased by around 5% only, when the pH was altered from 3 to 11. However, when looked at more deeply, it was seen that the decrease in removal efficiency was not uniform overall, but was uniform between pH of 3–9 and a drastic decrease was observed, when pH approached to 11. Authors attributed this effect to the fact that when pH increased, decomposition of hydrogen peroxide decreased along with the conversion of carbonate and bicarbonates to their corresponding acid, which caused low reaction with OH^- radicals, which finally led to the decrease in solubility of iron that was present in the biochar. Therefore, in this particular case observed by [93], we see that the decrease in removal efficiency, due to changes in pH, is not as pronounced as in the other cases. In the experiment pertaining to adsorption of methyl violet dye using biochar conducted by [98], for pH values > 6, it was found that the adsorption of dye was favored, and the trend observed was due to the fact that at very low pH, the concentration of H^+ ions is significant and, hence, they compete along with the cationic dye (methyl violet) for the active adsorption sites on the biochar, thereby decreasing the percentage of removal of the dye. When an anionic dye, such as Congo red, is to be removed, the trend relating to the effect of pH may vary compared to other commonly seen dyes. In another study [99] focusing on the removal of dye using biochar, it was observed that when pH increased from 2 to 11, a significant decrease in removal percentage of dye was observed. Authors of this study [99] inferred from the observations that the decrease in removal efficiency between pH of 2 and 6 was due to the fact that at low pH < 2, the number of H^+ ions were significantly more and, hence, the adsorbent molecules acquired a positive charge and became cationic, increasing the adsorption of an anionic dye, such as Congo red, significantly. We see from the above-mentioned studies that the nature of dyes has played a significant role in determining the optimum pH for adsorption. When a dye is anionic, it has been observed that acidic pH (<2) is favored since the adsorbent surface (biochar) being positively charged due to the increase in presence of H^+ ions and it electrostatically favors attraction of anionic dyes and when a dye is cationic, increase in pH (>2) is favored as higher pH increases the presence of OH^- ions, which in turn makes the surface of biochar negative, which promotes the electrostatic attraction between the positively charged cationic dye and the negatively charged biochar surface [100,101]. From the studies we discussed above, it can be said that the interdependence between pH and adsorption is a key concept needed to understand the process of adsorption and that a large number of factors are responsible for different trends that may be observed. Figure 2 provides the schematic route of adsorption of dye from wastewater by biochar.

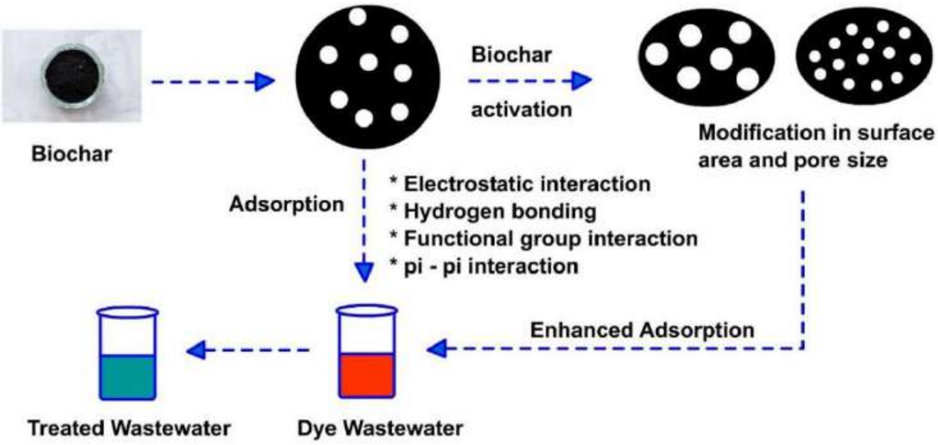

Figure 2. Schematic diagram of dye adsorption mechanism using biochar.

The dosage of adsorbent as well as adsorbate influence the extent of adsorption of dye and are important parameters to be considered. In a study of adsorption of dye using biochar [102], the removal percentage and capacity of adsorption were influenced heavily by the dosage of adsorbent. Even for a small increase in dosage of adsorbent caused the removal percentage to increase significantly (almost an 80 percent increase) and remained constant after a certain maximum dosage was reached. This phenomenon, according to authors [102], was due to the fact that at higher dosages of adsorbent, the number of active sites, as well as surface area of adsorption, will increase drastically, which in turn will increase the removal percentages of the dye present in water. A similar increase in percentage of dye removal with increase in adsorbent dosage was also observed in other studies [99,103,104]. The removal percentage of dye increased significantly for a very small increase in adsorbent (<1 g/100 mL) in all of the above-mentioned studies. This was similar to another study [102], which concluded that the increase in percentage of dye removal was because of the increase in dosage of adsorbent, which in turn increased the active sites for adsorption as well the surface area of adsorbent. However, the percentage of dye removal remained constant after a certain dosage of biochar due to the decrease in amount of dye molecules adsorbed per unit mass of adsorbent and the decrease in specific uptake [99]. Therefore, there will be no change in overall removal efficiency of dye by biochar after an equilibrium point has been reached. A similar conclusion was also achieved by [105], where switchgrass biochar was used as an adsorbent. It was observed that an increase in the dosage of biochar increased the removal percentage of dye and it reached an equilibrium percentage at around 50 mg of adsorbent dosage. Authors of this study [105] related this behavior to the increase in active binding sites and surface area due to the increase in dosage, which is similar to what has been concluded previously by other researchers [97,106]. When we assume the contrary, i.e., if the amount of dye is increased with the constant dosage of the adsorbent, the kinetics will depend on the equilibrium point, where the rate of adsorption of dye is equal to the desorption of already existing dye molecules [99]. The percentage removal will initially increase, and a small decrease may be seen, owing to the fact that the active sites present on the adsorbent (biochar) are completely occupied and the surface area that is free for adsorption decreases, while the number of dye molecules/reactive species adsorbed increases [99,106,107]. However, there are cases where the increase in concentration of dye indirectly increases the adsorption capacity of biochar until an equilibrium point after which no more adsorption is observed as all active sites on the biochar surfaces have been completely occupied by dye molecules, leaving no room for further adsorption [101]. The trends we discussed above, more or less, are similar in many aspects when it comes to the reason behind the increase/decrease in efficiency of dye removal. The operational parameters under which biochar works are of vital importance in order to understand and interpret the process of adsorption or other similar processes that might occur.

5.2. Adsorption Kinetic Studies

In order to understand the adsorption process and the rate of adsorption, kinetic studies are conducted. Kinetic studies have been extensively used by many researchers in order to study the mechanism by which adsorption takes place. Most adsorption kinetic studies apply pre-existing models, which act as guide to illustrate the adsorption mechanism. Pseudo first order, pseudo second order, and particle diffusion models are among the widely used models to describe the adsorption process. A wide range of standard models are available that describe adsorption at different conditions and the most suitable can be chosen for the given experimental conditions [108]. Adsorption of dyes using rice husks biochar was investigated, and from various kinetic models that were tested, pseudo second order model was the most suitable one to describe the experimental observations of the adsorption of malachite green dye using biochar [104], and the Elovich model was used in order to conclude that the mechanism of adsorption was chemisorption. In comparison, a similar study conducted on adsorption of Congo red by manganese composite biochar, it was observed that pseudo first order model was able to explain the kinetics of adsorption for a fixed amount of adsorbent and adsorbate [103]. These kinetic models not only can be used to describe the experimental observations of adsorption capacity, but they also indirectly indicate a way to describe the mechanism of adsorption.

In a study [109], the adsorption of methylene blue was examined using sugarcane bagasse biochar, and it was observed that pseudo second order kinetic model fitted well to the experimental results. It was also inferred that the mechanism of adsorption was chemisorption. Hence, the use of kinetic models is not restricted to only a mathematical result, but can also provide information regarding the mechanism of action. Factors, such as nature of biochar and the nature of the dye to be removed, also play key roles in determining the adsorption kinetics. The adsorption kinetics varied depending on the biochar used and the rate of adsorption varied progressively (fast to slow) [110]. Authors inferred that it was because of inherent properties, such as pore volume and size, that caused the discrepancy in the rate of adsorption and choice of kinetic model, which was in conjunction to similar observations made by other researchers [111–113]. In examination of adsorption of reactive red dye using ball-milled biochar, the adsorption rate was initially fast and then gradually became slower [111]. From calculating the values of coefficient of determination (R^2), it was able to conclude that intra particular diffusion model had the most appropriate fit and hence, the mechanism of adsorption was primarily diffusion, and the removal of dye was influenced mainly by the external surface area [111].

Adsorption of acid chrome blue K onto Cetyl trimethyl ammonium bromide modified magnetic biochar was reported in [112]. The first 600 min showed a rapid increase in adsorption of the dye by biochar until it slowed down and reached an equilibrium stage after 60 min. In most cases, we see that the increase in dosage increases the rate of the adsorption (Section 5.1), i.e., removal efficiency of dye and, hence, the kinetics vary correspondingly. Another study involved the adsorption and degradation of acid red 88 dye from solution using Fe-Mn composite biochar [114]. In this study, authors observed that the change of dosage of biochar increased the removal efficiency and increased the rate of adsorption, which agreed with the pseudo first order kinetic model theoretically. Similar to the method used by [111,115], which inferred using a pseudo second order kinetic model that, in the adsorption of methylene blue using biochar (municipal waste derived biochar), the rate limiting step was the chemisorption step, and that the pseudo second order kinetic model was much more efficient than the other models in describing the particulate and liquid film diffusion and surface adsorption processes.

Thus, we see that the use of kinetic models is not entirely restricted to just correlating the experimental and theoretical values of adsorption efficiency, rate of adsorption and equilibrium adsorption, but can also be used to infer various possible mechanisms of adsorption based on the numerical values that are obtained. Contrary to previous observations by a large number of researchers, it is not always possible to obtain the mechanism of adsorption by using a suitable kinetic model [116]. The reason for this discrepancy stated by [116] was that the mechanisms of dye adsorption by hydrogen bonding (as dyes are present in the solution phase) may have been misrepresented diagrammatically in the previously established standards, which researchers often refer to. Therefore, if we look at what has been observed and concluded by the various researchers of this specific topic (adsorption of dyes using biochar), we see that, even though adsorption kinetic studies have their merits, they may be inherently flawed, if they are not studied extensively and deeply.

Table 2 elaborates the description of different kinetic models that are used in adsorption studies for dyes removal. To summarize, we see that the knowledge regarding kinetics of adsorption is an extremely helpful and intuitive way of understanding how adsorption takes place. Primarily a mathematical concept, one can infer various aspects regarding adsorption from kinetic studies. Considering all the influencing factors and different experimental conditions, one can apply kinetic studies to study the adsorption of dyes or any such pollutant using biochar and gain a much deeper and greater understanding of the concept [108].

Table 2. Adsorption kinetic studies of different dyes onto biochar.

Adsorbent	**Adsorbate**	**Applicable Kinetic Models**	**Reference**
Steam activated spent mushroom substrate (SMS)	Congo red and crystal violet	Pseudo first order Pseudo second order	[100]
Nickel aluminum layered double oxides modified magnetic biochar	Acridine orange	Pseudo first order and Pseudo second order	[101]
Chemically modified lychee seed biochar	Methylene blue	Pseudo second order	[117]
Triethylenetetramine biochar	Sunset yellow dye	Pseudo second order	[94]
Orange peel waste microwave activated biochar	Congo red dye	Pseudo second order	[92]
Fe_2O_3/TiO_2 functionalized biochar	Methylene blue, Methyl orange, Rhodamine B	Pseudo first order	[91]
Switchgrass biochar	Methylene Blue, Orange G, Congo red	Pseudo first and second order model, Intra particular diffusion model	[90]
Biochar derived from *Opuntia ficus-indica* (OFI) cactus	Malachite green	Pseudo second order model, Elovich model	[118]
N-doped biochar	Acid red 18	Intra particular diffusion model	[113]
Ag-TiO_2 biochar	Methyl orange	Pseudo first order kinetic model	[119]
Biochar derived from mixed municipal discarded material	Methylene blue	Pseudo first and second order model Intra particular diffusion model	[115]
Mesoporous nano-zerovalent manganese (nZVMn) and *Phoenix dactylifera* leaves biochar (PBC) composite.	Congo red	Pseudo first and second order model	[103]
Cetyl trimethyl ammonium bromide modified magnetic biochar derived from pine nutshells	Acid chrome blue K	Pseudo first order model Pseudo second order model	[112]
Pristine and ball milled biochar	Reactive red 120	Pseudo-second order kinetic model Intra-particle diffusion model	[111]
Wood based biochar	Acid orange 7	Langmuir-Hinshelwood (L-H) kinetic mode	[107]
Pyrolyzed rice husk biochar	Malachite green	Intraparticle Diffusion Model Elovich models Pseudo second order model Pseudo-first order model	[104]
Animal waste biochar	Basic red 9	Pseudo first order model Pseudo second order model Pseudo Nth order model	[110]

5.3. Adsorption Isotherm Studies

An adsorption isotherm is an empirical equation, which relates the equilibrium concentration of solute, and is adsorbed on the surface of an adsorbent to the concentration of solute present in the liquid solution with which it is in contact with, as a function of pressure under constant temperature. For choosing the optimal isotherm model for the adsorption process, the following criteria must be fulfilled: (1) the isotherm model and the calculated equilibrium data must have a good fit; (2) the function of isotherm must be thermodynamically realistic; and the (3) analytical calculation of concentration from capacity and vice versa must be possible even in ideal scenarios [120].

A biochar prepared from pyrolyzed rice husk showed that the maximum removal of Malachite green dye by the biochar was 99.98% with an adsorbent dosage of 0.2 mg/L, dye concentration of 20 mg/L at pH of 6.2 over a period of 2 h [104]. Freundlich, Dubinin–Radushkevich, Langmuir, and Temkin isotherms were studied in order to determine the best fitting of the models. Langmuir isotherm model was found to have the best fit. This led to the inference that Malachite green dye had uniform binding energy with the active sites on the biochar, which was distributed homogeneously across the adsorbent via the mechanism of physisorption. An eco-friendly biochar was synthesized by the pyrolysis of Ashe Juniper and, thereafter, functionalized by sulfuric acid for the removal of methylene blue, a hazardous dye [121]. The Langmuir model had a higher correlation coefficient (R^2) value of 0.96 compared to the Freundlich model, which only had an R^2 value of 0.94. Since the Langmuir model was determined as the better fit, it implied that the biochar was monolayered, had identical binding sites distributed equally across its surface for dye adsorptive removal.

The fallen leaves from Magnolia Grandiflora L. were converted into biochar by subjecting it to slow pyrolysis for the removal of methylene blue dye [122]. Maximum dye adsorption was observed as 101.27 mg/g at an ionic strength (NaCl) of 0.1 M, pH level of 12 and at 303 K. Langmuir, Freundlich, Temkin, and Harkins–Jura models were tested. The experiments were performed at three temperatures (293 K, 298 K, and 303 K). Langmuir isotherm model was the best-fitted one and the adsorption process of methylene blue onto the biochar was found to be endothermic process. Furthermore, the dimensionless separation factor (R_L) had values of 0.139, 0.273, and 0.139, respectively, which clearly ranged between 0 and 1 for all three temperatures, suggesting favorability for the adsorption process. Freundlich isotherm model also proved favorable as the Freundlich adsorption intensity (1/n) values were 0.12, 0.09, 0.14, respectively, which were also between 0 and 1 for all three different temperatures. Temkin model had shown binding energies of 33.98, 51.36, and 46.78 kJ/mol, respectively, at the above different temperatures, implying that the adsorption process not only consists of an ion-exchange mechanism, as the binding energy should be within the range of 8–16 kJ/mol for the model to be accepted. For the Harkins–Jura model, the correlation coefficient (R^2) values were the lowest compared to other models, implying that multi-layer adsorption process had low correlation. The Langmuir model was concluded to be the best fitted among other models due to a high R^2 value of >0.99. This demonstrated that the biochar surface was homogenous and methylene blue was adsorbed as monolayer, distributed equally throughout its surface.

Empty-fruit bunch fibers were activated by chemo-physical processes to prepare the biochar for the removal of Cibacron Blue 3G-A dye from aqueous solution [123]. The maximum dye removal was 99.05% by the biochar at optimal conditions of an adsorption dosage of 0.10 g/100 mL, dye concentration of 100 mg/L at a pH value of 10, temperature at 343 K over a period of 45 min of contact time. The adsorption isotherm models considered in this study were only Langmuir and Freundlich models. The correlation coefficient (R^2) for both models was greater than 0.9. The dimensionless separation factor (R_L) for Langmuir isotherm was found to be between 0 and 1, suggesting that the adsorption process was feasible. For the Freundlich isotherm, the Freundlich adsorption intensity (1/n) was also between 0 and 1, which was a good indication of favorability of the adsorption process. It was finally concluded that Freundlich isotherm was a better fit compared to Langmuir, due to its high R^2 value compared to the latter. This also led to the inference that the surface of the biochar was heterogeneous, multilayer and the mechanism of adsorption was physisorption. Table 3 summarizes the most common isotherms studies in dye removal studies. Table 4 elaborates the detailed literature on the adsorption capacity of biochar adsorbents on dye removal.

Table 3. Adsorption isotherm studies of different dyes onto biochar.

Adsorbent	Adsorbate	Applicable Isotherm Models	Reference
Mg-Al-layered hydroxide intercalated date-palm biochar composites	Methylene blue	Langmuir, Freundlich	[124]
Rice husk biochar	Congo red	Langmuir, Freundlich	[125]
Cow dung biochar	Congo red	Langmuir, Freundlich	[125]
Magnetic chicken bone biochar	Rhodamine B	Freundlich	[126]
Chitin derived biochar	Methyl violet	Freundlich, Langmuir, Liu	[98]
Switchgrass biochar	Methylene blue	Langmuir, Freundlich	[90]
Switchgrass biochar	Orange G	Langmuir, Freundlich	[90]
Switchgrass biochar	Congo red	Langmuir, Freundlich	[90]
Banana peel extract and $FeSO_4$	Methylene blue	Langmuir, Freundlich, Dubinin-Radushkevich	[127]
Chemically modified lychee seed biochar	Methylene blue	Langmuir, Freundlich, Temkin, Dubinin-Radushkevich	[117]
Bamboo shoot shell biochar	Rhodamine B	Langmuir, Freundlich	[128]
Cetyl trimethyl ammonium bromide modified magnetic biochar from pine nut shells	Acid chrome blue K	Langmuir, Freundlich	[112]
Bovine bone biochar	Basic Red 9	Langmuir, Freundlich	[110]
Fish scale biochar	Basic Red 9	Langmuir, Freundlich	[110]

Table 4. Adsorption capacities of various biochar adsorbents for the removal of different dyes from water.

Adsorbent	Adsorbate	Adsorbent Dose	Contact Time (min)	Adsorption Capacity (mg/g)	Temperature (°C)	pH	References
Chitosan Based Material	Basic Blue 7	0.3 g/L	60	1174 mg/g	25	6	[57]
Wet-torrefied microalgal biochar	Methylene blue	1 g/L	7200	113.00 mg/g	25	6	[129]
Wet-torrefied microalgal biochar	Congo red	2 g/L	240	164.35 mg/g	25	6–8	[129]
Surfactant Modified Chitosan Beads	Crystal violet	0.36 g/L	120	97.09 mg/g	50	6	[130]
Surfactant Modified Chitosan Beads	Tartrazine	0.72 g/L	120	30.03 mg/g	50	3	[130]
Calcium rich biochar from Crab Shell	Malachite green	0.5 g/L	150	12,501.98 mg/g	25	7	[131]
Calcium rich biochar from Crab Shell	Congo red	0.5 g/L	2	20,317 mg/g	25	4	[131]
Ziziphus Lotus stones	Basic Yellow 28	0.5 g/L	180	424 mg/g	20	8	[132]
Ziziphus Lotus stones	Basic Red 46	0.5 g/L	180	307 mg/g	20	8	[132]
Date palm petiole derived biochar	Crystal violet	NA	15	209 mg/g	30	7	[133]
Activated wakame biochar material	Methylene blue	0.06 g/50 mL	NA	841.64 mg/g	20	2–12	[96]
Activated wakame biochar material	Rhodamine B	0.06 g/50 mL	NA	533.77 mg/g	20	2–12	[96]
Activated wakame biochar material	Malachite green	0.06 g/50 mL	NA	4066.96 mg/g	20	2–7	[96]
Activated biochar derived from *Opuntia ficus-indica*	Malachite green	60 mg/100 mL	120	1341.38 mg/g	30	6	[118]
Biochar derived from Caulerpa scalpelliformis	Remazol brilliant blue R	2 g/L	300	129.00 mg/g	30	2	[134]
Biochar derived from Caulerpa scalpelliformis	Remazol brilliant orange 3R	2 g/L	300	130.11 mg/g	30	2	[134]
Biochar derived from Caulerpa scalpelliformis	Remazol brilliant violet 5R	2 g/L	300	139.76 mg/g	30	2	[134]
Biochar derived from Caulerpa scalpelliformis	Remazol black B	2 g/L	300	159.08 mg/g	30	2	[134]

5.4. Mechanisms of Dyes Adsorption onto Biochar

The mechanism of removal of dyes from wastewater using biochar involves many complex interactions (both chemisorption and physisorption) between the adsorbate (dye) and adsorbent (biochar). Current literature leads us to a conclusion that the adsorption involves multiple mechanisms working together, some dominating, others based on prevailing conditions of the system. Depending on the dyes, biochar and solvent, mechanisms, such as pore-filling effect, van der Waals interaction, electrostatic interaction, chemical action, ion exchange, surface complexation, π-π interactions, cation-π interactions could play important roles in the adsorption process [135].

Adsorption of positively charged methylene blue dye (MBD) using municipal sewage sludge and tea waste derived biochar was investigated [11]. The impact of pH on adsorption showed that adsorption was influenced by the pH; for pH lower than 2, the removal efficiency of MBD was only 80%, while it was nearly 100% at a pH of 11 [11]. This strongly suggests that the adsorption mechanism involved electrostatic interaction. At low pH, the abundant H^+ ions occupied the limited bonding sites on biochar and repelled the positively charged MBD molecules, but as pH was increased, the bonded sites were deprotonated and were free for the MBD molecules to interact, thus, greatly increasing the adsorption capacity. The alternate mechanism could involve ion exchange; as the concentration of released metal cations (Ca^{2+}, Na^+, K^+, Mg^{2+}) by the biochar in the equilibrium solution was recorded and it was found that concentration of these ions was greatly increased after MBD adsorption, especially Na^+ and K^+ ions, indicating that these ions were involved in the ion exchange process.

A study of malachite green dye (MGD) on activated biochar, derived from Opuntia ficus-indica, possessing a meso-porous structure showed increased physical adsorption capabilities; which indicated that the pore filling effect was the main mechanism [118]. Hydrogen bonding between the MGD functional groups and the biochar could have supplemented the adsorption process. The activated biochar also possessed amine and hydroxyl groups (according to XRD and FTIR analyses), which are electron rich in nature, while the MGD possessed electron-deficient functional groups as part of the aromatic ring. Thus, depending on the pH of the solution, π-π electron donor–acceptor (EDA) interactions and cation- π interactions would have also been possible.

A study of surface and structural parameters of biochar and their impacts on Q_m (maximum adsorption capacity) of MBD was conducted using biochar, derived from cashew nut shells [136]. It was found that Q_m varied linearly with the volume of pores having a diameter between 1.6 and 2 nm, and adsorption capacity was mainly dependent on these pores. This was because this pore size diameter closely corresponds with the size of the MBD molecule; thus, biochar adsorption can be very selective in the wastewater treatment by closely controlling the volumes and diameter of surface pores. The study also found high correlation between Q_m and presence of weakly acidic phenolic groups on the surface of the biochar. These groups attract MBD molecules by dipole-dipole interactions or hydrogen bonding, both facilitated by the aforementioned phenolic groups.

Removal of MGD, MBD, and Rhodamine B dye (RBD) using biochar was examined and it was found that the intramolecular diffusion process, involved in adsorption, is rate-limiting [96]. The first step is fast, getting progressively slower due to the reduced adsorption intensity and decrease of unoccupied active sorption sites on biochar surface. Fourier Transform Infrared Spectroscopy (FTIR) analysis also showed the presence of hydroxyl and carbonyl groups leading to adsorption by hydrogen bonding and π-π stacking. Biochar derived from crab shells, which were rich in calcium, was studied to adsorb MGD and Congo red Dye (CRD) [131]. Zeta potential analysis showed normal electrostatic interaction activity for both dyes but FTIR and XPS analysis of biochar showed a marked difference before and after adsorption, with typical calcite bands (1440, 873 and 710 cm^{-1}) in biochar missing after CR adsorption, corroborated with the results of XPS spectra (decreased intensity of peaks at 348 and 438 eV) [131]. This suggested that calcite and CaO were involved in CR adsorption by biochar; this theory was further proven by the fact that crab shell biochar was more efficient without acid washing, indicating that the calcium ion interactions in adsorption had a positive effect in dye adsorption.

From the current literature review, it is apparent that there is a lack of studies to assess biochar performance in systems with more than one dye. Studies thus far have only utilized single dyes, adsorbed using batch processes. While studies such as [137,138] used textile effluents, which contained more than one particular dye, they failed to enumerate them and thus, the influence of the interactions of multiple dyes and biochar is unknown. It is essential, in an industrial wastewater treatment setting to determine the performance of biochar while simultaneously adsorbing multiple dyes. As [139] suggests, depending on the type of effluent, multiple treatment technologies could be combined to treat wastewater.

5.5. Potential Drawbacks of Using Biochar as an Adsorbent

In the above-mentioned sections, we extensively reviewed the potential of biochar as an adsorbent for the removal of dyes; however, the use of biochar possesses certain drawbacks. In most of the research that has been citied, we see that biochar is used under extremely specific conditions of dosage, temperature, etc., which determine how the process takes place. Hence, subsequent steps need to be performed to remove the biochar from the wastewater before reusing it for other applications, which can increase the cost of treatment. Few studies [116,126] which investigated the use of biochar as an adsorbent for dyes removal, concluded that in both cases, the efficiency of biochar decreased after prolonged usage. Therefore, we see that biochar as an adsorbent may require additional processes of desorption and that this could cause potentially economic drawbacks. Most commonly used biochars contain a significant amount of heavy metals, thereby increasing the risk of pollution due to excess desorption of these heavy metals [140–142]. Moreover, ref. [142] studied the environmental risk associated with different types of biochar containing heavy metals (derived from sludge of swine wastewater) and examined how they may affect the environment during the application of the biochar. Authors observed that the temperature, at which the biochar was prepared, played a crucial role in immobilization of heavy metal ions and it was found that 600 degrees Celsius was the ideal temperature for immobilization and heavy metals seemed to contaminate the environment at other undesirable temperatures. Moreover, ref. [140] extensively studied the effects of environmentally persistent free radicals on wastewater and soil. The free radicals (produced under certain carbonization and pyrolysis conditions), which may mobilize, may pose a significant threat to the environment if they are not monitored and managed. Furthermore, [140] research led to the conclusion that even though biochar finds a plethora of applications in various fields, it still possesses a significant threat as a pollutant to the environment if not used properly. A similar study was conducted by [141], in which the effect of temperature and raw material on biochar toxicity was studied. Their study suggested that at certain temperatures, heavy metals tend to diffuse and, hence, pollute the surrounding environment (wastewater in this case). It was observed that at exceedingly high temperatures, the heavy metals tend to volatize and temperatures of around 400 degrees proved to increase the volatility of cadmium in comparison to the other heavy metals, hence enabling pollution of the surroundings through heavy metal contamination. Therefore, we see heavy metals diffusion into the surroundings, while biochar is used as an adsorbent, is of crucial environmental concern, and despite its wide application, it does possess certain drawbacks, which need to be taken into account before its usage.

6. Conclusions and Future Perspective

Biochar was found to be an outstanding candidate for the remediation of dyes from wastewater, as evident by the literature reviewed herein. Advanced oxidation processes (AOPs), such as ozonation and Fenton oxidation processes, provide a good removal of dyes and colorants, ranging from 85% to 95% within a time span of 30 min to 1 h. However, these processes have disadvantages, such as being expensive and skill intense. Whereas, the membrane-based processes, such as nanofiltration and forward osmosis, are highly effective, and result in more than 99% removal rates within a few minutes. These membranes are highly vulnerable and need replacement very often. Biochar produced in hydrothermal processing of biomass, upon surface modification, would act as an effective adsorbent that could remove dyes from synthetic and real industrial wastewater. Pyrolysis and hydrothermal carbonization have been the most preferred techniques to processing various types of feedstocks (agricultural waste, algae biomass, sludge, plant residue, etc.) for biochar production. Most of the biochar-based adsorption processes exhibit chemisorption mechanism. Kinetic studies were exclusively carried out to these systems. Pseudo first or second order kinetic models fit well with experimental data. Furthermore, adsorption isotherm studies were also carried out by many researchers. Of all the isotherm models studied, Langmuir or Freundlich isotherm models fit most of the systems with R^2 values higher than 0.95, showing it as a good fit. The adsorption capacities of biochar-based adsorbents sometimes resulted in as low as 30.03 mg/g to as high as 20,317 mg/g. pH values play an important role in deciding the adsorption capacity of the biochar. Many studies were carried out to study the threshold pH values and results showed that in most of the cases, biochar could tolerate lower pH values up to 2 and higher pH values up to 11. Still, the removal efficiencies reached more than 80%.

The future scope in using biochar as adsorbent is huge. Engineered biochar and selective modifications will improve the efficiency of the biochar. Embedding metal frameworks derive catalyst quality biochar, which can be used for many advanced oxidation processes as a cheap catalyst. Moreover, regeneration and reuse of spent biochar adsorbent is a prominent niche in the research of biochar adsorbents. Very few studies have emerged in using spent biochar as soil amendment and additive in various biological degradation processes. Biochar can also be used as biocarriers after using as adsorbents. Studies on biochar–dye interaction will be important, as the problem of dye contamination in water is growing in most of countries worldwide.

Supplementary Materials: The following are available online at http://www.mdpi.com/2073-4441/12/12/3561/s1, Table S1: Summary of most preferred synthesis routes for biochar production from different feedstocks.

Author Contributions: P.S.: Conceptualization, Data curation; B.S.B.: Writing—original draft; V.S.: Writing—original draft; J.A.: Conceptualization; K.P.G.: Project administration, Supervision; A.B.: Review & editing. All authors have read and agreed to the published version of the manuscript.

Funding: This research received no external funding.

Acknowledgments: The authors wish to thank management of SSN College of Engineering and Sathyabama Institute of Science and Technology for the support.

Conflicts of Interest: The authors declare no conflict of interest.

References

1. Lin, Y.T.; Kao, F.Y.; Chen, S.H.; Wey, M.Y.; Tseng, H.H. A facile approach from waste to resource: Reclaimed rubber-derived membrane for dye removal. *J. Taiwan Inst. Chem. Eng.* **2020**, *112*, 286–295. [CrossRef]
2. Kazemi Shariat Panahi, H.; Dehhaghi, M.; Ok, Y.S.; Nizami, A.S.; Khoshnevisan, B.; Mussatto, S.I.; Aghbashlo, M.; Tabatabaei, M.; Lam, S.S. A comprehensive review of engineered biochar: Production, characteristics, and environmental applications. *J. Clean. Prod.* **2020**, *270*, 122462. [CrossRef]
3. Chi, N.T.L.; Anto, S.; Ahamed, T.S.; Kumar, S.S.; Shanmugam, S.; Samuel, M.S.; Mathimani, T.; Brindhadevi, K.; Pugazhendhi, A. A review on biochar production techniques and biochar based catalyst for biofuel production from algae. *Fuel* **2020**, 119411. [CrossRef]
4. Dai, Y.; Zhang, N.; Xing, C.; Cui, Q.; Sun, Q. The adsorption, regeneration and engineering applications of biochar for removal organic pollutants: A review. *Chemosphere* **2019**, *223*, 12–27. [CrossRef] [PubMed]
5. Rodriguez, J.A.; Lustosa Filho, J.F.; Melo, L.C.A.; de Assis, I.R.; de Oliveira, T.S. Influence of pyrolysis temperature and feedstock on the properties of biochars produced from agricultural and industrial wastes. *J. Anal. Appl. Pyrolysis* **2020**, *149*, 104839. [CrossRef]
6. Xu, Y.; Luo, G.; He, S.; Deng, F.; Pang, Q.; Xu, Y.; Yao, H. Efficient removal of elemental mercury by magnetic chlorinated biochars derived from co-pyrolysis of Fe(NO3)3-laden wood and polyvinyl chloride waste. *Fuel* **2019**, *239*, 982–990. [CrossRef]
7. Yang, H.; Ye, S.; Zeng, Z.; Zeng, G.; Tan, X.; Xiao, R.; Wang, J.; Song, B.; Du, L.; Qin, M.; et al. Utilization of biochar for resource recovery from water: A review. *Chem. Eng. J.* **2020**, *397*. [CrossRef]

8. Amen, R.; Yaseen, M.; Mukhtar, A.; Ullah, S.; Al-sehemi, A.G.; Ra, S.; Babar, M.; Lai, C.; Ibrahim, M.; Asif, S.; et al. Lead and cadmium removal from wastewater using eco-friendly biochar adsorbent derived from rice husk, wheat straw, and corncob. *Clean. Eng. Technol.* **2020**. [CrossRef]
9. Santos, G.E.D.S.D.; Lins, P.V.D.S.; Oliveira, L.M.T.D.M.; Da Silva, E.O.; Anastopoulos, I.; Erto, A.; Giannakoudakis, D.A.; De Almeida, A.R.F.; Duarte, J.L.D.S.; Meili, L. Layered double hydroxides/biochar composites as adsorbents for water remediation applications: Recent trends and perspectives. *J. Clean. Prod.* **2020**, 124755. [CrossRef]
10. Leichtweis, J.; Silvestri, S.; Carissimi, E. New composite of pecan nutshells biochar-ZnO for sequential removal of acid red 97 by adsorption and photocatalysis. *Biomass Bioenergy* **2020**, *140*, 105648. [CrossRef]
11. Fan, S.; Tang, J.; Wang, Y.; Li, H.; Zhang, H.; Tang, J.; Wang, Z.; Li, X. Biochar prepared from co-pyrolysis of municipal sewage sludge and tea waste for the adsorption of methylene blue from aqueous solutions: Kinetics, isotherm, thermodynamic and mechanism. *J. Mol. Liq.* **2016**, *220*, 432–441. [CrossRef]
12. Xiang, W.; Zhang, X.; Chen, J.; Zou, W.; He, F.; Hu, X.; Tsang, D.C.W.; Ok, Y.S.; Gao, B. Biochar technology in wastewater treatment: A critical review. *Chemosphere* **2020**, *252*, 126539. [CrossRef] [PubMed]
13. Benkhaya, S.; M' rabet, S.; El Harfi, A. A review on classifications, recent synthesis and applications of textile dyes. *Inorg. Chem. Commun.* **2020**, *115*, 107891. [CrossRef]
14. Bhuiyan, M.A.R.; Islam, A.; Ali, A.; Islam, M.N. Color and chemical constitution of natural dye henna (Lawsonia inermis L) and its application in the coloration of textiles. *J. Clean. Prod.* **2017**, *167*, 14–22. [CrossRef]
15. Zerin, I.; Farzana, N.; Sayem, A.S.M.; Anang, D.M.; Haider, J. *Potentials of Natural Dyes for Textile Applications*; Hashmi, S., Choudhury, I.A., Eds.; Elsevier: Oxford, UK, 2020; pp. 873–883. ISBN 978-0-12-813196-1.
16. Nambela, L.; Haule, L.V.; Mgani, Q. A review on source, chemistry, green synthesis and application of textile colorants. *J. Clean. Prod.* **2020**, *246*, 119036. [CrossRef]
17. Saxena, S.; Raja, A.S.M. *Natural Dyes: Sources, Chemistry, Application and Sustainability Issues BT—Roadmap to Sustainable Textiles and Clothing: Eco-friendly Raw Materials, Technologies, and Processing Methods*; Muthu, S.S., Ed.; Springer Singapore: Singapore, 2014; pp. 37–80. ISBN 978-981-287-065-0.
18. Degano, I.; Mattonai, M.; Sabatini, F.; Colombini, M.P. A mass spectrometric study on tannin degradation within dyed woolen yarns. *Molecules* **2019**, *24*, 2318. [CrossRef]
19. Christie, R. *Colour Chemistry*; Royal Society of Chemistry: Cambridge, UK, 2014; ISBN 1849733287.
20. Raman, C.D.; Kanmani, S. Textile dye degradation using nano zero valent iron: A review. *J. Environ. Manag.* **2016**, *177*, 341–355. [CrossRef]
21. Gürses, A.; Açıkyıldız, M.; Güneş, K.; Gürses, M.S. *Classification of Dye and Pigments BT—Dyes and Pigments*; Gürses, A., Açıkyıldız, M., Güneş, K., Gürses, M.S., Eds.; Springer International Publishing: Cham, Switzerland, 2016; pp. 31–45. ISBN 978-3-319-33892-7.
22. Clark, M. Fundamental Principles of Dyeing. In *Handbook of Textile and Industrial Dyeing*; Woodhead Publishing: Cambridge, UK, 2011; Volume 1, pp. 1–27.
23. Burkinshaw, S.M. *Physico-Chemical Aspects of Textile Coloration*; SDC-Society of Dyers and Colourists; Wiley: Hoboken, NJ, USA, 2015; ISBN 9781118725634.
24. Roy Choudhury, A.K. 2—Dyeing of synthetic fibres. In *Woodhead Publishing Series in Textiles*; Clark, M., Ed.; Woodhead Publishing: Cambridge, UK, 2011; Volume 2, pp. 40–128. ISBN 978-1-84569-696-2.
25. Jamil, A.; Bokhari, T.H.; Javed, T.; Mustafa, R.; Sajid, M.; Noreen, S.; Zuber, M.; Nazir, A.; Iqbal, M.; Jilani, M.I. Photocatalytic degradation of disperse dye Violet-26 using TiO2 and ZnO nanomaterials and process variable optimization. *J. Mater. Res. Technol.* **2020**, *9*, 1119–1128. [CrossRef]
26. Broadbent, A. Basic principles of textile coloration. *Color Res. Appl.* **2003**, *28*, 230–231. [CrossRef]
27. Chattopadhyay, D.P. 4—Chemistry of dyeing. In *Woodhead Publishing Series in Textiles*; Clark, M., Ed.; Woodhead Publishing: Cambridge, UK, 2011; Volume 1, pp. 150–183. ISBN 978-1-84569-695-5.
28. Jalandoni-Buan, A.C.; Decena-Soliven, A.L.A.; Cao, E.P.; Barraquio, V.L.; Barraquio, W.L. Characterization and identification of Congo red decolorizing bacteria from monocultures and consortia. *Philipp. J. Sci.* **2010**, *139*, 71–78.
29. Pereira, L.; Alves, M. *Dyes—Environmental Impact and Remediation BT—Environmental Protection Strategies for Sustainable Development*; Malik, A., Grohmann, E., Eds.; Springer: Dordrecht, The Netherlands, 2012; pp. 111–162, ISBN 978-94-007-1591-2.

30. Pal, P. *Chapter 6—Industry-Specific Water Treatment: Case Studies*; Pal, P., Ed.; Butterworth-Heinemann: Oxford, UK, 2017; pp. 243–511, ISBN 978-0-12-810391-3.
31. Khatri, A.; Peerzada, M.H.; Mohsin, M.; White, M. A review on developments in dyeing cotton fabrics with reactive dyes for reducing effluent pollution. *J. Clean. Prod.* **2015**, *87*, 50–57. [CrossRef]
32. Chavan, R.B. 16—Environmentally friendly dyes. In *Woodhead Publishing Series in Textiles*; Clark, M., Ed.; Woodhead Publishing: Cambridge, UK, 2011; Volume 1, pp. 515–561. ISBN 978-1-84569-695-5.
33. Desore, A.; Narula, S.A. An overview on corporate response towards sustainability issues in textile industry. *Environ. Dev. Sustain.* **2018**, *20*, 1439–1459. [CrossRef]
34. Liang, Z.; Wang, J.; Zhang, Y.; Han, C.; Ma, S.; Chen, J.; Li, G.; An, T. Removal of volatile organic compounds (VOCs) emitted from a textile dyeing wastewater treatment plant and the attenuation of respiratory health risks using a pilot-scale biofilter. *J. Clean. Prod.* **2020**, *253*, 120019. [CrossRef]
35. Khatri, J.; Nidheesh, P.V.; Anantha Singh, T.S.; Suresh Kumar, M. Advanced oxidation processes based on zero-valent aluminium for treating textile wastewater. *Chem. Eng. J.* **2018**, *348*, 67–73. [CrossRef]
36. Lellis, B.; Fávaro-Polonio, C.Z.; Pamphile, J.A.; Polonio, J.C. Effects of textile dyes on health and the environment and bioremediation potential of living organisms. *Biotechnol. Res. Innov.* **2019**, *3*, 275–290. [CrossRef]
37. Vikrant, K.; Giri, B.S.; Raza, N.; Roy, K.; Kim, K.-H.; Rai, B.N.; Singh, R.S. Recent advancements in bioremediation of dye: Current status and challenges. *Bioresour. Technol.* **2018**, *253*, 355–367. [CrossRef]
38. Xiang, X.; Chen, X.; Dai, R.; Luo, Y.; Ma, P.; Ni, S.; Ma, C. Anaerobic digestion of recalcitrant textile dyeing sludge with alternative pretreatment strategies. *Bioresour. Technol.* **2016**, *222*, 252–260. [CrossRef]
39. Issa Hamoud, H.; Finqueneisel, G.; Azambre, B. Removal of binary dyes mixtures with opposite and similar charges by adsorption, coagulation/flocculation and catalytic oxidation in the presence of CeO_2/H_2O_2 Fenton-like system. *J. Environ. Manag.* **2017**, *195*, 195–207. [CrossRef]
40. Furlan, F.R.; de Melo da Silva, L.G.; Morgado, A.F.; de Souza, A.A.U.; Guelli Ulson de Souza, S.M.A. Removal of reactive dyes from aqueous solutions using combined coagulation/flocculation and adsorption on activated carbon. *Resour. Conserv. Recycl.* **2010**, *54*, 283–290. [CrossRef]
41. Babu, D.S.; Srivastava, V.; Nidheesh, P.V.; Kumar, M.S. Detoxification of water and wastewater by advanced oxidation processes. *Sci. Total Environ.* **2019**, *696*, 133961. [CrossRef]
42. Nidheesh, P.V.; Zhou, M.; Oturan, M.A. An overview on the removal of synthetic dyes from water by electrochemical advanced oxidation processes. *Chemosphere* **2018**, *197*, 210–227. [CrossRef] [PubMed]
43. Colindres, P.; Yee-Madeira, H.; Reguera, E. Removal of Reactive Black 5 from aqueous solution by ozone for water reuse in textile dyeing processes. *Desalination* **2010**, *258*, 154–158. [CrossRef]
44. Muniyasamy, A.; Sivaporul, G.; Gopinath, A.; Lakshmanan, R.; Altaee, A.; Achary, A.; Velayudhaperumal Chellam, P. Process development for the degradation of textile azo dyes (mono-, di-, poly-) by advanced oxidation process—Ozonation: Experimental & partial derivative modelling approach. *J. Environ. Manag.* **2020**, *265*. [CrossRef]
45. Mascolo, G.; Lopez, A.; Bozzi, A.; Tiravanti, G. By-products formation during the ozonation of the reactive dye uniblu-A. *Ozone Sci. Eng.* **2002**, *24*, 439–446. [CrossRef]
46. Xu, X.; Geng, A.; Yang, C.; Carabineiro, S.A.C.; Lv, K.; Zhu, J. One-pot synthesis of La—Fe—O @ CN composites as photo-Fenton catalysts for highly e ffi cient removal of organic dyes in wastewater. *Ceram. Int.* **2020**, *46*, 10740–10747. [CrossRef]
47. Jin, J.; Du, X.; Yu, J.; Qin, S.; He, M.; Zhang, K.; Chen, G. High performance nanofiltration membrane based on SMA-PEI cross-linked coating for dye/salt separation. *J. Memb. Sci.* **2020**, *611*, 118307. [CrossRef]
48. Qi, Y.; Zhu, L.; Shen, X.; Sotto, A.; Gao, C.; Shen, J. Polythyleneimine-modified original positive charged nano filtration membrane: Removal of heavy metal ions and dyes. *Sep. Purif. Technol.* **2019**, *222*, 117–124. [CrossRef]
49. Meng, L.; Wu, M.; Chen, H.; Xi, Y.; Huang, M.; Luo, X. Rejection of antimony in dyeing and printing wastewater by forward osmosis. *Sci. Total Environ.* **2020**, *745*. [CrossRef]
50. Lin, C.; Tung, K.; Lin, Y.; Dong, C.; Wu, C. l P re of. *Process Saf. Environ. Prot.* **2020**. [CrossRef]
51. Marzbali, M.H.; Mir, A.A.; Pazoki, M.; Pourjamshidian, R.; Tabeshnia, M. Removal of direct yellow 12 from aqueous solution by adsorption onto spirulina algae as a high-efficiency adsorbent. *J. Environ. Chem. Eng.* **2017**, *5*, 1946–1956. [CrossRef]

52. Ihsanullah, I.; Jamal, A.; Ilyas, M.; Zubair, M.; Khan, G.; Atieh, M.A. Bioremediation of dyes: Current status and prospects. *J. Water Process Eng.* **2020**, *38*, 101680. [CrossRef]
53. Shao, H.; Li, Y.; Zheng, L.; Chen, T.; Liu, J. Removal of methylene blue by chemically modified defatted brown algae Laminaria japonica. *J. Taiwan Inst. Chem. Eng.* **2017**, *80*, 525–532. [CrossRef]
54. Cui, D.; Guo, Y.Q.; Lee, H.S.; Cheng, H.Y.; Liang, B.; Kong, F.Y.; Wang, Y.Z.; Huang, L.P.; Xu, M.Y.; Wang, A.J. Efficient azo dye removal in bioelectrochemical system and post-aerobic bioreactor: Optimization and characterization. *Chem. Eng. J.* **2014**, *243*, 355–363. [CrossRef]
55. Sirajudheen, P.; Karthikeyan, P.; Vigneshwaran, S.; Meenakshi, S. Synthesis and characterization of La(III) supported carboxymethylcellulose-clay composite for toxic dyes removal: Evaluation of adsorption kinetics, isotherms and thermodynamics. *Int. J. Biol. Macromol.* **2020**, *161*, 1117–1126. [CrossRef] [PubMed]
56. Saxena, M.; Sharma, N.; Saxena, R. Highly efficient and rapid removal of a toxic dye: Adsorption kinetics, isotherm, and mechanism studies on functionalized multiwalled carbon nanotubes. *Surf. Interfaces* **2020**, *21*, 100639. [CrossRef]
57. Morais da Silva, P.M.; Camparotto, N.G.; Grego Lira, K.T.; Franco Picone, C.S.; Prediger, P. Adsorptive removal of basic dye onto sustainable chitosan beads: Equilibrium, kinetics, stability, continuous-mode adsorption and mechanism. *Sustain. Chem. Pharm.* **2020**, *18*. [CrossRef]
58. Deniz, F. Adsorption Properties of Low-Cost Biomaterial Derived from *Prunus amygdalus* L. for Dye Removal from Water. *Sci. World J.* **2013**, *2013*, 961671. [CrossRef]
59. Fan, H.; Ma, Y.; Wan, J.; Wang, Y.; Li, Z.; Chen, Y. Adsorption properties and mechanisms of novel biomaterials from banyan aerial roots via simple modification for ciprofloxacin removal. *Sci. Total Environ.* **2020**, *708*, 134630. [CrossRef]
60. Niinipuu, M.; Latham, K.G.; Boily, J.F.; Bergknut, M.; Jansson, S. The impact of hydrothermal carbonization on the surface functionalities of wet waste materials for water treatment applications. *Environ. Sci. Pollut. Res.* **2020**, *27*, 24369–24379. [CrossRef]
61. Sharma, H.B.; Sarmah, A.K.; Dubey, B. Hydrothermal carbonization of renewable waste biomass for solid biofuel production: A discussion on process mechanism, the influence of process parameters, environmental performance and fuel properties of hydrochar. *Renew. Sustain. Energy Rev.* **2020**, *123*, 109761. [CrossRef]
62. Stirling, R.J.; Snape, C.E.; Meredith, W. The impact of hydrothermal carbonisation on the char reactivity of biomass. *Fuel Process. Technol.* **2018**, *177*, 152–158. [CrossRef]
63. Yusuf, I.; Flagiello, F.; Ward, N.I.; Arellano-García, H.; Avignone-Rossa, C.; Felipe-Sotelo, M. Valorisation of banana peels by hydrothermal carbonisation: Potential use of the hydrochar and liquid by-product for water purification and energy conversion. *Bioresour. Technol. Rep.* **2020**, 100582. [CrossRef]
64. Bisinoti, C.; Moreira, A.B.; Laranja, J.; Renata, C.J.; Ferreira, O.P.; Melo, C.A. Semivolatile organic compounds in the products from hydrothermal carbonisation of sugar cane bagasse and vinasse by gas chromatography-mass spectrometry. *Bioresour. Technol. Rep.* **2020**, *12*. [CrossRef]
65. Fregolente, L.G.; Miguel, T.B.A.R.; de Castro Miguel, E.; de Almeida Melo, C.; Moreira, A.B.; Ferreira, O.P.; Bisinoti, M.C. Toxicity evaluation of process water from hydrothermal carbonization of sugarcane industry by-products. *Environ. Sci. Pollut. Res.* **2019**, *26*, 27579–27589. [CrossRef] [PubMed]
66. Ischia, G.; Fiori, L. Hydrothermal Carbonization of Organic Waste and Biomass: A Review on Process, Reactor, and Plant Modeling. *Waste Biomass Valorization* **2020**. [CrossRef]
67. Marzbali, M.H.; Paz-ferreiro, J.; Kundu, S.; Ramezani, M.; Halder, P.; Patel, S.; White, T.; Madapusi, S.; Shah, K. Investigations into distribution and characterisation of products formed during hydrothermal carbonisation of paunch waste. *Biochem. Pharmacol.* **2020**, 104672. [CrossRef]
68. Zhang, Z.; Zhu, Z.; Shen, B.; Liu, L. Insights into biochar and hydrochar production and applications: A review. *Energy* **2019**, *171*, 581–598. [CrossRef]
69. Wang, L.; Chang, Y.; Liu, Q. Fate and distribution of nutrients and heavy metals during hydrothermal carbonization of sewage sludge with implication to land application. *J. Clean. Prod.* **2019**, *225*, 972–983. [CrossRef]
70. Maniscalco, M.P.; Volpe, M.; Messineo, A. Hydrothermal carbonization as a valuable tool for energy and environmental applications: A review. *Energies* **2020**, *13*, 4098. [CrossRef]
71. Ponnusamy, V.K.; Nagappan, S.; Bhosale, R.R.; Lay, C.H.; Duc Nguyen, D.; Pugazhendhi, A.; Chang, S.W.; Kumar, G. Review on sustainable production of biochar through hydrothermal liquefaction: Physico-chemical properties and applications. *Bioresour. Technol.* **2020**, *310*, 123414. [CrossRef]

72. Mathimani, T.; Mallick, N. A review on the hydrothermal processing of microalgal biomass to bio-oil-Knowledge gaps and recent advances. *J. Clean. Prod.* **2019**, *217*, 69–84. [CrossRef]
73. Brindhadevi, K.; Anto, S.; Rene, E.R.; Sekar, M. Effect of reaction temperature on the conversion of algal biomass to bio-oil and biochar through pyrolysis and hydrothermal liquefaction. *Fuel* **2021**, *285*, 119106. [CrossRef]
74. Liu, H.; Ma, M.; Xie, X. New materials from solid residues for investigation the mechanism of biomass hydrothermal liquefaction. *Ind. Crop. Prod.* **2017**, *108*, 63–71. [CrossRef]
75. Sun, Y.; Yang, G.; Zhang, L.; Sun, Z. Preparation of high performance H2S removal biochar by direct fluidized bed carbonization using potato peel waste. *Process Saf. Environ. Prot.* **2017**, *107*, 281–288. [CrossRef]
76. Li, F.; Gui, X.; Ji, W.; Zhou, C. Effect of calcium dihydrogen phosphate addition on carbon retention and stability of biochars derived from cellulose, hemicellulose, and lignin. *Chemosphere* **2020**, *251*, 126335. [CrossRef]
77. Li, J.; Li, Y.; Wu, Y.; Zheng, M. A comparison of biochars from lignin, cellulose and wood as the sorbent to an aromatic pollutant. *J. Hazard. Mater.* **2014**, *280*, 450–457. [CrossRef]
78. Kim, D.; Lee, K.; Park, K.Y. Upgrading the characteristics of biochar from cellulose, lignin, and xylan for solid biofuel production from biomass by hydrothermal carbonization. *J. Ind. Eng. Chem.* **2016**, *42*, 95–100. [CrossRef]
79. Qin, L.; Wu, Y.; Hou, Z.; Jiang, E. Influence of biomass components, temperature and pressure on the pyrolysis behavior and biochar properties of pine nut shells. *Bioresour. Technol.* **2020**, *313*, 123682. [CrossRef]
80. Muppaneni, T.; Reddy, H.K.; Selvaratnam, T.; Dandamudi, K.P.R.; Dungan, B.; Nirmalakhandan, N.; Schaub, T.; Omar Holguin, F.; Voorhies, W.; Lammers, P.; et al. Hydrothermal liquefaction of Cyanidioschyzon merolae and the influence of catalysts on products. *Bioresour. Technol.* **2017**, *223*, 91–97. [CrossRef]
81. Cui, Z.; Cheng, F.; Jarvis, J.M.; Brewer, C.E.; Jena, U. Roles of Co-solvents in hydrothermal liquefaction of low-lipid, high-protein algae. *Bioresour. Technol.* **2020**, *310*, 123454. [CrossRef]
82. Shen, Y.; Yu, S.; Yuan, R.; Wang, P. Biomass pyrolysis with alkaline-earth-metal additive for co-production of bio-oil and biochar-based soil amendment. *Sci. Total Environ.* **2020**, *743*, 140760. [CrossRef] [PubMed]
83. Yuan, S.; Hong, M.; Li, H.; Ye, Z.; Gong, H.; Zhang, J.; Huang, Q.; Tan, Z. Contributions and mechanisms of components in modified biochar to adsorb cadmium in aqueous solution. *Sci. Total Environ.* **2020**, *733*, 139320. [CrossRef] [PubMed]
84. Wu, L.; Zhang, S.; Wang, J.; Ding, X. Phosphorus retention using iron (II/III) modified biochar in saline-alkaline soils: Adsorption, column and field tests. *Environ. Pollut.* **2020**, *261*, 114223. [CrossRef] [PubMed]
85. Nakarmi, A.; Bourdo, S.E.; Ruhl, L.; Kanel, S.; Nadagouda, M.; Kumar Alla, P.; Pavel, I.; Viswanathan, T. Benign zinc oxide betaine-modified biochar nanocomposites for phosphate removal from aqueous solutions. *J. Environ. Manag.* **2020**, *272*, 111048. [CrossRef] [PubMed]
86. Li, Y.; Xing, B.; Ding, Y.; Han, X.; Wang, S. A critical review of the production and advanced utilization of biochar via selective pyrolysis of lignocellulosic biomass. *Bioresour. Technol.* **2020**, *312*, 123614. [CrossRef] [PubMed]
87. Elkhalifa, S.; Al-Ansari, T.; Mackey, H.R.; McKay, G. Food waste to biochars through pyrolysis: A review. *Resour. Conserv. Recycl.* **2019**, *144*, 310–320. [CrossRef]
88. Tripathi, M.; Sahu, J.N.; Ganesan, P. Effect of process parameters on production of biochar from biomass waste through pyrolysis: A review. *Renew. Sustain. Energy Rev.* **2016**, *55*, 467–481. [CrossRef]
89. Wang, X.; Li, C.; Li, Z.; Yu, G.; Wang, Y. Effect of pyrolysis temperature on characteristics, chemical speciation and risk evaluation of heavy metals in biochar derived from textile dyeing sludge. *Ecotoxicol. Environ. Saf.* **2019**, *168*, 45–52. [CrossRef]
90. Park, J.H.; Wang, J.J.; Meng, Y.; Wei, Z.; DeLaune, R.D.; Seo, D.C. Adsorption/desorption behavior of cationic and anionic dyes by biochars prepared at normal and high pyrolysis temperatures. *Colloids Surf. A Physicochem. Eng. Asp.* **2019**, *572*, 274–282. [CrossRef]
91. Chen, X.L.; Li, F.; Chen, H.Y.; Wang, H.J.; Li, G.G. Fe_2O_3/TiO_2 functionalized biochar as a heterogeneous catalyst for dyes degradation in water under Fenton processes. *J. Environ. Chem. Eng.* **2020**, *8*, 103905. [CrossRef]
92. Yek, P.N.Y.; Peng, W.; Wong, C.C.; Liew, R.K.; Ho, Y.L.; Wan Mahari, W.A.; Azwar, E.; Yuan, T.Q.; Tabatabaei, M.; Aghbashlo, M.; et al. Engineered biochar via microwave CO_2 and steam pyrolysis to treat carcinogenic Congo red dye. *J. Hazard. Mater.* **2020**, *395*. [CrossRef] [PubMed]

93. Chu, J.H.; Kang, J.K.; Park, S.J.; Lee, C.G. Application of magnetic biochar derived from food waste in heterogeneous sono-Fenton-like process for removal of organic dyes from aqueous solution. *J. Water Process Eng.* **2020**, *37*, 101455. [CrossRef]
94. Mahmoud, M.E.; Abdelfattah, A.M.; Tharwat, R.M.; Nabil, G.M. Adsorption of negatively charged food tartrazine and sunset yellow dyes onto positively charged triethylenetetramine biochar: Optimization, kinetics and thermodynamic study. *J. Mol. Liq.* **2020**, *318*, 114297. [CrossRef]
95. Zhang, H.; Lu, T.; Wang, M.; Jin, R.; Song, Y.; Zhou, Y.; Qi, Z.; Chen, W. Inhibitory role of citric acid in the adsorption of tetracycline onto biochars: Effects of solution pH and Cu^{2+}. *Colloids Surf. A Physicochem. Eng. Asp.* **2020**, *595*. [CrossRef]
96. Yao, X.; Ji, L.; Guo, J.; Ge, S.; Lu, W.; Chen, Y.; Cai, L.; Wang, Y.; Song, W. An abundant porous biochar material derived from wakame (Undaria pinnatifida) with high adsorption performance for three organic dyes. *Bioresour. Technol.* **2020**, *318*, 124082. [CrossRef] [PubMed]
97. Rubeena, K.K.; Prasad, P.H.; Laiju, A.R.; Nidheesh, P. V Iron impregnated biochars as heterogeneous Fenton catalyst for the degradation of acid red 1 dye. *J. Environ. Manag.* **2018**, *226*, 320–328. [CrossRef] [PubMed]
98. Zazycki, M.A.; Borba, P.A.; Silva, R.N.F.; Peres, E.C.; Perondi, D.; Collazzo, G.C.; Dotto, G.L. Chitin derived biochar as an alternative adsorbent to treat colored effluents containing methyl violet dye. *Adv. Powder Technol.* **2019**, *30*, 1494–1503. [CrossRef]
99. Nautiyal, P.; Subramanian, K.A.; Dastidar, M.G. Adsorptive removal of dye using biochar derived from residual algae after in-situ transesteri fi cation: Alternate use of waste of biodiesel industry. *J. Environ. Manag.* **2016**, *182*, 187–197. [CrossRef]
100. Damertey, D.; Jung, H.; Soo, S.; Sung, D.; Han, S. Decolorization of cationic and anionic dye-laden wastewater by steam- activated biochar produced at an industrial-scale from spent mushroom substrate. *Bioresour. Technol.* **2019**, *277*, 77–86. [CrossRef]
101. Wang, H.; Zhao, W.; Chen, Y.; Li, Y. Nickel aluminum layered double oxides modified magnetic biochar from waste corncob for efficient removal of acridine orange. *Bioresour. Technol.* **2020**, *315*, 123834. [CrossRef]
102. Yu, K.L.; Lee, X.J.; Ong, H.C.; Chen, W.-H.; Chang, J.-S.; Lin, C.-S.; Show, P.L.; Ling, T.C. Adsorptive removal of cationic methylene blue and anionic Congo red dyes using wet-torrefied microalgal biochar: Equilibrium, kinetic and mechanism modeling. *Environ. Pollut.* **2020**, 115986. [CrossRef] [PubMed]
103. Iqbal, J.; Shah, N.S.; Sayed, M.; Niazi, N.K.; Imran, M.; Khan, J.A.; Khan, Z.U.H.; Hussien, A.G.S.; Polychronopoulou, K.; Howari, F. Nano-zerovalent manganese/biochar composite for the adsorptive and oxidative removal of Congo-red dye from aqueous solutions. *J. Hazard. Mater.* **2021**, *403*, 123854. [CrossRef]
104. Ganguly, P.; Sarkhel, R.; Das, P. Synthesis of pyrolyzed biochar and its application for dye removal: Batch, kinetic and isotherm with linear and non-linear mathematical analysis. *Surf. Interfaces* **2020**, *20*, 100616. [CrossRef]
105. Kumar, S.; Abdel-fattah, T.M. Kinetics, isotherm, and thermodynamic studies of the adsorption of reactive red 195 A dye from water by modified Switchgrass Biochar adsorbent. *J. Ind. Eng. Chem.* **2016**. [CrossRef]
106. Sahu, S.; Pahi, S.; Tripathy, S.; Singh, S.K.; Behera, A.; Sahu, U.K.; Patel, R. Adsorption of methylene blue on chemically modified lychee seed biochar: Dynamic, equilibrium, and thermodynamic study. *J. Mol. Liq.* **2020**, *315*, 113743. [CrossRef]
107. Zhu, K.; Wang, X.; Chen, D.; Ren, W.; Lin, H.; Zhang, H. Wood-based biochar as an excellent activator of peroxydisulfate for Acid Orange 7 decolorization. *Chemosphere* **2019**, *231*, 32–40. [CrossRef] [PubMed]
108. Wang, J.; Guo, X. Adsorption kinetic models: Physical meanings, applications, and solving methods. *J. Hazard. Mater.* **2020**, *390*, 122156. [CrossRef] [PubMed]
109. Biswas, S.; Mohapatra, S.S.; Kumari, U.; Meikap, B.C.; Sen, T.K. Batch and continuous closed circuit semi-fluidized bed operation: Removal of MB dye using sugarcane bagasse biochar and alginate composite adsorbents. *J. Environ. Chem. Eng.* **2020**, *8*, 103637. [CrossRef]
110. Côrtes, L.N.; Druzian, S.P.; Streit, A.F.M.; Godinho, M.; Perondi, D.; Collazzo, G.C.; Oliveira, M.L.S.; Cadaval, T.R.S.; Dotto, G.L. Biochars from animal wastes as alternative materials to treat colored effluents containing basic red 9. *J. Environ. Chem. Eng.* **2019**, *7*. [CrossRef]
111. Xu, X.; Xu, Z.; Huang, J.; Gao, B.; Zhao, L.; Qiu, H.; Cao, X. Sorption of reactive red by biochars ball milled in different atmospheres: Co-effect of surface morphology and functional groups. *Chem. Eng. J.* **2020**, 127468. [CrossRef]

112. Wang, H.; Wang, S.; Gao, Y. Cetyl trimethyl ammonium bromide modified magnetic biochar from pine nut shells for efficient removal of acid chrome blue K. *Bioresour. Technol.* **2020**, *312*, 123564. [CrossRef] [PubMed]
113. Wang, L.; Yan, W.; He, C.; Wen, H.; Cai, Z.; Wang, Z.; Chen, Z.; Liu, W. Microwave-assisted preparation of nitrogen-doped biochars by ammonium acetate activation for adsorption of acid red 18. *Appl. Surf. Sci.* **2018**, *433*, 222–231. [CrossRef]
114. Chen, L.; Jiang, X.; Xie, R.; Zhang, Y.; Jin, Y.; Jiang, W. A novel porous biochar-supported Fe-Mn composite as a persulfate activator for the removal of acid red 88. *Sep. Purif. Technol.* **2020**, *250*, 117232. [CrossRef]
115. Hoslett, J.; Ghazal, H.; Mohamad, N.; Jouhara, H. Removal of methylene blue from aqueous solutions by biochar prepared from the pyrolysis of mixed municipal discarded material. *Sci. Total Environ.* **2020**, *714*, 136832. [CrossRef] [PubMed]
116. Tran, H.N. Comments on "High-efficiency removal of dyes from wastewater by fully recycling litchi peel biochar". *Chemosphere* **2020**, *257*, 126444. [CrossRef] [PubMed]
117. Ang, T.N.; Young, B.R.; Taylor, M.; Burrell, R.; Aroua, M.K.; Chen, W.-H.; Baroutian, S. Enrichment of surface oxygen functionalities on activated carbon for adsorptive removal of sevoflurane. *Chemosphere* **2020**, *260*, 127496. [CrossRef] [PubMed]
118. Choudhary, M.; Kumar, R.; Neogi, S. Activated biochar derived from Opuntia ficus-indica for the efficient adsorption of malachite green dye, Cu^{+2} and Ni^{+2} from water. *J. Hazard. Mater.* **2020**, *392*, 122441. [CrossRef]
119. Shan, R.; Lu, L.; Gu, J.; Zhang, Y.; Yuan, H.; Chen, Y.; Luo, B. Photocatalytic degradation of methyl orange by Ag/TiO2/biochar composite catalysts in aqueous solutions. *Mater. Sci. Semicond. Process.* **2020**, *114*, 105088. [CrossRef]
120. Al-Ghouti, M.A.; Da'ana, D.A. Guidelines for the use and interpretation of adsorption isotherm models: A review. *J. Hazard. Mater.* **2020**, *393*, 122383. [CrossRef]
121. Choi, J.; Won, W.; Capareda, S.C. The economical production of functionalized Ashe juniper derived-biochar with high hazardous dye removal efficiency. *Ind. Crop. Prod.* **2019**, *137*, 672–680. [CrossRef]
122. Ji, B.; Wang, J.; Song, H.; Chen, W. Removal of methylene blue from aqueous solutions using biochar derived from a fallen leaf by slow pyrolysis: Behavior and mechanism. *J. Environ. Chem. Eng.* **2019**, *7*, 103036. [CrossRef]
123. Jabar, J.M.; Odusote, Y.A. Removal of cibacron blue 3G-A (CB) dye from aqueous solution using chemo-physically activated biochar from oil palm empty fruit bunch fiber. *Arab. J. Chem.* **2020**, *13*, 5417–5429. [CrossRef]
124. Zubair, M.; Manzar, M.S.; Mu'azu, N.D.; Anil, I.; Blaisi, N.I.; Al-Harthi, M.A. Functionalized MgAl-layered hydroxide intercalated date-palm biochar for Enhanced Uptake of Cationic dye: Kinetics, isotherm and thermodynamic studies. *Appl. Clay Sci.* **2020**, *190*, 105587. [CrossRef]
125. Khan, N.; Chowdhary, P.; Ahmad, A.; Giri, B.S.; Chaturvedi, P. Hydrothermal liquefaction of rice husk and cow dung in Mixed-Bed-Rotating Pyrolyzer and application of biochar for dye removal. *Bioresour. Technol.* **2020**, *309*, 123294. [CrossRef]
126. Oladipo, A.A.; Ifebajo, A.O. Highly efficient magnetic chicken bone biochar for removal of tetracycline and fluorescent dye from wastewater: Two-stage adsorber analysis. *J. Environ. Manag.* **2018**, *209*, 9–16. [CrossRef]
127. Zhang, P.; O'Connor, D.; Wang, Y.; Jiang, L.; Xia, T.; Wang, L.; Tsang, D.C.W.; Ok, Y.S.; Hou, D. A green biochar/iron oxide composite for methylene blue removal. *J. Hazard. Mater.* **2020**, *384*, 121286. [CrossRef]
128. Hou, Y.; Huang, G.; Li, J.; Yang, Q.; Huang, S.; Cai, J. Hydrothermal conversion of bamboo shoot shell to biochar: Preliminary studies of adsorption equilibrium and kinetics for rhodamine B removal. *J. Anal. Appl. Pyrolysis* **2019**, *143*, 104694. [CrossRef]
129. Muhammad, N.Z.; Qamar, D.; Faisal, N.; Muhammad, N.Z.; Munawar, I.; Muhammad, F.N. Effective adsorptive removal of azo dyes over spherical ZnO nanoparticles. *J. Mater. Res. Technol.* **2019**, *8*, 713–725.
130. Pal, P.; Pal, A. Dye removal using waste beads: Efficient utilization of surface-modified chitosan beads generated after lead adsorption process. *J. Water Process Eng.* **2019**, *31*. [CrossRef]
131. Dai, L.; Zhu, W.; He, L.; Tan, F.; Zhu, N.; Zhou, Q.; He, M.; Hu, G. Calcium-rich biochar from crab shell: An unexpected super adsorbent for dye removal. *Bioresour. Technol.* **2018**, *267*, 510–516. [CrossRef]
132. Boudechiche, N.; Fares, M.; Ouyahia, S.; Yazid, H.; Trari, M.; Sadaoui, Z. Comparative study on removal of two basic dyes in aqueous medium by adsorption using activated carbon from Ziziphus lotus stones. *Microchem. J.* **2019**, *146*, 1010–1018. [CrossRef]

133. Chahinez, H.-O.; Abdelkader, O.; Leila, Y.; Tran, H.N. One-stage preparation of palm petiole-derived biochar: Characterization and application for adsorption of crystal violet dye in water. *Environ. Technol. Innov.* **2020**, *19*, 100872. [CrossRef]
134. Gokulan, R.; Avinash, A.; Prabhu, G.G.; Jegan, J. Remediation of remazol dyes by biochar derived from Caulerpa scalpelliformis—An eco-friendly approach. *J. Environ. Chem. Eng.* **2019**, *7*, 103297. [CrossRef]
135. Kah, M.; Sigmund, G.; Xiao, F.; Hofmann, T. Sorption of ionizable and ionic organic compounds to biochar, activated carbon and other carbonaceous materials. *Water Res.* **2017**, *124*, 673–692. [CrossRef] [PubMed]
136. Spagnoli, A.A.; Giannakoudakis, D.A.; Bashkova, S. Adsorption of methylene blue on cashew nut shell based carbons activated with zinc chloride: The role of surface and structural parameters. *J. Mol. Liq.* **2017**, *229*, 465–471. [CrossRef]
137. Del Bubba, M.; Anichini, B.; Bakari, Z.; Bruzzoniti, M.C.; Camisa, R.; Caprini, C.; Checchini, L.; Fibbi, D.; El Ghadraoui, A.; Liguori, F.; et al. Physicochemical properties and sorption capacities of sawdust-based biochars and commercial activated carbons towards ethoxylated alkylphenols and their phenolic metabolites in effluent wastewater from a textile district. *Sci. Total Environ.* **2020**, *708*, 135217. [CrossRef]
138. Santra, B.; Ramrakhiani, L.; Kar, S.; Ghosh, S.; Majumdar, S. Ceramic membrane-based ultrafiltration combined with adsorption by waste derived biochar for textile effluent treatment and management of spent biochar. *J. Environ. Health Sci. Eng.* **2020**. [CrossRef]
139. De Gisi, S.; Notarnicola, M. *Industrial Wastewater Treatment*; Abraham, M., Ed.; Elsevier: Oxford, UK, 2017; pp. 23–42, ISBN 978-0-12-804792-7.
140. Odinga, E.S.; Waigi, M.G.; Gudda, F.O.; Wang, J.; Yang, B.; Hu, X.; Li, S.; Gao, Y. Occurrence, formation, environmental fate and risks of environmentally persistent free radicals in biochars. *Environ. Int.* **2020**, *134*, 105172. [CrossRef]
141. Zhang, Y.; Chen, Z.; Xu, W.; Liao, Q.; Zhang, H.; Hao, S.; Chen, S. Pyrolysis of various phytoremediation residues for biochars: Chemical forms and environmental risk of Cd in biochar. *Bioresour. Technol.* **2020**, *299*, 122581. [CrossRef]
142. Zhang, Q.; Ye, X.; Li, H.; Chen, D.; Xiao, W.; Zhao, S.; Xiong, R.; Li, J. Cumulative effects of pyrolysis temperature and process on properties, chemical speciation, and environmental risks of heavy metals in magnetic biochar derived from coagulation-flocculation sludge of swine wastewater. *J. Environ. Chem. Eng.* **2020**, *8*, 104472. [CrossRef]

water

Review

An Overview and Evaluation of Highly Porous Adsorbent Materials for Polycyclic Aromatic Hydrocarbons and Phenols Removal from Wastewater

Zakariyya Uba Zango [1,2,*], Nonni Soraya Sambudi [3,*], Khairulazhar Jumbri [1], Anita Ramli [1], Noor Hana Hanif Abu Bakar [4], Bahruddin Saad [1], Muhammad Nur' Hafiz Rozaini [1], Hamza Ahmad Isiyaka [1], Abubaker Mohammed Osman [5] and Abdelmoneim Sulieman [6]

[1] Fundamental and Applied Sciences Department, Universiti Teknologi PETRONAS, Seri Iskandar 32610, Perak, Malaysia; khairulazhar.jumbri@utp.edu.my (K.J.); anita_ramli@utp.edu.my (A.R.); bahrudsaad@gmail.com (B.S.); Muhammad_18000735@utp.edu.my (M.N.H.R.); hamza_18001996@utp.edu.my (H.A.I.)
[2] Chemistry Department, Colllege of Natural and Applied Sciences, Al-Qalam University, 2137 Katsina, Nigeria
[3] Chemical Engineering Department, Universiti Teknologi PETRONAS, Seri Iskandar 32610, Perak, Malaysia
[4] School of Chemical Sciences, Universiti Sains Malaysia, Pinang 11800, Malaysia; hana_hanif@usm.my
[5] Chemistry Department, College of Science, King Khalid University, Abha 62529, Saudi Arabia; abubaker123@gmail.com
[6] Radiology and Medical Imaging Department, College of Applied Medical Sciences, Prince Sattam Bin Abduaziz University, Alkharj 16278, Saudi Arabia; a.sulieman@psau.edu.sa
* Correspondence: zakariyyazango4@gmail.com (Z.U.Z.); soraya.sambudi@utp.edu.my (N.S.S.); Tel.: +60-174269144 (Z.U.Z.); +60-18957481 (N.S.S.)

Received: 15 September 2020; Accepted: 13 October 2020; Published: 19 October 2020

Abstract: Polycyclic aromatic hydrocarbons (PAHs) and phenolic compounds had been widely recognized as priority organic pollutants in wastewater with toxic effects on both plants and animals. Thus, the remediation of these pollutants has been an active area of research in the field of environmental science and engineering. This review highlighted the advantage of adsorption technology in the removal of PAHs and phenols in wastewater. The literature presented on the applications of various porous carbon materials such as biochar, activated carbon (AC), carbon nanotubes (CNTs), and graphene as potential adsorbents for these pollutants has been critically reviewed and analyzed. Under similar conditions, the use of porous polymers such as Chitosan and molecularly imprinted polymers (MIPs) have been well presented. The high adsorption capacities of advanced porous materials such as mesoporous silica and metal-organic frameworks have been considered and evaluated. The preference of these materials, higher adsorption efficiencies, mechanism of adsorptions, and possible challenges have been discussed. Recommendations have been proposed for commercialization, pilot, and industrial-scale applications of the studied adsorbents towards persistent organic pollutants (POPs) removal from wastewater.

Keywords: adsorption; phenols; polycyclic aromatic hydrocarbons; wastewater

1. Introduction

Organic pollutants, such as polycyclic aromatic hydrocarbons (PAHs), phenols, and their derivatives, are one of the major pollutants that are frequently detected in wastewater. They are usually originated from both natural and anthropogenic sources, such as bush-burning, volcanic eruptions, petroleum exploration and refining, mining etc. [1,2]. They are usually run-off into the water bodies where they reside in the ground and surface water, thus resulting into environmental problem for decades. They are highly lipophilic, semi volatile, and accumulative in water and can be transported into various water compartments due to their non-biodegradable and persistent nature [3,4]. They are categorized as persistent organic pollutants (POP's) in the water. When present in the living cells, they are capable of undergoing bioaccumulating and biomagnifying through food webs into different trophic levels of organisms, and subsequently into humans [5].

PAHs are organic compounds consisting of two or more fused benzene ring molecules. They mostly result from petroleum refining, fuel combustion, coal mining and processing, coke production, oil shale pyrolysis, chemicals production, and other industrial processes. Various research conducted in different parts of the world have shown considerable increase in the PAHs concentrations in the receiving water bodies. Thus, PAHs could be ubiquitously transported into the rivers [6,7], fresh and terrestrial water [8], municipal wastewater treatment plants [9], and consequently exposed to the human being and aquatic organism. They are classified based on the number of rings they contained into low molecular weight (LMW-PAHs) and higher molecular weight (HMW-PAHs). The former comprised those PAHs with two to three benzene rings, while the latter are made of four to six rings. In comparisons, the latter are more toxic and persistent to the water due to their low solubility [10,11]. The United States Protection Agency (USEPA) has listed 16 PAHs as potential toxic and carcinogenic and thus they have priority concerned. The structures, molecular weight, and log *p* values of the PAHs are highlighted in Table 1.

Table 1. Chemical structures and log *p* values of polycyclic aromatic hydrocarbons (PAHs).

Compound	Formula	Abbreviation	Structure	Molecular Weight (g/mol)	Partition Coefficient
Naphthalene	$C_{10}H_8$	NAP	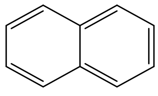	128.17	3.37
Acenaphthylene	$C_{12}H_8$	ACE	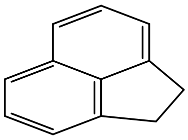	152.1	4.0
Acenaphthene	C_1H_{10}	ACE	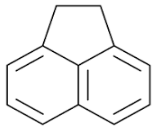	154.21	3.92
Fluorene	$C_{13}H_{10}$	FLU	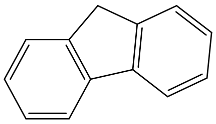	166.22	4.18
Phenanthrene	$C_{14}H_{10}$	PHE	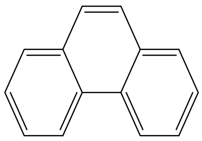	178.23	4.57
Anthracene	$C_{14}H_{10}$	ANT	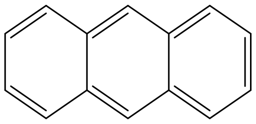	178.23	4.54

Table 1. *Cont.*

Compound	Formula	Abbreviation	Structure	Molecular Weight (g/mol)	Partition Coefficient
Fluoranthene	$C_{16}H_{10}$	FL	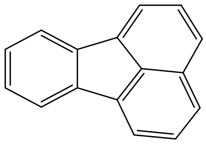	202.25	4.58
Pyrene	$C_{16}H_{10}$	PYR	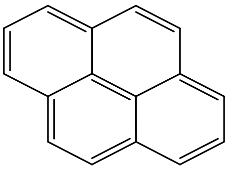	202.25	4.58
Benz[a]anthracene	$C_{18}H_{12}$	B[a]A	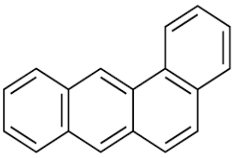	228.3	6.14
Chrysene	$C_{18}H_{12}$	CRY		228.29	5.30
Benzo[b]fluoranthene	$C_{20}H_{12}$	BbF	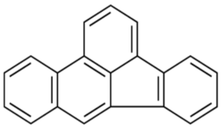	252.3	5.74
Benz[k]fluoranthene	$C_{20}H_{12}$	BkF	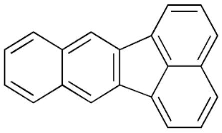	252.3	5.74
Benz[a]pyrene	$C_{20}H_{12}$	BaP	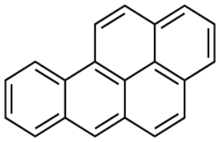	252.3	6.74
Benzo[ghi]perylene	$C_{22}H_{12}$	BhP		276.3	6.52
Dibenz[a,h]anthracene	$C_{22}H_{14}$	DahA	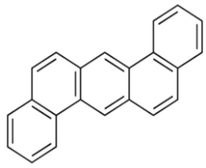	278.4	6.20
Indeno[1,2,3-c,d]pyrene	$C_{22}H_{12}$	IP	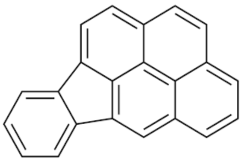	276.3	6.20

Phenols are a class of organic compounds having hydroxyl group (–OH) attached to the carbon atom that is part of the aromatic ring. They have found numerous applications as intermediates for industrial production of petrochemicals, dyes, herbicides, pesticides, pharmaceuticals and cosmetics, etc. [12]. Apart from that, they are also used in household products such as flavorings, cleaners and mouthwash. Thus, they are usually discharged in the wastewater and effluents from those industries [13,14]. Even though small quantity of phenols are produced from the decomposition of plants and animals, but anthropogenic sources has been a major contributor of phenols in the environment wastewater effluents in high concentration up to even several thousands of mg/L [15,16]. Considering their adverse effect to living organisms in the environment, they are also classified as priority pollutants [17,18]. The frequent discharge of phenolics without treatment leads to environmental toxicities to the extent that they are posing serious threats to human health. Some of their toxic effects includes; skin and eyes irritations, respiratory complications, weight loss, diarrhea, vertigo, salivation, and dark coloration of urine etc. [19,20]. Table 2 presents some of the most frequently reported phenols and their dissociation constants (PKa).

Table 2. Chemical structures and log *p* values of polycyclic aromatic hydrocarbons studied.

Compound	Formula	Structure	Molecular Weight (g/mol)	Partition Coefficient
Phenol	C_6H_6O	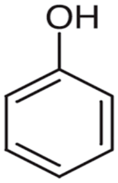	94.11	10.0
Cresol	C_7H_8O	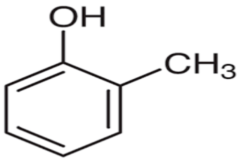	108.14	10.28
Resorcinol	$C_6H_6O_2$	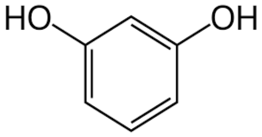	110.1	19.15
Hydroquinone	$C_6H_6O_2$	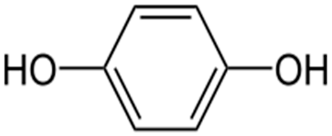	110.11	9.9
Pyrogallol	$C_6H_6O_3$	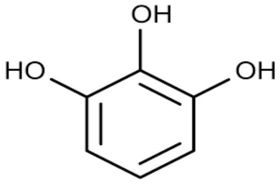	126.11	9.03
Naphthol	C_6H_8O	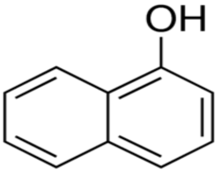	144.17	9.51
Salicylic acid	$C_7H_6O_3$	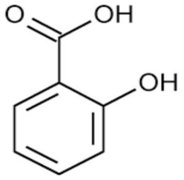	178.23	2.97

Table 2. *Cont.*

Compound	Formula	Structure	Molecular Weight (g/mol)	Partition Coefficient
Picric acid	$C_6H_3N_3O_7$	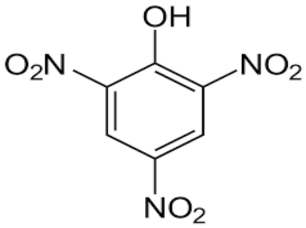	229.1	0.38
Bisphenol A	$C_{15}H_{16}O_2$	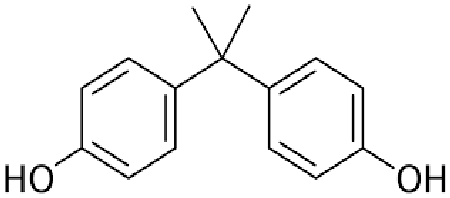	228.29	10.29
Chlorophenol	C_6H_5ClO	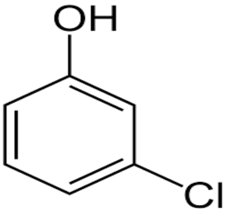	128.6	9.12
Nitrophenol	$C_6H_5NO_3$	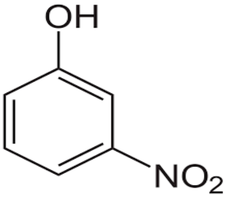	139.10	7.15

In recognition of the mobilities and high toxicities of these pollutants in environmental waters, a prompt response from various environmental monitoring and protection is needed to reduce their concentrations, or to ideally completely eliminate them. Thus, considerable attention has been paid to develop suitable techniques for their effective remediation [21,22]. Over the last three decades, extensive studies have been conducted using different technologies including coagulation and flocculation, phytoremediation, reverse and forward osmosis, chemical oxidation, photocatalytic degradation and adsorption [23–25]. Table 3 highlights the pros and cons of some of the remediation techniques employed. Generally, most of these techniques failed to address the persistent problem, partly because the pollutants are highly lipophilic. In a conventional wastewater treatment plant (WWTPs), they are resistant to bioremediation and photolysis is insignificant for their degradations [26]. Additionally, the excessive chemical remediation might cause secondary pollution because of the unreasonable proportions of the reagents used and formation of oxygenated species that are potentially hazardous [27,28]. Photocatalytic degradation has been limited by the semi conducting property of the materials and the utilization of light energy. Additionally, most of the techniques are non-feasible and non-economical.

Table 3. Pros and Cons of Wastewater treatments process used for PAHs and phenols remediation.

Method	Pros	Cons
Coagulation	– The colloidal particles are easily settled down by the coagulants added to the wastewater	– It is time-consuming – Incomplete removal of the organic pollutants are always the case – It resulted in secondary pollution inform of sludge
Flocculation	– Availability of various flocculants that have been commercialized. – Some of the flocculants have shown a high affinity to the organic pollutants.	– It is highly dependent on the physicochemical parameters of the pollutants; such as pH and ionic strength. – The flocculants often resulted in secondary pollution.
Bioremediation; including the use of microbes such as bacteria, fungi, and algae.	– It was employed for the treatments of PAHs at the contamination site and wastewater treatment plants – Availability and low-cost of various microbes. – It is a simple process	– The method requires nutrients for the microbes to flourish. – Temperature optimization for the condition has been a challenge. – A long time is required to degrade organic pollutants.
Reverse Osmosis	– No chemicals are added to the pollutants; hence no secondary pollutants are generated. – It is available for large scale application using sophisticated reverse osmosis membranes systems	– It is costly, especially for small and medium-scale applications. – It is a time-consuming process.
Chemical oxidations	– The organic pollutants such as PAHs and phenols are easily oxidized to carbon dioxide and water. – No sludge is generated in the process; thus, it is environmentally friendly.	– The high cost of operation and maintenance – Since it involved the use of hydrogen peroxide, it may result in harmful effects to humans if not considerably removed.

Table 3. *Cont.*

Method	Pros	Cons
Solvent extraction and ion exchange process	– It is a rapid process with high efficiency for the removal of PAHs and phenols in wastewater. – The cost of operation is cheap – The extractants are mostly reusable, thus, it is economical.	– Some solvents are toxic; thus, cross-contamination may occur. – The use of volatile solvents may result in fire emission. – Not suitable at the low concentration of the pollutants.
Photocatalytic degradation	– Complete mineralization of the pollutants to carbon dioxide and water – The photocatalysts are upon reusable from the economic point of view. – It is an environmentally friendly technique. – It is mostly operated under room temperature.	– A sufficient light source of energy is required to excite the photocatalyst. – Some of the photocatalysts are expensive, thus not economical for industrial-scale applications. – The photocatalytic reactor is expensive for both purchasing and maintenance.
Adsorption process	– It is simple to design and operate. – Availability of various forms of locally synthetic adsorbents materials. – Low-cost adsorbents and commercial adsorbents are available. – Complete adsorption of the pollutants can be achieved within a short time. – It is an environmentally friendly technique. – Reusability of the adsorbents.	– Adsorbent regeneration is often difficult and costly. – A high temperature is needed to dissolve high molecular weight pollutants. – Spent adsorbent may be considered hazardous but are usually incinerated.

However, adsorption has been recognized as the major technique for the effective removal due to the high affinity the various adsorbents for the organic pollutants. Additionally, the process has been recognized for its simplicity, low-cost, availability of various adsorbents materials, non-environmental toxicity, ease of design, etc. Figure 1 presents the literature survey conducted via web of science and for publications reported and patents for various remediation for PAHs and phenols. The prominence of adsorption is clearly seen among the techniques. It is thus justifiable that this review was conducted for the removal of PAHs and phenols using adsorption techniques. Critical analysis was conducted using various advanced porous adsorbents and the adsorptive performance of the materials have been highlighted. To some extent, the mechanism for the adsorptions have been discussed.

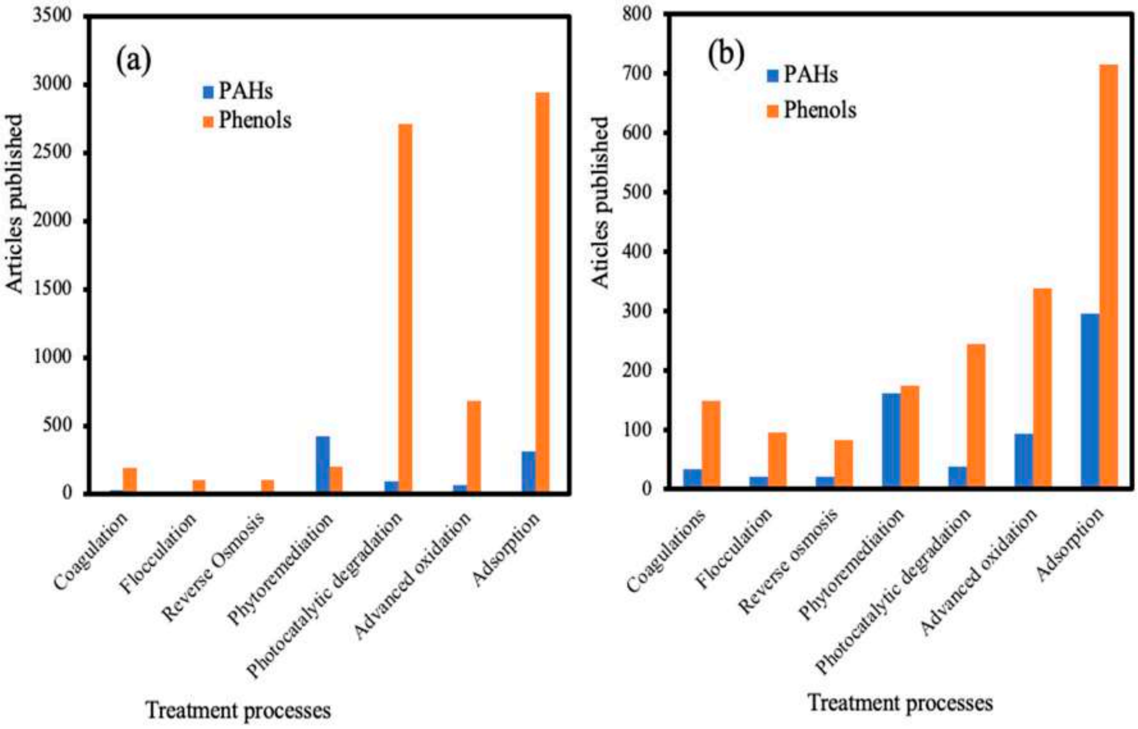

Figure 1. Trends of (**a**) publications and (**b**) patents on various treatment techniques for PAHs and phenols remediation: Data obtained from the web of science using keywords: Adsorptions, Advanced oxidation, Coagulation, Flocculation, PAHs, Phenols, Phytoremediation, Photocatalytic degradation, Reverse osmosis.

1.1. Sources of PAHs and Phenols

Industrial activities driving by energy and power demands have been the major source of PAHs and phenolic compounds in the environment. In particular, the refining of crude oil is usually associated with the production of various by-products such as petrol, diesel, coal tar, etc. [29]. Crude and refined oil leakage have also been widely recognized as one of the major sources of PAHs and phenols in the water [30]. It has been estimated, around 5–30 million tons of crude oil spilt into the ocean every year [31], as a result of either accident or leakage oil tankers. One of the most recent ones is the oil spill which occurred in Ambarnaya river and Mauritius coast in May and July 2020, respectively. In both cases, the spills were reported to occupy large area and consequently washed into the oceans. Petroleum and industrial sludges have also been a major deposit of PAHs and phenols [32,33].

Apart from petroleum and petrochemicals, coal processing to generate heat and power, as well as coke production, has also been identified as another way through which PAHs and phenolic compounds get into the water [34]. The generation of electricity from coal has been widely practiced, taking about one third of the total electricity generation [35]. According to the Environmental Protection Agency, coal fire plants contributed to about a third of the total global water pollution due to the various toxic chemicals such as PAHs, phenolic compound, and heavy metals discharged into the rivers, streams, and other water bodies [36]. Thus, the concentrations of these pollutants in the coal wastewater is high when discharged into the atmosphere and are said to be contributing to the persistent problem of global warming [37].

PAHs and phenols have been identified as one of the major contaminants in wastewater, ans usually exist in complex. The textile and dyeing industry have been a major contributor to PAHs. According to the China environmental statistics yearbook of 2012, discharge of wastewater from dyeing industries was about 2.37 billion. Accordingly, Ning et al., (2014), reported that the total number of 16 different PAHs with concentration range of 1463–16,714 ng/g has been detected in textile dyeing sludge from Guangdong [38]. Natural and anthropogenic sources of phenols have been discussed by Anku et al., (2016), highlighting the contribution of dissolved organic matter in increasing the phenols concentrations in the environment [39]. Floodwater is another source of which PAHs and phenolic compounds get into wastewater. The catastrophe of flooding has been a common phenomenon in different places of the world, particularly in the tropical areas, where rainfall is very high over a long period of the year [40]. For example, Chukwujindu et al. (2017) reported on the prevalent occurrences of flood along the River Niger and River Benue in Nigeria, as a result of excessive rainfall during the wet season [41]. Even though no established finding between the magnitude and frequency of a flood event has been found (especially large floods), the resulting environmental changes has been reported. However, Ciesielczuk et al. (2014) described that PAHs and phenols are usually adsorbed on the humic acids in the floodwaters and thus migrated to the water [42].

1.2. PAHs and Phenols in Wastewater Treatment Plants (WWTPs)

WWTPs has been the secondary source of PAHs and phenols. WWTPs serve as the major reservoir of wastewater collected from a wide range of domestic and industrial sources. Thus, various pollutants from these sources have been found to concentrate along with the solid particles in the wastewater [25]. According to the J. Liu et al. (2011), PAHs were detected in domestic WWTP in Xian, China for a period of one year, originated from domestic usage of petrochemical substances such as oil and grease, cosmetics, etc. Therefore, WWTPs is acting as the secondary source of PAHs from the different sources [43].

1.3. Toxicities of PAHs and Phenols to Humans

Much attention has been given to the study of toxicities of PAHs and phenols to humans. The source of human exposure has been mostly linked to consumption of contaminated water, air inhalation or from infected foods [44,45]. The exposure is more pronounced to communities living at the site of petroleum exploration and refining or near the coastal areas where discharged wastewater is released into rivers, oceans or seas [46]. Industrial water has higher risk of contaminations than the municipal WWTPs as in the former, the wastewater is directly coming from the source such as coke production plants which contains mixture of complex compounds such as PAHs, phenols and nitrogen containing aromatics [47].

The level of bioaccumulation of PAHs in humans is determined by the toxicities which increased with molecular weight. Long term exposure usually resulted in acute toxicities, associated with carcinogenicity and mutagenicity [48]. High exposure increased the risk of cancer of various organs such as lung, breast, prostate, kidney, bladder, stomach, and skin [26]. They are also reported to suppress the immune of the body, thus they are labeled as endocrine disruptors [49]. Chukwujindu et al. (2017), studied the effect of exposure to PAHs due to overflooding of PAH contaminated water with the associated health risk. They employed the technique of incremental lifetime cancer risk (ILCR) to determine the extent of the PAHs exposure among various age groups in the study area. The finding shows that on the average, the total ILCR values obtained in 2014 were 443 and 308 chances in a million among the children and adults, respectively, and that the number of the risk of cancer was 6450 and 4480 chances for children and adults, respectively, about a 15-fold decrease in the average total

ILCR values. Thus, they estimated high risk of exposure among adults than children, attributed to the prolong duration of exposure for the adults [41].

On the other hand, phenols are potential human carcinogens. They are found to exert toxic effects even at lower concentrations. At higher concentrations, phenols has the tendency to coagulate with the proteins in the body, which may result in cellular and cytoplasmic permeability, hence, could cause damage of the sensitive cells, cardiovascular, and central nervous system [50]. Prolonged ingestion of phenols may result into mouth sore, dark urine, and even diarrhea [51].

1.4. Environmental Regulations on PAHs and Phenols

In an effort to eliminate the effect of PAH and other toxic chemicals into the environmental waters, the United Nation has set the regulation to stop the establishment of coal power plants around the globe to tackle the climate change and water pollution challenges [47,52]. The United States Protection Agency (USEPA) has categorized 16 PAHs as priority pollutants of carcinogenic and mutagenic effect in water [25]. To limit the PAHs and other toxic contaminants from the environmental water, E.U has regulations to forbid sludge disposal. The Ministry of Environmental Protection of China has set the level of toxic PAHs and B[a]PYR in wastewater treatment plant as 50 μg/L and 0.03 μg/L [2,9] respectively.

Phenol has been detected in various water samples ranging from hazardous waste sites, surface water, rainwater, ground water, sediments, industrial and urban runoff, as well as the drinking water. The level of toxicity of phenol in human and aquatic animals has been identified as 9–25 mg/L [53]. Considering the toxicity and environmental impact of phenolic compounds in water, the USEPA has included them under the listed of priority pollutants with limited environmental discharge of less than 1 mg/L in the treated effluents and set their maximum content in potable water as 0.5 mg/L [54]. Similarly, the World Health Organization (WHO) has regulated the concentration of phenol in potable drinking water at 0.001 mg/L [55].

2. PAHs and Phenols Remediation in Wastewater

Considering the negative impact of PAHs and phenols with their derivatives in wastewater, various forms of remediation have been proposed. Some of these techniques reported includes conventional methods such as coagulation, flocculation, activated sludge, and bioremediation [42,56]. Other techniques such as membrane technology, photocatalytic degradation, advanced oxidation, and electrochemical catalysis have also been reviewed [57,58]. Some of these techniques have shown considerable promise [26], while some are facing challenges of incomplete removal or degradation of the pollutants, generations of other toxic contaminants [24,59], complexity of the method, as well as the cost of application and maintenance. Hence, the quest for more alternative techniques has seemed endless.

Adsorption techniques using various adsorbent materials from natural and synthetic origins have been well studied due to their prospects to effectively removed the pollutants from water. These technique are simple, economical, and practicable [60]. The ease of operation and non-generation of secondary pollutants are other advantages enjoyed by the method.

2.1. PAHs and Phenols Removal by Adsorption

In the adsorption process, pollutants in the solution are trapped on the surface of suspended particles, known as the adsorbent materials. Adsorption technology is motivated by the availability of a broad spectrum of low-cost adsorbents obtained from abundant naturally occurring and waste substances such as mineral deposits, agricultural waste products, particulate organic matters, and solid industrial wastes [61]. Thus, it provides an alternative for transforming waste materials into useful material for environmental sustainability.

Apart from the naturally occurring materials, synthesized particles with higher surface area and pore volumes such as organic and inorganic polymers, porous carbon materials, graphene, silica-based materials, have been successfully utilized as adsorbents for the PAHs and phenols removal from the wastewater [62,63]. Adsorption process is usually carried out in a batch reactor on a small scale, non-continuous process such as in research laboratories [64], or using a more advanced technique of fixed bed reactors or column for a pilot-scale industrial and water treatment plants application [65]. Villegas et al. (2016) [53] discussed on various methods for phenols removal in wastewater, however, emphasis was laid mainly on activated carbon (AC), those other highly porous adsorbents such as silica and metal-organic frameworks (MOFs) have not been considered.

In this article, we aimed at reviewing and discussing past and present scenario of using various adsorbent materials for the removal of PAHs and phenols from water. The review also provides scientific analysis and propose future research directions on the use of promising adsorbent materials for PAHs and phenols adsorptive removals in the water.

2.2. Adsorption of PAHs and Phenols onto Porous Carbon Materials

The use of porous carbon materials as adsorbents for organic pollutants removal from aquatic environment was first mentioned by Walters and Luthy (1984) [66]. They argued that porous carbon adsorbents are superior to soils, sediments, and suspended organic matters in terms of removal of PAHs. This claim has catalyzed discoveries of various porous carbon materials for wastewater remediation. The use of porous carbon materials such as activated carbon (AC) prepared from various agricultural waste materials [67,68], biochar [69,70], carbon nanotubes (CNTs) [71,72], and other derived carbon materials for the adsorption of PAHs have been studied.

2.2.1. Biochar

Biochar is a carbonaceous solid obtained from waste materials such as agricultural wastes, sewage sludge (SSL), and petroleum sludge (PS). For example, sewage sludge is generated as a by-product of sewage treatment. It is composed of many organic and inorganic substances as well as hazardous biological materials [73,74]. Thus, these solid wastes are harmful to the environment and requires proper disposal. Interestingly, pyrolysis is used as an alternative thermochemical technique to convert the waste sludge into useful biochar for effective industrial and environmental applications. It has been identified as one of the major forms of porous derived carbon. Godlewsky et al. (2019) investigated the effect of atmosphere nitrogen (N_2) and carbon dioxide (CO_2) for the production of sludge derived-biochar under pyrolysis temperatures of 500–700 °C. The use of CO_2 atmosphere was able to generate biochar with improved properties such as higher BET surface area, porosity as compared to those obtained under N_2 atmosphere [56].

Biochar that are derived from biomass-derived is by far the most important means to produce the porous carbon materials. It has been estimated that, the world production of dry biomass is about 220 billion tons annually [75], thus pyrolysis treatment to energy and biochar is interesting option [76,77]. Agricultural waste materials such as rice husk [78], wheat straw [79], and palm kernel seeds [80] have been reportedly used for PAHs and phenol adsorption in water.

The review by Bedia et al. (2018) focused mainly on the use of biomass derived biochar for emerging contaminants adsorptions in water streams [81]. In comparison to sludge derived-biochar, biomass derived-biochar has been found to possess higher specific surface area and pore volumes which was attributed to the higher carbon content in the latter [77]. Thus, high removal of PAHs (pyrene and benzo[a]pyrene) has been reported by Qiao et al. (2018) using biomass derived biochar generated from *Enteromorpha prolifera* at 200 °C. The Langmuir monolayer maximum adsorption capacities were estimated to be 187.27 μg/g and 80.00 μg/g, for the pyrene and benzo[a]pyrene, respectively [82]. Recently, Arshad et al. (2019) reported on response surface method (RSM) optimizations of phenol adsorption onto oil–palm bunch derived biochar [80]. Lee et al. (2019) reported on the effective removal of phenol using biochar generated from food waste Factors that affect the adsorption of PAHs and phenols onto biochar include pore size and volume of the adsorbent as well as the concentration of the pollutants [20]. The review by Lamichhane et al., 2016 [25] also highlighted some advantages of biochar in the removal of PAHs. Different biochars for the adsorptions of PAHs and phenols in water streams are summarized in Table 4.

Table 4. Adsorptions of PAHs and phenols using biochars.

Adsorbent	Pollutant	Concentration (mg/L)	Q_e (mg/g)	Equilibrium Time	Ref
RHB	PHE	5	17	1 h	[78]
Magnetic modified RHB			42		
Biochar	PHE	1	2	3 days	[83]
graphene/biochar composite			3		
Rice-350-M	PHE	1	43	24 h	[69]
Elephant grass biochar	BaA	0.1	19	250 min	[84]
	BkF		19		
	BaP		18		
	DahA		8		
Poplar Catkins biochar	PHE	30	384	1120 min	[85]
Sewage sludge char	PHE	0.8	-	24 h	[56]
	PYR		-		
Wood biochar	PYR				
Wheat straw biochar	PHE	9.1	-	48 h	[79]
	FLU	10.0	-		
	PYR	11	-		
Chitin biochar	phenol	500	184	12 h	
	2-nitrphenol		206		
Hizikia fusiformis biochar	phenol	50	30	1440 min	[86]
Black spruce biochar	phenol	200	233	18 h	[87]
White birch biochar			150	4 h	
Chinese herb biochar	phenol	50	-	360 min	[88]
scots pine bark biochar	phenol	500	149	24 h	[89]
spruce bark biochar			84		
Bamboo biochar	phenol	10	17	24 h	[90]
Oak wood biochar			13		
Food waste biochar	phenol	10	3	30 min	[20]
Japanese red pine char	Phenol	200	6	30 min	[61]
Yellow poplar char	Phenol		7		
Pine fruit shell biochar	Phenol	50	27	24 h	[91]

2.2.2. Activated Carbon (AC)

AC are highly porous carbon materials obtained from agricultural wastes, with high carbon contents such as cellulose, hemicellulose, lignin, lipids, proteins, simple sugars, and starch [67,92]. The production of AC involved thermal decomposition of these materials under limited supply of air, followed by the activation to generate highly porous carbon material. Thus, precursors for AC are usually low-cost agricultural waste materials such as husk [93], shells [94], wood [95], sawdust [96], rice husk [66], etc. The use of other materials such as bones, cartilages, coke etc. have also been employed [97]. It has been widely employed for a variety of industrial applications such as gas separations and purifications, liquid and gas storage, super capacitors, electrodes, catalysis, and removal of toxic substances in contaminated wastewater etc. [98]. They are usually characterized by a large surface area and large porosity than most of the conventional adsorbents ever reported. However, the properties are largely dependent on the precursor material, pyrolysis temperature, and the activation conditions. In some cases, the AC produced might contain heteroatoms and mineral matter (ash content) depending on the nature of the raw material used as precursor. A literature has shown that over 26,000 articles have been published by Elsevier on the use of AC for the adsorption of pollutants in aqueous medium. Danish and Ahmad 2018, has reviewed on the production of AC from wood biomass as adsorbent materials. Pore size, pore diameter distribution, of AC as the major contributing factor for the adsorption of the pollutants [92].

Different forms of AC such as AC powdered activated carbons (PAC) and granular activated carbons (GAC) [99,100] from different biomass has been reportedly used for organic pollutants removal from water (Figure 2). Additionally, the use of modified AC to regulate its pore structure and chemical properties for the effective removal has been studied [101]. Wu et al. (2020) recently reported on the preparation of walnut shell AC (WAC) with a surface area of 438.5 m^2/g via microwave-assisted KOH activation process at 900 W for the competitive adsorption of NAP and PHE in aqueous medium. Equilibrium adsorption of 40 min, with the adsorption capacities of 39.58 and 63.37 mg/g for the NAP and PHE respectively were obtained [98]. More porous AC were produced via modified coal-base AC (MCAC) and iron-modified coal-base AC (Fe-MCAC) with BET surface area of 1062 and 1079.67 m^2/g respectively for PAHs adsorption [102]. Similarly, optimizations studies for the phenols adsorption was studied using AC obtained from *Terminalia chebula* (TCAC). Equilibrium time of 24 h with the monolayer adsorption capacity of 36.77 mg/g were observed. Table 5 presented more literature on the application of AC as adsorbent for PAHs and phenols removal.

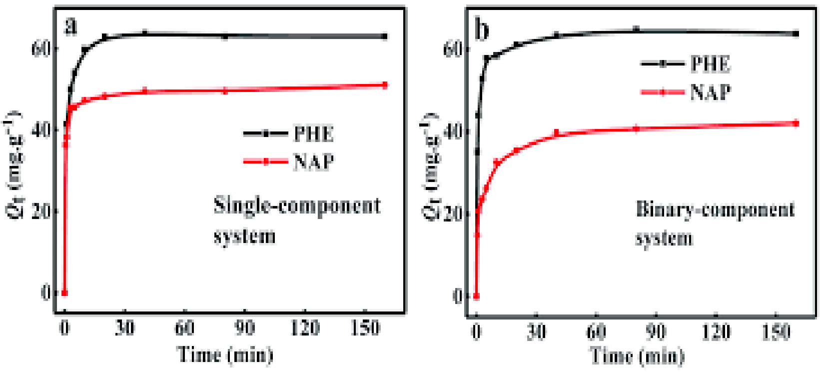

Figure 2. Kinetic studies and adsorption capacities for the removal of NAP and PHE using walnut shell activated carbon (WAC) under (**a**) single and (**b**) binary systems [103]. Copyright: Royal Society of Chemistry (2020).

Table 5. Adsorptions of PAHs and phenols using different forms activated carbon (AC).

Adsorbent	Pollutant	Concentration (mg/g)	Q_e (mg/g)	Equilibrium Time	Ref
Commercial PAC	ANT	-	143	4 h, 5 min	[68]
	PYR		142	4 h, 10 min	
Commercial AC	PHE	120	46	24 h	[104]
	FLA	80	36		
	BaA	12	9.7		
Rice husk AC	NAP	8	14	24 h	[66]
	PHE		17		
	PYR		18		
Flamboyant pod back AC	ACE	50	4.7	2 h	[105]
Milk bush kernel AC			4		
Rice husk AC			5.6		
Rice husk AC	NAP	8	15	24 h	[106]
	PHE		17.5		
	PYR		18		
Rice husk AC	PHE	10	-	60 min	[107]
	FLU		-	30 min	
Rice husk AC	ACE	50	46	3 h	[93]
Vitis vinifera leaf AC ($ZnCl_2$)	PHE	1	94	180 min	[108]
Vitis vinifera leaf AC (H_3PO_4)			89		

Table 5. *Cont.*

Adsorbent	Pollutant	Concentration (mg/g)	Q_e (mg/g)	Equilibrium Time	Ref
Walnut shell AC	NAP	10	49.6	40 min	[103]
	PHE	10	63.8		
flamboyant pod AC	NAP	50	294.2	2 h	[94]
milk bush kernel shell AC			63.3		
Coal-based AC	NAP	200	78.2	20 min	[98]
	PHE		111.4		
	PYR		117.2		
Fe-modified Coal-based AC	NAP	30	167.8	40 min	[101]
	PHE		190.4		
	PYR		20.3		
Terminalia chebula AC	phenol	100	26.2	24 h	[109]
Commercial AC	phenol	1000	132.3	360 min	[110]
Commercial AC	phenol				
Miswak root AC	phenol	100	142.2	120 min	[111]
Coal-based GAC	phenol	300	169.9	180 min	[112]
Coal-based PAC			176.6		
Coconut shell PAC			213		
Cherry stone AC	phenol	25	80	24 h	[113]
Agave Utahensis AC	Phenol	14	1.7	3h	[114]
Euphorbia Resinifira AC			1.9		
Banana peel AC			2.0		
Oily sludge AC	phenol	100	434	30 min	[115]
Tea waste AC	phenol	100	132.5	4 h	[67]
Babul sawdust AC	phenol	50	15.3	60 min	[96]
Olive stone AC	phenol	800	44,269	4 h	[116]
Palm oil bunch AC	phenol	40	55.3	2 h	[117]
Wood fiberboard AC	phenol	250	208	120 min	[95]
Avocado kernel AC	phenol	0.7	3.3	100 min	[118]
Date pit AC	Phenol	50	46	1 h	[119]
Sugar cane bagasse AC	Phenol	100	27	30 min	[120]
Lantana camara AC	Phenol	150	112.5	7 h	[121]
Magnetic AC	phenol	80	107.5	15 min	[122]
Granular activated carbon (GAC)	Phenol,	50	4.9	60 min	[123]
	2-chlorophenol		4.3		
	4-chlorophenol		4.5		
Red pine AC	Phenol	200	454.5	30 min	[61]
Yellow poplar AC			625		
Commercial AC			500		

Generally, AC produced from agricultural wastes displayed better removal capacity and shorter equilibrium time for the adsorption of PAHs and phenols in the aqueous medium as compared to biochar. This is perhaps associated with the higher porosities of the AC. However, in terms of sources, biochar can be generated from different varieties and abundant agricultural waste feedstocks [70]. Additionally, from economic point of view, biochar has cheaper production cost than the AC. Unlike in the latter, the former consumes less energy and activation is necessary in most cases [79]. However, both materials are considered superior to raw biomass in their affinity towards PAHs and phenols [124]. In both cases, the adsorption occurs via hydrogen bonding and π–π electron- donor–acceptor interactions between the active sites on the surface of the AC with the benzene rings of the organic pollutants and the functional groups on the phenol as seen in the Figure 3. For both AC and biochar, better removal capacities are achieved by surface modifications of the porous carbon materials. Additionally, the surface modifications could result in more stable adsorbents [98].

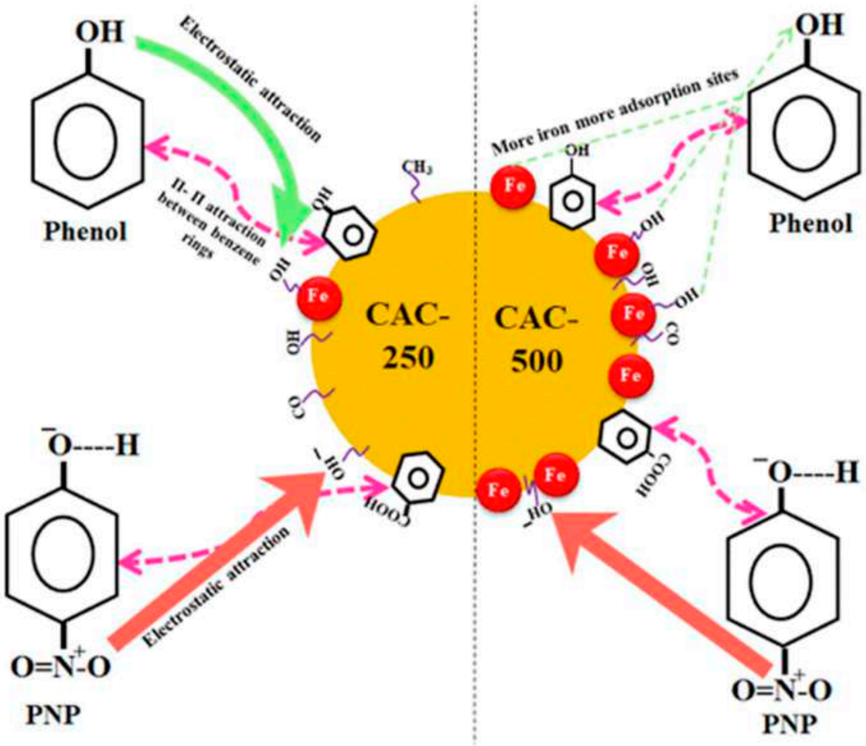

Figure 3. Mechanism for the adsorption of phenols onto activated carbons via hydrogen bonding and π–π interactions [125]. Copyright: Korean Society of Chemical Engineers (2020).

2.3. Other Porous Carbon Materials as Adsorbents for PAHs and Phenols

Apart from biochar and AC, other porous carbon nanomaterials such as graphene, carbon nanotubes (CNTs), nanohorns, nanofibers, fullerenes, soot, molecular carbon sieves, and other carbonaceous-derived materials [126] have been studied. They are chemically heterogenous and high carbon content materials that are usually obtained from either partial or complete combustion of plant materials [127]. Many of the carbon-based nanomaterials have been investigated as adsorption material for water remediation. The most widely employed are graphene and CNTs. They are recognized with extra-ordinary physical and chemical properties that are superior to other carbon-based materials. They possess good chemical and thermal stability with much higher surface area than AC and biochar [62,128]. Their improved surface properties allow them to interact with organic pollutants via covalent and non-covalent bond formation such as hydrogen bonding, electrostatic forces, π-π stacking, van der Waals forces, and hydrophobic interactions [14].

2.3.1. Graphene, Graphene Oxides, and Reduced Graphene Oxides

Graphene is a form of nanomaterial having a honeycomb-like structure of sp^2 hybridized carbon atoms with single atom of graphite layer. The allotrope of graphene is called graphite, having a planar structure [129]. It exhibits outstanding physical and chemical properties, such as good electrical and thermal conductivity, high strength, high specific surface area and pore volumes, flexibility, and negligible thickness [130,131]. Apart from that, graphene chemical mobility, which allow for its modification to form other functionalized advanced carbon materials. Graphene oxides (GOs) and reduced graphene oxide (rGO) are among the most advanced graphene-based engineering materials (Figure 4) [132,133] They are regarded as the fascinating forms of graphene materials and thus have versatile applications in various fields such as biomedicines, sensors, metrology, electronic devices, as well as environmental pollutant's remediation in environmental waters [134].

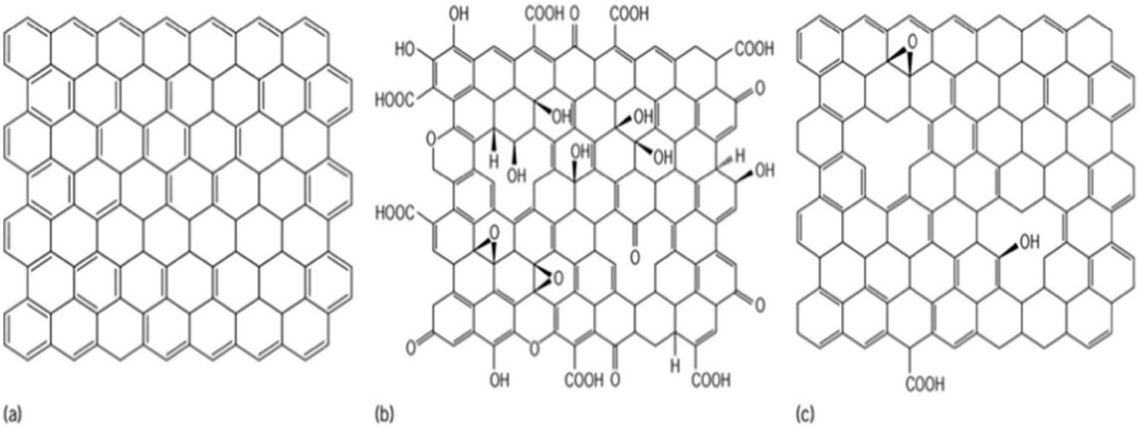

Figure 4. Chrystal structures of (**a**) graphene, (**b**) graphene oxide, and (**c**) reduced graphene oxide [133]. Copyright: Elsevier (2020).

In adsorption studies, their unique chemical properties and high specific surface area has been emphasized. Sun et al. (2013), has reported on the batch adsorptions of NAP, ANT, NAP, and PYR onto graphite, GOs and RGOs. The performance of the materials in decreasing order were rGOs > GOs > graphite, with the former having adsorption capacities of 15.92, 247.17, and 369.06 mg/g for NAP, ANT, and PYR, respectively [135]. Recently, application of graphene wool for the removal of PHE and PYR from aqueous environment has been reported by Adedapo et al. (2019). Effective removal of 99.9 and 99.1% were achieved for PHE and PYR respectively, within 24 h of contact between the PAHs and the adsorbent. The adsorbent material can be repeatedly used with little or no decreased in percentage removals over 8 successive cycles [136].

In the case of phenols removal, graphene and functionalized graphene materials have been reportedly used as adsorbents. Zhou et al. (2017) reported on the fabrication of graphene composite Fe_3O_4@PANI-GO for the batch removal of bisphenol A, t-octyl phenol and α-naphthol in water. The complete removal of the pollutants within shortest time (5 min) for bisphenol A, t-octyl phenol respectively, whereas the α-naphthol experienced slightly longer time, (300 min) to equilibrium. The promising application of the material was demonstrated by its effective reusability (10 successive cycles) without decreased in the removal capacity of the pollutants [137]. The report of Wang et al., (2018) have shown that the adsorption of phenols pollutants; 2-phenylphenol (PPE), bisphenol A (BPA), 4-isopropylphenol (IPE), 4-methylphenol (ME), and phenol (PE) were more effective onto the rGO (Figure 5) as compared to the GO, attributed to the decreased in electron density in the latter, hence the strong π-π interactions between the phenols and the adsorbent [138]. Tian et al. (2019), reported on the rapid adsorption of bisphenol A (3.4 s), onto hybrid material of graphene oxide with amino functionalized polypropylene (PP-g-DMAEMA/GO). The adsorbent possessed dual channel structure which allows bisphenol A to easily access the surface of the GO through the nanochannels of the propylene molecule [139].

In most cases, graphene was shown to have better performance in terms of adsorption capacity as compared to GO and rGO. In comparison to rGO, GO has more oxygen containing functional groups and lesser π electron density [138]. It has been established that the hydrophobic effects of the organic contaminants were the reasons for their strong absorption onto the graphene which occur though π-π interactions [63,140]. In the case of GO, the dense carbonyl groups at the edge of the carbon layers were responsible for the strong adsorption of hydrophobic organic pollutants onto the surface of the material through electrostatic, hydrogen bonding, and anion-π interactions. More details of the adsorptions of PAHs and phenols onto the graphene, GO, rGO, and their derivatives have been highlighted in Table 6.

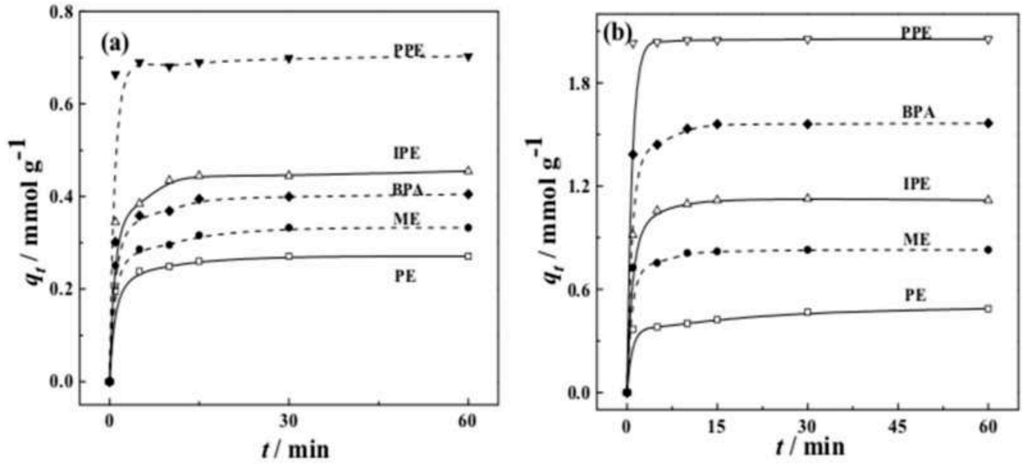

Figure 5. Adsorption capacity (**a**) graphene and (**b**) graphene oxide for phenols removal. Reproduced from ref [138].

Table 6. Adsorptions of PAHs and phenols onto graphene, GO and reduced graphene oxide (rGO) and their composites.

Adsorbent	**Pollutant**	**Concentration (mg/L)**	**Q_e (mg/g)**	**Equilibrium Time**	**Ref**
Graphene wool	PHE	0.8	5	24 h	[126]
	PYR	5	200		
rGO	NAP	30	16	7 days	[125]
	ANT	0.05	247		
	PYR	0.1	369		
GO/FeO·Fe_2O_3	NAP	0.1	6	48 h	[64]
Graphene	NAP	4.6	1	4 h	[63]
GO			66		
Graphene	NAP	-	9	10 min	[141]
GO			8		
Sulfonated graphene	NAP	0.39	2	5 days	[142]
rGO@Sand	NAP	0.8	4	120 min	[143]
	ACE		6		
Magnetic graphene nanosheet	PHE	0.5	0.02	1 h	[72]
Magnetic GO	PHE	1	14	24 h	[60]
Magnetic chemically GO			30		
Magnetic rG			26		
TiO_2-Graphene	PHE	4.2	1.2	180 min	[59]
	FLAN	4.5	0.9		
	BaP	2.5	0.5		
GO	NAP	20	21	24 h	[144]
rG			52		
Reduced graphene			145		
Fe_3O_4@PANI-GO	Bisphenol A	5	14	5 min	[137]
	t-octyl phenol	5	31	5 min	
	α-naphthol	10	23	300 min	
rGO	2-phenylphenol	0.470	12	60 min	[138]
	bisphenol A	0.350	1.56		
	4-isopropylphenol	0.587	1.117		
	4-methylphenol	0.550	0.841		
	phenol	0.850	0.483		
CTAB-modified graphite	bisphenol A	300	125	10 min	[129]
Amino-functionalized GO	Bisphenol A	1	2.3	3.4 s	[139]

Table 6. *Cont.*

Adsorbent	Pollutant	Concentration (mg/L)	Q_e (mg/g)	Equilibrium Time	Ref
rGO GO	phenol	50	16 23		
GO	bisphenol A 4-nonylphenol tetrabromobisphenol A 2,4,6-trichlorophenol	20	21 10 11 18	1400 min	[14]
Graphene	4-chloro-2-nitrophenol	10	25	60 min	[145]
GO rGO	Phenol	50	23 16.32	100 min	[146]
MGO-IL	phenol	30	741	12 min	[147]
Graphene	Bisphenol A	10	87	5 h	[62]
Sulfonated graphene	1-naphthol	0.7	2.41	5 days	[142]
Graphene	phenol	50	28	400 min	[148]
GO sheet GO sponge	2,4,6-trichlorophenol	5	10 21	30 min 12 min	[149]
GO	Bisphenol A	-	49	30 min	[150]
GO	tetrabromobisphenol A	1	41	120 min	[151]
GO	p-nitrophenol	200	138	24 h	[51]
GO Chemically GO rG	1-naphthol	50	21 52 145	24 h	[144]
GO Ultrasonic GO Conventional GO Ultrasonic GO	2-chlorophenol	50	32 134 50 209	50 min	[152]

2.3.2. Carbon Nanotubes (CNTs)

CNTs are sheets of pure form of carbon atoms covalently bonded to one another in hexagonal arrays which are rolled into a hollow cylindrical shape, with the outer diameter ranging between 1–100 nm, while the size up to several tens of micrometers [153]. Since its discovery in 1992, CNT have been identified with unique physical and chemical properties such as high strength and specific gravity, good conductivity and thermal stability, high porosity [154,155], making them potential materials have for various applications such as in optical appliances, energy conversion, electrochemical sensors, catalyst and adsorbent, micro analytical devices, biomedical devices, and drug delivery [156,157]. The application of CNTs in environmental remediation have also been investigated [158,159]. CNTs have been employed as potential adsorbents for organic and inorganic pollutants removal from wastewater due to its superior properties and more tailored surface chemistry, presenting higher surface porosities and strong chemical and physical interactions with the organic pollutants than the AC and corresponding carbon-derived adsorbents [160,161]. The surface morphology of the CNTs and the functional groups present in the organic pollutant has been contributing factor for their higher affinity for the pollutants, thus, rapid removal with higher adsorption capacities [162].

The potential of CNTs for environmental remediation of organic pollutants has been well studied. Wu et al. (2016) explored on the affinity of various aromatic compounds onto CNTs. About 22 different organic pollutants including phenols, substituted benzenes, and PAHs, have been considered and the findings confirmed positive correlations between the adsorption capacities of the CNTs based on their mesoporous surfaces to the properties of the pollutants [163]. A review on the prospects and applications of carbon nanostructured materials in water treatment was presented by Selvaraj et al. (2020) [164]. Apur et al. (2015) discussed the adsorption of organic pollutants including PAHs and phenols onto the CNTs [165]. Another report was presented by Ahmad et al. (2019) on the removal of organic pollutants in wastewater by CNTs [166]. The preparations, properties, and modifications of the CNTs have been discussed. The adsorptions of PAHs, pharmaceutical and personal care products, surfactants and pesticides has been explored and the nature of the interactions between the pollutants and the CNTs has been highlighted. However, in most of the review articles written detailed of the optimized adsorption conditions of phenols and PAHs onto the CNTs were not mentioned.

Earlier work on the removal of PAHs from wastewater was conducted by Yang et al. (2006) using commercially obtained single-walled carbon nanotubes (SWCNTs) and multi-walled carbon nanotubes (MWCNTs). The adsorptions were found to be pH independent due to the neutral nature of the PAHs [167]. The adsorption modeling of PAHs onto CNTs has been studied by Kah et al. (2011). Various concentrations of the PAHs were analyzed, achieving higher adsorption capacities at both lower and higher concentrations, attributed to the higher surface area of the CNTs in the range of 200–500 m^2/g [168]. Zhang et al. (2019) reported the use of magnetic CNTs for the removal of PHE from water. The magnetization of the CNTs has been shown to increase the removal efficiency as well as ease of the regeneration and reusability of the adsorbents [72]. The non-linearity of the PAHs and their non-ionic and hydrophobic nature, enable them to interact with CNTs through π-π bonding [169]. Hybrid simulation analysis was employed by Yali et al. (2019) to predict the adsorption coefficient of PAHs onto MWCNT using quantitative structure-property relationship (QSPR) using genetic algorithm-multiple linear regression (GA-MLR). The data was subjected to training and testing. The explanation given was that the electrostatic and steric parameters of PAHs were the major factors responsible for the higher adsorption capacities for the MWCNT. Hence the molecular docking simulation was accurate and reliable to predict the sorption efficiency [170]. Wu et al. (2020), studied the sorption mechanisms for PAHs onto CNTs through density functional theory (DFT) and molecular dynamics simulation. The sorption energies for the individual PAHs (NAP and PHE, −33.48 and −42 kcal/mol, respectively) were calculated from the compass force field. The simulation studies were able to predict that CNTs and PAHs interacted through π-π stacking and the Van der Waals interactions [171].

For the adsorption phenol onto CNTs, researchers have identified multiple interactions via π-π, hydrogen bonds, and electrostatic interactions. Kragulj et al. (2015) reported on the removal of chlorinated phenols (2,4-dichlorophenols, 2,4,6-trichlorophenols, and 2,3,4,5-tetrachlorophenols) onto originally synthesized MWCNT via catalytic chemical vapor deposition (CCVD) and acid functionalization (FMWCNTs). The FMWCNTs has outstanding performance compared to the pristine form as shown by the increased in the BET surface area functionalization (61.3 m^2/g and 600 m^2/g for MWCNT and FMWCNT, respectively). Except for 2,4,6-trichlorophenol, which was slightly lower than 2,4-dichlorophenol, the adsorption was found to be positively correlated with molecular weight of the pollutants [172]. The mechanism for phenol adsorption onto SWCNTs and MWCNTs using quantum mechanics molecular modeling was investigated by Rezakazemi et al. (2018) [136]. The strong affinity of CNTs onto the phenols has been emphasized by the formation of π-π interactions between the delocalized π electrons in the surface of the sp^2 hybridized carbon structure of the CNTs. However, modified CNTs such as oxidized CNT (CNTO) can form hydrogen bonding with the phenol, thus better affinity than the pristine CNT (Figure 6). Other factors affecting the adsorption of phenols onto the CNTs include pH, ionic strength, as well as the dispersion of the CNTs in the solution. Table 7 discussed the adsorptions of phenols and PAHs onto various CNTs.

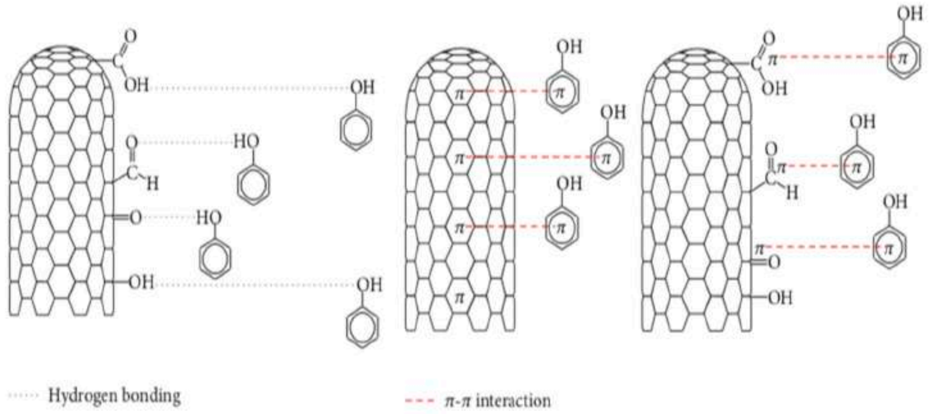

Figure 6. Schematic diagram for the mechanism of phenol adsorption onto carbon nanotubes (CNT). Reproduced from ref [146].

Table 7. Adsorptions of PAHs and phenols onto CNTs and their composites.

Adsorbent	Pollutant	Concentration (mg/L)	Q_e (mg/g)	Equilibrium Time	Ref
MWCNT	NAP	200	69.2	5 days	[173]
Commercial MWCNT	NAP	-	10.9	5 days	[167]
	PHE		10.6		
	PYR		10.6		
Magnetic SWCNT	PHE	500	24.82	30 min	[72]
Magnetic MWCNT			19.37		
MWCNT	phenol	0.147	0.13	3 days	[174]
	3-chlorophenol	1.25	0.38		
CNT-polymer bead	p-chlorophenol	100	24	1200 min	[71]
CNT-polyethylene glycol	phenol	20	27	40 min	[54]
CNT-polymer composite	phenol	30	262	50 min	[162]
SWCNT	phenol	50	51	54 min	[127]
MWCNT			65	36 min	
CNT	phenol	2	1.1	2 h	[175]
CNT-Fe_2O_3			2.8		
Magnetic-N_2H_4-SH/MWCNT	phenol	40	39	700 min	[176]
Chitosan hydrogel-CNT	phenol	200	404	120 min	[177]
CNT	phenol	2	1.1	120 min	[34]
	4-chlorophenol		1.3		
CNT-Al_2O_3	phenol		2.8		
	4-chlorophenol		2.8		
CNT	phenol	50	62	24 h	[13]
CNT-deep eutectic solvent			120		
Chitosan-MWCNT	phenol	150	88	24 h	[17]
CNT	phenol	150	24	50 min	[178]
	2-chlorophenol		86	50 min	
	4-chlorophenol		52	30 min	
CNT-activated	phenol		64	50 min	
	2-chlorophenol		240	50 min	
	4-chlorophenol		105	30 min	
MWCNT	bisphenol A	0.37	111	3 days	[179]
Nitrogen doped-MWCNT			440		
MWCNT	phenol	25	32	300 min	[180]
SWCNT	phenol	50	20	100 min	[146]
SWCNTO			21		
MWCNT			18		
MCNTO			16		
CNT-Mg-Al hydroxide	phenol	50	13		[181]
	4-chlorophenol		14		
MWCNT	2,4,6-trichlorophenol	120	2.3	48 h	[182]

Thus, the efficiency of the carbon-based materials as adsorbents for PAHs and phenols removal has been well established. AC to a larger extent has been the most widely reported adsorbent. It has been prepared from the various agricultural waste materials under different conditions. Additionally, the commercial AC has been available in the markets. Thus, their removal efficiency towards the PAHs and phenols is superior to that of the corresponding biochar derived from similar agricultural waste. Generally, CNTs have been shown to offer better removal efficiency than their corresponding graphene adsorbents. This is attributed to their remarkable high surface area. The strong affinity of the materials to the pollutants is made possible by the presence of hydrogen and π-π bonding interactions as illustrated in Figure 5.

2.4. Other Porous Materials for PAHs and Phenols Adsorption

Porous polymers (e.g., polymer beads, molecular imprinted polymers (MIPs)) [27], mesoporous chitosan [183], and advanced porous materials, such as mesoporous silica (examples; MCM-41, MCM-48 and SBA-15) [184], metal-organic frameworks (MOFs) [185], and other corresponding composites materials synthesized or are usually synthesized from other known materials. They have been known to possess physical and chemical properties superior to that of precursor components and that of the conventional porous materials. They have ultra-high porosity and surface area, high crystallinity, uniform surface morphology, high chemical and thermal stabilities, and other promising features. Thus, they have found numerous applications in various fields such as catalysis, gas storage, sensors, actuators, drug delivery, microextraction, and wastewater remediation [186,187].

The applications of synthesized polymers and advanced porous materials as adsorbents for PAHs and phenol removals have been investigated by various researchers. In most cases, the efficiency of these materials surpasses that of carbon-based materials such as AC, due to their larger pore size and volumes providing more adsorption sites for the pollutants [188,189]. Additionally, some of these materials have displayed good selectively for the PAHs and other phenolic compounds with the formation of hydrogen bonding and π-π interactions.

2.4.1. Chitosan

The applications of chitosan, a polymer material obtained from the shell of seafoods and natural substances for adsorption of pollutants from wastewater have received considerable attention. The advantages of the material are the low-cost and large content of hydroxyl functional groups on the surface of the materials [190]. The price of commercial chitosan is much lower compared to that of the AC and zeolites and it can be easily synthesized with much less energy consumption [191]. The adsorptions of PAHs and phenols onto the chitosan are predominated by hydrogen bonding, hydrophobic, and π-π interactions [192,193].

Bibi et al. (2015) used membranes synthesized from chitosan and poly vinyl pyrrolidone (CW) and carbon nanotube (CNT). The membranes with a surface area of 246 and 253 m^2/g were used for the adsorption of NAP from aqueous solution. The membranes were applied for the adsorption of NAP from aqueous solution with the removal efficiency of 93 and 97% were achieved within 120 and 150 min, respectively [194]. Crisafully et al. (2008) reported on the comparisons of various natural and commercial adsorbents materials including chitosan for the removal of PAHs [4]. Filho et al. (2018) reported on the synthesis of pectin/chitosan and pectin/chitosan/cyclodextrin polymers for the adsorption of 3 PAHs, PYR, B[b]F, and B[a]P. The adsorption of PAHs and phenols onto chitosan is summarized in Table 8. Efficient removal of the pollutants was achieved with good reusability of the adsorbents [195].

Alves et al. (2019) reported on the modification of chitosan with carbon nanotube composite with enhanced BET surface area of 1130 m^2/g for the adsorption of phenol. Equilibrium was reached within 120 min with adsorption capacity of 404.2 mg/g [177]. A similar finding was reported Bahmani et al. (2019) using chitosan grafted with ZIF-8 for the phenol removal, achieving adsorption capacity of 152.3 mg/g within 30 min [196]. Guo et al. (2019) comprised the of adsorption of phenol using chitosan and MWCNT modified chitosan. The composite material achieved higher adsorption capacity of (86.96 mg/g) than the pristine chitosan with (61.69 mg/g) [17]. Karamipour et al. (2020) reported the adsorption of phenol using cellulose acetate/chitosan (CA/Chitosan) composite. The adsorption capacity achieved was 97.43 mg/g within 9 h. A modification of the CA/Chitosan with iron (III) oxide, (Fe_2O_3-CA/Chitosan) improved the physical stability of the adsorbent, achieving good reusability with the adsorption capacity to 163 mg/g [197].

2.4.2. Molecularly Imprinted Polymers (MIPs)

MIPs are obtained from the interactions of organic and or inorganic monomers of polymerizable capabilities which are assembled around a specific template known as the 'imprint', resulting into crosslinking of the monomers to form a solid framework [198]. They are well known for their high porosity resulting from the removal of the template molecules, forming large cavities allows for the easy access of the molecules to the recognition sites [27,199]. The MIPs of inorganic molecularly imprinted materials are more flexible in comparison to those obtained from the organic monomers due to the more availability of the inorganic monomers to be selected from, hence the rigidity of the solid network as well as the adaptable porosity [200].

The adsorptive properties of the MIP towards pollutants removals in wastewater has been emphasized on their large porosity, providing more adsorption sites for the pollutants [201], as highlighted in Table 6. They also offer high selectivity to the pollutants, mainly via hydrogen bonding, ion-pair interactions, hydrophobic interactions, and Van der Waals forces [28]. The adsorptions of PAHs onto the functionalized silica aerogels has been recently reported by Saad et al., (2020). The adsorbent material has proven to be effective in the removal of NAP, ANT, and PYR, with the fluorescence measurements showing effective adsorption and selectivity of the material in the highest order of NAP, ANT, and PYR, respectively [200]. Wei et al. (2015) reported on the selective recognition of PAHs by MIPs. In comparison to the hydrophilic MIP (H-MIP) and co-monomer glycidyl methacrylate (G-MIP), the conventional MIP has higher binding capacity to the PAHs, attributed to the hydrophobic nature of the material [202].

Bhatnagar and Anastopoulos (2017) reported the adsorption of bisphenol A and other phenolic compounds in water [190]. Bayramoglu et al. (2016) reported on the synthesis and selectivity of MIP and non-imprinted polymer (NIP) for the adsorption of bisphenol A, 4-aminophenol, p-toluidine, and 2-napthol in the binary and multiple component system. The adsorption capacity of bisphenol A for the MIP and NIP were 76.7 and 59.9 mg/g, respectively, indicating the selectivity and removal efficiency of the latter [203]. Adsorptive recognition of phenolic compounds bisphenol A, phenol, 4-nitrophenol, 2-amino-4-chlorophenol and 2-napthol has been reported by Lyu et al. (2020), using MIP and ionic liquid mediated MIP (IL-MIP). Higher selective of the bisphenol A has been achieved by the IL-MIP as compared to the conventional MIP, attributed to the complementary of the imprinted cavity of the IL-MIP to the bisphenol structure [198].

Table 8. Adsorption of PAHs and phenols using chitosan and molecularly imprinted polymers (MIPs).

Adsorbent	Pollutant	Concentration (mg/L)	Q_e (mg/g)	Equilibrium Time	Ref
		Chitosan			
Pec-β-CD/Chitosan	PYR	2	0.1	1200 min	[195]
	B[b]F		0.2		
	B[a]P		0.2		
Chitosan	phenol				
Chitosan/CNT	phenol	400	404	120 min	[177]
Chitosan-cyclodextrin	phenol	150	34	-	[193]
	p-chlorophenol	157	180		
	p-nitrophenol	150	21		

Table 8. *Cont.*

Adsorbent	Pollutant	Concentration (mg/L)	Q_e (mg/g)	Equilibrium Time	Ref
chitosan-g-PNVCL/ZIF-8	Phenol	20	152	30 min	[196]
CA/Chitosan	phenol	100	97	5 h	[197]
Fe_2O_3-CA/Chitosan			163		
Chitosan	phenol	150	62	24 h	[16]
MWCNT-Chitosan			87		
Fe-EDA/β-CD/Chitosan	phenol	50	243	120 min	[204]
	p-nitrophenol		274		
	p-cresol		298		
Magnetic chitosan	phenol	15	52	50 min	[19]
Resin-chitosan	phenol	50	189	200 min	[205]
	4-chlorophenol		99	350 min	
EDTA/Chitosan/TiO_2	phenol	50	209	240 min	[206]
Chitosan-Carbon composite	phenol	10	34	1 h	
Magnetic graphene-Chitosan	2-napthol	40	169	60 min	[207]
β-cyclodextrin-chitosan	phenol	120	60	3 h	[22]
	2-chlorophenol		71		
	4-chlorophenol		96		
	2,4-dichlorophenol		315		
	2,4,6-trichlorophenol		376		
Magnetic-Chitosan	bisphenol A	100	55	120 min	[208]
Glutaraldehyde-Chitosan	phenol	50	21	60 min	[209]
	phenol	100	71	240 min	[210]
	o-chlorophenol		51		
MIPs					
MIP	BaP	1	75.9	3 h	[211]
	PYR		7		
	CHR		7		
MIP	PHE	0.6	16	90 min	[212]
MIP	PYR	1	11	90 min	[213]
MIP	bisphenol A	150	77	120 min	[203]
vermiculite MP	bisphenol A	1000	217	90 min	[214]
magnetic vermiculite MP			274		
Surface-MIP	phenol	0.75	86	4 h	[50]
	p-nitrophenol		8		
	p-tert-butylphenol		7		
MIP/PES/SiO_2	phenol	4000	47	8 h	[215]
	p-nitrophenol		37		
AMPS-Am-MIP	Phenol	50	97	180 min	[18]
MIP	Bisphenol A	100	87	20 min	[198]
IL-MIP			116		
Fe_3O_4@SiO_2@PNP-SMIP	4-nitophenol	210	134	60 min	[216]
MIP	bisphenol-A	20	24	240 min	[217]
SMIP			23		

However, it should be stressed that pristine chitosan, upon long term usage as adsorbents, swells. This has drastically limited its application as potential adsorbent material in wastewater remediation. However, surface modification of the chitosan with other ideal functional materials helps to improve the performance of the material and improve its long-term usage. Some reported chitosan composites used for PAHs and phenols adsorption have been highlighted in Table 6.

2.4.3. Mesoporous Silica

With the advancement in nanotechnology and the attempted reproduction of silica nanoparticles in 1990 in Japan [218], researchers all over the world continue to explore the potential of the materials in various areas. Mesoporous nano silica particles such as Mobil Crystalline Materials (such as MCM-41 and MCM-48) and Santa Barbara Amorphous (such as SBA-15 and SBA-16) have been synthesized from rice husks, characterized and commercialized for various applications such as gas storage, drug delivery, oil–water separations, catalysis, and pollutant remediation [186].

Mesoporous silica has well-defined pore structures (hexagonal mesopores), narrow pore size distributions (4–12 nm), as well as high BET and Langmuir surface-area. Table 6 shows mesoporous silica that have been used for the PAHs and phenols adsorption. The adsorption capacity and equilibrium time have been stated.

Nasreen et al. (2018) synthesized highly porous mesoporous silica SBA-15 and MSU-H with BET surface area of 521 and 580 units, respectively. Both SBA-15 and MSU-H were found to be effective in the removal of NAP and PHE with the complete removal achieved within 20 min [218]. Costa et al. (2020) have reported the adsorptions of PAHs from aqueous solution using mesoporous silica MCM-41-NH_2 that have been hydrothermally synthesized, possessing high retention rate of the pollutants with efficiency in the range of 93–98% [219]. Comparison for the removal efficiency of MCM-48 and SBA-15 for the adsorption of NAP was investigated by Balati et al. (2014) with the latter having better efficiency, attributed to its higher larger pore diameter [220]. Yuan et al. (2018) investigated the mechanism for the PAHs adsorption onto the mesoporous silica. They have identified π-π as the predominant interactions between the pollutants and the adsorbents [221].

The applications of mesoporous silica materials for phenols adsorptions has been investigated. Nasreen et al. (2018) reported that SBA-15 and MSU-H were able to adsorb 4-aminophenol and p-nitrophenol from the aqueous medium. The removal efficiency achieved was above 90% within 20 min. It was suggested that the initial properties of the silica has been retained even after a series of regeneration and reusability, attributed to the high silicon content in the materials [218]. Highly porous mesoporous silica SBA-10 and PA-10 with a BET surface area of 925 and 353 m^2/g were synthesized by Yangui et al. (2017) for the adsorption of phenolic compounds. Adsorption efficiency of 75% and 67% for phenol removal were reported within 2 h when the SBA-15 and PA-10 were modified with amine functional groups [222].

2.4.4. Metal-Organic Frameworks (MOFs)

The application of MOFs in wastewater remediation have recently gained more recognitions due to the great potential of these materials. They are made from the coordination interaction of the metal ion with organic moieties [223]. The metal node is the central building block, while organic moiety is the ligand and together forming a framework of higher tunability [224]. They are known to possess ultra-high porosity (over 90% by volume is empty) with BET surface area higher than that of AC and mesoporous silica (up to 9000 m^2/g) [225]. MOFs have higher crystallinity, thermal and moisture stability, and they can be easily regenerated from the aqueous medium through simple decantation or magnetic separation [226]. The topology of the framework also made it possible to modify the MOFs with other functional groups and materials for versatile and particular applications.

The use of MOFs for PAHs adsorptions recently been published by our groups [227]. The application of Zr-based MOFs; UiO-66(Zr) and NH_2-UiO-66(Zr) have been reported for ANT and CRY adsorptions from the aqueous medium. The BET surface area of the MOFs was 1420 and 985 m^2/g for the UiO-66(Zr) and NH_2-UiO-66(Zr), respectively. Higher removal efficiency has been achieved within short equilibrium time (25–30 min) with percentage removals of 98.6 and 97.9% for the ANT and CRY, respectively, using UiO-66(Zr) MOF. Interestingly, all the reported MOFs have displayed good reusability for the PAHs adsorption. We have also reported on the molecular docking interaction of the Fe-based MOFs, MIL-88(Fe) and NH_2-MIL-88(Fe) with CRY. Figure 7 has illustrated the binding interaction of the MOFs with the CRY molecules with the MIL-88(Fe) having the most stable complex structure with the higher binding energy (ΔG_{bind}) of −3.88 kcal/mol and lower inhibition constant (*Ki*) of 1.58 mM. Thus, the CRY molecules preferred to reside in the internal pores of the MOF. However, for the NH_2-MIL-88(Fe), the binding energy is slightly lower, and the inhibition constant is higher, −3.80 kcal/mol and 1.65 mM respectively, resulting into lower binding stability of the complex. In the NH_2-MIL-88(Fe), the CRY molecules preferred to adsorb on the outer pores of the MOFs. The high selectivity of the MIL-88(Fe) has been emphasized by the larger BET surface area and pore size of 1242 m^2/g and 12.5 nm respectively. The BET surface area and the pore size of the NH_2-MIL-88(Fe) was 941 m^2/g and 8.8 nm respectively [228]. Table 9 highlights the various MOFs used for PAHs and phenols adsorptions in wastewater.

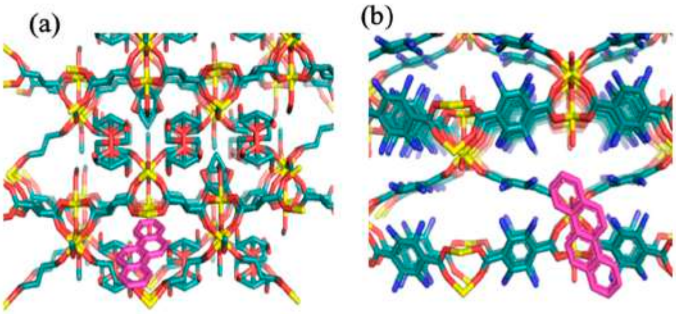

Figure 7. The molecular docking structure of (**a**) MIL-88(Fe) and (**b**) NH_2-MIL-88(Fe) with the CRY molecule, for the binding interactions [229]. Copyright: Elsevier (2020). Metal (Fe), carbon (C), oxygen (O), and nitrogen (N) are colored as yellow, green, red, and blue, respectively. The CRY is indicated in purple.

Adsorptions of phenolic compounds onto MOFs have also been studied. Most of the reported MOFs are promising adsorbents for the removal of the pollutants studied. The famous HKUST-1 has shown good removal efficiency for the p-nitrophenol, with complete removal achieved within 40 min (equilibrium adsorption capacity of 400 mg/g). The high adsorption capacity of the MOF for the p-nitrophenol was attributed to the high affinity of the MOF to the NO_2 side of the pollutant, resulting into hydrogen bonding interactions [229]. The high selectivity and removal efficiency of the crystalline and water stable Zr-based MOF, NH_2-UiO-66(Zr) for the adsorptions of 2,4,6-trinitrophenol, 2,4-dinitrophenol, 2,4,6-tri-nitrotoluene, and 2,4-dinitrotoluene in water was also investigated. Higher equilibrium adsorption capacities was achieved with the hydrogen bonding formation between the MOF and the pollutants [230]. Luo et al. (2019) reported on the enhanced removal of bisphenol A using Al-based composite Al-MOF/SA-CS. The adsorption capacity was 136 mg/g. The adsorption mechanism has been explained by the formation of hydrogen bonding, π-π stacking and cation-π interactions [231].

Table 9. Adsorption of PAHs and phenols onto mesoporous silica and metal-organic frameworks (MOFs).

Adsorbent	Pollutant	Concentration (mg/L)	Q_e (mg/g)	Equilibrium Time	Ref
Mesoporous Silica					
MCM-41	NAP	15	61	20 min	[184]
Periodic mesoporous organosilica	NAP	10	1.5	24 h	
	ACE		0.9		
	FLU		0.9		
	FLUO		0.7		
	PYR		1.3		
Fe-SBA-15	PYR	0.1	0.034	20 min	[188]
NH_2-SBA-15	NAP	1	1.9	24 h	[232]
	ACE		1.4		
	PHE		0.8		

Table 9. *Cont.*

Adsorbent	Pollutant	Concentration (mg/L)	Q_e (mg/g)	Equilibrium Time	Ref
MCM-41-PABA	NAP	200 μg/L	17.83	24 h	[233]
	B[b]FLUO		20		
	B[k]FLUO		19		
	B[b]PYR		19		
MCM-48	NAP	7	0.7	24 h	[220]
SBA-15			0.4		
NH_2-SBA-15	4-chlorophenol	250	141	6 h	[234]
	4-bromophenol		115		
	4-iodophenol		72		
MCM-41-	phenol	50	12	24 h	[222]
	o-chlorophenol		30		
MCM-48-Chitosan	Phenol	500	149	24 h	[183]
SBA-15	4-aminophenol	-	10	20 min	[235]
	4-nitrophenol		8		
Rice husk silica	phenol	15	4	60 min	[236]
MCM-41	phenol	60			
MOFs					
	ANT	4	24	30 min	[227]
UiO-66(Zr)	CRY		24	25 min	
NH_2-UiO-66(Zr)	ANT		22	30 min	
	CRY		19	25 min	
MIL-88(Fe)	CRY	4	24	25 min	[228]
NH_2-MIL-88(Fe)			22		
MIL-88(Fe)	ANT	4	24	30 min	[237]
Mixed-MIL-88(Fe)			23		
NH_2-MIL-88(Fe)			21		
MIL-88(Fe)	PYR	4	24	40 min	[238]
NH_2-MIL-88(Fe)			23		
MIL-53(Al)	bisphenol A	250	329	90 min	[239]
MIL-53(Al)-F127			473	30 min	
MIL-68(Al)/PVDF	p-nitrophenol	10	126	720 min	[240]
HKUST-1(Cu)	p-nitrophenol	200	400	30 min	[229]
SiO_2@MIL-68(Al)	aniline	3000	532	40 s	[241]
[Zn(ATA)(BPD)]	2,4-dichlorophenol	60	-	90 min	[242]
MOF-VII			-		
[Zn(TDC) MOF	2, 4-dichloropheno	60	-	180 min	[243]
MIL-68(Al)	phenol	1000	118	120 min	[244]
CNT@MIL-68(Al)	phenol		257		
NH_2-UiO-66(Zr)	2,4,6-trinitrophenol	100	23	36 h	[230]
	Styphnic acid		24		
	2,4-dinitrophenol		30		
	2,4,6-tri- nitrotoluene		0.5		
	2,4-dinitrotoluene		2		
MIL-53(Al)	dichlorophenoxyacetic acid	150	556	1 h	[245]
MIL–68(Al)	p–nitrophenol	300	271	17 h	[51]
MIL–68(Al)/GO			332	17 h	
NH_2-MIL-88(Fe)	2,4,6-trinitrophenol	35	164	40 min	[246]
MOF-199(Cu)	Phenol	500	58	300 min	[247]
	p-nitro phenol		68	30 min	
Al-MOF/SA-CS	bisphenol A	50	137	18 h	[231]
Cu-BDC MOF	bisphenol A	200	60	40 min	[248]
Cu-BDC@GrO			182		
Cu-BDC@CNT			164		
laccase@HKUST-1	bisphenol A	200	-	4 h	[249]

2.5. Pilot and Industrial Scale Adsorption of PAHs and Phenol in Wastewater

Pilot and industrial wastewater treatment plants have been the major repository of PAHs and phenols. In most cases, these pollutants are washed from the soil by heavy rain or directly emitted from petroleum refineries, petrochemical industries, and coal mining and processing areas. Thus, they are deposited into the municipal wastewater and wastewater treatment plants. Various studies have shown the presence of these pollutants at much higher concentrations than the maximum tolerable limit in the water. Thus, the target of wastewater remediation technologies has been the wastewater for both industrial and municipal treatment plants. Application of adsorption technologies at pilot and industrial wastewater has been well explored [250].

Activated carbon has been the adsorbent most widely used for the post-treatment of non-biodegradable pollutants such as PAHs and phenols in the wastewater treatment plants due to its large surface area and uniformity of surface microspores [251]. With the availability of various low-cost and highly porous adsorbents materials, some researchers have endeavored to explore the adsorptive removals of the PAHs and phenols at both pilot and industrial scale treatment plants. Kalmykova et al. (2014) have explored the performance of sand, granular activated carbon (GAC), and peat moss filters for PAHs and phenol adsorption at pilot-plant. The performance of each filter has been assessed with the GAC achieving complete removal of phenols, while the peat filter was able to remove 50–80% of the phenols. For PAHs removal, the percentage achieved by GAC and peat were 50% and 63%, respectively [252]. The application of resin adsorbent, Amberlite XAD16, was reported by Frascari et al. (2016) for the removal of phenols from olive mill wastewater using continuous flow column at pilot-scale. The Amberlite XAD16 was well characterized with BET surface area of 800 m^2/g and average particle size of 0.63 mm. The adsorption capacity of the material was evaluated by the Langmuir model at 40 mg/g with over 70% removal efficiency achieved by the material [253]. El-Nass et al. (2016) have reported on the pilot-scale removal of phenol from refinery wastewater. About 250 kg of GAC with a particle size of 1.5 mm was used as the bed in the packed column of 1.8 m and 0.6 m length and internal diameter respectively. Over 90% removal of the phenols was achieved by the adsorbent, indicating the efficiency of GAC in removal of organic pollutants from the refinery wastewater [251].

3. Conclusions

Ubiquitous transport, distributions, and the fate of PAHs and phenols in wastewater has been a major environmental challenge for decades. These pollutants have been well identified as highly toxic to both fauna and flora and pose carcinogenic and mutagenic effects to humans. Hence, their environmental abatement, particularly from industrial, municipal, and wastewater treatment plants (WWTPs), has been highly desired. Various wastewater remediation technologies have been proposed. This article presented comprehensive review on the use of adsorption technology for PAHs and phenols remediation from water. The application of various porous adsorbents materials has been studied.

Porous carbon materials biochar and AC have discovered various applications in environmental remediation. Those materials have been successfully prepared from various agricultural wastes and been widely used as adsorbents for PAHs and phenols removal. In comparison to biochar, AC has shown more promising and potential removal capacity, attributed to the higher porosity of the AC. Apart from the biochar and AC, other derived porous carbons such as the graphene and CNTs have been widely employed. Their potentially higher removal efficiencies have been commended. This is attributed to their remarkable high surface area and strong affinity to the pollutants through the formation of hydrogen and π-π bonding interactions, as we have illustrated.

Under similar conditions, the use of synthetic polymers, chitosan and MIPs, have been presented. Despite the selectivity of the polymers, the swelling effect of the chitosan limits their applications. However, modified chitosan has been shown to offer better removal capacity than the pristine form. To the larger extent, the potentials of advanced porous materials; mesoporous silica (such as MCM-41, MCM-48, and SBA-15), and MOFs had been discussed. The superior adsorption capacity of the silica and MOFs adsorbents had been in all way connected to their ultra-porosities and high stability of the materials. Their strong affinity to the PAHs and phenol has been highlighted.

Thus, application of various porous adsorbents has been presented. Findings from previous works from literature have been compiled and analyzed. This review thus highlighted the potential of adsorption technique for the removal of PAHs and phenols from environmental wastewater.

Author Contributions: Conceptualization, Z.U.Z. and N.S.S.; software, K.J.; validation, M.N.H.R.; formal analysis, H.A.I.; investigation, N.H.H.A.B.; resources, N.S.S.; data.; writing—original draft preparation, Z.U.Z.; writing—review and editing, A.R. and A.M.O.; visualization, A.S.; supervision, B.S.; project administration, N.S.S.; funding acquisition, N.S.S., A.R. All authors have read and agreed to the published version of the manuscript.

Funding: This research was funded by YUTP and UTP-UIR, grant number 015LCO-211 and 015MEO-166 and The APC was funded by King Khalid University.

Acknowledgments: We would like to acknowledge the grants received from Universiti Teknologi PETRONAS under YUTP and UTP-UIR with cost centers 015LCO-211 and 015MEO-166 respectively. We also wish to acknowledge King Khalid University, Abha, Kingdom of Saudi Arabia.

Conflicts of Interest: The authors declare no conflict of interest.

References

1. Oh, J.Y.; Choi, S.D.; Kwon, H.O.; Lee, S.E. Leaching of polycyclic aromatic hydrocarbons (PAHs) from industrial wastewater sludge by ultrasonic treatment. *Ultrason. Sonochem.* **2016**, *33*, 61–66. [CrossRef] [PubMed]
2. Zhang, Y.; Zhang, L.; Huang, Z.; Li, Y.; Li, J.; Wu, N.; He, J.; Zhang, Z.; Liu, Y.; Niu, Z. Pollution of polycyclic aromatic hydrocarbons (PAHs) in drinking water of China: Composition, distribution and influencing factors. *Ecotoxicol. Environ. Saf.* **2019**, *177*, 108–116. [CrossRef] [PubMed]
3. Tian, W.; Bai, J.; Liu, K.; Sun, H.; Zhao, Y. Occurrence and removal of polycyclic aromatic hydrocarbons in the wastewater treatment process. *Ecotoxicol. Environ. Saf.* **2012**, *82*, 1–7. [CrossRef] [PubMed]
4. Crisafully, R.; Milhome, M.A.L.; Cavalcante, R.M.; Silveira, E.R.; De Keukeleire, D.; Nascimento, R.F. Removal of some polycyclic aromatic hydrocarbons from petrochemical wastewater using low-cost adsorbents of natural origin. *Bioresour. Technol.* **2008**, *99*, 4515–4519. [CrossRef]
5. Zhang, Y.; Tao, S. Global atmospheric emission inventory of polycyclic aromatic hydrocarbons (PAHs) for 2004. *Atmos. Environ.* **2009**, *43*, 812–819. [CrossRef]
6. Liu, Y.; Zarfl, C.; Basu, N.B.; Cirpka, O.A. Turnover and legacy of sediment-associated PAH in a baseflow-dominated river. *Sci. Total Environ.* **2019**, *671*, 754–764. [CrossRef]
7. Andrade, M.V.F.; Santos, F.R.; Oliveira, A.H.B.; Nascimento, R.F.; Cavalcante, R.M. Influence of sediment parameters on the distribution and fate of PAHs in an estuarine tropical region located in the Brazilian semi-arid (Jaguaribe River, Ceará coast). *Mar. Pollut. Bull.* **2019**, *146*, 703–710. [CrossRef]
8. Zhao, W.; Sui, Q.; Huang, X. Removal and fate of polycyclic aromatic hydrocarbons in a hybrid anaerobic–anoxic–oxic process for highly toxic coke wastewater treatment. *Sci. Total Environ.* **2018**, *635*, 716–724. [CrossRef]
9. Sun, S.; Jia, L.; Li, B.; Yuan, A.; Kong, L.; Qi, H.; Ma, W.; Zhang, A.; Wu, Y. The occurrence and fate of PAHs over multiple years in a wastewater treatment plant of Harbin, Northeast China. *Sci. Total Environ.* **2018**, *624*, 491–498. [CrossRef]
10. De Gisi, S.; Lofrano, G.; Grassi, M.; Notarnicola, M. Characteristics and adsorption capacities of low-cost sorbents for wastewater treatment: A review. *Sustain. Mater. Technol.* **2016**, *9*, 10–40. [CrossRef]
11. Qiao, M.; Qi, W.; Liu, H.; Qu, J. Oxygenated, nitrated, methyl and parent polycyclic aromatic hydrocarbons in rivers of Haihe River System, China: Occurrence, possible formation, and source and fate in a water-shortage area. *Sci. Total Environ.* **2014**, *481*, 178–185. [CrossRef] [PubMed]
12. Zango, Z.U.; Garba, Z.N.; Abu Bakar, N.H.H.; Tan, W.L.; Abu Bakar, M. Adsorption studies of Cu^{2+}–Hal nanocomposites for the removal of 2,4,6-trichlorophenol. *Appl. Clay Sci.* **2016**, *132–133*, 68–78. [CrossRef]
13. Lawal, I.A.; Lawal, M.M.; Azeez, M.A.; Ndungu, P. Theoretical and experimental adsorption studies of phenol and crystal violet dye on carbon nanotube functionalized with deep eutectic solvent. *J. Mol. Liq.* **2019**, *288*. [CrossRef]

14. Catherine, H.N.; Ou, M.H.; Manu, B.; Shih, Y. hsin Adsorption mechanism of emerging and conventional phenolic compounds on graphene oxide nanoflakes in water. *Sci. Total Environ.* **2018**, *635*, 629–638. [CrossRef] [PubMed]
15. Bazrafshan, E.; Mostafapour, F.K.; Mahvi, A.H. Phenol removal from aqueous solutions using pistachio-nut shell ash as a low cost adsorbent. *Fresenius Environ. Bull.* **2012**, *21*, 2962–2968.
16. Soni, U.; Bajpai, J.; Singh, S.K.; Bajpai, A.K. Evaluation of chitosan-carbon based biocomposite for efficient removal of phenols from aqueous solutions. *J. Water Process Eng.* **2017**, *16*, 56–63. [CrossRef]
17. Guo, M.; Wang, J.; Wang, C.; Strong, P.J.; Jiang, P.; Ok, Y.S.; Wang, H. Carbon nanotube-grafted chitosan and its adsorption capacity for phenol in aqueous solution. *Sci. Total Environ.* **2019**, *682*, 340–347. [CrossRef]
18. Zhang, Y.; Qin, L.; Cui, Y.; Liu, W.; Liu, X.; Yang, Y. A hydrophilic surface molecularly imprinted polymer on a spherical porous carbon support for selective phenol removal from coking wastewater. *New Carbon Mater.* **2020**, *35*, 220–231. [CrossRef]
19. Salari, M.; Dehghani, M.H.; Azari, A.; Motevalli, M.D.; Shabanloo, A.; Ali, I. High performance removal of phenol from aqueous solution by magnetic chitosan based on response surface methodology and genetic algorithm. *J. Mol. Liq.* **2019**, *285*, 146–157. [CrossRef]
20. Lee, C.G.; Hong, S.H.; Hong, S.G.; Choi, J.W.; Park, S.J. Production of Biochar from Food Waste and its Application for Phenol Removal from Aqueous Solution. *Water Air Soil Pollut.* **2019**, *230*. [CrossRef]
21. Wang, F.; Haftka, J.J.H.; Sinnige, T.L.; Hermens, J.L.M.; Chen, W. Adsorption of polar, nonpolar, and substituted aromatics to colloidal graphene oxide nanoparticles. *Environ. Pollut.* **2014**, *186*, 226–233. [CrossRef]
22. Zhou, L.C.; Meng, X.G.; Fu, J.W.; Yang, Y.C.; Yang, P.; Mi, C. Highly efficient adsorption of chlorophenols onto chemically modified chitosan. *Appl. Surf. Sci.* **2014**, *292*, 735–741. [CrossRef]
23. Blanchard, M.; Teil, M.J.; Ollivon, D.; Legenti, L.; Chevreuil, M. Polycyclic aromatic hydrocarbons and polychlorobiphenyls in wastewaters and sewage sludges from the Paris area (France). *Environ. Res.* **2004**, *95*, 184–197. [CrossRef] [PubMed]
24. Mojiri, A.; Zhou, J.L.; Ohashi, A.; Ozaki, N.; Kindaichi, T. Comprehensive review of polycyclic aromatic hydrocarbons in water sources, their effects and treatments. *Sci. Total Environ.* **2019**, *696*. [CrossRef] [PubMed]
25. Lamichhane, S.; Bal Krishna, K.C.; Sarukkalige, R. Polycyclic aromatic hydrocarbons (PAHs) removal by sorption: A review. *Chemosphere* **2016**, *148*, 336–353. [CrossRef] [PubMed]
26. Alegbeleye, O.O.; Opeolu, B.O.; Jackson, V.A. Polycyclic Aromatic Hydrocarbons: A Critical Review of Environmental Occurrence and Bioremediation. *Environ. Manag.* **2017**, *60*, 758–783. [CrossRef]
27. Ndunda, E.N.; Mizaikoff, B. Molecularly imprinted polymers for the analysis and removal of polychlorinated aromatic compounds in the environment: A review. *Analyst* **2016**, *141*, 3141–3156. [CrossRef]
28. Kumar, V.; Kim, K.H.; Park, J.W.; Hong, J.; Kumar, S. Graphene and its nanocomposites as a platform for environmental applications. *Chem. Eng. J.* **2017**, *315*, 210–232. [CrossRef]
29. de Souza, C.V.; Corrêa, S.M. Polycyclic aromatic hydrocarbons in diesel emission, diesel fuel and lubricant oil. *Fuel* **2016**, *185*, 925–931. [CrossRef]
30. Akinpelu, A.A.; Ali, M.E.; Johan, M.R.; Saidur, R.; Qurban, M.A.; Saleh, T.A. Polycyclic aromatic hydrocarbons extraction and removal from wastewater by carbon nanotubes: A review of the current technologies, challenges and prospects. *Process Saf. Environ. Prot.* **2019**, *122*, 68–82. [CrossRef]
31. Redondo, J.M.; Platonov, A.K. Self-similar distribution of oil spills in European coastal waters. *Environ. Res. Lett.* **2009**, *4*. [CrossRef]
32. Lai, X.; Ning, X.-A.; He, Y.; Yuan, Y.; Sun, J.; Ke, Y.; Man, X. Treatment of a simulated sludge by ultrasonic zero-valent iron/EDTA/Air process: Interferences of inorganic salts in polyaromatic hydrocarbon removal. *Waste Manag.* **2019**, *85*, 548–556. [CrossRef] [PubMed]
33. Lu, Y.; Zheng, G.; Zhou, W.; Wang, J.; Zhou, L. Bioleaching conditioning increased the bioavailability of polycyclic aromatic hydrocarbons to promote their removal during co-composting of industrial and municipal sewage sludges. *Sci. Total Environ.* **2019**, *665*, 1073–1082. [CrossRef]
34. Ihsanullah; Asmaly, H.A.; Saleh, T.A.; Laoui, T.; Gupta, V.K.; Atieh, M.A. Enhanced adsorption of phenols from liquids by aluminum oxide/carbon nanotubes: Comprehensive study from synthesis to surface properties. *J. Mol. Liq.* **2015**, *206*, 176–182. [CrossRef]
35. Marañón, E.; Vázquez, I.; Rodríguez, J.; Castrillón, L.; Fernández, Y.; López, H. Treatment of coke wastewater in a sequential batch reactor (SBR) at pilot plant scale. *Bioresour. Technol.* **2008**, *99*, 4192–4198. [CrossRef]

36. Bargieł, P.; Zabochnicka-Świątek, M. Technologies of Coke Wastewater Treatment in the Frame of Legislation in Force. *Ochr. Sr. Zasobow Nat.* **2018**, *29*, 11–15. [CrossRef]
37. Pal, P.; Kumar, R. Treatment of coke wastewater: A critical review for developing sustainable management strategies. *Sep. Purif. Rev.* **2014**, *43*, 89–123. [CrossRef]
38. Ning, X.A.; Lin, M.Q.; Shen, L.Z.; Zhang, J.H.; Wang, J.Y.; Wang, Y.J.; Yang, Z.Y.; Liu, J.Y. Levels, composition profiles and risk assessment of polycyclic aromatic hydrocarbons (PAHs) in sludge from ten textile dyeing plants. *Environ. Res.* **2014**, *132*, 112–118. [CrossRef]
39. Anku, W.W.; Mamo, M.A.; Govender, P.P. Phenolic Compounds in Water: Sources, Reactivity, Toxicity and Treatment Methods. *Intech Open* **2016**, 419–443. [CrossRef]
40. Agarwal, T.; Khillare, P.S.; Shridhar, V. PAHs contamination in Bank sediment of the Yamuna River, Delhi, India. *Environ. Monit. Assess.* **2006**, *123*, 151–166. [CrossRef]
41. Iwegbue, C.M.A.; Tesi, G.O.; Overah, L.C.; Emoyan, O.O.; Nwajei, G.E.; Martincigh, B.S. Effects of Flooding on the Sources, Spatiotemporal Characteristics and Human Health Risks of Polycyclic Aromatic Hydrocarbons in Floodplain Soils of the Lower Parts of the River Niger, Nigeria. *Polycycl. Aromat. Compd.* **2017**, *6638*, 1–17. [CrossRef]
42. Ciesielczuk, T.; Kusza, G.; Poluszyńska, J.; Kochanowska, K. Pollution of flooded arable soils with heavy metals and polycyclic aromatic hydrocarbons (PAHs). *Water Air Soil Pollut.* **2014**, *225*. [CrossRef] [PubMed]
43. Liu, J.J.; Wang, X.C.; Fan, B. Characteristics of PAHs adsorption on inorganic particles and activated sludge in domestic wastewater treatment. *Bioresour. Technol.* **2011**, *102*, 5305–5311. [CrossRef] [PubMed]
44. Jin, J.; Wang, S.; Hu, J.; Wu, J.; Li, M.; Wang, Y.; Jin, J. Polychlorinated naphthalenes in human serum samples from an industrial city in Eastern China: Levels, sources, and sex differences. *Ecotoxicol. Environ. Saf.* **2019**, *177*, 86–92. [CrossRef]
45. Liang, X.; Junaid, M.; Wang, Z.; Li, T.; Xu, N. Spatiotemporal distribution, source apportionment and ecological risk assessment of PBDEs and PAHs in the Guanlan River from rapidly urbanizing areas of Shenzhen, China. *Environ. Pollut.* **2019**, *250*, 695–707. [CrossRef] [PubMed]
46. McDonough, C.A.; Khairy, M.A.; Muir, D.C.G.; Lohmann, R. Significance of population centers as sources of gaseous and dissolved PAHs in the lower Great Lakes. *Environ. Sci. Technol.* **2014**, *48*, 7789–7797. [CrossRef] [PubMed]
47. Zhang, W.; Wei, C.; Chai, X.; He, J.; Cai, Y.; Ren, M.; Yan, B.; Peng, P.; Fu, J. The behaviors and fate of polycyclic aromatic hydrocarbons (PAHs) in a coking wastewater treatment plant. *Chemosphere* **2012**, *88*, 174–182. [CrossRef]
48. Li, J.; Dong, H.; Xu, X.; Han, B.; Li, X.; Zhu, C.; Han, C.; Liu, S.; Yang, D.; Xu, Q.; et al. Prediction of the bioaccumulation of PAHs in surface sediments of Bohai Sea, China and quantitative assessment of the related toxicity and health risk to humans. *Mar. Pollut. Bull.* **2016**, *104*, 92–100. [CrossRef]
49. de Jesus, J.H.F.; Cunha, G.d.C.; Cardoso, E.M.C.; Mangrich, A.S.; Romão, L.P.C. Evaluation of waste biomasses and their biochars for removal of polycyclic aromatic hydrocarbons. *J. Environ. Manag.* **2017**, *200*, 186–195. [CrossRef]
50. Qu, Y.; Qin, L.; Liu, X.; Yang, Y. Reasonable design and sifting of microporous carbon nanosphere-based surface molecularly imprinted polymer for selective removal of phenol from wastewater. *Chemosphere* **2020**, *251*. [CrossRef]
51. Wu, Z.; Yuan, X.; Zhong, H.; Wang, H.; Zeng, G.; Chen, X.; Wang, H.; Zhang, L.; Shao, J. Enhanced adsorptive removal of p-nitrophenol from water by aluminum metal-organic framework/reduced graphene oxide composite. *Sci. Rep.* **2016**, *6*, 25638. [CrossRef] [PubMed]
52. Kong, Q.; Wu, H.; Liu, L.; Zhang, F.; Preis, S.; Zhu, S.; Wei, C. Solubilization of polycyclic aromatic hydrocarbons (PAHs) with phenol in coking wastewater treatment system: Interaction and engineering significance. *Sci. Total Environ.* **2018**, *628–629*, 467–473. [CrossRef]
53. Villegas, L.G.C.; Mashhadi, N.; Chen, M.; Mukherjee, D.; Taylor, K.E.; Biswas, N. A Short Review of Techniques for Phenol Removal from Wastewater. *Curr. Pollut. Rep.* **2016**, *2*, 157–167. [CrossRef]
54. Bin-Dahman, O.A.; Saleh, T.A. Synthesis of carbon nanotubes grafted with PEG and its efficiency for the removal of phenol from industrial wastewater. *Environ. Nanotechnol. Monit. Manag.* **2020**, *13*. [CrossRef]
55. Saleh, T.A.; Elsharif, A.M.; Asiri, S.; Mohammed, A.R.I.; Dafalla, H. Synthesis of carbon nanotubes grafted with copolymer of acrylic acid and acrylamide for phenol removal. *Environ. Nanotechnol. Monit. Manag.* **2020**, *14*. [CrossRef]

56. Godlewska, P.; Siatecka, A.; Kończak, M.; Oleszczuk, P. Adsorption capacity of phenanthrene and pyrene to engineered carbon-based adsorbents produced from sewage sludge or sewage sludge-biomass mixture in various gaseous conditions. *Bioresour. Technol.* **2019**, *280*, 421–429. [CrossRef] [PubMed]
57. Giwa, A.; Daer, S.; Ahmed, I.; Marpu, P.R.; Hasan, S.W. Experimental investigation and artificial neural networks ANNs modeling of electrically-enhanced membrane bioreactor for wastewater treatment. *J. Water Process Eng.* **2016**, *11*, 88–97. [CrossRef]
58. Lin, M.; Ning, X.-a.; An, T.; Zhang, J.; Chen, C.; Ke, Y.; Wang, Y.; Zhang, Y.; Sun, J.; Liu, J. Degradation of polycyclic aromatic hydrocarbons (PAHs) in textile dyeing sludge with ultrasound and Fenton processes: Effect of system parameters and synergistic effect study. *J. Hazard. Mater.* **2016**, *307*, 7–16. [CrossRef]
59. Bai, H.; Zhou, J.; Zhang, H.; Tang, G. Enhanced adsorbability and photocatalytic activity of TiO_2-graphene composite for polycyclic aromatic hydrocarbons removal in aqueous phase. *Colloids Surf. B Biointerfaces* **2017**, *150*, 68–77. [CrossRef]
60. Huang, D.; Xu, B.; Wu, J.; Brookes, P.C.; Xu, J. Adsorption and desorption of phenanthrene by magnetic graphene nanomaterials from water: Roles of pH, heavy metal ions and natural organic matter. *Chem. Eng. J.* **2019**, *368*, 390–399. [CrossRef]
61. Hwang, H.; Sahin, O.; Choi, J.W. Manufacturing a super-active carbon using fast pyrolysis char from biomass and correlation study on structural features and phenol adsorption. *RSC Adv.* **2017**, *7*, 42192–42202. [CrossRef]
62. Xu, J.; Wang, L.; Zhu, Y. Decontamination of bisphenol A from aqueous solution by graphene adsorption. *Langmuir* **2012**, *28*, 8418–8425. [CrossRef] [PubMed]
63. Wang, J.; Chen, Z.; Chen, B. Adsorption of polycyclic aromatic hydrocarbons by graphene and graphene oxide nanosheets. *Environ. Sci. Technol.* **2014**, *48*, 4817–4825. [CrossRef] [PubMed]
64. Yang, X.; Li, J.; Wen, T.; Ren, X.; Huang, Y.; Wang, X. Adsorption of naphthalene and its derivatives on magnetic graphene composites and the mechanism investigation. *Colloids Surf. A Physicochem. Eng. Asp.* **2013**, *422*, 118–125. [CrossRef]
65. Mohammad, A.T.; Al-Obaidi, M.A.; Hameed, E.M.; Basheer, B.N.; Mujtaba, I.M. Modelling the chlorophenol removal from wastewater via reverse osmosis process using a multilayer artificial neural network with genetic algorithm. *J. Water Process Eng.* **2020**, *33*. [CrossRef]
66. Yakout, S.M.; Daifullah, A.A.M.; El-Refeey, S.A. Adsorption of Naphthalene, Phenanthrene and Pyrene from Aqueous Solution Using Low-Cost Activated Carbon Derived from Agricultural. *Adsorpt. Sci. Technol.* **2013**, *31*, 293–302. [CrossRef]
67. Gundogdu, A.; Duran, C.; Senturk, H.B.; Soylak, M.; Ozdes, D.; Serencam, H.; Imamoglu, M. Adsorption of phenol from aqueous solution on a low-cost activated carbon produced from tea industry waste: Equilibrium, kinetic, and thermodynamic study. *J. Chem. Eng. Data* **2012**, *57*, 2733–2743. [CrossRef]
68. Rasheed, A.; Farooq, F.; Rafique, U.; Nasreen, S.; Aqeel Ashraf, M. Analysis of sorption efficiency of activated carbon for removal of anthracene and pyrene for wastewater treatment. *Desalin. Water Treat.* **2016**, *57*, 145–150. [CrossRef]
69. Feng, Z.; Zhu, L. Sorption of phenanthrene to biochar modified by base. *Front. Environ. Sci. Eng.* **2018**, *12*, 1–11. [CrossRef]
70. Tong, Y.; McNamara, P.J.; Mayer, B.K. Adsorption of organic micropollutants onto biochar: A review of relevant kinetics, mechanisms and equilibrium. *Environ. Sci. Water Res. Technol.* **2019**, *5*, 821–838. [CrossRef]
71. Xu, L.; Wang, Z.; Ye, S.; Sui, X. Removal of p-chlorophenol from aqueous solutions by carbon nanotube hybrid polymer adsorbents. *Chem. Eng. Res. Des.* **2017**, *123*, 76–83. [CrossRef]
72. Zhang, J.; Li, R.; Ding, G.; Wang, Y.; Wang, C. Sorptive removal of phenanthrene from water by magnetic carbon nanomaterials. *J. Mol. Liq.* **2019**, *293*. [CrossRef]
73. Zielińska, A.; Oleszczuk, P. The conversion of sewage sludge into biochar reduces polycyclic aromatic hydrocarbon content and ecotoxicity but increases trace metal content. *Biomass Bioenergy* **2015**, *75*, 235–244. [CrossRef]
74. Smith, K.M.; Fowler, G.D.; Pullket, S.; Graham, N.J.D. Sewage sludge-based adsorbents: A review of their production, properties and use in water treatment applications. *Water Res.* **2009**, *43*, 2569–2594. [CrossRef]

75. Azargohar, R.; Jacobson, K.L.; Powell, E.E.; Dalai, A.K. Evaluation of properties of fast pyrolysis products obtained, from Canadian waste biomass. *J. Anal. Appl. Pyrolysis* **2013**, *104*, 330–340. [CrossRef]
76. Qiu, M.; Sun, K.; Jin, J.; Gao, B.; Yan, Y.; Han, L.; Wu, F.; Xing, B. Properties of the plant- and manure-derived biochars and their sorption of dibutyl phthalate and phenanthrene. *Sci. Rep.* **2014**, *4*, 5295. [CrossRef]
77. Askeland, M.; Clarke, B.; Paz-Ferreiro, J. Comparative characterization of biochars produced at three selected pyrolysis temperatures from common woody and herbaceous waste streams. *PeerJ* **2019**, *7*, e6784. [CrossRef]
78. Guo, W.; Wang, S.; Wang, Y.; Lu, S.; Gao, Y. Sorptive removal of phenanthrene from aqueous solutions using magnetic and non-magnetic rice husk-derived biochars. *R. Soc. Open Sci.* **2018**, *5*, 1–11. [CrossRef] [PubMed]
79. Li, H.; Qu, R.; Li, C.; Guo, W.; Han, X.; He, F.; Ma, Y.; Xing, B. Selective removal of polycyclic aromatic hydrocarbons (PAHs) from soil washing effluents using biochars produced at different pyrolytic temperatures. *Bioresour. Technol.* **2014**, *163*, 193–198. [CrossRef]
80. Md Arshad, S.H.; Ngadi, N.; Wong, S.; Saidina Amin, N.; Razmi, F.A.; Mohamed, N.B.; Inuwa, I.M.; Abdul Aziz, A. Optimization of phenol adsorption onto biochar from oil palm empty fruit bunch (EFB). *Malays. J. Fundam. Appl. Sci.* **2019**, *15*, 1–5. [CrossRef]
81. Bedia, J.; Peñas-Garzón, M.; Gómez-Avilés, A.; Rodriguez, J.; Belver, C. A Review on the Synthesis and Characterization of Biomass-Derived Carbons for Adsorption of Emerging Contaminants from Water. *J. Carbon Res.* **2018**, *4*, 63. [CrossRef]
82. Qiao, K.; Tian, W.; Bai, J.; Dong, J.; Zhao, J.; Gong, X.; Liu, S. Preparation of biochar from Enteromorpha prolifera and its use for the removal of polycyclic aromatic hydrocarbons (PAHs) from aqueous solution. *Ecotoxicol. Environ. Saf.* **2018**, *149*, 80–87. [CrossRef]
83. Tang, J.; Lv, H.; Gong, Y.; Huang, Y. Preparation and characterization of a novel graphene/biochar composite for aqueous phenanthrene and mercury removal. *Bioresour. Technol.* **2015**, *196*, 355–363. [CrossRef] [PubMed]
84. de Jesus, J.H.F.; Matos, T.T.d.S.; Cunha, G.d.C.; Mangrich, A.S.; Romão, L.P.C. Adsorption of aromatic compounds by biochar: Influence of the type of tropical biomass precursor. *Cellulose* **2019**. [CrossRef]
85. Liu, X.; Sun, J.; Duan, S.; Wang, Y.; Hayat, T.; Alsaedi, A.; Wang, C.; Li, J. A Valuable Biochar from Poplar Catkins with High Adsorption Capacity for Both Organic Pollutants and Inorganic Heavy Metal Ions. *Sci. Rep.* **2017**, *7*, 10033. [CrossRef]
86. Shin, W. seok Adsorption characteristics of phenol and heavy metals on biochar from Hizikia fusiformis. *Environ. Earth Sci.* **2017**, *76*, 782. [CrossRef]
87. Braghiroli, F.L.; Bouafif, H.; Hamza, N.; Neculita, C.M.; Koubaa, A. Production, characterization, and potential of activated biochar as adsorbent for phenolic compounds from leachates in a lumber industry site. *Environ. Sci. Pollut. Res.* **2018**, *25*, 26562–26575. [CrossRef]
88. Zhang, Y.; Tang, Z.; Liu, S.; Xu, H.; Song, Z. Study on adsorption of phenol from aqueous media using biochar of Chinese herb residue. *IOP Conf. Ser. Mater. Sci. Eng.* **2018**, *394*. [CrossRef]
89. Siipola, V.; Pflugmacher, S.; Romar, H.; Wendling, L.; Koukkari, P. Low-Cost Biochar Adsorbents for Water Purification Including Microplastics Removal. *Appl. Sci.* **2020**, *10*, 788. [CrossRef]
90. Jin, D.F.; Xu, Y.Y.; Zhang, M.; Jung, Y.S.; Ok, Y.S. Comparative evaluation for the sorption capacity of four carbonaceous sorbents to phenol. *Chem. Speciat. Bioavailab.* **2016**, *28*, 18–25. [CrossRef]
91. Mohammed, N.A.S.; Abu-Zurayk, R.A.; Hamadneh, I.; Al-Dujaili, A.H. Phenol adsorption on biochar prepared from the pine fruit shells: Equilibrium, kinetic and thermodynamics studies. *J. Environ. Manag.* **2018**, *226*, 377–385. [CrossRef] [PubMed]
92. Danish, M.; Ahmad, T. A review on utilization of wood biomass as a sustainable precursor for activated carbon production and application. *Renew. Sustain. Energy Rev.* **2018**, *87*, 1–21. [CrossRef]
93. Alade, A.O.; Amuda, O.S.; Ibrahim, A.O. Isothermal studies of adsorption of acenaphthene from aqueous solution onto activated carbon produced from rice (Oryza sativa) husk. *Elixir Chem. Eng.* **2012**, *46*, 87–95. [CrossRef]
94. Alade, A.O.; Amuda, O.S.; Afolabi, T.J.; Okoya, A.A. Adsorption of naphthalene onto activated carbons derived from milk bush kernel shell and flamboyant pod. *J. Environ. Chem. Ecotoxicol.* **2012**, *4*, 124–132. [CrossRef]
95. Jin, X.J.; Zhu, Y.M. Absorption of Phenol on Nitrogen-Enriched Activated Carbon from Wood Fiberboard Waste with Chemical Activation by Potassium Carbonate. *J. Chem. Eng. Process Technol.* **2014**, *5*, 4. [CrossRef]
96. Ingole, R.S.; Lataye, D.H. Adsorptive removal of phenol from aqueous solution using activated carbon prepared from Babul sawdust. *J. Hazard. Toxicol. Radioact. Waste* **2015**, *19*, 1–9. [CrossRef]

97. Dąbrowski, A.; Podkościelny, P.; Hubicki, Z.; Barczak, M. Adsorption of phenolic compounds by activated carbon—A critical review. *Chemosphere* **2005**, *58*, 1049–1070. [CrossRef]
98. Xiao, X.; Liu, D.; Yan, Y.; Wu, Z.; Wu, Z.; Cravotto, G. Preparation of activated carbon from Xinjiang region coal by microwave activation and its application in naphthalene, phenanthrene, and pyrene adsorption. *J. Taiwan Inst. Chem. Eng.* **2015**, *53*, 160–167. [CrossRef]
99. Eeshwarasinghe, D.; Loganathan, P.; Vigneswaran, S. Simultaneous removal of polycyclic aromatic hydrocarbons and heavy metals from water using granular activated carbon. *Chemosphere* **2019**, *223*, 616–627. [CrossRef]
100. Rakowska, M.I.; Kupryianchyk, D.; Grotenhuis, T.; Rijnaarts, H.H.M.; Koelmans, A.A. Extraction of sediment-associated polycyclic aromatic hydrocarbons with granular activated carbon. *Environ. Toxicol. Chem.* **2013**, *32*, 304–311. [CrossRef]
101. Ge, X.; Wu, Z.; Wu, Z.; Yan, Y.; Cravotto, G.; Ye, B.C. Enhanced PAHs adsorption using iron-modified coal-based activated carbon via microwave radiation. *J. Taiwan Inst. Chem. Eng.* **2016**, *64*, 235–243. [CrossRef]
102. Ge, X.; Tian, F.; Wu, Z.; Yan, Y.; Cravotto, G.; Wu, Z. Adsorption of naphthalene from aqueous solution on coal-based activated carbon modified by microwave induction: Microwave power effects. *Chem. Eng. Process.* **2015**, *91*, 67–77. [CrossRef]
103. Wu, Z.; Sun, Z.; Liu, P.; Li, Q.; Yang, R.; Yang, X. Competitive adsorption of naphthalene and phenanthrene on walnut shell based activated carbon and the verification via theoretical. *RSC Adv.* **2020**, *10*, 10703–10714. [CrossRef]
104. Liu, J.; Chen, J.; Jiang, L.; Yin, X. Adsorption of mixed polycyclic aromatic hydrocarbons in surfactant solutions by activated carbon. *J. Ind. Eng. Chem.* **2014**, *20*, 616–623. [CrossRef]
105. Alade, A.O.; Amuda, O.S.; Afolabi, A.O.; Adelowo, F.E. Adosrption of Acenaphthene unto Ativated Crabon Produced from Agricultural Wastes. *J. Envion. Sci. Technol.* **2012**, *5*, 192–209.
106. Yakout, S.M.; Daifullah, A.A.M.; El-Reefy, S.A. Equilibrium and kinetic studies of sorption of polycyclic aromatic hydrocarbons from water using rice husk activated carbon. *Asian J. Chem.* **2013**, *25*, 10037–10042. [CrossRef]
107. Rinawati; Hidayat, D.; Supriyanto, R.; Permana, D.F. Yunita Adsorption of Polycyclic Aromatic Hydrocarbons using Low-Cost Activated Carbon Derived from Rice Husk. *J. Phys. Conf. Ser.* **2019**, *1338*. [CrossRef]
108. Awe, A.A.; Opeolu, B.O.; Fatoki, O.S.; Ayanda, O.S.; Jackson, V.A.; Snyman, R. Preparation and characterisation of activated carbon from Vitis vinifera leaf litter and its adsorption performance for aqueous phenanthrene. *Appl. Biol. Chem.* **2020**, *63*, 12. [CrossRef]
109. Khare, P.; Kumar, A. Removal of phenol from aqueous solution using carbonized Terminalia chebula-activated carbon: Process parametric optimization using conventional method and Taguchi's experimental design, adsorption kinetic, equilibrium and thermodynamic study. *Appl. Water Sci.* **2012**, *2*, 317–326. [CrossRef]
110. Lin, J.Q.; Yang, S.E.; Duan, J.M.; Wu, J.J.; Jin, L.Y.; Lin, J.M.; Deng, Q.L. The Adsorption Mechanism of Modified Activated Carbon on Phenol. *MATEC Web Conf.* **2016**, *67*. [CrossRef]
111. Biglari, H.; Afsharnia, M.; Javan, N.; Sajadi, S.A. Phenol Removal from Aqueous Solutions by Adsorption on Activated Carbon of Miswak's Root Treated with KMnO4. *Iran. J. Health Sci.* **2016**, *42*, 20–30. [CrossRef]
112. Xie, B.; Qin, J.; Wang, S.; Li, X.; Sun, H.; Chen, W. Adsorption of Phenol on Commercial Activated Carbons: Modelling and Interpretation. *Int. J. Environ. Res. Public Health* **2020**, *17*, 789. [CrossRef]
113. Beker, U.; Ganbold, B.; Dertli, H.; Gülbayir, D.D. Adsorption of phenol by activated carbon: Influence of activation methods and solution pH. *Energy Convers. Manag.* **2010**, *51*, 235–240. [CrossRef]
114. Germain, T.; Lynda, E.; Tchirioua, E. Adsorption of Phenol on Carbon Based on Cactus and Banana Peel. *Aust. J. Basic Appl. Sci.* **2019**, *13*, 64–70. [CrossRef]
115. Mojoudi, N.; Mirghaffari, N.; Soleimani, M.; Shariatmadari, H.; Belver, C.; Bedia, J. Phenol adsorption on high microporous activated carbons prepared from oily sludge: Equilibrium, kinetic and thermodynamic studies. *Sci. Rep.* **2019**, *9*, 19352. [CrossRef]
116. Nouha, S.; Souad, N.S.; Abdelmottalab, O. Enhanced adsorption of phenol using alkaline modified activated carbon prepared from olive stones. *J. Chil. Chem. Soc.* **2019**, *64*, 4352–4359. [CrossRef]
117. Siti Hadjar, M.A.; Astimar, A.A.; Norzita, N.; Noraishah, S.A. Phenol adsorption by activated carbon of different fibre size derived from empty fruit bunches. *J. Oil Palm Res.* **2012**, *24*, 1524–1532.
118. Dejene, K.; Siraj, K.; Kitte, S.A. Kinetic and Thermodynamic Study of Phenol Removal from Water Using Activated Carbon Synthesizes from Avocado Kernel Seed. *Int. Lett. Nat. Sci.* **2016**, *54*, 42–57. [CrossRef]

119. Banat, F.; Al-Asheh, S.; Al-Makhadmeh, L. Utilization of raw and activated date pits for the removal of phenol from aqueous solutions. *Chem. Eng. Technol.* **2004**, *27*, 80–86. [CrossRef]
120. Mohtashami, S.A.; Asasian Kolur, N.; Kaghazchi, T.; Asadi-Kesheh, R.; Soleimani, M. Optimization of sugarcane bagasse activation to achieve adsorbent with high affinity towards phenol. *Turk. J. Chem.* **2018**, *42*, 1720–1735. [CrossRef]
121. Girish, C.R.; Murty, V.R. Adsorption of Phenol from Aqueous Solution Using Lantana camara, Forest Waste: Packed Bed Studies and Prediction of Breakthrough Curves. *Environ. Process.* **2014**, *2*, 773–796. [CrossRef]
122. Mohammadi, S.Z.; Darijani, Z.; Karimi, M.A. Fast and efficient removal of phenol by magnetic activated carbon-cobalt nanoparticles. *J. Alloys Compd.* **2020**, *832*. [CrossRef]
123. Gholizadeh, A.; Kermani, M.; Gholami, M.; Farzadkia, M. Kinetic and isotherm studies of adsorption and biosorption processes in the removal of phenolic compounds from aqueous solutions: Comparative study. *J. Environ. Health Sci. Eng.* **2013**, *11*, 29. [CrossRef] [PubMed]
124. Ioannou, Z.; Simitzis, J. Adsorption kinetics of phenol and 3-nitrophenol from aqueous solutions on conventional and novel carbons. *J. Hazard. Mater.* **2009**, *171*, 954–964. [CrossRef] [PubMed]
125. Yadav, N.; Narayan Maddheshiaya, D.; Rawat, S.; Singh, J. Adsorption and equilibrium studies of phenol and para-nitrophenol by magnetic activated carbon synthesised from cauliflower waste. *Environ. Eng. Res.* **2019**, *25*, 742–752. [CrossRef]
126. Atieh, M.A. Removal of Phenol from Water Different Types of Carbon—A Comparative Analysis. *APCBEE Procedia* **2014**, *10*, 136–141. [CrossRef]
127. Dehghani, M.H.; Mostofi, M.; Alimohammadi, M.; McKay, G.; Yetilmezsoy, K.; Albadarin, A.B.; Heibati, B.; AlGhouti, M.; Mubarak, N.M.; Sahu, J.N. High-performance removal of toxic phenol by single-walled and multi-walled carbon nanotubes: Kinetics, adsorption, mechanism and optimization studies. *J. Ind. Eng. Chem.* **2016**, *35*, 63–74. [CrossRef]
128. Rezakazemi, M.; Kurniawan, T.A.; Albadarin, A.B.; Shirazian, S. Molecular modeling investigation on mechanism of phenol removal from aqueous media by single- and multi-walled carbon nanotubes. *J. Mol. Liq.* **2018**, *271*, 24–30. [CrossRef]
129. Wang, L.C.; Ni, X.J.; Cao, Y.H.; Cao, G.Q. Adsorption behavior of bisphenol A on CTAB-modified graphite. *Appl. Surf. Sci.* **2018**, *428*, 165–170. [CrossRef]
130. Chowdhury, S.; Balasubramanian, R. Recent advances in the use of graphene-family nanoadsorbents for removal of toxic pollutants from wastewater. *Adv. Colloid Interface Sci.* **2014**, *204*, 35–56. [CrossRef]
131. Li, B.; Ou, P.; Wei, Y.; Zhang, X.; Song, J. Polycyclic aromatic hydrocarbons adsorption onto graphene: A DFT and AIMD study. *Materials* **2018**, *11*, 726. [CrossRef] [PubMed]
132. Fraga, T.J.M.; Carvalho, M.N.; Ghislandi, M.G.; Da Motta Sobrinho, M.A. Functionalized graphene-based materials as innovative adsorbents of organic pollutants: A concise overview. *Braz. J. Chem. Eng.* **2019**, *36*, 1–31. [CrossRef]
133. Ali, I.; Basheer, A.A.; Mbianda, X.Y.; Burakov, A.; Galunin, E.; Burakova, I.; Mkrtchyan, E.; Tkachev, A.; Grachev, V. Graphene based adsorbents for remediation of noxious pollutants from wastewater. *Environ. Int.* **2019**, *127*, 160–180. [CrossRef]
134. Bano, Z.; Mazari, S.A.; Saeed, R.M.Y.; Majeed, M.A.; Xia, M.; Memon, A.Q.; Abro, R.; Wang, F. Water decontamination by 3D graphene based materials: A review. *J. Water Process Eng.* **2020**, *36*, 101404. [CrossRef]
135. Sun, Y.; Yang, S.; Zhao, G.; Wang, Q.; Wang, X. Adsorption of polycyclic aromatic hydrocarbons on graphene oxides and reduced graphene oxides. *Chemistry* **2013**, *8*, 2755–2761. [CrossRef]
136. Adeola, A.O.; Forbes, P.B.C. Optimization of the sorption of selected polycyclic aromatic hydrocarbons by regenerable graphene wool. *Water Sci. Technol.* **2020**, *80*, 1931–1943. [CrossRef]
137. Zhou, Q.; Wang, Y.; Xiao, J.; Fan, H. Fabrication and characterisation of magnetic graphene oxide incorporated Fe_3O_4@polyaniline for the removal of bisphenol A, t-octyl-phenol, and α-naphthol from water. *Sci. Rep.* **2017**, *7*, 11316. [CrossRef]
138. Wang, X.; Hu, Y.; Min, J.; Li, S.; Deng, X.; Yuan, S.; Zuo, X. Adsorption characteristics of phenolic compounds on graphene oxide and reduced graphene oxide: A batch experiment combined theory calculation. *Appl. Sci.* **2018**, *8*, 1950. [CrossRef]

139. Tian, J.; Wei, J.; Zhang, H.; Kong, Z.; Zhu, Y.; Qin, Z. Graphene oxide-functionalized dual-scale channels architecture for high-throughput removal of organic pollutants from water. *Chem. Eng. J.* **2019**, *359*, 852–862. [CrossRef]
140. Apul, O.G.; Wang, Q.; Zhou, Y.; Karanfil, T. Adsorption of aromatic organic contaminants by graphene nanosheets: Comparison with carbon nanotubes and activated carbon. *Water Res.* **2013**, *47*, 1648–1654. [CrossRef]
141. Das, P.; Goswami, S.; Maiti, S. Removal of naphthalene present in synthetic waste water using novel Graphene /Graphene Oxide nano sheet synthesized from rice straw: Comparative analysis, isotherm and kinetics. *Front. Nanosci. Nanotechnol.* **2016**, *2*, 38–42. [CrossRef]
142. Zhao, G.; Jiang, L.; He, Y.; Li, J.; Dong, H.; Wang, X.; Hu, W. Sulfonated graphene for persistent aromatic pollutant management. *Adv. Mater.* **2011**, *23*, 3959–3963. [CrossRef]
143. Mortazavi, M.; Baghdadi, M.; Seyed Javadi, N.H.; Torabian, A. The black beads produced by simultaneous thermal reducing and chemical bonding of graphene oxide on the surface of amino-functionalized sand particles: Application for PAHs removal from contaminated waters. *J. Water Process Eng.* **2019**, *31*, 100798. [CrossRef]
144. Wang, J.; Chen, B. Adsorption and coadsorption of organic pollutants and a heavy metal by graphene oxide and reduced graphene materials. *Chem. Eng. J.* **2015**, *281*, 379–388. [CrossRef]
145. Mehrizad, A.; Gharbani, P. Decontamination of 4-chloro-2-nitrophenol from aqueous solution by graphene adsorption: Equilibrium, kinetic, and thermodynamic studies. *Pol. J. Environ. Stud.* **2014**, *23*, 2111–2116. [CrossRef]
146. De La Luz-Asunción, M.; Sánchez-Mendieta, V.; Martínez-Hernández, A.L.; Castaño, V.M.; Velasco-Santos, C. Adsorption of phenol from aqueous solutions by carbon nanomaterials of one and two dimensions: Kinetic and equilibrium studies. *J. Nanomater.* **2015**, *2015*, 405036. [CrossRef]
147. Gholami-Bonabi, L.; Ziaefar, N.; Sheikhloie, H. Removal of phenol from aqueous solutions by magnetic oxide graphene nanoparticles modified with ionic liquids using the Taguchi optimization approach. *Water Sci. Technol.* **2020**, *81*, 228–240. [CrossRef]
148. Li, Y.; Du, Q.; Liu, T.; Sun, J.; Jiao, Y.; Xia, Y.; Xia, L.; Wang, Z.; Zhang, W.; Wang, K.; et al. Equilibrium, kinetic and thermodynamic studies on the adsorption of phenol onto graphene. *Mater. Res. Bull.* **2012**, *47*, 1898–1904. [CrossRef]
149. Wang, J.; Gao, X.; Wang, Y.; Gao, C. Novel Graphene Oxide Sponge synthesized by Freeze-Drying Process for the Removal of 2,4,6-Trichlorophenol. *RSC Adv.* **2014**, *4*, 57476–57482. [CrossRef]
150. Phatthanakittiphong, T.; Seo, G.T. Characteristic evaluation of graphene oxide for bisphenol a adsorption in aqueous solution. *Nanomaterials* **2016**, *6*, 128. [CrossRef]
151. Zhang, Y.; Tang, Y.; Li, S.; Yu, S. Sorption and removal of tetrabromobisphenol A from solution by graphene oxide. *Chem. Eng. J.* **2013**, *222*, 94–100. [CrossRef]
152. Soltani, T.; Lee, B.K. Mechanism of highly efficient adsorption of 2-chlorophenol onto ultrasonic graphene materials: Comparison and equilibrium. *J. Colloid Interface Sci.* **2016**, *481*, 168–180. [CrossRef] [PubMed]
153. Zhou, L.; Zhang, X.; Chen, Y. Modulated synthesis of zirconium metal—Organic framework UiO-66 with enhanced dichloromethane adsorption capacity. *Mater. Lett.* **2017**, *197*, 167–170. [CrossRef]
154. Ong, Y.T.; Ahmad, A.L.; Zein, S.H.S.; Tan, S.H. A review on carbon nanotubes in an environmental protection and green engineering perspective. *Braz. J. Chem. Eng.* **2010**, *27*, 227–242. [CrossRef]
155. Sarkar, B.; Mandal, S.; Tsang, Y.F.; Kumar, P.; Kim, K.H.; Ok, Y.S. Designer carbon nanotubes for contaminant removal in water and wastewater: A critical review. *Sci. Total Environ.* **2018**, *612*, 561–581. [CrossRef]
156. ALOthman, Z.A.; Wabaidur, S.M. Application of carbon nanotubes in extraction and chromatographic analysis: A review. *Arab. J. Chem.* **2019**, *12*, 633–651. [CrossRef]
157. Mallakpour, S.; Khadem, E. Carbon nanotube–metal oxide nanocomposites: Fabrication, properties and applications. *Chem. Eng. J.* **2016**, *302*, 344–367. [CrossRef]
158. Krstić, V.; Urošević, T.; Pešovski, B. A review on adsorbents for treatment of water and wastewaters containing copper ions. *Chem. Eng. Sci.* **2018**, *192*, 273–287. [CrossRef]
159. Zhang, W.; Zeng, Z.; Liu, Z.; Huang, J.; Xiao, R.; Shao, B.; Liu, Y.; Liu, Y.; Tang, W.; Zeng, G.; et al. Effects of carbon nanotubes on biodegradation of pollutants: Positive or negative? *Ecotoxicol. Environ. Saf.* **2020**, *189*. [CrossRef]
160. Yu, J.G.; Zhao, X.H.; Yang, H.; Chen, X.H.; Yang, Q.; Yu, L.Y.; Jiang, J.H.; Chen, X.Q. Aqueous adsorption and removal of organic contaminants by carbon nanotubes. *Sci. Total Environ.* **2014**, *482–483*, 241–251. [CrossRef]

161. Jung, C.; Son, A.; Her, N.; Zoh, K.D.; Cho, J.; Yoon, Y. Removal of endocrine disrupting compounds, pharmaceuticals, and personal care products in water using carbon nanotubes: A review. *J. Ind. Eng. Chem.* **2015**, *27*, 1–11. [CrossRef]
162. Saleh, T.A.; Sarı, A.; Tuzen, M. Carbon nanotubes grafted with poly(trimesoyl, m-phenylenediamine) for enhanced removal of phenol. *J. Environ. Manag.* **2019**, *252*. [CrossRef]
163. Wu, W.; Yang, K.; Chen, W.; Wang, W.; Zhang, J.; Lin, D.; Xing, B. Correlation and prediction of adsorption capacity and affinity of aromatic compounds on carbon nanotubes. *Water Res.* **2016**, *88*, 492–501. [CrossRef]
164. Selvaraj, M.; Hai, A.; Banat, F.; Haija, M.A. Application and prospects of carbon nanostructured materials in water treatment: A review. *J. Water Process Eng.* **2020**, *33*. [CrossRef]
165. Apul, O.G.; Karanfil, T. Adsorption of synthetic organic contaminants by carbon nanotubes: A critical review. *Water Res.* **2015**, *68*, 34–55. [CrossRef] [PubMed]
166. Ahmad, J.; Naeem, S.; Ahmad, M.; Usman, A.R.A.; Al-Wabel, M.I. A critical review on organic micropollutants contamination in wastewater and removal through carbon nanotubes. *J. Environ. Manag.* **2019**, *246*, 214–228. [CrossRef] [PubMed]
167. Yang, K.; Zhu, L.; Xing, B. Adsorption of polycyclic aromatic hydrocarbons by carbon nanomaterials. *Environ. Sci. Technol.* **2006**, *40*, 1855–1861. [CrossRef]
168. Kah, M.; Zhang, X.; Jonker, M.T.O.; Hofmann, T. Measuring and modeling adsorption of PAHs to carbon nanotubes over a six order of magnitude wide concentration range. *Environ. Sci. Technol.* **2011**, *45*, 6011–6017. [CrossRef]
169. Gotovac, S.; Yang, C.M.; Hattori, Y.; Takahashi, K.; Kanoh, H.; Kaneko, K. Adsorption of polyaromatic hydrocarbons on single wall carbon nanotubes of different functionalities and diameters. *J. Colloid Interface Sci.* **2007**, *314*, 18–24. [CrossRef]
170. Pahlavan Yali, Z.; Fatemi, M.H. Prediction of the sorption coefficient for the adsorption of PAHs on MWCNT based on hybrid QSPR-molecular docking approach. *Adsorption* **2019**, *25*, 737–743. [CrossRef]
171. Hu, B.; Gao, Z.; Wang, H.; Wang, J.; Cheng, M. Computational insights into the sorption mechanism of polycyclic aromatic hydrocarbons by carbon nanotube through density functional theory calculation and molecular dynamics simulation. *Comput. Mater. Sci.* **2020**, *179*. [CrossRef]
172. Kragulj, M.; Tričković, J.; Kukovecz, Á.; Jović, B.; Molnar, J.; Rončević, S.; Kónya, Z.; Dalmacija, B. Adsorption of chlorinated phenols on multiwalled carbon nanotubes. *RSC Adv.* **2015**, *5*, 24920–24929. [CrossRef]
173. Yang, K.; Wu, W.; Jing, Q.; Jiang, W.; Xing, B. Competitive adsorption of naphthalene with 2,4-dichlorophenol and 4-chloroaniline on multiwalled carbon nanotubes. *Environ. Sci. Technol.* **2010**, *44*, 3021–3027. [CrossRef] [PubMed]
174. Tóth, A.; Törocsik, A.; Tombácz, E.; László, K. Competitive adsorption of phenol and 3-chlorophenol on purified MWCNTs. *J. Colloid Interface Sci.* **2012**, *387*, 244–249. [CrossRef]
175. Asmaly, H.A.; Abussaud, B.; Ihsanullah; Saleh, T.A.; Gupta, V.K.; Atieh, M.A. Ferric oxide nanoparticles decorated carbon nanotubes and carbon nanofibers: From synthesis to enhanced removal of phenol. *J. Saudi Chem. Soc.* **2015**, *19*, 511–520. [CrossRef]
176. Jiang, L.; Li, S.; Yu, H.; Zou, Z.; Hou, X.; Shen, F.; Li, C.; Yao, X. Amino and thiol modified magnetic multi-walled carbon nanotubes for the simultaneous removal of lead, zinc, and phenol from aqueous solutions. *Appl. Surf. Sci.* **2016**, *369*, 398–413. [CrossRef]
177. Alves, D.C.S.; Gonçalves, J.O.; Coseglio, B.B.; Burgo, T.A.L. Adsorption of phenol onto chitosan hydrogel scaffold modified with carbon nanotubes. *J. Environ. Chem. Eng.* **2019**, *7*, 103460. [CrossRef]
178. Strachowski, P.; Bystrzejewski, M. Comparative studies of sorption of phenolic compounds onto carbon-encapsulated iron nanoparticles, carbon nanotubes and activated carbon. *Colloids Surf. A Physicochem. Eng. Asp.* **2015**, *467*, 113–123. [CrossRef]
179. Yi, L.; Zuo, L.; Wei, C.; Fu, H.; Qu, X.; Zheng, S.; Xu, Z.; Guo, Y.; Li, H.; Zhu, D. Enhanced adsorption of bisphenol A, tylosin, and tetracycline from aqueous solution to nitrogen-doped multiwall carbon nanotubes via cation-π and π-π electron-donor-acceptor (EDA) interactions. *Sci. Total Environ.* **2020**, *719*. [CrossRef]
180. Abdel-Ghani, N.T.; El-Chaghaby, G.A.; Helal, F.S. Individual and competitive adsorption of phenol and nickel onto multiwalled carbon nanotubes. *J. Adv. Res.* **2015**, *6*, 405–415. [CrossRef]
181. Zhang, Z.; Sun, D.; Li, G.; Zhang, B.; Zhang, B.; Qiu, S.; Li, Y.; Wu, T. Calcined products of Mg–Al layered double hydroxides/single-walled carbon nanotubes nanocomposites for expeditious removal of phenol

and 4-chlorophenol from aqueous solutions. *Colloids Surf. A Physicochem. Eng. Asp.* **2019**, *565*, 143–153. [CrossRef]

182. Chen, G.C.; Shan, X.Q.; Wang, Y.S.; Wen, B.; Pei, Z.G.; Xie, Y.N.; Liu, T.; Pignatello, J.J. Adsorption of 2,4,6-trichlorophenol by multi-walled carbon nanotubes as affected by Cu(II). *Water Res.* **2009**, *43*, 2409–2418. [CrossRef] [PubMed]
183. Fathy, M.; Selim, H.; Shahawy, A.E.L. Chitosan/MCM-48 nanocomposite as a potential adsorbent for removing phenol from aqueous solution. *RSC Adv.* **2020**, *10*, 23417–23430. [CrossRef]
184. Albayati, T.M.; Kalash, K.R. Polycyclic aromatic hydrocarbons adsorption from wastewater using different types of prepared mesoporous materials MCM-41in batch and fixed bed column. *Process Saf. Environ. Prot.* **2020**, *133*, 124–136. [CrossRef]
185. Connolly, B.M.; Mehta, J.P.; Moghadam, P.Z.; Wheatley, A.E.H.; Fairen-Jimenez, D. From synthesis to applications: Metal–organic frameworks for an environmentally sustainable future. *Curr. Opin. Green Sustain. Chem.* **2018**, *12*, 47–56. [CrossRef]
186. Jiang, N.; Shang, R.; Heijman, S.G.J.; Rietveld, L.C. High-silica zeolites for adsorption of organic micro-pollutants in water treatment: A review. *Water Res.* **2018**, *144*, 145–161. [CrossRef]
187. Wen, Y.; Zhang, J.; Xu, Q.; Wu, X.; Zhu, Q. Pore surface engineering of metal—Organic frameworks for heterogeneous catalysis. *Coord. Chem. Rev.* **2018**, *376*, 248–276. [CrossRef]
188. Zhang, Z.; Hou, X.; Zhang, X.; Li, H. The synergistic adsorption of pyrene and copper onto Fe(III) functionalized mesoporous silica from aqueous solution. *Colloids Surf. A Physicochem. Eng. Asp.* **2017**, *520*, 39–45. [CrossRef]
189. Nadar, S.S.; Varadan, N.; Suresh, S.; Rao, P.; Ahirrao, D.J.; Adsare, S. Recent progress in nanostructured magnetic framework composites (MFCs): Synthesis and applications. *J. Taiwan Inst. Chem. Eng.* **2018**, *91*, 653–677. [CrossRef]
190. Bhatnagar, A.; Anastopoulos, I. Adsorptive removal of bisphenol A (BPA) from aqueous solution: A review. *Chemosphere* **2017**, *168*, 885–902. [CrossRef]
191. Mahmodi, G.; Zarrintaj, P.; Taghizadeh, A.; Taghizadeh, M.; Manouchehri, S.; Dangwal, S.; Ronte, A.; Ganjali, M.R.; Ramsey, J.D.; Kim, S.J.; et al. From microporous to mesoporous mineral frameworks: An alliance between zeolite and chitosan. *Carbohydr. Res.* **2020**, *489*. [CrossRef] [PubMed]
192. Ahmed, M.J.; Hameed, B.H.; Hummadi, E.H. Review on recent progress in chitosan/chitin-carbonaceous material composites for the adsorption of water pollutants. *Carbohydr. Polym.* **2020**, *247*. [CrossRef] [PubMed]
193. Li, J.M.; Meng, X.G.; Hu, C.W.; Du, J. Adsorption of phenol, p-chlorophenol and p-nitrophenol onto functional chitosan. *Bioresour. Technol.* **2009**, *100*, 1168–1173. [CrossRef]
194. Bibi, S.; Yasin, T.; Hassan, S.; Riaz, M.; Nawaz, M. Chitosan/CNTs green nanocomposite membrane: Synthesis, swelling and polyaromatic hydrocarbons removal. *Mater. Sci. Eng. C* **2015**, *46*, 359–365. [CrossRef] [PubMed]
195. Filho, C.M.C.; Bueno, P.V.A.; Matsushita, A.F.Y.; Rubira, A.F.; Muniz, E.C.; Durães, L.; Murtinho, D.M.B.; Valente, A.J.M. Synthesis, characterization and sorption studies of aromatic compounds by hydrogels of chitosan blended with β-cyclodextrin- and PVA-functionalized pectin. *RSC Adv.* **2018**, *8*, 14609–14622. [CrossRef]
196. Bahmani, E.; Koushkbaghi, S.; Darabi, M.; ZabihiSahebi, A.; Askari, A.; Irani, M. Fabrication of novel chitosan-g-PNVCL/ZIF-8 composite nanofibers for adsorption of Cr(VI), As(V) and phenol in a single and ternary systems. *Carbohydr. Polym.* **2019**, *224*. [CrossRef]
197. Karamipour, A.; Parsi, P.K.; Zahedi, P.; Moosavian, S.M.A. Using Fe_3O_4-coated nanofibers based on cellulose acetate/chitosan for adsorption of Cr(VI), Ni(II) and phenol from aqueous solutions. *Int. J. Biol. Macromol.* **2020**, *154*, 1132–1139. [CrossRef] [PubMed]
198. Lyu, H.; Hu, K.; Chu, Q.; Su, Z.; Xie, Z. Preparation of ionic liquid mediated molecularly imprinted polymer and specific recognition for bisphenol A from aqueous solution. *Microchem. J.* **2020**, *158*. [CrossRef]
199. Ncube, S.; Kunene, P.; Tavengwa, N.T.; Tutu, H.; Richards, H.; Cukrowska, E.; Chimuka, L. Synthesis and characterization of a molecularly imprinted polymer for the isolation of the 16 US-EPA priority polycyclic aromatic hydrocarbons (PAHs) in solution. *J. Environ. Manag.* **2017**, *199*, 192–200. [CrossRef]
200. Saad, N.; Chaaban, M.; Patra, D.; Ghanem, A.; El-rassy, H. Molecularly imprinted phenyl-functionalized silica aerogels: Selective adsorbents for methylxanthines and PAHs. *Microporous Mesoporous Mater.* **2020**, *292*, 109759. [CrossRef]
201. Azizi, A.; Bottaro, C.S. A critical review of molecularly imprinted polymers for the analysis of organic pollutants in environmental water samples. *J. Chromatogr. A* **2020**, *1614*. [CrossRef] [PubMed]

202. Wei, W.; Liang, R.; Wang, Z.; Qin, W. Hydrophilic molecularly imprinted polymers for selective recognition of polycyclic aromatic hydrocarbons in aqueous media. *RSC Adv.* **2015**, *5*, 2659–2662. [CrossRef]
203. Bayramoglu, G.; Arica, M.Y.; Liman, G.; Celikbicak, O.; Salih, B. Removal of bisphenol A from aqueous medium using molecularly surface imprinted microbeads. *Chemosphere* **2016**, *150*, 275–284. [CrossRef] [PubMed]
204. Balbino, T.A.C.; Bellato, C.R.; da Silva, A.D.; de Marques Neto, J.O.; de Guimarães, L.M. Magnetic cross-linked chitosan modified with ethylenediamine and β-cyclodextrin for removal of phenolic compounds. *Colloids Surf. A Physicochem. Eng. Asp.* **2020**, *602*. [CrossRef]
205. Heydaripour, J.; Gazi, M.; Oladipo, A.A.; Gulcan, H.O. Porous magnetic resin-g-chitosan beads for adsorptive removal of phenolic compounds. *Int. J. Biol. Macromol.* **2019**, *123*, 1125–1131. [CrossRef] [PubMed]
206. Alizadeh, B.; Delnavaz, M.; Shakeri, A. Removal of Cd(II) and phenol using novel cross-linked magnetic EDTA/chitosan/TiO_2 nanocomposite. *Carbohydr. Polym.* **2018**, *181*, 675–683. [CrossRef] [PubMed]
207. Rebekah, A.; Bharath, G.; Naushad, M.; Viswanathan, C.; Ponpandian, N. Magnetic graphene/chitosan nanocomposite: A promising nano-adsorbent for the removal of 2-naphthol from aqueous solution and their kinetic studies. *Int. J. Biol. Macromol.* **2020**, *159*, 530–538. [CrossRef] [PubMed]
208. Zhou, A.; Chen, W.; Liao, L.; Xie, P.; Zhang, T.C.; Wu, X.; Feng, X. Comparative adsorption of emerging contaminants in water by functional designed magnetic poly(N-isopropylacrylamide)/chitosan hydrogels. *Sci. Total Environ.* **2019**, *671*, 377–387. [CrossRef]
209. Nguyen, M.L.; Huang, C.; Juang, R.S. Synergistic biosorption between phenol and nickel(II) from Binary mixtures on chemically and biologically modified chitosan beads. *Chem. Eng. J.* **2016**, *286*, 68–75. [CrossRef]
210. Nadavala, S.K.; Swayampakula, K.; Boddu, V.M.; Abburi, K. Biosorption of phenol and o-chlorophenol from aqueous solutions on to chitosan-calcium alginate blended beads. *J. Hazard. Mater.* **2009**, *162*, 482–489. [CrossRef]
211. Krupadam, R.J.; Korde, B.A.; Ashokkumar, M.; Kolev, S.D. Novel molecularly imprinted polymeric microspheres for preconcentration and preservation of polycyclic aromatic hydrocarbons from environmental samples. *Anal. Bioanal. Chem.* **2014**, *406*, 5313–5321. [CrossRef] [PubMed]
212. Li, H.; Wang, L. Highly selective detection of polycyclic aromatic hydrocarbons using multifunctional magnetic-luminescent molecularly imprinted polymers. *ACS Appl. Mater. Interfaces* **2013**, *5*, 10502–10509. [CrossRef] [PubMed]
213. Tiu, B.D.B.; Krupadam, R.J.; Advincula, R.C. Pyrene-imprinted polythiophene sensors for detection of polycyclic aromatic hydrocarbons. *Sens. Actuators B Chem.* **2016**, *228*, 693–701. [CrossRef]
214. Saleh, T.A.; Tuzen, M.; Sari, A. Magnetic vermiculite-modified by poly(trimesoyl chloride-melamine) as a sorbent for enhanced removal of bisphenol A. *J. Environ. Chem. Eng.* **2019**, *7*. [CrossRef]
215. An, F.; Gao, B.; Feng, X. Adsorption and recognizing ability of molecular imprinted polymer MIP-PEI/SiO2 towards phenol. *J. Hazard. Mater.* **2008**, *157*, 286–292. [CrossRef]
216. Liang, W.; Lu, Y.; Li, N.; Li, H.; Zhu, F. Microwave-assisted Synthesis of Magnetic Surface Molecular Imprinted Polymer for Adsorption and Solid Phase Extraction of 4-nitrophenol in wastewater. *Microchem. J.* **2020**, 105316. [CrossRef]
217. Zhao, Z.; Fu, D.; Zhang, B. Novel molecularly imprinted polymer prepared by palygorskite as support for selective adsorption of bisphenol A in aqueous solution. *Desalin. Water Treat.* **2016**, *57*, 12433–12442. [CrossRef]
218. Nasreen, S.; Rafique, U.; Ehrman, S.; Ashraf, M.A. Synthesis and characterization of mesoporous silica nanoparticles for environmental remediation of metals, PAHs and phenols. *Ekoloji* **2018**, *27*, 1625–1637.
219. Costa, J.A.S.; Sarmento, V.H.V.; Romão, L.P.C.; Paranhos, C.M. Removal of polycyclic aromatic hydrocarbons from aqueous media with polysulfone/MCM-41 mixed matrix membranes. *J. Membr. Sci.* **2020**, *601*. [CrossRef]
220. Balati, A.; Shahbazi, A.; Amini, M.M.; Hashemi, S.H.; Jadidi, K. Comparison of the efficiency of mesoporous silicas as absorbents for removing naphthalene from contaminated water. *Eur. J. Environ. Sci.* **2014**, *4*, 69–76. [CrossRef]
221. Yuan, P.; Li, X.; Wang, W.; Liu, H.; Yang, H.; Yue, Y.; Bao, X. Tailored design of differently modified mesoporous materials to deeply understand the adsorption mechanism for PAHs. *Langmuir* **2018**. [CrossRef] [PubMed]

222. Yangui, A.; Abderrabba, M.; Sayari, A. Amine-modified mesoporous silica for quantitative adsorption and release of hydroxytyrosol and other phenolic compounds from olive mill wastewater. *J. Taiwan Inst. Chem. Eng.* **2017**, *70*, 111–118. [CrossRef]
223. Zou, D.; Liu, D. Understanding the modifications and applications of highly stable porous frameworks via UiO-66. *Mater. Today Chem.* **2019**, *12*, 139–165. [CrossRef]
224. Elsabawy, K.M.; Fallatah, A.M. New advanced approach of ultra-fast synthesis of ultrahigh-BET-surface area crystalline metal-organic-frameworks MOFs. *Mater. Lett.* **2018**, *224*, 71–74. [CrossRef]
225. Jiang, D.; Chen, M.; Wang, H.; Zeng, G.; Huang, D.; Cheng, M.; Liu, Y.; Xue, W.; Wang, Z.W. The application of different typological and structural MOFs-based materials for the dyes adsorption. *Coord. Chem. Rev.* **2019**, *380*, 471–483. [CrossRef]
226. Mahmoodi, N.M.; Oveisi, M.; Asadi, E. Synthesis of NENU metal-organic framework-graphene oxide nanocomposites and their pollutant removal ability from water using ultrasound. *J. Clean. Prod.* **2019**, *211*, 198–212. [CrossRef]
227. Zango, Z.U.; Sambudi, N.S.; Jumbri, K.; Abu Bakar, N.H.H.; Abdullah, N.A.F.; Negim, E.S.M.; Saad, B. Experimental and molecular docking model studies for the adsorption of polycyclic aromatic hydrocarbons onto UiO-66(Zr) and NH_2-UiO-66(Zr) metal-organic frameworks. *Chem. Eng. Sci.* **2020**, *220*, 115608. [CrossRef]
228. Zango, Z.U.; Abu Bakar, N.H.H.; Sambudi, N.S.; Jumbri, K.; Abdullah, N.A.F.; Abdul Kadir, E.; Saad, B. Adsorption of chrysene in aqueous solution onto MIL-88(Fe) and NH_2-MIL-88(Fe) metal-organic frameworks: Kinetics, isotherms, thermodynamics and docking simulation studies. *J. Environ. Chem. Eng.* **2019**. [CrossRef]
229. Lin, K.A.; Hsieh, Y. Copper-based metal organic framework (MOF), HKUST-1, as an efficient adsorbent to remove p-nitrophenol from water. *J. Taiwan Inst. Chem. Eng.* **2015**, *50*, 223–228.
230. Xu, Z.; Wen, Y.; Tian, L.; Li, G. Efficient and selective adsorption of nitroaromatic explosives by Zr-MOF. *Inorg. Chem. Commun.* **2017**, *77*, 11–13. [CrossRef]
231. Luo, Z.; Chen, H.; Wu, S.; Yang, C.; Cheng, J. Enhanced removal of bisphenol A from aqueous solution by aluminum-based MOF/sodium alginate-chitosan composite beads. *Chemosphere* **2019**, *237*. [CrossRef] [PubMed]
232. Balati, A.; Shahbazi, A.; Amini, M.M.; Hashemi, S.H. Adsorption of polycyclic aromatic hydrocarbons from wastewater by using silica-based organic–inorganic nanohybrid material. *J. Water Reuse Desalin.* **2015**, *5*, 50–63. [CrossRef]
233. Costa, J.A.S.; Sarmento, V.H.V.; Romão, L.P.C.; Paranhos, C.M. Synthesis of functionalized mesoporous material from rice husk ash and its application in the removal of the polycyclic aromatic hydrocarbons. *Environ. Sci. Pollut. Res.* **2019**, *26*, 25476–25490. [CrossRef] [PubMed]
234. Anbia, M.; Amirmahmoodi, S. Adsorption of phenolic compounds from aqueous solutions using functionalized SBA-15 as a nano-sorbent. *Sci. Iran.* **2011**, *18*, 446–452. [CrossRef]
235. Nasreen, S.; Rafique, U.; Ehrman, S.; Ashraf, M.A. Hybrid mesoporous silicates: A distinct aspect to synthesis and application for decontamination of phenols. *Saudi J. Biol. Sci.* **2019**, *26*, 1161–1170. [CrossRef]
236. Asgharnia, H.; Nasehinia, H.; Rostami, R.; Rahmani, M.; Mehdinia, S.M. Phenol removal from aqueous solution using silica and activated carbon derived from rice husk. *Water Pract. Technol.* **2019**, *14*, 897–907. [CrossRef]
237. Zango, Z.U.; Jumbri, K.; Sambudi, N.S.; Abu Bakar, N.H.H.; Abdullah, N.A.F.; Basheer, C.; Saad, B. Removal of anthracene in water by MIL-88(Fe), NH_2-MIL-88(Fe), and mixed-MIL-88(Fe) metal–organic frameworks. *RCS Adv.* **2019**, *9*, 41490–41501. [CrossRef]
238. Zango, Z.U.; Sambudi, N.S.; Jumbri, K.; Abu Bakar, N.H.H.; Saad, B. Removal of Pyrene from Aqueous Solution Using Fe-based Metal-organic Frameworks. *IOP Conf. Ser. Earth Environ. Sci.* **2020**, *549*, 012061. [CrossRef]
239. Zhou, M.; Wu, Y.-n.; Qiao, J.; Zhang, J.; McDonald, A.; Li, G.; Li, F. The removal of bisphenol A from aqueous solutions by MIL-53(Al) and mesostructured MIL-53(Al). *J. Colloid Interface Sci.* **2013**, *405*, 157–163. [CrossRef]
240. Tan, Y.; Sun, Z.; Meng, H.; Han, Y.; Wu, J.; Xu, J.; Xu, Y.; Zhang, X. A new MOFs/polymer hybrid membrane: MIL-68(Al)/PVDF, fabrication and application in high-efficient removal of p-nitrophenol and methylene blue. *Sep. Purif. Technol.* **2019**, *215*, 217–226. [CrossRef]

241. Han, T.; Li, C.; Guo, X.; Huang, H.; Liu, D.; Zhong, C. In-situ synthesis of SiO_2@MOF composites for high-efficiency removal of aniline from aqueous solution. *Appl. Surf. Sci.* **2016**, *390*, 506–512. [CrossRef]
242. Abazari, R.; Salehi, G.; Mahjoub, A.R. Ultrasound-assisted preparation of a nanostructured zinc(II) amine pillar metal-organic framework as a potential sorbent for 2,4-dichlorophenol adsorption from aqueous solution. *Ultrason. Sonochem.* **2018**, *46*, 59–67. [CrossRef] [PubMed]
243. Abazari, R.; Mahjoub, A.R. Ultrasound-assisted synthesis of Zinc(II)-based metal organic framework nanoparticles in the presence of modulator for adsorption enhancement of 2,4-dichlorophenol and amoxicillin. *Ultrason. Sonochem.* **2018**, *42*, 577–584. [CrossRef] [PubMed]
244. Han, T.; Xiao, Y.; Tong, M.; Huang, H.; Liu, D.; Wang, L.; Zhong, C. Synthesis of CNT@MIL-68(Al) composites with improved adsorption capacity for phenol in aqueous solution. *Chem. Eng. J.* **2015**, *275*, 134–141. [CrossRef]
245. Jung, B.K.; Hasan, Z.; Jhung, S.H. Adsorptive removal of 2,4-dichlorophenoxyacetic acid (2,4-D) from water with a metal–organic framework. *Chem. Eng. J.* **2013**, *234*, 99–105. [CrossRef]
246. Guo, H.; Niu, B.; Wu, X.; Zhang, Y.; Ying, S. Effective removal of 2,4,6-trinitrophenol over hexagonal metal–organic framework NH_2-MIL-88B(Fe). *Appl. Organomet. Chem.* **2018**, *33*, e4580. [CrossRef]
247. Giraldo, L.; Bastidas-Barranco, M.; Húmpola, P.; Moreno-Piraján, J.C. Design, synthesis and characterization of MOF-199 and ZIF-8: Applications in the adsorption of phenols derivatives in aqueous solution. *Eur. J. Chem.* **2017**, *8*, 293–304. [CrossRef]
248. Ahsan, M.A.; Jabbari, V.; Islam, M.T.; Turley, R.S.; Dominguez, N.; Kim, H.; Castro, E.; Hernandez-Viezcas, J.A.; Curry, M.L.; Lopez, J.; et al. Sustainable synthesis and remarkable adsorption capacity of MOF/graphene oxide and MOF/CNT based hybrid nanocomposites for the removal of Bisphenol A from water. *Sci. Total Environ.* **2019**, *673*, 306–317. [CrossRef]
249. Zhang, R.; Wang, L.; Han, J.; Wu, J.; Li, C.; Ni, L.; Wang, Y. Improving laccase activity and stability by HKUST-1 with cofactor via one-pot encapsulation and its application for degradation of bisphenol A. *J. Hazard. Mater.* **2020**, *383*. [CrossRef]
250. Kamali, M.; Persson, K.M.; Costa, M.E.; Capela, I. Sustainability criteria for assessing nanotechnology applicability in industrial wastewater treatment: Current status and future outlook. *Environ. Int.* **2019**, *125*, 261–276. [CrossRef]
251. El-Naas, M.H.; Surkatti, R.; Al-Zuhair, S. Petroleum refinery wastewater treatment: A pilot scale study. *J. Water Process Eng.* **2016**, *14*, 71–76. [CrossRef]
252. Kalmykova, Y.; Moona, N.; Strömvall, A.M.; Björklund, K. Sorption and degradation of petroleum hydrocarbons, polycyclic aromatic hydrocarbons, alkylphenols, bisphenol A and phthalates in landfill leachate using sand, activated carbon and peat filters. *Water Res.* **2014**, *56*, 246–257. [CrossRef] [PubMed]
253. Frascari, D.; Bacca, A.E.M.; Zama, F.; Bertin, L.; Fava, F.; Pinelli, D. Olive mill wastewater valorisation through phenolic compounds adsorption in a continuous flow column. *Chem. Eng. J.* **2016**, *283*, 293–303. [CrossRef]

water

MDPI

Review

Chemically Modified Biosorbents and Their Role in the Removal of Emerging Pharmaceutical Waste in the Water System

Adewale Adewuyi

Department of Chemical Sciences, Faculty of Natural Sciences, Redeemer's University, P.M.B 230, Ede, Osun State, Nigeria; walexy62@yahoo.com; Tel.: +234-8035826679

Received: 29 April 2020; Accepted: 26 May 2020; Published: 29 May 2020

Abstract: Presence of pharmaceutically active compounds (PACs) as emerging contaminants in water is a major concern. Recent reports have confirmed the presence of PACs in natural and wastewater systems, which have caused several problems indicating the urgent need for their removal. The current review evaluates the role of chemically modified biosorbents in the removal of PACs in water. Reported biosorbents include plant and animal solid waste, microorganisms and bio-composite. Bio-composites exhibited better prospects when compared with other biosorbents. Types of chemical treatment reported include acid, alkaline, solvent extraction, metal salt impregnation and surface grafting, with alkaline treatment exhibiting better results when compared with other treatments. The biosorption processes mostly obeyed the pseudo-second-order model and the Langmuir isotherm model in a process described mainly by ionic interaction. Desorption and regeneration capacity are very important in selecting an appropriate biosorbent for the biosorption process. Depending on the type of biosorbent, the cost of water treatment per million liters of water was estimated as US $10–US $200, which presents biosorption as a cheap process compared to other known water treatment processes. However, there is a need to conduct large-scale studies on the biosorption process for removing PACs in water.

Keywords: algae; bacteria; biosorbent; biosorption; pharmaceutical waste

---

1. Introduction

Lack of sufficient clean drinking water is a growing challenge in many countries. Most surface and groundwater bodies are contaminated and are not directly safe for consumption without being treated. Surface and ground waters in rural communities that were once clean are now contaminated due to industrialization and abuse in the use and disposal of pharmaceutically active compounds (PACs). Contamination has severely affected the quality of freshwater. This undesired effect harms humans, animals and the ecosystem. Although several measures, such as creating awareness of water quality problems, promoting advanced water cleaning techniques and establishing preventive systems, have been put in place in some countries, the challenge is still persistent with different levels of impact in different countries. Several organic compounds have been reported in water systems; however, the presence of PACs continues to pose a severe problem among these organic compounds. Most PACs are considered as emerging contaminants, since their regulation and limit in domestic and industrial wastewater handling and treatment criteria, in most countries of the world, are not yet specified, most notably in developing countries [1]. They occur in small amounts and are capable of bioaccumulating over a period to cause harm. The danger ascribed to PACs necessitates the development of an environmentally friendly and cost-effective means for their removal in water systems. The consumption of pharmaceutical compounds has increased over the past decade across the world. Their use includes application in disease control and eradication in both human and animals. One major problem of this is the uncontrolled use of antimicrobial agents in veterinary medicine as well as the use of over-the-counter drugs in self-medication [2,3]. The abuse of PACs has led to their presence in the environment. They enter the environment when they are excreted from the body system and sometimes when inappropriately disposed of or applied. Having entered the environment, they are capable of transforming into metabolites under certain environmental conditions, temperature, pressure, light, etc., in a process, which can be described as biodegradation and photodegradation. The metabolites are sometimes more toxic than the parent PACs. This transformation makes it difficult to monitor the presence of PACs in their parent forms in surface and groundwater. The presence of PACs and possibly their metabolites have made pathogenic organisms develop resistance against them and, over time, they lose their potency against these disease-causing microorganisms. These emerging contaminants have gained attention as previous researchers have reported toxic and adverse effect even at low concentration [4]. Apart from the development of drug resistance by pathogenic microorganisms, previous studies have linked feminization of fish species to the presence of natural and synthetic estrogens in water [5–7].

PACs are a wide range of chemical compounds, which may include anti-inflammatories, antibiotics, cytotoxins, birth control pills, synthetic hormones, and statins. They are different from other chemical contaminants found in water because innumerable complex molecules may form them; the molecules are absorbed in the human body and may undergo metabolic reactions that can modify their chemical structure; they may persist in the environment and may be amphiphilic [8]. Several PACs have been detected in surface water, which varies from region to region, as shown in Table 1. Many sources may have contributed to their presence in surface water; primary sources are urban, industrial, domestic and hospital wastewater. Intensive livestock farming, liquid livestock manure, sewage sludge from agricultural practice and effluents from sewage treatment plants may also serve as sources.

Table 1. Pharmaceutically active compounds (PACs) reported in surface water.

PACs	Country	Concentration (ng L^{-1}) *	Reference
Antibiotics			
Erythromycin	Bangladesh	6.46	[9]
Metronidazole	China	5.10	[10]
Sulfamethoxazole	USA	14.73	[11]
Trimethoprim	Mexico	74.00	[12]
Ciprofloxacin	India	6,500,000	[13]
Amoxicillin	Ghana	2.70	[14]
Trimethoprim	Kenya	2650	[15]
Tetracyclin	Ghana	30.00	[14]
Anti-hyperglycemic			
Metformin	Sweden	8.40	[16]
Lipid regulator			
Gemfibrozil	Spain	3735.00	[17]
Analgesics and Anti-inflammatories			
Acetaminophen	UK	9822.00	[18]
Diclofenac	Malaysia	15.49	[19]
Ibuprofen	South-Africa	846.00	[20]
Ketoprofen	Portugal	86.90	[21]
Naproxen	Poland	13.40	[22]
Anti-depressives			
Diazepam	India	305.00	[23]
Fluoxetine	Portugal	25.37	[21]

* = Maximum concentration reported.

The different pathways for the introduction of PACs into the environment can be described as reported by Silva et al. [24] in Figure 1. Apart from their presence in surface water, they have percolated into groundwater, and their presence has also been documented in coastal seawater [25]. The consequences of the presence of PACs in water goes beyond the reduction in water quality to environmental persistence and detrimental effect on aquatic life [26].

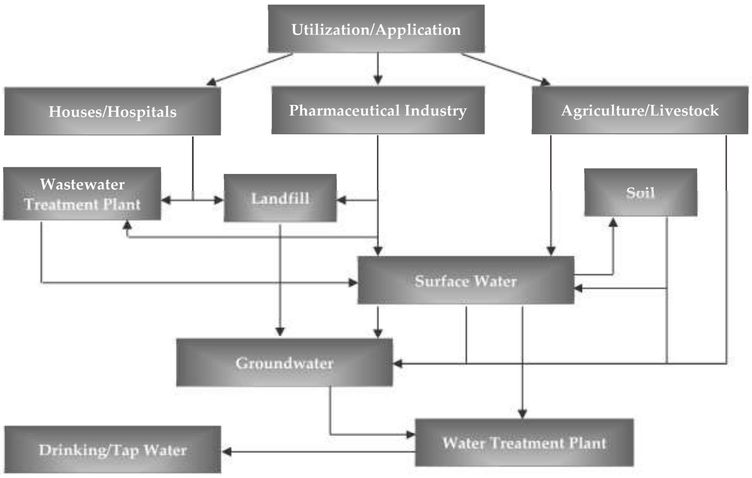

Figure 1. Pathways of PACs' introduction into the environment [24].

There is a need to develop procedures and technology for the complete removal of PACs in water or in wastewater before they are discharged into the environment. Previous techniques used for the removal of PACs from water include chemical, physical and biological approaches, e.g., coagulation, membrane filtration, bioremediation, volatilization, ozonation, flocculation, advance oxidation, photocatalysis, sedimentation, microbial degradation, electrochemical processes and adsorption [27–34]. These approaches differ in effectiveness, sustainability and cost and have different advantages and disadvantages. Unfortunately, sedimentation, coagulation and flocculation processes are not so suitable and effective for the removal of PACs due to the high solubility and mobility of some PACs in water [35]. However, separation processes such as ultra-, nano- and micro-filtrations have been suggested, but their efficiency is mainly dependent on the molecular weight and size of the PACs. Other studies have also shown that the filtration processes might further depend on ionic interaction, membrane functional groups, hydrophobic interaction and age of the membrane [36–38]. Use of advanced electrochemical oxidation has been shown to have the limitation of producing more toxic and recalcitrant by-products than the parent PACs [39,40]. Although ozonation processes have been useful, the toxicity of the intermediate compounds formed during the process is not well understood. It becomes necessary to develop an additional unit operation to remove the intermediate molecules formed, which increases production cost and the need for expertise. The biological process has been useful, but the main challenges are incomplete degradation of PACs and production of intermediate compounds, which either need another procedure to remove them or whose toxicity is not well known.

Several steps have been taken to upgrade these techniques, e.g., attempts at combined advanced oxidation processes, ultrasonic irradiation, electrochemical degradation, photodegradation, adsorption, photo-Fenton, etc. [41–44]; however, the upgrade results from the sophistication of these processes. The biosorption process remains relevant because of its process characteristics such as ease of maintenance, simplicity, ease of modification of biosorbents, inexpensive cost, efficiency of uptake even when the adsorbates (PACs) are in low concentrations, lower selectivity and consistency [26,45]. The outstanding performance of biosorption gives it an edge over the other known processes, most notably the ease of modification, which simplifies the process design. For this reason, this review aims to consider the role of chemically modified biosorbents in the removal of PACs from the water system.

2. Biosorption as a Process for Removing PACs in Water

Biosorption is a mass transfer process that moves substances from the fluid phase to the solid phase. It is a physicochemical and metabolically independent process with mechanisms such as ion exchange, precipitation, absorption, adsorption and surface complexation [46]. It has found application in water treatment and, in this case, removal of PACs from the water system. During this process, substances (adsorbate) in the fluid phase interact with the solid phase and are transferred from the fluid to the solid phase (biosorbent). PACs are the adsorbate in the fluid phase while a suitable material capable of interacting with PACs is the solid phase (biosorbent). The process may be conducted in batch (stirred systems) or continuous mode system (fixed-bed column). The process entails three stages: (I) transport of adsorbate in the fluid phase to the surface of the biosorbent, known as film diffusion, (II) movement of the adsorbate to the pores of the biosorbent, or intraparticle diffusion and (III) fixing of the adsorbate on the surface of the biosorbent, surface bonding. The rate-determining step is at stage I or II, while the III stage is usually very fast [8,47]. Biosorption has been used to remove a wide range of contaminants in water, which has included PACs [29,47,48]. One significant advantage over other processes is that it does not lead to the formation of intermediates [26,27]. The process is reversible, and the adsorbent used can be regenerated by desorption for reuse. However, biosorption may be influenced by certain factors, including pH, temperature, particle size and surface area of the biosorbent. Apart from the surface being large, the surface chemistry must also be appropriate, and the pore size distribution towards PACs must also be correct. Biosorption has received high interest because of the wide range of materials that could be used as biosorbent [49]. The biosorbent used will depend on solubility in water, surface functionality, molecular size and distribution, although it is difficult to predict the performance of any biosorbent at a glance [24,50]. The economic viability of the biosorption process will depend on the adsorbate, biosorbent and the process variable employed, although the biosorbent plays a significant role in this regard. Economic feasibility will depend on the biosorption capacity, regeneration and possible modification of the biosorbent [27,50].

The development of cheap and efficient biosorbent is critical as many of the conventional ones lack satisfactory performance [51], which is the reason for introducing processes such as chemical modification to enhance their performance. Although some materials have been used as adsorbents for the purification of wastewater in the past despite their high purification capacities, the challenge is that a few of them are not biodegradable, which gives natural adsorbents priority over synthetic. Over time, several biosorbents have been modified to improve their capacity for the removal of PACs in the water system. Attention has been placed on biosorbents for water treatment because they are from a natural source, are biodegradable, easy to modify, and most are from renewable sources. Attempts have been made also to make use of waste materials as feedstock for the production of biosorbents. This way, waste from wood, agricultural and food industries are converted to useful and cheap low-cost biosorbents, which has emerged as a cost-effective and efficient alternative for water and wastewater treatment.

2.1. Biosorbents

Biosorbents are biological materials used to remove pollutants passively from a solution. They include biomaterials like agricultural wastes, algae, bacterial, and industrial wastes. They have been receiving encouraging attention because they are from renewable sources, cheap, biodegradable and, after complete usage, do not generate secondary contaminants [52]. Being biological, they contain lots of functional groups, which is the driving force of the hydrophobic interaction they exhibit during the sorption process, which is mostly pH-dependent [53,54]. Many natural materials have been suggested as promising biosorbents for the removal of pollutants in water. These materials can be inactive or dead microbial biomass, as well as living microorganisms. The mechanism by which this is achieved is fully understood for some biosorbents, whereas some require more detailed study. However, the toxicity of some of these biomaterials remains a subject of discussion, which also requires a detailed study.

Biomaterials of various sorption capacities are known. The use of these materials depends on not only their sorption capacity but also reusability over time, which forms the basis for selecting them as biosorbents. One of the major challenges is the selection of the best performing type of biosorbent from a large pool of promising and cheap biomaterials. Although most lignocellulosic materials have a small surface area, effort is focused on how to improve their activity as biosorbents. This does not only include sorption capacity but also improvement in regeneration. Comparison of sorption capacity or efficiency of modified and unmodified biosorbents is essential. The modification might be in the form of pretreatment because the use of untreated biosorbents, most especially plant waste materials, can cause the release of organic compounds into the water being treated. Untreated biosorbents may create high chemical oxygen demand, biological oxygen demand and total organic carbon [55], which leads to depletion of water oxygen content. Therefore, modification of the biosorbent is expected to be encompassing; this cleans the biomaterial by preventing the introduction of unwanted organic compounds into the treated water as well as enhancing the ability of the biomaterial to remove PACs. Different types of chemical modification reported for biosorbents are compared in Table 2.

Table 2. Types of chemical modifications and targeted PACs.

Biosorbent	Type of Chemical Modification	PAC	Qe (mg g^{-1})	pH	Kinetic Model	Time (min)	Reference
Scenedesmus obliquus (Alga)	Alkaline (NaOH)	CEFA	68.00	7.80	PS	45	[56]
		PARA	58.00	7.80	PS	45	
		IBU	42.00	7.80	PS	45	
		TRAM	42.00	7.80	PS	45	
		CIP	39.00	7.80	PS	45	
Waste apricot	Metal salt ($ZnCl_2$) impregnation	Naproxen	106.38	5.8	PS	60	[57]
Bone char	Acid (H_2SO_4)	Ibuprofen	56.78	4.00	PS	360	[58]
Spent tea	Unmodified	Aspirin	-	3.00	-	30	[59]
Modified Spent tea	Surface grafting (Polyethyleneimine)	Aspirin	-	3.00	-	30	
cork waste	Alkaline (K_2CO_3)	Ibuprofen	416.70	2–4	PS	360	[60]
Olive waste	Acid impregnation (H_3PO_4)	Ibuprofen	12.60	4.12	PS	1560	[61]
		Ketoprofen	24.70	4.12	PS	1560	
		Naproxen	39.50	4.12	PS	1560	
		Diclofenac	56.20	4.12	PS	1560	
Parthenium hysterophorus weed	Alkaline (NaOH)	Ibuprofen	90.46	4.00	PS	120	[62]
Pine wood chips	Pyrolysis followed by organic solvent	Salicylic acid	22.70	2.00	PS	960	[63]
		Ibuprofen	10.74		PS	960	
Sisal waste	Alkaline (K_2CO_3)	Ibuprofen	140.10	4.00	PS	1440	[64]
		Paracetamol	124.30	6.00	PS	1440	
Sugar cane bagasse	H_2O (Extraction)	Paracetamol	0.12	7.00	-	-	[65]
Vegetable sponge	H_2O (Extraction)	Paracetamol	0.04	7.00	-	-	

CEFA = Cefadroxil, PARA = Paracetamol, IBU = Ibuprofen, TRAM = Tramadol, CIP = Ciprofloxacin, PS = Pseudo-Second-Order, - = Not determined, Qe = Adsorption capacity.

As shown in Table 2, the use of organic solvent after pyrolysis of pine wood chips removed substances that may have leached from the biosorbent into treated water [63]. Similarly, use of water (H_2O) in the pretreatment of sugar cane bagasse and vegetable sponge before the treatment of water contaminated with paracetamol also removed substances that might have interfered with the use of the biosorbents [65]. Use of alkaline in chemical modification of biosorbents showed better adsorption capacity when compared with other methods. The authors argued that the use of alkaline opens up pores in the biosorbents, which are capable of interacting and trapping the targeted PACs. The kinetic model described the biosorption process for the modified biosorbents as reaching equilibrium in less than 60 min. However, most of the authors allowed the process to keep running for over 60 min to ascertain the consistency of the equilibria process. Moreover, all the sorption processes obeyed pseudo-second-order kinetics at a pH in the range 2–7.8. Most authors claimed that biosorption of PACs is favored at acidic or neutral pH. Unmodified and modified spent teas were evaluated for the removal of aspirin from the water system [58]. The study confirmed that the use of polyethyleneimine surface grafted spent tea performed better at a 65% aspirin removal than unmodified spent tea, which achieved just 1% removal of aspirin. This further shows that chemical modification has the capacity to improve the performance of biosorbents. Many biosorbents are known for the removal of PACs in water. Based on their numerous forms, they may be classified into four categories: natural, industrial wastes, agricultural wastes and forest wastes [66,67].

2.2. Plant and Animal Solid Waste Biosorbent

Plant and animal solid wastes are readily available, cheap and renewable resource materials. They are produced in large amount yearly and usually disposal is a problem. Finding meaningful use of these materials is an important area of research. Making use of these waste materials can help reduce waste load as well as produce economically valuable products [68,69]. The plant-sourced wastes are composed mainly of cellulose with the presence of lignin, proteins, hemicellulose, sugars, lipids and starch, which serve as structural components [70]. Studies have shown the capacity of waste materials to remove PACs from water; the different types of waste reported as biosorbents by the authors of these studies for the removal of PACs in water are presented in Table 3.

The table reveals the importance of pH in the biosorption process. The pH of the solution plays an important role in the sorption process. The pH was related to the pH_{pzc} (point of zero charges) of the studied biosorbents. The pH_{pzc} helps in determining surface properties of the biosorbents. If the pH of the solution is above pH_{pzc}, then the functional groups on the surface of the biosorbents may be protonated by excess H^+ ions whereas if the solution pH is lower than the pHpzc, the surface of the biosorbents may become deprotonated by excess OH^- ions in solution [73]. It was obvious that very high pH did not work well for most PACs; however, most works in the literature reported pH around 5–7. This goes a long way in helping to explain the mechanism of action of the biosorbents towards PACs. Most of the reported mechanisms involved electronic interactions between the surface of the biosorbents and PACs. The concentration of the PACs studied in Table 3 varies. Chen et al. [71] reported a concentration range of 5–20 mg L^{-1} for tetracycline while Wang et al. [75] reported a range of 0.5–32 mg L^{-1}, and a range of 0–100 mg dm^{-3} for diclofenac [72], and Pouretedal et al. [73], for some PACs, reported a range of 20–200 mg L^{-1}. The concentration range studied has an influence on the biosorption capacity exhibited by the biosorbents. The studies further show that biosorption capacity exhibited increases with increase in concentration. However, most PACs are not expected to be present in the environment at very high concentrations; they are expected to occur in the ng L^{-1} but, surprisingly, most authors conducted their studies in ranges (mg L^{-1}), which are higher than reported concentrations of most PACs in surface water as shown in Table 1. The concentration range in the studies may have contributed to the high capacity exhibited by the studied biosorbents. In fact, a range as high as 300 mg L^{-1} was reported in the study of chemically prepared carbon from date palm leaflets towards the sorption of ciprofloxacin, which was higher than the amount expected in an environmental sample. However, attention must be focused on the use of low concentration range to understand further the exact behavior of chemically modified biosorbents at low concentrations, which reflects the precise concentration of these PACs in the environment. PAC solutions used in most studies are synthetic in nature and studies on sorption efficiency of biosorbents in real water samples are lacking. Most reported studies using synthetic PAC solutions did not also consider the effect of salts, organic matters, surfactants, inorganic molecules, etc., which influences the biosorption capacity or process. Therefore, more studies should be conducted to be able to know the exact capacity and prospects of biosorbents.

Table 3. Removal of PACs by some selected biosorbents and their sorption capacity.

Biosorbent	PACs	Adsorption Capacity (mg g^{-1})	Kinetic Model	Mechanism	pH Used	Con (mg L^{-1})	Reference
Rice husk ash	Tetracycline	8.37	PS	Complexation	>7.7	5–20	[71]
Potato peel waste (activated carbon)	Diclofenac	74.00	PS	π-π electron donor-acceptor interaction	5	0–100	[72]
Vine wood	Amoxicillin, Cephalexin, Tetracycline and Penicillin G	1.98–8.41	PS	-	2	20–200	[73]
Bamboo biochar	Sulfamethazine, sulfamethoxazole, and sulfathiazole	25.11–40.11	PS	Lewis acid-base interactions, hydrogen bonding and π-π Electron-donor-acceptor interactions	3–6.5	1–50	[74]
Rice husk	Tetracycline	3.89–13.85	-	π–π electron-donor acceptor	5.5	0.5–32	[75]
Reed straw	Sulfamethoxazole	23.35	-	Hydrogen bonding and π-π electron donor–acceptor	4	5–30	[76]
Date palm	Ciprofloxacin	25.30–53.20	PS	Cation exchange and hydrogen bonding	6	50–300	[77]
Canola biomass	Metronidazole	21.42	PS	Electrostatic interaction	7	0–100	[78]
Groundnut shell	Paracetamol	3.02	-	-	-	10–100	[79]
Brassica nigra	Acetic acid	0.96	-	-	-	0.5 *	[80]

- = Not reported, PS = Pseudo-Second-Order, * = Concentration (N), Con = Concentration.

Table 4 presents the BET (Brunauer-Emmett-Teller) surface area obtained for some biosorbents. The value varies for the different adsorbents depending on the modification process. Plant materials, which are lignocellulose, have low S_{BET} as shown by Silva et al. [81], which demonstrated that plant waste-based biosorbents are feasible alternatives to commercial adsorbents for the removal of PACs in solution. The team reported use of NaOH modified spent coffee grounds, pine bark and cork waste for the removal of fluoxetine from the water with biosorption capacities ranging from 4.74 to 14.31 mg g^{-1}. The sorption capacities exhibited by commercially prepared materials, activated carbon (233.5 mg g^{-1}), zeolite 13 × (32.11 mg g^{-1}) and zeolite 4 A (21.86 mg g^{-1}) were higher than those of spent coffee grounds G (14.31 mg g^{-1}), pine bark (6.53 mg g^{-1}), and cork waste (4.74 mg g^{-1}). However, the NaOH modified biosorbents reflect economic feasibility through cost analysis (0.16–6.85 € g^{-1}) as they are cheaper than the commercial materials, zeolite 4 A (6.85 € g^{-1}), zeolite 13 × (3.13 € g^{-1}) and activated carbon (1.07 € g^{-1}). Apart from economic feasibility, the biosorbents have a positive environmental impact by not introducing solid or liquid waste into the environment. As a form of chemical modification, NaOH-activated carbon was prepared from macadamia nutshell for the removal of tetracycline from the water system [82]. The material showed a microporous structure with a BET surface area of 1524 m^2 g^{-1}. It exhibited an adsorption capacity of 455.33 mg g^{-1} towards tetracycline in a process that can be described by the Elovich kinetic model. The capacity was higher than what was reported for rice husk ash [71]. It has become obvious that antibiotics are the most studied classes of PACs with respect to biosorption onto newly sourced biosorbents. This might be because they are the most commonly found in the surface water system and due to the possibility of the emergence of drug-resistant microorganisms. Ciprofloxacin, tetracycline and sulfamethoxazole are among the most reported. The PACs and biosorbents exist in different ionic states (neutral, cationic or anionic) as pH changes. The different states of existence determine their speciation, and thus their π-electron-donating behavior, hydrophobicity and PAC-biosorbent interaction. Biosorption is most favourable when the PAC and biosorbent have different surface charges, which promotes electrostatic interaction. It is important to understand state of existence when designing and planning the removal of PACs in water systems. Study on date palm (*Phoenix dactylifera*) by El-Shafey et al. [77] revealed its capacity to adsorb ciprofloxacin from aqueous media by a sorption mechanism that is mainly related to cation exchange and hydrogen bonding. Previous studies have shown that modified plant-sourced material can exhibit both biosorption and photocatalysis. In this case, the surface of the material breaks down the PACs into smaller molecules and, at the same time, adsorbs. This observation was reported for reed straw supported titanium dioxide, which used synthesis by sol-gel method and was applied for the removal of sulfamethoxazole [76]. The material exhibited both biosorption and photocatalysis properties toward sulfamethoxazole with an adsorption capacity of 23,347 mg g^{-1}, which can be described by Langmuir isotherm. Similarly, Kumar et al. [83] demonstrated the degradation and biosorption of ibuprofen and 2,4-dichlorophenoxyacetic acid using biochar. The degradation was monitored using LC-MS (Liquid chromatography-mass spectrometry) while the toxicity of the degraded products was analyzed by the viability of human peripheral blood cells. This has also shown that biosorbents modified with transition metal salts like Ti, Zn, etc., have the capacity to degrade the PACs, apart from the biosorption of the PACs taking place at the surface of the biosorbent. It is of note that most reported degradation processes did not lead to complete degradation to CO_2 and H_2O. Biosorbents of this class are considered dual-functional because of their ability to exhibit both biosorption and degradation in a single process of water treatment.

Other studies have also shown that biomaterial could be incorporated with nanomaterials to improve on performance. Wang et al. [84] reported this in a study on the removal of ciprofloxacin from aqueous solution by magnetic chitosan grafted graphene oxide. The material exhibited a high sorption capacity of 282.9 mg g^{-1}; the process was pH-dependent. The authors further reported the influence of other ions (Ca and Na), which was significant on the sorption of ciprofloxacin in a process controlled by electrostatic attraction and π-π electron interaction. It has become so obvious that functionalization plays an important role in improving the ability of plant-sourced materials to perform significantly as biosorbents. The authors reported the synthesis of magnetic chitosan grafted graphene oxide nanocomposite as an efficient biosorbent for the removal of ciprofloxacin. The modification led to a reduction in the surface area of graphene oxide from 1685.7m^2 g^{-1} to 388.3 m^2 g^{-1} due to aggregation resulting from chitosan. The average pore diameter was 13.98 nm, which suggested that the biosorbent composite was a mesoporous material. This also revealed that care must be taken when selecting a chemical modification method in order to prevent the selection of methods or steps that may lead to the formation of aggregates, which reduces the surface area. Since both Langmuir and Freundlich isotherms can describe the process, the authors argued that the process of biosorption was likely to be a complex chemisorption process. The bio-composite was regenerated using 100% methanol; the performance was above 80% in the first cycle. However, the biosorption capacity remained at 72% at 4th regeneration. Unfortunately, most authors did not report the regeneration of biosorbents in their studies. Attention should be given to regeneration studies to understand the worth of low-cost biosorbents.

Table 4. Mode of study, S_{BET}, Isotherm, Qe, Isotherm, Desorption and ΔG° for the sorption of PACs on biosorbents.

Biosorbent	**PAC**	**Mode of Study**	**S_{BET} (m^2 g^{-1})**	**Qe (mg g^{-1})**	**Isotherm**	**Desorption (%)**	**ΔG° (kJ mol^{-1})**	**Reference**
CA-Al-KABs	Ciprofloxacin	Batch	10.595	68.36	Langmuir	-	−0.944	[32]
SCG CW PB	Fluoxetine	Batch	<4 <4 <4	14.31 4.74 6.53	Sips	-	-	[81]
MNS	Tetracycline	Batch	1524	455.33	Temkin	-	-	[82]
MCGO	Ciprofloxacin		388.3	282.9	Freundlich and Langmuir	>80	-	[84]
WPK	Naproxen	Batch	601.9	73.14	Langmuir	-	-	[85]
GS YB CB	Paracetamol	Batch	- - -	1.74 0.77 0.99	Langmuir	-	-	[86]
CTCBW	Acetaminophen	Batch	80.586	-	Freundlich	-		[87]
CBP	Clarithromycin Atenolol		19.26	34.5 39.5	Freundlich Langmuir	-	−838	[88]
ASCK	Paracetamol Amoxicillin	Batch and fixed bed	1908	502.26 282.42	L-F L-F	-	-	[89]
ASK	Paracetamol Amoxicillin	Batch and fixed bed	1635	453.39 228.39	L-F L-F	-	-	[89]
ASP	Paracetamol Amoxicillin	Batch and fixed bed	420	318.84 198.73	L-F L-F	-	-	[89]

CA-Al-KABs = Aluminum-pillared kaolin sodium alginate beads, ΔG^0 = Free Gibbs energy, CW = Cork waste, PB = Pine bark, SCG = Spent coffee grounds, MNS = macadamia nut shells, MCGO = Magnetic chitosan grafted graphene oxide nanocomposite, WPK = Wild plum kernels, GS = Grape stalk, YB = Yohimbe bark, CB = Cork bark, CTCBW = Chemically treated chicken bone waste, CBP = Cuttlefish bone powder, ASCK = NaOH modified Argan waste carbon, ASK = NaOH modified Argan waste, ASP = Phosphoric acid modified Argan waste, L-F = Langmuir-Freundlich isotherm, S_{BET} = Surface area.

Recently, a study by Paunovic et al. [85] documented microwave-functionalized biochar derived from novel lignocellulosic waste biomass for the sorption of ionizable emerging pharmaceuticals in solution. They achieved this by preparing a functionalized biochar from wild plum kernels using simultaneous pyrolysis and microwave potassium hydroxide functionalization. The material removed naproxen from solution at a pH 5–7 having a maximum adsorption capacity of 73.14 mg g^{-1}. The removal was driven by electrostatic attraction as the main mechanism of the process, as shown in Figure 2. Chemical modification by way of first converting biomass to biochar before it is chemically activated or functionalized has received attention for the removal of PACs in a water system. More recently, microwave-assisted techniques have been gaining relevance because of their advantage over the conventional pyrolysis method. Biosorbents prepared through this method have a higher surface area as reported by Paunovic et al. [85] when compared with other direct, simple modifications as reported by Silva et al. [81] in Table 4. The microwave-assisted method is of advantage because the conventional pyrolysis method involves heat transfer to the biomass particles by convection, conduction and radiation mechanisms. During the conventional method, the surface of the biomass is heated first in comparison with the internal zones, resulting in a temperature gradient from the biomass surface to the interior of each particle. The method requires high temperatures, meaning high-energy involvement, which makes it expensive to run. However, the microwave-assisted methods make use of radiation that utilizes volumetric heating within a short time. A relatively low amount of energy is required; the processing time is short with high production yield, which makes it cheaper than the conventional pyrolysis method. The surface area of natural biosorbents has been improved via this means as a way of enhancing sorption capacity for PACs.

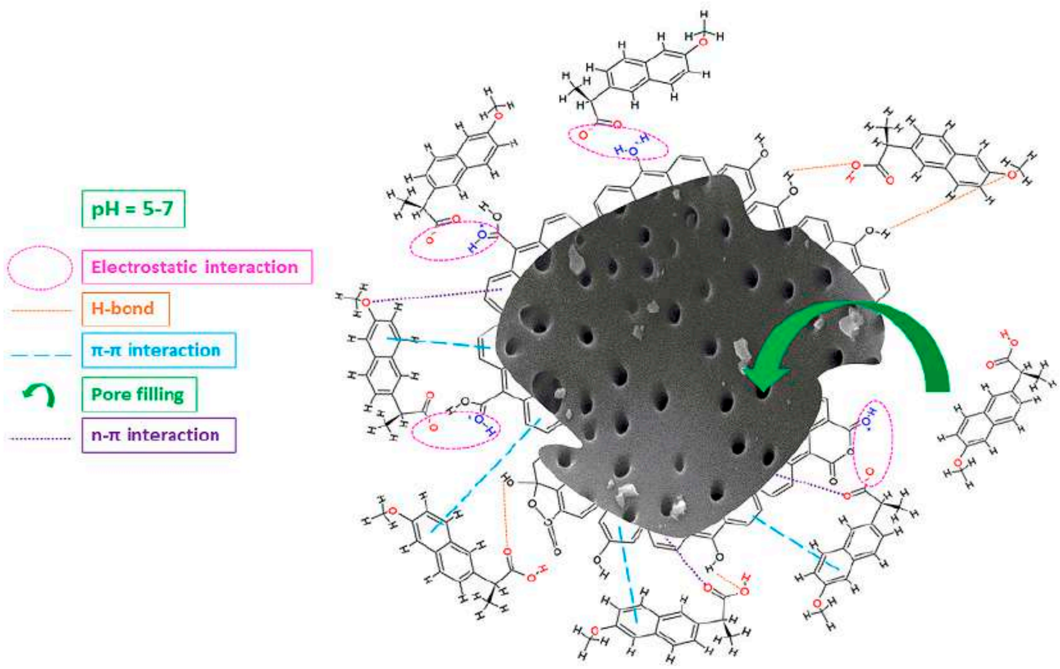

Figure 2. Proposed key sorption mechanisms for the sorption of naproxen on microwave-functionalized biochar [85].

Use of plant waste after simple pretreatment have also been reported. An example of this is the use of grape stalk, yohimbe bark, and cork bark for the removal of paracetamol reported by Villaescusa et al. [86]. The removal process was found not to depend on pH. The grape stalk waste exhibited the best adsorption capacity with a modelling capacity that reflected π-stacking interactions among the lignin, syringyl and guaiacyl moieties in grape stalk and the aromatic ring in paracetamol. Adewuyi et al. [90] also reported the pretreatment of *Adenopus breviflorus* for the removal of 2-chlorophenol in solution. The pretreatment was achieved using different solvent systems. The treatment prevented the introduction of organic molecules from the seed biosorbent into the treated solution in a process which followed the pseudo-second-order model, with isotherm plots fitting well for Freundlich, Langmuir and Temkin models.

Animal waste such as fish bones, cow bones, crab shells, eggshells, etc., have been explored as biosorbents or precursor materials for biosorption. The study by Kizilkaya et al. [91] reported pretreated fish bones obtained from bluefish (*Pomatomus saltotrix*), bogue (*Boop boops*), European anchovy (*Engraulis encrasicolus*) and gilthead seabream (*Sparus aurata*) as low-cost biosorbents. Dahiya et al. [92] also reported the use of pretreated crab and arca shell biomass for biosorption. Ojedokun and Bello [93] published a review on the use of cow dung as biosorbent for the removal of pollutants in water. This has shown an affinity for cations, which suggests that the material may be useful for the removal of positively charged PACs in solution. The review showed cow dung as a bioorganic waste, eco-friendly and inexpensive biosorbent. Previous studies [93,94] showed cow dung to contain calcium sulphate (0.312%), aluminum oxide (20%), calcium oxide (12.48%), magnesium oxide (0.9%), iron oxide (20%) and silica (61%). Another study by El Haddad et al. [95] revealed the use of animal bone meal as biosorbent for the removal of organic compounds in water. The material had an adsorption capacity of 57.15 mg g^{-1} towards reactive yellow 84 dye in a process that is endothermic, and that can be described by Langmuir isotherm. Dyes and PACs are organic molecules; the ability of the material to remove yellow 84 dye in solutions is an indication that the material may be useful for the removal of organic molecules like PACs in solution. Previous work [87] has reported the use of chemically modified chicken bone waste as a biosorbent efficient for the removal of acetaminophen. The process fitted well for both pseudo-second-order kinetic and Freundlich isotherm models. Interestingly, a mixture of activated animal bones from cow, donkey, chicken and horse has also been evaluated as an efficient biosorbent for wastewater treatment [96]. Use of human hair as a biosorbent for the removal of phenol was reported to achieve a removal of 92% in a batch process [97]. The study leveraged on the fact that human hair contains keratin, which is a fibrous proteinaceous material with a large surface area. It reveals the ability of human hair as a possible means for the removal of micro-organic pollutants such as PACs in water. It is a pointer towards finding application for human hair waste produced in large quantities in barbers, serving as a means of converting waste to wealth. Clarithromycin and atenolol, which are common PACs in surface water, were reportedly biosorbed onto cuttlefish bone powder treated with HCl [88]. The biosorbent showed an adsorption capacity of 34.5 mg g^{-1} towards clarithromycin and 39.5 mg g^{-1} towards atenolol in a process that was found to be spontaneous. The $\Delta G°$ for the process was negative (−838 kJ mol^{-1}), which suggests that the process was spontaneous. A similar negative value (−0.944 kJ mol^{-1}) was reported for the sorption of ciprofloxacin on CA-Al-KABs [32]. However, most recent works found in the literature did not consider the effect of temperature on the biosorption of PACs. Most of the published works on biosorption of PACs were carried out focusing on batch operation mode under agitation, which created a gap for limited fixed-bed mode and pilot studies. This makes it difficult to better estimate the potential of biosorbents. It was also evident that most studies did not compare the capacity of the considered low-cost biosorbents with commercially available materials for effective comparison. It is important that future studies consider this.

2.3. *Microorganisms as Biosorbents*

At the early stage of involving microorganisms in the biosorption process, the effort by researchers revealed that inactive/dead microbial biomass could passively bind metal ions. The dead microbial biomass has several advantages over the living microbial biomass such as being cheap, limitation of toxicity, ease of regeneration, exhibiting ion exchange and with a wide range of operational pH and temperature. Subsequently, the effort began to move towards investigating the removal of dyes and other organic pollutants in the water system. Over time, it became evident that biosorption exhibited by microbial biomass does not only depend on the chemical composition of the microbial biomass but also the external physicochemical factors and the matrix chemistry. This mechanism has been reported to be one or a combination of chelation, complexation, adsorption, ion exchange, degradation, electrostatic interaction, microprecipitation, coordination and donor-acceptor interaction [52,98]. Strains of microorganisms have been shown with the capacity to bio-transform toxic compounds into less hazardous forms [99]. The sorption tendency exhibited by a microorganism further depends on the microbial genus, which on the long run defines its cellular composition. They can be used in the form of fine powder or wet cells, which makes resistance to mass transfer negligible. Some biomass has been tested and reported as biosorbent. They include algae, yeast, bacteria and fungi with well-defined structures.

2.3.1. Bacterial

Based on the cell wall and gram staining, bacteria can be divided into Gram-negative and Gram-positive. The cell ranged in diameter between 0.5 to 1.0 μm, and most are unicellular, belonging to the prokaryotes. The cell has four major components: cytoplasm, cell wall, nuclear and cell membrane. The proportions of lipid and protein in the cell membrane vary from one species to the other. They have different shapes such as spiral, rod, cocci and filamentous. The cell wall differs from those of other microorganisms due to the presence of peptidoglycan, which determines its shape and the rigidity of the cell wall. A description of the cell wall of Gram-positive and negative bacterial is shown in Figure 3.

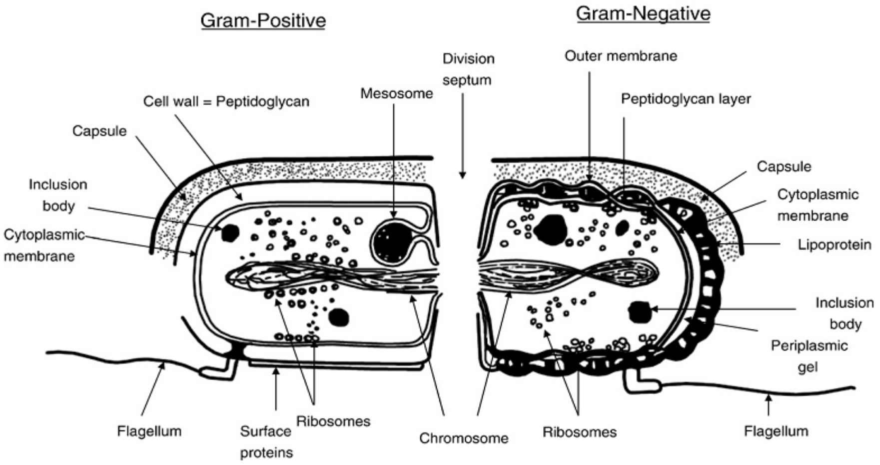

Figure 3. Structure of Gram-positive and negative s [52].

During biosorption by bacteria, the cell wall encounters the PACs first in an interaction where PACs are deposited on its surface. The functional groups such as amine, hydroxyl, carboxyl and phosphonate groups of the cell wall play an important role in the biosorption process since the uptake of the PACs is extracellular [52,100]. Characterization and the biosorption mechanism of bacteria have been studied using different methods such as X-ray diffraction, potentiometric titrations, scanning electron microscopy, Fourier transform infrared spectroscopy, transmission electron microscopy and energy dispersive X-ray microanalysis [101–104]. This has revealed the types, nature and number of binding sites on the surface of the bacteria. Use of Fourier transform infrared spectroscopy has shown band transformations, which enabled the prediction of possible functional groups involved in the biosorption, as well as the acidity and basicity of the bacterial surface involved in the interaction. Energy-dispersive X-ray microanalysis had helped in predicting the chemical and elemental composition of the bacterial, which helps in confirming the involvement of ion exchange mechanism during the biosorption process. X-ray diffraction analysis helps in predicting the chemical nature, while the morphology of the cell surface can be studied using scanning electron microscopy. Both the surface chemistry of the biosorbent and the water chemistry plays an important role in the removal of PACs while certain factors such as solution pH, ionic strength, particle size, concentration and temperature influences the removal rate as well as the adsorption capacity of the bacterial.

Studies have reported different means of enhancing the capacity of bacterial to act as biosorbents. Methods include chemical and genetic modification. Some focused on improving the active binding sites to improve biosorption capacity while less consideration was given to the inhibition sites on the surface of the bacteria. A study by Vijayaraghavan and Yun [105] revealed that the amine group are active towards biosorption of organic compounds via electrostatic interaction. However, on the contrary, the presence of carboxyl functional groups on the same surface repels biosorption from taking place at the surface. The study by Martins et al. [106] reported the use of anaerobic microorganisms to remove ciprofloxacin, 17β-estradiol and sulfamethoxazole from solution as well as elucidate their bio-removal mechanisms. The work provided new insight into the anaerobic bioremediation of ciprofloxacin, 17β-estradiol and sulfamethoxazole. During the process condition used (nitrate- and sulfate-reducing conditions), ciprofloxacin was biodegraded to 80 % under both conditions. Degradation of 17β-estradiol reached 84 % under nitrate-reducing conditions whereas no biodegradation was achieved with respect to sulfamethoxazole. The study further revealed that bioremediation might occur by four mechanisms: (i) extracellular bio-removal by metabolites produced during growth, (ii) biodegradation by co-metabolism, (iii) biodegradation by sole substrate consumption, or (iv) biosorption to the bacterial cells. Sorption steps and biodegradation characteristics of lomefloxacin, ofloxacin, enrofloxacin, ciprofloxacin and norfloxacin have been reported [107]. The study reported sorption of these PACs as the lead process followed by biodegradation. The biodegradation was favored under aerobic condition by temperature increase, which may have been achieved during nitrification through co-metabolism. Co-metabolic activities of heterotrophic denitrifying bacteria and ammonia-oxidizing bacteria in the removal of nitrogen and pharmaceutical and personal care products have been investigated [108]. The study revealed biodegradation as the dominant process for removal of ibuprofen while removal of triclosan was via an equal contribution from adsorption and biodegradation.

Commonly used bacterial strains for remediation of wastewater include *Pseudomonas, Enterobactor, Streptomonas, Aeromonas, Acinetobactor* and *Klebsiella*. Several membrane bioreactors have been developed for large-scale treatment of domestic and industrial wastewater.

Use of membrane reactor has shown several advantages such as flexibility in operation, prolonged microorganism retention, complete removal of suspended solids, low rate of sludge production, treatment of both toxic inorganic and organic pollutants, compact plant size and high rate of degradation [109]. *E-coli* biofilm built on activated carbons was reported [89] for the removal of paracetamol and amoxicillin present in water. The prepared material is microporous with a high surface area. The performance of the material was compared with when the *E-coli* biofilm was not built into the activated carbon. The sorption process without the biofilm showed a rapid kinetic, with sorption capacity being 319 mg g^{-1} in a process that can be described by Langmuir isotherm. Interestingly, the process changed significantly when the biofilm was introduced to the activated carbon. Although the kinetic was slow, the performance changed remarkably with the material exhibiting a biosorption capacity of 465 mg g^{-1} and the process best represented by Langmuir-Freundlich isotherm model having three different stages. This has shown that the use of bacteria in the biosorption process for the removal of PACs in water has a positive impact. As shown in Table 4, the authors focused on the removal of paracetamol and amoxicillin. They argued that the size of PAC plays an important role in its removal; in this case, paracetamol has a lower molecular weight (151.16 g mol^{-1}) compared to amoxicillin (365.4 g mol^{-1}), which may have contributed to the greater sorption capacity exhibited towards paracetamol in the study.

2.3.2. Fungi

This includes yeasts and molds. They are filamentous, with mycelium, which contains a complex mass of filaments. The cell wall is rigid, which gives structural support and shape, mainly consisting of polysaccharide, with polyphosphates, proteins, lipids and inorganic ions. The composition of the cell wall may have contributed significantly to its use as biosorbent for the removal of PACs. Fungi have a promising ability to serve as biosorbents because of its various functional groups, due to the high amount of cell wall materials. It is readily available due to the ease of cultivation in large scale with high yield. Previous work has shown that the use of yeast for environmental research is attractive because it can be genetically modified. It is well characterized, which helps in understanding the biosorption mechanism. The ease of modification shows that it can be manipulated for removing PACs in solution. Four factors that can influence the biosorption of fungi have been reported as: biomass dose in solution, type and nature of biomass, physicochemical factors like temperature, pH, ionic strength, and initial solute concentration [110]. They can be modified chemically or physically to improve capacity to act as biosorbent. The modification can be achieved via improving surface characteristics by exfoliating or masking the functional groups or by making the biosorption sites readily available for sorption [111,112]. They are pretreated chemically to modify the cell wall by creating derivatives with altered sorption abilities and affinities [112]. When fungi are used in water treatment, the free cells have small particle size and low mechanical strength, which creates the need for the application of hydrostatic pressure for a suitable flow rate. However, this leads to disintegration and attrition. Although this material might work well when subjected to the batch process, due to the hydrostatic pressure they become unsuitable for the column packing process, which is applicable in the industrial process [113]. Due to the disintegration and attrition challenge, immobilization techniques have been recommended as means of modification, which may include crosslinking and entrapment.

When this takes place on polymeric matrix, the biosorbent exhibits improvement and advantage in particle size, high biomass loading, minimal clogging, high regeneration and ease of separation [114].

Table 5 shows the different types of fungi reported in the past for the removal of PACs in water. As shown in the table, it is evident that when using fungi for water treatment, biosorption and biodegradation mostly take place together.

Table 5. Selected fungi previously reported for the removal of PACs.

PACs	Fungi	Mechanism of Action	Reference
Estrone, 17 β-estradiol, 17 α-ethinyl-estradiol and estriol	*Myceliophthora thermophile and Trametes versicolor*	Biodegradation Adsorption	[115]
Carbamazepine	*Phanerochaete chrysosporium*	Biodegradation Biosorption	[116]
Sulfapyridine, sulfapyridine, and sulfamethazine	*Trametes versicolor*	Biodegradation Biosorption	[117]
Diclofenac, ibuprofen, naproxen, carbamazepine, and diazepam	*Phanerochaete chrysosporium*	Biodegradation Biosorption	[118]
Carbamazepine, diclofenac, iopromide and venlafaxine	*Trametes versicolor* *Irpex lacteus* *Ganoderma lucidum* *Stropharia rugosoannulata* *Gymnopilus luteofolius* *Agrocybe erebia*	Biosorption	[119]

Sorption of carbamazepine, diclofenac, iopromide and venlafaxine by fungi was reported in a bioreactor treatment [119]. The sorption process was likened to active transport in living cells, which plays an essential role in the sorption process. The removal of the PACs was by both sorption and biodegradation. Recently, *Aspergillus sydowii* and *Aspergillus destruens* were reported for their use under saline conditions for the removal of PACs [120]. Benzo-α-pyrene and phenanthrene were used as a sole carbon source during the study. They achieved a removal of over 90% in a process described to be biodegradation (*Aspergillus sydowii*) and biosorption (*Aspergillus destruens*). Furthermore, a study [121] on the efficiency of *Trametes versicolor* and *Ganoderma lucidum*, to remove thirteen pharmaceutical pollutants with concomitant biodiesel production from the accumulating lipid content after treatment, revealed a 100% removal for diclofenac, gemfibrozil, ibuprofen, progesterone and ranitidine, whereas it showed low removal towards 4-acetamidoantipyrin, clofibric acid, atenolol, caffeine, carbamazepine, hydrochlorothiazide, sulfamethoxazole and sulpiride. However, the combination of *Trametes versicolor* and *Ganoderma lucidum* enhanced efficiency, which was attributed to the interactions developed between both strains. In general, white-rot fungi belonging to the Basidiomycota family has been used in several studies to evaluate potential as a means of removing PACs in water [115,122–125]. They are well known for their ability to degrade lignin. Interestingly, their enzyme system is based on free radicals; they are non-selective and non-specific; they tend to degrade pollutants either by extracellular or intracellular enzymatic route [126]. This capacity and mechanism of degrading lignin is also extended towards PACs. This ability gives them an outstanding edge and attraction in the treatment of wastewater.

2.3.3. Microalgae

There is growing interest in the use of microalgae-based remediation biotechnologies as a means of removing PACs in water. The microalgae-based remediation biotechnology is green, driven by solar energy, eco-friendly, shows fixation and turnover of carbon, and can serve as a source of other useful products [127,128]. Figure 4a shows the different species of microalgae commonly used in bioremediation of wastewater and PACs [129]. The fact that mixotrophic microalgae can maneuver their metabolism process between autotrophic and heterotrophic, making them survive and thrive in extreme environments, gives them an edge over bacteria and fungi that need carbon and other nutrients for growth and degradation of PACs. Just like bacterial and fungi, algae make use of their cell wall for the removal of PACs in solution. The cell wall contains several substances like lignin, pectins, protein, cellulose, hemicellulose and extensin. Due to the main functional groups in the cell wall being phosphoryl, amine and carboxyl groups, the cell wall is negatively charged, which makes them attractive towards cations via electrostatic interaction. Apart from the charge playing an essential role in biosorption, the hydrophobicity, species and structure are also crucial in selecting microalgae for biosorption activities. Studies have shown their ability to remove carbamazepine, ibuprofen, metoprolol, estrone, β-estradiol, etc., from solution. A report by Matamoros et al. [130] showed that mixed microalgae species such as Chlorella and Scenedesmus species could remove tris(2-chloroethyl) phosphate, caffeine, tributyl phosphate, carbamazepine, galaxolide, 4-octylphenol and ibuprofen from solution. The removal of the pollutant was high at a capacity that was not less than 99%. However, the aerated batch reactors inoculated with the mixed microalgae could only efficiently remove 4-octylphenol, galaxolide, and tributyl phosphate as well as ibuprofen and caffeine, but expressed difficulties removing carbamazepine and tris(2-chloroethyl) phosphate. Interestingly, the authors argued that it was the first time that the enhancing effect of microalgae in water treatment had been evaluated. The findings showed that microalgae improved the removal efficiency of ibuprofen by 40%, which further reduced the lag phase of caffeine by three days. It was further shown that microalgae improved the removal efficiency of ibuprofen and caffeine either by releasing exudates, which enhanced the biodegradation processes, or by microalgae biosorption. Studies of *Scenedesmus obliquus* and *Chlorella pyrenoidosa* dead cells have shown their ability to remove progesterone and norgestrel [131]. When PACs are biosorbed by microalgae, they can bioaccumulate with the possibility of causing damage to the cell; however, the concentration at which PACs are present in the environment is safe enough for the microalgae and do not exhibit lethal inhibition [129,132]. *Chlamydomonas Mexicana* and *Scenedesmus obliquus* are examples of species that bioaccumulated carbamazepine [133]. Microalgae have shown biodegradation to be an effective mechanism for the removal of PACs in water. They have biodegraded carbamazepine, ibuprofen, caffeine and tris(2-chloroethyl) phosphate in previous studies [134,135]. Several types of enzymatic reactions have been brought forward to describe the degradation exhibited by microalgae towards PACs, and some of these reactions include oxidation, ring cleavage, demethylation, hydroxylation, hydrogenation, carboxylation, halogenation, decarboxylation and glycosylation [129–135]. The degradation of PACs, as described in Figure 4b may occur in a two phase enzyme system known as phase I and II. In phase I, initial attacks take place using enzyme cytochrome P450, which increases the hydrophilicity of PACs or promote hydrolysis, reduction or oxidation reactions. During phase II reaction, enzymes such as glutathione-S-transferases catalyze the reaction between glutathione and electrophilic molecules; this reaction also protects the system against oxidative damage [129]. Escapa et al. [136] reported the removal of salicylic acid, paracetamol, phosphate and nitrate using *Chlorella sorokiniana*. This study further revealed its use for the biodegradation of metoprolol, diclofenac, paracetamol and ibuprofen.

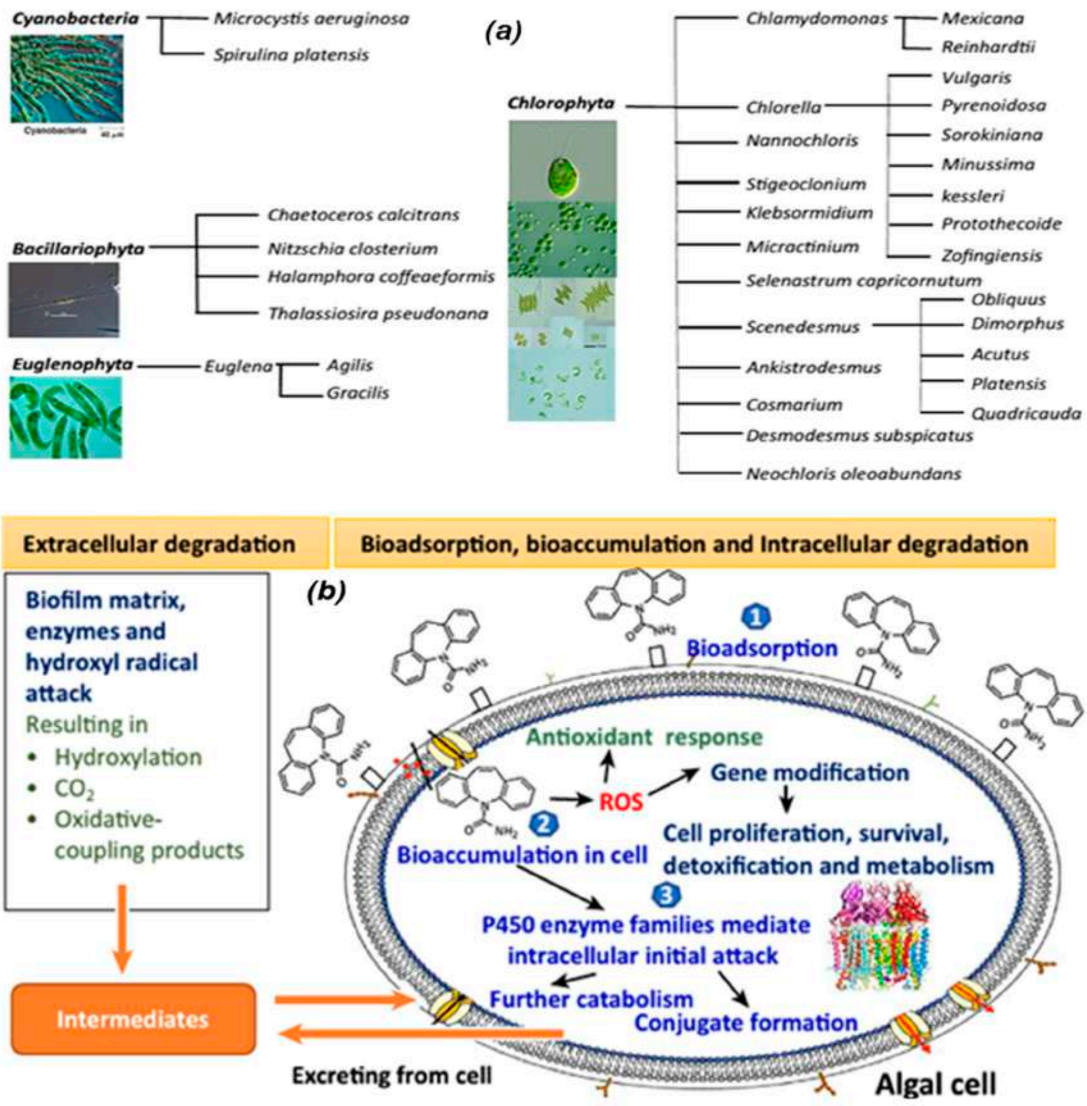

Figure 4. (**a**) Microalgae species commonly used for bioremediation of wastewater, (**b**) Proposed mechanisms of removal of pharmaceutical contaminants and microalgae metabolism [129]. ROS = Reactive oxygen species.

The complete role of these enzymes in the two phase enzyme system is not well understood as research is currently ongoing on how to understand the biotransformation of PACs in the microalgae system. However, metagenomics and meta-transcriptomics analyses are playing a leading role in this regard. Co-metabolism has also been effective in enhancing the ability of microalgae in the removal of PACs. The introduction of organic substrates to the degradation process serves as a means of supporting activities of specific catabolic enzymes in charge of the degradation process. This was demonstrated in the degradation of monooxygenase and N-deethylase with the introduction of acetate [137]. It is important to evaluate the influence of organic substrate before it is introduced into the degradation process because some substrate is capable of having a negative effect on the process by reducing enzyme activity. However, a few factors are understood, such as the role of electron-donating groups, e.g., amine, hydroxyl and alkoxy, in enhancing susceptibility to electrophilic attack by enzymes. It has also become clear that the presence of groups such as nitro, halogen and amide decreases enzymatic biotransformation ability [53,138]. This is also an indication that it is better to understand the structure and functional group composition of PACs before selecting species of microorganisms for its removal. It is also essential to understand the functionality of any organic substrate before inclusion in the degradation process.

2.4. Biocomposite

Bio-composites are materials containing two or more distinct substances, which are brought together to produce a new material with improved performance better than the individual constituent materials. They are biomass-based-materials that can be used for wastewater treatment; they are receiving much attention now because of their biodegradability, high performance and eco-friendliness. Biopolymers remain the major component of bio-composites; these biopolymers are cellulose, chitosan, starch, chitin, alginate, etc. The merit of these biopolymers lies in their non-toxicity, abundance, cost-effectiveness and environmental friendliness [139]. Cellulose, chitin and chitosan are similar in their chemical structure. The only difference is the N-acetyl, amino and hydroxyl functional groups at the C-2 position, as shown in Figure 5.

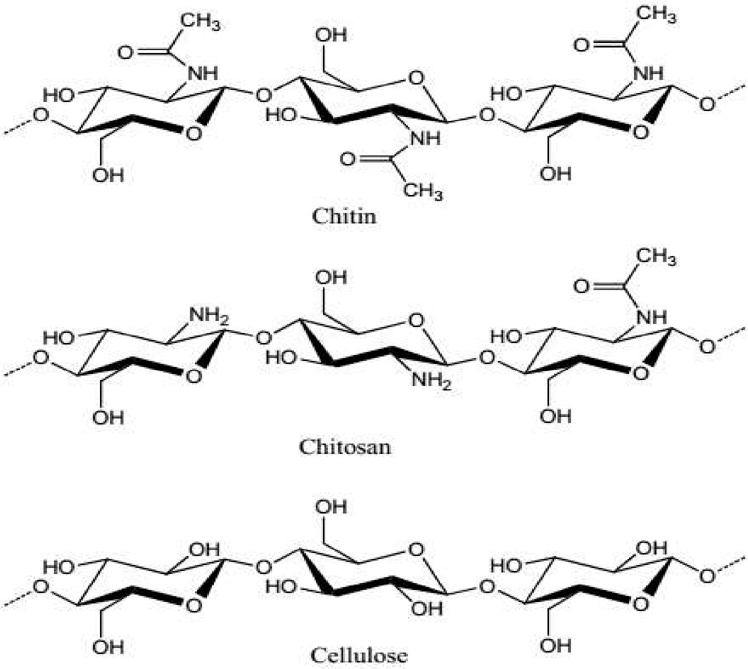

Figure 5. Structure of chitosan, chitin and cellulose [140].

These materials have been prepared in combination with other materials such as clay (commonly used clays include kaolinite, vermiculite, montmorillonite and illite), graphene, carbon, etc. Use of biopolymer alone may not be so effective in the removal of PACs from water. However, the combination of these materials (clay, carbon, graphene and natural polymer) plays an important role. Clay and graphene have large surface areas that can enhance removal; moreover, the cation exchange capacity of clays is also essential. An appropriate bio-composite should be inexpensive, abundant, efficient, environmentally friendly, biocompatible and reusable.

Table 6 presents different bio-composites reported in the literature. Karoui et al. [141] reported the preparation of enhanced biosorbent from Tunisian-reed (*Phragmites-Australis) and its use in the removal of* ciprofloxacin antibiotic and methylene blue dye. The composite was designed under response surface methodology. The study revealed a 76.66% removal for ciprofloxacin and 100% removal for methylene blue dye in a process that can be described by the Brouers-Sotolongo-fractal model. A study reported the removal of parabens from wastewater using magnetic waste tyre activated carbon-chitosan composite [142]. The composite has a surface area of 1281 m^2 g^{-1} and pore size of 4.05 nm, which exhibited a high sorption capacity with 100% removal in a process described by Langmuir and Redlich-Peterson isotherm models. Figure 6 shows the adsorption of parabens and the TEM (Transmission electron microscopy) images. The composite contains chitosan, which is the most deacetylated form of chitin. The presence of hydroxyl and amine groups makes it highly reactive with other compounds. The regeneration capacity of the biosorbent was carried out using methanol. The results obtained for the regeneration showed that recovery and adsorption were not affected for up to seven adsorption/desorption cycles. The result of the regeneration demonstrated the outstanding reusability of the bio-composite and its potential use in wastewater treatment.

Table 6. Bio-composites reported for water treatment.

Bio-composite	PAC	S_{BET} ($m^2\ g^{-1}$)	Qe ($mg\ g^{-1}$)	Removal (%)	Desorption (%)	Solvent for Desorption	Reference
CCGC	Metamizol	-	6.29	>70	>55	Ethanol and water	[3]
	Acetylsalicylic acid	-	9.92	>85	>85		[3]
	Acetaminophen	-	7.52	>60	>55		[3]
	Caffeine	-	8.21	>80	>80		[3]
NMVC	4-aminoantipyrine	96	6.53	98.40	76	Water	[30]
MCGO	Ciprofloxacin	388.30	282.90		>80	Methanol	[84]
Phragmites-Australis	Ciprofloxacin	8.90	17.30	76.66	-	-	[141]
MWACC	Methylparaben	1281	85.90	100	>95	Methanol	[142]
	Propylparaben		90.00	100	>95		
APB	Norfloxacin	90.40	5.24	92.70	>84	Methanol	[143]
RGO-M	Ciprofloxacin	-	18.22	-	-	-	[144]
	Norfloxacin	-	22.20	-	-	-	[144]
CBM	Diclofenac sodium	27.54	164.00	>70	>60	Ethanol and water	[145]
	Tetracycline hydrochloride		40.20	>55	>60		

CCGC = Chitosan/waste coffee-grounds composite, MWACC = Magnetic waste tyre activated carbon-chitosan, APB = Clay-biochar composite with potato stem and natural attapulgite, - = Not determined, NMVC = Nanocellulose modified vermiculite clay, MCGO = Magnetic chitosan grafted graphene oxide nanocomposite, RGO-M = Graphene oxide/magnetite composites, CBM = Chitosan-based magnetic composite, Qe = Adsorption capacity, S_{BET} = Surface area.

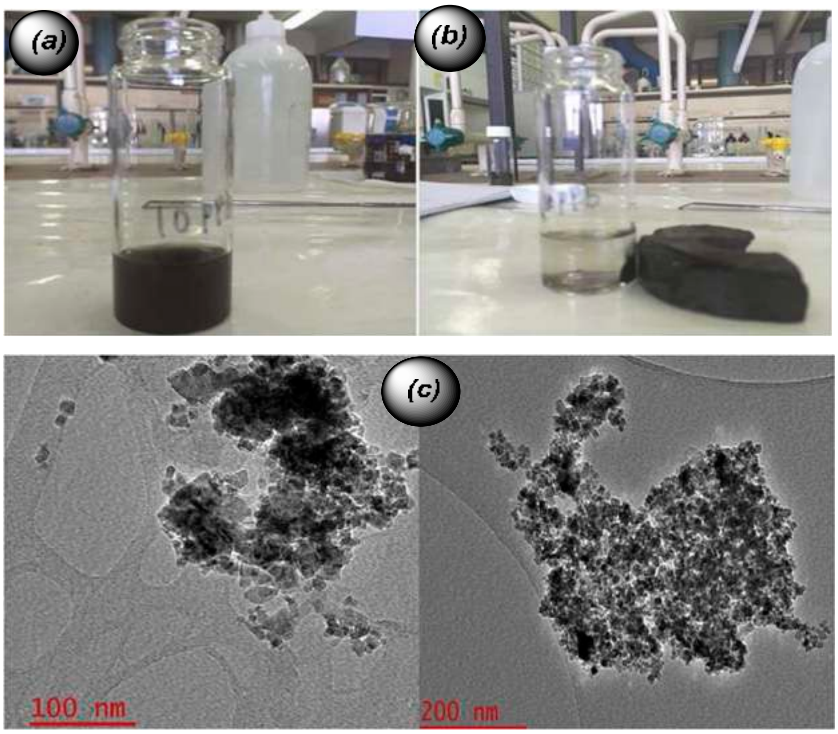

Figure 6. (**a**) Magnetic adsorbent dispersed in sample solution during the adsorption process, (**b**) Separation of sorbent using external magnet and (**c**) TEM of magnetic waste tyre coated activated carbon-chitosan under different magnifications [142].

Clays are hydrous aluminosilicates, which can be categorized mainly into montmorillonite, smectite, kaolinite, ilite, and chlorite. Among these categories, kaolinite, montmorillonite and ilite are mostly used, due to their physicochemical, structural and mechanical properties. The price is low as the cost of clay ranges between \$0.005–0.46 per kg [146,147]. It contains exchangeable cations and anions such as Ca^{2+}, Mg^{2+}, H^+, K^+, Na^+, NH_4^+, Cl^-, PO_4^{3-} and NO^{3-}, which are easily exchanged with other ions without altering the clay structure [147]. Report from the previous study has shown that faces and edges of clay particles can adsorb charged (cations and anions) and neutral pollutants in water [147]. These properties qualify it as a material that can be combined with biopolymer to produce bio-composite. Clay-biochar composites have been produced for the enhancement of sorption capacity of biochar for certain contaminants [148]. Even though several methods have been used for the production of clay-biochar composites, the most frequently used method is pyrolysis [148,149]. Clay-biochar composite prepared by potato stem and natural attapulgite has shown higher sorption capacity for norfloxacin in the pH range of 2.0–11.0 [143]. Major sorption mechanisms involved were electrostatic attraction, hydrogen bonding, hydrophobic interaction, and π-π interactions [150]. The sorption capacity was demonstrated in double distilled tap and river water, and the composite exhibited a removal of 84.14, 82.17 and 87.37%, respectively. The regeneration of the bio-composite with methanol was stable up to the 5th cycle with a capacity greater than 84%. This capacity relates well with values reported for the regeneration of magnetic waste tyre activated carbon-chitosan bio-composite [141], which presents bio-composites as promising materials for wastewater treatment.

Waste coffee-grounds, a poorly explored source of bio-compounds, were combined with chitosan and poly (vinyl alcohol) in order to obtain composite [3]. The composite exhibited a noticeable enhancement for the sorption of metamizol (6.29 mg g^{-1}), acetylsalicylic acid (9.92 mg g^{-1}), acetaminophen (7.52 mg g^{-1}) and caffeine (8.21 mg g^{-1}). The highest removal efficiency was registered at pH 6, which obeyed the pseudo-second-order model and Freundlich isotherm. The composite is cost-effective with remarkable reusability of at least five consecutive biosorption/desorption cycles. Surfactant modified cellulose-montmorillonite composite has also been prepared as a biosorbent [151]. Aluminum-pillared kaolin sodium alginate beads (CA-Al-KABs) were prepared by gelling and solidification processes, which were used for the removal of ciprofloxacin in solution [32]. Sorption of ciprofloxacin was found to be pH-dependent, pseudo-first-order kinetics model controlled and obeyed the Langmuir isotherm model with an adsorption capacity of 68.36 mg g^{-1}. The mechanism for the sorption of ciprofloxacin is electrostatic attraction, as described in Figure 7a. Starch modified smectite clay composite has also been prepared and used for the removal of PACs from wastewater treatment plant effluent [152]. It is evident that most regeneration processes made use of polar solvents or a mixture of organic solvent with water as a means of an aqueous system for the regeneration of bio-composite. Alcohol is the most commonly used organic solvent, which might be due to the polar solubility of most of the PACs.

Graphene is a one-atom-thick, two-dimensional layer of sp^2-hybridized carbon [153]. Its physicochemical, thermal, mechanical and electrical properties are extraordinary, which makes it suitable for different applications. The surface area is large, and its large delocalized π-electron system promotes interaction with other molecules [154,155]. This interaction is a pointer for its use as a material in the removal of PACs in the water system. It can hold oxygen-containing functional groups in its molecule to form reduced graphene (rGO) or graphene oxide (GO). This is an indication that it can be modified by grafting other functional groups onto it or by combination with other materials such as biopolymers. Its exceptional properties such as large surface area, short intra-particle diffusion path-length, high sorption site, low-temperature modification and ease of regeneration present graphene as an excellent material for composite preparation. When such composites are prepared in combination with a biopolymer, they are classified as a new class of fascinating bio-composite. One disadvantage that limits the use of graphene is the possibility of aggregation. However, this challenge is overcome by intercalating particles within the layers of graphene [144]. rGO/magnetite was prepared by Tang et al. [156] and used for the removal of norfloxacin and ciprofloxacin. The process was spontaneous and exothermic with sorption capacity of 22.20 and 18.22 mg g^{-1} for norfloxacin and ciprofloxacin, respectively. The process obeyed Temkin isotherm, Langmuir isotherm and pseudo-second-order kinetic models. It is pH-dependent, and the removal mechanism consisted of electrostatic repulsions and π-π interactions. GO may be incorporated into polymer membrane to boost performance in water treatment. A few reports cover the incorporation of GO into particular; poly (*N*-vinylcarbazole), polyamide; and polysulfone membranes [157]. Inclusion of GO and activated carbon in polymer ultrafiltration membrane has shown improvement in hydrophilicity, electrostatic repulsion and pore size, which remarkably enhance removal of PACs in water [158]. Li et al. [159] reported the degradation of amoxicillin using magnetic TiO_2-GO-Fe_3O_4 composite with a submerged magnetic separation membrane photocatalytic reactor. TiO_2-GO-Fe_3O_4 was prepared with high Photo-Fenton catalytic performance and capability of magnetic recovery. Fe_3O_4 not only enhanced Fenton degradation of amoxicillin but also contributed to the magnetism of the photocatalyst for magnetic separation from treated water. The study revealed an excellent degradation of amoxicillin in a photodegradation process that is described in Figure 7b. It is also obvious in Table 6 that bio-composite prepared with the inclusion of GO exhibited high surface area and high adsorption capacity when compared with other bio-composites which did not include GO. The high surface area exhibited by the bio-composite might be due to the high surface area of GO, although the authors reported that the initial high surface area of GO reduced after inclusion for the preparation of bio-composite, which may be due to the aggregation resulting from the interaction with biomass. Most bio-composites remained steady in their regeneration and adsorption capacity up to 5–8 cycles, which makes them outstanding. Unfortunately, there is limited information on desorption studies or regeneration of plant-based biosorbents, as shown in Table 4, unlike the case for bio-composite. Apart from this, the introduction of magnetic properties into some of the reported bio-composites [142] as described in Figure 6 makes them stand out. The magnetic properties demonstrated by such bio-composites makes it easy to separate the biosorbent from the treated water system, unlike other biosorbents which required filtration and other steps, which adds extra cost to the actual treatment cost.

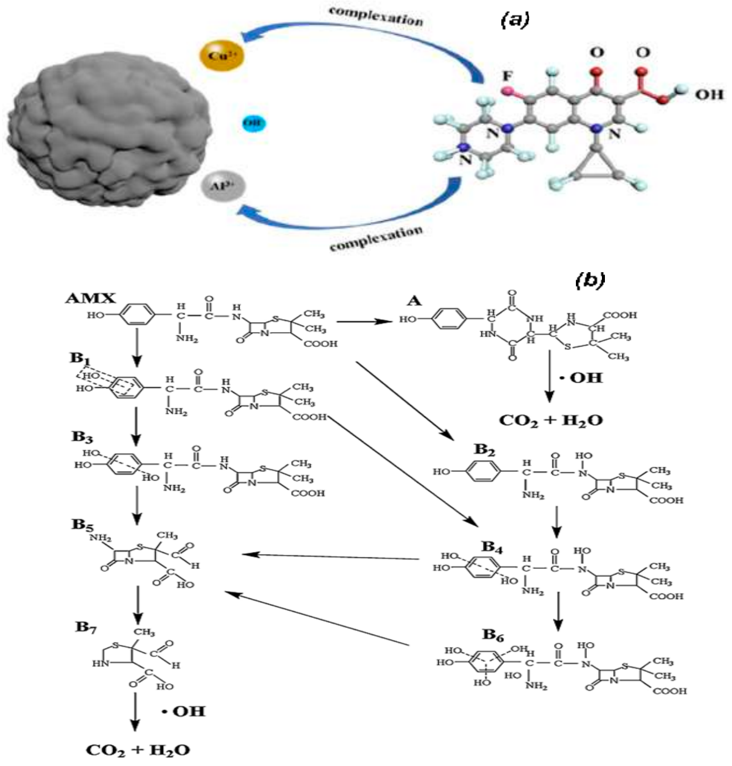

Figure 7. (**a**) The mechanism of ciprofloxacin loaded on CA-Al-KABs [32], (**b**) Mineralization pathways of amoxicillin (AMX) in water by submerged magnetic separation membrane photocatalytic reactor [159].

2.5. Desorption and Regeneration

The reusability of biosorbent is essential. This involves the removal of adsorbate from the surface of the biosorbent after use and the biosorbent should return to almost its original form in morphology and effectiveness. The number of cycles in which biosorbents can be reused goes a long way in determining their economic value and viability. One of the key achievements of biosorbents is their recovery after usage. Developing a suitable system for desorption is very important. It is not sufficient for a biosorbent to exhibit high performance alone, but reusability is equally essential. Therefore, desorption and regeneration are the fundamental processes to check when selecting biosorbents. Many materials have been developed in the past as biosorbents for removal of PACs from the water system. However, some of them are not easily regenerated, which makes their continuous use questionable, as they will have to be discarded after completing a circle or two. Discarding such material may also lead to an environmental pollution problem. It is very important that, after the sorption process, spent biosorbents are separated from the medium, regenerated and recycled. Several methods have been developed for the desorption process. However, the use of eluents is still the most commonly used process. Ability to select the most suitable eluent is very vital, a process, which depends on the type of biosorbent, adsorbate and mechanism of biosorption. An appropriate eluent should not damage or change the structure of the biosorbent, should be environmentally friendly, cheap, have high affinity for the adsorbate, not alter the adsorbate or biosorbent and should easily separate from the adsorbate.

Previously used eluents include mineral acids [30], organic acids and solvents [160], and complexing agents [161]. Desorption may be performed in batch or column, although the desorption process is easier in a packed column arrangement. When the sorption process is in a column, it is better to perform the desorption in the column as well. For example, once the sorption process becomes saturated, it is better to switch to desorption by allowing the eluent to flow through the column. It is important to carefully monitor the process so as not to overstretch the biosorbent; however, this also depends on the strength of the biosorbent. The potential of a desorption process relies on the removal mechanisms and the mechanical stability of the biosorbent. Since most biosorbents exhibit ion-exchange or ionic interaction towards positively charged PACs, use of mild to strong acidic systems should sufficiently achieve the desorption. This becomes beneficial since acidic solutions are common waste, generated in most industries. Therefore, acidic solutions generated during industrial processes can find an application by serving as a means of regenerating spent biosorbents. Chakraborty et al. [162] reported the desorption of ibuprofen from bidirectional activated biochar from sugarcane bagasse. The desorption was carried out using 0.1 N methanol under continuous agitation at 130 rpm for 24 h at 25 °C. It was efficient even after 4 cycles up to values above 65%. Desorption of diclofenac sodium and tetracycline hydrochloride from chitosan-based magnetic composite was achieved using ethanol and water (volume ratio of 1:1) with 1 wt % of NaOH [145]. For effective desorption, the alkaline condition was maintained since Fe_3O_4 is unstable at very low pH. Furthermore, the solution of ethanol-water was used in order to dissolve diclofenac sodium and tetracycline hydrochloride. The process attained a regeneration efficiency of five cycles. Desorption and regeneration of biosorbent are carefully considered when selecting biosorbent for water treatment. Care should be taken to ensure that the integrity of the biosorbent is intact after desorption and regeneration. It has become apparent that selecting the most suitable system for desorption is a challenging task, which requires a detailed understanding of the biosorbent as well as the PACs.

3. Cost Evaluation

Estimating the cost of biosorption and biosorbent is not an easy task, and it is not often reported. Process treatment, transportation, energy consumption, maintenance, process optimization, regeneration, disposal and desorption are factors considered when making an estimate. It depends on the nature of water or wastewater to be treated, as well as volume. However, capital expenditure and running cost will depend on the type and size of the treatment plant. It is better to make use of waste as feedstock for biosorbent production to minimize process cost. Wastes generated from farm produce, domestic and industrial wastes such as bacterial waste from fermentation industries, fungal wastes from food processing industries and sludge from other processing industries are applicable in biosorbent production. Waste disposal is a major problem, therefore making use of these wastes solves the environmental problem and at the same time helps reduce the cost of producing biosorbents for water treatment. One factor that increases production cost is pretreatment given to feedstock. Some of these materials require some pretreatments before processing, and the extra pretreatment may increase production cost. However, it is important to consider an effective but cheap and affordable treatment. It is vital to ensure that the treatment facility is close to the source of waste to minimize cost. Disposal cost should be factored into the cost of biosorption because once the biosorbent is completely utilized in a repeated cycle, it has to be replaced, although the spent biosorbent might find application in other fields like in the production of particleboard, cement, biogas, etc.

Cost evaluation depends on several factors, which makes it difficult to generalize. Therefore, the cost may vary from one biosorbent to the other depending on composition. This will also include whether it is sourced from waste or neat feedstock. Biosorption cost will also depend on the capacity and behavior of the biosorbent used. For example, if the removal process is fast and completed within a short time, less energy is consumed, unlike a biosorbent with slow uptake and long sorption time. The more the energy consumption, the higher the cost of production. The biosorption process is economically feasible compared to other methods such as reverse osmosis, electrodialysis, advance oxidation and electrothermal methods, which cost about US $450 per million liters whereas, depending on the type of biosorbent, the cost of water treatment per million liters is estimated as US $10–US $200 [163]. Use of chemicals is reduced, and when microorganisms are used, they can mineralize and degrade the PACs to forms that are readily adsorbed or wholly converted to CO_2 and H_2O. Different costs have been reported in the literature, for example, bagasse fly ash costs US $0.02 per kg [164], biochar costs US $2.65 per kg [165], chitosan-based biosorbent costs US $8–10 per kg [166] and kaolinite clay costs $0.005–0.46 per kg. The price may change depending on several economic factors.

Future Perspectives for Biosorption

With the current challenge of how to get rid of PACs in the environment, the government needs to develop a policy that will regulate the use of pharmaceutical products. Most countries do not have functional regulations to monitor and control the emergence of PACs in water. Moreover, current emerging PACs in water were not envisaged to occur in the water system; therefore, most of the currently used techniques for water treatment were not developed to cater for them. There is a need to develop efficient technologies that will help remove PACs entirely. However, biosorption has this advantage over other known methods. Nonetheless, most reported works on biosorption were laboratory-based and not on a large scale, which should be an area of focus. For biosorption to gain full operation, there is a need to conduct sufficient research on its use on a large scale for industrial purposes. To apply biosorption in real large-scale situation, there is a need to understand the response of biosorbent to operating parameters such as pH, temperature, particle size and load on a large scale. Most published works were conducted on a small scale in the laboratory. Therefore, it is crucial to know whether the biosorbent will behave differently when subjected to these parameters on a large scale. This information is currently missing.

The fact that it is cheaper to produce biosorbents from waste is an indication that there would be a socio-economic viability for large tons of waste generated from bio-based industrial processes. The waste generated from agriculture is massive. Investing in the conversion of such waste to biosorbents will create jobs and a new avenue for developing biosorption to full industrial scale, although there is the possibility of competition between using agricultural wastes as biosorbent and as feedstock for biogas production. However, the biosorbent can still be used for biogas production after it is completely used up and has repeatedly completed its utilization cycle, which makes it a win-win situation. Even though biosorbents can find use in biogas production, it is crucial to develop good disposal practice for spent biosorbents. It may also be essential to develop other ways of making use of spent biosorbents. Microorganisms as biosorbents have shown exciting results in biosorption, biodegradation and bioaccumulation of PACs. Care must be taken when using living organisms not to create strains that would be resistant by mutating. It is important not to end up creating a new problem while trying to solve environmental challenges. The possibility of using microorganisms creates a new area of research of screening for novel strains of bacteria, fungi and algae that will be useful and efficient in wastewater purification. There is a need to pay more attention to understanding the mechanism by which these microorganisms remove PACs from water. The use of bio-composite has proven very useful for the removal of PACs in water, but the complexity and chemical reagent involved in its production increases cost. There is a need to research more on reducing production cost by reducing production steps and using simple and cheap chemical reagents for bio-composite preparation.

4. Conclusions

This review considers the role of chemically modified biosorbent in removing PACs in water. It identified a few biosorbents and their role. It revealed that modification of biosorbents is vital to improving their capacity. Most biosorbents are prepared from waste, which plays a crucial role in cost reduction. Bio-composites exhibited better prospect as biosorbents when compared with other biosorbents because they contain two or more distinct materials brought together to produce a new material with improved performance better than individual constituent materials. During the sorption process, pH plays an important role; most of the sorption processes were pH-dependent. Use of living microorganisms showed that, apart from biosorption, the organisms are capable of bioaccumulating and biodegrading PACs. The majority of the sorption processes reported followed the pseudo-second-order model and can be described by the Langmuir isotherm model. Production of biosorbents was considered relatively cheap, efficient, and a promising means of removing PACs in the water system. Despite the numerous studies of biosorption, most of the works reported were laboratory-based (small-scale), and there is a need to conduct large-scale studies on the biosorption process for removing PACs in water.

Funding: This research received no external funding

Acknowledgments: Thanks for the support from the Department of Chemical Sciences, Redeemer's University.

Conflicts of Interest: There is no conflict of interest.

References

1. Tran, N.H.; Gin, K.Y.H. Occurrence and removal of pharmaceuticals, hormones, personal care products, and endocrine disrupters in a full-scale water reclamation plant. *Sci. Total Environ.* **2017**, *599–600*, 1503–1516.
2. Kostich, M.S.; Batt, A.L.; Lazorchak, J.M. Concentrations of prioritized pharmaceuticals in effluents from 50 large wastewater treatment plants in the US and implications for risk estimation. *Environ. Pollut.* **2014**, *184*, 354–359. [PubMed]
3. Lessa, E.F.; Nunes, M.L.; Fajardo, A.R. Chitosan/waste coffee-grounds composite: An efficient and eco-friendly adsorbent for removal of pharmaceutical contaminants from water. *Carbohydr. Polym.* **2018**, *189*, 257–266. [PubMed]
4. Larsson, D.G.J. Pollution from drug manufacturing: Review and perspectives. *Philos. Trans. R. Soc. B Biol. Sci.* **2014**, *369*, 1656. [CrossRef] [PubMed]
5. Yan, Z.; Lu, G.; Liu, J.; Jin, S. An integrated assessment of estrogenic contamination and feminization risk in fish in Taihu Lake, China. *Ecotoxicol. Environ. Saf.* **2012**, *84*, 334–340. [CrossRef] [PubMed]
6. Ikhwanuddin, M.; Bahar, H.; Ma, H.; Manan, H. Effect of estrogen hormone, 17β-estradiol on feminization of banana shrimp, *Penaeus merguiensis* (de Man, 1888) postlarvae and the identification of the age of external sex differentiation. *Aquac. Rep.* **2019**, *13*, 100177. [CrossRef]
7. Porseryd, T.; Larsson, J.; Kellner, M.; Bollner, T.; Dinnetz, P.; Hallstrom, I.P. Altered non-reproductive behavior and feminization caused by developmental exposure to 17α-ethinylestradiol persist to adulthood in three-spined stickleback (*Gasterosteus aculeatus*). *Aquatic Toxicol.* **2019**, *207*, 142–152. [CrossRef]

8. Quesada, H.B.; Baptista, A.T.A.; Cusioli, L.F.; Seibert, D.; Bezerra, C.O.; Bergamasco, R. Surface water pollution by pharmaceuticals and an alternative of removal by low-cost adsorbents: A review. *Chemosphere* **2019**, *222*, 766–780. [CrossRef]
9. Hossain, A.; Nakamichi, S.; Habibullah-Al-Mamun, M.; Tani, K.; Masunaga, S.; Matsuda, H. Occurrence and ecological risk of pharmaceuticals in river surface water of Bangladesh. *Environ. Res.* **2018**, *165*, 258–266. [CrossRef]
10. Asghar, M.A.; Zhu, Q.; Sun, S.; Peng, Y.; Shuai, Q. Suspect screening and target quantification of human pharmaceutical residues in the surface water of Wuhan, China, using UHPLC-Q-Orbitrap HRMS. *Sci. Total Environ.* **2018**, *635*, 828–837. [CrossRef]
11. Bean, T.G.; Rattner, B.A.; Lazarus, R.S.; Day, D.D.; Burket, S.R.; Brooks, B.W.; Haddad, S.P.; Bowerman, W.W. Pharmaceuticals in water, fish and osprey nestlings in Delaware River and Bay. *Environ. Pollut.* **2018**, *232*, 533–545. [CrossRef] [PubMed]
12. Rivera-Jaimes, J.A.; Postigo, C.; Melgoza-Aleman, R.M.; Acena, J.; Barcelo, D.; Lopez de Alda, M. Study of pharmaceuticals in surface and wastewater from Cuernavaca, Morelos, Mexico: Occurrence and environmental risk assessment. *Sci. Total Environ.* **2018**, *613–614*, 1263–1274. [CrossRef] [PubMed]
13. Fick, J.; Söderström, H.; Lindberg, R.H.; Phan, C.; Tysklind, M.; Larsson, D.G.J. Contamination of surface, ground, and drinking water from pharmaceutical production. *Environ. Toxicol. Chem.* **2009**, *28*, 2522–2527. [CrossRef] [PubMed]
14. Azanu, D.; Styrishave, B.; Darko, G.; Weisser, J.J.; Abaidoo, R.C. Occurrence and risk assessment of antibiotics in water and lettuce in Ghana. *Sci. Total Environ.* **2018**, *622–623*, 293–305. [CrossRef] [PubMed]
15. Madikizela, L.M.; Tavengwa, N.T.; Chimuka, L. Status of pharmaceuticals in African water bodies: Occurrence, removal and analytical methods. *J. Environ. Manag.* **2017**, *193*, 211–220.
16. Lindim, C.; van Gils, J.; Georgieva, D.; Mekenyan, O.; Cousins, I.T. Evaluation of human pharmaceutical emissions and concentrations in Swedish river basins. *Sci. Total Environ.* **2016**, *572*, 508–519.
17. Carmona, E.; Andreu, V.; Pico, Y. Occurrence of acidic pharmaceuticals and personal care products in Turia River Basin: From waste to drinking water. *Sci. Total Environ.* **2014**, *484*, 53–63.
18. Burns, E.E.; Carter, L.J.; Kolpin, D.W.; Thomas-Oates, J.; Boxall, A.B.A. Temporal and spatial variation in pharmaceutical concentrations in an urban river system. *Water Res.* **2018**, *137*, 72–85. [CrossRef]
19. Praveena, S.M.; Shaifuddin, S.N.M.; Sukiman, S.; Nasir, F.A.M.; Hanafi, Z.; Kamarudin, N.; Ismail, T.H.T.; Aris, A.Z. Pharmaceuticals residues in selected tropical surface water bodies from Selangor (Malaysia): Occurrence and potential risk assessments. *Sci. Total Environ.* **2018**, *642*, 230–240.
20. Matongo, S.; Birungi, G.; Moodley, B.; Ndungu, P. Pharmaceutical residues in water and sediment of msunduzi river, KwaZulu-Natal, South Africa. *Chemosphere* **2015**, *134*, 133–140. [CrossRef]
21. Pereira, A.M.P.T.; Silva, L.J.G.; Laranjeiro, C.S.M.; Meisel, L.M.; Lino, C.M.; Pena, A. Human pharmaceuticals in Portuguese rivers: The impact of water scarcity in the environmental risk. *Sci. Total Environ.* **2017**, *609*, 1182–1191. [PubMed]
22. Caban, M.; Lis, E.; Kumirska, J.; Stepnowski, P. Determination of pharmaceutical residues in drinking water in Poland using a new SPE-GC-MS(SIM) method based on Speedisk extraction disks and DIMETRIS derivatization. *Sci. Total Environ.* **2015**, *538*, 402–411. [CrossRef] [PubMed]
23. Mutiyar, P.K.; Gupta, S.K.; Mittal, A.K. Fate of pharmaceutical active compounds (PhACs) from River Yamuna, India: An ecotoxicological risk assessment approach. *Ecotoxicol. Environ. Saf.* **2018**, *150*, 297–304. [CrossRef]
24. Silva, A.; Delerue-Matos, C.; Figueiredo, S.A.; Freitas, O.M. The use of algae and fungi for removal of pharmaceuticals by bioremediation and biosorption processes: A Review. *Water* **2019**, *11*, 1555.
25. Bottoni, P.; Caroli, S.; Caracciolo, A.B. Pharmaceuticals as priority water contaminants. *Toxicol. Environ. Chem.* **2010**, *92*, 549–565. [CrossRef]
26. Akhtar, J.; Amin, N.A.S.; Shahzad, K. A review on removal of pharmaceuticals from water by adsorption. *Desalin. Water Treat.* **2016**, *57*, 12842–12860. [CrossRef]
27. Hokkanen, S.; Bhatnagar, A.; Sillanpää, M. A review on modification methods to cellulose-based adsorbents to improve adsorption capacity. *Water Res.* **2016**, *91*, 156–173. [CrossRef]
28. Xu, Y.; Liu, T.; Zhang, Y.; Ge, F.; Steel, R.M.; Sun, L. Advances in technologies for pharmaceuticals and personal care products removal. *J. Mater. Chem. A* **2017**, *5*, 12001–12014.

29. Silva, C.P.; Jaria, G.; Otero, M.; Esteves, V.I.; Calisto, V. Waste-based alternative adsorbents for the remediation of pharmaceutical contaminated waters: Has a step forward already been taken? *Bioresour. Technol.* **2018**, *250*, 888–901.
30. Adewuyi, A.; Oderinde, R.A. Chemically modified vermiculite clay: A means to removing emerging contaminant from polluted water system in developing nation. *Polym. Bull.* **2019**, *76*, 4967–4989.
31. Lach, J. Adsorption of chloramphenicol on commercial and modified activated carbons. *Water* **2019**, *11*, 1141. [CrossRef]
32. Hu, Y.; Pan, C.; Zheng, X.; Liu, S.; Hu, F.; Xu, L.; Xu, G.; Peng, X. Removal of ciprofloxacin with aluminum-pillared kaolin sodium alginate beads (CA-Al-KABs): Kinetics, isotherms, and BBD model. *Water* **2020**, *12*, 905. [CrossRef]
33. Rodriguez, A.Z.; Wang, H.; Hu, L.; Zhang, Y.; Xu, P. Treatment of produced water in the permian basin for hydraulic fracturing: Comparison of different coagulation processes and innovative filter media. *Water* **2020**, *12*, 770. [CrossRef]
34. Zhang, G.; Yang, Y.; Lu, Y.; Chen, Y.; Li, W.; Wang, S. Effect of heavy metal Ions on steroid estrogen removal and transport in SAT using DLLME as a detection method of steroid estrogen. *Water* **2020**, *12*, 589. [CrossRef]
35. Jiang, M.; Yang, W.; Zhang, Z.; Yang, Z.; Wang, Y. Adsorption of three pharmaceuticals on two magnetic ion-exchange resins. *J. Environ. Sci.* **2015**, *31*, 226–234.
36. Nghiem, L.D.; Schafer, A.I.; Elimelech, M. Removal of natural hormones by nanofiltration membranes: Measurement, modeling, and mechanisms. *Environ. Sci. Technol.* **2004**, *15*, 1888–1896. [CrossRef] [PubMed]
37. Rana, D.; Scheier, B.; Narbaitz, R.M.; Matsuura, T.; Tabe, S.; Jasim, S.Y.; Khulbe, K.C. Comparison of cellulose acetate (CA) membrane and novel CA membranes containing surface modifying macromolecules to remove pharmaceutical and personal care product micropollutants from drinking water. *J. Membr. Sci.* **2012**, *409*, 346–354.
38. Rajapaksha, A.U.; Premarathna, K.S.D.; Gunarathne, V.; Ahmed, A.; Vithanage, M. Sorptive removal of pharmaceutical and personal care products from water and wastewater. In *Pharmaceuticals and Personal Care Products: Waste Management and Treatment Technology*; Butterworth–Heinemann, Elsevier: Oxford, UK, 2019; pp. 213–238.
39. Feng, Y.; Wang, C.; Liu, J.; Zhang, Z. Electrochemical degradation of 17-alphaethinylestradiol (EE2) and estrogenic activity changes. *J. Environ. Monit.* **2010**, *12*, 404–408. [CrossRef]
40. Sires, I.; Brillas, E. Remediation of water pollution caused by pharmaceutical residues based on electrochemical separation and degradation technologies: A review. *Environ. Int.* **2012**, *40*, 212–229. [CrossRef]
41. Méndez-Arriaga, F.; Torres-Palma, R.; Pétrier, C.; Esplugas, S.; Gimenez, J.; Pulgarin, C. Ultrasonic treatment of water contaminated with ibuprofen. *Water Res.* **2008**, *42*, 4243–4248. [CrossRef]
42. Ciríaco, L.; Anjo, C.; Correia, J.; Pacheco, M.; Lopes, A. Electrochemical degradation of ibuprofen on Ti/Pt/PbO 2 and Si/BDD electrodes. *Electrochim. Acta* **2009**, *54*, 1464–1472. [CrossRef]
43. Madhavan, J.; Grieser, F.; Ashokkumar, M. Combined advanced oxidation processes for the synergistic degradation of ibuprofen in aqueous environments. *J. Hazard. Mater.* **2010**, *178*, 202–208. [CrossRef] [PubMed]
44. Salaeh, S.; Perisic, D.J.; Biosic, M.; Kusic, H.; Babic, S.; Stangar, U.L.; Dionysiou, D.D.; Bozic, A.L. Diclofenac removal by simulated solar assisted photocatalysis using TiO_2-based zeolite catalyst; mechanisms, pathways and environmental aspects. *Chem. Eng. J.* **2016**, *304*, 289–302. [CrossRef]
45. Hasan, Z.; Jhung, S.H. Removal of hazardous organics from water using metalorganic frameworks (MOFs): Plausible mechanisms for selective adsorptions. *J. Hazard. Mater.* **2015**, *283*, 329–339. [CrossRef]
46. Fomina, M.; Gadd, G.M. Biosorption: Current perspectives on concept, definition and application. *Bioresour. Technol.* **2014**, *160*, 3–14. [CrossRef]
47. Worch, E. *Adsorption Technology in Water Treatment*; de Gruyter, W., Ed.; Deutscher Kunstverlag: Berlin, Germany, 2012; p. 332.
48. Rostamian, R.; Behnejad, H. A comprehensive adsorption study and modeling of antibiotics as a pharmaceutical waste by graphene oxide nanosheets. *Ecotoxicol. Environ. Saf.* **2018**, *147*, 117–123. [CrossRef]
49. Basu, S.; Balakrishnan, M. Polyamide thin film composite membranes containing ZIF-8 for the separation of pharmaceutical compounds from aqueous streams. *Sep. Purif. Technol.* **2017**, *179*, 118–125. [CrossRef]

50. Qian, K.; Kumar, A.; Zhang, H.; Bellmer, D.; Huhnke, R. Recent advances in utilization of biochar. *Renew. Sustain. Energy Rev.* **2015**, *42*, 1055–1064. [CrossRef]
51. Šolic, M.; Maletic, S.; Isakovski, M.K.; Nikic, J.; Watson, M.; Kónya, Z.; Trickovic, J. Comparing the adsorption performance of multiwalled carbon nanotubes oxidized by varying degrees for removal of low levels of copper, nickel and chromium (VI) from aqueous solutions. *Water* **2020**, *12*, 723. [CrossRef]
52. Vijayaraghavan, K.; Yun, Y.S. Bacterial biosorbents and biosorption. *Biotechnol. Adv.* **2008**, *26*, 266–291. [CrossRef]
53. Tadkaew, N.; Hai, F.I.; Mcdonald, J.A.; Khan, S.J.; Nghiem, L.D. Removal of trace organics by MBR treatment: The role of molecular properties. *Water Res.* **2011**, *45*, 2439–2451. [CrossRef] [PubMed]
54. Adewuyi, A.; Pereira, F.V. Underutilized *Luffa cylindrica* sponge: A local bio-adsorbent for the removal of Pb (II) pollutant from water system. *Beni-Suef Uni. J. Basic Appl. Sci.* **2017**, *6*, 118–126.
55. Ngah, W.S.W.; Hanafiah, M.A.K.M. Removal of heavy metal ions from wastewater by chemically modified plant wastes as adsorbents: A review. *Bioresour. Technol.* **2008**, *99*, 3935–3948.
56. Ali, M.E.M.; Abd El-Aty, A.M.; Badawy, M.I.; Ali, R.K. Removal of pharmaceutical pollutants from synthetic wastewater using chemically modified biomass of green alga Scenedesmus obliquus. *Ecotoxicol. Environ. Saf.* **2018**, *151*, 144–152. [PubMed]
57. Onal, Y.; Akmil-Basar, C.; Sarıcı-Ozdemir, C. Elucidation of the naproxen sodium adsorption onto activated carbon prepared from waste apricot: Kinetic, equilibrium and thermodynamic characterization. *J. Hazard. Mater.* **2007**, *148*, 727–734. [PubMed]
58. Cazetta, A.L.; Martins, A.C.; Pezoti, O.; Bedin, K.C.; Beltrame, K.K.; Asefa, T.; Almeida, V.C. Synthesis and application of N–S-doped mesoporous carbon obtained from nanocasting method using bone char as heteroatom precursor and template. *Chem. Eng. J.* **2016**, *300*, 54–63.
59. Rosli, N.; Ngadi, N.; Azman, M.A. Synthesis of modified spent tea for aspirin adsorption in aqueous solution. *Inter. J. Rec. Technol. Eng.* **2019**, *8*, 531–534.
60. Mestre, A.S.; Pires, J.; Nogueira, J.M.F.; Carvalho, A.P. Activated carbons for the adsorption of ibuprofen. *Carbon* **2007**, *45*, 1979–1988. [CrossRef]
61. Baccar, R.; Sarrà, M.; Bouzid, J.; Feki, M.; Blánquez, P. Removal of pharmaceutical compounds by activated carbon prepared from agricultural by-product. *Chem. Eng. J.* **2012**, *211–212*, 310–317. [CrossRef]
62. Mondal, S.; Aikat, K.; Halder, G. Biosorptive uptake of ibuprofen by chemically modified Parthenium hysterophorus derived biochar: Equilibrium, kinetics, thermodynamics and modeling. *Ecol. Eng.* **2016**, *92*, 158–172. [CrossRef]
63. Essandoh, M.; Kunwar, B.; Pittman, C.U.; Mohan, D.; Mlsna, T. Sorptive removal of salicylic acid and ibuprofen from aqueous solutions using pine wood fast pyrolysis biochar. *Chem. Eng. J.* **2015**, *265*, 219–227. [CrossRef]
64. Mestre, A.S.; Bexiga, A.S.; Proença, M.; Andrade, M.; Pinto, M.L.; Matos, I.; Fonseca, I.M.; Carvalho, A.P. Activated carbons from sisal waste by chemical activation with K_2CO_3: Kinetics of paracetamol and ibuprofen removal from aqueous solution. *Bioresour. Technol.* **2011**, *102*, 8253–8260. [CrossRef] [PubMed]
65. Ribeiro, A.V.F.N.; Belisário, M.; Galazzi, R.M.; Balthazar, D.C.; Pereira, M.G.; Ribeiro, J.N. Evaluation of two bioadsorbents for removing paracetamol from aqueous media. *Electron. J. Biotechnol.* **2011**, *14*, 1–10.
66. Ornek, A.; Ozacar, M.; Sengil, I.A. Adsorption of Pb(II) onto formaldehyde or sulphuric acid treated acorn waste: Equilibrium and kinetic studies. *Biochem. Eng. J.* **2007**, *37*, 192–200. [CrossRef]
67. Saka, C.; Sahin, O.; Kucuk, M.M. Applications on agricultural and forest waste adsorbentsfor the removal of lead (II) from contaminated waters. *Int. J. Environ. Sci. Technol.* **2012**, *9*, 379–394. [CrossRef]
68. Ramachandran, V.; Pujari, N.; Matey, T.; Kulkarni, S. Enzymatic hydrolysis of cassava using wheat seedlings. *Int. J. Sci. Eng. Technol. Res.* **2014**, *3*, 1216–1219.
69. Kulkarni, S.J. Use of biotechnology for synthesis of various products from different feedstocks-a review. *Int. J. Adv. Res. Bio-Technol.* **2014**, *2*, 1–3.
70. Rajapaksha, A.U.; Vithanage, M.; Ahmad, M.; Seo, D.C.; Cho, J.S.; Lee, S.E.; Lee, S.S.; Ok, Y.S. Enhanced sulfamethazine removal by steam-activated invasive plant-derived biochar. *J. Hazard. Mater.* **2015**, *290*, 43–50.
71. Chen, Y.; Wang, F.; Duan, L.; Yang, H.; Gao, J. Tetracycline adsorption onto rice husk ash, an agricultural waste: Its kinetic and thermodynamic studies. *J. Mol. Liq.* **2016**, *222*, 487–494. [CrossRef]

72. Bernardo, M.; Rodrigues, S.; Lapa, N.; Matos, I.; Lemos, F.; Batista, M.K.S.; Carvalho, A.P.; Fonseca, I. High efficacy on diclofenac removal by activated carbon produced from potato peel waste. *Int. J. Environ. Sci. Technol.* **2016**, *13*, 1989–2000. [CrossRef]
73. Pouretedal, H.R.; Sadegh, N. Effective removal of amoxicillin, cephalexin, tetracycline and penicillin G from aqueous solutions using activated carbon nanoparticles prepared from vine wood. *J. Water Process Eng.* **2014**, *1*, 64–73. [CrossRef]
74. Ahmed, M.B.; Zhou, J.L.; Ngo, H.H.; Guo, W.; Johir, M.A.H.; Sornalingam, K. Single and competitive sorption properties and mechanism of functionalized biochar for removing sulfonamide antibiotics from water. *Chem. Eng. J.* **2017**, *311*, 348–358.
75. Wang, H.; Chu, Y.; Fang, C.; Huang, F.; Song, Y.; Xue, X. Sorption of tetracycline on biochar derived from rice straw under different temperatures. *PLoS ONE* **2017**, *12*, e0182776.
76. Zhang, H.; Wang, Z.; Li, R.; Guo, J.; Li, Y.; Zhu, J.; Xie, X. TiO_2 supported on reed straw biochar as an adsorptive and photocatalytic composite for the efficient degradation of sulfamethoxazole in aqueous matrices. *Chemosphere* **2017**, *185*, 351–360. [CrossRef] [PubMed]
77. El-Shafey, E.S.I.; Al-Lawati, H.; Al-Sumri, A.S. Ciprofloxacin adsorption from aqueous solution onto chemically prepared carbon from date palm leaflets. *J. Environ. Sci.* **2012**, *24*, 1579–1586.
78. Balarak, D.; Mostafapour, F.K. Canola residual as a biosorbent for antibiotic metronidazole removal. *Pharm. Chem. J.* **2016**, *3*, 12–17.
79. N'diaye, A.D.; Bollahi, M.A.; Kankou, M.S.A. Sorption of paracetamol from aqueous solution using groundnut shell as a low cost sorbent. *J. Mater. Environ. Sci.* **2019**, *10*, 553–562.
80. Aziz, S.S.; Mushtaq, S.; Begum, N. Adsorption studies of acetic acid removal from waste water using seeds of *Brassica nigra*. *Int. J. Eng. Res. Appl.* **2017**, *7*, 1–3.
81. Silva, B.; Martins, M.; Rosca, M.; Rocha, V.; Lago, A.; Neves, I.C.; Tavares, T. Waste-based biosorbents as cost-effective alternatives to commercial adsorbents for the retention of fluoxetine from water. *Sep. Purif. Technol.* **2020**, *235*, 116–139.
82. Martins, A.C.; Pezoti, O.; Cazetta, A.L.; Bedin, K.C.; Yamazaki, D.A.S.; Bandoch, G.F.G.; Asefa, T.; Visentainer, J.V.; Almeida, V.C. Removal of tetracycline by NaOH-activated carbon produced from macadamia nut shells: Kinetic and equilibrium studies. *Chem. Eng. J.* **2015**, *260*, 291–299. [CrossRef]
83. Kumar, A.; Sharma, G.; Naushad, M.; Al-Muhtaseb, A.; Hira, I.; Ahamad, T.; Kumar, A.; Ghfar, A.A.; Stadler, F.J. Visible photodegradation of ibuprofen and 2,4-D in simulated waste water using sustainable metal free-hybrids based on carbon nitride and biochar. *J. Environ. Manag.* **2019**, *231*, 1164–1175. [CrossRef]
84. Wang, F.; Yang, B.; Wang, H.; Song, Q.; Tan, F.; Cao, Y. Removal of ciprofloxacin from aqueous solution by a magnetic chitosan grafted graphene oxide composite. *J. Mol. Liq.* **2016**, *222*, 188–194.
85. Paunovic, O.; Pap, S.; Maletic, S.; Taggart, M.A.; Boskovic, N.; Sekulic, M.T. Ionisable emerging pharmaceutical adsorption onto microwave functionalised biochar derived from novel lignocellulosic waste biomass. *J. Colloid Interface Sci.* **2019**, *547*, 350–360. [CrossRef]
86. Villaescusa, I.; Fiol, N.; Poch, J.; Bianchi, A.; Bazzicalupi, C. Mechanism of paracetamol removal by vegetable wastes: The contribution of π-π interactions, hydrogen bonding and hydrophobic effect. *Desalination* **2011**, *270*, 135–142. [CrossRef]
87. Yusoff, N.A.; Ngadi, N.; Alias, H.; Jusoh, M. Chemically treated chicken bone waste as an efficient adsorbent for removal of acetaminophen. *Chem. Eng. Trans.* **2017**, *56*, 925–930.
88. Khazri, H.; Ghorbel-Abid, I.; Kalfat, R.; Trabelsi-Ayadi, M. Extraction of clarithromycin and atenolol by cuttlefish bone powder. *Environ. Technol.* **2018**, *38*, 2662–2668. [CrossRef]
89. Benjedim, S.; Romero-Cano, L.A.; Pérez-Cadenas, A.F.; Bautista-Toledo, M.I.; Lotfi, E.; Carrasco-Marín, F. Removal of emerging pollutants present in water using an E-coli biofilm supported onto activated carbons prepared from argan wastes: Adsorption studies in batch and fixed bed. *Sci. Total Environ.* **2020**, *720*, 137491. [CrossRef]
90. Adewuyi, A.; Göpfert, A.; Adewuyi, O.A.; Wolff, T. Adsorption of 2-chlorophenol onto the surface of underutilized seed of *Adenopus breviflorus*: A potential means of treating waste water. *J. Environ. Chem. Eng.* **2016**, *4*, 664–672. [CrossRef]
91. Kizilkaya, B.; Tekinay, A.A.; Dilgin, Y. Adsorption and removal of Cu (II) ions from aqueous solution using pretreated fish bones. *Desalination* **2010**, *264*, 37–47.

92. Dahiya, S.; Tripathi, R.M.; Hegde, A.G. Biosorption of lead and copper from aqueous solutions by pre-treated crab and arca shell biomass. *Bioresour. Technol.* **2008**, *99*, 179–187. [CrossRef]
93. Ojedokun, A.T.; Bello, O.S. Sequestering heavy metals from wastewater using cow dung. *Water Resour. Ind.* **2016**, *13*, 7–13. [CrossRef]
94. Vasanthakumar, K.; Bhagavanalu, D.V.S. Adsorption of basic dye from its aqueous solution on to bio-organic waste. *J. Ind. Pollut. Control* **2003**, *19*, 20–28.
95. El Haddad, M.; Mamouni, R.; Slimani, R.; Saffaj, N.; Ridaoui, M.; ElAntri, S.; Lazar, S. Adsorptive removal of reactive yellow 84 dye from aqueous solutions onto animal bone meal. *J. Mater. Environ. Sci.* **2012**, *3*, 1019–1026.
96. Nworu, J.S.; Enemose, E.A.; Osideru, O.O.; Emmanuel, O.A. Efficiency of animal (Cow, Donkey, Chicken and Horse) bones, in removal of hexavalent chromium from aqueous solution as a low cost adsorbent. *Am. J. Appl. Chem.* **2019**, *7*, 1–9.
97. Banat, F.A.; Al-Asheh, S. The use of human hair waste as a phenol biosorbent. *Adsorp. Sci. Technol.* **2001**, *19*, 599–608. [CrossRef]
98. Volesky, B.; Schiewer, S. Biosorption of metals. In *Encyclopedia of Bioprocess Technology*; Flickinger, M., Drew, S.W., Eds.; Wiley: New York, NY, USA, 1999; pp. 433–453.
99. Aydin, S. Enhanced biodegradation of antibiotic combinations via the sequential treatment of the sludge resulting from pharmaceutical wastewater treatment using white-rot fungi *Trametes versicolor* and *Bjerkandera adusta*. *Appl. Microbiol. Biotechnol.* **2016**, *100*, 6491–6499. [CrossRef]
100. Doyle, R.J.; Matthews, T.H.; Streips, U.N. Chemical basis for selectivity of metal ions by the Bacillus subtilis cell wall. *J. Bacteriol.* **1980**, *143*, 471–480. [CrossRef]
101. Phoenix, V.R.; Martinez, R.E.; Konhauser, K.O.; Ferris, F.G. Characterization and implications of the cell surface reactivity of Calothrixsp. strain KC97. *Appl. Environ. Microbiol.* **2002**, *68*, 4827–4834. [CrossRef]
102. Kazy, S.K.; Das, S.K.; Sar, P. Lanthanum biosorption by a Pseudomonassp.: Equilibrium studies and chemical characterization. *J. Ind. Microbiol. Biotechnol.* **2006**, *33*, 773–783. [CrossRef]
103. Vannela, R.; Verma, S.K. Cu^{2+} removal and recovery by SpiSORB: Batch stirred and up-flow packed bed columnar reactor systems. *Bioprocess Biosyst. Eng.* **2006**, *29*, 7–17. [CrossRef]
104. Vijayaraghavan, K.; Han, M.H.; Choi, S.B.; Yun, Y.S. Biosorption of reactive black 5 by *Corynebacterium glutamicum* biomass immobilized in alginate and polysulfone matrices. *Chemosphere* **2007**, *68*, 1838–1845. [CrossRef]
105. Vijayaraghavan, K.; Yun, Y.S. Chemical modification and immobilization of *Corynebacterium glutamicum* for biosorption of reactive black 5 from aqueous solution. *Ind. Eng. Chem. Res.* **2007**, *46*, 608–617. [CrossRef]
106. Martins, M.; Sanches, S.; Pereira, I.A.C. Anaerobic biodegradation of pharmaceutical compounds: New insights into the pharmaceutical-degrading bacteria. *J. Hazard. Mater.* **2018**, *357*, 289–297.
107. Wang, L.; Qiang, Z.; Li, Y.; Ben, W. An insight into the removal of fluoroquinolones in activated sludge process: Sorption and biodegradation characteristics. *J. Environ. Sci.* **2017**, *56*, 263–271. [CrossRef]
108. Sun, H.; Wang, T.; Yang, Z.; Yu, C.; Wu, W. Simultaneous removal of nitrogen and pharmaceutical and personal care products from the effluent of waste water treatment plants using aerated solid-phase denitrification system. *Bioresour. Technol.* **2019**, *287*, 121389.
109. Rana, R.S.; Singh, P.; Kandari, V.; Singh, R.; Dobhal, R.; Gupta, S. A review on characterization and bioremediation of pharmaceutical industries' wastewater: An Indian perspective. *Appl. Water Sci.* **2017**, *7*, 1–12. [CrossRef]
110. Yu, J.; Tong, M.; Sun, X.; Li, B. A simple method to prepare poly (amic acid)-modified biomass for enhancement of lead and cadmium adsorption. *Biochem. Eng. J.* **2007**, *33*, 126–133. [CrossRef]
111. Göksungur, Y.; Üren, S.; Güvenc, U. Biosorption of cadmium and lead ion by ethanol treated waste baker's yeast biomass. *Bioresour. Technol.* **2005**, *96*, 103–109. [CrossRef]
112. Dhankhar, R.; Hooda, A. Fungal biosorption—An alternative to meet the challenges of heavy metal pollution in aqueous solutions. *Environ. Technol.* **2011**, *32*, 467–491. [CrossRef]
113. Ridvan, S.; Nalan, Y.; Adil, D. Biosorption of cadmium, lead, mercury and arsenic ions by fungus Penicillium purpurogenum. *Sep. Sci. Technol.* **2003**, *39*, 2039–2053.
114. Gadd, G.M. Accumulation and transformation of metals by microorganisms. In *Biotechnology: A Multi-Volume Comprehensive Treatise, Vol. 10 Special Processes*; Rehm, H.J., Reed, G., Puhler, A., Stadler, P., Eds.; Wiley: Weinheim, Germany, 2001; pp. 225–264.

115. Becker, D.; Rodriguez-Mozaz, S.; Insa, S.; Schoevaart, R.; Barceloó, D.; de Cazes, M.; Belleville, M.P.; Sanchez-Marcano, J.; Misovic, A.; Oehlmann, J.; et al. Removal of endocrine disrupting chemicals in wastewater by enzymatic treatment with fungal laccases. *Org. Process Res. Dev.* **2017**, *21*, 480–491. [CrossRef]
116. Zhang, Y.; Geißen, S.U. Elimination of carbamazepine in a nonsterile fungal bioreactor. *Bioresour. Technol.* **2012**, *112*, 221–227. [CrossRef] [PubMed]
117. Rodriguez-Rodriguez, C.E.; García-Galán, M.J.; Blánquez, P.; Díaz-Cruz, M.S.; Barceló, D.; Caminal, G.; Vicent, T. Continuous degradation of a mixture of sulfonamides by Trametes versicolor and identification of metabolites from sulfapyridine and sulfathiazole. *J. Hazard. Mater.* **2012**, *213–214*, 347–354. [CrossRef] [PubMed]
118. Rodarte-Moralez, A.I.; Feijoo, G.; Moreira, M.T.; Lema, J.M. Operation of stirred tank reactors (STRs) and fixed-bed reactors (FBRs) with free and immobilized Phanerochaete chrysosporium for the continuous removal of pharmaceutical compounds. *Biochem. Eng. J.* **2012**, *66*, 38–45.
119. Lucas, D.; Castellet-Rovira, F.; Villagrasa, M.; Badia-Fabregat, M.; Barceló, D.; Vicent, T.; Caminal, G.; Sarràb, M.; Rodríguez-Mozaz, S. The role of sorption processes in the removal of pharmaceuticals by fungal treatment of wastewater. *Sci. Total Environ.* **2018**, *610–611*, 1147–1153.
120. González-Abradelo, D.; Pérez-Llano, Y.; Peidro-Guzmán, H.; Sánchez-Carbente, M.R.; Folch-Mallol, J.L.; Aranda, E.; Vaidyanathan, V.K.; Cabana, H.; Gunde-Cimerman, N.; Batista-García, R.A. First demonstration that ascomycetous halophilic fungi (*Aspergillus sydowii* and *Aspergillus destruens*) are useful in xenobiotic mycoremediation under high salinity conditions. *Bioresour. Technol.* **2019**, *279*, 287–296. [PubMed]
121. Vasiliadou, I.A.; Sanchez-Vazquez, R.; Molina, R.; Martínez, F.; Melero, J.A.; Bautista, L.F.; Iglesias, J.; Morales, G. Biological removal of pharmaceutical compounds using white-rotfungi with concomitant FAME production of the residual biomass. *J. Environ. Manag.* **2016**, *180*, 228–237. [CrossRef]
122. Badia-Fabregat, M.; Lucas, D.; Pereira, M.A.; Alves, M.A.; Pennanen, T.; Fritze, H.; Rodríguez-Mozaz, S.; Barceló, D.; Vicent, T.; Caminal, G. Continuous fungal treatment of non-sterile veterinary hospital effluent: Pharmaceuticals removal and microbial community assessment. *Appl. Microbiol. Biotechnol.* **2016**, *100*, 2401–2415. [CrossRef]
123. Becker, D.; Varela Della Giustina, S.; Rodriguez-Mozaz, S.; Schoevaart, R.; Barcelo, D.; de Cazes, M.; Belleville, M.P.; Sanchez-Marcano, J.; de Gunzburg, J.; Couillerot, O.; et al. Removal of antibiotics in wastewater by enzymatic treatment with fungal laccase—Degradation of compounds does not always eliminate toxicity. *Bioresour. Technol.* **2016**, *219*, 500–509.
124. Esterhuizen-Londt, M.; Schwartz, K.; Pflugmacher, S. Using aquatic fungi for pharmaceutical bioremediation: Uptake of acetaminophen by Mucor hiemalis does not result in an enzymatic oxidative stress response. *Fungal Biol.* **2016**, *120*, 1249–1257.
125. Palli, L.; Castellet-Rovira, F.; Péerez-Trujillo, M.; Caniani, D.; Sarrá-Adroguer, M.; Gori, R. Preliminary evaluation of *Pleurotus ostreatus* for the removal of selected pharmaceuticals from hospital wastewater. *Biotechnol. Prog.* **2017**, *33*, 1529–1537.
126. Pointing, S.B. Feasibility of bioremediation by white-rot fungi. *Appl. Microbiol. Biotechnol.* **2001**, *57*, 20–33.
127. Wijffels, R.H.; Kruse, O.; Hellingwerf, K.J. Potential of industrial biotechnology with cyanobacteria and eukaryotic microalgae. *Curr. Opin. Biotechnol.* **2013**, *24*, 405–413.
128. Xiong, J.Q.; Govindwar, S.; Kurade, M.B.; Paeng, K.J.; Roh, H.S.; Khan, M.A.; Jeon, B.H. Toxicity of sulfamethazine and sulfamethoxazole and their removal by a green microalga, Scenedesmus obliquus. *Chemosphere* **2019**, *218*, 551–558. [CrossRef]
129. Xiong, J.Q.; Kurade, M.B.; Jeon, B.H. Can microalgae remove pharmaceutical contaminants from water? *Trends Biotechnol.* **2017**, *36*, 30–44. [CrossRef]
130. Matamoros, V.; Uggetti, E.; García, J.; Bayona, J.M. Assessment of the mechanisms involved in the removal of emerging contaminants by microalgae from wastewater: A laboratory scale study. *J. Hazard. Mater.* **2016**, *301*, 197–205. [CrossRef]
131. Peng, F.Q.; Ying, G.G.; Yang, B.; Liu, S.; Lai, H.J.; Liu, Y.S.; Chen, Z.F.; Zhou, G.J. Biotransformation of progesterone and norgestrel by two freshwater microalgae (Scenedesmus obliquus and Chlorella pyrenoidosa): Transformation kinetics and products identification. *Chemosphere* **2014**, *95*, 581–588. [CrossRef]
132. González-Pleiter, M.; Gonzalo, S.; Rodea-Palomares, I.; Leganés, F.; Rosal, R.; Boltes, K.; Marco, E.; Fernández-Piñas, F. Toxicity of five antibiotics and their mixtures towards photosynthetic aquatic organisms: Implications for environmental risk assessment. *Water Res.* **2013**, *47*, 2050–2064. [CrossRef]

133. Xiong, J.Q.; Kurade, M.B.; Abou-Shanab, R.A.I.; Ji, M.K.; Choi, J.; Kim, J.O.; Jeon, B.H. Biodegradation of carbamazepine using freshwater microalgae *Chlamydomonas mexicana* and *Scenedesmus obliquus* and the determination of its metabolic fate. *Bioresour. Technol.* **2016**, *205*, 183–190. [CrossRef]
134. Ding, T.; Yang, M.; Zhang, J.; Lin, K.; Li, J.; Gan, J. Toxicity, degradation and metabolic fate of ibuprofen on freshwater diatom Naviculasp. *J. Hazard. Mater.* **2017**, *330*, 127–134.
135. Hom-Diaz, A.; Jaen-Gil, A.; Bello-Laserna, I.; Rodríguez-Mozaz, S.; Vincent, T.; Barceló, D.; Blánquez, P. Performance of a microalgal photobioreactor treating toilet wastewater: Pharmaceutically active compound removal and biomass harvesting. *Sci. Total Environ.* **2017**, *592*, 1–11. [CrossRef]
136. Escapa, C.; Coimbra, R.; Paniagua, S.; García, A.; Otero, M. Paracetamol and salicylic acid removal from contaminated water by microalgae. *J. Environ. Manag.* **2017**, *203*, 799. [CrossRef] [PubMed]
137. Amorim, C.L.; Moreira, I.S.; Maia, A.S.; Tiritan, M.E.; Castro, P.M.L. Biodegradation of ofloxacin, norfloxacin, and ciprofloxacin as single and mixed substrates by Labrys portucalensis F11. *Appl. Microbiol. Biotechnol.* **2014**, *98*, 3181–3190. [CrossRef] [PubMed]
138. Yang, S.; Hai, F.I.; Nghiem, L.D.; Nguyen, L.N.; Roddick, F.; Price, W.E. Removal of bisphenol a and diclofenac by a novel fungal membrane bioreactor operated under non-sterile conditions. *Int. Biodeterior. Biodegrad.* **2013**, *85*, 483–490. [CrossRef]
139. Zhang, L.; Xia, W.; Teng, B.; Liu, X.; Zhang, W. Zirconium cross-linked chitosan composite: Preparation, characterization and application in adsorption of Cr(VI). *Chem. Eng. J.* **2013**, *229*, 1–8. [CrossRef]
140. Rahim, M.; Haris, M.R.H.M. Application of biopolymer composites in arsenic removal from aqueous medium: A review. *J. Radiat. Res. Appl. Sci.* **2015**, *8*, 255–263. [CrossRef]
141. Karoui, S.; Ben, A.R.; Mougin, K.; Ghorbal, A.; Assadi, A.; Amrane, A. Synthesis of novel biocomposite powder for simultaneous removal of hazardous ciprofloxacin and methylene blue: Central composite design, kinetic and isotherm studies using Brouers-Sotolongo family models. *J. Hazard. Mater.* **2020**, *387*, 121675. [CrossRef]
142. Mashile, G.P.; Mpupa, A.; Nqombolo, A.; Dimpe, K.M.; Nomngongo, P.N. Recyclable magnetic waste tyre activated carbon-chitosan composite as an effective adsorbent rapid and simultaneous removal of methylparaben and propylparaben from aqueous solution and wastewater. *J. Water Process Eng.* **2020**, *33*, 101011. [CrossRef]
143. Li, Y.; Wang, Z.; Xie, X.; Zhu, J.; Li, R.; Qin, T. Removal of norfloxacin from aqueous solution by clay-biochar composite prepared from potato stem and natural attapulgite. *Colloids Surf. A* **2017**, *514*, 126–136. [CrossRef]
144. Wang, H.; Yuan, X.; Wu, Y.; Huang, H.; Peng, X.; Zeng, G.; Zhong, H.; Liang, J.; Ren, M.M. Graphene-based materials, fabrication, characterization and application for the decontamination of wastewater and waste gas and hydrogen storage/generation. *Adv. Colloid Interface Sci.* **2013**, *195–196*, 19–40. [CrossRef]
145. Zhang, S.; Dong, Y.; Yang, Z.; Yang, W.; Wu, J.; Dong, C. Adsorption of pharmaceuticals on chitosan-based magnetic composite particles with core-brush topology. *Chem. Eng. J.* **2016**, *304*, 325–334. [CrossRef]
146. Babel, S.; Kurniawan, T. A Low-cost adsorbents for heavy metals uptake from contaminated water: A review. *J. Hazard. Mater.* **2003**, *97*, 219–243. [CrossRef]
147. Srinivasan, R. Advances in application of natural clay and its composites in removal of biological, organic, and inorganic contaminants from drinking water. *Adv. Mater. Sci. Eng.* **2011**, *2011*, 1–17. [CrossRef]
148. Yao, Y.; Gao, B.; Fang, J.; Zhang, M.; Chen, H.; Zhou, Y.; Creamer, A.E.; Sun, Y.; Yang, L. Characterization and environmental applications of clay-biochar composites. *Chem. Eng. J.* **2014**, *242*, 136–143. [CrossRef]
149. Fosso-Kankeu, E.; Waanders, F.B.; Steyn, F.W. The preparation and characterization of clay-biochar composites for the removal of metal pollutants. In Proceedings of the Seventh International Conference on Latest Trends in Engineering & Technology, Irene, Pretoria, South Africa, 26–27 November 2015.
150. Wang, W.; Zheng, B.; Deng, Z.; Feng, Z.; Fu, L. Kinetics and equilibriums for adsorption of poly(vinyl alcohol) from aqueous solution onto natural bentonite. *Chem. Eng. J.* **2013**, *214*, 343–354. [CrossRef]
151. Kumar, A.S.K.; Kalidhasan, S.; Rajesh, V.; Rajesh, N. Application of cellulose-clay composite biosorbent toward the effective adsorption and removal of chromium from industrial wastewater. *Ind. Eng. Chem. Res.* **2012**, *51*, 58–69. [CrossRef]
152. Amin, M.F.M.; Heijman, S.G.J.; Rietveld, L.C. Clay–starch combination for micropollutants removal from wastewater treatment plant effluent. *Water Sci. Technol.* **2016**, *73*, 1719–1727. [CrossRef] [PubMed]
153. Sophia, A.C.; Lima, E.C.; Allaudeen, N.; Rajan, S. Application of graphene based materials for adsorption of pharmaceutical traces from water and wastewater-a review. *Desalin. Water Treat.* **2016**, *57*, 27573–27586.

154. Stoller, M.D.; Park, S.; Zhu, Y.; An, J.; Ruoff, R.S. Graphene-based ultracapacitors. *Nano Lett.* **2008**, *8*, 3498–3502. [CrossRef]
155. Georgakilas, V.; Otyepka, M.; Bourlinos, A.B.; Chan-dra, V.; Kim, N.; Kemp, K.C.; Hobza, P.; Zboril, R.; Kim, K.S. Functionalization of graphene: Covalent andnon-covalent approaches, derivatives and applications. *Chem. Rev.* **2012**, *112*, 6156–6214. [CrossRef]
156. Tang, Y.; Guo, H.; Xiao, L.; Yu, S.; Gao, N.; Wang, Y. Synthesis of reduced graphene oxide/magnetite composites and investigation of their adsorption performance of fluoroquinolone antibiotics. *Colloids Surf. A Physicochem. Eng. Asp.* **2013**, *424*, 74–80. [CrossRef]
157. Cao, B.; Ansari, A.; Yi, X.; Rodrigues, D.F.; Hu, Y. Gypsum scale formation on graphene oxide modified reverse osmosis membrane. *J. Membr. Sci.* **2018**, *552*, 132–143. [CrossRef]
158. Chu, K.H.; Fathizadeh, M.; Yu, M.; Flora, J.R.V.; Jang, A.; Jang, M.; Park, C.M.; Yoo, S.S.; Her, N.; Yoon, Y. Evaluation of removal mechanisms in a graphene oxide-coated ceramic ultrafiltration membrane for retention of natural organic matter, pharmaceuticals, and inorganic salts. *ACS Appl. Mater. Interfaces* **2017**, *9*, 40369–40377. [CrossRef] [PubMed]
159. Li, Q.; Kong, H.; Li, P.; Shao, J.; He, Y. Photo-Fenton degradation of amoxicillin via magnetic TiO_2-graphene oxide-Fe_3O_4 composite with a submerged magnetic separation membrane photocatalytic reactor (SMSMPR). *J. Hazard. Mater.* **2019**, *373*, 437–446. [CrossRef] [PubMed]
160. Chen, L.; Li, X.; Tanner, E.E.L.; Compton, R.G. Catechol adsorption on graphene nanoplatelets, isotherm, flat to vertical phase transition and desorption kinetics. *Chem. Sci.* **2017**, *8*, 4771–4778. [CrossRef] [PubMed]
161. Oyetibo, G.O.; Ishola, S.T.; Ikeda-Ohtsubo, W.; Miyauchi, K.; Ilori, M.O.; Endo, G. Mercury bioremoval by Yarrowia strains isolated from sediments of mercury polluted estuarine water. *Appl. Microbiol. Biotechnol.* **2015**, *99*, 3651–3657. [CrossRef]
162. Chakraborty, P.; Show, S.; Banerjee, S.; Halder, G. Mechanistic insight into sorptive elimination of ibuprofen employing bidirectional activated biochar from sugarcane bagasse: Performance evaluation and cost estimation. *J. Environ. Chem. Eng.* **2018**, *6*, 5287–5300. [CrossRef]
163. de Andrade, J.l.R.; Oliveira, M.F.; da Silva, M.G.; Vieira, M.G. Adsorption of pharmaceuticals from water and wastewater using nonconventional low-cost materials: A Review. *Ind. Eng. Chem. Res.* **2018**, *57*, 3103–3127. [CrossRef]
164. Gupta, V.K.; Ali, I. Removal of lead and chromium from wastewater using bagasse fly ash a sugar industry waste. *J. Colloid Interface Sci.* **2004**, *271*, 321–328. [CrossRef]
165. Ahmed, M.B.; Zhou, J.L.; Ngo, H.H.; Guo, W. Insight into biochar properties and its cost analysis. *Biomass Bioenergy* **2016**, *84*, 76–86. [CrossRef]
166. Gandhi, M.R.; Meenakshi, S. Recent advancement in heavy metal removal onto silica-based adsorbents and chitosan composites−A review. In *A Book on Ion Exchange, Adsorption and Solvent Extraction*; Naushad, M., Al-Othman, Z.A., Eds.; Nova Science Publishers, Inc.: New York, NY, USA, 2013; pp. 201–230.

water

MDPI

Article

Adsorption by Granular Activated Carbon and Nano Zerovalent Iron from Wastewater: A Study on Removal of Selenomethionine and Selenocysteine

Stanley Onyinye Okonji [1], Linlong Yu [2], John Albino Dominic [2], David Pernitsky [3] and Gopal Achari [2,*]

[1] Department of Mechanical & Manufacturing Engineering, University of Calgary, ICT 402, 2500 University Drive NW, Calgary, AB T2N 1N4, Canada; stanley.okonji@ucalgary.ca
[2] Department of Civil Engineering, University of Calgary, ENF 262, 2500 University Drive NW, Calgary, AB T2N 1N4, Canada; linyu@ucalgary.ca (L.Y.); johnalbino.dominic@ucalgary.ca (J.A.D.)
[3] Stantec, 200-325 25 Street SE, Calgary, AB T2A 7H8, Canada; David.Pernitsky@stantec.com
* Correspondence: gachari@ucalgary.ca

Abstract: Selenomethionine (SeMet) and selenocysteine (SeCys) are the most common forms of organic selenium, which is often found in the effluent of industrial wastewater. These organic selenium compounds are toxic, bioavailable and most likely to bioaccumulate in aquatic organisms. This study investigated the use of two adsorbent candidates (granular activated carbon (GAC) and nano zerovalent iron (nZVI)) as treatment technologies for SeMet and SeCys removal. Batch experiments were performed and inductively coupled plasma optical emission spectrometer (ICP-OES) was used for sample analysis. Experimental data showed GAC demonstrated a higher affinity towards the removal of SeMet and SeCys compared to nZVI. The removal efficiency of SeCys and SeMet by GAC was 96.1% and 86.7%, respectively. NZVI adsorption capacity for SeCys was 39.4% and SeMet < 1.1%. Irrespective of the adsorbent, SeMet is more refractory to be adsorbed compared to SeCys. Kinetics data of GAC and nZVI agreed well with the pseudo-second-order model ($R^2 > 0.990$). The experimental data of SeCys was characterized by Langmuir model, indicating monolayer adsorption. The adsorption capacity of nZVI for SeCys increased significantly by about 35%, with a decrease in pH from 9.0 to 4.0, indicating that SeCy removal by nZVI is pH dependent. While electrostatic attraction is considered the driving mechanism for nZVI adsorption, GAC uptake capacity is controlled by weak van der Waal forces. The adsorption of binary adsorbates (SeMet and SeCys) exhibited an inhibitory effect due to the competitive interaction between contaminant molecules.

Keywords: adsorption; nano zerovalent iron; granular activated carbon; organoselenium; water; wastewater; treatment

Citation: Okonji, S.O.; Yu, L.; Dominic, J.A.; Pernitsky, D.; Achari, G. Adsorption by Granular Activated Carbon and Nano Zerovalent Iron from Wastewater: A Study on Removal of Selenomethionine and Selenocysteine. *Water* **2021**, *13*, 23. https://dx.doi.org/10.3390/w13010023

Received: 26 November 2020
Accepted: 22 December 2020
Published: 25 December 2020

1. Introduction

Organoselenium simply refers to compounds that contain selenium (Se) in combination with other elements, such as carbon, oxygen, hydrogen, and nitrogen as part of their structure. The primary form of organic Se is selenoamino acids and selenoproteins [1]. SeMet and SeCys are the most common forms by which Se-amino acids exist in the environment and are uptaken by plants and aquatic organisms [2,3]. Naturally, SeMet and SeCys are organically bound in foods, such as nuts, yeast, eggs, liver, garlic [1,3]. In general, Se is a trace element essential for living organism physiological processes at a concentration range from 63–135 μg/L but exhibits toxicity outside this range of concentration [4].

In aqueous environments, organic selenium can be categorized as an emerging contaminant. It exists in the form of SeMet and SeCys in the effluent of industrial wastewaters [5], emanating from mostly mining, oil and gas refineries and coal-fired power plants. SeMet and SeCys are known to have higher bioavailability than inorganic selenium species as it is readily absorbed [3,5]. As a result, the ecotoxicological effect of organic Se (SeMet and SeCys) in aqueous environments is increased. One of the major concerns of organic selenium is the tendency to accumulate in aquatic organisms for an extended period of time, resulting in the contamination of fish and wildlife diets [6]. Public health is at risk if humans consume selenium-contaminated fish and wildlife [7]. The US EPA recently set environmental Se threshold regulations to be reliant on biotic tissue-based concentration rather than the traditional aqueous concentration limit [8]. This regulation is key to preventing organic Se propensity to bioaccumulate within the food-web. Therefore, it is essential to remove organic selenium contaminants from industrial wastewaters in order to decrease the bioaccumulation of selenium in aquatic life, the adverse impact on the ecosystem and the threat to public health. However, there are limited options available for the industries to meet this regulation.

To date, research on selenium remediation in aqueous media has largely focused on inorganic selenium removal. Various treatment technologies have been explored to remove Se from industrial wastewater. These are broadly classified into physical, chemical and biological treatment processes [9,10]. The following studies investigated these removal technologies: elemental selenium (Se^0) precipitation [11,12], iron coprecipitation methods [13], ion-exchange [14], adsorption using mineral adsorbents [15–21], coagulation [22], electrocoagulation [14] and photocatalytic reduction [23,24]. The biological treatment method is the most commonly used remediation technology for inorganic Se removal [10]. The process relies on the use of microbial mediation for selenium species removal [25–28]. However, the presence of SeMet has been reported in the effluents of an industrial biological treatment system [5]. It stands to reason that biological treatment techniques are among the primary sources of organic Se pollution in wastewaters. The transformation of inorganic selenium species to the organic form is mainly due to the microbial activities [5,29]. As a result, the existence of organic Se (SeMet and SeCys) in wastewaters remains an environmental contaminant of concern and the remediation techniques have rarely been researched.

So far, very few studies had investigated organic selenium removal from wastewaters. Alain (1997) investigated the removal of selenocyanate ($SeCN^-$) from sour crude oil produced wastewater by copper (II) salt precipitation [30]. Meng 2002 [31] studied the removal of selenocyanate ($SeCN^-$) from wastewater using Fe(0) filings through the formation of elemental selenium (Se^0). Sanna (2003) studied seleno-DL-methionine separation from inorganic selenium solution using magnesium-loaded activated charcoal [32]. However, besides our earlier study on SeMet removal [33], no previous research has investigated the removal of SeMet and SeCys from wastewater.

This study was conducted to determine the removal of SeMet and SeCys from wastewaters by (granular activated carbon (GAC) and nano zerovalent iron (nZVI)) adsorption, which have shown promise in treating inorganic selenium [34–36]. In this research, adsorption kinetics and isotherms of the two adsorbents were investigated. The effects of pH, initial adsorbate concentrations on adsorption capacities and the influence of binary adsorption were evaluated. SeMet and SeCys were selected as probe contaminants due to its toxicity and bioavailability in the wastewater, while the choice of adsorbents was driven by inexpensive cost and their being environmental benign [37,38]. This is the first study investigating the mechanism of GAC and nZVI to remove organic selenium from industrial wastewater. The knowledge gain in this study will benefit the development of efficient treatment processes for SeMet and SeCys using GAC and nZVI.

2. Materials and Methods

2.1. Chemicals

All chemicals employed in this study were used as received. Selenomethionine (>98%) and selenocysteine (>98%) were purchased from TCI America. Hydrochloric acid (HCl) (>98%), sodium hydroxide (NaOH) (>98%), nano zerovalent iron (nZVI 60–80 nm >99%) were procured from Sigma-Aldrich Chemical Company. Granular activated carbon was acquired from Evoqua (Pittsburgh).

2.2. Characterization of Adsorbents

The morphological properties of the adsorbents were obtained on a scanning electron microscope (SEM, ThermoFisher, Quanta FEG 250), as shown in Figure 1. BET surface area and total pore volume were obtained by N_2 adsorption at 77 K on a PMI Automated Brunauer–Emmett–Teller (BET), Quantachrome ChemBet (3000 CB-SCL).

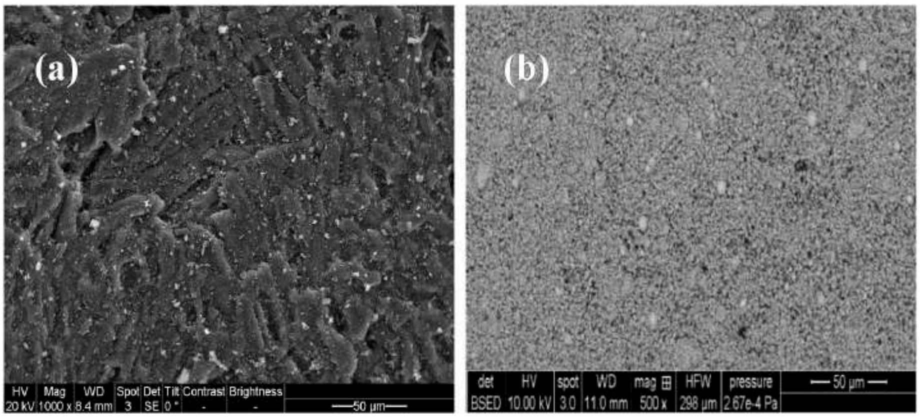

Figure 1. SEM images of granular activated carbon (**a**) and nZVI (**b**).

2.3. Batch Adsorption Studies

Selenocysteine ($C_3H_7NO_2Se$) and Selenomethionine ($C_5H_{11}NO_2Se$) stock solution were prepared separately by dissolving 0.5 g of both compounds in 100 mL of deionized water. The stock solution was diluted appropriately to obtain working solutions of various concentrations, as needed. The concentration of SeMet and SeCys in working solutions, used for adsorbent dose studies, pH studies, initial adsorbate concentrations and adsorption kinetics, was 5 mg/L. Table 1 illustrates the summary of experimental conditions with respect to the adsorbents and their respective concentrations used for evaluating adsorbent dose studies. The effect of pH on the adsorption of SeMet and SeCys was investigated by conducting experiments with different pH conditions (4.0, 7.0 and 9.0). Batch experiments were performed using straight-wall glass jars of 150 mL volume. A magnetic stirrer (VWR 200 model) was used to stir the solutions; the mixtures was agitated at a constant shaking speed of 180 rpm in a temperature-controlled orbital shaker. All experiments were conducted at ambient temperature. The initial pH of the solution was adjusted by adding HCl or NaOH (1 M). At different time intervals, aliquots of 10 mL samples were periodically taken and immediately filtered using 0.22 µm PTFE syringe filter. The collected samples were acidified using 50% nitric acid for a resulting strength of 2% and stored at 4 °C before analysis. For statistical reliability, all the experiments were conducted in duplicate, the samples were analyzed in triplicate and standard deviation was used for error analysis.

Table 1. Summary of experimental conditions for adsorbent dose.

	SeCys		**SeMet**	
Adsorbent Type	**GAC**	**nZVI**	**GAC**	**nZVI**
Dosage (g/L)	1	-	1	-
	2	2	2	-
	3	-	3	-
	5	-	5	-
	7	7	7	7
	14	14	14	-

2.4. Analysis and Equipment

The total Se concentration in the samples was analyzed using an inductively coupled plasma optical emission spectrometer (ICP-OES) (Thermo Scientific icap 7000 series). The limit of detection and quantitation for selenium was estimated as 0.005 and 0.01 mg/L, respectively. The pH fluctuations in the system with time were measured with a pH digital instrument symphony B20PI VWR. The analysis in this study did not distinguish between the species of organic selenium. The total selenium concentration was measured and analyzed.

2.5. Adsorption Kinetics

Adsorption kinetics were examined for an SeMet and SeCys initial concentration of 5 mg/L using nZVI and GAC adsorbent. An adsorbent loading rate of 7 g/L was used and the adsorption capacity $q_e\ (mg/g)$ was calculated using the expression (Equation (1)):

$$q_e = \frac{C_o\ -\ C_e}{M} V \tag{1}$$

where C_o and C_e represent initial and equilibrium concentrations (mg/L), respectively; M is the mass of the adsorbent (g); V is the volume of the solution (L). A pseudo-second-order kinetic model was applied to the kinetic data; the mathematical expression is shown in Equation (2):

$$\frac{t}{q_t} = \frac{1}{k_2 q_e^2} + \frac{t}{q_e} \tag{2}$$

where q_e and q_t (mg/g) represent the amount of adsorbate adsorbed at equilibrium and time (t), respectively; k_2 is pseudo-second-order kinetic rate constant (g·mg^{-1}min^{-1}) and adsorption time (min). The initial adsorption rate h of the system is equal to $k_2 q_e^2$ (mg·g^{-1} min^{-1}). Equation (3) shows the pseudo-first-order kinetic model:

$$q_t = q_e\left(1 - e^{-kt}\right) \tag{3}$$

where k (min^{-1}) is the rate constant; other parameters in the expression have been defined above.

2.6. Adsorption Isotherm Studies

Adsorption isotherm studies were conducted with various initial concentrations (5 to 47.2 mg/L) for SeMet and SeCys. Freundlich and Langmuir isotherm models were used to evaluate the adsorption isotherm. The Freundlich model describes the relationship between the equilibrium concentration and the adsorption capacity. Equation (4) describes the nonlinear Freundlich adsorption isotherm model [39]:

$$\frac{(C_o - C_e)}{M} V = K_f C_e^{\frac{1}{n}} \tag{4}$$

where C_e is the equilibrium concentration (mg/L), C_o is the initial concentration (mg/L), M is the mass of adsorbent (g), V is the volume of the solution (L), K_f and n are Freundlich constants. The left-hand side of the Equation can be determined from experimental data, and it denotes the mass of adsorbate adsorbed per unit mass of adsorbent. The mathematical expression of Langmuir isotherm model [40] is given in Equation (5):

$$q_e = q_m K_c \frac{C_e}{1 + K_c C_e} \tag{5}$$

where q_e is the adsorption capacity at equilibrium (mgSe/g), q_m (mgSe/g) is the maximum adsorption capacity, K_c (L/mg) defined the equilibrium adsorption constants and C_e is the equilibrium concentration (mg/L). The Langmuir isotherm is based on the assumption that adsorption can occur at a finite number of specific localized sites (monolayer) [40]. Equation (6) can be used to evaluate the Langmuir model further [41].

$$R_L = \frac{1}{1 + K_c C_o} \tag{6}$$

The value of R_L defines the adsorption process as irreversible when $(R_L = 0)$, favorable $(1 > R_L > 0)$, unfavorable $(R_L > 1)$ and linear $(R_L = 1)$.

2.7. Parameter Study

The impact of various parameters, including adsorbent dose, pH and initial adsorbate concentration on organic selenium adsorption were evaluated. The experimental conditions were described in Section 2.3 and are summarized in Table 1 (adsorbent dose). The adsorbent amount of 7 g/L was chosen for all experiments based on the optimum dose determined in the dosage studies. For the binary adsorption experiment, a solution containing a mixture of SeMet and SeCys was used to study the effect of organic selenium coexistence. The initial concentration of the organoselenium was 5 mg/L each.

3. Results and Discussion

3.1. Adsorption of Organic Selenium by nZVI and GAC

The batch experiments result for the adsorption of organic selenium species (SeMet and SeCys) using 7 g/L of nZVI and GAC are presented in Figure 2. As shown, the removal of SeCys and SeMet by GAC is more effective than nZVI. After 3 h of adsorption experiments, it was observed that 96% of SeCys and 86.76% of SeMet was removed from water by activated carbon, while 39.44% of SeCys and less than 1.05% of SeMet was transferred to nZVI from the aqueous phase. Physisorption and chemisorption are the two major mechanisms for activated carbon adsorption. The former is caused by relatively weak van der Waals forces formed between the adsorbates and activated carbon's surface. In contrast, the latter is driven by a chemical reaction between the adsorbate molecules and the adsorbent surface [42].

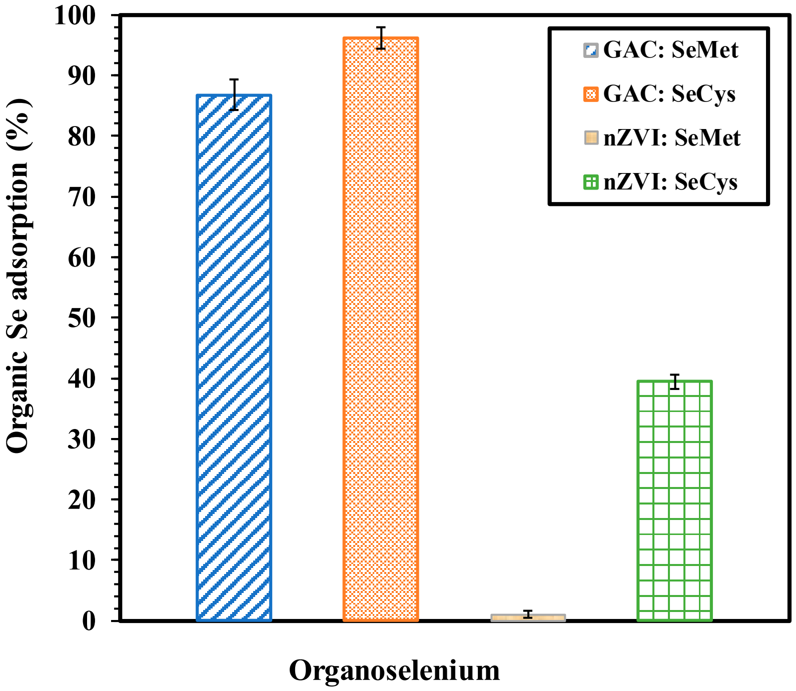

Figure 2. Comparison of organic selenium removal using 7 g/L of GAC and nZVI, pH 7.0, at 25 °C for 3 h period.

Conversely, the elemental iron (nZVI) removal mechanism for organic selenium (selenoyanate) is driven by a corrosion process, which removes the dense oxide layer and activates Fe(0) [31]. Meng [31] demonstrated that, when Fe(0) is mixed in water in the presence of dissolved oxygen (DO), Fe(0) is oxidized to ferrous ions. The oxidation process will give rise to ferric ions, which subsequently form loose ferric hydroxide in water. This phenomenon is referred to as the Fe(0) adsorption process [34], and it describes the nZVI removal mechanism of selenocyanates. In light of selenocyanate being an organic selenium compound and has similar characteristics, such as SeMet and SeCys, it is expected that a similar removal process may be applicable.

In comparison, GAC has better performance and can be attributed to the following reasons—(1) activated carbon possesses a microporous structure, which can lead to large active surface area (~1000 m^2/g) [43], with BET pore volume 0.500 (cm^3/g), and average pore width 2.138 (nm). The second reason is that activated carbon-oxygen surface functional groups (e.g., carboxylic and phenolic groups) can react with SeCys and SeMet to form chemical bonds. SeMet and SeCys are known to contain amino and a carboxylic acid; the functional groups can create hydrogen-bonding with activated carbon surface oxygen [44,45]. Additionally, selenium has an electronegativity similar to sulfur and is capable of forming strong hydrogen bonds identical to sulfur and oxygen [46].

On the other hand, nZVI adsorption was weak; it can be ascribed to the limited number of active sites. The surface area is much smaller than GAC, usually less than 100 m^2/g [47,48]. The adsorption of SeCys and SeMet on metals has not been reported in the literature. However, the mechanism can possibly be understood through the published studies on the interaction between metals, cysteine and methionine. Selenocysteine is an analogue of cysteine with selenium in place of the sulfur, while selenomethionine is analogue of methionine with selenium in place of the sulfur. Therefore, it is expected that the contaminants would have similar behavior and interactions with iron. Generally, the first steps in the adsorption of cysteine or methionine on an iron surface involve the replacement of one or more water molecules adsorbed at the iron surfaces, followed by the formation of iron-cysteine/methionine complexes, as shown in Equations (7)–(9) [49]. It is reported that cysteine can bond to the metal surface through sulfur, two oxygen, and a nitrogen atom in a four-point ″quadrangular footprint″, while methionine adsorbs on the surface with two oxygen and a nitrogen atom in a ″triangular footprint″ [50]. The sulfur atom within the methionine molecule does not interact with the metal surface. The reaction between the sulfur atom and the metal substrate can form a strong bond [50,51], indicating that cysteine's adsorption is stronger than methionine. Similar to methionine, the selenium atom in SeMet is not expected to react with iron's surface, hence no strong bond; which explains the weak adsorption of SeMet on the surface of iron compared to selenocysteine.

$$\text{Cystein/methione(sol)} + x\text{H}_2\text{O(ads)} \rightarrow \text{Cystein/methione (ads)} + x\text{H}_2\text{O(sol)} \quad (7)$$

$$\text{Fe} \rightarrow \text{Fe}^{2+} + 2e \quad (8)$$

$$\text{Fe}^{2+} + \text{Cystein/methione (ads)} \rightarrow [\text{Fe} - \text{Cystein/methione}]^{2+}\text{(ads)} \quad (9)$$

3.2. Adsorbent Dosage

Figure 3 presents the result of the adsorbent amount study on the uptake of SeMet and SeCys by GAC and nZVI with an initial concentration of 5 mg/L at pH 7.0. The removal percentage of organoselenium increased with an increase in the dose of GAC and nZVI. As shown in Figure 3, the effect of adsorbent dose on the organic selenium removal was more significant at the lower adsorbent loadings. Approximately 86.3% of SeCys and 57.1% of SeMet were removed by 1.0 g/L of GAC in 3 h. While 12.2% of SeCys was removed by nZVI within the same time frame. About 72.6% and 90% of SeMet was swiftly removed when the GAC dose was increased from 2 to 14 g/L, respectively. While 93% and 97.9% of SeCys were adsorbed from the solution with the same GAC loading. About 39.4% and

56.6% of SeCys were adsorbed by 7 and 14 g/L of nZVI, respectively. The increase in the adsorption capacity of the adsorbent candidates (GAC and nZVI) is attributed to the availability of greater surface area that drives an increase in the number of active adsorption sites; therefore, resulting in a higher removal rate [35,38]. In contrast to nZVI adsorption, an optimum dose of 7 g/L of GAC significantly adsorbed both contaminants.

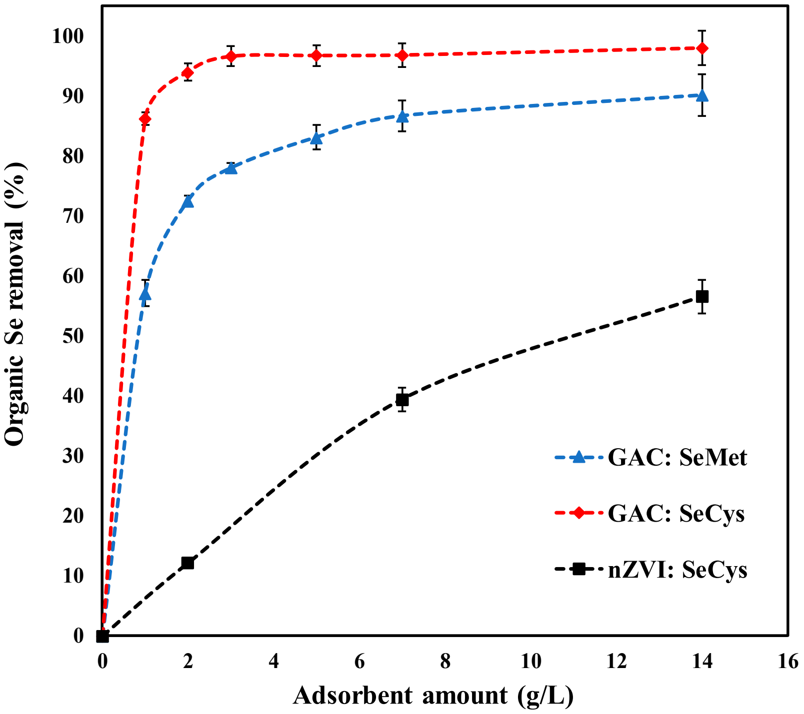

Figure 3. Effect of adsorbent dosage on organic selenium removal, by GAC and nZVI (initial concentration of 5 mg/L, pH 7.0, at 25 °C).

3.3. Effect of pH

Figure 4 depicts the results of experiments conducted to determine the pH influence on organic selenium adsorption by GAC and nZVI. The solutions pH level was measured at pH 4.0, 7.0 and 9.0 during mixing for 3 h. As shown in Figure 4, the amount of SeMet and SeCys adsorbed onto GAC for acidic, neutral and alkaline pH was significant. The removal efficiency of SeCys by GAC occurred in the order of 94.7%, 96.1% and 96.8% for pH 4.0, 7.0 and 9.0, respectively. The acidic condition was observed to be slightly less favorable for the adsorption of SeMet by GAC, corresponding to 80.3% removal. The removal of SeMet at pH 7.0 and 9.0 solution was 86.7% and 86.6%, respectively. SeCys and SeMet are zwitterions, containing both amino groups and carboxyl groups. The isoelectric point (Ip) for SeMet and SeCys are 5.75 and 5.54, respectively [51,52]. Increasing the pH from 4.0 to 9.0 would change the net charge of SeCys and SeMet solution from positive to negative and also influence the surface charge of activated carbon, leading to different electrostatic interactions between SeCys and SeMet molecules and activated carbon. In this study, the investigated pHs insignificantly impacted the adsorption of the two organic selenium compounds by GAC, indicating that the adsorption of SeCys and SeMet by GAC was not dominated by electrostatic force. The adsorption of SeCys and SeMet could potentially occur as a result of the hydrogen bonding or the hydrophobic interaction that exists between the hydrophobic part of SeCys and SeMet molecules and the hydrophobic part of the adsorbent, which have been reported as mechanisms for the adsorption of amino acids on the surface of activated carbon [53].

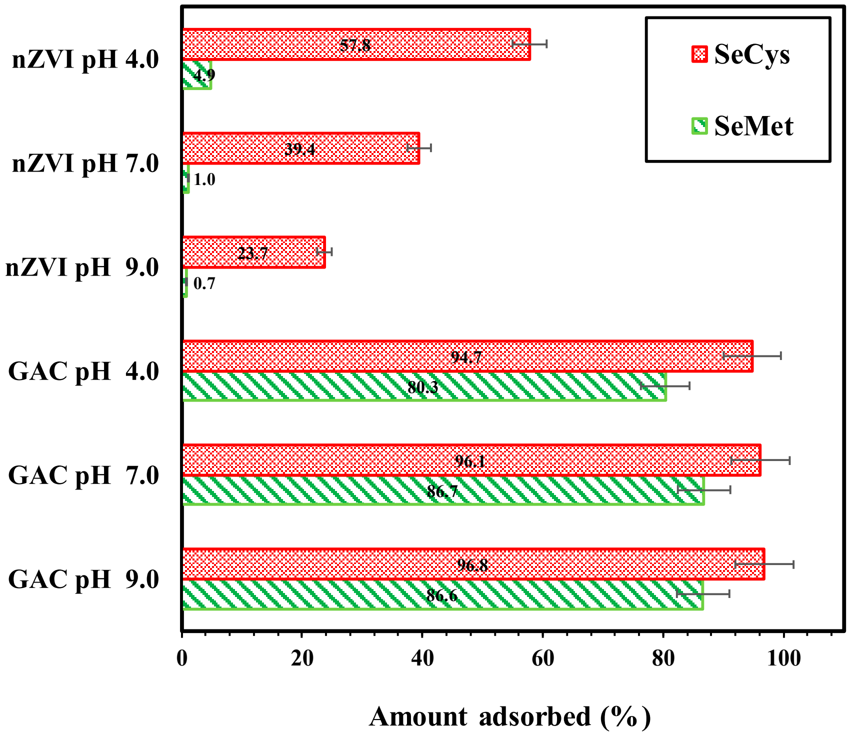

Figure 4. Effect of pH on SeMet and SeCys adsorption by GAC and nZVI, (initial concentration 5 mg/L, 7 g/L, pH 4.0, 7.0 and 9.0, at 25 °C).

On the other hand, the removal of SeCys and SeMet by nZVI decreased remarkably with increasing pH, as shown in Figure 4. The percentages of SeCys adsorbed on nZVI under different pHs are 57.8% for pH 4.0, 39.4% for pH 7.0 and 23.7% for pH 9.0. SeMet removal rate decreased from 4.9% to less than 1% when pH was increased from 4.0 to 9.0, indicating a negative effect of an increase in pH condition. Similar findings have been reported on selenocyanate adsorption (an organic selenium species) by nZVI [31]. Meng et al. [31] demonstrated that selenocyanate's removal rate increased from 50% to 97% when pH was decreased from 8.5 to 5.5.

3.4. Effect of Initial Concentration

GAC performance in treating water containing different concentrations of SeMet and SeCys at pH 7.0 is presented in Figure 5. For SeMet, 4.9 mg/L and 46.8 mg/L of initial concentration were evaluated, while SeCys, 3.8 and 38 mg/L of initial concentration were examined. Both forms of organoselenium were adsorbed continuously as a function of time until equilibrium was reached. However, SeMet appears to have some desorption after 1 h, which was typical in both concentrations (4.9 and 46.8 mg/L). The pseudo-second-order kinetic model adequately describes the data depicted in Table 2. The correlation coefficients (R^2) value was evaluated between 0.999–1.000 (Table 2). As illustrated in Table 2, the rate constant is between 2.50 to 1.80 for SeMet C_o (4.9 and 46.8 mg/L) and 1.30 to 0.25 for SeCys C_o (3.8 and 38 mg/L), respectively. The result demonstrates that the rate constant (K_2) decreased with an increase in SeMet and SeCys concentration. When the initial concentration is increased, the solution takes more time to attain equilibrium. The decrease in K_2, with respect to an increase in the initial concentration, can be attributed to a longer duration that is required for the solution to attain equilibrium; a similar phenomenon has been reported in the literature [54,55].

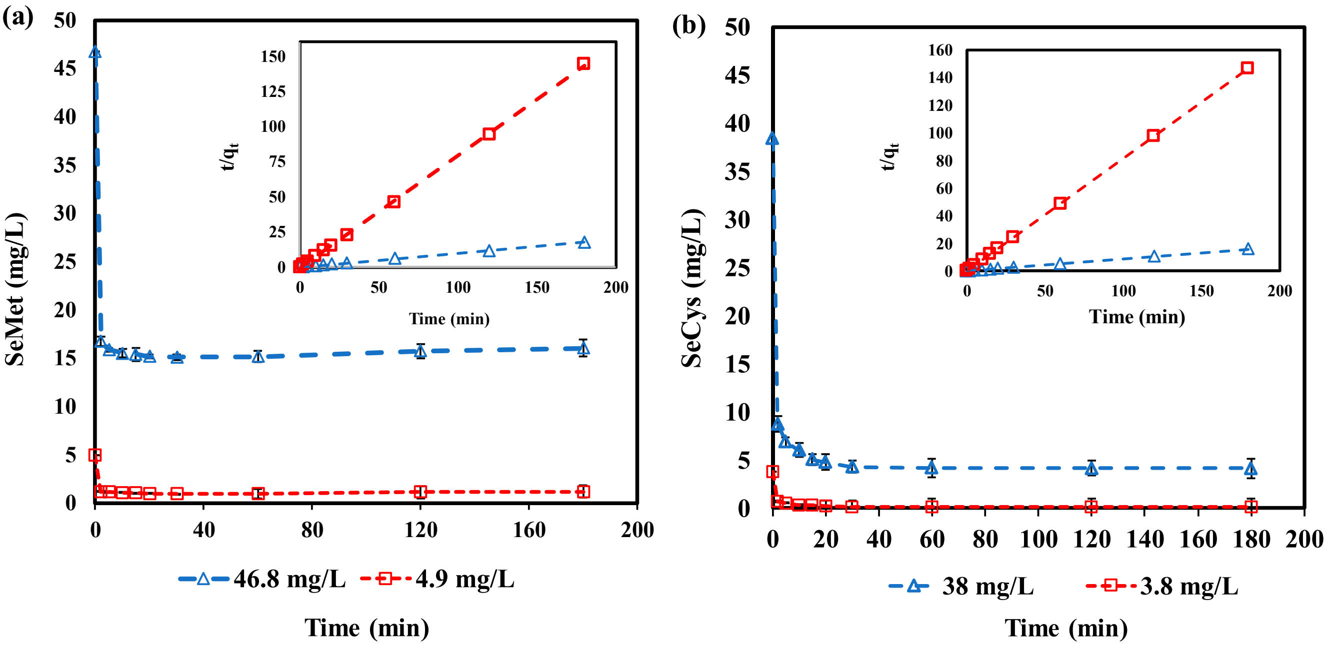

Figure 5. Effect of initial concentration by GAC: (**a**) SeMet (C_o: 46.8 and 4.9 mg/L); (**b**) SeCys (C_o: 38 and 3.8 mg/L); all experiments were conducted at pH 7.0, 7 g/L and 25 °C.

Table 2. Experimental data for adsorbate initial concentration studies with GAC adsorbent, at pH 7.0.

	SeMet		SeCys	
C_o (mg/L)	4.9	46.8	3.8	38
q_e (mg·g^{-1})	1.32	10.54	1.23	11.40
K_2 (g·mg^{-1}·min^{-1})	2.50	1.80	1.30	0.25
R^2	1.000	0.999	1.000	1.000

Furthermore, the experimental data also show that q_e increases with higher C_o, the increment was significant about eight times higher as the initial concentrations of SeMet and SeCys were varied. It can be deduced that the increase in C_o provides the driving force to overcome the mass transfer resistance between the adsorbate and solid phases [56]. It was observed that GAC completely removed 3.8 mg/L of SeCys in 30 min, while the initial concentration of 38 mg/L was reduced to 4.2 mg/L in 3 h. About 30.7 and 3.6 mg/L of SeMet were adsorbed from the initial concentration of 46.8 and 4.9 mg/L, respectively. An upsurge in adsorption capacity as a result of an increase in adsorbate initial concentration has been reported by Aksu [57] and Al-Ghouti [58].

3.5. Adsorption Isotherm

The adsorption data for GAC were evaluated using Langmuir and Freundlich isotherm models. The results of both Langmuir and Freundlich models for SeMet and SeCys adsorption are summarized in Table 3. Freundlich and Langmuir models fitted well with the experimental data (R^2 > 0.950). Figure 6a shows that the Freundlich model provided a better fit for SeMet adsorption data compared to the Langmuir model. The correlation coefficient (R^2 > 0.996) was higher for the Freundlich model, suggesting that the adsorption of SeMet might occur in multilayers. The parameter K_f of the Freundlich model was calculated to be 1.85, which is related to the adsorption capacity. As reflected in Table 3, the constant n, representing the adsorption intensity, was equal to 1.55, indicating pseudo linear adsorption [59].

Table 3. Adsorption isotherm parameters for organoselenium by GAC.

	Langmuir Model			**Freundlich Model**		
	q_m **(mg/g)**	K_c **(L/mg)**	$\mathbf{R^2}$	K_f	n	$\mathbf{R^2}$
SeMet	18.9	0.10	0.967	1.85	1.55	0.996
SeCys	10.0	0.32	0.999	2.52	2.14	0.950

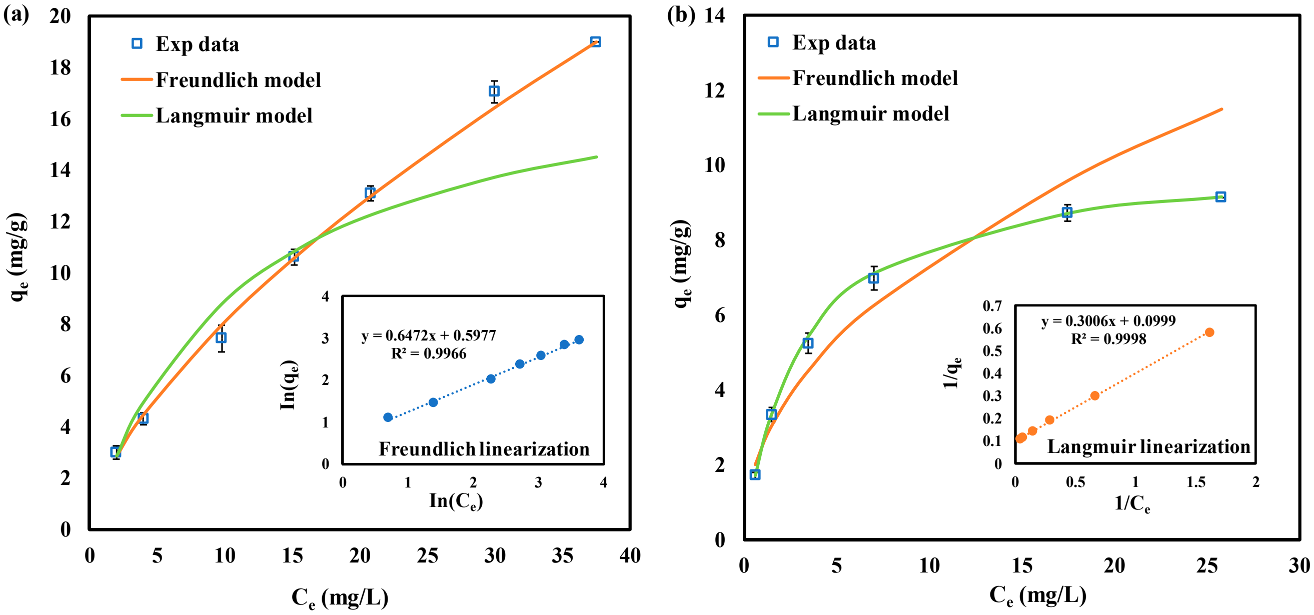

Figure 6. Organic selenium adsorption isotherms by GAC, pH 7.0, at 25 °C. (**a**) SeMet; (**b**) SeCys. The solid lines represent model fits; inset shows a linearization fit.

On the other hand, SeCys adsorption by GAC with corresponding Langmuir plots is presented in Figure 6b. Freundlich isotherm was also used to normalize the adsorption data. As stated in Table 3, the isotherm data fitted better with the Langmuir model (higher coefficients of determination $R^2 = 0.990$) in contrast to the Freundlich model, suggesting that the adsorption of SeCys is monolayer and it occurred at localized sites [53,57]. The maximum uptake capacity for the Langmuir parameter q_m is 10 mg/g. The dimensionless constant $R_L = 0.082$, an indication that SeCys adsorption process can be considered as favorable [41].

3.6. Adsorption Kinetics

Figure 7a shows the time-dependent data of SeMet and SeCys adsorption by GAC. As shown in the results (Figure 7a), the equilibrium time for SeMet was 20 min, while SeCys took longer than 50 min to achieve equilibrium, indicating that the SeCys adsorption process was progressive. The pseudo-second-order (PSO) kinetics model (inset of Figure 6a) was used to investigate the adsorption kinetics, the rate constant (k_2) values and the maximum adsorption capacity (q_e) for SeMet and SeCys, as presented in Table 4. The correlation coefficients ($R^2 > 0.999$) suggest that the PSO model was a good fit for the adsorbents tested. However, when parameter h, which accounts for the initial adsorption rate, was calculated, the value shows that SeCys adsorption was faster than SeMet adsorption (h value of SeMet is about 33% less than SeCys).

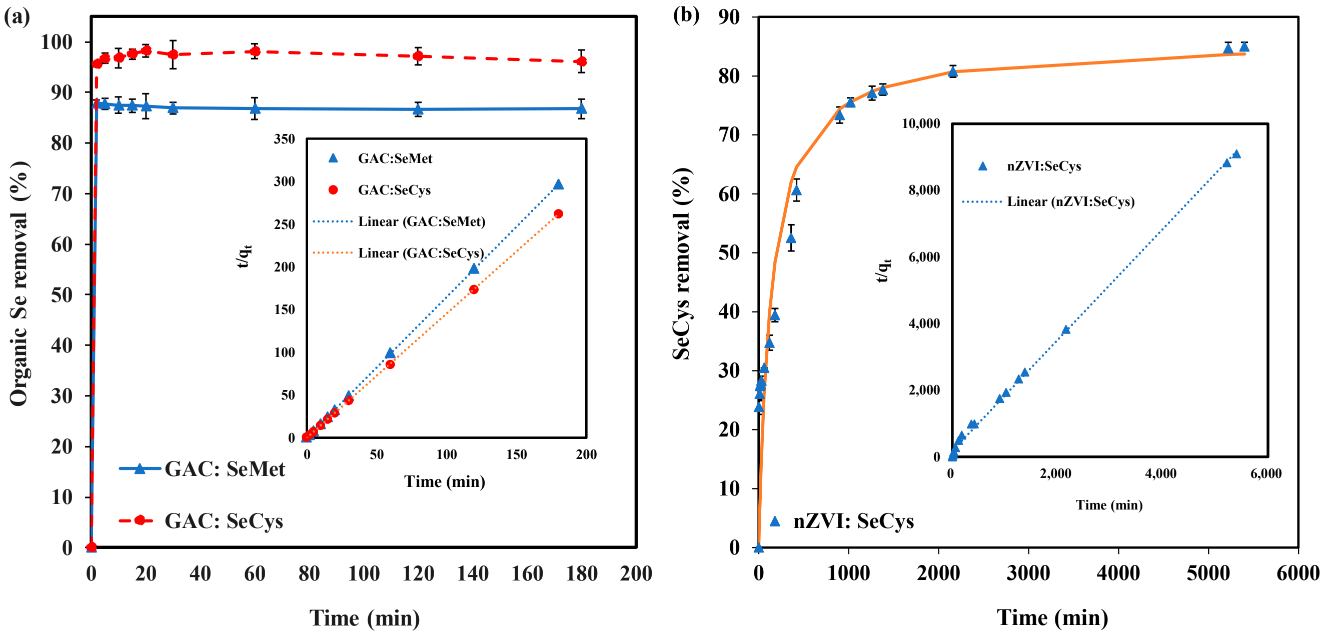

Figure 7. (**a**) Organic selenium adsorption kinetics using 7 g/L of GAC. (**b**) SeCys adsorption kinetics using 7 g/L of nZVI. All experiments were conducted at pH 7.0, 25 °C with an initial concentration of 5 mg/L.

Table 4. Kinetic parameters of pseudo-second-order models for SeMet and SeCys adsorption.

Kinetic Parameter	pH	SeMet	SeCys	
		GAC	nZVI	GAC
q_e (mg·g^{-1})	7	0.61	0.59	0.70
k_2 (g·mg^{-1}·min^{-1})		24	0.012	28
R^2		1.000	0.998	0.999
h (mg·g^{-1}·min^{-1})		8.81	0.004	13.27

The adsorption kinetics of SeCys by nZVI are depicted in Figure 7b. The experiment was performed for 54 h to allow enough time for equilibrium. However, equilibrium was not achieved because the adsorption process was very slow (Table 4). The pseudo-second-order kinetics model showed a good fit for SeCys adsorption data ($R^2 > 0.998$). Contrary to GAC adsorption, nZVI removal efficiency was found to increase slowly until a final adsorption efficiency of 85% was achieved. Overall, GAC kinetics was very swift compared to nZVI, which can be explained as an outcome of a more significant adsorption site [43].

3.7. Binary Adsorption of SeMet and SeCys

The effect of the coexistence of SeMet and SeCys on wastewaters was investigated using 7 g/L of GAC and nZVI. The initial concentration of organic selenium in the mixture was 10 mg/L (comprising 5 mg/L of SeMet and SeCys each), and the pH of the solution was 7.0. The result presented in Figure 8 shows that GAC and nZVI removed 8.9 mg/L and 1.5 mg/L of Se from the mixture of SeMet and SeCys, respectively, in 3 h. On an individual basis, GAC removed 4.8 mg/L of Se from SeCys solution and 4.3 mg/L of Se from SeMet solution. While nZVI adsorbed 1.9 mg/L of Se from SeCys and 0.1 mg/L of Se from SeMet. The result shows that the total Se removed by GAC from the mixture of SeMet and SeCys solution was lower compared to the sum of Se adsorbed in a single solute system. This phenomenon is an indication of competition between different molecules for available adsorption sites on GAC surface [60,61]. Conversely, the adsorption of SeMet by nZVI in a single solute system was very weak, indicating that the competing effect for active sites on the surface of nZVI was negligible. The inhibition effect of SeMet on the adsorption of

SeCys by GAC and nZVI can possibly occur as a result of the interaction between SeCys and SeMet in the binary system. Organic selenium speciation was not determined in this study; hence, the selenium species removed from the mixture was unknown.

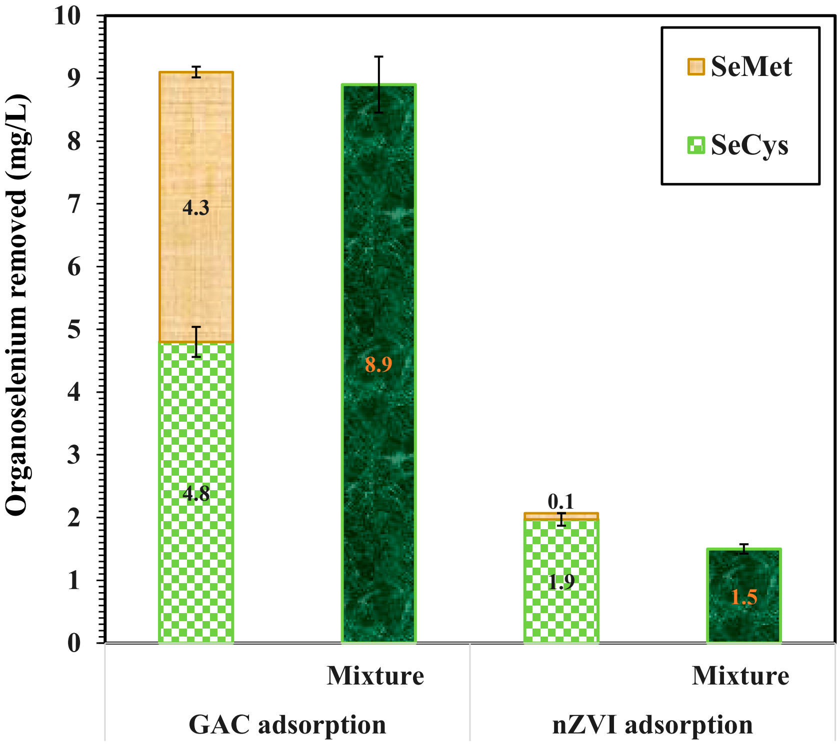

Figure 8. Binary adsorption of SeMet and SeCys by nZVI and GAC, initial concentration of 10 mg/L, 7 g/L at pH 7.0 and 25 °C.

4. Conclusions

The adsorption of SeMet and SeCys by GAC and nZVI under various conditions—different pHs, adsorbate initial concentration, adsorbent dosage, and binary adsorption were investigated. GAC demonstrated a higher affinity towards the removal of SeMet and SeCys, and was, therefore, considered a better adsorbent candidate. An optimum dose of 7 g/L of GAC was found to remove both contaminants effectively. Change in pH had no significant impact on SeCys removal by GAC; nevertheless, more than 93.99% removal was achieved at all pH tested. In the case of nZVI, pH change substantially influenced the adsorption capacity—at pH 4.0, about 57.8% of SeCys was removed. An increase in adsorption capacity with a decrease in pH value was observed for SeMet removal by nZVI. SeCys adsorbed more readily into nZVI compared to SeMet—for all conditions evaluated, SeMet removal by nZVI was less than 5%. The pseudo-second-order kinetics model characterized the adsorption of organoselenium by both adsorbents. The fastest adsorption kinetics was observed with GAC under neutral pH, where an instantaneous removal of organic selenium was observed. Binary adsorption of SeCys and SeMet indicates an inhibitory effect on SeCys removal by SeMet. The adsorption data fitted well with both Langmuir and Freundlich isotherm models.

Author Contributions: Conceptualization, S.O.O., G.A. and D.P.; methodology, S.O.O.; experimental design, S.O.O. and L.Y.; formal analysis, S.O.O. and J.A.D.; investigation, S.O.O.; resources, G.A; writing—original draft preparation, S.O.O.; writing—review and editing, G.A, L.Y., D.P. and J.A.D.; supervision, G.A; project administration, J.A.D.; funding acquisition, G.A. All authors have read and agreed to the published version of the manuscript.

Funding: Natural Sciences and Engineering Research Council of Canada (NSERC).

Data Availability Statement: The data presented in this study are available on request from the corresponding author.

Acknowledgments: The authors gratefully acknowledge the funding support provided by National Sciences and Engineering Research Council of Canada (NSERC) through an Engage grant.

Conflicts of Interest: The authors declare no conflict of interest.

References

1. Maseko, T.; Callahan, D.L.; Dunshea, F.R.; Doronila, A.; Kolev, S.D.; Ng, K. Chemical characterisation and speciation of organic selenium in cultivated selenium-enriched Agaricus bisporus. *Food Chem.* **2013**, *141*, 3681–3687. [CrossRef] [PubMed]
2. Dumont, E.; Vanhaecke, F.; Cornelis, R. Selenium speciation from food source to metabolites: A critical review. *Anal. Bioanal. Chem.* **2006**, *385*, 1304–1323. [CrossRef] [PubMed]
3. Amoako, P.O.; Uden, P.C.; Tyson, J.F. Speciation of selenium dietary supplements; formation of S-(methylseleno) cysteine and other selenium compounds. *Anal. Chim. Acta* **2009**, *652*, 315–323. [CrossRef] [PubMed]
4. Albert, M.; Demesmay, C.; Rocca, J. Analysis of organic and non-organic arsenious or selenious compounds by capillary electrophoresis. *Fresenius' J. Anal. Chem.* **1995**, *351*, 426–432. [CrossRef]
5. LeBlanc, K.L.; Wallschläger, D. Production and release of selenomethionine and related organic selenium species by microorganisms in natural and industrial waters. *Environ. Sci. Technol.* **2016**, *50*, 6164–6171. [CrossRef] [PubMed]
6. Lemly, A.D. Environmental implications of excessive selenium: A review. *Biomed. Environ. Sci.* **1997**, *10*, 415–435.
7. Fan, A.M.; Book, S.A.; Neutra, R.R.; Epstein, D.M. Selenium and human health implications in California's San Joaquin Valley. *J. Toxicol. Environ. Health Part A Curr. Issues* **1988**, *23*, 539–559. [CrossRef]
8. Delos, C. *Draft Aquatic Life Water Quality Criteria for Selenium*; US Environmental Protection Agency: Washington, DC, USA, 2004.
9. CH2M HILL. Review of available technologies for the removal of selenium from water. In *Final Report, Prepared for North American Metals Council (NAMC)*; CH2M HILL: Charlotte, NC, USA; Bellevue, WA, USA, 2010.
10. Khamkhash, A.; Srivastava, V.; Ghosh, T.; Akdogan, G.; Ganguli, R.; Aggarwal, S. Mining-related selenium contamination in Alaska, and the state of current knowledge. *Minerals* **2017**, *7*, 46. [CrossRef]
11. Zhang, Y.; Amrhein, C.; Frankenberger, W.T., Jr. Effect of arsenate and molybdate on removal of selenate from an aqueous solution by zero-valent iron. *Sci. Total Environ.* **2005**, *350*, 1–11. [CrossRef]
12. Mondal, K.; Jegadeesan, G.; Lalvani, S.B. Removal of selenate by Fe and NiFe nanosized particles. *Ind. Eng. Chem. Res.* **2004**, *43*, 4922–4934. [CrossRef]
13. Montgomery, J.M.; Engineers, C. *Water Treatment Principles and Design*; Wiley: New York, NY, USA, 1985.
14. Mavrov, V.; Stamenov, S.; Todorova, E.; Chmiel, H.; Erwe, T. New hybrid electrocoagulation membrane process for removing selenium from industrial wastewater. *Desalination* **2006**, *201*, 290–296. [CrossRef]
15. Balistrieri, L.S.; Chao, T. Selenium Adsorption by Goethite. *Soil Sci. Soc. Am. J.* **1987**, *51*, 1145–1151. [CrossRef]
16. Balistrieri, L.S.; Chao, T. Adsorption of selenium by amorphous iron oxyhydroxide and manganese dioxide. *Geochim. Cosmochim. Acta* **1990**, *54*, 739–751. [CrossRef]
17. Zhang, Y.; Frankenberger, W.T. Factors affecting removal of selenate in agricultural drainage water utilizing rice straw. *Sci. Total Environ.* **2003**, *305*, 207–216. [CrossRef]
18. Peak, D. Adsorption mechanisms of selenium oxyanions at the aluminum oxide/water interface. *J. Colloid Interface Sci.* **2006**, *303*, 337–345. [CrossRef]
19. El-Shafey, E. Sorption of Cd (II) and Se (IV) from aqueous solution using modified rice husk. *J. Hazard. Mater.* **2007**, *147*, 546–555. [CrossRef]
20. Zhang, N.; Gang, D.; Lin, L.-S. Adsorptive removal of parts per million level Selenate using iron-coated GAC Adsorbents. *J. Environ. Eng.* **2010**, *136*, 1089–1095. [CrossRef]
21. Zhang, N.; Lin, L.-S.; Gang, D. Adsorptive selenite removal from water using iron-coated GAC adsorbents. *Water Res.* **2008**, *42*, 3809–3816. [CrossRef]
22. Hu, C.; Chen, Q.; Chen, G.; Liu, H.; Qu, J. Removal of Se (IV) and Se (VI) from drinking water by coagulation. *Sep. Purif. Technol.* **2015**, *142*, 65–70. [CrossRef]
23. Tan, T.; Beydoun, D.; Amal, R. Effects of organic hole scavengers on the photocatalytic reduction of selenium anions. *J. Photochem. Photobiol. A Chem.* **2003**, *159*, 273–280. [CrossRef]
24. Nguyen, V.N.H.; Beydoun, D.; Amal, R. Photocatalytic reduction of selenite and selenate using TiO_2 photocatalyst. *J. Photochem. Photobiol. A Chem.* **2005**, *171*, 113–120. [CrossRef]
25. Zhang, Y.; Moore, J.N. Environmental conditions controlling selenium volatilization from a wetland system. *Environ. Sci. Technol.* **1997**, *31*, 511–517. [CrossRef]
26. Amweg, E.; Stuart, D.; Weston, D. Comparative bioavailability of selenium to aquatic organisms after biological treatment of agricultural drainage water. *Aquat. Toxicol.* **2003**, *63*, 13–25. [CrossRef]
27. Zhang, Y.; Okeke, B.C.; Frankenberger, W.T., Jr. Bacterial reduction of selenate to elemental selenium utilizing molasses as a carbon source. *Bioresour. Technol.* **2008**, *99*, 1267–1273. [CrossRef] [PubMed]

28. Presser, T.S.; Ohlendorf, H.M. Biogeochemical cycling of selenium in the San Joaquin Valley, California, USA. *Environ. Manag.* **1987**, *11*, 805–821. [CrossRef]
29. Ohlendorf, H.M. Bioaccumulation and Effects of Selenium in Wildlife. *Selenium Agric. Environ.* **1989**, *23*, 133–177.
30. Manceau, A.; Gallup, D.L. Removal of Selenocyanate in Water by Precipitation: Characterization of Copper−Selenium Precipitate by X-ray Diffraction, Infrared, and X-ray Absorption Spectroscopy. *Environ. Sci. Technol.* **1997**, *31*, 968–976. [CrossRef]
31. Meng, X.; Bang, S.; Korfiatis, G.P. Removal of selenocyanate from water using elemental iron. *Water Res.* **2002**, *36*, 3867–3873. [CrossRef]
32. Latva, S.; Peräniemi, S.; Ahlgrén, M. Study of metal-loaded activated charcoals for the separation and determination of selenium species by energy dispersive X-ray fluorescence analysis. *Anal. Chim. Acta* **2003**, *478*, 229–235. [CrossRef]
33. Okonji, S.O.; Dominic, J.A.; Pernitsky, D.; Achari, G. Removal and recovery of selenium species from wastewater: Adsorption kinetics and co-precipitation mechanisms. *J. Water Process Eng.* **2020**, *38*, 101666. [CrossRef]
34. Yoon, I.-H.; Kim, K.-W.; Bang, S.; Kim, M.G. Reduction and adsorption mechanisms of selenate by zero-valent iron and related iron corrosion. *Appl. Catal. B Environ.* **2011**, *104*, 185–192. [CrossRef]
35. Wasewar, K.L.; Prasad, B.; Gulipalli, S. Removal of selenium by adsorption onto granular activated carbon (GAC) and powdered activated carbon (PAC). *CLEAN–Soil Air Water* **2009**, *37*, 872–883. [CrossRef]
36. Das, S.; Lindsay, M.B.; Essilfie-Dughan, J.; Hendry, M.J. Dissolved selenium (VI) removal by zero-valent iron under oxic conditions: Influence of sulfate and nitrate. *ACS Omega* **2017**, *24*, 1513–1522. [CrossRef] [PubMed]
37. Zhang, Y.; Wang, J.; Amrhein, C.; Frankenberger, W.T. Removal of selenate from water by zerovalent iron. *J. Environ. Qual.* **2005**, *34*, 487–495. [CrossRef] [PubMed]
38. Liang, L.; Jiang, X.; Yang, W.; Huang, Y.; Guan, X.; Li, L. Kinetics of selenite reduction by zero-valent iron. *Desalination Water Treat.* **2015**, *53*, 2540–2548. [CrossRef]
39. Zelmanov, G.; Semiat, R. Selenium removal from water and its recovery using iron (Fe3+) oxide/hydroxide-based nanoparticles sol (NanoFe) as an adsorbent. *Sep. Purif. Technol.* **2013**, *103*, 167–172. [CrossRef]
40. Langmuir, I. The constitution and fundamental properties of solids and liquids. Part I. Solids. *J. Am. Chem. Soc.* **1916**, *38*, 2221–2295. [CrossRef]
41. Zeng, G.; Liu, Y.; Tang, L.; Yang, G.; Pang, Y.; Zhang, Y.; Zhou, Y.; Li, Z.; Li, M.; Lai, M. Enhancement of Cd (II) adsorption by polyacrylic acid modified magnetic mesoporous carbon. *Chem. Eng. J.* **2015**, *259*, 153–160. [CrossRef]
42. Bansal, R.; Goyal, M. Activated carbon adsorption and environment: Adsorptive removal of organic from water. In *Activated Carbon Adsorption*; Taylor & Francis: Boca Raton, FL, USA, 2005; pp. 297–372.
43. Yang, Y.; Yu, L.; Iranmanesh, S.; Keir, I.; Achari, G. Laboratory and Field Investigation of Sulfolane Removal from Water Using Activated Carbon. *J. Environ. Eng.* **2020**, *146*, 04020022. [CrossRef]
44. Ahnert, F.; Arafat, H.A.; Pinto, N.G. A study of the influence of hydrophobicity of activated carbon on the adsorption equilibrium of aromatics in non-aqueous media. *Adsorption* **2003**, *9*, 311–319. [CrossRef]
45. López-Velandia, C.; Moreno-Barbosa, J.J.; Sierra-Ramirez, R.; Giraldo, L.; Moreno-Piraján, J.C. Adsorption of volatile carboxylic acids on activated carbon synthesized from watermelon shells. *Adsorpt. Sci. Technol.* **2014**, *32*, 227–242. [CrossRef]
46. Mundlapati, V.R.; Sahoo, D.K.; Ghosh, S.; Purame, U.K.; Pandey, S.; Acharya, R.; Pal, N.; Tiwari, P.; Biswal, H.S. Spectroscopic evidence for strong hydrogen bonds with selenomethionine in proteins. *J. Phys. Chem. Lett.* **2017**, *8*, 794–800. [CrossRef] [PubMed]
47. Adusei-Gyamfi, J.; Acha, V. Carriers for nano zerovalent iron (nZVI): Synthesis, application and efficiency. *RSC Adv.* **2016**, *6*, 91025–91044. [CrossRef]
48. Wang, Q.; Kanel, S.R.; Park, H.; Ryu, A.; Choi, H. Controllable synthesis, characterization, and magnetic properties of nanoscale zerovalent iron with specific high Brunauer–Emmett–Teller surface area. *J. Nanoparticle Res.* **2009**, *113*, 749–755. [CrossRef]
49. Oguzie, E.; Li, Y.; Wang, F. Corrosion inhibition and adsorption behavior of methionine on mild steel in sulfuric acid and synergistic effect of iodide ion. *J. Colloid Interface Sci.* **2007**, *310*, 90–98. [CrossRef] [PubMed]
50. Thomsen, L.; Wharmby, M.; Riley, D.; Held, G.; Gladys, M. The adsorption and stability of sulfur containing amino acids on Cu {5 3 1}. *Surf. Sci.* **2009**, *603*, 1253–1261. [CrossRef]
51. Mishra, B.; Priyadarsini, K.; Mohan, H. One-Electron Oxidation of Selenomethionine in Aqueous Solutions. *Barc Newslett.* **2005**, *261*, 115.
52. Bettelheim, F.A.; Brown, W.H.; Campbell, M.K.; Farrell, S.O.; Torres, O. *Introduction to General, Organic and Biochemistry*; Nelson Education: Toronto, ON, Canada, 2012.
53. Cermakova, L.; Kopecka, I.; Pivokonsky, M.; Pivokonska, L.; Janda, V. Removal of cyanobacterial amino acids in water treatment by activated carbon adsorption. *Sep. Purif. Technol.* **2017**, *173*, 330–338. [CrossRef]
54. Gupta, S.S.; Bhattacharyya, K.G. Kinetics of adsorption of metal ions on inorganic materials: A review. *Adv. Colloid Interface Sci.* **2011**, *162*, 39–58. [CrossRef]
55. Allen, S.J.; Gan, Q.; Matthews, R.; Johnson, P.A. Kinetic modeling of the adsorption of basic dyes by kudzu. *J. Colloid Interface Sci.* **2005**, *286*, 101–109. [CrossRef]
56. Wang, W.; Wang, J.; Guo, Y.; Zhu, C.; Pan, F.; Wu, R.; Wang, C. Removal of multiple nitrosamines from aqueous solution by nanoscale zero-valent iron supported on granular activated carbon: Influencing factors and reaction mechanism. *Sci. Total Environ.* **2018**, *639*, 934–943. [CrossRef] [PubMed]

57. Aksu, Z.; Dönmez, G. A comparative study on the biosorption characteristics of some yeasts for Remazol Blue reactive dye. *Chemosphere* **2003**, *50*, 1075–1083. [CrossRef]
58. Al-Ghouti, M.A.; Khraisheh, M.A.; Ahmad, M.N.; Allen, S. Adsorption behaviour of methylene blue onto Jordanian diatomite: A kinetic study. *J. Hazard. Mater.* **2009**, *165*, 589–598. [CrossRef] [PubMed]
59. Tseng, R.-L.; Wu, F.-C. Inferring the favorable adsorption level and the concurrent multi-stage process with the Freundlich constant. *J. Hazard. Mater.* **2008**, *155*, 277–287. [CrossRef]
60. Jain, J.S.; Snoeyink, V.L. Adsorption from bisolute systems on active carbon. *J. Water Pollut. Control Fed.* **1973**, *45*, 2463–2479.
61. Noroozi, B.; Sorial, G.; Bahrami, H.; Arami, M. Adsorption of binary mixtures of cationic dyes. *Dyes Pigment.* **2008**, *76*, 784–791. [CrossRef]

water

Article

Removal of Arsenic(III) Ion from Aqueous Media Using Complex Nickel-Aluminum and Nickel-Aluminum-Zirconium Hydroxides

Fumihiko Ogata [1], Noriaki Nagai [1], Megumu Toda [2], Masashi Otani [2], Chalermpong Saenjum [3,4], Takehiro Nakamura [1] and Naohito Kawasaki [1,5,*]

[1] Faculty of Pharmacy, Kindai University, 3-4-1 Kowakae, Higashi-Osaka, Osaka 577-8502, Japan; ogata@phar.kindai.ac.jp (F.O.); nagai_n@phar.kindai.ac.jp (N.N.); nakamura@phar.kindai.ac.jp (T.N.)
[2] Kansai Catalyst Co. Ltd., 1-3-13, Kashiwagi-cho, Sakai-ku, Sakai, Osaka 590-0837, Japan; megumu.toda@kansyoku.co.jp (M.T.); masashi.ootani@kansyoku.co.jp (M.O.)
[3] Faculty of Pharmacy, Chiang Mai University, Suthep Road, Muang District, Chiang Mai 50200, Thailand; chalermpong.saenjum@gmail.com
[4] Cluster of Excellence on Biodiversity-based Economics and Society (B.BES-CMU), Chiang Mai University, Suthep Road, Muang District, Chiang Mai 50200, Thailand
[5] Antiaging Center, Kindai University, 3-4-1 Kowakae, Higashi-Osaka, Osaka 577-8502, Japan
* Correspondence: kawasaki@phar.kindai.ac.jp; Tel.: +81-6-4307-4012

Received: 12 May 2020; Accepted: 12 June 2020; Published: 14 June 2020

Abstract: The technology of wastewater treatment involving removal of heavy metals using complex metal hydroxides is reported. In this study, complex nickel-aluminum (NA11 and NA12) and nickel-aluminum-zirconium (NAZ1 and NAZ2) hydroxides were prepared for the removal of arsenite ions, As(III), from aqueous solution. The characteristics of each adsorbent were evaluated, and the adsorption capacity and adsorption mechanism were determined. The adsorption capacity of As(III) on NAZ1 (15.3 mg g^{-1}) was greater than that on NA11 (9.3 mg g^{-1}). Coverage is directly related to the specific surface area with a correlation coefficient of 0.921. Ion exchange involving sulfate ions in the interlayer of the adsorbent also plays a role in the mechanism of As(III) adsorption as demonstrated by correlation coefficients of 0.797 and 0.944 for the NA11 and NAZ1, respectively. The results demonstrate the usefulness of NAZ1 in removing As(III) from aqueous media.

Keywords: complex nickel-aluminum-zirconium hydroxide; arsenic ion; adsorption

1. Introduction

The United Nations has adopted 17 goals as part of its 2030 agenda to develop a sustainable future for all. Issues of clean water and sanitation (Goal No. 6) and undersea water (Goal No. 14) are particularly relevant to the development of an acceptable global water environment [1]. Heavy metals and their compounds are useful in many areas of human endeavor [2]. However, their excessive use leads to an increasing presence in aqueous environments [3]. Arsenic (As) pollution in aquatic systems is a global issue owing to its high toxicity and chronic effects on human health [4,5]. Arsenic pollution in drinking water is a major concern in developing countries. Previous studies have identified a relationship between arsenic exposure and diseases such as asthma and hyperglycemia [6,7]. Arsenic and inorganic arsenic compounds are classified as Group 1 human carcinogens by the International Agency for Research on Cancer [8]. The World Health Organization has established 0.01 mg L^{-1} as the maximum permissible arsenic content in potable water to protect human health [9]. The predominant forms of inorganic arsenic in aquatic systems are As(V) (arsenate) and As(III) (arsenite). Arsenic is a ubiquitous element, occurring from natural sources (such as wearing of arsenic bearing minerals and volcanic eruptions) and anthropogenic activities (such as mining, glassware production, dyes, drugs, and pesticide industries) [10–12]. As(III) is highly toxic, soluble, and mobile compared to As(V) [13,14]. Therefore, there is a need for simple, efficient, and inexpensive techniques to remove As(III) from aquatic systems.

Adsorption techniques using a variety of materials have been shown to be superior to conventional techniques such as precipitation, reverse osmosis, filtration, and biological treatment for As(III) removal [2,15]. Complex metal hydroxides are useful adsorbents for the removal of heavy metals from aqueous systems [16,17]. A complex metal hydroxide, or layered double hydroxide, contains divalent and trivalent cations at the octahedral positions of brucite-like layers. Anions are incorporated in the interlayer region for charge neutrality [18,19]. Multi-metal hydroxides exhibit substantially different physicochemical characteristics than their single-metal counter parts. Their properties depend on the identities and molar ratios of the constituent metals [20]. Many researchers have reported As(III) removal using adsorbents such as a Mn-oxide-doped Al oxide [15], an iron-zirconium binary oxide [13], a calcined Mg-Fe-La hydrotalcite-like compound [21], a nickel-aluminum hydroxide [16], and an Fe-Mg type hydrotalcite [17].

Incorporation of zirconium (Zr^{4+}) into a complex metal hydroxide such as a Mg-Al-layered double hydroxide has recently been examined [22,23]. Incorporation increases the charge in the metal layer and promises to be an attractive means of generating unique physicochemical properties. Positively charged brucite-like sheets have been prepared containing Zr^{4+}, which randomly occupies the octahedral holes in a close-packed configuration of hydroxide ions [22]. Adsorption of phosphate ion from aqueous media using the Zr^{4+}-containing complex metal hydroxide has been reported [22,23]. However, there have been no reports regarding As(III) adsorption from aqueous media. Arsenic as As(V) (arsenate) or As(III) (arsenite) adopts chemical forms similar to those of phosphorus as P(V) (phosphate) or P(III) (phosphite). We previously reported that nickel-aluminum-zirconium hydroxide is useful in the removal of phosphate ions from an aqueous phase [24]. This paper focuses on the relationship between As(III) adsorption and the complex nickel-aluminum and nickel-aluminum-zirconium hydroxides. The objectives of this work are to determine the physicochemical characteristics of complex nickel-aluminum and nickel-aluminum-zirconium hydroxides as a function of composition, to evaluate their ability to adsorb As(III) from aqueous media, and to investigate the mechanism of As(III) adsorption.

2. Materials and Methods

2.1. Materials and Chemicals

Nickel-aluminum and nickel-aluminum-zirconium hydroxides of different compositions were obtained from Kansai Catalyst Co., Ltd., Japan. Nickel-to-aluminum molar ratios of 1 and 0.5 are designated as NA11 and NA12, respectively. Nickel:aluminum:zirconium molar ratios of 0.9:1.0:0.09 and 0.9:0.2:0.09 are denoted as NAZ1 and NAZ2, respectively. Sulfate was included as an exchangeable anion in the interlayer of NA and NAZ. These materials were synthesized by the following method. Nickel(II) sulfate hexahydrate, aluminum sulfate octahydrate, and zirconium(IV) sulfate tetrahydrate were mixed with distilled water (230 g) at heating. The reaction mixture was added to the distilled water (400 g) at pH 9.0 for 800 rpm at 25 °C. The solution pH was adjusted using a 25% sodium hydroxide solution. After mixing for 2 h, the suspension was filtered, washed, and dried at 110 °C for 12 h. Arsenic(III) standard solution (As(III), As_2O_3 and NaOH in water pH 5.0 with HCl), hydrochloric acid, and sodium hydroxide were purchased from FUJIFILM Wako Pure Chemical Co., Japan. The purity grade of all reagents was special grade and the quality of water (resistivity) was 18.2 MΩ·cm at 25 °C.

2.2. Physicochemical Properties of Adsorbents

The NA11, NA12, NAZ1, and NAZ2 adsorbents were characterized as follows. The morphologies and crystallinities of the adsorbents were determined by scanning electron microscopy with an SU1510 instrument (Hitachi High-technologies Co., Tokyo, Japan) and a Mini Flex II X-ray diffraction analyzer (Rigaku Co., Tokyo, Japan), respectively. The surface area was determined by a specific surface analyzer N42-25E (Quantachrome Instruments Japan G.K., Kanagawa, Japan). Surface hydroxyl groups were assayed using the fluoride-ion adsorption method [25]. Briefly, the adsorbent (0.125 g) was mixed with a 0.01 mol L^{-1} NaF solution (50 mL) at pH 4.6. The solution pH was adjusted by 0.2 mol L^{-1} acetic acid solution and 0.2 mol L^{-1} acetate buffer solution. The reaction mixture was shaken for 24 h at 100 rpm and 25 °C and filtered through a 0.45-μm membrane filter. The concentration of fluoride ion before and after adsorption was measured using absorption spectrophotometry (DR890, HACH, Loveland, CO, USA). The amount of fluoride ion adsorbed was calculated (the ratio of the concentration of fluoride ion and the concentration of hydroxyl group is 1:1). The surface pH of the adsorbent was measured as follows. A 0.1-g quantity of adsorbent was added to 50 mL distilled water at pH 7.0. The suspension was shaken for 2 h at 100 rpm and 25 °C and filtered through a 0.45-μm membrane filter. The solution pH was measured with a digital pH meter (F-73, Horiba, Ltd., Kyoto, Japan) [26].

2.3. Adsorption Experiments

NA11, NA12, NAZ1, and NAZ2 in 0.1-g quantities were mixed with 50 mL of 100 mg L^{-1} As(III) solution to determine the extent of As(III) adsorption. Mixtures were shaken for 24 h at 100 rpm and filtered through a 0.45-μm membrane filter. The As(III) concentration of the filtrate was measured by inductively coupled plasma optical emission spectrometry using an iCAP 7600 Duo instrument (ICP-OES, Thermo Fisher Scientific Inc., Kanagawa, Japan). The quantity of As(III) adsorbed was calculated from the difference in As(III) concentration before and after adsorption. To examine the effect of contact time, 0.1-g quantities of NA11 and NAZ1 were mixed with 50 mL of a 100 mg L^{-1} As(III) solution and shaken for 0.5, 1, 3, 6, 9, 12, 16, 20, and 24 h at 100 rpm and 25 °C. The effect of pH was studied by mixing the same adsorbents with 50 mL of 100 mg L^{-1} As(III) and adjusting the solution pH from 2 to 10 using hydrochloric acid or sodium hydroxide. The same adsorbents were mixed with 50 mL of 1, 10, 30, 50, 70, and 100 mg L^{-1} As(III) solutions to study the effect of concentration. These solutions also were shaken for 24 h at 100 rpm and 25 °C. The quantity of sulfate ion released from adsorbent was measured to elucidate the adsorption mechanism of As(III).

Sulfate ion concentration was determined by ion chromatography using a DIONEX ICS-900 instrument (Thermo Fisher Scientific Inc., Tokyo, Japan), an IonPac AS12A system (4 × 200 mm, Thermo Fisher Scientific Inc., Tokyo, Japan), and an AMMS 300 (4 mm, Thermo Fisher Scientific Inc., Tokyo, Japan) micro-membrane filter suppressor. The regenerant and mobile phase were 12.5 mmol L^{-1} H_2SO_4, and 2.7 mmol L^{-1} Na_2CO_3 + 0.3 mmol L^{-1} $NaHCO_3$, respectively. The flow rate and sample volume were 1.0 mL min^{-1} and 10 μL under ambient conditions. The quantity of sulfate ions released from adsorbent were calculated using the levels before and after adsorption in Equation (1):

$$q = (C_e - C_0)V/W, \tag{1}$$

where q is the quantity of sulfate ion released (mg g^{-1}); C_0 is the concentration before adsorption (mg L^{-1}); C_e is the concentration after adsorption (mg L^{-1}); V is the solvent volume (L); and W is the weight of the adsorbent (g). Data are presented as the mean ± standard deviation from 2–3 experiments.

3. Results and Discussion

3.1. Physicochemical Properties of Adsorbents

The SEM images of each adsorbent are shown in Figure 1. The adsorbents are not perfectly spherical in shape, but no significant differences are observed in the appearance of the adsorbents in this study.

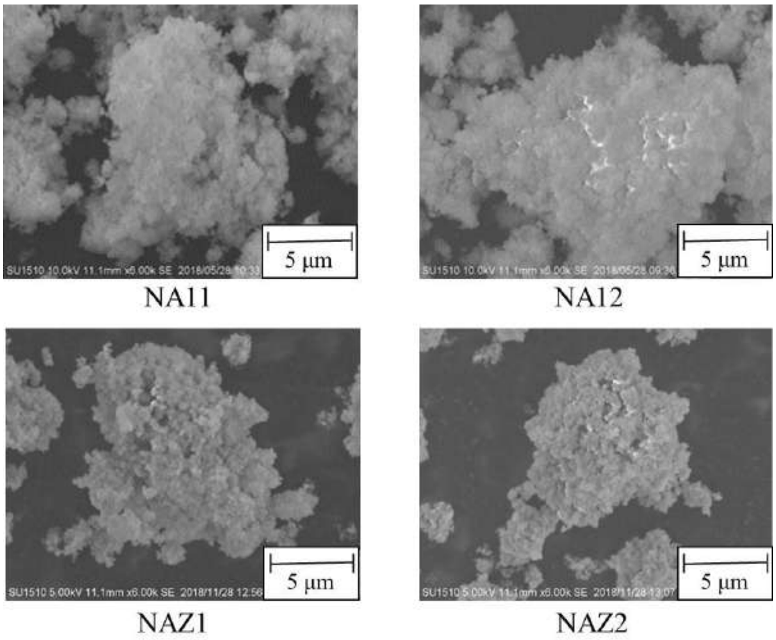

Figure 1. SEM images of adsorbents.

Figure 2 contains the X-ray diffraction patterns. Peaks at (003), (006), (015), and (113) are observed for all adsorbents indicating that they can be indexed to the crystal structure of the complex metal hydroxide. Peaks (003) and (006) are attributed to basal reflections that correspond to the stacking of the brucite-like sheets [27]. Some NAZ peaks are comparable to those in NA, which indicates that Zr^{4+} has been successfully incorporated into the octahedral layer of the complex nickel-aluminum hydroxide. Zirconium(IV) insertion alters the distances between metals and between the octahedral layers. Similar trends have been reported in previous investigations [22,23].

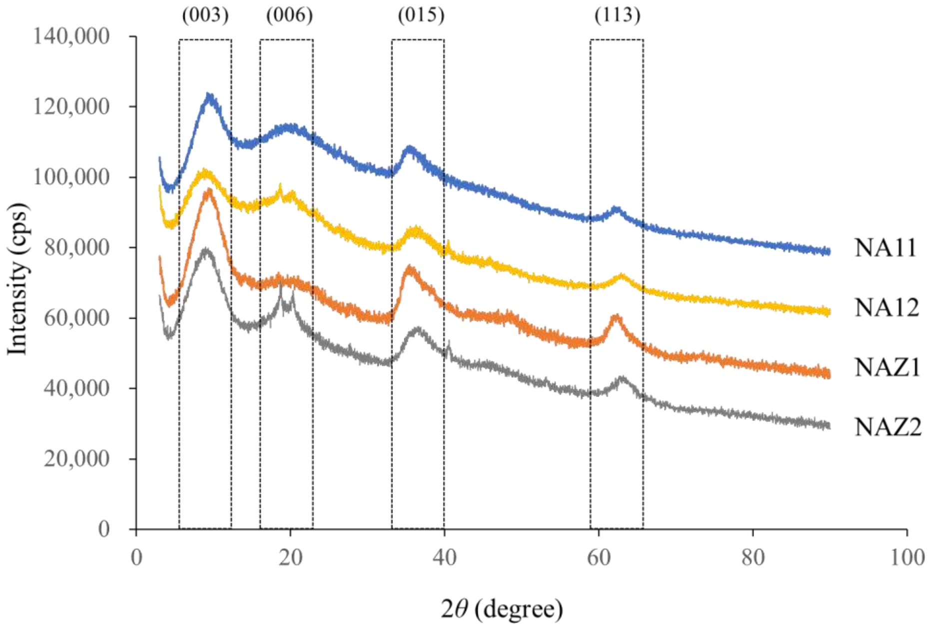

Figure 2. XRD patterns of adsorbents.

Some characteristics of the adsorbents are shown in Table 1. Surface pH and the number of hydroxyl groups of NA are higher than those of NAZ. However, the specific surface area of NAZ is greater than that of NA. The specific surface area of NAZ1 (51.9 m^2 g^{-1}) is greater than that of previously reported (Mg(AlZr)-LDHs(CO_3 or Cl) = 2.2–39 m^2 g^{-1} and Zr-MgAl = 49 m^2 g^{-1}) adsorbents, but not of (Zr-MgAl-HT = 154 m^2 g^{-1}) [17,18]. These results indicate that incorporation of Zr^{4+} into the octahedral layer of the complex nickel-aluminum hydroxide results in an increase of the specific surface area.

Table 1. Characteristics of adsorbents.

Adsorbents	Surface pH	Number of Hydroxyl Groups (mmol g^{-1})	Specific Surface Area (m^2 g^{-1})
NA11	7.98	1.92	22.8
NA12	7.63	1.62	26.4
NAZ1	6.18	1.08	51.9
NAZ2	6.21	1.51	27.8

3.2. Adsorption Capability of As(III)

The quantities of As(III) adsorbed onto each adsorbent are shown in Figure 3. The amount adsorbed increases as NA11 < NA12 < NAZ2 < NAZ1, which indicates that NAZ1 should be the most useful for removal of As(III) from aqueous media. Relationships between the quantity of As(III) adsorbed and the three parameters in Table 1 were statistically assessed. The correlation coefficients between the amount adsorbed and the surface pH, amount of hydroxyl groups, and specific surface area were negative 0.570, negative 0.738, and positive 0.921, respectively. Therefore, specific surface area most strongly influences As(III) adsorption capability in solution. The surface properties of adsorbents are very important in the interactions with As(III) in the aqueous phase. Additionally, the effect of zirconium incorporation on the characteristic of adsorbent and adsorption capability of As(III) was evaluated in detail. Thus, NA11 and NAZ1 were selected to evaluate As(III) adsorption in the following experiments.

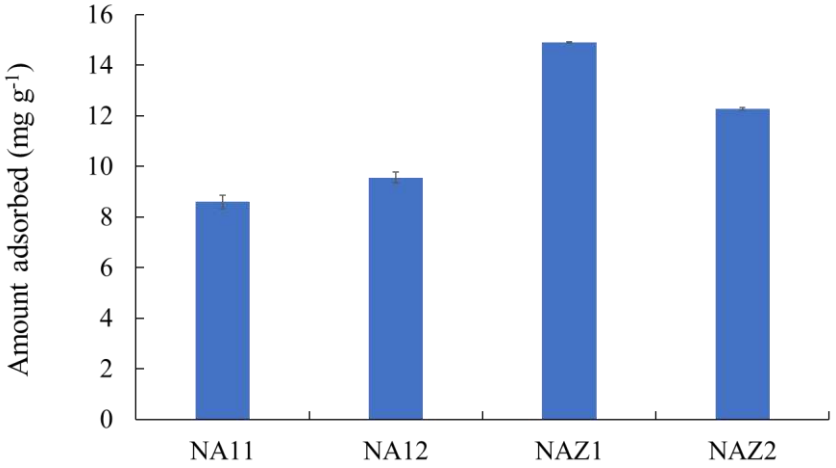

Figure 3. Amount of As(III) adsorbed. Initial concentration: 100 mg L^{-1}, solvent volume: 50 mL, adsorbent: 0.1 g, contact time: 24 h, temperature: 25 °C, agitation speed: 100 rpm.

3.3. Adsorption Kinetics

The kinetics of As(III) adsorption onto NA11 and NAZ1 were conducted at an initial concentration of 100 mg L^{-1}. Adsorption equilibrium was reached within 24 h under the experimental conditions (Figure 4). It is clear that adsorption of As(III) onto NA11 and NAZ1 is complicated, because the time to reach equilibrium would be short if the process were controlled by a single factor [21]. Thus, the adsorption mechanism was investigated by comparing results to both pseudo-first-order (2) and pseudo-second-order models (3) [28,29]:

$$\ln(q_e - q_t) = \ln q_e - k_1 t, \tag{2}$$

$$\frac{t}{q_t} = \frac{t}{q_e} + \frac{1}{k_2 \times q_e{}^{2'}} \tag{3}$$

where q_e and q_t are the amounts of As(III) adsorbed (mg g^{-1}) at equilibrium and given time t, and k_1 and k_2 are the pseudo-first-order (h^{-1}) and pseudo-second-order (g mg^{-1} h^{-1}) rate constants. Table 2 shows the results of fitting the experimental data to the pseudo-first-order (coefficient of determination = 0.817–0.961) and pseudo-second-order (coefficient of determination = 0.978–0.992) models. The adsorption of As(III) onto NA11 and NAZ1 appears to occur by a process of chemisorption. The value of k_2 with NAZ1 is less than that with NA11, which indicates that As(III) adsorption is favored at NAZ1. This conclusion is supported by the result in Figure 3, which shows that a greater amount of As(III) is adsorbed by NAZ1. Adsorption equilibrium also tends to be established more rapidly using NA11 than NAZ1. Similar trends have been reported in previous studies [13,30]. Additionally, a previous study pointed out the fact that more caution should be exercised in the analysis of kinetic data [31]. Thus, the chi-square analysis (χ^2) was conducted for the evaluation of kinetic models to avoid including errors. The low value of χ^2 indicates that the kinetic model fits to the experimental data [32]. The value of χ^2 in the pseudo-first-order model was higher than that in the pseudo-second-order model (Table 2), which indicates that the pseudo-second-order model is considered to be better for the obtained data in this study.

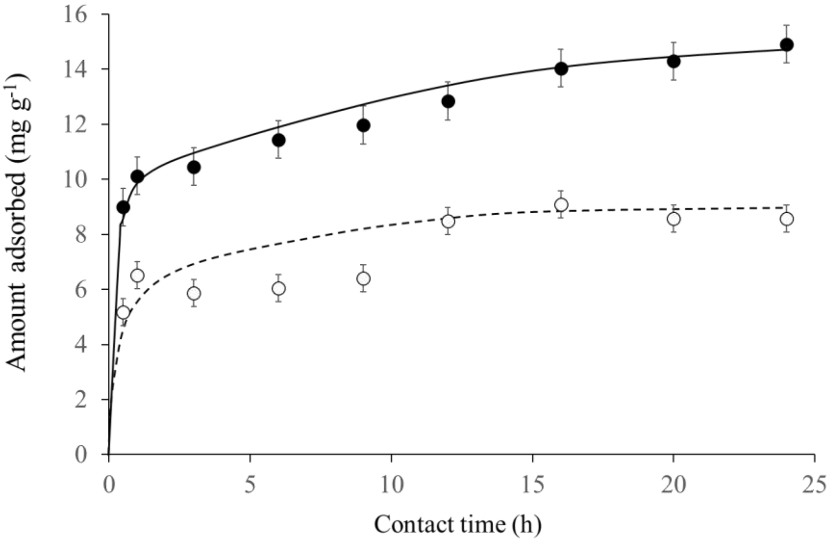

Figure 4. Effect of contact time on the adsorption of As(III) using NA11 and NAZ1. Initial concentration 100 mg L^{-1}, solvent volume 50 mL, adsorbent 0.1 g, contact time 0.5, 1, 3, 6, 9, 12, 16, 20, and 24 h, temperature 25 °C, agitation speed 100 rpm, ●: NAZ1, ○: NA11.

Table 2. Kinetic parameters for the adsorption of As(III).

Adsorbents	q_e	**Pseudo-First-Order Model**				**Pseudo-Second-Order Model**			
		k_1 (h^{-1})	q_e (mg g^{-1})	r^2	χ^2	k_2 (g mg^{-1} h^{-1})	q_e (mg g^{-1})	r^2	χ^2
NA11	8.6	0.093	3.9	0.817	1.8×10^2	0.110	9.1	0.978	1.8
NAZ1	14.9	6.4	6.4	0.961	2.9×10	0.066	15.2	0.992	1.4

3.4. Effect of pH on the Adsorption of As(III)

Solution pH is a critical factor in the removal of As(III) from aqueous solution. Figure 5 shows the effect of pH on As(III) adsorption using NA11 and NAZ1. The quantity of As(III) adsorbed tends to increase with increasing pH. A similar trend using zirconium oxide-ethanolamine has been reported in a previous study [12]. Here, solution pH tends to increase or decrease slightly after adsorption indicating that the surface of NA11 and NAZ1 may be useful as a neutralizing agent in the wastewater treatment of highly acidic or basic As(III) samples [12,33]. The $pK_{a,1}$ of H_3AsO_3 is 9.2, which indicates that As(III) is a neutral species at pH 9.2. At pH > 9.2, anionic forms of As(III) are produced that undergo ion exchange with sulfate ion from NA11 and NAZ11 under the experimental conditions (see Section 3.5).

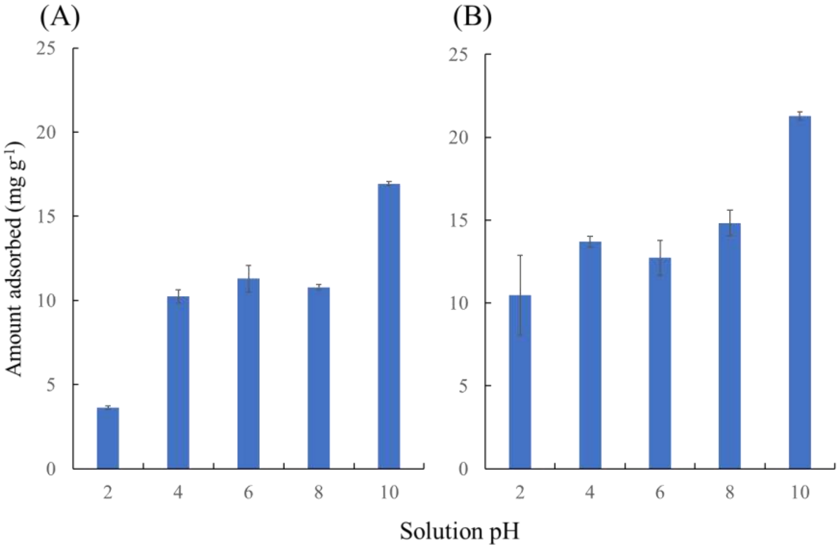

Figure 5. Effect of pH on the adsorption of As(III) using NA11(**A**) and NAZ1(**B**). Initial concentration 100 mg L^{-1}, solvent volume 50 mL, adsorbent 0.1 g, pH 2, 4, 6, 8, and 10, contact time 24 h, temperature 25 °C, agitation speed 100 rpm.

3.5. As(III) Adsorption Isotherms

Figure 6 displays adsorption isotherms of As(III) at different temperatures. The data provide considerable insight to the adsorptive behavior of NA11 and NAZ1 towards As(III) in aqueous solution. The quantities of As(III) adsorbed increase with increasing temperatures (10 < 25 < 45 °C), which indicates that chemisorption is involved in the adsorption of As(III) on NA11 and NAZ1. The solution pH was 5.5–6.4 and 5.9–6.2 for NA11 and NAZ1 in all experimental temperatures. Thus, the predominant form of As(III) was not affected by the temperature under our experimental conditions.

Langmuir and Freundlich models were applied to provide a more quantitative description of the relationship between the quantity of As(III) adsorbed and the solute concentration. The Langmuir model is described by Equation (4) [34]:

$$1/q = 1/(W_s a C_e) + 1/W_s, \tag{4}$$

where q is the quantity of As(III) adsorbed (mg g^{-1}), W_s is the maximum amount of As(III) adsorbed (mg g^{-1}), a is the Langmuir isotherm constant (binding energy) (L mg^{-1}), and C_e is the equilibrium concentration (mg L^{-1}). The Langmuir isotherm is applicable to monolayer coverage by the adsorbate. The Freundlich model is described by Equation (5) [35]:

$$\log q = \frac{1}{n} \log C + \log k, \tag{5}$$

where k and $1/n$ are the adsorption capacity and strength of adsorption, respectively. The Freundlich model describes systems where the surface of the adsorbent is heterogeneous and has sites of different energy [13]. Table 3 shows that the Freundlich model (≥0.970) provides better correlation than the Langmuir model (≥0.965) except for NAZ1 at 25 °C. Previous studies have reported similar behavior using Fe-based backwashing sludge and polymer adsorbents [33,36]. The maximum adsorption capacity (W_s) of As(III) increases from 10 °C to 45 °C. It is worth noting that in the experimental conditions used, equilibrium data (Figure 6) suggest that the plateau for maximum adsorption was not reached. The maximum adsorbed amounts calculated in the Langmuir fitting, however, are lower than some values measured experimentally, which may be due to the use of a linearized equation (Equation (4)) to mathematically model the results. This indicates that the adsorption of As(III) on NA11 and NAZ1 is an endothermic process, which was supported by the results in Figure 6. In the Freundlich model, n is the heterogeneity factor. Therefore, when $1/n$ = 0.1–0.5, adsorption occurs easily, and when $1/n > 2$, adsorption is difficult [37]. The values of $1/n$ = 0.13−0.97 obtained in this study indicate that As(III) adsorption onto NA11 and NAZ1 is favored in aqueous solution.

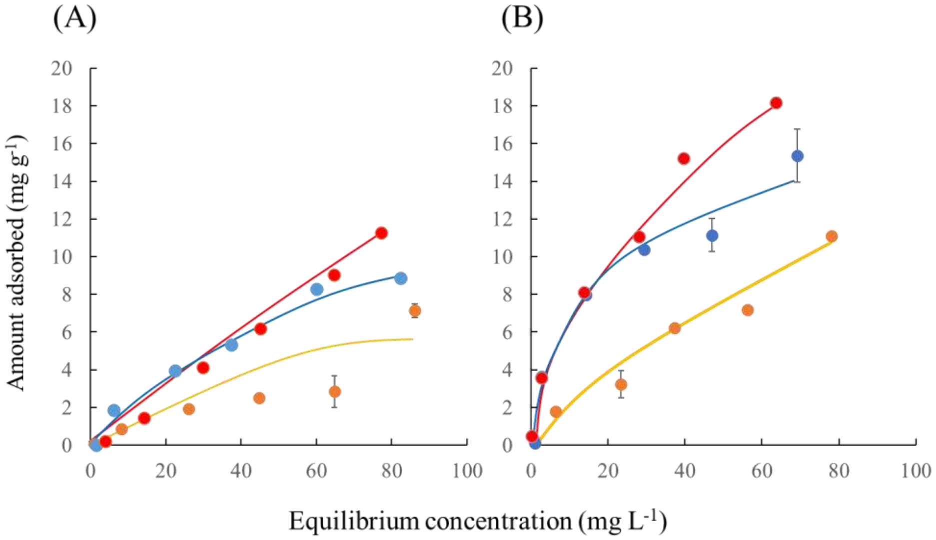

Figure 6. Effect of temperature on the adsorption of As(III) using NA11 (**A**) and NAZ1 (**B**). Initial concentration 1, 10, 30, 50, 70, and100 mg L^{-1}, solvent volume 50 mL, adsorbent 0.1 g, contact time 24 h, pH 5.5-6.4 and 5.9-6.2 for NA11 and NAZ1, temperature 10 (●), 25 (●), and 45 °C (●), agitation speed 100 rpm.

Table 3. Langmuir and Freundlich constants for the adsorption of As(III).

Adsorbents	Temperature (°C)	Langmuir Constants			Freundlich Constants		
		W_s (mg g^{-1})	a (L mg^{-1})	r^2	log$k$	$1/n$	r^2
NA11	10	6.1	0.02	0.965	−0.1	0.91	0.970
	25	9.3	0.04	0.982	−0.1	0.56	0.991
	45	15.4	0.006	0.989	−1.4	0.13	0.996
NAZ1	10	6.3	0.09	0.996	−0.3	0.70	0.989
	25	15.3	0.01	0.935	−0.4	0.97	0.768
	45	16.6	0.10	0.977	0.29	0.54	0.999

In this study, sulfate ions are present in the interlayer of the NA11 and NAZ1 absorbents. Figure 7 shows the relationship between the amount of As(III) adsorbed and the amount of sulfate ion released from NA11 and NAZ1. The correlation coefficients for release from NA11 and NAZ1 are 0.797 and 0.944, respectively. The results indicate that the release of sulfate from NA11 and NAZ1 by ion exchange has a role in the adsorption mechanism of As(III).

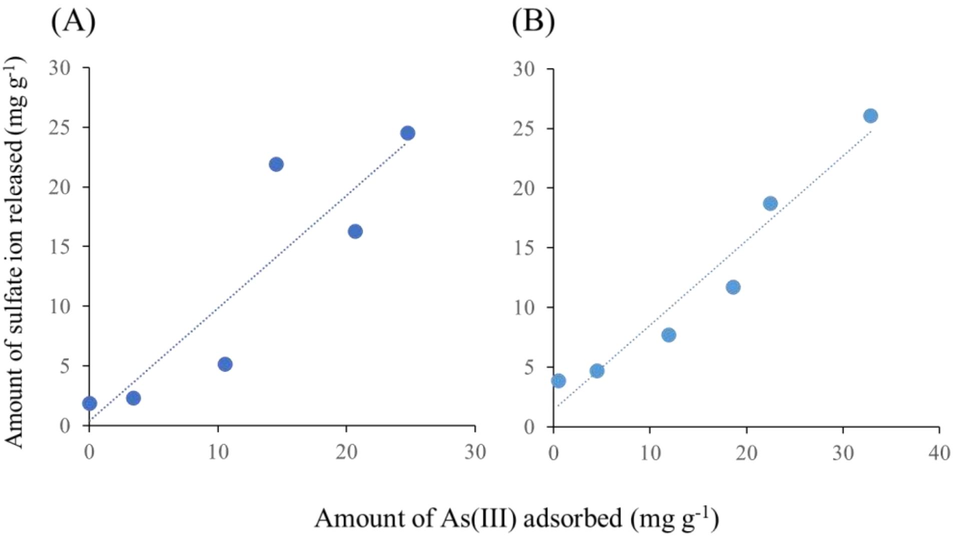

Figure 7. Relationship between amount of As(III) adsorbed and amount of sulfate ion released using NA11 (**A**) and NAZ1 (**B**). Initial concentration 1, 10, 30, 50, 70, and100 mg L^{-1}, solvent volume 50 mL, adsorbent 0.1 g, pH 10, contact time 24 h, temperature 25 °C, agitation speed 100 rpm.

3.6. Comparison of Adsorption Capability of As(III)

Table 4 summarizes comparisons of As(III) adsorption capability of NA11 and NAZ1 with other reported adsorbents [38–41]. The NAZ1 exhibited a good potential to be used for removal of As(III) from aqueous media compared to other reported adsorbents (except for drinking-water treatment residuals (WTRs)). From these comparisons, NAZ1 is expected to be employed in a commercial process in the future for As(III) adsorption.

Table 4. Comparison of As(III) adsorption capacity of NA11 and NAZ1 with other reported adsorbents.

Adsorbents	Adsorption Capability (mg/g)	pH	Temp. (°C)	Initial Concentration (mg/L)	Contact Time (h)	Adsorbent (g/L)	Ref.
ZrPACM-43	0.8	<5	50	100	2	13	[3]
Al-HDTMA-sericite	0.433	4.5	-	2	Approximately 6.7	1	[38]
Iron hydroxide-coated alumina	9.0	6.6	20 × 0.5	7.5–135	48	1–25	[39]
Silica gel impregnated with ferric hydroxide	4.5	7.0	20–23	1	15	-	[40]
WTRs	15	6.0–6.5	23	375–3000	48	25–200	[41]
NA11	9.3	5.5–6.4	25	100	24	2	This study
NAZ1	15.3	5.9–6.2	25	100	24	2	This study

4. Conclusions

The complex metal hydroxides NA11 and NAZ1 were prepared to study As(III) removal from aqueous media. The specific surface area of NAZ1 (51.9 m^2 g^{-1}) was greater than that of NA11 (22.8 m^2 g^{-1}). The quantity of As(III) adsorbed onto NAZ1 (15.3 mg g^{-1}) was also greater than that adsorbed onto NA11 (9.3 mg g^{-1}). The correlation coefficient between the quantity adsorbed and the specific surface area was 0.921. The adsorption kinetics followed the pseudo-second-order model (coefficient of determination using NA11 and NAZ1 was 0.978 and 0.992, respectively). Adsorption isotherms data established that As(III) adsorption was an endothermic process. Ion exchange with sulfate ions in the interlayer of the adsorbent was also involved in the As(III) adsorption mechanism.

Author Contributions: Conceptualization, N.K. and F.O.; investigation, N.N., C.S., and T.N.; resources, M.T. and M.O.; writing—original draft preparation, F.O.; writing—review and editing, F.O. and C.S.; project administration, N.K. All authors have read and agreed to the published version of the manuscript.

Funding: This research was funded by The Research Foundation for Pharmaceutical Sciences.

Conflicts of Interest: The authors declare no conflict of interest.

References

1. Transforming Our World: The 2030 Agenda for Sustainable Development. Available online: https://sustainabledevelopment.un.org/post2015/transformingourworld (accessed on 8 May 2020).
2. Mohan, D.; Charles, P. Arsenic removal from water/wastewater using adsorbents-a critical review. *J. Hazard. Mater.* **2007**, *142*, 1–53. [CrossRef]
3. Mandal, S.; Sahu, M.K.; Patel, R.K. Adsorption studies of arsenic(III) removal from water by zirconium polyacrylamide hybrid material (ZrPACM-34). *Water Resour. Ind.* **2013**, *4*, 51–67. [CrossRef]
4. Hughes, M.F. Arsenic toxicity and potential mechanisms of action. *Toxicol. Lett.* **2002**, *133*, 1–16. [CrossRef]
5. Mandal, B.K.; Suzuki, K.T. Arsenic round the world: A review. *Talanta* **2002**, *58*, 201–235. [CrossRef]
6. Siddique, A.E.; Rahman, M.; Hossain, M.I.; Karim, Y.; Hasibuzzaman, M.M.; Biswas, S.; Islam, M.S.; Rahman, A.; Hossen, F.; Mondal, V.; et al. Association between chronic arsenic exposure and the characteristic features of asthma. *Chemosphere* **2020**, *246*, 129750. [CrossRef]
7. Paul, S.K.; Islam, M.S.; Hasibuzzaman, M.M.; Hossain, F.; Anjum, A.; Saud, Z.A.; Haque, M.M.; Sultana, P.; Haque, A.; Andric, K.B.; et al. Higher risk of hyperglycemia with greater susceptibility in females in chronic arsenic-exposed individuals in Bangladesh. *Sci. Total Environ.* **2019**, *668*, 1004–1012. [CrossRef]
8. IARC Monographs on the Identification of Carcinogenic Hazards to Human. Available online: https://monographs.iarc.fr/agents-classified-by-the-iarc/ (accessed on 31 May 2020).
9. Arsenic in Drinking Water. Available online: https://www.who.int/water_sanitation_health/water-quality/guidelines/arsenic-information/en/ (accessed on 31 May 2020).
10. Vaishya, R.C.; Gupta, S.K. Modeling arsenic(III) adsorption from water by sulfate-modified iron oxide-coated sand (SMIOCS). *J. Chem. Technol. Biotechnol.* **2002**, *89*, 73–80. [CrossRef]
11. Martinson, C.A.; Reddy, K.J. Adsorption of arsenic(III) and arsenic(V) by cupric oxide nanoparticles. *J. Colloid Interf. Sci.* **2009**, *336*, 406–411. [CrossRef]
12. Mandal, S.; Padhi, T.; Patel, R.K. Studies on the removal of arsenic(III) from water by a novel hybrid material. *J. Hazard. Mater.* **2011**, *192*, 899–908. [CrossRef]
13. Ren, Z.; Zhang, G.; Paul Chen, J. Adsorptive removal of arsenic from water by an iron-zirconium binary oxide adsorbent. *J. Colloid Interf. Sci.* **2011**, *358*, 230–237. [CrossRef]
14. Ferguson, J.F.; Gavis, J. A review of arsenic cycle in natural waters. *Water Res.* **1972**, *6*, 1259–1274. [CrossRef]
15. Wu, K.; Liu, T.; Xue, W.; Wang, X. Arsenic(III) oxidation/adsorption behaviors on a new bimetal adsorbent of Mn-oxide-doped Al oxide. *Chem. Eng. J.* **2012**, *192*, 343–349. [CrossRef]
16. Ogata, F.; Nakamura, T.; Toda, M.; Otani, M.; Kawasaki, N. Evaluation of nickel-aluminum complex hydroxide for adsorption of chromium(VI) ion. *Chem. Pharm. Bull.* **2020**, *68*, 70–76. [CrossRef]
17. Ogata, F.; Ueta, E.; Kawasaki, N. Characteristics of a novel adsorbent Fe-Mg-type hydrotalcite and its adsorption capability of As(III) and Cr(VI) from aqueous solution. *J. Ind. Eng. Chem.* **2018**, *59*, 56–63. [CrossRef]
18. Zhang, X.; Guo, L.; Huang, H.; Jiang, Y.; Li, M.; Leng, Y. Removal of phosphorus by the core-shell bio-ceramic/Zn-layered double hydroxides (LDHs) composites for municipal wastewater treatment in constructed rapid infiltration system. *Water Res.* **2016**, *96*, 280–291. [CrossRef]
19. Radha, A.V.; Kamath, P.V. Aging of trivalent metal hydroxide/oxide gels in divalent metal salt solutions: Mechanism of formation of layered double hydroxides (LDHs). *Bull. Mater. Sci.* **2003**, *26*, 661–666. [CrossRef]
20. Ogata, F.; Nagai, N.; Toda, M.; Otani, M.; Nakamura, T.; Kawasaki, N. Evaluation of the interaction between borate ions and nickel-aluminum complex hydroxide for purification of wastewater. *Chem. Pharm. Bull.* **2019**, *67*, 487–492. [CrossRef]

21. Wu, P.; Xia, L.; Liu, Y.; Wu, J.; Chen, Q.; Song, S. Simultaneous sorption of arsenate and fluoride on calcined Mg-Fe-La hydrotalcite-like compound from water. *ACS Sustain. Chem. Eng.* **2018**, *6*, 16287–16297. [CrossRef]
22. Chitrakar, R.; Tezuka, S.; Sonoda, A.; Sakane, K.; Ooi, K.; Hirotsu, T. Synthesis and phosphate uptake behavior of Zr4+ incorporated MgAl-layered double hydroxides. *J. Colloid Interf. Sci.* **2007**, *313*, 53–63. [CrossRef]
23. Miyauchi, H.; Yamamoto, T.; Chitrakar, R.; Makita, Y.; Wang, Z.; Kawai, J.; Hirotsu, T. Phosphate adsorption site on zirconium ion modified MgAl-layered double hydroxides. *Top Catal.* **2009**, *52*, 714–723. [CrossRef]
24. Ogata, F.; Iijima, S.; Toda, M.; Otani, M.; Nakamura, T.; Kawasaki, N. Characterization and phosphate adsorption capability of novel nickel-aluminum-zirconium complex hydroxide. *Chem. Pharm. Bull.* **2020**, *68*, 292–297. [CrossRef]
25. Ymashita, T.; Ozawa, Y.; Nakajima, N.; Murata, T. Collection of uranium from sea water with hydrous oxide adsorbents. 1. Ion exchange properties and uranium adsorption of hydrous titanium(IV) oxide. *Nippon Kagaku Kaishi* **1978**, *8*, 1057–1061. [CrossRef]
26. Ogata, F.; Ueta, E.; Toda, M.; Otani, M.; Kawasaki, N. Adsorption of phosphate ions from an aqueous solution by calcined nickel-cobalt binary hydroxide. *Water Sci. Technol.* **2017**, *75*, 94–105. [CrossRef]
27. Türk, T.; Alp, İ. Arsenic removal from aqueous solutions with Fe-hydrotalcite supported magnetite nanoparticle. *J. Ind. Eng. Chem.* **2014**, *20*, 732–738. [CrossRef]
28. Lagergren, S. Zur theorie der sogenannten adsorption geloster stoffie, *Kunglia Svenska Vetenskapsakademiens. Handlingar* **1898**, *24*, 1–39.
29. Ho, Y.S.; McKay, G. Pseudo-second order model for sorption process. *Pro Biochem.* **1999**, *34*, 451–465. [CrossRef]
30. Raven, K.P.; Jain, A.; Loeppert, R.H. Arsenite and arsenate adsorption on ferrihydrite: Kinetics, equilibrium, and adsorption evelopes. *Environ. Sci. Technol.* **1998**, *32*, 344–349. [CrossRef]
31. Simonin, J.P. On the comparison of pseudo-first order and pseudo-second order rate laws in the modeling of adsorption kinetics. *Chem. Eng. J.* **2016**, *300*, 254–263. [CrossRef]
32. Ho, Y.S. Selection of optimum sorption isotherm. *Carbon* **2004**, *42*, 2115–2116. [CrossRef]
33. Wu, K.; Liu, R.; Li, T.; Liu, H.; Peng, J.; Qu, J. Removal of arsenic(III) from aqueous solution using a low-cost by-product in Fe-removal plants-Fe-based backwashing sludge. *Chem. Eng. J.* **2013**, *226*, 292–401. [CrossRef]
34. Langmuir, I. The constitution and fundamental properties of solids and liquids. *J. Am. Chem. Soc.* **1916**, *38*, 2221–2295. [CrossRef]
35. Freundlich, H.M.T. Over the adsorption in solution. *J. Phys. Chem.* **1906**, *57*, 385–471.
36. Li, H.T.; Xu, M.C.; Shi, Q.; He, B.L. Isotherm analysis of phenol adsorption on polymeric adsorbents from nanoaqueous solution. *J. Colloid. Interf. Sci.* **2004**, *271*, 47–54. [CrossRef]
37. Abe, I.; Hayashi, K.; Kitagawa, M. Studies on the adsorption of surfactants on activated carbons. I. Adsorption of nonionic surfactants. *Yukagaku* **1976**, *25*, 145–150.
38. Tiwari, D.; Lee, S.M. Novel hybrid materials in the remediation of ground waters contaminated with As(III) and As(V). *Chem. Eng. J.* **2012**, *204-206*, 23–31. [CrossRef]
39. Hlavay, J.; Polyak, K. Determination of surface properties of iron hydroxide-coated alumina adsorbent prepared for removal of arsenic from drinking water. *J. Colloid Interf. Sci.* **2005**, *284*, 71–77. [CrossRef]
40. Yoshida, I.; Kobayashi, H.; Ueno, K. Selective adsorption of arsenic ions on silica gel impregnated with ferric hydroxide. *Anal. Lett.* **1976**, *9*, 1125–1133. [CrossRef]
41. Makris, K.C.; Sarkar, D.; Datta, R. Evaluating a drinking-water waste by-product as a novel sorbent for arsenic. *Chemosphere* **2006**, *64*, 730–741. [CrossRef]

water

Article

Uptake and Recovery of Gold from Simulated Hydrometallurgical Liquors by Adsorption on Pine Bark Tannin Resin

Maria Beatriz Q. L. F. Torrinha, Hugo A. M. Bacelo, Sílvia C. R. Santos *, Rui A. R. Boaventura and Cidália M. S. Botelho

Laboratory of Separation and Reaction Engineering—Laboratory of Catalysis and Materials (LSRE-LCM), Chemical Engineering Department, Faculdade de Engenharia da Universidade do Porto, Rua Dr. Roberto Frias, 4200-465 Porto, Portugal; up201305818@fe.up.pt (M.B.Q.L.F.T.); up201204895@fe.up.pt (H.A.M.B.); bventura@fe.up.pt (R.A.R.B.); cbotelho@fe.up.pt (C.M.S.B.)

* Correspondence: scrs@fe.up.pt

Received: 6 November 2020; Accepted: 7 December 2020; Published: 9 December 2020

Abstract: The recovery of critical and precious metals from waste electrical and electronic equipment (WEEE) is an environmental and economic imperative. Biosorption has been considered a key technology for the selective extraction of gold from hydrometallurgical liquors obtained in the chemical leaching of e-waste. In this work, the potential of tannin resins prepared from *Pinus pinaster* bark to sequester and recover gold(III) from hydrochloric acid and aqua regia solutions was assessed. Equilibrium isotherms were experimentally determined and maximum adsorption capacities of 343 ± 38 and 270 ± 19 mg g^{-1} were found for Au uptake from HCl and HCl/HNO_3 (3:1 *v/v*) solutions containing 1.0 mol L^{-1} H^+. Higher levels of acidity (and chloride ligands) significantly impaired the adsorption of gold from both kinds of leaching solutions, especially in the aqua regia system, in which the adsorbent underperformed. Pseudo-first and pseudo-second order models successfully described the kinetic data. The adsorbent presented high selectivity towards gold. Actually, in simulated aqua regia WEEE liquors, Au(III) was extensively adsorbed, compared to Cu(II), Fe(III), Ni(II), Pd(II), and Zn(II). In three adsorption–desorption cycles, the adsorption capacity of the regenerated adsorbent moderately decreased (19%), although the gold elution in acidic thiourea solution had been quite limited. Future research is needed to examine more closely the elution of gold from the exhausted adsorbents. The results obtained in this work show good perspectives as regards the application of pine bark tannin resins for the selective extraction of Au from electronic waste leach liquors.

Keywords: precious metals; hydrometallurgical processing; biosorption; selectivity; pine bark

---

1. Introduction

Gold is a precious metal commonly used in jewellery and electronics [1], but also in medicine and as a catalyst in various chemical processes [2]. Waste electrical and electronic equipment (WEEE) is a fast-growing waste stream. In 2019, 53.6 Mt of e-waste were generated in the world, corresponding to an average of 7.3 kg per capita [3]. Globally, however, only 17.4% was documented to be formally collected and recycled [3]. In Europe, the management of WEEE is regulated by the Directive 2012/19/EU [4], which states that, from 2019, member states should achieve an annual collection rate of WEEE of 65% of the average weight of EEE placed on the market in the three preceding years. Although Europe was the continent presenting the highest rate (42.5%), collection and recycling must increase even further to meet the target [3]. WEEE contains bulky metals, along with plastics and toxic elements, but also technology metals which, in the frame of a circular economy, should be recovered. The content of precious/critical metals in WEEE vary considerably, but in certain types of WEEE can even exceed those found in primary sources [5–7]. For instance, levels of 250–2050 ppm of gold have been reported in waste printed circuit boards [8]. However, greener and more economically competitive routes are necessary to extract metals from WEEE and achieve sustainable processes.

The recovery of precious metals from e-waste usually involves dismantling, comminution, and separation [8–10], chemical pre-treatments to dissolve base metals [10,11], followed by pyrometallurgical and/or hydrometallurgical processes. Despite the challenges related to the use of strong acids in leaching processes, and the need to minimise the loss of chemicals, hydrometallurgical processes have been considered a cleaner option to be integrated at the back-end of a recycling scheme for the recovery and production of high purity metals [6,7,12]. They also have lower capital costs and benefit from easier implementation at the small scale. Cyanide has been the dominating leaching reagent of Au from primary resources [13] and possibly the most reliable and economic for WEEE [10]. However, the toxicity of cyanide makes its use prohibitive in modern processes. Alternative leaching reagents have been proposed to dissolve Au from WEEE, including chloride, aqua regia, thiourea and thiosulfate [13]. The subsequent stage of a typical flowsheet is the extraction of gold from leaching liquors. Among the various techniques that can be implemented, adsorption has been the dominant one, especially in cyanide liquors, and due to a favourable cost-effectiveness [14], in which activated carbon has been for decades the adsorbent of choice [15,16]. The current interest in moving forward a more benign recovery has been motivating the search for alternative adsorbents, at more competitive prices and able to sequester gold from non-cyanide leach liquors. The use of bio-derived adsorbents has been regarded as a key technology [17], offering advantages related to the ready availability of the biomass, to the simple synthesis and chemical functionality, which usually make them good sequestrants of metals. Important criteria to be met by biosorbents for gold recovery include: (i) high uptake capacity of the metal from actual matrices; (ii) selectivity, i.e., adsorbents should be able to uptake gold to the detriment of other base metals and noble metals coexisting in solution; (iii) fast adsorption kinetics; and (iv) feasible subsequent recovery of the adsorbed metal. In addition, the adsorbents should have particle sizes suitable for use in fixed bed systems, avoiding pressure drop and column clogging, and should have also good chemical stability in strong acidic solutions, considering this is the condition of typical gold-bearing liquors [18]. Various adsorbents have been investigated for gold recovery, including commercial resins [19,20], crosslinked polyethyleneimine resin [19], and a wide range of natural-derived adsorbents such as polyethylenimine modified Ca^{2+}-alginate fibres [18], polyethylenimine modified *Lagerstroemia speciosa* leaves [21], banana peel derivatives [22], raw date pits [23], and tannin-derived materials [6,24–26]. The successful uptake of gold has been explained by electrostatic interaction between the gold complexes in solution and the adsorbent surface, followed by a reduction mechanism, involving amine, hydroxyl, and aldehyde groups of the adsorbents [18,21,27,28].

Tannins are natural polyphenolic macromolecules present in leaves, wood, bark, seeds and fruits of various plants. Their abundance in nature, easy extraction with water, richness in hydroxyl groups and easy tailoring have made tannin materials interesting biosorbents for the removal of contaminants from water and for the uptake and recovery of precious metals [26]. Tannin resins may be prepared through a crosslinking reaction (gelification) with aldehydes [24,25]. Further chemical modifications, such as anchoring of amine groups [24,29] are possible to improve the adsorptive performance of the materials. Immobilization in support materials [28,30] and magnetization [24] have been also investigated to enhance solid-liquid separation. Outstanding uptake capacities of gold have been reported for different tannin-derived biosorbents [24,27,29], explained by the oxidation of polyhydroxyl groups and the reduction of the metal to its elemental form [24,28]. Literature on the recovery of gold by tannin adsorbents has been however limited to few sources of the precursor, namely tannin acid, commercial tannins, valonea, and persimmon tannins [26,28–30]. Despite the fact that pine bark tannin resins have been investigated to remove pollutants from water, in a remediation perspective [31–33], no studies were found in the literature evaluating the uptake of precious metals by this material and subsequent recovery. More research is also needed to obtain results in aqua regia solutions and stronger chloride and acidic media.

This work comes in response to the need of economical and environmentally competitive processes for the recovery of precious metals from WEEE. The adsorption of gold(III) by a tannin resin prepared from bark of maritime pine (*Pinus pinaster*) is studied. The bark of this native Mediterranean tree is a forest residue and a by-product of wood conversion industry, which can give a contribute to bioeconomy. Chloride and aqua regia solutions were used, and the uptake of gold was investigated from single and multi-metal systems, simulating actual hydrometallurgical liquors. The final recovery of the metal was achieved by elution.

2. Materials and Methods

2.1. Adsorbent

A tannin resin, prepared from maritime pine (*P. pinaster*) bark, was used in this work as adsorbent. *P. pinaster* bark was collected (direct sampling) from the coastal North region of Portugal, milled using a regular coffee grinder resulting a final particle size distribution of (percentages by mass, % *w/w*): 40% in the fraction <0.15 mm, 24% in the range 0.15–0.50 mm, 29% of 0.50–1.0 mm, and 7% of 1.0–2.0 mm. Tannins were extracted from the pine bark in batch mode, using an alkaline aqueous solution of 7.5 % NaOH (% *w/w*, in respect to the bark), and a bark-to-liquid ratio of 1:6 (*w/w*). The extraction was carried out under magnetic stirring at a temperature of 90 °C and for a contact time of 60 min. These extraction conditions were the best found in a previous work [33]. After solid-liquid separation (suction filtration, using a vacuum pump), the resulting solution was neutralized with HCl 2.0 mol L^{-1} and subjected to freeze-drying (FreeZone 2.5 Plus, Labconco, Kansas City, MO, USA). NaOH and HCl solutions were prepared from analytical grade salt and acid, respectively. The obtained solid extract was converted into an insoluble material by a cross-linking reaction (gelification). For this purpose, 3.0 g of tannin extract were solubilized in 12.0 mL of a 0.25 mol L^{-1} NaOH solution and mixed with 0.6 mL of formaldehyde (36% *w/w*, analytical grade). The reaction was carried out at 80 °C in digestion vessels for 8 h. The precipitate was dried, milled, washed with HCl 0.05 mol L^{-1} (prepared from analytical grade 37% *w/w* acid) and distilled water, and dried at 65 °C. These operating conditions were also selected according to the optimization studies previously conducted [33]. Particle size analysis was performed by laser diffraction (Coulter LS230, Beckman Coulter, Pasadena, CA, USA): 32%, 43%, 14%, and 11%, respectively found for particles sizes < 0.15 mm, 0.15–0.50 mm, 0.50–1.0 mm, and 1.0–2.0 mm. The fraction 0.15–0.50 mm was selected and used as adsorbent in the present work. The point of zero charge of the pine bark tannin resin was 6.2 ± 0.1 [33]. The high chemical stability of the adsorbent at acidic conditions was demonstrated by low values of dissolved organic carbon concentration at pH 2.0 (4.98 ± 0.07 mg-C L^{-1}), for a tannin resin dosage of 2.0 g L^{-1} and a contact time of 24 h [33].

Scanning electron microscopy (SEM) and energy dispersion spectroscopy (EDS) were used to observe the morphology and detect the chemical elemental composition in the tannin adsorbent surface, before and after adsorption of gold. The SEM/EDS exam was performed at CEMUP-LMEV (Materials Centre of the University of Porto—Laboratory for Scanning Electron Microscopy and X-ray Microanalysis) using a high resolution (Schottky) environmental scanning electron microscope with X-ray microanalysis and electron backscattered diffraction analysis (Quanta 400 FEG ESEM/EDAX Genesis X4M). Samples were coated with a gold/palladium thin film by sputtering, using the SPI Module Sputter Coater equipment.

2.2. Gold Solutions

In this work, gold(III) was used as adsorbate. Aqueous solutions of the metal, with concentrations ranging from 10 to 550 mg-Au L^{-1}, were prepared by dilution of a commercial standard 1000 mg-Au L^{-1}, containing 2 mol L^{-1} HCl. Considering the aim of the study, to evaluate the uptake of Au(III) from chloride and aqua regia liquors, two types of strong acidic solutions containing different levels of H^+ were used as aqueous matrices: hydrochloric acid (HCl) and a mixture of hydrochloric acid and nitric acid (HCl/HNO_3 in a ratio of 3:1 (*v/v*), molar ratio of 2.6:1.0). The desired HCl and HNO_3 concentrations were obtained by the addition of analytical grade commercial acid solutions (HCl 37% *w/w*, density 1.19 g mL^{-1}; HNO_3 65% *w/w*, density 1.39 g mL^{-1}) and taking into account the pre-existing HCl concentration in the gold standard solution.

2.3. Analytic Methods

The analysis of dissolved metals (Au and Cu, Fe, Ni, Pd, Zn—multi-metal experiments) in aqueous solutions was performed by AAS (Atomic Absorption Spectroscopy), with flame atomization (GBC Scientific 932 Plus, Australia). The calibration plots were taken daily and accepted for coefficients of determination (R^2) higher than 0.995. In particular, the dissolved gold was measured by air-acetylene flame, using a hollow-cathode lamp operating at 242.8 nm, intensity of 4.0 mA. Potassium nitrate (analytical grade) was added to the standards and samples at final concentrations of 2000 mg-K L^{-1}, in order to suppress ionization.

2.4. Adsorption Studies

Adsorption studies were conducted in batch mode. Accurately measured volumes of Au solutions (15.0 mL) were put in contact with the required amount of adsorbent (depending on the adsorbent dosages defined in the Sections 2.4.1–2.4.4) in Erlenmeyer closed flasks. Suspensions were stirred in an orbital shaker, operating at 280 rpm. Samples taken from the suspensions were filtered using cellulose acetate membranes (0.45 μm porosity), the liquid phase was diluted when necessary and analysed for metal concentration. All the experiments were made in duplicate and results presented as the average values with corresponding uncertainties (absolute deviations or propagated errors).

2.4.1. Effect of the Leaching Reagent

Aqueous solutions of 100 mg-Au L^{-1} were prepared in HCl, using acid concentrations varying from 0.2 to 3.7 mol L^{-1}, and in aqua regia (HCl/HNO_3) dilutions with total H^+ varying from 0.3 to 4.2 mol L^{-1}. These solutions were mixed with the tannin resin (adsorbent dosage of 2.0 g L^{-1}) and stirred for two days. The uptake percentages of gold from the initial solution was calculated by Equation (1), where C_0 and C_e denote gold concentrations (mg L^{-1}) in the initial and the final solutions, respectively.

$$\text{Uptake } (\%) = \frac{C_0 - C_e}{C_0} \times 100 \tag{1}$$

2.4.2. Adsorption Equilibrium Isotherms

Adsorption equilibrium data allow for the design and optimization of the adsorption systems and provide information on the capacity of an adsorbent to accumulate the adsorbate on its surface. Equilibrium isotherms were obtained for the adsorption of Au(III) by the tannin resin at 20 °C and for different aqueous matrices: HCl 1.0 mol L^{-1} and 2.0 mol L^{-1}, and aqua regia (3:1 *v/v* HCl/HNO_3) dilutions corresponding to 1.0, 1.4 and 2.0 mol L^{-1} total H^+ levels. The experimental data was obtained using solutions with initial concentrations of Au in the range 10–550 mg L^{-1} and a constant solid-to-liquid ratio (*S/L* = 1.0 g L^{-1}). Adsorbent dosages in the range 0.3–3.0 g L^{-1} have been reported in literature [34–36] for gold uptake. Usually, a higher adsorbent dosage provides a higher uptake efficiency, but a lower usage capacity of the solid [31]. Considering the results obtained with 2.0 g L^{-1} (effect of leaching reagent, previous subsection), it was decided to use a lower solid-to-liquid ratio (1.0 g L^{-1}) to ensure that final measurable gold concentrations (significantly different from zero) would be obtained to plot the isotherm. Suspensions were stirred for 72 h (enough to attain the steady state). The amount of metal adsorbed per gram of adsorbent in the equilibrium (q_e, in mg

Au per g of tannin resin) was calculated as a function of the final Au concentration in equilibrium (C_e, mg L^{-1}) by the mass balance expressed by Equation (2).

$$q_e = \frac{C_0 - C_e}{S/L} \tag{2}$$

Langmuir [37] and Freundlich [38] models, expressed by Equations (3) and (4), respectively, were fitted to experimental data by non-linear regression. In Equation (3), Q_m (mg g^{-1}) symbolizes the maximum uptake capacity, corresponding to the monolayer coverage assumed by the Langmuir model, and K_L denotes a constant related to the energy of adsorption. In Equation (4), K_F and n are constants related to the adsorption capacity and adsorption intensity, respectively.

$$q_e = \frac{Q_m K_L C_e}{1 + K_L C_e} \tag{3}$$

$$q_e = K_F {C_e}^{1/n} \tag{4}$$

2.4.3. Kinetic Study

The contact time effect on the amount of adsorbed Au was studied using 1.0 mol L^{-1} HCl solution and aqua regia at the same HCl level (total H$^+$ concentration of 1.4 mol L^{-1}), adsorbent dosages of 0.5, 1.0 and 2.0 g L^{-1}, and different initial Au concentrations (100 mg L^{-1} and 300 mg L^{-1}). The liquid solutions were stirred with the tannin resin for different periods of time, at room temperature (20 ± 2 °C). Control assays (with no adsorbent) were conducted in parallel. After designated times, suspensions were immediately filtered, and the liquid phase analysed for Au concentration (C). The amount of Au adsorbed per gram of tannin resin (q, mg g^{-1}) at each contact time (t) was calculated by Equation (5).

$$q = \frac{C_0 - C}{S/L} \tag{5}$$

Lagergren's pseudo-first order and pseudo-second order reaction-based models have been widely applied in numerous adsorption systems, due to their simplicity and the commonly good fittings generated. Despite their questionable significance and fairly empirical nature [39], these models were also employed in the present work. Lagergren's pseudo-first order [40] and pseudo-second order models [41,42] are represented by Equations (6) and (7). In these expressions, q and q_e (mg g^{-1}) symbolize the amount of gold adsorbed per mass unit of adsorbent, at time t (h) and at equilibrium, respectively, and k_1 (h^{-1}) and k_2 (g mg^{-1} h^{-1}) are the kinetic constants.

$$q = q_e[1 - exp(-k_1 t)] \tag{6}$$

$$q = q_e \frac{q_e k_2 t}{1 + q_e k_2 t} \tag{7}$$

In addition, an intraparticle diffusion model was also used. Linear Driving Force (LDF) approximation (Equation (8)) [43] assumes that the uptake rate of an adsorbate is proportional to the difference between the adsorbed phase concentration at the solid/fluid interface (q*, given by Langmuir model) and the average adsorbed phase concentration in the particle (q). The calculation of the LDF constant (k_{LDF}) was done using the explicit equation (Equation (12)) that results from Equation (8), combined with the use of the variables expressed in Equations (9)–(11) [44]. The solver tool in Excel was used to obtain k_{LDF} constants, by minimizing the sum of squared residuals. The calculation of D_h, based on Equation (13) [45], assumes spherical adsorbent particles (r_p denotes the average particle radius) and a parabolic profile of metal concentration inside the particle.

$$\frac{\partial q}{\partial t} = k_{LDF} \times (q^* - q) \tag{8}$$

$$\xi = \frac{Q_m}{C_0} \times S/L \tag{9}$$

$$y = \frac{C}{C_0} \tag{10}$$

$$a = \xi - 1 + \frac{1}{K_L \cdot C_0};\ b = \frac{1}{K_L \cdot C_0};\ \alpha = \frac{-a + \sqrt{a^2 + 4b}}{2};\ \beta = \frac{-a - \sqrt{a^2 + 4b}}{2} \tag{11}$$

$$t = -\frac{1}{k_{LDF}}\left\{\frac{1}{2b} \times ln\left[\frac{y^2 + ay - b}{a - b + 1}\right] + \left(1 - \frac{a}{2b}\right)\left(\frac{1}{\alpha - \beta}\right) \times ln\left[\frac{(1-\beta)(y-\alpha)}{(1-\alpha)(y-\beta)}\right]\right\} \tag{12}$$

$$k_{LDF} = \frac{15D_h}{{r_p}^2} \tag{13}$$

2.4.4. Competitive Adsorption and Selectivity

The dissolution of precious metals from WEEE is usually preceded by chemical pre-treatments to dissolve base metals (e.g., copper, lead) [10]. However, certain amounts of these metals remain in the residue, together with the precious metals, and are leached out with gold in the subsequent steps. The presence of these metals in solution may affect the adsorption capacity of the adsorbent, due to possible competition. In addition, if an adsorbent sequesters significant amounts of other metals, besides gold, the generation of a final high purity recovered product may be compromised. Assessing the performance of an adsorbent in a multi-metal solution simulating an actual hydrometallurgical liquor is therefore important. Multi-metal solutions containing Au(III) (200 mg L^{-1}), Cu(II) (200 mg L^{-1}), Fe(III) (150 mg L^{-1}), Ni(II) (80 mg L^{-1}), Zn(II) (10 mg L^{-1}) and Pd(II) (40 mg L^{-1}) were prepared in aqua regia (0.75, 1.3 and 2.0 mol L^{-1} H^+ solutions). The desired concentration of each metal was obtained by the dilution of commercial metal standards (1000 mg L^{-1}) or, in the case of Cu(II), by the dissolution of $CuCl_2{\cdot}2H_2O$ salt. The metal composition of the simulated solutions was based on the levels reported in literature for aqua regia liquors of WEEE [25,29]. Simulated leaching solutions were then mixed with the tannin resin at an adsorbent dosage of 1.0 g L^{-1}. After 72 h of stirring, the concentration of each metal was analysed in the liquid and uptake percentages and adsorbed amounts calculated (Equations (1) and (2)). Control assays were conducted in parallel, in similar conditions, but using single-metal solutions (200 mg-Au L^{-1}).

2.5. Desorption and Regeneration

Desorption and regeneration studies were conducted in order to evaluate the recovery of gold by elution from exhausted adsorbents and the possibility to reuse the regenerated material. A sample of Au-loaded adsorbent was prepared by stirring the tannin resin (1.0 g L^{-1}) with 500 mg L^{-1} Au solution, prepared in HCl 1.0 mol L^{-1} H^+. After the saturation with gold, the adsorbent was separated from the remaining liquid by vacuum filtration, washed with distilled water and dried at 50 °C overnight. The first desorption stage was conducted using a solid-to-liquid ratio of 2.5 g L^{-1} and two different eluents: acid thiourea solution (0.5 mol L^{-1} thiourea and 0.5 mol L^{-1} HCl) and HCl 50% (*v/v*). After 3 days stirring, the liquid phase was analysed for Au and the desorbed percentage calculated. Adsorption and desorption steps were repeated for 3 cycles, using the thiourea solution as eluent.

3. Results and Discussion

3.1. Effect of the Leaching Solution

Figure 1 presents the results on gold(III) uptake from aqueous matrices containing different levels of HCl and HCl/HNO_3. In both aqueous systems, the acidity of the medium affects the amount of gold adsorbed by tannin resin.

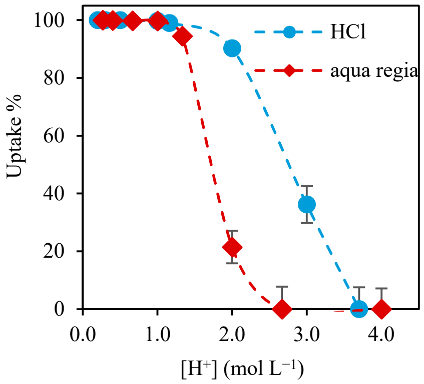

Figure 1. Effect of hydrogen ion concentration ([H$^+$]) on the uptake of gold by the pine bark tannin resin from HCl and HCl/HNO$_3$ (aqua regia) aqueous solutions.

Total removal of gold from HCl solutions is achieved up to 1.2 mol L^{-1} H$^+$. Above 2.0 mol L^{-1} HCl, the uptake of the metal is seriously affected, and for 3.7 mol L^{-1} HCl is practically suppressed. Results can be explained considering the effect of H$^+$, but also the presence of Cl- ligands, and their effect on the adsorbate species (gold complexes) and on the adsorbent surface. The adsorption mechanism that has been proposed for the uptake of gold by tannin materials is based on an electrostatic attraction followed by the reduction of Au(III) and the oxidation of hydroxyl groups [19,24]. The redox reaction is expressed by Equation (14), where the reduction of the chlorogold complex is accompanied by the oxidation of hydroxyl to carbonyl groups [46].

$$AuCl_4^- + 3\ R\text{-}OH \rightarrow Au^0 + 3\ R = O + 3\ H^+ + 4\ Cl^- \quad (14)$$

Under the HCl concentrations used in this study, Au should be present in solution as tetrachloroaurate(III) complex ($AuCl_4^-$) (speciation diagram presented in [47]), and the resin surface should present a high positive charge. These conditions favour the uptake of Au complexes by electrostatic attraction, which explains the good results observed up to 1.2 mol L^{-1} HCl. However, an excessive increase in HCl concentration (and consequently, in H$^+$ and Cl$^-$ levels) impairs the reduction of gold (Equation (14)), and chloride ions, abundantly present in solution, may also compete with $AuCl_4^-$ to the active sites of the adsorbent [19,24]. This explains the marked reduction in the gold uptake observed for HCl levels above 2.0 mol L^{-1}.

With regards to the aqua regia, Figure 1 shows that 100% of gold in HCl/HNO$_3$ solutions is sequestered by the tannin resin for acidic levels below 1.0 mol-H$^+$ L^{-1}. The adsorptive ability sharply decreased for higher acid concentrations and ceases at 2.7 mol L^{-1} H$^+$ (corresponding to 2.0 and 0.7 mol L^{-1} of HCl and HNO$_3$, respectively), results that can be explained in the same way as for the HCl solutions. As it can be seen, for acidity levels higher than 1.2 mol-H$^+$ L^{-1}, the tannin resin exhibits a higher performance for the uptake of Au(III) from HCl solutions than from aqua regia, and it is much more affected by the acid concentration in the latter system than in the former. This means that the presence of nitric acid in solution impairs the uptake of Au by the adsorbent, being a result of the strong oxidizing capacity of aqua regia which hinders the reduction of Au(III) [25].

The results here obtained are generally in line with those reported in literature. Fan et al. [25] studied the adsorption of Au(III) by a persimmon tannin in HCl and HNO$_3$ media. Under the studied conditions, the adsorbent performance was only significantly reduced for HCl and HNO$_3$ concentrations higher than 3.74 and 3 mol L^{-1}, respectively. The adsorbent performed better in HCl than in HNO$_3$ aqueous medium. Yi et al. [29] studied the effect of HCl concentration on the adsorption of gold(III) by ethylenediamine modified persimmon tannin adsorbent and reported a gradual decrease in the Au uptake when the H$^+$ concentration rose from 0.1 to 5.82 mol L^{-1}. Al-Saidi [23] reported an increase in Au(III) removal by raw date pits for HCl concentrations up to 0.5 mol L^{-1}, but a decrease in the uptake efficiency above this level. Most of literature studies were conducted using HCl aqueous matrices. In the present study we have investigated also the use of aqua regia because it is also employed as leaching solution for WEEE, superior to chloride leaching in some criteria [10,13]. Several works have also evaluated the uptake of gold under HCl levels equal and lower than 0.1 mol L^{-1}, corresponding to pH values between 1 and 5–6 [18,21,22], which are weaker acidic conditions than those used in the present work. In fact, our experiments were carried out by using 1.0–2.0 mol H^+ L^{-1} (HCl and HCl/HNO_3 solutions), closer to the H^+ concentration in actual leach liquors of WEEE, even though that acid levels below 1.0 mol L^{-1} would assure a greater adsorbent performance.

3.2. Adsorption Equilibrium Isotherms

Figure 2 shows adsorption isotherms obtained for the uptake of gold by the tannin resin, in different acidic systems (HCl and aqua regia).

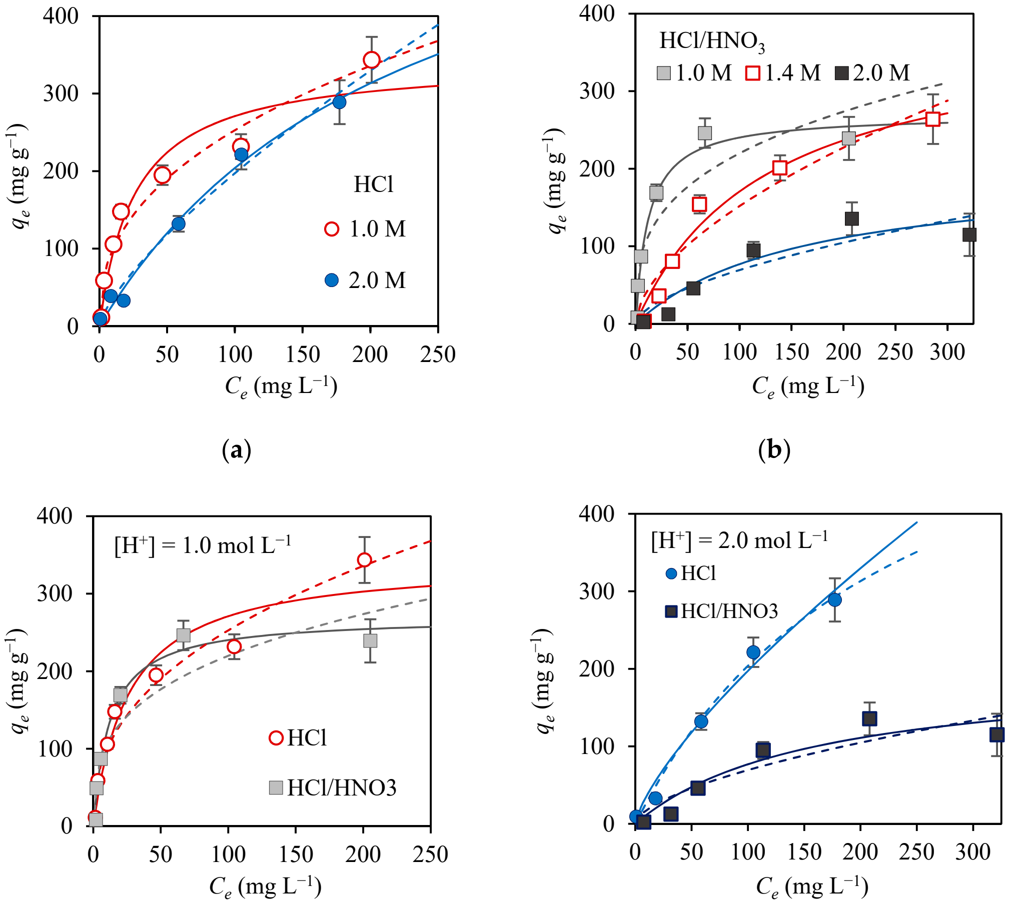

(**a**)

(**b**)

(**c**)

(**d**)

Figure 2. Equilibrium isotherms for the adsorption of gold by the pine bark tannin resin from different acidic matrices (20 °C, $S/L = 1.0$ g L^{-1}): effect of H^+ concentration in (**a**) HCl and (**b**) aqua regia solutions; effect of the leaching solution for a total H^+ concentration of (**c**) 1.0 and (**d**) 2.0 mol L^{-1}. C_e denotes the gold concentration in the liquid phase, in equilibrium with the metal adsorbed amount, q_e. Langmuir and Freundlich models are represented by solid and dashed lines, respectively.

In line with the previous results, Figure 2a,b shows a negative effect of increasing the solution acidity. The slope of the isotherms for low equilibrium concentrations gives indication about the affinity adsorbent/adsorbate, and in both charts (Figure 2a,b), the decrease of adsorption is evident for higher H^+ concentrations. However, the results show that the negative influence of acid concentrations tends to cease as the Au concentration increases. The adsorbed amounts of Au from 1.0 mol L^{-1} HCl solution are significantly higher than the ones recorded at 2.0 mol L^{-1} only for equilibrium gold concentrations below 100 mg L^{-1}, but are practically the same for higher adsorbate levels (Figure 2a). The same happens when it comes to aqua regia (Figure 2b), as the isotherms measured at 1.0 and 1.4 mol L^{-1} H^+ get closer for Au concentrations of ca. 200 mg L^{-1}. This is reflected by the similarity of the maximum adsorbed amounts obtained experimentally ($q_{e,m}$, Table 1) for 1.0 and 2.0 mol L^{-1} HCl, and for 1.0 and 1.4 mol L^{-1} H^+ aqua regia. The use of 2.0 mol L^{-1} of H^+, however, impaired more dramatically the uptake ability, as even for higher Au levels the adsorbed amounts remained significantly below the values obtained at 1.0 and 1.4 mol L^{-1}.

Table 1. Parameters of Langmuir and Freundlich isotherms for the adsorption of gold from HCl and aqua regia solutions using pine bark tannin resin, at 20 °C, and comparison between the maximum adsorbed amounts obtained experimentally ($q_{e,m}$) and from Langmuir modelling (Q_m).

	exp.	**Langmuir**				**Freundlich**			
	$q_{e,m}$ **(mg g^{-1})**	Q_m **(mg g^{-1})**	$K_L \times 10^3$ **(L mg^{-1})**	**R**	**SE (mg g^{-1})**	K_F **($mg^{1-1/n}g^{-1}L^{1/n}$)**	**n**	**R**	**SE (mg g^{-1})**
				HCl Solution					
1.0 mol L^{-1} H^+	344 ± 30	343 ± 38	38 ± 13	0.97	31.0	38 ± 7	2.4 ± 0.3	0.98	23.7
2.0 mol L^{-1} H^+	289 ± 28	675 ± 152	4 ± 2	1.00	12.6	7 ± 2	1.4 ± 0.1	0.99	15.7
				Aqua Regia Solution					
1.0 mol L^{-1} H^+	246 ± 19	270 ± 19	81 ± 21	0.99	19.3	51 ± 21	3 ± 2	0.91	47.2
1.4 mol L^{-1} H^+	264 ± 32	386 ± 62	8 ± 3	0.98	20.9	10 ± 6	1.7 ± 0.3	0.96	31.5
2.0 mol L^{-1} H^+	136 ± 21	200 ± 65	6 ± 4	0.95	19.3	5 ± 4	1.7 ± 0.5	0.92	24.8

Figure 2d compares isotherms measured from HCl and aqua regia matrices, under the same total H^+ concentrations. For 1.0 mol L^{-1} H^+, the two isotherms are quite similar, mainly for low gold concentrations. For 2.0 mol L^{-1} H^+, the performance of the tannin resin is unquestionably worst under aqua regia solutions (Figure 2d). In this case, the maximum adsorbed amounts, recorded within the experimental conditions were 289 mg g^{-1} in HCl solution and 136 mg g^{-1} in aqua regia solution (Table 1). Such behaviour should be related to the strong oxidizing power of aqua regia that inhibits the reduction of Au and limits the sequestering ability of the adsorbent. Therefore, the use of HCl as a leaching agent for gold in hydrometallurgical processes has proven to create more favourable conditions than aqua regia, considering its subsequent uptake and recovery.

The parameters of Langmuir and Freundlich models are shown in Table 1. The coefficients of correlation (R) and the standard error of the regressions (SE) are also presented, as measures of the quality of the fittings. Modelled curves are illustrated in Figure 2. As it can be seen, both equilibrium models described quite well the experimental data. Considering the higher correlation coefficients and the lower standard errors, the Langmuir model provided better fittings (exception is the isotherm measured at 1.0 mol L^{-1} HCl). Despite this, in the experimental range of concentrations studied and in certain conditions (e.g., 2.0 mol L^{-1} HCl; 1.4 and 2.0 mol L^{-1} HNO_3/HCl), the maximum experimental adsorbed amounts (denoted as $q_{e,m}$, in Table 1) are lower than the Q_m values predicted by Langmuir model. This is an indication that the monolayer capacity was not attained, which means that the adsorbent still has capacity to sequester more gold ions from solution. Indeed, other studies present similar observations. A continuous rise of the isotherm curve, even for Au equilibrium concentrations of 1500–2000 mg L^{-1}, has been reported for the adsorption of gold by crosslinked polyethylenimine/calcium-alginate fibres, and attributed to a continuous reduction process of Au(III) [18].

In a general way, and despite the negative effect of H^+ and aqua regia, pine bark tannin resin showed an excellent ability to sequester and accumulate gold on its surface in all the conditions tested. Table 2 presents maximum adsorption capacities of gold(III) reported in the literature for different adsorbents. In order to allow a suitable comparison, maximum adsorbed amounts obtained experimentally ($q_{e,m}$) and from Langmuir modelling (Q_m) are presented, together with the most relevant operating conditions. The pine bark tannin resin presents adsorbed amounts in the range of the reported values for other biosorbents. Looking only at the uptake capacities of gold, its performance seems to be comparable to the banana peel derived adsorbent and PEI-modified *L. speciosa* leaves, superior to some other biosorbents or synthetic polymers (e.g., commercial resin Lewatit TP214, raw date pits, activated rice husk), but worse than other tannin adsorbents. However, it is worth noting that the adsorption capacity of the pine bark tannin resin was evaluated here under more harsh acidic conditions (1.0 mol L^{-1} acid solutions) than most of the data collected from literature and referred in Table 2. Although strong acidic conditions are more representative of the actual conditions found industrially, it is known that they impair the uptake of gold (Figure 1; [25,29]). On this basis, it can be said that pine bark tannin resin proved to be a promising material for gold uptake.

Table 2. Maximum adsorption capacities reported in literature for the adsorption of gold from chloride media by different adsorbents: maximum adsorbed amounts, obtained experimentally ($q_{e,m}$) and calculated monolayer capacities (Q_m) by Langmuir modelling.

Adsorbent	T (K)	pH or [H^+]	C_e (mg L^{-1})	$q_{e,m}$ (mg g^{-1})	Q_m (mg g^{-1})	Ref.
Commercial resin IRA400		pH 2	0–215		902.3	[19]
Commercial resin Lewatit TP214	298	pH 6.1	35–225		108.7	[20]
Polyaniline modified by TMP	298	pH 4	0–300	881	883	[48]
Crosslinked PEI resins		pH 2	0–210		943.5	[19]
NIPA gel	323	1 mol L^{-1}	0–790		125.5	[49]
Activated rice husk	298	pH 6.1	50–260		93.46	[20]
PEI-alginate fibers	298	0.1 mol L^{-1}	0–2000	1240	1404	[18]
GA-PEI-alginate fibers	298	0.1 mol/L	0–1500	2325	2182	[18]
Cellulose acetate fibers	298	2 mol L^{-1}	0–800	110		[50]
Raw date pits	298	0.5 mol L^{-1}	0–35	78	61	[23]
Banana peel	298	pH 1	0–1200	370.18	377.2	[22]
Banana peel (lipid extraction)	298	pH 1	0–1000	475.48	448.4	[22]
Oil palm trunk (dewaxed)	303	pH 2	0–120	91.47	95.16	[35]
PEI-modified *L. speciosa* leaves	298	pH 1	0–200	282	286	[21]
Persimmon resin	303	pH 2	150–351	≈965	1905	[36]
Persimmon peel gel	303	0.1 mol L^{-1}	0–11 × 10^3	1.8 × 10^3		[51]
Crosslinked persimmon tannin gel	303	0.1 mol L^{-1}	0–2.4 × 10^3	1517		[34]
TEPA-persimmon tannin gel	303	0.1 mol L^{-1}	0–1.2 × 10^3		1168	[6]
EDA-modified persimmon tannin	303	0.1 mol L^{-1}	0–1.5 × 10^3		1550.4	[29]
persimmon tannin onto Fe3O4@SiO2 microspheres	298	pH 5	(0.2–1.8) × 10^3	860	917.4	[24]
persimmon tannin functionalized viscose fiber	298	pH 2	0–120	528	536	[28]
Sericin and alginate particles chemically crosslinked by proanthocyanidins	298	pH 2.5–3	0–140	196.1	188.4	[27]
Pine bark tannin resin	298	1 mol L^{-1}	0–200	344	343	This work
Pine bark tannin resin	298	1 mol L^{-1} (HCl/HNO_3)	0–200	246	270	This work

EDA—ethylenediamine; GA–glutaraldehyde; NIPA–N-isopropylacrylamide; PEI–polyethylenimine; TEPA–tetraethylenepentamine; TMP–trimethyl phosphate.

3.3. Kinetic Study

The effect of contact time on the uptake of gold was studied at 20 °C, for different adsorbate concentrations, solid-to-liquid ratios and acidic aqueous matrices. The kinetic profiles are presented in Figure 3 and show a relatively slow adsorptive process, with equilibrium times of two or three days. Similar contact times were found by Gurung et al. [34], with persimmon tannin resins, although other authors report considerably lower values (8 h) [36]. The slow kinetics on the gold uptake appears to be a shortcoming of many biosorbents, but this has been explained by the reductive process of gold, which is essential for high uptake capacities.

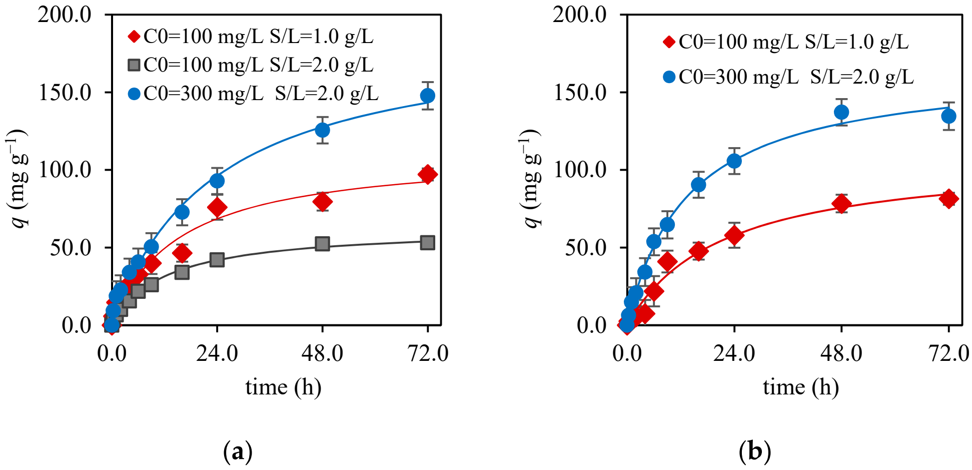

(**a**) (**b**)

Figure 3. Effect of contact time on the uptake of gold by the pine bark tannin resin at 20 °C, different initial gold concentrations, adsorbent dosages and using aqueous solutions of (**a**) 1.0 mol L^{-1} HCl (**a**) and (**b**) aqua regia 1.0 mol L^{-1} H^+: experimental data and pseudo-second order modelling.

The adsorption dynamics is a result of a multi-step process involving [52,53]: (i) transport through the external film up to the surface of the adsorbent, (ii) intraparticle diffusion (in pores and/or over the surface), and (iii) final adsorption reaction on the active sites. The last step is usually very fast and do not determine the overall adsorption rate [52]. In well-stirred batch systems, the external resistance of mass transfer can be also considered negligible. Despite the fact that the adsorption reaction is also usually fast, Lagergren's pseudo-first order and pseudo-second order reaction-based models have been widely applied in numerous adsorption systems, due to their simplicity and the commonly good fittings generated. Table 3 presents kinetic parameters for Lagergren's pseudo-first and pseudo-second order models. As it can be seen, both models describe very well the experimental data, with all coefficients of correlation equal or higher than 0.98. Despite the fact that the pseudo-second order model (Figure 3) has mostly provided the lowest SE, the pseudo-first order predicted equilibrium adsorbed amounts (q_e) closest to the experimental values.

Table 3. Kinetic parameters of reaction-based models (*k*, kinetic constants; q_e, equilibrium adsorbed amounts) for the adsorption of gold from HCl and aqua regia solutions by the pine bark tannin resin, at 20 °C and for different initial Au(III) concentrations (C_0) and adsorbent dosages (*S/L*).

		Pseudo-First Order Model				**Pseudo-Second Order Model**			
C_0 **(mg L^{-1})**	*S/L* **(g L^{-1})**	q_e **(mg g^{-1})**	$k_1 \times 10^2$ **(h^{-1})**	**R**	**SE (mg g^{-1})**	q_e **(mg g^{-1})**	$k_2 \times 10^4$ **(g mg^{-1} h^{-1})**	**R**	**SE (mg g^{-1})**
				1.0 mol L^{-1} HCl					
100	1.0	91 ± 6	6 ± 1	0.98	7.2	112 ± 9	6 ± 2	0.98	6.2
100	2.0	52 ± 2	7.7 ± 0.6	0.99	2.2	63 ± 2	1.3 ± 0.1	1.00	1.4
300	2.0	147 ± 8	4.7 ± 0.6	0.99	7.5	190 ± 12	2.3 ± 0.5	0.99	6.0
				1.4 mol L^{-1} H$^+$ Aqua Regia Solution					
100	1.0	84 ± 4	5.3 ± 0.7	0.99	4.5	109 ± 9	4 ± 1	0.99	4.8
300	2.0	136 ± 3	7.2 ± 0.5	1.0	4.2	167 ± 5	4.4 ± 0.5	1.0	3.8

The kinetics of gold uptake by the tannin resin was also analysed considering an intraparticle diffusion-controlled process. Assuming a negligible mass transfer resistance in the outer layer and considering that intraparticle resistance is governed by surface diffusion (as this adsorbent is essentially a non-porous material), homogeneous solid diffusion model (HSDM) combined with Linear Driving Force (LDF) approximation were used to model kinetic data and to calculate the average values of the homogeneous diffusion coefficients (D_h) (equations in Section 2.4.3). Table 4 presents k_{LDF} and D_h estimated values. The good agreement between the LDF fitting and the experimental data (coefficients of correlation equal or higher than 0.98) shows that this model can also successfully describe the adsorption of gold by the tannin resin. The homogeneous solid diffusivity coefficients calculated were in the range 10^{-14}–10^{-13} m^2 s^{-1}. Saman et al. [35] reported values in the order of magnitude of 10^{-13} m^2 s^{-1} for the adsorption of Au(III) by oil palm trunk biosorbents. For the same adsorbent dosage, the results show an increase in D_h with the initial adsorbate concentration, which has been reported in various adsorptive systems [44,54], including on the uptake of gold cyanide by activated carbon [16]. For the same initial adsorbate concentrations and adsorbent dosages, lower k_{LDF} and D_h values were obtained for the aqua regia solutions, in comparison to HCl, which indicates slower adsorption kinetics.

Table 4. Kinetic constant (k_{LDF}) of LDF approximation and solid diffusivity coefficients (D_h) calculated by HSDM model for the adsorption of gold from HCl and aqua regia solutions by the pine bark tannin resin.

C_0 (mg L^{-1})	*S/L* (g L^{-1})	R	k_{LDF} (h^{-1})	D_h (m^2 s^{-1})
1.0 mol L^{-1} HCl				
100	1.0	0.98	0.076	3.6×10^{-14}
100	2.0	0.98	0.051	2.5×10^{-14}
300	2.0	0.99	0.215	1.1×10^{-13}
1.4 mol L^{-1} H^+ Aqua Regia Solution				
100	1.0	1.00	0.021	1.0×10^{-14}
300	2.0	0.99	0.087	4.3×10^{-14}

3.4. Competitive Adsorption and Selectivity

The tannin resin was tested in multi-metal solutions containing Cu(II), Fe(III), Ni(II), Zn(II), Pd(II), and Au(III). The results are depicted in Figure 4.

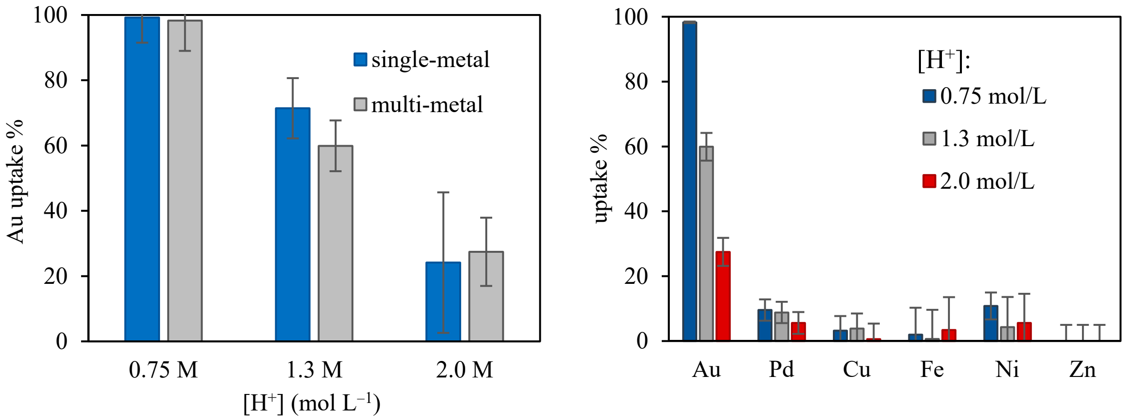

(**a**) (**b**)

Figure 4. Percentages of metals extracted from simulated liquors containing aqua regia in different H^+ concentrations by the pine bark tannin resin from (20 °C, *S/L* 1.0 g L^{-1}, initial Au concentration 200 mg L^{-1}): (**a**) comparison of Au uptake from single and multi-metal solutions; (**b**) uptake of metals from the multi-metal solution.

As it can be seen (Figure 4a), the ability of the tannin resin to uptake gold from the simulated liquors is practically the same as that found in single-metal solutions. The uptake percentages of gold obtained in multi-metal systems (Figure 4b) were noticeably higher than those of the other metals (which has never surpassed 11%), particularly for total acidities of 1.0 and 1.4 mol L^{-1}. For instance, at acidic level of 0.75 mol L^{-1} H^+, almost 100% of the gold in solution was adsorbed by the tannin resin, whereas Ni and Pd were very weakly extracted (11 ± 4% and 10 ± 3%, respectively), and other metals remained practically solubilized (uptake percentages < 3%). In the presence of high chloride concentrations and low pH, gold and platinum group metals are present as anionic chloro-complexes, which favour their uptake by the positively charged adsorbent surface. Palladium has similar properties and behaviour as Au, namely a low reduction potential. It has been reported that $PdCl_4^-$ can be also adsorbed by tannin-adsorbents through the oxidation of the functional groups of tannins and reduction to Pd(0) [24], which justify its co-adsorption. Base metals, on the other hand, are present in solution as cationic species and are electrostatically repelled. Indeed, in biosorption processes, anions are typically adsorbed at low pH (1.0–3.0), whereas metal cations are typically adsorbed under optimum conditions of pH 5.0–5.5 [55]. This explains the reduced competition observed between gold and base metals. The present results are generally in line with results published in literature, which have shown very good selectivity for gold over other metals for different HCl and HNO_3 media [25].

3.5. SEM and EDS Analysis

Figure 5 presents the SEM images of the tannin resin adsorbent, before and after gold uptake. As it can be observed, the adsorbent particles present an irregular shape and a faceted non-porous surface (Figure 5a). After adsorbing gold from HCl (Figure 5b) and aqua regia solutions (Figure 5d,e), the adsorbent surface presented an accumulation of metal particles, identified as gold through the EDS spectra performed in the micro areas denoted as Z1 and Z2 (Figure 5f). These images are in line with the quantitative adsorption results previously obtained, considering that Figure 5d (Au-loaded adsorbents in HCl and aqua regia solutions 1.0 mol L^{-1} H^+, respectively) show high amounts of gold particles, whereas Figure 5e shows a much scarce distribution. The EDS spectra obtained in areas not covered by gold particles (not illustrated) showed an abundance of carbon and oxygen (also observed before adsorption), but the additional presence of chlorine. This confirms the competition between chloride and gold to the adsorbent surface.

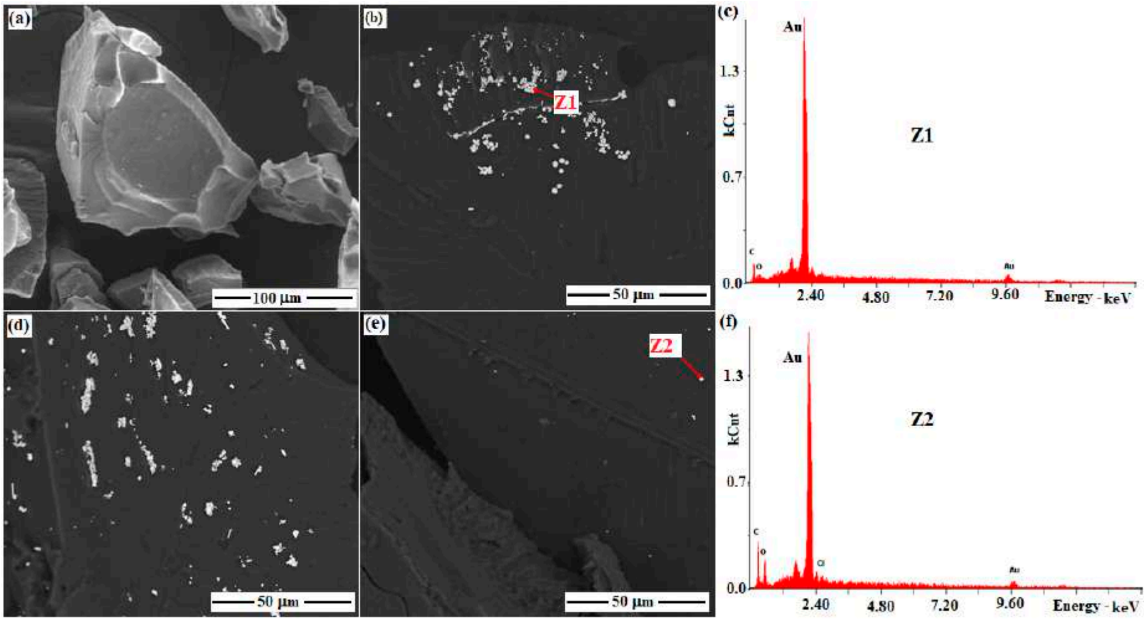

Figure 5. SEM images obtained for the pine bark tannin resin (**a**) before contact with gold, and after adsorption of gold (**b**) from 1.0 mol L^{-1} HCl, and from aqua regia solutions (**d**) 1.0 mol L^{-1} H^+ and (**e**) 2.0 mol L^{-1} H^+. EDS spectra obtained in the areas denoted as (**c**) Z1 and (**f**) Z2.

3.6. Desorption and Regeneration

The final recovery of gold from the loaded adsorbent and the regeneration of the adsorbent are important for industrial applications. A first desorption test of gold(III) was conducted using HCl 50%

(*v/v*) and 0.5 mol L^{-1} acidic thiourea as eluents. Negligible desorption percentage (<1%) was obtained in HCl eluent, whereas 57% was registered using the acidic thiourea solution. In fact, formulations of thiourea with HCl have been identified in literature as the most effective desorbing solutions for gold [18,22,27,56]. The desorption mechanism of the process is based on the displacement of the electrostatically adsorbed Au(III), that complexes with chloride in the HCl eluent, and on the oxidation of the elemental gold forming the gold(I)-thiourea $Au(CS[NH_2]_2)_2^+$ [18,56]. Details about the reactions of gold dissolution through the use of acid thiourea solution can be found in literature [57,58].

Adsorption–desorption assays were then conducted for three cycles, using the acidic thiourea solution. The results are presented in Figure 6.

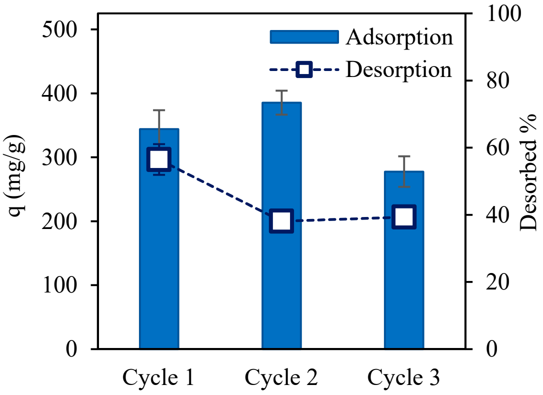

Figure 6. Results obtained in the adsorption (C_0 = 500 mg L^{-1}, *S/L* = 1.0 g L^{-1}, 20 °C) and desorption cycles (eluent: 0.5 mol L^{-1} thiourea and 0.5 mol L^{-1} HCl solution, *S/L* = 2.5 g L^{-1}, 20 °C).

As it can be seen, the desorption efficiency observed in the first cycle (57%) decreased to 38% and 39% in the two subsequent desorption steps. In spite of that, the regeneration ability of the tannin resin was quite good, as the adsorbed amount remained practically constant in two cycles and reduced moderately (19%) in the third one, indicating that the regenerated tannin resin still has capacity to accumulate gold in its surface. These results are promising, but the necessity of more research is evident to find an improved solution (e.g., increasing HCl concentration) to desorb gold more efficiently from the pine bark tannin resins. Although from environmental and cost-effectiveness points of view, the desorption and regeneration seem to be the most interesting options to recover gold, incineration could be considered in future as it is a direct way to obtain metallic gold.

4. Conclusions

Tannin resins prepared from maritime pine (*Pinus pinaster*) bark were evaluated for the uptake and recovery of gold from simulated e-waste hydrometallurgical liquors. Higher extraction efficiencies of gold were obtained from HCl solutions, in comparison to aqua regia, but excessive levels of HCl caused a severe impact in the metal uptake from both aqueous systems. Even though, at strong acidic levels and in both acidic systems, the pine bark tannin resin presented a good performance, with maximum adsorption capacities ranging from 200 and 343 mg g^{-1} (2.0 and 1.0 mol L^{-1} H^+, respectively). The adsorption process was found to be a rather slow process (2–3 days to be completed) and successfully described by the homogeneous solid diffusion model and LDF approximation. The selectivity of the adsorbent towards gold was evaluated using simulated hydrometallurgical liquors. The amount of gold extracted by the tannin resin from multi-metal solutions was similar to the values registered in the single-metal solutions and the co-adsorption of Pd(II), Cu(II), Fe(II), Ni(II) and Zn(II) was in general low. Desorption and regeneration studies conducted through three adsorption–desorption cycles, using a solution of 0.5 mol L^{-1} thiourea and 0.5 mol L^{-1} HCl as eluent, indicate desorption percentages of 38–57%, although with only a mild loss of the adsorption capacity of the regenerated adsorbent.

Considering the harsher conditions at which the pine bark tannin resin was evaluated, it can be said that it presents analogous or even better performance when compared to other biosorbents or synthetic resins. A deeper analysis on the final recovery of gold from the exhausted adsorbents will be considered in forthcoming work. More research is needed in this field to improve the circularity in WEEE, particularly by the promotion of benign practices.

Author Contributions: Investigation, M.B.Q.L.F.T., H.A.M.B., and S.C.R.S.; conceptualization, S.C.R.S.; formal analysis, S.C.R.S., M.B.T. and H.A.M.B.; funding acquisition and resources, C.M.S.B. and R.A.R.B.; project administration, C.M.S.B.; methodology, S.C.R.S.; supervision, S.C.R.S., R.A.R.B., and C.M.S.B.; validation, S.C.R.S., C.M.S.B., and R.A.R.B.; visualization, M.B.Q.L.F.T., H.A.M.B., and S.C.R.S.; writing—original draft—S.C.R.S.; writing—review and editing—M.B.Q.L.F.T., H.A.M.B., R.A.R.B., and C.M.S.B. All authors have read and agreed to the published version of the manuscript.

Funding: This work was financially supported by: Base Funding—UIDB/50020/2020 of the Associate Laboratory LSRE-LCM—funded by national funds through FCT/MCTES (PIDDAC). S. Santos acknowledges postdoctoral scholarship (SFRH/BPD/117387/2016), awarded by the Portuguese Science and Technology Foundation (FCT) and financed by National Funds and by the European Social Fund (ESF) through the Human Capital Operational Programme (POCH). H. Bacelo acknowledges PhD scholarship (PD/BD/135062/2017) funded by FCT.

Conflicts of Interest: The authors declare no conflict of interest.

References

1. Perez, J.P.H.; Folens, K.; Leus, K.; Vanhaecke, F.; Van Der Voort, P.; Du Laing, G. Progress in hydrometallurgical technologies to recover critical raw materials and precious metals from low-concentrated streams. *Resour. Conserv. Recycl.* **2019**, *142*, 177–188. [CrossRef]
2. Falahati, M.; Attar, F.; Sharifi, M.; Saboury, A.A.; Salihi, A.; Aziz, F.M.; Kostova, I.; Burda, C.; Priecel, P.; Lopez-Sanchez, J.A.; et al. Gold nanomaterials as key suppliers in biological and chemical sensing, catalysis, and medicine. *Biochim. Biophys. Acta BBA Gen. Subj.* **2020**, *1864*, 129435. [CrossRef] [PubMed]
3. Forti, V.; Baldé, C.P.; Kuehr, R.; Bel, G. *The Global E-waste Monitor 2020: Quantities, Flows and the Circular Economy Potential*; United Nations University (UNU)/United Nations Institute for Training and Research (UNITAR)–co-hosted SCYCLE Programme, International Telecommunication Union (ITU) & International Solid Waste Association (ISWA): Bonn, Germany; Geneva, Switzerland; Rotterdam, The Netherlands, 2020.
4. European Parliament and Council. *Directive 2012/19/EU of the European Parliament and of the Council of 4 July 2012 on Waste Electrical and Electronic Equipment (WEEE)*; European Parliament and Council: Brussels, Belgium, 2012.
5. Akcil, A.; Erust, C.; Gahan, C.S.; Ozgun, M.; Sahin, M.; Tuncuk, A. Precious metal recovery from waste printed circuit boards using cyanide and non-cyanide lixiviants-A review. *Waste Manag.* **2015**, *45*, 258–271. [CrossRef] [PubMed]
6. Gurung, M.; Adhikari, B.B.; Kawakita, H.; Ohto, K.; Inoue, K.; Alam, S. Recovery of gold and silver from spent mobile phones by means of acidothiourea leaching followed by adsorption using biosorbent prepared from persimmon tannin. *Hydrometallurgy* **2013**, *133*, 84–93. [CrossRef]
7. Rao, M.D.; Singh, K.K.; Morrison, C.A.; Love, J.B. Challenges and opportunities in the recovery of gold from electronic waste. *RSC Adv.* **2020**, *10*, 4300–4309. [CrossRef]
8. Kaya, M. Recovery of metals and nonmetals from electronic waste by physical and chemical recycling processes. *Waste Manag.* **2016**, *57*, 64–90. [CrossRef]
9. Ventura, E.; Futuro, A.; Pinho, S.C.; Almeida, M.; Dias, J.M. Physical and thermal processing of Waste Printed Circuit Boards aiming for the recovery of gold and copper. *J. Environ. Manag.* **2018**, *223*, 297–305. [CrossRef]
10. Zhang, Y.; Liu, S.; Xie, H.; Zeng, X.; Li, J. Current Status on Leaching Precious Metals from Waste Printed Circuit Boards. *Procedia Environ. Sci.* **2012**, *16*, 560–568. [CrossRef]
11. Camelino, S.; Rao, J.; Padilla, R.L.; Lucci, R. Initial Studies about Gold Leaching from Printed Circuit Boards (PCB's) of Waste Cell Phones. *Procedia Mater. Sci.* **2015**, *9*, 105–112. [CrossRef]
12. Diaz, L.A.; Lister, T.E. Economic evaluation of an electrochemical process for the recovery of metals from electronic waste. *Waste Manag.* **2018**, *74*, 384–392. [CrossRef]
13. Birich, A.; Mohamed, S.R.; Friedrich, B. Screening of Non-cyanide Leaching Reagents for Gold Recovery from Waste Electric and Electronic Equipment. *J. Sustain. Met.* **2018**, *4*, 265–275. [CrossRef]

14. Korolev, I.; Kolehmainen, E.; Haapalainen, M.; Yliniemi, K.; Lundström, M. Gold Recovery from Chloride Leaching Solutions by Electrodeposition-Redox Replacement Method. In Proceedings of the 10th European Metallurgical Conference (EMC 2019), Düsseldorf, Germany, 23–26 June 2019.
15. Sayiner, B.; Acarkan, N. Effect of Silver, Nickel and Copper Cyanides on Gold Adsorption on Activated Carbon in Cyanide Leach Solutions. *Physicochem. Probl. Miner. Process.* **2014**, *50*, 277–287. [CrossRef]
16. Leroux, J.D.; Bryson, A.W.; Young, B.D. A Comparison of Several Kinetic-Models for the Adsorption of Gold Cyanide onto Activated Carbon. *J. S. Afr. Inst. Min. Metall.* **1991**, *91*, 95–103.
17. Dodson, J.R.; Parker, H.L.; García, A.M.; Hicken, A.; Asemave, K.; Farmer, T.J.; He, H.; Clark, J.H.; Hunt, A.J. Bio-derived materials as a green route for precious & critical metal recovery and re-use. *Green Chem.* **2015**, *17*, 1951–1965. [CrossRef]
18. Bediako, J.K.; Lin, S.; Sarkar, A.K.; Zhao, Y.; Choi, J.-W.; Song, M.-H.; Wei, W.; Reddy, D.H.K.; Cho, C.-W.; Yun, Y.-S. Benignly-fabricated crosslinked polyethylenimine/calcium-alginate fibers as high-performance adsorbents for effective recovery of gold. *J. Clean. Prod.* **2020**, *252*, 119389. [CrossRef]
19. Liu, F.; Zhou, L.; Wang, W.; Yu, G.; Huang, J. Adsorptive recovery of Au(III) from aqueous solution using crosslinked polyethyleneimine resins. *Chemosphere* **2019**, *241*, 125122. [CrossRef]
20. Morcali, M.H.; Zeytuncu, B.; Ozlem, E.; Aktas, S. Studies of Gold Adsorption from Chloride Media. *Mater. Res.* **2015**, *18*, 660–667. [CrossRef]
21. Choudhary, B.C.; Choudhary, B.C.; Borse, A.U.; Garole, D.J. Surface functionalized biomass for adsorption and recovery of gold from electronic scrap and refinery wastewater. *Sep. Purif. Technol.* **2018**, *195*, 260–270. [CrossRef]
22. Bediako, J.K.; Choi, J.-W.; Song, M.-H.; Zhao, Y.; Lin, S.; Sarkar, A.K.; Cho, C.-W.; Yun, Y.-S. Recovery of gold via adsorption-incineration techniques using banana peel and its derivatives: Selectivity and mechanisms. *Waste Manag.* **2020**, *113*, 225–235. [CrossRef]
23. Al-Saidi, H. The fast recovery of gold(III) ions from aqueous solutions using raw date pits: Kinetic, thermodynamic and equilibrium studies. *J. Saudi Chem. Soc.* **2016**, *20*, 615–624. [CrossRef]
24. Fan, R.; Min, H.; Hong, X.; Yi, Q.; Liu, W.; Zhang, Q.; Luo, Z. Plant tannin immobilized Fe3O4@SiO2 microspheres: A novel and green magnetic bio-sorbent with superior adsorption capacities for gold and palladium. *J. Hazard. Mater.* **2019**, *364*, 780–790. [CrossRef] [PubMed]
25. Fan, R.; Xie, F.; Guan, X.; Zhang, Q.; Luo, Z. Selective adsorption and recovery of Au(III) from three kinds of acidic systems by persimmon residual based bio-sorbent: A method for gold recycling from e-wastes. *Bioresour. Technol.* **2014**, *163*, 167–171. [CrossRef] [PubMed]
26. Santos, S.C.; Bacelo, H.A.M.; Boaventura, R.A.R.; Botelho, C.M.S. Tannin-Adsorbents for Water Decontamination and for the Recovery of Critical Metals: Current State and Future Perspectives. *Biotechnol. J.* **2019**, *14*, e1900060. [CrossRef] [PubMed]
27. Santos, N.T.D.G.; Moraes, L.F.; Da Silva, M.G.C.; Vieira, M.G.A. Recovery of gold through adsorption onto sericin and alginate particles chemically crosslinked by proanthocyanidins. *J. Clean. Prod.* **2020**, *253*, 119925. [CrossRef]
28. Liu, F.; Wang, S.; Chen, S. Adsorption behavior of Au(III) and Pd(II) on persimmon tannin functionalized viscose fiber and the mechanism. *Int. J. Biol. Macromol.* **2020**, *152*, 1242–1251. [CrossRef]
29. Yi, Q.; Fan, R.; Xie, F.; Min, H.; Zhang, Q.; Luo, Z. Selective Recovery of Au(III) and Pd(II) from Waste PCBs Using Ethylenediamine Modified Persimmon Tannin Adsorbent. *Procedia Environ. Sci.* **2016**, *31*, 185–194. [CrossRef]
30. Wang, Z.; Li, X.; Liang, H.; Ning, J.; Zhou, Z.; Li, G. Equilibrium, kinetics and mechanism of Au^{3+}, Pd^{2+} and Ag^{+} ions adsorption from aqueous solutions by graphene oxide functionalized persimmon tannin. *Mater. Sci. Eng. C* **2017**, *79*, 227–236. [CrossRef]
31. Bacelo, H.A.; Vieira, B.R.; Santos, S.C.; Boaventura, R.A.; Botelho, C.M. Recovery and valorization of tannins from a forest waste as an adsorbent for antimony uptake. *J. Clean. Prod.* **2018**, *198*, 1324–1335. [CrossRef]
32. Sánchez-Martín, J.; Beltrán-Heredia, J.; Gibello-Pérez, P. Adsorbent biopolymers from tannin extracts for water treatment. *Chem. Eng. J.* **2011**, *168*, 1241–1247. [CrossRef]
33. Bacelo, H.A.; Santos, S.C.; Botelho, C.M. Removal of arsenic from water by an iron-loaded resin prepared from Pinus pinaster bark tannins. *Euro-Mediterr. J. Environ. Integr.* **2020**, *5*, 1–17. [CrossRef]
34. Gurung, M.; Adhikari, B.B.; Kawakita, H.; Ohto, K.; Inoue, K.; Alam, S. Recovery of Au(III) by using low cost adsorbent prepared from persimmon tannin extract. *Chem. Eng. J.* **2011**, *174*, 556–563. [CrossRef]

35. Saman, N.; Tan, J.-W.; Mohtar, S.S.; Kong, H.; Lye, J.W.P.; Johari, K.; Hassan, H.; Mat, H. Selective biosorption of aurum(III) from aqueous solution using oil palm trunk (OPT) biosorbents: Equilibrium, kinetic and mechanism analyses. *Biochem. Eng. J.* **2018**, *136*, 78–87. [CrossRef]
36. Xie, F.; Fan, Z.; Zhang, Q.; Luo, Z. Selective adsorption of Au3+from aqueous solutions using persimmon powder-formaldehyde resin. *J. Appl. Polym. Sci.* **2013**, *130*, 3937–3946. [CrossRef]
37. Langmuir, I. The Adsorption of Gases on Plane Surfaces of Glass, Mica and Platinum. *J. Am. Chem. Soc.* **1918**, *40*, 1361–1403. [CrossRef]
38. Freundlich, H.M.F. Over the adsorption in solution. *J. Phys. Chem.* **1906**, *57*, 385–471.
39. Tien, C. Batch Adsorption Models and Model Applications. In *Introduction to Adsorption*; Tien, C., Ed.; Elsevier: Amsterdam, The Netherlands, 2019; Chapter 5; pp. 119–153. [CrossRef]
40. Zur Theorie der sogenannten Adsorption gelöster Stoffe. *Z. Chem. Ind. Kolloide* **1907**, *2*, 15. [CrossRef]
41. Blanchard, G.; Maunaye, M.; Martin, G. Removal of heavy metals from waters by means of natural zeolites. *Water Res.* **1984**, *18*, 1501–1507. [CrossRef]
42. Ho, Y.S. Adsorption of Heavy Metals from Waste Streams by Peat. Ph.D. Thesis, The University of Birmingham, Birmingham, UK, 1995.
43. Glueckauf, E. Theory of chromatography. Part 10-Formulae for diffusion into spheres and their application to chromatography. *Trans. Faraday Soc.* **1955**, *51*, 1540–1551. [CrossRef]
44. Santos, S.C.; Boaventura, R. Adsorption of cationic and anionic azo dyes on sepiolite clay: Equilibrium and kinetic studies in batch mode. *J. Environ. Chem. Eng.* **2016**, *4*, 1473–1483. [CrossRef]
45. Tien, C. Adsorbate Uptake and Equations Describing Adsorption Processes. In *Introduction to Adsorption*; Tien, C., Ed.; Elsevier: Amsterdam, The Netherlands, 2019; Chapter 4; pp. 87–118.
46. Ogata, T.; Nakano, Y. Mechanisms of gold recovery from aqueous solutions using a novel tannin gel adsorbent synthesized from natural condensed tannin. *Water Res.* **2005**, *39*, 4281–4286. [CrossRef]
47. Bergamini, M.F.; Santos, D.P.; Zanoni, M.V.B. Screen-printed carbon electrode modified with poly-L-histidine applied to gold(III) determination. *J. Braz. Chem. Soc.* **2009**, *20*, 100–106. [CrossRef]
48. Wang, C.; Zhao, J.; Zhang, L.; Wang, C.; Wang, S. Efficient and Selective Adsorption of Gold Ions from Wastewater with Polyaniline Modified by Trimethyl Phosphate: Adsorption Mechanism and Application. *Polymers* **2019**, *11*, 652. [CrossRef] [PubMed]
49. Tokuyama, H.; Kanehara, A. Temperature swing adsorption of gold(III) ions on poly(N-isopropylacrylamide) gel. *React. Funct. Polym.* **2007**, *67*, 136–143. [CrossRef]
50. Yang, J.; Kubota, F.; Baba, Y.; Kamiya, N.; Goto, M. Application of cellulose acetate to the selective adsorption and recovery of Au(III). *Carbohydr. Polym.* **2014**, *111*, 768–774. [CrossRef] [PubMed]
51. Parajuli, D.; Kawakita, H.; Inoue, K.; Ohto, K.; Kajiyama, K. Persimmon peel gel for the selective recovery of gold. *Hydrometallurgy* **2007**, *87*, 133–139. [CrossRef]
52. Malash, G.F.; El-Khaiary, M.I. Piecewise linear regression: A statistical method for the analysis of experimental adsorption data by the intraparticle-diffusion models. *Chem. Eng. J.* **2010**, *163*, 256–263. [CrossRef]
53. Yao, C.; Chen, T. A new simplified method for estimating film mass transfer and surface diffusion coefficients from batch adsorption kinetic data. *Chem. Eng. J.* **2015**, *265*, 93–99. [CrossRef]
54. Da Silva, J.S.; Da Rosa, M.P.; Beck, P.H.; Peres, E.C.; Dotto, G.L.; Kessler, F.; Grasel, F.D.S. Preparation of an alternative adsorbent from Acacia Mearnsii wastes through acetosolv method and its application for dye removal. *J. Clean. Prod.* **2018**, *180*, 386–394. [CrossRef]
55. Mack, C.; Wilhelmi, B.; Duncan, J.; Burgess, J. Biosorption of precious metals. *Biotechnol. Adv.* **2007**, *25*, 264–271. [CrossRef]
56. Wei, W.; Reddy, D.H.K.; Bediako, J.K.; Yun, Y.-S. Aliquat-336-impregnated alginate capsule as a green sorbent for selective recovery of gold from metal mixtures. *Chem. Eng. J.* **2016**, *289*, 413–422. [CrossRef]
57. Li, J.; Miller, J. Reaction kinetics for gold dissolution in acid thiourea solution using formamidine disulfide as oxidant. *Hydrometallurgy* **2002**, *63*, 215–223. [CrossRef]

58. Đurović, M.; Puchta, R.; Bugarčić, Ž.D.; Van Eldik, R. Studies on the reactions of [AuCl4]− with different nucleophiles in aqueous solution. *Dalton Trans.* **2014**, *43*, 8620–8632. [CrossRef]

water

Article

Cd(II) and Pb(II) Adsorption Using a Composite Obtained from *Moringa oleifera* Lam. Cellulose Nanofibrils Impregnated with Iron Nanoparticles

Adriana Vázquez-Guerrero [1], Raúl Cortés-Martínez [2,*], Ruth Alfaro-Cuevas-Villanueva [3], Eric M. Rivera-Muñoz [4] and Rafael Huirache-Acuña [1,*]

[1] División de Estudios de Posgrado, Facultad Ingeniería Química, Universidad Michoacana de San Nicolás de Hidalgo Edificio M, Ciudad Universitaria, C.P. 58030 Morelia, Mexico; adris.mokona@gmail.com
[2] Facultad de Químico Farmacobiología, Universidad Michoacana de San Nicolás de Hidalgo, Tzintzuntzan 173, Colonia Matamoros, C.P. 58240 Morelia, Mexico
[3] Instituto de Investigaciones en Ciencias de la Tierra, Universidad Michoacana de San Nicolás de Hidalgo, Edificio U5, Ciudad Universitaria, C.P. 58030 Morelia, Mexico; racv11@gmail.com
[4] Centro de Física Aplicada y Tecnología Avanzada, Universidad Nacional Autónoma de México, Campus Juriquilla, C.P. 76230 Querétaro, Mexico; emrivera@fata.unam.mx
* Correspondence: raulcortesmtz@gmail.com (R.C.-M.); rafael_huirache@yahoo.it (R.H.-A.)

Abstract: This work informs on the green synthesis of a novel adsorbent and its adsorption capacity. The adsorbent was synthesized by the combination of iron nanoparticles and cellulose nanofibers (FeNPs/NFCs). Cellulose nanofibers (NFCs) were obtained from Moringa (*Moringa oleifera* Lam.) by a pulping Kraft process, acid hydrolysis, and ultrasonic methods. The adsorption method has advantages such as high heavy metal removal in water treatment. Therefore, cadmium (Cd) and lead (Pb) adsorption with FeNP/NFC from aqueous solutions in batch systems was investigated. The kinetic, isotherm, and thermodynamic parameters, as well as the adsorption capacities of FeNP/NFC in each system at different temperatures, were evaluated. The adsorption kinetic data were fitted to mathematical models, so the pseudo-second-order kinetic model described both Cd and Pb. The kinetic rate constant (K_2), was higher for Cd than for Pb, indicating that the metal adsorption was very fast. The adsorption isotherm data were best described by the Langmuir–Freundlich model for Pb multilayer adsorption. The Langmuir model described Cd monolayer sorption. However, experimental maximum adsorption capacities ($q_{e\ exp}$) for Cd (>12 mg/g) were lower than those for Pb (>80 mg/g). In conclusion, iron nanoparticles on the FeNP/NFC composite improved Cd and Pb selectivity during adsorption processes, indicating the process' spontaneous and exothermic nature.

Keywords: cadmium; lead; adsorption; cellulose nanofibrils; iron nanoparticles

Citation: Vázquez-Guerrero, A.; Cortés-Martínez, R.; Alfaro-Cuevas-Villanueva, R.; Rivera-Muñoz, E.M.; Huirache-Acuña, R. Cd(II) and Pb(II) Adsorption Using a Composite Obtained from *Moringa oleifera* Lam. Cellulose Nanofibrils Impregnated with Iron Nanoparticles. *Water* **2021**, *13*, 89. https://doi.org/10.3390/w13010089

Received: 26 November 2020
Accepted: 28 December 2020
Published: 3 January 2021

1. Introduction

Water pollution by heavy metals is one of the most severe environmental problems, with industrial processes being their main anthropogenic sources. Heavy metals can be distinguished from other pollutants because they are not biodegradable, and they can be bioaccumulated in different food chains. Furthermore, these metals have been linked to carcinogenic, embryotoxic, teratogenic, and mutagenic effects [1,2]. Consequently, the permissible limits for cadmium (Cd) and lead (Pb) in drinking water established in 2017 by the World Health Organization's (WHO) standards are 0.003 and 0.01 mg/L, respectively. The United States Environmental Protection Agency (USEPA) has set the maximum contaminant levels (MCLs) in drinking water at 0.015 mg/L for lead and 0.005 mg/L for cadmium [3–5]. Cadmium and lead are some of the heavy metals introduced as anthropogenic pollutants worldwide by various processes. Cadmium contamination may occur due to the manufacture of alloys, batteries, pigments, plastics, mining, and refining processes [6]. Cadmium causes severe damage to kidneys and bones. Its accumulation in the human body leads to nausea, headaches, fatigue, salivation, diarrhea, muscular cramps, renal degradation, chronic pulmonary problems, skeletal deformity, low levels of iron in the blood, and breathlessness (dyspnea) [7,8].

On the other hand, common anthropogenic causes of lead contamination in groundwater are mining, smelting, fossil fuel combustion, solid waste incineration, batteries, paints, cables, ceramics, and glass manufacturing [9]. In children, overexposure to lead causes swelling of the optic nerve, ataxia, brain damage (encephalopathy), convulsions, seizures, and impaired consciousness. In adults, lead exposure causes high blood pressure, damage to the reproductive organs, fever, headaches, fatigue, vomiting, anorexia, abdominal pain, constipation, joint pain, incoordination, insomnia, irritability, and various symptoms related to the nervous systems [7].

Many techniques have been employed to reduce the adverse effects of cadmium and lead in water bodies, including chemical oxidation/reduction, chemical precipitation, electrochemical processes, ion exchange, membrane filtration, and others [10,11]. These processes can be difficult to operate, and they show low selectivity. However, among these methods, adsorption is flexible, low cost, and a high-efficiency technique [12]. Adsorption is a mass transfer process by which a substance is transferred from the liquid phase to the solid's surface by physical or chemical interactions.

Other studies have demonstrated the use of biomaterials as efficient, low-cost, abundant, biodegradable, and highly stable adsorbents [13]. Cellulose is an abundant natural polymer and is commonly found in wood, seeds, algae, and agro-industrial waste. The Moringa tree (*Moringa oleifera* Lam), a member of the Moringaceae family, can grow around the tropics. It is native to sub-Himalayan areas of northwestern India. It can be easily cultivated and adapts to semiarid climates, as it is a polyvalent tropical tree. In Michoacan, Mexico, the generation of residual biomass product from its plantation along the Pacific coast has been reported, with an average of 300 to 500 kg per hectare. This waste from leaves, stems, and branches concentrates wasted cellulose in large amounts [14,15]. Among the various functional polymers exist cellulose nanofibers (NFCs). Such fibers are large flexible fiber structures consisting of alternating crystalline and amorphous domains in a net-like structure. NFCs can be extracted from a cellulosic material, moderately degraded by chemical methods, thermal processes, and mechanical processes. Additionally, NFCs have been obtained from combined pulping Kraft process, acid hydrolysis, and ultrasonic methods [16,17].

The adsorption of metals by this type of material can be attributed to their structural compounds with various functional groups, such as carboxyl, carbonyl, sulfide, and hydroxyl. Many of these hydroxyl groups allow chemical modification and improve adsorption performance [18]. Cellulose tends to form an aggregate structure due to the hydrogen bonds being present, limiting adsorption; hence, modification of the cellulose structure and surface can help to avoid adsorption restraints. One of these modifications involves impregnation with metallic nanoparticles. Such a change can enhance adsorption properties in the biopolymer [19]. It has been reported that many metal oxide nanoparticles and other inorganic nanoparticles (i.e., zeolite nanoparticles) effectively and quickly remove metal contaminants in wastewater treatment processes [11,20].

The appearance of iron nanoparticles in remediation is attributed to their low toxicity and redox capacity when reacting with water. They have a large surface areas and high reactivity [21]. The use of iron nanoparticles has been reported in different carbon-based materials, such as starch and biopolymers, as well as in mineral adsorbents, such as clays. These materials act as supports for obtaining nanocomposites [22–26]. Moreover, functionalization with organic solvents helps to mitigate nanoparticles' agglomeration on the composite and improves dispersion. Different modifiers are used to abate nanoparticles' mobility in water, such as carboxymethyl cellulose or cellulose, since they are negatively charged molecules. These nanoparticles (NPs) are generally considered to be the most mobile in aqueous solutions due to electrostatic repulsion [27].

Several processes have been utilized to prepare nanoadsorbents. These are often considered as time-consuming processes, have high reagent requirements, and release toxic substances into the environment [28]. Otherwise, nanoparticles synthesized by plant products or extracts are more stable. These green syntheses are more manageable than conventional techniques. Such ecological approaches are cost-effective, simple, and sustainable and do not involve any toxic agents [29]. Different green synthesis routes use agro-industrial wastes, biopolymers, solvent replacement, plants, microorganisms, etc. [30]. Nanoparticles can be incorporated into the biopolymer through different mechanisms, such as chemical coprecipitation, to obtain the final composite material. Still, the use of plant extracts (organic compounds) can influence the reduction process. They can also stabilize the nanoparticles, promoting bonding to the biopolymer [31].

Fruits, seeds, stem, and leaf extracts from different plants contain useful polyphenols for metal reduction. These substances have been researched as bioreducing agents to synthesize nanoparticles, such as *Vitex negundo* L., *E. condylocarpa*, and *Amaranthus dubius* [32–35]; including *Rumex acetosa* [36], *Eucalyptus globulus* [37], *Mukia maderaspatana* [38], *Camellia sinensis* [39], *Rosemarinus officinalis* [40], *Citrus maxima* [41], *Azadirachta Indica* [30,42], green tea [43], eucalyptus [44], and *Canna indica* [21]. Additionally, waste materials such as banana peel and citrus juice waste have also been used.

Green plant leaves have recently been studied for the eco-friendly synthesis of iron nanoparticles, using Fe(II) or Fe(III) chloride solutions as precursors [30]. This synthesis is possible because these plants contain bioactive components, mostly polyphenols, that act as reducing and capping agents. Moreover, several applications and syntheses of metal oxide nanoparticles, particularly for iron, have been reported [45–49]. Jitendra et al. [50] reported that *A. indica* leaf extract assisted in the green synthesis of highly crystalline α-Fe_2O_3 nanomaterials with well-defined unique morphologies. Similarly, the green-synthesized mesoporous α-Fe_2O_3 had a surface area four times larger than the commercial α-Fe_2O_3 nanoparticles [39]. Moringa leaf contains various photochemical type-like flavonoids, such as polyphenols, rutin, kaempferol, chlorogenic acid, quercetin-malonyl-glucoside, glucosinolate, and isothiocyanates, with high antioxidant capacities. These are an alternative reducing agent for synthesizing iron oxide NPs [51,52].

Therefore, the present study aims to evaluate the iron nanoparticles and cellulose nanofibers (FeNPs/NFCs) performance for the removal of Cd(II) and Pb(II) from aqueous solutions and to examine the structure of the composite obtained from the cellulose nanofiber's (from branch wood residues) contact with iron nanoparticles (from green synthesis with $FeCl_3$ and leaf tea extract). Furthermore, the influence of contact time, temperature, and pH on adsorption experiments was determined, as were the adsorption mechanisms and thermodynamic, kinetic, and isothermal parameters of the studied systems.

2. Materials and Methods

2.1. Preparation of FeNP/NFC Composite

Large amounts of wood residues obtained from the pruning of the Moringa tree were collected from an orchard located in the municipality of Nueva Italia in the State of Michoacán, Mexico. These wood residues were used for cellulose extraction by Kraft pulping, followed by acid hydrolysis.

The cellulose nanofibrils (NFCs) were obtained using a high-intensity ultrasonication technique combined with cryo-crushing with liquid nitrogen. Wood chips from *Moringa oleifera* Lam. were cooked by Kraft pulping in a Kamir digester (METROTEC, model LB-16) with a capacity of 15 L and a speed of 5.16 r.p.m. The Kraft Pulping process was carried out with the following operating parameters: the temperature ranged from 160 to 170 °C with a boiling time of 20–30 min, a white liquor with sulfidity levels between 20 and 27% was used, using 200 g of wood chips (dry basis).

Chemical post-treatment to wood fibers by acid hydrolysis was performed with an H_2SO_4 solution 40% (*v/v*) at 80 °C for 2 h. The separation of fibers was carried out using a high-intensity ultrasonication technique combined with cryo-crushing with liquid nitrogen.

The mechanical cryo-crushing with ice crystal formation slashed the vegetal fiber wall and released wall fragments. The ultrasonic treatment was carried out for 40 min at 60 kHz, and then the material was dried in an oven. Mechanical fibrillation was performed using liquid nitrogen and applying high shear forces.

The synthesis of the composite material (FeNP/NFC) was carried out by putting in contact 4 g of cellulose (Kraft pulp) and 40 mL of leaf extract. Fresh *Moringa oleifera* Lam. leaves were collected and carefully washed with deionized water, and they were dried at room temperature with constant ventilation. Then, 20 g of dried leaves sample were mixed with 150 mL distilled water at 60 °C for 45 min. The supernatant was filtered with a Whatman filter paper to produce the leaf extract, and was stored at 4 °C in the refrigerator. A 0.5 M solution of $FeCl_3.6H_2O$ was subsequently adjusted at pH 8, using 0.1 N HCl and 0.1 N NaOH solutions. The leaf extract (pH 5.6) was added dropwise to the $FeCl_3$ solution with continuous stirring at 60 °C for 180 min. The modified material FeNP/NFC was filtered and washed several times with distilled water to eliminate any excess of reactive components from the material; the modified material was allowed to dry and it was stored in a desiccator.

2.2. Characterization of FeNP/NFC Composite

Different methods were used to perform the characterization of Kraft pulp and composite material in order to determine their morphologies, semiquantitative elemental properties, and surface properties. Scanning Electron Microscopy (SEM) images were obtained using a JEOL JSM IT300LV microscope (Tokyo, Japan).

Fourier Transform Infrared Spectroscopy (FTIR) was used to examine the changes in the functional groups induced by the adsorbent synthesis and the adsorption process. The samples were analyzed in a Bruker® Tensor 27 FTIR spectrophotometer (Bruker Optics Inc., Billerica, MA, USA).

The zeta potential (ZP) was used to measure the electrical potential on the adsorbent's surface. From the values of the zeta potential at different values 3 to 10 pH, the surface acidity or basicity and the isoelectric point were determined [16]. The FeNP/NFC material's zeta potential was measured with a Nano Brook 90 Plus Zeta instrument.

X-ray Diffraction (XRD) measurements were conducted to determine the presence of the cellulose crystalline phase in the samples, using a Rigaku Ultima IV (Rikagu, Tokio, Japan). The diffracted intensity of the Cu-Kα (λ = 1.54 Å) was measured in a 2θ range. Data analysis to identify crystalline and amorphous phases was carried out using Match V. 1.10^a 2003–2010 Software (Crystal Impact, Bonn, Germany).

The FeNP/NFC composite oxides were analyzed on an energy dispersive X-Ray fluorescence spectrometer model Bruker S2PUMA with an Ag tube. Samples were analyzed to define the form of oxides.

2.3. Adsorption Experiments

2.3.1. Kinetics

Batch-type experiments with FeNP/NC were performed to determine Cd and Pb removal. Samples with 10 mL aliquots of a 2 mg/L metal solution were put in contact with 0.05 g of composite material in plastic flasks. The pHs of the initial solution for Pb and Cd were 2 and 3, respectively. The solutions' pHs were adjusted to and maintained at 5 (by adding 0.01 M HCl or 0.05 M NaOH to the solutions) due to the cationic chemical species (II) present in the solution. The flasks were shaken, separately, at 100 rpm and 25 °C. The solutions' concentrations were 2 mg/L for both $Pb(NO_3)_2$ and $Cd(NO_3)_2{\cdot}4H_2O$. The contact times ranged from 5 to 150 min to acquire the equilibrium time. After the contact time was achieved, the supernatants were separated by filtration, and the residual solution was analyzed for each metal by Flame Atomic Absorption Spectrometry (FAAS) (model Perkin Elmer® AANALYST 200, Waltham, MA, USA). The solutions were refrigerated at 4 °C and stored in amber bottles (plastic and glass) to avoid precipitation and oxidation during analysis. The experiments were performed in triplicate to determine reproducibility.

The Cd and Pb adsorption concentrations at equilibrium time during adsorption were calculated by:

$$q_t = \frac{(C_o - C_t)V}{m} \tag{1}$$

where q_t is the amount of ion adsorbed, at a time (t), per weight of adsorbent (mg/g); C_o is the initial concentration of heavy metal (mg/L); C_t is the concentration of heavy metal at that equilibrium time (mg/L); V is the volume of solution (L), and m is the mass of the adsorbent (g).

A batch removal system requires information about the optimum conditions that can only be acquired from kinetic models. Moreover, adsorption kinetics studies and their adjustment to empirical models allow the evaluation of removal mechanisms and are fundamental for selecting optimal design parameters for future effluent treatments. The data obtained from the kinetics tests were fitted to the Elovich, Lagergren (pseudo-first-order), and pseudo-second-order kinetic models by nonlinear regression analysis using Statistica 7.0 software. Such kinetic models were used in this research due to their wide use and acceptance in heavy metals removal studies.

The general expression of the pseudo-first-order rate, also known as the Lagergren model, is represented by the following equation [53].

$$q_t = q_e\left(1 - e^{-K_l t}\right) \tag{2}$$

where K_L is the Lagergren rate constant (1/min), q_t is the amount of ions adsorbed, at a time (*t*), per weight of adsorbent (mg/g), and q_e is the amount of ions adsorbed at the equilibrium (mg/g).

The pseudo-second-order model is based on the assumption that the rate-limiting step may be chemisorption [54]. Alternatively, the pseudo-second-order model is expressed in its linear form as follows:

$$q_t = \frac{K_2 q_e^2 t}{1 + 2K_2 q_e t} \tag{3}$$

where K_2 is the pseudo-second-order rate constant for adsorption (g/mg min), q_t is the amount of ions adsorbed, at a time (*t*), per weight of adsorbent (mg/g), and q_e is the amount of ions adsorbed at the equilibrium (mg/g).

The Elovich equation is represented by the following [55], commonly used in the kinetics of the chemisorption of gases on solids:

$$q_t = \frac{1}{b}\ln(1 + abt) \tag{4}$$

where q_t is the amount of ion adsorbed, at a time (*t*), per weight of adsorbent (mg/g), q_e is the concentration of solute removed at the equilibrium per weight of adsorbent (mg/g), K_L is the pseudo-first-order kinetic constant (1/min), K_2 is the pseudo-second-order rate constant of sorption (g/mg.min), and *a* and *b* are the Elovich constants related to the initial adsorption rate (mg/g min) and desorption rate (g/mg), respectively.

2.3.2. Isotherms

Adsorption isotherms were performed with Cd and Pb aqueous solutions at different concentrations to determine the systems' equilibrium parameters. Plastic vials were used to put 0.05 g of FeNP/NC in contact with 10 mL of Pb and Cd solutions, separately, at different concentrations, ranging from 5 to 500 mg/L. Then, the vials were placed in a thermostat-adjusted water bath agitator. They were shaken at 100 rpm at different temperatures (25, 30, and 40 °C). All experiments were performed in triplicate. According to the chemical equilibrium diagram for cation ions in an aqueous solution, the pH values were selected. Cd ions predominate at pH values between 2 and 8 and Pb ions with pH values between 3 and 5.5. The pH 5 value was then set and adjusted with 0.01 M HCl and 0.05 M NaOH solutions, as required, before the adsorption experiments.

The experimental data from sorption isotherms of Pb and Cd were fitted to the following isotherm models by nonlinear regression analysis. The equation that expresses the Freundlich model is:

$$Q_e = K_f C_e^{\frac{1}{n}} \tag{5}$$

where Q_e is the adsorption capacity of Pb(II) and Cd(II) of the adsorbents (mg/g), C_e is the equilibrium concentration of the metal ion in solution (mg/L), K_f is the equilibrium constant indicative of adsorption capacity, and n is the adsorption equilibrium constant whose reciprocal is indicative of adsorption intensity. The Freundlich model assumes that the adsorption process happened on heterogeneous surfaces [56].

Langmuir model could be represented by Equation (6) [57]:

$$Q_e = \frac{Q_0 K_L C_e}{1 + K_L C_e} \tag{6}$$

where Q_0 represents the maximum monolayer adsorption capacity of Pb and Cd, and K_L is the Langmuir constant (L/g). The Langmuir model is established based on forming a complete monolayer on the surface (mg/g).

Langmuir–Freundlich model is represented by Equation (7) [58]:

$$Q_e = \frac{K_{LF} C_e^{\frac{1}{n}}}{1 + a_{LF} C_e^{\frac{1}{n}}} \tag{7}$$

where K_{LF} and a_{LF} are empirical constants.

2.4. Thermodynamic Studies

The thermodynamic results were calculated from isotherm data of Pb and Cd at 25, 30, and 40 °C. The thermodynamic parameters were estimated to analyze the influence of temperature on metal ion adsorption, such as Gibb's free energy change ΔG (kJ/mol), enthalpy change ΔH (kJ/mol), and entropy change ΔS (J/mol K) [4,59], using the following thermodynamic equations:

$$K_c = \frac{C_{ad}}{C_e} \tag{8}$$

$$C_e = C_i\,(1 - F_e) \tag{9}$$

$$C_{ad} = C_i\,F_e \tag{10}$$

$$K_c = \frac{F_e}{1 - F_e} \tag{11}$$

$$\Delta G^\circ = -RTlnK_c \tag{12}$$

$$\Delta H^\circ = R\left(\frac{T_1 T_2}{T_1 - T_2}\right)\ln\frac{K_{c1}}{K_{c2}} \tag{13}$$

$$\Delta S^\circ = \frac{\Delta H^\circ - \Delta G^\circ}{T} \tag{14}$$

where R = 8.314 J/mol K is the universal gas constant; K_c (mL/g) is the equilibrium constant; C_e is the concentration of the metal in the solution at equilibrium (mg/L); C_i is the initial concentration of the metal in the solution at equilibrium (mg/L); F_e is the fractional conversion of the sorption at equilibrium, and T is the thermodynamic temperature (K).

Van't Hoff's equation [59] allowed us to obtain the ΔH° and ΔS° values graphically:

$$lnK_C = \frac{-\Delta H^\circ}{R\;x\;T} + \frac{\Delta S^\circ}{R} \tag{15}$$

A graph of lnK_c on the abscissa axis and $1/T$ on the ordinate axis should be linear, and the intercept would be equivalent to $\Delta S°/R$, while the slope would be numerically equal to $\Delta H°/R$.

3. Results and Discussion

3.1. Characterization of FeNP/NFC Composite

As shown in Figure 1, the surface morphology is significantly different before and after NFC impregnation with iron nanoparticles. After the hydrolysis and cryo-crushing process, NFC exhibited a cavernous network structure that has a smooth surface. Figure 1a,b, show the formation of several clefts or folds, which will help distribute the nanoparticles on the support material. The spaces between the microfibers collapse for wood and plant cellulose sources due to water molecules' outflow. When the microfibers dry, all the hydrogen bonds between the fibrils are displaced, forming weak links. It is essential to indicate the effect of pH on the material because hydrolysis was generated in an acidic medium. The concentration of hydronium ions incorporated into the material increased and, therefore, they are attributed to agglomeration behavior [60,61]. Cellulose nanofibers tend to aggregate due to hydrogen bonding between the OH and COOH- groups [62,63].

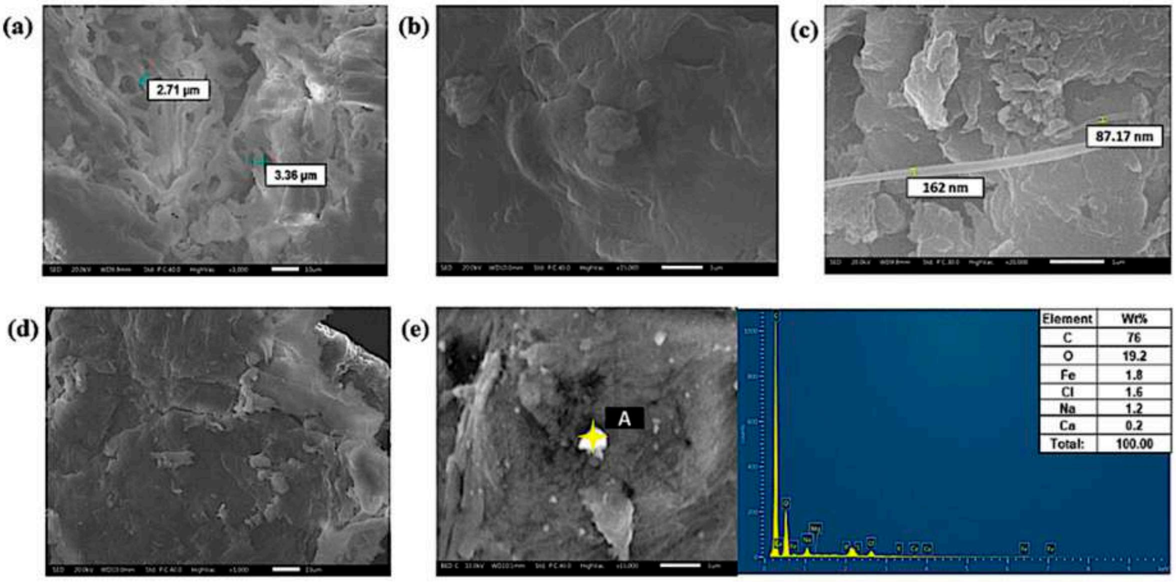

Element	Wt%
C	76
O	19.2
Fe	1.8
Cl	1.6
Na	1.2
Ca	0.2
Total:	100.00

Figure 1. Scanning electron microscopy (SEM) micrographs of Cellulose nanofibers (NFCs): (**a**) X1000, (**b**) X15,000, (**c**) X20,000; iron nanoparticles and cellulose nanofibers (FeNPs/NFCs): (**d**) X1000, (**e**) X1500.

The cryo-crushing process formed ice crystals that helped to slash vegetal fiber and expose more surfaces, which allowed access to chemical activation of various functional groups. Because of nanofibers' exposure (Figure 1c), it can be established that the mechanical cryo-crushing and ultrasonic treatment were suitable for defibrillation of Moringa's Kraft pulp. The average diameter of nanofibers reported in other studies ranged from 50 to 100 nm, depending on the cellulose source [63–66]. In this case, the nanofibers' diameters ranged from 80 to 160 nm, as shown in Figure 1c, indicating nanofibers' presence. These nanofibers are not clearly seen in Figure 1a,b due to the micrographs' magnification. However, a nonhomogeneous accumulation of fibers can be observed in these micrographs (Figure 1a,b), which can also be denominated as microfibrillated cellulose (depending on the size and production process), consisting of cellulose nanofibers and nanofiber bundles [67,68].

Moreover, an increase in cellulose crystallinity has also been reported in NFC production from various sources [63,67]. In this case, such an increase was observed after the Moringa's NFC synthesis process, compared to the Kraft pulp cellulose crystallinity, due to the breaking down of the hierarchical structure of the cellulose into individualized nanofibers of high crystallinity, with a reduction in amorphous parts [67]. The crystallinity of the Moringa's NFC will be discussed further below. Furthermore, FTIR analyses of several NFC samples from different sources proved that chemical treatment also led to partial removal of hemicelluloses and lignin from the fibers' structures. Still, the molecular structure of cellulose remained unchanged after chemical and mechanical treatments [64,67]. This behavior was also observed in the NFC from Moringa and will also be discussed further. Based on the above, the presence of cellulose nanofibrils in the Moringa composite can be confirmed.

In Figure 1d,e, micrographs of FeNP/NFC are observed. The surface showed a distribution of small particles which are related to NPs. Results for punctual Energy Dispersive X-Ray Spectroscopy (EDS) analysis (point A in Figure 1e) indicate high concentrations of carbon (C), oxygen (O), iron (Fe), chlorine (Cl), sodium (Na), and calcium (Ca), Figure 1e. Chlorine comes from the reactive solution used in FeNP/NCF preparation. The results indicate a certain percentage of Fe adhered to the surface, which is related to the synthesis of NPs. The alkaline pH system adjusted in the synthesis of nanoparticles helps incorporate hydroxyl groups (–OH) and NPs to the matrix. Hemicelluloses that still partially persist in the structure can inhibit nanofibrils' coalescence during the synthesis of iron nanoparticles. The formation of several slits is observed, which helped distribute the nanoparticles on the support material and capture these ions [61].

The elemental mapping was performed to the FeNP/NFC samples after the adsorption process. In Figure 2a,b, the main elements present on the materials' surfaces are carbon and oxygen in a higher proportion in weight, and low concentrations of dispersed forms of Cd and Pb. The sulfate (S), Ca, and Fe compounds contribute to Cd aggregates' adsorption on the surface of the material observed at various sites. Sodium comes from cooking liquors of the Kraft pulping process: NaOH, NaS, and Na_2CO_3. Calcium and potassium are the main elements present in the wood. The sample's composition with adhered particles of Cd is shown in Figure 3b at 5000×, where the spot analysis indicates solid Cd particles. The results demonstrate the presence of Cd at around 11% (*w/w*), forming various phases on the material. The sample analysis shows a decrease in Fe (with values <0.15%) compared to the samples before Cd adsorption, indicating a possible ion-exchange sorption mechanism. The spot analysis of the sample that adsorbed Pb (Figure 3a) reached a concentration near 1.05% (*w/w*). The carboxylic acids, phenols, and alcohols on the surface of the adsorbent were protonated, and the surface was negatively charged, allowing adsorption.

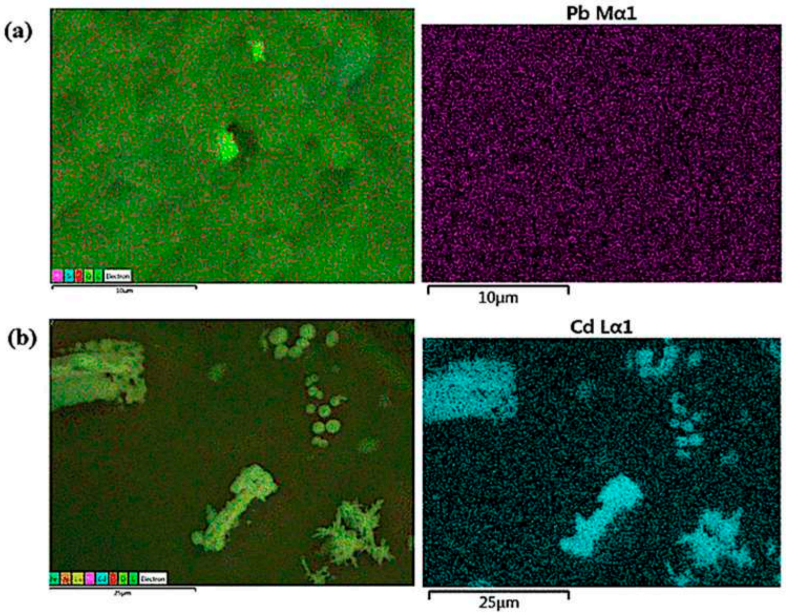

Figure 2. Elemental mapping of FeNP/NFC samples after adsorption of (**a**) lead (Pb) and (**b**) cadmium (Cd).

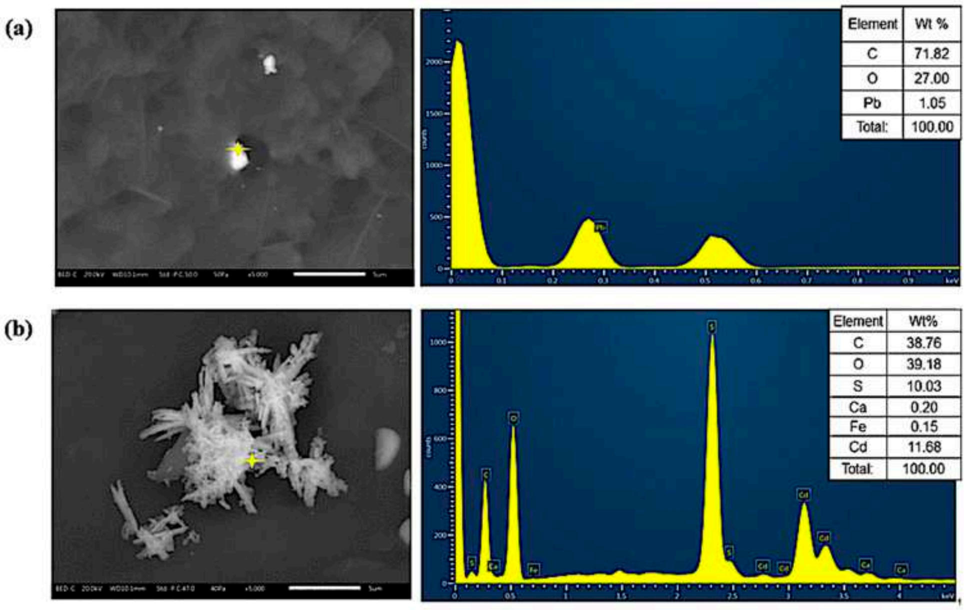

Element	Wt %
C	71.82
O	27.00
Pb	1.05
Total:	100.00

Element	Wt%
C	38.76
O	39.18
S	10.03
Ca	0.20
Fe	0.15
Cd	11.68
Total:	100.00

Figure 3. Spot analysis of composite samples after adsorption of (**a**) Pb and (**b**) Cd.

Figure 4 shows the FTIR spectra of NFC and FeNP/NFC. For both spectra, the broad peaks at 3406 and 3374 cm^{-1} are associated with -OH stretching vibration. The bands at 1636 and 1611 cm^{-1} are attributed to the water bending vibration. Displacement of these peaks is observed due to their intervention during the synthesis of the new material. In the case of the FeNP/NFC sample, the smaller peak at 2909 cm^{-1} corresponds to the -CH stretching of the aromatic rings and methylene (-CH_2), which are associated with functional groups involved in the green synthesis of nanoparticles. The appearance of a band at 1456 cm^{-1} can be assigned to a -CH_2 bending vibration and -OH deformation vibration, for the phenolic or alcoholic group.

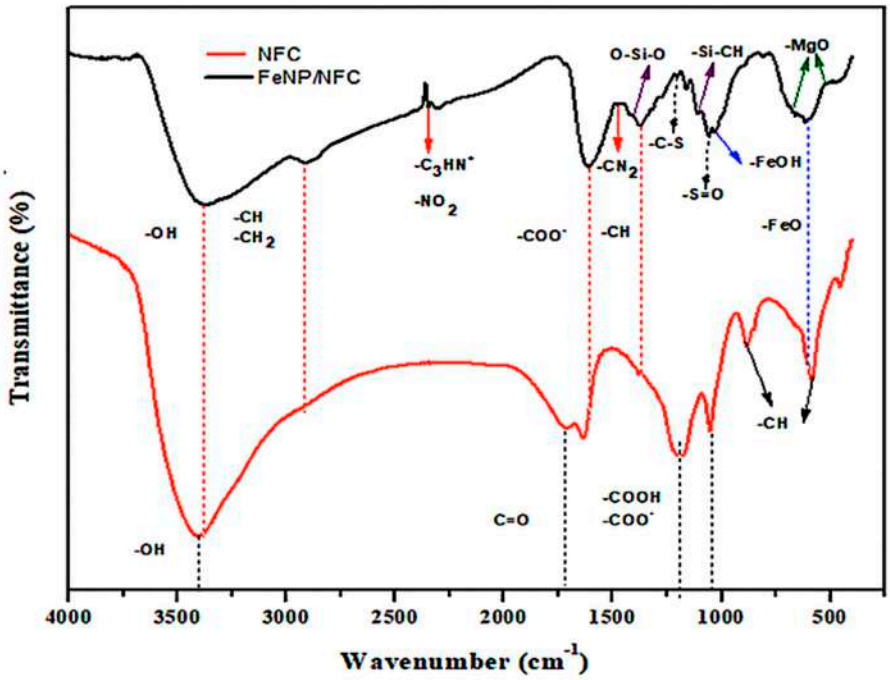

Figure 4. Fourier Transform Infrared Spectroscopy (FTIR) spectra of NFC and FeNP/NFC samples.

Significant changes were observed in the bands from 1500 to 1000 cm^{-1}. The bands from 1502 to 1418 cm^{-1} correspond to the aromatic elongation of C=C bonds and aromatic deformation vibration of C-C bonds. The stretching of carboxylic acids and esters peak is present at 1271 cm^{-1}. Ether and free alcohol C-O stretching can also be observed at the bands from 1000 to 1280 cm^{-1}. The adsorption peaks at 1161 and 661 cm^{-1} are attributed to asymmetric C-O-C and deformation of out-of-plane hydrogen of the C-H bond in the aromatic ring [69].

After the Fe nanoparticles' impregnation on NFC, some peaks' intensities increased in the spectrum of the FeNP/NFC composite (Figure 4)—mainly the bands that appeared in the region between 600 and 400 cm^{-1}, which correspond to Fe oxides. The FTIR spectrum of FeNP/NFC exhibited peaks at 1611, 1551, 1463, 1376, 1031, and 600 cm^{-1}. The broad peak at 601 cm^{-1} was attributed to stretching vibrations of Fe-O.

On the other hand, the O-Si-O and Si-CH functional groups were observed in the cellulosic material; thus, main peaks with stretching and bending vibrations from 1430 to 1100 cm^{-1} were noticed. The Si can also react with the noncellulosic components, where it can contribute to the Fe-O bond from 580 to 603 cm^{-1} due to the formation of the Fe-O-Si bond [70]. Furthermore, the peaks with lower intensities, at 511 and 675 cm^{-1}, such as -MgO, are related to other oxides present in the material. These sites intervened in the adsorption and were largely attributed to the wood's inorganic portion, and a smaller portion to the final material [71]

The peaks around 1376 and 1463 cm^{-1} increased their intensity; these are attributed to the -CH symmetric vibration of the polymeric matrix of NFC, mainly due to a strong hydrogen bond between the NFC groups and iron nanoparticles. The broad peak at 1031 cm^{-1} was associated with Fe-OH vibration; it indicates the incorporation of iron onto the surface [69]. The stretching vibration of O=S=O was observed at 1384 cm^{-1}; the C-S group was found at 1200 cm^{-1} and the S=O group was identified at 1053 cm^{-1}. These bands confirmed the presence of the sulfonic group. The effect of alkaline and acid treatments on cellulosic materials leads to surface activation with various functional groups such as -SH, -SOH_2, -SO, -$(CH_3O)_2SO_2$, and C-S, which can help in the adsorption process [4,56]. Bands at 2340, 2346, and 1478 cm^{-1} are typical of N vibrations, such as -NO_2, C_3HN^+, and CN_2; these groups were formed by the cellulose synthesis and extraction [72].

The Fourier Transform Infrared Spectroscopy (FTIR) analysis reveals (Figure 4) that the FeNP/NFC was esterified during the synthesis process at 1721 cm^{-1}; this band is usually attributed to C=O stretching vibration, and a decrease in this band was observed for the FeNP/NFC sample. A new weak absorption peak appeared at 1427 cm^{-1}, which could be attributed to the bending vibration of OH in carboxyl groups. On the other hand, a large amount of -COOH groups had been introduced to cellulose after the modification; these groups possess strong adsorption properties for heavy metal ions [73].

Figure 5 shows the FTIR spectra of FeNP/NFC adsorbent after Pb adsorption (PbRM) and after Cd adsorption (CdRM). It was observed that metal adsorption generated slight displacements in some bands and significant changes in the band frequencies of groups such as -OH, -COO-, C=O, C-O, and C-O-C; this suggests that such ionizable functional groups on the adsorbent surface can bond with the metal ion. For CdRM and PbRM, the stretching vibration peak of C-H observed at bands from 2800 to 3000 cm^{-1} disappeared, indicating that C-H may participate in the cross-linking reaction. Moreover, at the 1630 cm^{-1} wavenumber, band intensity changes can be attributed to the $Pb(NO_2)$ stretching vibration. Therefore, it can be established that amine groups in FeNP/NFC play an essential role in lead adsorption on this material by sharing one electron pair of the nitrogen atom with the Pb ions. The decrease in free carboxylic acid, iron oxide, iron hydroxides, amide, nitrogen dioxide, magnesium oxide, sulfur groups, and other possible sites indicates the same type changes upon sorption of Pb and Cd ions.

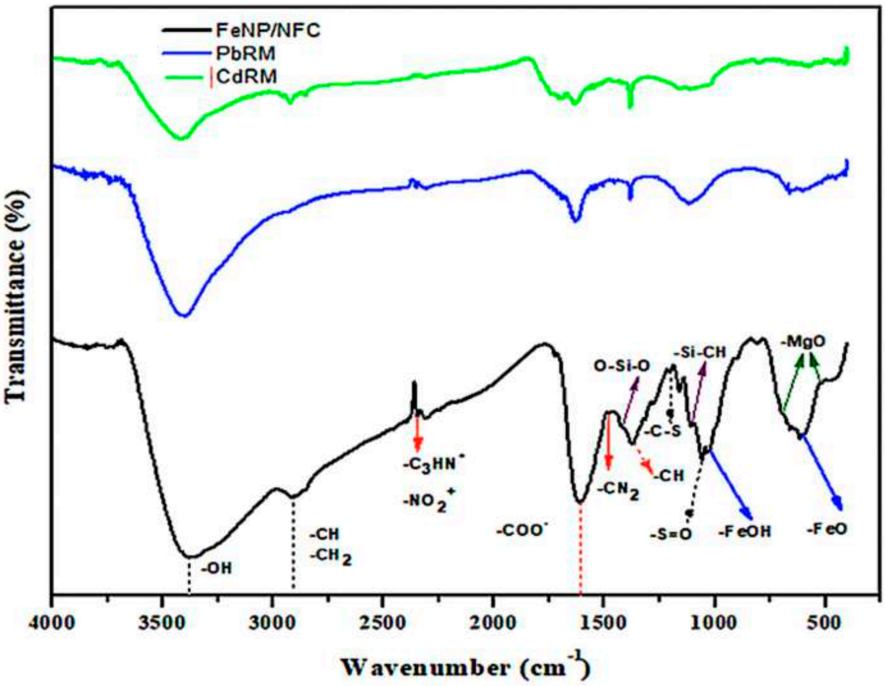

Figure 5. FTIR spectra of FeNP/NFC, adsorbent after Pb adsorption (PbRM) and after Cd adsorption (CdRM).

The zeta potential (ZP) value of FeNP/NFC increased from −11 to −23 mV; this lower negative value is due both to the polyphenolic components present in the extract during the synthesis of the material and also to the cellulose structure of the support material for the Fe nanoparticles (Figure 6) [34]. Different modification strategies create ionic groups on the surfaces of NFCs. Carboxymethylation, oxidation, and sulfonation are three routes that can add ionic groups on the surface of the cellulose. Carboxymethylation causes surfaces to be negatively charged, promoting stable suspension from carboxymethylated fibers. The oxidation process includes hydroxyl groups, which oxidize to aldehyde groups, followed by carboxyl groups. Sulfonation is considered as a way to induce an anionic charge on the surface with different functional groups such as -SO, -SH, and $-HSO_3^-$ [74,75].

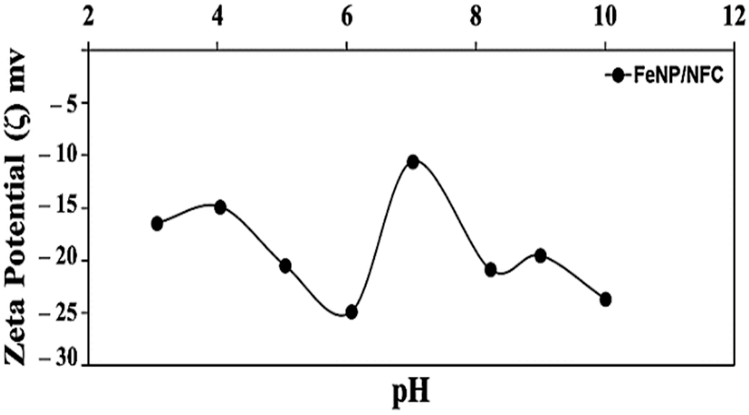

Figure 6. Zeta potential (ZP) of FeNP/NFC composite.

There is no evidence of an isoelectric point in the sample, which confirms that charge dissociation is virtually independent of pH. Under acidic conditions, as the pH decreases, the -COO- groups are converted to -COOH resulting in a lower density of surface charge, and therefore a reduction in mobility. Additionally, an increase in pH did not change the particle mobility significantly. In all of the pH ranges, the Zeta potential values were negative; therefore, it can be considered that the pH does not affect the surface loading properties of the material. Particles with low zeta potential have tended to agglomerate, while particles with high zeta potentials have been electrically stable.

On the other hand, the crystalline structure of cellulose is one of the most studied structural problems in polymer science, and its accurate description of the crystal structure remains a topic of discussion [76,77]. Therefore, an analysis of the crystal structure by XRD was carried out to determine the composite material's crystalline state.

As shown in XRD patterns (Figure 7), there is strong diffraction at 14.63°, 16.7°, and 22.42° of FeNP/NFC, corresponding to the (101), (10 $\bar{1}$), and (002) crystalline planes for cellulose II, into the sample. The acid hydrolysis and cryo-crushing methods destroy the stable hydrogen bonds, generate free hydroxyl groups, and increase cellulose reactivity [73]. They were indexed in the structure of cellulose (JCPDS No. 50-2241). The diffraction intensity was weak for the (101) and (10 $\bar{1}$) crystal planes. These two peaks overlap with each other because they have a lower amount of lignin and hemicellulose, resulting from the adsorbent's synthesis process.

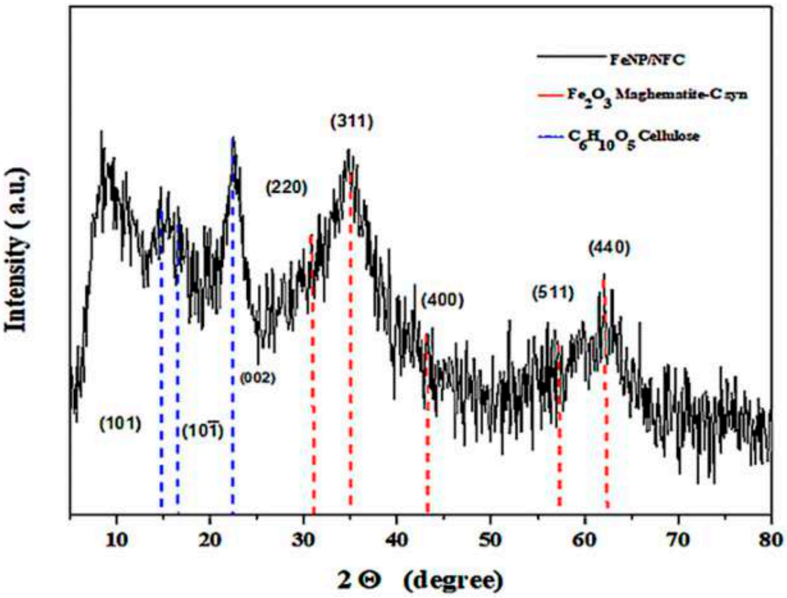

Figure 7. X-ray Diffraction (XRD) patterns of the FeNP/NFC, prepared with Moringa leaf extract.

It is difficult for chemical reactions to take place in the crystalline region because of its stable structure. Hence, it becomes an easily accessible and penetrable amorphous structure, increasing iron nanoparticles' introduction [4,73]. XRD patterns show peaks related to amorphous and crystalline compounds (Figure 7). The nanoparticles in the material presented peaks at around 30° to 62°, which could be due to crystalline materials on organic matter.

The iron oxide phase in FeNP/NFC shows some intense XRD peaks—identified as maghematite (Fe_2O_3). These peaks and indices were 30.79° (220), 35.63° (311), 43.51° (400), 57.22° (511), and 62.79° (440), as can be observed in Figure 7. The diffraction peaks belong to iron oxide maghematite-C syn (No. 00-024-0081) with a rhombohedral structure. Different amorphous materials impregnated with nanoparticles have been reported, finding that the iron nanoparticles prepared with green tea extract were efficient in different aspects [34]. The polyphenolic compounds from tea do not possess a reduction potential negative enough to reduce from Fe^{3+} to Fe^0 but can reduce Fe^{3+} to Fe^{2+}, forming oxide/hydroxide nanoparticles.

The Energy Dispersive X-ray Fluorescence (EDXRF) analysis is shown in the spectrum of Figure 8. The peaks around 0.8, 6.4, and 7.05 keV are related to the Fe binding energies. Therefore, the EDXRF spectrum for Fe_2O_3 from the FeNP/NFC material, synthesized with aqueous extract of Moringa leaves, confirmed nanoparticles' presence. The number of radicals present in the hybrid sample revealed the photocatalytic activity of the nanoparticles. The other intense peaks shown in the EDXRF spectrum are marked as salts' structures derived from the extraction of the cellulose and its initial composition from the raw material derived from Moringa wood (Figure 8). The signal peak at 2.98 keV is assigned to silver (Ag), derived from its presence on the sample holder and tube in the instrument employed for the analysis; hence, the peak of iron looks smaller than silver. Potassium is essential for the growth of the tree, which can be seen in the graph's 3.16 keV intensity. The EDXRF spectrum analysis indicates that the sample has a composition of approximately 32.81% Fe_2O_3 and is only one of the existing oxide groups in the material (Table 1). According to this result, the weight percent of metal oxides on cellulose increased, confirming that the iron nanoparticles were successfully incorporated. Other than iron, different compounds were identified, such as MgO, SiO_2, P_2O_5, SO_3, and Cl (Table 1). Inorganic material in wood is found as carbonates, oxalates, silicates, phosphates, and sulfates; or organized as carboxyl groups in the cellulosic materials [78].

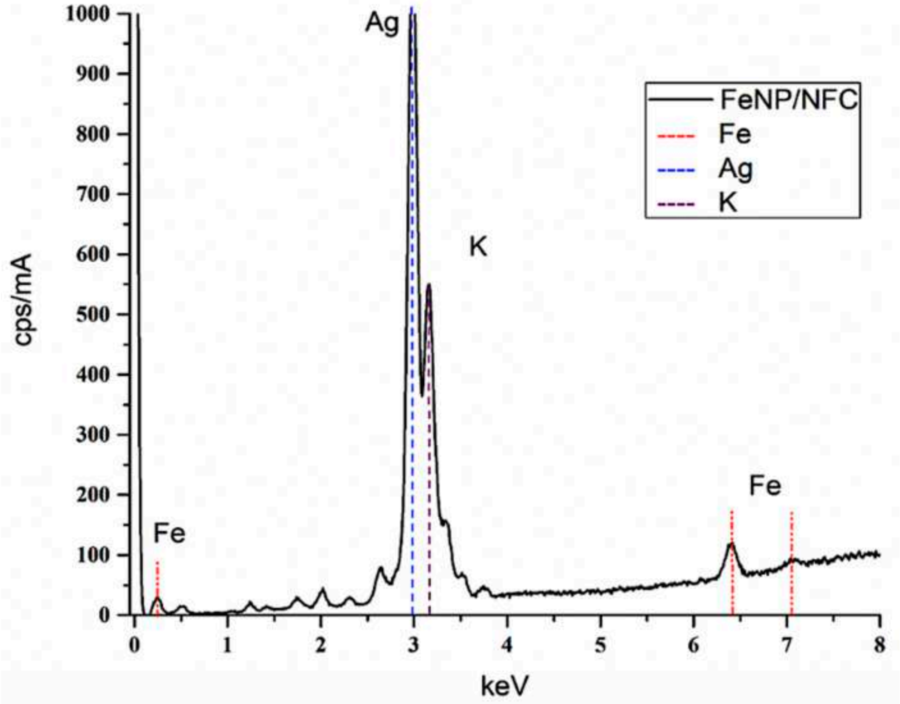

Figure 8. Energy Dispersive X-ray Fluorescence (EDXRF) spectrum of the FeNP/NFC composite.

Table 1. Composition of oxide groups in iron nanoparticles and cellulose nanofibers (FeNPs/NFCs).

Formula	
Concentration (%)	
Formula	**Concentration (%)**
MgO	13.55
SiO_2	20.65
P_2O_5	24.04
SO_3	3.68
Cl	5.26
Fe_2O_3	32.81

Generally, tropical woods contain inorganic salts of calcium, potassium, and magnesium [78,79]. Mineral transport into the plants can occur through natural routes from the soil, where minerals are in abundance. Silica, phosphorus, magnesium, and potassium components of biomass contribute to the plant´s rigidness, growth, and posture [78,80,81]. Sulfur oxide is attributed to cooking Kraft pulp in the composition of the reagents in the white liquor. Chlorine can be attributed to the reagent used ($FeCl_3$) in the nanoparticle synthesis process [82–84]. The inorganic substances found contributed to the various chemical reaction processes that took place during the synthesis of the composite, such as carboxymethylation, oxidation, hydrolysis, and sulfonation.

3.2. Adsorption Experiments

3.2.1. Kinetics

The adsorption kinetics results are shown in Figure 9. The adsorption kinetics of Pb(II) and Cd(II) ions in FeNP/NFC were significantly different. Cd's adsorption in the initial stage was very fast in the first 5 min, where 22% of the total cadmium elimination was obtained. Still, it gradually slowed down and finally reached equilibrium with a maximum efficiency of 32%. In the case of Pb, the adsorption capacity was slow in the first 5 min, rapidly increased between 5 and 20 min, and then slowed down—being more constant up to 75 min (with adsorption of 40%). This adsorption system had an efficiency above 58%. The equilibrium time was selected after 150 min for both cations, and it was ensured that the adsorption equilibrium was reached in later experiments.

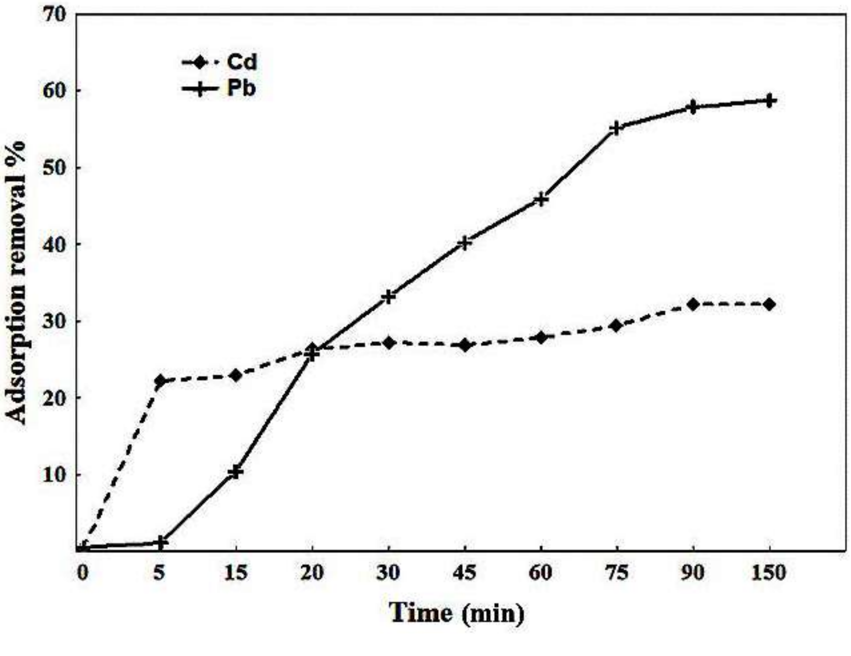

Figure 9. Cd and Pb adsorption onto FeNP/NFC composite as a function of time.

The adsorption phenomenon occurs at the surface, where the transport process and the diffusion of the adsorption are carried out between the film and the adsorbent. Moreover, the second phase is characterized by a slow adsorption rate due to the ions' slow diffusion and surface phenomena, which indicates the rate-limiting step and the type of adsorption governing the system. The effective adsorption area on the adsorbent's surface has many vacant bonding sites for the metal ions, and all resulted in easy adsorption. As adsorption proceeded, the concentration of metal ions and active sites decreased, resulting in a lower adsorption rate when the systems reached equilibrium.

The adsorption kinetic data were fitted to Pseudo-first-order, pseudo-second-order, and Elovich models. The correspondent parameters for each model are shown in Table 2. The high correlation coefficient values (R = 0.9858) obtained by the pseudo-first-order model for Pb adsorption indicates that sorption occurs exclusively at one site per ion and involves physisorption. This model suggests that the adsorption is superficial, and one solute molecule is adsorbed at one defined specific site. These sites were made up of the same type of functional groups. For both adsorption kinetics, the calculated values (qe_{calc}) and experimental values ($q_{e\ \mathrm{exp}}$) were similar. The theoretical or estimated values are considered the adsorption capacity calculated by kinetic modeling. Thus, $q_{e\ \mathrm{calc}}$ from the pseudo-first-order model resulted in 0.1348 mg/g for Cd and 0.3401 mg/g for Pb. Adsorption capacity experimental values ($q_{e\ \mathrm{exp}}$) were obtained from the experimental data graphs (Figure 9). Consequently, $q_{e\ \mathrm{exp}}$ for Cd sorption was 0.1513 mg/g and 0.3109 mg/g for Pb.

Table 2. Parameters of kinetic models for cadmium (Cd) and lead (Pb) adsorption onto FeNP/NFC.

Model	**Parameters**	**Metal Ions**	
		Cd	**Pb**
	$q_{e\ \mathrm{exp.}}$ [1] (mg/g)	0.1513	0.3109
Pseudo-first-order	K_L (1/min)	0.2445	0.0220
	$q_{e\ \mathrm{calc.}}$ (mg/g)	0.1348	0.3401
	R	0.9197	0.9858
Pseudo-second-order	K_2 (1/min)	0.4486	0.0170
	$q_{e\ \mathrm{calc.}}$ (mg/g)	0.2937	0.7781
	R	0.9611	0.9734
Elovich	a (1/min)	0.8112	0.00478
	b (mg/g)	59.077	2.4590
	R	0.9895	0.9204

[1] Obtained from experimental data.

The pseudo-first-order model can only be applied to describe the initial stage of adsorption. However, the pseudo-second-order model can predict the entire period of the adsorption behaviors. Therefore, the pseudo-second-order model can describe the adsorption behavior of the ions studied. In this model, the individual molecules join in two adsorption sites of the surface. They indicate that the sorption processes are entirely controlled by chemical processes and highlight their particularity in the electrical charge during equilibrium, such as the exchange of electrons or covalent forces.

According to the pseudo-second-order model constant (K_2), it can be observed that the adsorption rate is higher for Cd (K_2 = 0.4486 1/min) than for Pb (K_2 = 0.0170 1/min). This fact corroborates the differences found for both cations' adsorption kinetics, Cd, which implies a different equilibrium reaction for Cd compared to Pb. Cd's kinetic reaction rate indicates that it is only involved with the functional groups on the external surface. Pb's kinetics consist of multiple slow reactions between the outer surface and the material's internal pores. Additionally, the adsorption of Cd ions by the adsorbent was described with the Elovich equation (R = 0.9895). However, when the Elovich model fitted Pb data, low correlation coefficients were observed. This model indicates that the adsorbent's active sites are heterogeneous and exhibit different activation energies, based on a second-order reaction mechanism for a heterogeneous reaction process. Consequently, this model suggests that Cd removal occurs by a chemisorption process concerning the transfer or exchange of electrons, taking into account the metal's oxidation state and the possible formation of complexes involved in it [85].

3.2.2. Isotherms

Figure 10 shows the adsorption isotherms of Cd in FeNP/NFC at different temperatures. Considering the Langmuir, Freundlich, and Langmuir–Freundlich models presented, the three models had a good fit for the three different temperatures, with R values > 0.9700 (Table 3). However, in solid–liquid systems, many factors come into play, such as hydration forces, mass transfer, etc., which makes it more complicated to define equilibrium behavior in a sorption system, and obeying a single isotherm does not fully reflect the entire adsorption process. Moreover, the isotherm's suitability may be affected by experimental conditions, mainly the solute's concentration range. Both Langmuir and Freundlich isotherms may adequately describe the same set of liquid–solid adsorption data at specific concentration ranges. The Langmuir–Freundlich isotherm model gives information about the adsorption on homogeneous and heterogeneous surfaces with the possibility of multilayer adsorption.

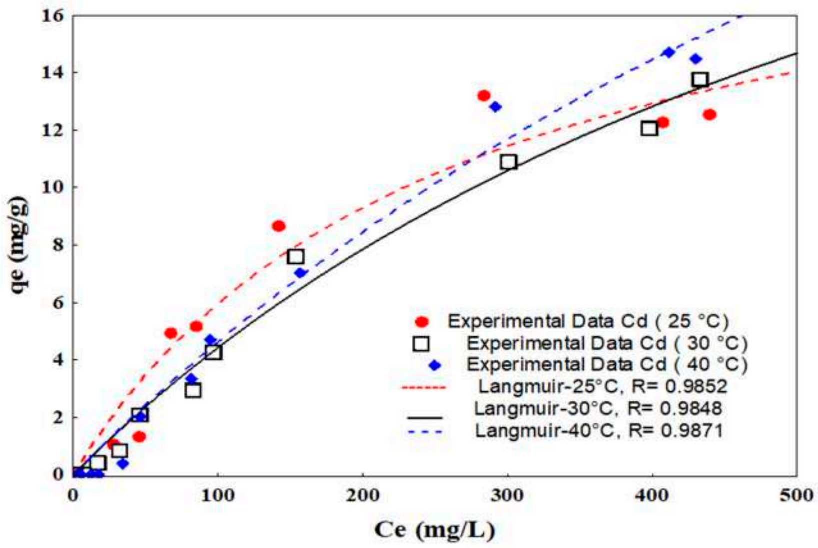

Figure 10. Cd adsorption isotherms onto FeNP/NFC composite at 25, 30, and 40 °C.

Table 3. Parameters of kinetic models for Cd and Pb adsorption onto FeNP/NFC.

Model	**Parameters**	**Metal Ions**					
		Cd			**Pb**		
		25 °C	**30 °C**	**40 °C**	**25 °C**	**30 °C**	**40 °C**
	$q_{e\text{ exp.}}$[1] (mg/g)	12.538	13.7377	14.4896	81.4064	89.2212	89.0882
Langmuir	$Q_{0\text{ calc.}}$ (mg/g)	21.233	34.999	49.697	467.307	956.02	357.549
	b	0.0040	0.0014	0.0010	0.0131	0.0084	0.0263
	R	0.9789	0.9929	0.9924	0.9149	0.7274	0.7294
Freundlich	K_F (mg/g) $(\text{L/mg})^{1/n}$	0.2601	0.0922	0.0775	4.1092	0.7209	1.4545
	n	1.5275	1.2117	1.1443	0.8916	0.4163	0.5055
	R	0.9617	0.9895	0.9891	0.9262	0.9180	0.8707
Langmuir–Freundlich	K_{LF} $(\text{mg/g})(\text{L/mg})^{1/\text{nLF}}$	0.8453	1.0635	0.2825	0.17961	0.3134	0.2995
	a_{LF} (mg/L)	1×10^{-4}	2×10^{-6}	3×10^{-6}	0.1394	0.1223	0.1511
	n_{LF}	0.4763	0.4052	0.6554	3.1486	3.0864	3.2310
	R	0.9234	0.8864	0.9731	0.9934	0.9390	0.9040

[1] Obtained from experimental data.

The Langmuir model was the one that best described all the isotherms of Cd at 25, 30, and 40 °C, with adsorption capacities of 21.233, 34.999, and 46.697 mg/g for each temperature, respectively. The Langmuir model was used to describe the monolayer adsorption at the adsorbent's surface, considering the similar types of vacancies and similar forces binding Cd molecules to the adsorbent's surface. The value of b in the Langmuir model suggests that the isotherm was favorable ($0 < b < 1$). In this context, the low b values reflect that adsorption is favorable: b > 1 is unfavorable, $b = 1$ is linear, $0 < b < 1$

is favorable or $b = 0$ is irreversible. In this case, the respective b values for each evaluated temperature indicate that the adsorption process was favorable [12,86]. The Langmuir equation is valid for monolayer sorption onto a completely homogeneous surface with a finite number of identical sites and little interaction between adsorbed molecules. This fact means that once a metal ion occupies a site, it cannot have another place for adsorption, so the adsorption behavior is gradually reflected in the different tested concentrations of Cd.

Lead (Pb) isotherm data were also fitted to the same models mentioned above. The results are shown in Figure 11. It was noticed that the Langmuir–Freundlich model best described such data at 25, 30, and 40 °C, according to their correlation coefficients (R), shown in Table 3. This model describes the equilibrium relationship between adsorbate binding and heterogeneous or homogeneous surfaces [72]. These surfaces have spaces with different forces, where the adsorbate molecules bind to the surface. The isotherm at high solute concentrations indicated a duality of both monolayer and multilayer adsorption [72]. This fact reinforces the idea that the governing mechanism is more complicated for Pb (II) than for the weak bond of Cd (II). As a result, a $Q_{0\ \mathrm{cal}}$ value of 467.307 mg/g was obtained for the Pb system at 25 °C, and the $Q_{0\ \mathrm{cal}}$ values at 30 and 40 °C were 956.02 and 357.549 mg/g, respectively, as shown in Table 3. Some discrepancies regarding Q_0 can be observed at 30 and 40 °C because of the relatively low R coefficients obtained in the Langmuir model's fittings in such cases. These results complement together with the Freundlich model, so the adsorption intensity (n) was always <1 for Pb adsorption cases (Table 3). These values ($0 < n < 1$) indicated favorable adsorption. These facts support that the lead adsorption was superficial and multilayered, considered as a heterogeneous adsorption type. Additionally, the adsorption mechanisms varied depending on the solution's concentrations. In this context, it is essential to emphasize that the FeNP/NFC composite can be considered highly efficient in removing Pb ions from aqueous solutions under these experimental conditions.

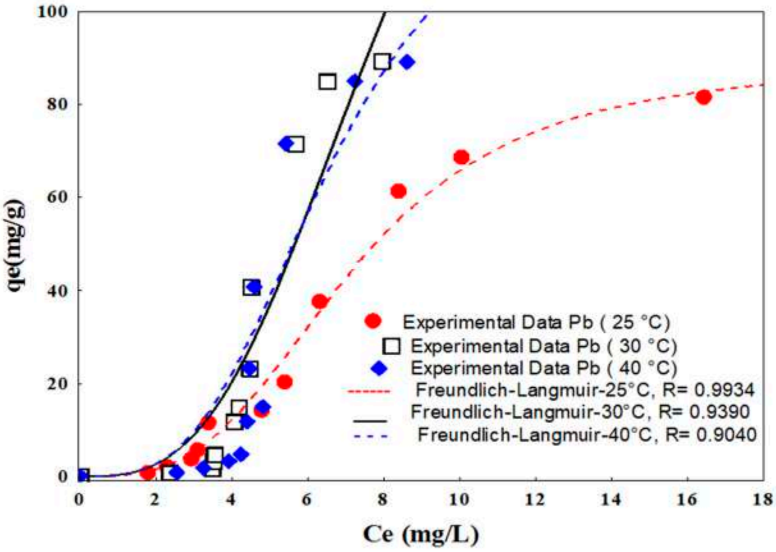

Figure 11. Pb adsorption isotherms onto FeNP/NFC composite at 25, 30, and 40 °C.

Polymers are heterogeneous materials containing sorption sites with various binding affinities and selectivities [45]. Hence, it can be suggested that the FeNP/NFC adsorbent has a heterogeneous surface, and Pb and Cd sorption onto this composite may present a multilayer behavior. The adsorption capacity of FeNP/NFC increased as the solute concentration rose until it reached the highest adsorption capacity. An increase in experimental adsorption capacity ($q_{e\ \mathrm{exp}}$) was observed in high-temperature conditions (Table 3) for both ions.

Previous studies indicated three explanations in the absorption behavior of specific metallic ions towards the adsorbent: radio, electronegativity, and charge [87]. It can be inferred from the results that the order of heavy metal ion removal efficiency under the experimental conditions was as follows: Pb(II) > Cd(II). The sizes of the ionic radius of the elements that are Pb (0.119 nm) > Cd (0.095 nm) should be taken into account. However, some studies conclude that the order of adsorption efficiency is due to the hydrated ionic radius of Pb (0.45 nm) < Cd (0.5 nm), highlighting a relatively smaller lead ion compared to cadmium. In aqueous solutions, ions form hydrate complexes with water, thus increasing the ionic size. Therefore, hydrated ions are transported to the surface of the material and diffuse into the pores [87–89].

The electronegativity is higher for lead ions (1.87–2.34) compared to cadmium (1.69). Phenomena, such as electrostatic interactions, covalent bonds, and ion exchange, could occur at the cellulose wall where cation bonding takes place. Adsorption or chelation involving hydroxyl functions, close to carboxylates or iron nanoparticles (-FeO, -FeOH), can increase the cation binding level [87].

The pH is an important parameter influencing the adsorption process at the water–sorbent interfaces. However, Pb and Cd's adsorption on this adsorbent is independent of the pH according to the zeta potential results of the material. As mentioned above, the solution's pH is reduced after the sorption process; this occurs because the deprotonation of the acidic functional groups of the adsorbent releases H_3O^+, allowing the metal cations to be adsorbed. The final pH value, obtained after the sorption experiments, was 3.6. Cd and Pb's removal by adsorption, reported in the literature, ranges from 3 to 8 for this type of sample [73,74]. Therefore, all further kinetic adsorption experiments were performed at a pH of 5.

Some polymers have shown that various surfaces are nonionogenic and acquire a negative charge in aqueous solutions. It has been shown that the electrokinetic charges of polymer surfaces become more negative as surface hydrophobicity increases. FeNP/NFC contains carboxyl (-COOH) and hydroxyl (-OH) functional groups as part of their polymer structures. Therefore, the negative electrokinetic charge acquired in the material can be explained by the dissociation of the mentioned functional groups [90]. The zeta potential was negative in all the pH values investigated; thus, this material can help remove Cd and Pb in some chemical species present in the solution. Both metals have the same charge (+2). It makes adsorption favorable in the system under study, though it depends on the chemical species present. Cadmium exists as a different form of Cd^{2+}, $Cd(OH)^+$, $Cd(OH)_2$, and $Cd(OH)_3{}^-$ at different pH values. At pH < 8.0, the predominant Cd species are Cd^{2+} [91]. Furthermore, Pb has a different form in aqueous solution at different pH values, such as Pb^{2+}, $Pb(OH)^+$, $Pb(OH)_2$, $Pb(OH)_3{}^-$, and $Pb(OH)_4{}^{2-}$. Pb^{2+} is the dominant species under acidic conditions because the Pb^{2+} and Cd^{2+} ions begin to hydrolyze and then form a minimal amount of other chemical species. Some of these species could be unfavorable for adsorption on negatively charged materials at pH < 3 in solution, so a value of 5 as the initial pH was selected for all adsorption experiments. The intense competition between hydronium ions and cations (Cd or Pb ions) decreases the metal ion interaction with the sorbent's binding sites by greater repulsive forces.

According to the Giles classification [92], sorption isotherms of Cd at 25, 30 and 40 °C can be included in S-type subgroup 2 (S-2). This fact indicates cooperative or complex adsorption with molecules that tend to be adsorbed in rows or groups. In celluloses, where free radical ions were involved in the adsorption, such as those present in this adsorbent, the solutes formed bonds with aromatic nuclei or their surroundings. Similarly, for the Pb isotherms at 25, 30, and 40 °C, the S-2 type can be described. The shapes of isotherms suggested one orientation of the adsorbed molecules stacked on the adsorbent's surface. The polymeric hydrocarbons in this material clearly cannot have simple surfaces because of their complex three-dimensional structures. Nevertheless, they produce S-curves. The cause is not, in this case, competition with water in the solvent, but it is possibly promoted by some form or interlocking of the adsorbed molecules [92,93]. Being classified in subgroup 2 indicates that monolayer capacity has reached its maximum. The plateau's height determines the surface cover for each solute molecule; additionally, electrostatic forces were involved in the adsorption. As seen in Figure 11, the length of the plateau showed an exposed surface, which easily attracted Cd and Pb ions. In nearly all cases, the isotherms have the S-shape. The adsorption sites appear to be isolated and negatively charged atoms.

A comparison of the maximum experimental adsorption capacities with similar adsorbents are shown in Table 4 for Cd and Pb. Differences in experimental conditions have been considered when comparing with other adsorbents. The advantage of using FeNP/NFC as an adsorbent is significant, and it can be observed that, compared with the other materials, it is highly efficient for removing Cd and, especially, Pb ions.

The adsorption capacities of synthesized nanocomposites in this study can be compared to other available adsorbents. Prasher et al. [94] indicated that the Pb(II) adsorption capacity obtained for the red algae biosorbent was superior compared to Cd(II) under similar experimental conditions. In some studies, this sorption behavior was also explained by the concepts of ionizing radio, electronegativity, and ion charge.

Table 4. Cd and Pb adsorption capacities of different adsorbents.

Adsorbent	**$q_{e\ exp.}$ (mg/g)**		**Temperature (°C)**	**pH**	**Adsorbent Mass (g)**	**Solution Volume (mL)**	**Reference**
	Cd	**Pb**					
FeNP/NFC	12.538 13.737 14.489	81.406 89.221 89.088	25 30 40	5 5 5	0.05 0.05 0.05	10 10 10	This study
Magnetic Bauhinia purpurea (Kaniar) powders	0.83 0.86 2.20	14.14 1.02 1.35	25 30 40	5	2	50	[4]
Biochar (waste agro-industry) FeSO4·7H2O	38.3 to 75.3	179-311	25	5	0.04	20	[95]
Banana peels	5.71	2.18	25	3	1.5	50	[96]
Polymer-modified magnetic nanoparticles	29.6	3.103	25	1 to 8	0.05	50	[97]
Chitosan/iron oxide nanocomposite	4.106	3.795	25	3	0.05	20,000	[98]
Sugar beet pulp	0.98	1.00	25	5	0.4	20	[99]
Sawdust (Fe3O_4/SC)	63 22 25	– – –	27	6.5	0.4 1.2 2	50	[100]
Fe3O4 nanoparticles onto cellulose acetate nanofibers	–	44	27	6	0.1	50	[101]

Biochar from agro-industrial wastes (nut shield, wheat straw, grape stalk, grape husk, and plum stone) was evaluated by Trakal et al. [95]. The results indicated that this material was strengthened after Fe oxide impregnation, increasing Cd and Pb sorption capacities. Such higher capacities were attributed to the surface complexation of metals with carboxyl and hydroxyl functional groups. In this case, Pb's adsorption capacity was higher than that of Cd, with different experimental conditions.

3.3. Thermodynamic Parameters

The analysis of these parameters allows the estimation of the feasibility of the adsorption process and the effect of temperature. The results of ΔH and ΔS were obtained from the slope and intercept of the graph lnK_c versus $1/T$ (Figure 12), using isotherm data. Parameters $\Delta G°$, $\Delta H°$, and $\Delta S°$ for the metal ions adsorption with FeNP/NFC are listed in Table 5.

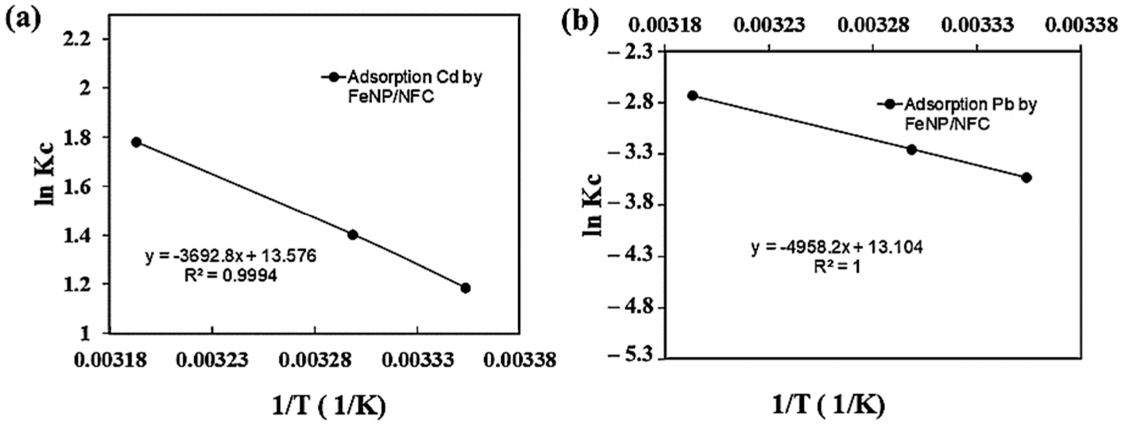

Figure 12. Van't Hoff's equation model for (**a**) Cd, and (**b**) Pb.

Table 5. Thermodynamic parameters for Pb and Cd adsorption on FeNP/NFC.

Metal Ions	**Δ*G*° (kJ/mol)**			**Δ*H*° (kJ/mol)**	**Δ*S*° (KJ/mol K)**
	25 °C	**30 °C**	**40 °C**		
Cd	−64.339	−64.904	−66.031	−30.701	0.1128
Pb	−73.704	−74.250	−75.339	−41.222	0.1089

The negative values of Δ*G* indicate a spontaneous reaction of the adsorption process for the FeNP/NFC. However, only a slight decrease in Pb and Cd maximum adsorption capacities was observed as temperature increased. Therefore, a large amount of heat was consumed for the Pb and Cd ions to transfer from water into the surface of FeNP/NFC [26]. The Δ*H*° results are negative for both cations, indicating that the adsorption process is exothermic; the values of $\Delta H° < 0$ and $\Delta S > 0$ imply that it is spontaneous at all temperatures. The positive value of Δ*S* suggests an increased disorder in the system during the process of adsorption. A redistribution of energy between the heavy metals and FeNP/NFC occurred, which suggests increasing randomness with structural or solvation changes occurring at the solid/liquid interface [4]. Acidic functional groups in the adsorbent, such as carboxylic and carboxylate, decreased. The solvent–sorbent interactions were similar; therefore, the change in entropy decreased [59].

3.4. Adsorption Mechanism

A possible mechanism of nanoparticle formation is illustrated in Figure 13. Ferric chloride hexahydrate hydrolyzes to form the ferric hydroxide, releasing H^+. The leaves extract partially reduces the ferric hydroxide to form NPs. Small Fe_2O_3 crystals were formed and placed at the coordination sites in a monodisperse form on the carrier. Physical or thermodynamic principles can also contribute to nanocrystals' self-assembly [3]. They can provide heterogeneous coordination or nucleation sites needed to form complexes with the ion. The aldehyde groups of the extract oxidize the cellulose material's corresponding structures [102,103]. The predominant flavonoids and polyphenols identified in the Moringa leaf extracts include rutin, kaempferol or isorhamnetin, isothiocyanates, chlorogenic acid, and quercetin-malonyl-glucoside. All these processes contribute to metal ion reduction [39,52]. The free radical scavenging activity of *Moringa oleifera* Lam leaf has been reported to be higher than synthetic antioxidant counterparts such as butylated hydroxytoluene (BHT), rutin, and ascorbic acid [51].

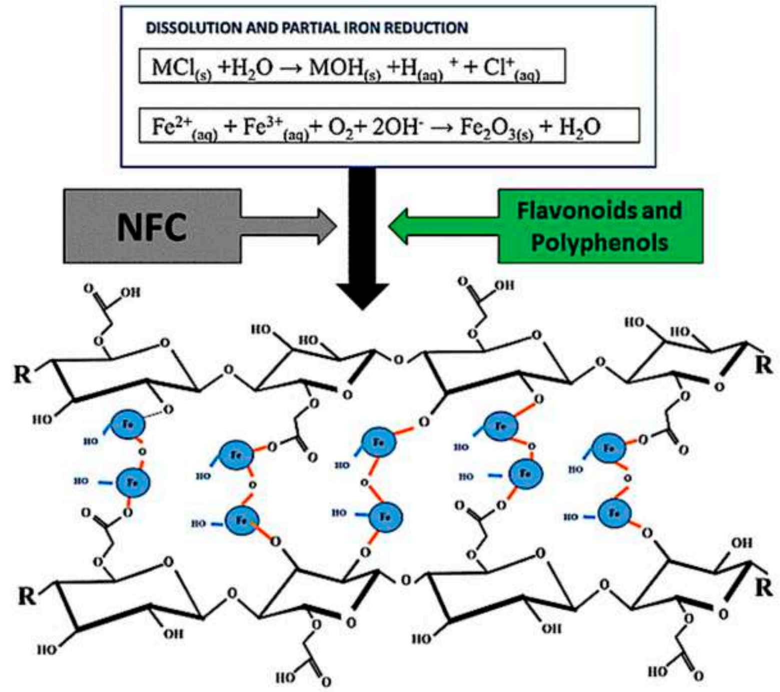

Figure 13. Schematic diagram of iron nanoparticle formation.

Cellulose nanofibers (NFCs) contain cellulose, simple sugars, and carbonaceous compounds that can bind to heavy metals. In nanoparticle synthesis, various compounds such as secondary metabolites and phytochemicals (phenolics, flavonoids, and fatty acids) have been introduced; these contribute to the metals' adsorptions. The significant importance of the polymeric matrix support and the nanoparticles' green synthesis processes can be attributed to carbonyl's complexation capacity with the metal ions. Therefore, it is observed that carbonyls are partially converted into carboxylic anions [97]. The FTIR confirmed this conversion in NFC and FeNP/NFC samples where functional groups such as carbonyl (-C=O), carboxylate (-COO), carboxyl (-COOH) in the range from 1000 to 1640 cm^{-1} are shown. These functional groups contribute to the adsorption mechanisms in the CdRM and PbRM samples of the FTIR spectra. They showed a significant reduction in the 1270, 1268, and 1610 cm^{-1} peaks of the carboxyl group (-COOH). Other groups also participated, such as the sulfonic group (-SO) with a band at 1059 cm^{-1}, iron hydroxide group (-FeOH) at 1023 cm^{-1}, and iron oxide group (-FeO) at 601 cm^{-1}.

The overall mechanism is a solid–liquid interfacial reaction, where Cd^{2+} and Pb^{2+} are represented as the metal ions (M^{2+}), Figure 14:

The mechanism for removing Pb^{2+} and Cd^{2+} ions was adsorption onto metallic oxides and nonmetallic sites through ion exchange, electrostatic bonds, and hydrogen bridge bonds. Some oxides (MgO, SiO_2, SO_3, Fe_2O_3) cause ligand chelation due to oxygen in the range from 4.5 to 5 pH used in these experiments (Figure 14b). The negative charge of the adsorbent, independently of the solution's pH, helps in the adsorption of these ions. These factors contribute to the formation of internal and external complexes by the various hydroxyl (-OH) groups present in the material, as shown in Figure 14c,d [56]. Electrostatic interactions would only occur with the weakest bound cations (Figure 14a). Hydroxyl (-OH) groups close to carboxyl (-COOH) groups would participate in the complexation of the highly bound cations and allow at least two functional carboxyl groups to contain a divalent cation.

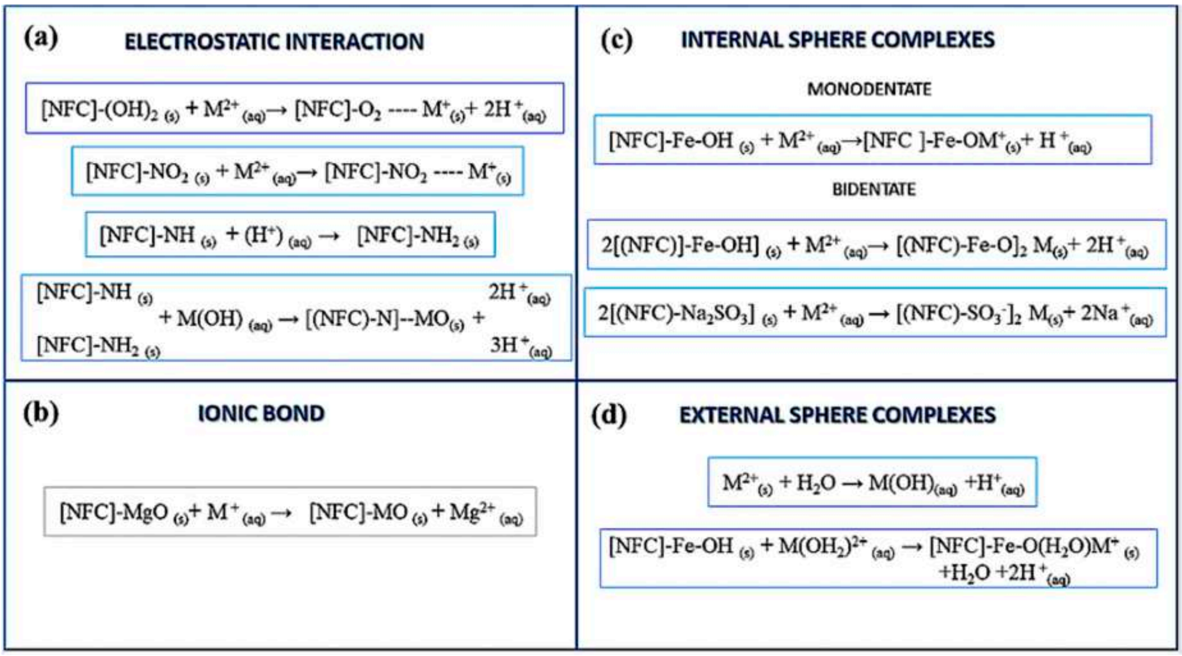

Figure 14. Metal ion (M^{2+}) adsorption mechanisms on composite adsorbent: (**a**) electrostatic interactions, (**b**) ionic bond formation, (**c**) internal sphere complexes formation, (**d**) external sphere complexes formation. [3,56,85,102,103].

The inner-sphere complex is formed by a covalent bond between the oxide's oxygen on the adsorbent's surface (-FeO) or the polymer's oxygen with the metal ion (M^{2+}). These possible mechanisms cause the loss of protons to the solutions, reducing the pH. Monodentate and bidentate complexes are formed depending on the presence of hydroxyl groups (Figure 15). The outer-sphere complex is formed when water is present between the adsorbed metal ion and the hydroxyl group on the iron (Fe-OH) surface. This complex can be distinguished because the bond is weaker than the inner-sphere complexes that form an electrostatic bond between the metal ions and the functional groups on the surface [3].

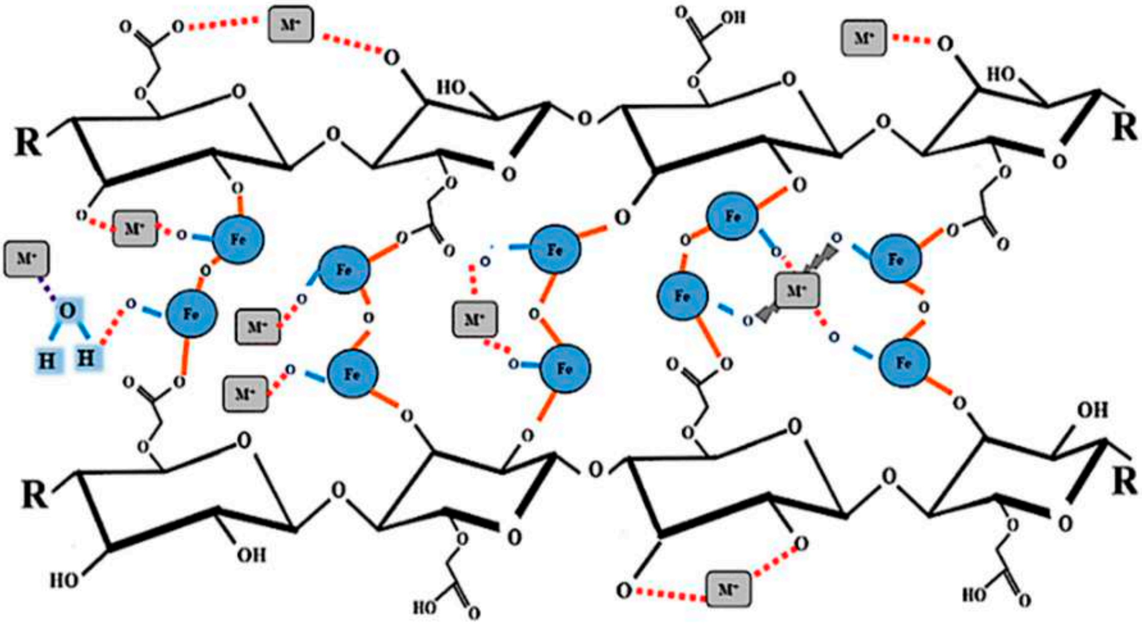

Figure 15. Scheme of adsorption mechanisms on FeNP/NFC.

The Kraft pulping and acid hydrolysis processes formed the anionic sulfonated cellulose derivatives, where the oxidation of the cellulose and sulfonation with the reagents used in these processes occurs. Material modifications, such as mercerization or sulfurization, increase the adsorption capacity of lignocellulosic materials. Sulfonated nanocelluloses have a large number of binding sites due to the different surfaces observed in the material. The participation in the adsorption of the sulfonic groups was important, as well as the carboxyl or hydroxyl groups. Sulfur forms complexes with ligands with a more covalent character instead of ionic, where metal ions (M^{2+}) bind with two oxygenates to form complexes, as illustrated in Figure 16a:

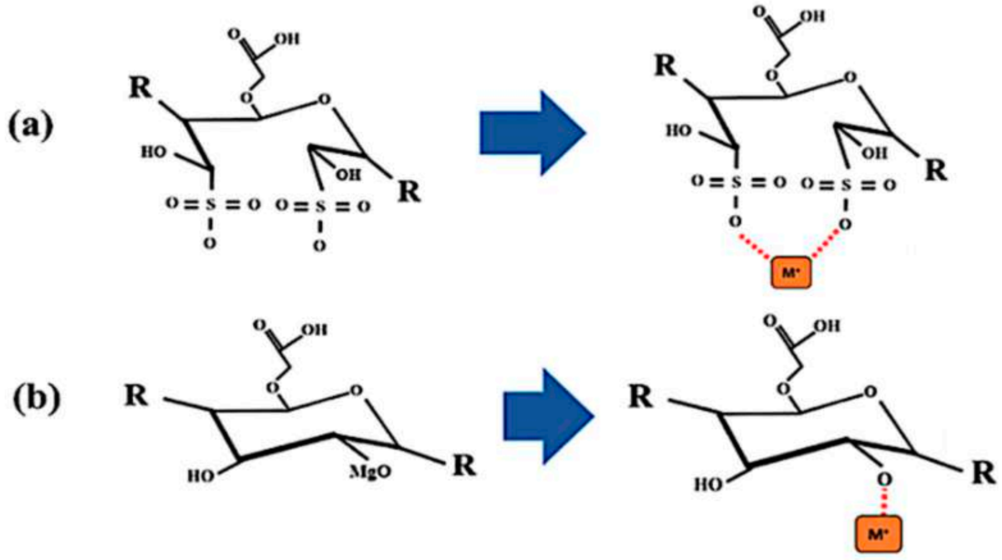

Figure 16. Adsorption mechanism on FeNP/NFC: (**a**) sulfur forms complexes and (**b**) ionic bonds.

The exchange of metal ions (M^2) with H^+ ions of hydroxyl groups on the surface occurs because the cations in the aqueous solutions are hydrated; therefore, they are attracted to the surface's functional group of interest. Mg^{2+} can participate in the adsorption. This result indicates that the magnesium ions, which were part of the MgO crystals in the FeNP/NFC composite, exchange with the M^{2+} during adsorption—Figure 16b [67]. As with many other adsorbent materials, there is the possibility that two or more mechanisms are involved in adsorption, as there are several active groups in FeNP/NFC.

The amino group on NFC, as mentioned above, influences the mechanism of lead removal. Metal ions can interact and bind with two binding sites on the surface [104]. There seems to be a significant impact on the ionization ability of –NH by pH, which affects the adsorption capacity of target ions. H^+ concentration is high in solution when pH is low; thus, –NH of material is protonated in this environment. This behavior will enhance the electrostatic attraction of anions, further increasing target ions' adsorption capacity [105].

4. Conclusions

Having Fe nanoparticles on the FeNP/NFC composite improved Cd and Pb selectivity during removal processes. The various chemical reaction processes (carboxymethylation, oxidation, hydrolysis, and sulfonation) occurred during the Kraft process, and acid hydrolysis increased the composite's heterogeneous surface. The chemical structure of the FeNP/NFC surface (adsorption sites and hydroxyl coordination) depends on the oxides' morphologies and the crystal structure. The high content of minerals or inorganic substances does not interfere with the adsorption process; otherwise, they helped to functionalize the material and diversify the adsorption mechanisms. Cd and Pb ions' speciation in an aqueous solution at pH 5 affects and determines the charge that will allow adsorption. As seen in the zeta potential results, the composite is negatively charged, so cations were easily adsorbed. Cd and Pb sorption mechanisms are related to electrostatic interactions, hydrogen bonding, and ion exchange with biopolymer structures. The strong electrostatic interactions between the -OH ions and the carboxyl groups were essential to form inner-sphere and outer-sphere complexes in the material. The thermodynamic results indicate that both processes have exothermic reactions which are irreversible and stable. The pseudo-first-order model describes Pb sorption kinetics well. Still, the Elovich equation was also a good model to describe Cd sorption kinetics. Based on the adsorption capacities obtained in this study, FeNP/NFC can be considered as a highly efficient adsorbent to remove these ions from aqueous solutions, particularly for Pb.

Author Contributions: Conceptualization, A.V.-G., R.C.-M., and R.H.-A.; methodology, A.V.-G. and R.C.-M.; software, A.V.-G.; validation, A.V.-G, R.A.-C.-V., and R.H.-A.; formal analysis, E.M.R.-M. and R.H.-A; investigation, A.V.-G. and E.M.R.-M.; resources, R.A.-C.-V., R.H.-A. and R.C.-M.; data curation, A.V.-G. and E.M.R.-M.; writing—original draft preparation, A.V.-G.; writing—review and editing, R.C.-M., R.H.-A., and R.A.-C.-V.; supervision, R.C.-M., R.H.-A., and R.A.-C.-V.; funding acquisition, R.A.-C.-V. All authors have read and agreed to the published version of the manuscript.

Funding: This research was funded by Coordinación de la Investigación Científica-UMSNH, grant number CIC-UMSNH-2020, and the APC was funded by PRODEP.

Institutional Review Board Statement: Not applicable.

Informed Consent Statement: Not applicable.

Acknowledgments: We appreciate the technical support provided by B. Millán-Malo from CFATA-UNAM.

Conflicts of Interest: The authors declare no conflict of interest. The funders had no role in the design of the study; in the collection, analyses, or interpretation of data; in the writing of the manuscript, or in the decision to publish the results.

References

1. Riani, E.; Cordova, M.R.; Arifin, Z. Heavy Metal Pollution and Its Relation to the Malformation of Green Mussels Cultured in Muara Kamal Waters, Jakarta Bay, Indonesia. *Mar. Pollut. Bull.* **2018**, *133*, 664–670. [CrossRef] [PubMed]
2. Fijałkowska, G.; Szewczuk-Karpisz, K.; Wiśniewska, M. Chromium(VI) and Lead(II) Accumulation at the Montmorillonite/Aqueous Solution Interface in the Presence of Polyacrylamide Containing Quaternary Amine Groups. *J. Mol. Liq.* **2019**, *293*, 111514. [CrossRef]
3. Kumari, M.; Pittman, C.U.; Mohan, D. Heavy Metals [Chromium (VI) and Lead (II)] Removal from Water Using Mesoporous Magnetite (Fe3O4) Nanospheres. *J. Colloid Interface Sci.* **2015**, *442*, 120–132. [CrossRef] [PubMed]
4. Sharma, R.; Sarswat, A.; Pittman, C.U.; Mohan, D. Cadmium and Lead Remediation Using Magnetic and Non-Magnetic Sustainable Biosorbents Derived from Bauhinia Purpurea Pods. *RSC Adv.* **2017**, *7*, 8606–8624. [CrossRef]
5. Koju, N.K.; Song, X.; Wang, Q.; Hu, Z.; Colombo, C. Cadmium Removal from Simulated Groundwater Using Alumina Nanoparticles: Behaviors and Mechanisms. *Environ. Pollut.* **2018**, *240*, 255–266. [CrossRef]
6. Chen, Z.; Zhang, J.; Huang, L.; Yuan, Z.; Li, Z.; Liu, M. Removal of Cd and Pb with Biochar Made from Dairy Manure at Low Temperature. *J. Integr. Agric.* **2019**, *18*, 201–210. [CrossRef]
7. Jaishankar, M.; Tseten, T.; Anbalagan, N.; Mathew, B.B.; Beeregowda, K.N. Toxicity, Mechanism and Health Effects of Some Heavy Metals. *Interdiscip. Toxicol.* **2014**, *7*, 60–72. [CrossRef]
8. Mohan, D.; Pittman, C.U.; Bricka, M.; Smith, F.; Yancey, B.; Mohammad, J.; Steele, P.H.; Alexandre-Franco, M.F.; Gómez-Serrano, V.; Gong, H. Sorption of Arsenic, Cadmium, and Lead by Chars Produced from Fast Pyrolysis of Wood and Bark during Bio-Oil Production. *J. Colloid Interface Sci.* **2007**, *310*, 57–73. [CrossRef]
9. Mager, E.M.; Brix, K.V.; Gerdes, R.M.; Ryan, A.C.; Grosell, M. Effects of Water Chemistry on the Chronic Toxicity of Lead to the Cladoceran, Ceriodaphnia Dubia. *Ecotoxicol. Environ. Saf.* **2011**, *74*, 238–243. [CrossRef]
10. Akinyeye, O.J.; Ibigbami, T.B.; Odeja, O.O.; Sosanolu, O.M. Evaluation of Kinetics and Equilibrium Studies of Biosorption Potentials of Bamboo Stem Biomass for Removal of Lead (II) and Cadmium (II) Ions from Aqueous Solution. *Afr. J. Pure Appl. Chem.* **2020**, *14*, 24–41. [CrossRef]
11. Isawi, H. Using Zeolite/Polyvinyl Alcohol/Sodium Alginate Nanocomposite Beads for Removal of Some Heavy Metals from Wastewater. *Arab. J. Chem.* **2020**, *13*, 5691–5716. [CrossRef]
12. Ahmad, R.; Mirza, A. Facile One Pot Green Synthesis of Chitosan-Iron Oxide (CS-Fe2O3) Nanocomposite: Removal of Pb(II) and Cd(II) from Synthetic and Industrial Wastewater. *J. Clean. Prod.* **2018**, *186*, 342–352. [CrossRef]
13. O'Connell, D.W.; Birkinshaw, C.; O'Dwyer, T.F. Heavy Metal Adsorbents Prepared from the Modification of Cellulose: A Review. *Bioresour. Technol.* **2008**, *99*, 6709–6724. [CrossRef] [PubMed]

14. Valdés Rodríguez, O.A.; Palacios Wassenaar, O.M.; Ruíz Hernández, R.; Pérez Vásquez, A. Moringa and Ricinus Association Potential in the Sub-Tropics of Veracruz. *Rev. Mex. Cienc. Agríc.* **2014**, *5*, 1673–1686.
15. Olson, M.E.; Fahey, J.W. Moringa oleifera: Un árbol multiusos para las zonas tropicales secas. *Rev. Mex. Biodivers.* **2011**, *82*, 1071–1082. [CrossRef]
16. Kargarzadeh, H.; Ahmad, I.; Abdullah, I.; Dufresne, A.; Zainudin, S.Y.; Sheltami, R.M. Effects of Hydrolysis Conditions on the Morphology, Crystallinity, and Thermal Stability of Cellulose Nanocrystals Extracted from Kenaf Bast Fibers. *Cellulose* **2012**, *19*, 855–866. [CrossRef]
17. Ramos-Vargas, S.; Huirache-Acuña, R.; Guadalupe Rutiaga-Quiñones, J.; Cortés-Martínez, R. Effective Lead Removal from Aqueous Solutions Using Cellulose Nanofibers Obtained from Water Hyacinth. *Water Supply* **2020**, *20*, 2715–2736. [CrossRef]
18. Mahfoudhi, N.; Boufi, S. Nanocellulose as a Novel Nanostructured Adsorbent for Environmental Remediation: A Review. *Cellulose* **2017**, *24*, 1171–1197. [CrossRef]
19. Rahmani, A.; Mousavi, H.Z.; Fazli, M. Effect of Nanostructure Alumina on Adsorption of Heavy Metals. *Desalination* **2010**, *253*, 94–100. [CrossRef]
20. Mondal, P.; Purkait, M.K. Green Synthesized Iron Nanoparticles Supported on PH Responsive Polymeric Membrane for Nitrobenzene Reduction and Fluoride Rejection Study: Optimization Approach. *J. Clean. Prod.* **2018**, *170*, 1111–1123. [CrossRef]
21. Bolade, O.P.; Williams, A.B.; Benson, N.U. Green Synthesis of Iron-Based Nanomaterials for Environmental Remediation: A Review. *Environ. Nanotechnol. Monit. Manag.* **2020**, *13*, 100279. [CrossRef]
22. Abujaber, F.; Zougagh, M.; Jodeh, S.; Ríos, Á.; Guzmán Bernardo, F.J.; Rodríguez Martín-Doimeadios, R.C. Magnetic Cellulose Nanoparticles Coated with Ionic Liquid as a New Material for the Simple and Fast Monitoring of Emerging Pollutants in Waters by Magnetic Solid Phase Extraction. *Microchem. J.* **2018**, *137*, 490–495. [CrossRef]
23. Krishna, R.; Dias, C.; Ventura, J.; Titus, E. Green and Facile Decoration of Fe3O4 Nanoparticles on Reduced Graphene Oxide. *Mater. Today Proc.* **2016**, *3*, 2807–2813. [CrossRef]
24. Ostovan, A.; Ghaedi, M.; Arabi, M. Fabrication of Water-Compatible Superparamagnetic Molecularly Imprinted Biopolymer for Clean Separation of Baclofen from Bio-Fluid Samples: A Mild and Green Approach. *Talanta* **2018**, *179*, 760–768. [CrossRef]
25. Soliemanzadeh, A.; Fekri, M. The Application of Green Tea Extract to Prepare Bentonite-Supported Nanoscale Zero-Valent Iron and Its Performance on Removal of Cr(VI): Effect of Relative Parameters and Soil Experiments. *Microporous Mesoporous Mater.* **2017**, *239*, 60–69. [CrossRef]
26. Wang, X.; Le, L.; Alvarez, P.J.J.; Li, F.; Liu, K. Synthesis and Characterization of Green Agents Coated Pd/Fe Bimetallic Nanoparticles. *J. Taiwan Inst. Chem. Eng.* **2015**, *50*, 297–305. [CrossRef]
27. Zhang, Y.; Chen, Y.; Westerhoff, P.; Hristovski, K.; Crittenden, J.C. Stability of Commercial Metal Oxide Nanoparticles in Water. *Water Res.* **2008**, *42*, 2204–2212. [CrossRef]
28. Liu, L.; Fan, S. Removal of Cadmium in Aqueous Solution Using Wheat Straw Biochar: Effect of Minerals and Mechanism. *Environ. Sci. Pollut. Res.* **2018**, *25*, 8688–8700. [CrossRef]
29. Bibi, I.; Nazar, N.; Ata, S.; Sultan, M.; Ali, A.; Abbas, A.; Jilani, K.; Kamal, S.; Sarim, F.M.; Khan, M.I.; et al. Green Synthesis of Iron Oxide Nanoparticles Using Pomegranate Seeds Extract and Photocatalytic Activity Evaluation for the Degradation of Textile Dye. *J. Mater. Res. Technol.* **2019**, *8*, 6115–6124. [CrossRef]
30. Bolade, O.P.; Akinsiku, A.A.; Adeyemi, A.O.; Williams, A.B.; Benson, N.U. Dataset on Phytochemical Screening, FTIR and GC–MS Characterisation of Azadirachta Indica and Cymbopogon Citratus as Reducing and Stabilising Agents for Nanoparticles Synthesis. *Data Brief* **2018**, *20*, 917–926. [CrossRef]
31. Akhtar, M.S.; Panwar, J.; Yun, Y.-S. Biogenic Synthesis of Metallic Nanoparticles by Plant Extracts. *ACS Sustain. Chem. Eng.* **2013**, *1*, 591–602. [CrossRef]
32. Kharissova, O.V.; Dias, H.V.R.; Kharisov, B.I.; Pérez, B.O.; Pérez, V.M.J. The Greener Synthesis of Nanoparticles. *Trends Biotechnol.* **2013**, *31*, 240–248. [CrossRef] [PubMed]
33. Nasrollahzadeh, M.; Mohammad Sajadi, S.; Rostami-Vartooni, A.; Khalaj, M. Green Synthesis of Pd/Fe3O4 Nanoparticles Using Euphorbia Condylocarpa M. Bieb Root Extract and Their Catalytic Applications as Magnetically Recoverable and Stable Recyclable Catalysts for the Phosphine-Free Sonogashira and Suzuki Coupling Reactions. *J. Mol. Catal. Chem.* **2015**, *396*, 31–39. [CrossRef]
34. Harshiny, M.; Iswarya, C.N.; Matheswaran, M. Biogenic Synthesis of Iron Nanoparticles Using Amaranthus Dubius Leaf Extract as a Reducing Agent. *Powder Technol.* **2015**, *286*, 744–749. [CrossRef]
35. Cai, Y.; Shen, Y.; Xie, A.; Li, S.; Wang, X. Green Synthesis of Soya Bean Sprouts-Mediated Superparamagnetic Fe3O4 Nanoparticles. *J. Magn. Magn. Mater.* **2010**, *322*, 2938–2943. [CrossRef]
36. Makarov, V.V.; Makarova, S.S.; Love, A.J.; Sinitsyna, O.V.; Dudnik, A.O.; Yaminsky, I.V.; Taliansky, M.E.; Kalinina, N.O. Biosynthesis of Stable Iron Oxide Nanoparticles in Aqueous Extracts of Hordeum Vulgare and Rumex Acetosa Plants. *Langmuir* **2014**, *30*, 5982–5988. [CrossRef]
37. Balamurugan, M.; Saravanan, S.; Soga, T. Synthesis of Iron Oxide Nanoparticles by Using *Eucalyptus Globulus* Plant Extract. *E-J. Surf. Sci. Nanotechnol.* **2014**, *12*, 363–367. [CrossRef]
38. Harshiny, M.; Matheswaran, M.; Arthanareeswaran, G.; Kumaran, S.; Rajasree, S. Enhancement of Antibacterial Properties of Silver Nanoparticles–Ceftriaxone Conjugate through Mukia Maderaspatana Leaf Extract Mediated Synthesis. *Ecotoxicol. Environ. Saf.* **2015**, *121*, 135–141. [CrossRef]

39. Ahmmad, B.; Leonard, K.; Shariful Islam, M.; Kurawaki, J.; Muruganandham, M.; Ohkubo, T.; Kuroda, Y. Green Synthesis of Mesoporous Hematite (α-Fe2O3) Nanoparticles and Their Photocatalytic Activity. *Adv. Powder Technol.* **2013**, *24*, 160–167. [CrossRef]
40. Wang, Z.; Fang, C.; Megharaj, M. Characterization of Iron–Polyphenol Nanoparticles Synthesized by Three Plant Extracts and Their Fenton Oxidation of Azo Dye. *ACS Sustain. Chem. Eng.* **2014**, *2*, 1022–1025. [CrossRef]
41. Li, J.; Hu, J.; Xiao, L.; Wang, Y.; Wang, X. Interaction Mechanisms between α-Fe2O3, γ-Fe2O3 and Fe3O4 Nanoparticles and Citrus Maxima Seedlings. *Sci. Total Environ.* **2018**, *625*, 677–685. [CrossRef] [PubMed]
42. Devatha, C.P.; K, J.; Patil, M. Effect of Green Synthesized Iron Nanoparticles by Azardirachta Indica in Different Proportions on Antibacterial Activity. *Environ. Nanotechnol. Monit. Manag.* **2018**, *9*, 85–94. [CrossRef]
43. Zhu, F.; Ma, S.; Liu, T.; Deng, X. Green Synthesis of Nano Zero-Valent Iron/Cu by Green Tea to Remove Hexavalent Chromium from Groundwater. *J. Clean. Prod.* **2018**, *174*, 184–190. [CrossRef]
44. Weng, X.; Guo, M.; Luo, F.; Chen, Z. One-Step Green Synthesis of Bimetallic Fe/Ni Nanoparticles by Eucalyptus Leaf Extract: Biomolecules Identification, Characterization and Catalytic Activity. *Chem. Eng. J.* **2017**, *308*, 904–911. [CrossRef]
45. Abdelghany, T.M.; Al-Rajhi, A.M.H.; Al Abboud, M.A.; Alawlaqi, M.M.; Ganash Magdah, A.; Helmy, E.A.M.; Mabrouk, A.S. Recent Advances in Green Synthesis of Silver Nanoparticles and Their Applications: About Future Directions. A Review. *BioNanoScience* **2018**, *8*, 5–16. [CrossRef]
46. Ahmed, S.; Ahmad, M.; Swami, B.L.; Ikram, S. A Review on Plants Extract Mediated Synthesis of Silver Nanoparticles for Antimicrobial Applications: A Green Expertise. *J. Adv. Res.* **2016**, *7*, 17–28. [CrossRef] [PubMed]
47. Iqbal, A.; Iqbal, K.; Li, B.; Gong, D.; Qin, W. Recent Advances in Iron Nanoparticles: Preparation, Properties, Biological and Environmental Application. *J. Nanosci. Nanotechnol.* **2017**, *17*, 4386–4409. [CrossRef]
48. Saif, S.; Tahir, A.; Chen, Y. Green Synthesis of Iron Nanoparticles and Their Environmental Applications and Implications. *Nanomaterials* **2016**, *6*, 209. [CrossRef]
49. Rauwel, P.; Küünal, S.; Ferdov, S.; Rauwel, E. A Review on the Green Synthesis of Silver Nanoparticles and Their Morphologies Studied via TEM. Available online: https://www.hindawi.com/journals/amse/2015/682749/ (accessed on 4 October 2020).
50. Sharma, J.K.; Srivastava, P.; Akhtar, M.S.; Singh, G.; Ameen, S. α-Fe2O3 Hexagonal Cones Synthesized from the Leaf Extract of Azadirachta Indica and Its Thermal Catalytic Activity. *New J. Chem.* **2015**, *39*, 7105–7111. [CrossRef]
51. Falowo, A.B.; Mukumbo, F.E.; Idamokoro, E.M.; Lorenzo, J.M.; Afolayan, A.J.; Muchenje, V. Multi-Functional Application of Moringa Oleifera Lam. in Nutrition and Animal Food Products: A Review. *Food Res. Int.* **2018**, *106*, 317–334. [CrossRef]
52. Waterman, C.; Cheng, D.M.; Rojas-Silva, P.; Poulev, A.; Dreifus, J.; Lila, M.A.; Raskin, I. Stable, Water Extractable Isothiocyanates from Moringa Oleifera Leaves Attenuate Inflammation in Vitro. *Phytochemistry* **2014**, *103*, 114–122. [CrossRef] [PubMed]
53. Lagergren, S. Zur theorie der sogenannten adsorption geloster stoffe. Kungliga Svenska Vetenskapsakademiens. *Handlingar* **1898**, *24*, 1–39.
54. Ho, Y.S.; McKay, G.; Wase, D.A.J.; Forster, C.F. Study of the Sorption of Divalent Metal Ions on to Peat. *Adsorpt. Sci. Technol.* **2000**, *18*, 639–650. [CrossRef]
55. Low, M.J.D. Kinetics of Chemisorption of Gases on Solids. Available online: https://pubs.acs.org/doi/pdf/10.1021/cr60205a003 (accessed on 3 October 2020).
56. Chen, K.; He, J.; Li, Y.; Cai, X.; Zhang, K.; Liu, T.; Hu, Y.; Lin, D.; Kong, L.; Liu, J. Removal of Cadmium and Lead Ions from Water by Sulfonated Magnetic Nanoparticle Adsorbents. *J. Colloid Interface Sci.* **2017**, *494*, 307–316. [CrossRef] [PubMed]
57. Langmuir, I. The Adsorption of Gases on Plane Surfaces of Glass, Mica and Platinum. *J. Am. Chem. Soc.* **1918**, *40*, 1361–1403. [CrossRef]
58. Papageorgiou, S.K.; Kouvelos, E.P.; Katsaros, F.K. Calcium Alginate Beads from Laminaria Digitata for the Removal of Cu^{+2} and Cd^{+2} from Dilute Aqueous Metal Solutions. *Desalination* **2008**, *224*, 293–306. [CrossRef]
59. Acemioğlu, B. Removal of Fe(II) Ions from Aqueous Solution by Calabrian Pine Bark Wastes. *Bioresour. Technol.* **2004**, *93*, 99–102. [CrossRef]
60. Sivarathnakumar, S.; Baskar, G.; Kumar, R.P.; Bharathiraja, B. Bioethanol Production by the Utilisation of Moringa Oleifera Stem with Sono-Assisted Acid/Alkali Hydrolysis Approach. *Int. J. Environ. Sustain. Dev.* **2016**, *15*, 392–403. [CrossRef]
61. Zhao, H.; Kwak, J.H.; Conrad Zhang, Z.; Brown, H.M.; Arey, B.W.; Holladay, J.E. Studying Cellulose Fiber Structure by SEM, XRD, NMR and Acid Hydrolysis. *Carbohydr. Polym.* **2007**, *68*, 235–241. [CrossRef]
62. Lavoine, N.; Desloges, I.; Dufresne, A.; Bras, J. Microfibrillated Cellulose—Its Barrier Properties and Applications in Cellulosic Materials: A Review. *Carbohydr. Polym.* **2012**, *90*, 735–764. [CrossRef]
63. Kumar, A.; Negi, Y.S.; Choudhary, V.; Bhardwaj, N.K. Characterization of Cellulose Nanocrystals Produced by Acid-Hydrolysis from Sugarcane Bagasse as Agro-Waste. *J. Mater. Phys. Chem.* **2014**, *2*, 1–8. [CrossRef]
64. Zhao, Y.; Xu, C.; Xing, C.; Shi, X.; Matuana, L.M.; Zhou, H.; Ma, X. Fabrication and Characteristics of Cellulose Nanofibril Films from Coconut Palm Petiole Prepared by Different Mechanical Processing. *Ind. Crops Prod.* **2015**, *65*, 96–101. [CrossRef]
65. Abdul Khalil, H.P.S.; Davoudpour, Y.; Islam, M.N.; Mustapha, A.; Sudesh, K.; Dungani, R.; Jawaid, M. Production and Modification of Nanofibrillated Cellulose Using Various Mechanical Processes: A Review. *Carbohydr. Polym.* **2014**, *99*, 649–665. [CrossRef] [PubMed]

66. Tonoli, G.H.D.; Teixeira, E.M.; Corrêa, A.C.; Marconcini, J.M.; Caixeta, L.A.; Pereira-da-Silva, M.A.; Mattoso, L.H.C. Cellulose Micro/Nanofibres from Eucalyptus Kraft Pulp: Preparation and Properties. *Carbohydr. Polym.* **2012**, *89*, 80–88. [CrossRef] [PubMed]
67. Kalia, S.; Dufresne, A.; Cherian, B.M.; Kaith, B.S.; Avérous, L.; Njuguna, J.; Nassiopoulos, E. Cellulose-Based Bio- and Nanocomposites: A Review. Available online: https://www.hindawi.com/journals/ijps/2011/837875/ (accessed on 27 December 2020).
68. Dong, H.; Snyder, J.F.; Tran, D.T.; Leadore, J.L. Hydrogel, Aerogel and Film of Cellulose Nanofibrils Functionalized with Silver Nanoparticles. *Carbohydr. Polym.* **2013**, *95*, 760–767. [CrossRef]
69. Sahu, U.K.; Mahapatra, S.S.; Patel, R.K. Synthesis and Characterization of an Eco-Friendly Composite of Jute Fiber and Fe_2O_3 Nanoparticles and Its Application as an Adsorbent for Removal of As(V) from Water. *J. Mol. Liq.* **2017**, *237*, 313–321. [CrossRef]
70. Nagappan, S.; Ha, H.M.; Park, S.S.; Jo, N.-J.; Ha, C.-S. One-Pot Synthesis of Multi-Functional Magnetite–Polysilsesquioxane Hybrid Nanoparticles for the Selective Fe^{3+} and Some Heavy Metal Ions Adsorption. *RSC Adv.* **2017**, *7*, 19106–19116. [CrossRef]
71. Cao, C.-Y.; Qu, J.; Wei, F.; Liu, H.; Song, W.-G. Superb Adsorption Capacity and Mechanism of Flowerlike Magnesium Oxide Nanostructures for Lead and Cadmium Ions. *ACS Appl. Mater. Interfaces* **2012**, *4*, 4283–4287. [CrossRef]
72. Xu, Q.; Jiang, L. Infrared Spectra of the M(NO)n (M = Sn, Pb; n = 1, 2) and PbNO- Molecules. *Inorg. Chem.* **2006**, *45*, 8648–8654. [CrossRef]
73. Qin, X.; Zhou, J.; Huang, A.; Guan, J.; Zhang, Q.; Huang, Z.; Hu, H.; Zhang, Y.; Yang, M.; Wu, J.; et al. A Green Technology for the Synthesis of Cellulose Succinate for Efficient Adsorption of Cd(II) and Pb(II) Ions. *RSC Adv.* **2016**, *6*, 26817–26825. [CrossRef]
74. Asmaly, H.A.; Abussaud, B.; Ihsanullah; Saleh, T.A.; Bukhari, A.A.; Laoui, T.; Shemsi, A.M.; Gupta, V.K.; Atieh, M.A. Evaluation of Micro- and Nano-Carbon-Based Adsorbents for the Removal of Phenol from Aqueous Solutions. *Toxicol. Environ. Chem.* **2015**, *97*, 1164–1179. [CrossRef]
75. Taipale, T.; Österberg, M.; Nykänen, A.; Ruokolainen, J.; Laine, J. Effect of Microfibrillated Cellulose and Fines on the Drainage of Kraft Pulp Suspension and Paper Strength. *Cellulose* **2010**, *17*, 1005–1020. [CrossRef]
76. Capron, I.; Rojas, O.J.; Bordes, R. Behavior of Nanocelluloses at Interfaces. *Curr. Opin. Colloid Interface Sci.* **2017**, *29*, 83–95. [CrossRef]
77. Visakh, P.M.; Mathew, A.P.; Oksman, K.; Thomas, S. Starch-Based Bionanocomposites: Processing and Properties. In *Polysaccharide Building Blocks*; John Wiley & Sons, Ltd.: Hoboken, NJ, USA, 2012; pp. 287–306. ISBN 978-1-118-22948-4.
78. Fengel, D.; Wegener, G. *Wood: Chemistry, Ultrastructure, Reactions*; Walter de Gruyter: Berlin, Germany, 2011; ISBN 978-3-11-083965-4.
79. Martínez-Pérez, R.; Pedraza-Bucio, F.E.; Orihuela-Equihua, R.; López-Albarrán, P.; Rutiaga-Quiñones, J.G. Calorific Value and Inorganic Material of Ten Mexican Wood Species. *Wood Res.* **2015**, *60*, 12.
80. Argyropoulos, D.S. Wood and Cellulosic Chemistry. Second Edition, Revised and Expanded Edited by David N.-S. Hon (Clemson University) and Nubuo Shiraishi (Kyoto University). Marcel Dekker: New York and Basel. 2001. Vii + 914 Pp. $250.00. ISBN 0-8247-0024-4. *J. Am. Chem. Soc.* **2001**, *123*, 8880–8881. [CrossRef]
81. Ngangyo-Heya, M.; Foroughbahchk-Pournavab, R.; Carrillo-Parra, A.; Rutiaga-Quiñones, J.G.; Zelinski, V.; Pintor-Ibarra, L.F. Calorific Value and Chemical Composition of Five Semi-Arid Mexican Tree Species. *Forests* **2016**, *7*, 58. [CrossRef]
82. Muthukumar, H.; Matheswaran, M. Amaranthus Spinosus Leaf Extract Mediated FeO Nanoparticles: Physicochemical Traits, Photocatalytic and Antioxidant Activity. *ACS Sustain. Chem. Eng.* **2015**, *3*, 3149–3156. [CrossRef]
83. Zhu, X.; Song, T.; Lv, Z.; Ji, G. High-Efficiency and Low-Cost α-Fe2O3 Nanoparticles-Coated Volcanic Rock for Cd(II) Removal from Wastewater. *Process Saf. Environ. Prot.* **2016**, *104*, 373–381. [CrossRef]
84. Tajik, E.; Naeimi, A.; Amiri, A. Fabrication of Iron Oxide Nanoparticles, and Green Catalytic Application of an Immobilized Novel Iron Schiff on Wood Cellulose. *Cellulose* **2018**, *25*, 915–923. [CrossRef]
85. Gupta, V.K.; Nayak, A. Cadmium Removal and Recovery from Aqueous Solutions by Novel Adsorbents Prepared from Orange Peel and Fe2O3 Nanoparticles. *Chem. Eng. J.* **2012**, *180*, 81–90. [CrossRef]
86. Foo, K.Y.; Hameed, B.H. Insights into the Modeling of Adsorption Isotherm Systems. *Chem. Eng. J.* **2010**, *156*, 2–10. [CrossRef]
87. Papageorgiou, S.K.; Katsaros, F.K.; Kouvelos, E.P.; Nolan, J.W.; Le Deit, H.; Kanellopoulos, N.K. Heavy Metal Sorption by Calcium Alginate Beads from Laminaria Digitata. *J. Hazard. Mater.* **2006**, *137*, 1765–1772. [CrossRef] [PubMed]
88. Wang, F.; Lu, X.; Li, X. Selective Removals of Heavy Metals (Pb2+, Cu2+, and Cd2+) from Wastewater by Gelation with Alginate for Effective Metal Recovery. *J. Hazard. Mater.* **2016**, *308*, 75–83. [CrossRef] [PubMed]
89. Pawar, R.R.; Lalhmunsiama; Kim, M.; Kim, J.-G.; Hong, S.-M.; Sawant, S.Y.; Lee, S.M. Efficient Removal of Hazardous Lead, Cadmium, and Arsenic from Aqueous Environment by Iron Oxide Modified Clay-Activated Carbon Composite Beads. *Appl. Clay Sci.* **2018**, *162*, 339–350. [CrossRef]
90. Elimelech, M.; Chen, W.H.; Waypa, J.J. Measuring the Zeta (Electrokinetic) Potential of Reverse Osmosis Membranes by a Streaming Potential Analyzer. *Desalination* **1994**, *95*, 269–286. [CrossRef]
91. Zirino, A.; Yamamoto, S. A pH-Dependent Model for The Chemical Speciation of Copper, Zinc, Cadmium, and Lead in Seawater. *Limnol. Oceanogr.* **1972**, *17*, 661–671. [CrossRef]
92. Giles, C.H.; D'Silva, A.P.; Easton, I.A. A General Treatment and Classification of the Solute Adsorption Isotherm Part. II. Experimental Interpretation. *J. Colloid Interface Sci.* **1974**, *47*, 766–778. [CrossRef]
93. Giles, C.H.; Smith, D.; Huitson, A. A General Treatment and Classification of the Solute Adsorption Isotherm. I. Theoretical. *J. Colloid Interface Sci.* **1974**, *47*, 755–765. [CrossRef]

94. Prasher, S.O.; Beaugeard, M.; Hawari, J.; Bera, P.; Patel, R.M.; Kim, S.H. Biosorption of Heavy Metals by Red Algae (Palmaria Palmata). *Environ. Technol.* **2004**, *25*, 1097–1106. [CrossRef]
95. Trakal, L.; Veselská, V.; Šafařík, I.; Vítková, M.; Číhalová, S.; Komárek, M. Lead and Cadmium Sorption Mechanisms on Magnetically Modified Biochars. *Bioresour. Technol.* **2016**, *203*, 318–324. [CrossRef]
96. Anwar, J.; Shafique, U.; Waheed-uz-Zaman; Salman, M.; Dar, A.; Anwar, S. Removal of Pb(II) and Cd(II) from Water by Adsorption on Peels of Banana. *Bioresour. Technol.* **2010**, *101*, 1752–1755. [CrossRef] [PubMed]
97. Ge, F.; Li, M.-M.; Ye, H.; Zhao, B.-X. Effective Removal of Heavy Metal Ions Cd2+, Zn2+, Pb2+, Cu2+ from Aqueous Solution by Polymer-Modified Magnetic Nanoparticles. *J. Hazard. Mater.* **2012**, *211–212*, 366–372. [CrossRef] [PubMed]
98. Keshvardoostchokami, M.; Babaei, L.; Zamani, A.A.; Parizanganeh, A.H.; Piri, F. Synthesized chitosan/iron oxide nanocomposite and shrimp shell in removal of nickel, cadmium and lead from aqueous solution. *Global J. Environ. Sci. Manag.* **2017**, *3*, 267–278.
99. Pehlivan, E.; Yanık, B.H.; Ahmetli, G.; Pehlivan, M. Equilibrium Isotherm Studies for the Uptake of Cadmium and Lead Ions onto Sugar Beet Pulp. *Bioresour. Technol.* **2008**, *99*, 3520–3527. [CrossRef] [PubMed]
100. Kataria, N.; Garg, V.K. Green Synthesis of Fe3O4 Nanoparticles Loaded Sawdust Carbon for Cadmium (II) Removal from Water: Regeneration and Mechanism. *Chemosphere* **2018**, *208*, 818–828. [CrossRef]
101. Shalaby, T.I.; El-Kady, M.F.; Zaki, A.E.H.M.; El-Kholy, S.M. Preparation and Application of Magnetite Nanoparticles Immobilized on Cellulose Acetate Nanofibers for Lead Removal from Polluted Water. *Water Supply* **2017**, *17*, 176–187. [CrossRef]
102. Mahdavi, M.; Namvar, F.; Ahmad, M.B.; Mohamad, R. Green Biosynthesis and Characterization of Magnetic Iron Oxide (Fe3O4) Nanoparticles Using Seaweed (Sargassum Muticum) Aqueous Extract. *Molecules* **2013**, *18*, 5954–5964. [CrossRef]
103. Gao, S.; Shi, Y.; Zhang, S.; Jiang, K.; Yang, S.; Li, Z.; Takayama-Muromachi, E. Biopolymer-Assisted Green Synthesis of Iron Oxide Nanoparticles and Their Magnetic Properties. *J. Phys. Chem. C* **2008**, *112*, 10398–10401. [CrossRef]
104. Hokkanen, S.; Repo, E.; Suopajärvi, T.; Liimatainen, H.; Niinimaa, J.; Sillanpää, M. Adsorption of Ni(II), Cu(II) and Cd(II) from Aqueous Solutions by Amino Modified Nanostructured Microfibrillated Cellulose. *Cellulose* **2014**, *21*, 1471–1487. [CrossRef]
105. Zhao, T.; Feng, T. Application of Modified Chitosan Microspheres for Nitrate and Phosphate Adsorption from Aqueous Solution. *RSC Adv.* **2016**, *6*, 90878–90886. [CrossRef]

water

Article

Removal of Pb^{2+} from Aqueous Solutions Using K-Type Zeolite Synthesized from Coal Fly Ash

Yuhei Kobayashi [1], Fumihiko Ogata [1], Chalermpong Saenjum [2,3], Takehiro Nakamura [1] and Naohito Kawasaki [1,4,*]

[1] Faculty of Pharmacy, Kindai University, 3-4-1 Kowakae, Higashi-Osaka, Osaka 577-8502, Japan; 1944420001t@kindai.ac.jp (Y.K.); ogata@phar.kindai.ac.jp (F.O.); nakamura@phar.kindai.ac.jp (T.N.)

[2] Faculty of Pharmacy, Chiang Mai University, Suthep Road, Muang District, Chiang Mai 50200, Thailand; chalermpong.saenjum@gmail.com

[3] Cluster of Excellence on Biodiversity-Based Economics and Society (B.BES-CMU), Chiang Mai University, Suthep Road, Muang District, Chiang Mai 50200, Thailand

[4] Antiaging Center, Kindai University, 3-4-1 Kowakae, Higashi-Osaka, Osaka 577-8502, Japan

[*] Correspondence: kawasaki@phar.kindai.ac.jp; Tel.: +81-6-4307-4012

Received: 29 July 2020; Accepted: 22 August 2020; Published: 24 August 2020

Abstract: In this study, a novel zeolite (K-type zeolite) was synthesized from coal fly ash (FA), and adsorption capacity on Pb^{2+} was assessed. Six types of zeolite (FA1, FA3, FA6, FA12, FA24, and FA48) were prepared, and their physicochemical properties, such as surface functional groups, cation exchange capacity, pH_{pzc}, specific surface area, and pore volume, were evaluated. The quantity of Pb^{2+} adsorbed by the prepared zeolites followed the order FA < FA1 < FA3 < FA6 < FA12 < FA24 < FA48. Current results indicate that the level of Pb^{2+} adsorbed was strongly related to the surface characteristics of the adsorbent. Additionally, the correlation coefficient between the amounts of Pb^{2+} adsorbed and K^+ released from FA48 was 0.958. Thus, ion exchange with K^+ in the interlayer of FA48 is critical for the removal of Pb^{2+} from aqueous media. The new binding energies of Pb(4f) at 135 and 140 eV were detected after adsorption. Moreover, FA48 showed selectivity for Pb^{2+} adsorption in binary solution systems containing cations. The results revealed that FA48 could be useful for removing Pb^{2+} from aqueous media.

Keywords: K-type zeolite; fly ash; lead; adsorption

1. Introduction

In recent years, issues faced by the aquatic environment, such as water wastage (Goal 6) and the presence of plastic bags in the ocean (Goal 14), have become major concerns for sustainable societal development [1]. Several heavy metals have been contaminating the aquatic environment through human activities, which are non-biodegradable and accumulate in the ecosystem via the food chain, causing various health problems and diseases [2]. Among these heavy metals, lead (Pb^{2+}), mercury (Hg^{2+}), and cadmium (Cd^{2+}) have been defined as the "big three" harmful heavy metals posing the greatest threat to humans, animals, and the environment [3,4]. Numerous studies have previously identified a relationship between Pb^{2+} exposure and human health impacts, such as neurotoxicity, cardiovascular problems, kidney damage, hormonal imbalances, and decreased musculoskeletal function [5,6]. Pb^{2+} has been classified by the International Agency for Research on Cancer as Group 2B which is possibly carcinogenic to humans. Additionally, drinking water problems involving Pb^{2+} have occurred in several countries [7–10]. Therefore, the World Health Organization and U.S. Environmental Protection Agency have established maximum permissible Pb^{2+} contents for drinking water of 0.01 and 0.015 mg L^{-1}, respectively. Thus, the removal of Pb^{2+} from aqueous media is an important global issue.

In Japan, the demand for coal-fired power plants increased after the Fukushima Daiichi Nuclear Power Station accident in 2001. Coal fly ash, a byproduct of coal combustion, is produced from coal-fired power plants (approximately 11.5 million tons in Japan in 2017) [11]. Approximately 750 million tons of coal fly ash are produced globally, and only 25% of this ash is recycled in cement, concrete, soil conditioner, and fertilizer materials [12–14]. Therefore, a recycling technology for coal fly ash must be developed to utilize its unused value [14]. SiO_2, Al_2O_3, and Fe_2O_3 were identified as the major chemical components of coal fly ash. Various studies have previously reported the adsorption capability of heavy metals using coal fly ash; however, they suggested a lower adsorption capacity than that of conventional adsorbents [15,16].

Different activation methods have been modified and developed to improve the adsorption capacity of coal fly ash [17]. Such methods include the conversion of coal fly ash to zeolite named hydrothermal activation, which is useful for decreasing the amount of coal fly ash and preparing an adsorbent with a high adsorption capacity for heavy metals. Zeolite is a general term for crystalline hydrous aluminosilicate, which consists of a three-dimensional network structure of SiO_4–AlO_4 tetrahedrons with Si and Al as basic constituents. Their structures contain channels and cavities of different sizes with unique physicochemical properties, such as their adsorption, ion exchange, molecular sieving, and catalytic abilities [18–21]. Additionally, the physicochemical properties of zeolite prepared from coal fly ash following the activation using hydrothermal technique are directly affected by certain parameters, such as the coal fly ash composition, alkaline solution concentration, reaction temperature, time, and pressure, volume ratio of the alkaline solution, and amount of coal fly ash [14,22–24]. Therefore, suitable conditions for preparing zeolite from coal fly ash generated by coal-fired power plants in Japan must be identified. Our previous studies elucidated the composition of coal fly ash generated from the Tachibana-Wan Thermal Power Station in Japan [25]. Moreover, Na-type zeolite could be produced from coal fly ash, and adsorption capability on heavy metals was studied and evaluated [26]. Additionally, various previous studies have also investigated the adsorption of Pb^{2+} from aqueous media using industrial/agriculture wastes such as wool, sawdust, sugar beet pulp, and *Azadirachta indiea* (Neem) leaf [27–30]. However, the physicochemical properties of other types of zeolite produced from coal fly ash generated by the Tachibana-wan Thermal Power Station and its heavy metals adsorption capacity have not yet been reported.

Sodium hydroxide is often used in the conversion of FA into zeolite by hydrothermal activation, and the ion in the prepared zeolite can then be exchanged with sodium ions in aqueous media. Some studies have already reported the synthesis and characterization of zeolite prepared from FA using a sodium hydroxide solution [12,18,19,23,24,26]. However, few have been conducted on the synthesis and physicochemical properties of zeolite prepared from fly ash using potassium hydroxide solution. The preparation of K-type zeolite from coal ash for use as a fertilizer in the agricultural field has been reported [14]. However, those studies did not sufficiently evaluate the adsorption capacity for heavy metals. Additionally, the cation exchange capacity (ion exchange capacity) in zeolite is one of the most important adsorption mechanisms. This indicates that sodium ion (or potassium ion) is exchanged with cation (Pb^{2+} in this study) using Na-type zeolite (or K-type zeolite). The ionic radii of sodium ion and potassium ion are 1.80 and 2.20 Å, respectively. In addition, the (hydrate) radii of lead ion is over 1.8 Å [17,31]. Therefore, it was expected that K-type zeolite would be useful for removal of Pb^{2+} from aqueous solution compared to Na-type zeolite.

Therefore, the aim of this study was to synthesize K-type zeolite from coal fly ash following the activation using hydrothermal technique and evaluate adsorption capability on Pb^{2+} from aqueous media. The influences of various parameters including initial concentration, temperature, pH, contact time, and selectivity were additionally explored, and the Pb^{2+} adsorption mechanism of K-type zeolite was elucidated.

2. Materials and Methods

2.1. Materials and Chemicals

Standard solutions of Pb^{2+} ($Pb(NO_3)_2$ in 0.1 mol L^{-1} HNO_3), Na^+ (NaCl in water), Mg^{2+} ($Mg(NO_3)_2$ in 0.1 mol L^{-1} HNO_3), K^+ (KCl in water), Ca^{2+} ($CaCO_3$ in 0.1 mol L^{-1} HNO_3), Ni^{2+} ($Ni(NO_3)_2$ in 0.1 mol L^{-1} HNO_3), Cu^{2+} ($Cu(NO_3)_2$ in 0.1 mol L^{-1} HNO_3), Zn^{2+} ($Zn(NO_3)_2$ in 0.1 mol L^{-1} HNO_3), Sr^{2+} ($SrCO_3$ in 0.1 mol L^{-1} HNO_3), and Cd^{2+} ($Cd(NO_3)_2$ in 0.1 mol L^{-1} HNO_3), potassium hydroxide, nitric acid, and sodium hydroxide were purchased from FUJIFILM Wako Pure Chemical Co., Osaka, Japan. Coal fly ash (FA, JIS Type-II) was obtained from the Tachibana-wan Thermal Power Station (Shikoku Electric Power, Inc., Takamatsu, Japan). K-type zeolites were produced following a previously reported method [32]. Briefly, FA (3.0 g) was mixed with 3-mol L^{-1} potassium hydroxide solution in the volume of 240 mL. The reaction solution was then shaken and heated at 93 °C for 1, 3, 6, 12, 24, and 48 h. Afterwards, the suspensions were filtered through a 0.45-µm membrane filter (Advantec MFS, Inc., Tokyo, Japan), and obtained samples were washed with distilled water and then dried at 50 °C for 1 day. The samples heated for different durations were denoted as FA1, FA3, FA6, FA12, FA24, and FA48, respectively.

2.2. Physicochemical Properties of the Adsorbents

The physicochemical properties of each adsorbent were analyzed as follows. The crystal structure and morphology were analyzed using a MiniFlex II (Rigaku, Tokyo, Japan) and SU1510 (Hitachi Ltd., Tokyo, Japan), respectively. The specific surface area and pore volume were measured using a NOVA4200*e* instrument (Yuasa Ionic, Kyoto, Japan). The cation exchange capacity (CEC) and pH_{pzc} were determined following the Japanese Industrial Standard Method (JIS K 1478: 2009) and the method reported by Faria et al. [33]. The concentrations of acidic or basic functional groups in the adsorbents were measured following the Boehm titration method [34]. Additionally, the binding energy was analyzed using an AXIS-NOVA instrument (Shimadzu Co., Ltd., Kyoto, Japan). Finally, the solution pH was measured using an F-73S digital pH meter (HORIBA, Ltd., Kyoto, Japan).

2.3. Adsorption Capacity of Pb^{2+}

Each adsorbent (0.01 g) was mixed with 50 mL of the Pb^{2+} solution at 50 mg L^{-1} (pH 3.0). The reaction solution was shaken at 100 rpm and 25 °C for 24 h, and then filtered through a 0.45-µm membrane filter. The concentration of Pb^{2+} was measured using an iCAP-7600 Duo (Thermo Fisher Scientific Inc., Tokyo, Japan). The quantity of Pb^{2+} adsorbed was calculated as the difference between the Pb^{2+} concentrations before and after adsorption.

2.4. Effect of Initial Concentration, Temperature, pH, Contact Time, and Coexisting Ions on Pb^{2+} Adsorption

First, 0.01 g of FA48 was mixed with a 50-mL Pb^{2+} solution at concentrations of 10, 20, 30, 40, and 50 mg L^{-1} (the concentration range was determined by ecological risk assessment of sediment and total concentrations of heavy metals in sewage sludge from wastewater discharging area) [35–37]. The reaction solution was shaken at 100 rpm and 7, 25, and 45 °C for 24 h using water bath shaker MM-10 (TAITEC Co., Nagoya, Japan), and then filtered through a 0.45-µm membrane filter. Second, to evaluate the pH, 0.01 g of FA48 was mixed with 50 mL of a Pb^{2+} solution at concentrations of 10, 30, and 50 mg L^{-1}. The pH of the solution was adjusted between 2, 3, 5, 7, and 9 using nitric acid or sodium hydroxide solutions. The reaction solution was then shaken at 100 rpm and 25 °C for 24 h. To evaluate the contact time, 0.01 g of FA48 was mixed with 50 mL of a Pb^{2+} at a concentration of 50 mg L^{-1}. The reaction solution was then shaken at 100 rpm and 25 °C for 0.5, 1, 3, 6, 18, 21, 24, 30, 42, and 48 h. The quantity of Pb^{2+} adsorbed in each case was calculated as described above, and the data are presented as the mean ± standard deviation. Additionally, to evaluate the adsorption mechanism, the quantity of K^+ released from FA48 in the adsorption isotherm experiment was also measured using an iCAP-7600 Duo device. Finally, to evaluate the Pb^{2+} adsorption selectivity of the zeolite, 0.01 g of FA48 was mixed with 50 mL of a binary solution system at a concentration of 10 mg L^{-1} (Pb^{2+} and Na^+, Mg^{2+}, K^+, Ca^{2+}, Ni^{2+}, Cu^{2+}, Zn^{2+}, Sr^{2+}, or Cd^{2+}). The reaction solution was shaken at 100 rpm and 25 °C for 24 h. The concentration of each metal was measured using an iCAP-7600 Duo device. The quantity of each metal adsorbed was also calculated based on the differences in concentration before and after adsorption.

3. Results and Discussion

3.1. Physicochemical Properties

Zeolite is a highly porous aluminosilicate containing various channels and cavities. Ion-exchangeable cations, such as sodium, potassium, and calcium were used to balance the negative charge [21,38]. The scanning electron microscopy (SEM) images of each zeolite are shown in Figure 1. Spherical particles with different diameters were observed in FA. The spheres and agglomerates of FA1, FA3, FA6, and FA12 could be maintained, and some changes on the surfaces of each type of FA were observed under the tested experimental conditions. The spheres and agglomerates of FA24 and FA48 significantly changed to different crystal shapes and their particle sizes decreased. The synthesis of zeolite from fly ash involves three steps, i.e., dissolution, condensation, and crystallization [39]. Similar trends were observed in previous studies [12,17].

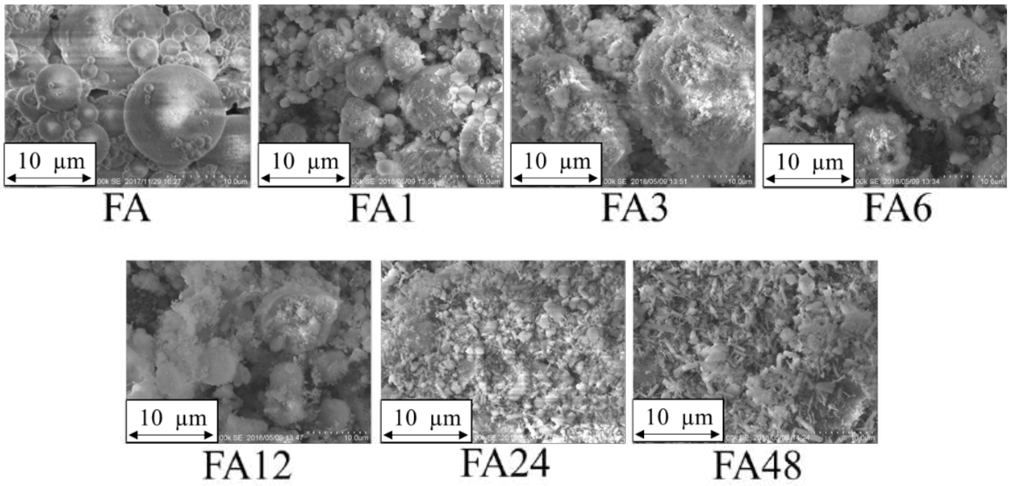

Figure 1. SEM images of adsorbents. Magnification is 3000 diameters.

The X-ray diffraction (XRD) patterns of the samples are shown in Figure 2. The FA was composed of quartz (SiO_2) and mullite ($3Al_2O_3 \cdot 2SiO_2$), and no significant changes in the XRD patterns of FA, FA1, FA3, FA6, and FA12 under our experimental conditions were observed. However, the structure of Zeolite F ($(K_{13.5}Si_{10}Al_{10}O_{40})(OH)_3 \cdot 13H_2O$) appeared in FA24 and FA48, indicating that FA was converted into zeolite. Less time was required to convert FA into zeolite using sodium hydroxide (approximately 6 h) than that required when using potassium hydroxide (approximately 24 h). Trends similarly were observed in a previous study [14]. The physicochemical properties of the adsorbents are shown in Table 1, and the concentrations of basic functional groups of FA24 and FA48 were higher than those of the other adsorbents. However, the concentrations of acidic functional groups decreased with raising the time of alkaline activation. The pH_{pzc} were not significantly different between the different types of FAs in this study. The CEC and pore volume ($d \leq 20$ (Å)), which greatly influence the adsorption capacity, of FA24 and FA48 were 12.4–26.4 times and 100 times higher than those of other FAs, indicating that the hydrothermal activation method significantly affected the CEC and pore volume ($d \leq 20$ (Å)) under our experimental conditions. Additionally, the specific surface area and pore volume (such as $20 < d \leq 500$ (Å), total, and mean pore diameter) of FA6 and FA12 were higher than those of the other FAs. Our previous study reported the characteristics of Na-type zeolite [26], and the CEC and pore volume ($d \leq 20$ (Å)) of the K-type zeolite prepared in this study exceeded those of the Na-type zeolite. Thus, hydrothermal activation using FA and potassium hydroxide was useful for producing novel zeolites to remove metals from aqueous media.

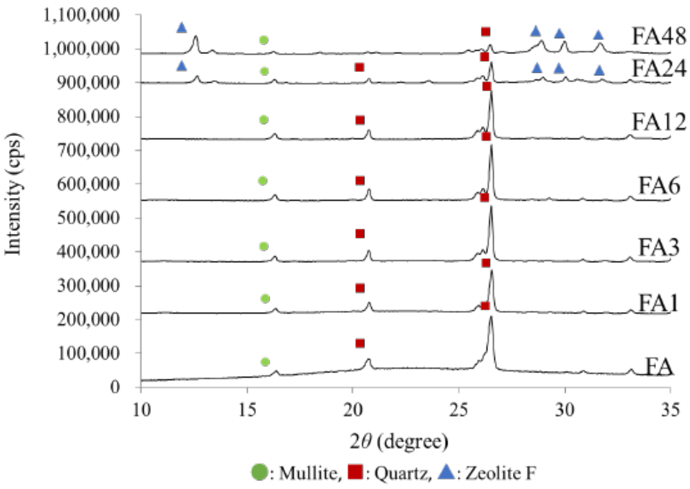

Figure 2. XRD patterns of adsorbents.

Table 1. Physicochemical properties of adsorbents.

Adsorbents		**FA**	**FA1**	**FA3**	**FA6**	**FA12**	**FA24**	**FA48**
Concentration of basic functional groups (mmol g^{-1})		0	0.41	0.77	1.38	1.36	1.48	1.43
Concentration of acidic functional groups (mmol g^{-1})		0.10	0.24	0.30	0.31	0.31	0.24	0.24
CEC (mmol g^{-1})	pH 5	0.34	1.98	1.17	1.63	2.27	7.90	8.98
	pH 10	0.19	0.65	1.55	2.09	3.46	11.17	11.17
pH_{pzc}		9.8	9.3	9.3	9.5	9.7	10.4	10.4
Specific surface area (m^2 g^{-1})		1.4	15.1	31.5	53.3	54.5	50.3	47.3
Pore volume (μL g^{-1})	$d \leq 20$ (Å)	0.1	0.9	0	0.5	0.2	10.0	10.0
	$20 < d \leq 500$ (Å)	2.0	41.9	97.4	161.5	185.0	105.0	99.0
	Total	2.2	63.0	139.0	221.0	220.0	151.0	131.0
Mean pore diameter (Å)		57.0	167.2	176.7	165.9	161.6	120.1	110.7

3.2. Adsorption Capacity of Pb^{2+}

FA, FA1, FA3, FA6, FA12, FA24, and FA48 adsorbed 1.04, 1.45, 4.87, 8.11, 13.54, 54.29, and 55.53 mg g^{-1} of Pb^{2+}, respectively. The relationships between the quantity of Pb^{2+} adsorbed and the parameters in Table 1 were statistically assessed (Table 2), and the correlation coefficients value between the level of Pb^{2+} adsorbed and CEC, pH_{pzc}, and pore volume ($d \leq 20$ (Å)) were positive, at 0.986–0.999, 0.921, and 0.980, respectively. Therefore, these properties have the greatest influence on the Pb^{2+} adsorption capacity in solution. Additionally, FA24 and FA48 adsorbed more Pb^{2+} than Na-type zeolite (approximately 30 mg g^{-1}) under the same experimental conditions [26]. This is because K-type zeolite has a high CEC and pore volume ($d \leq 20$ (Å)) than Na-type zeolite. In this study, FA48 was selected to study and evaluate the adsorption capability on Pb^{2+} in the following experiments.

3.3. Pb^{2+} Adsorption Isotherms

The Pb^{2+} adsorption isotherms are shown in Figure 3. The quantity of Pb^{2+} adsorbed increased with raising initial concentration. Amount adsorbed was 2.0 times (7 °C), 2.36 times (25 °C), and 2.44 times (45 °C) raised from 10 to 50 mg L^{-1} of initial concentration. Additionally, the quantity of Pb^{2+} adsorbed also increased with raising temperature, thereby indicating that Pb^{2+} adsorption using FA48 was endothermic. In this study, the distribution of Pb^{2+} between the aqueous media and FA48 was described using adsorption isotherms based on a set of assumptions related to the heterogeneity or homogeneity of the FA48 [24]. Thus, two useful isotherm models, i.e., Freundlich and Langmuir, were selected [40,41]. The Freundlich isotherm model is applicable to adsorption onto heterogeneous surfaces, whereas the Langmuir isotherm is applicable to monolayer and homogeneous adsorption [17]. The Freundlich and Langmuir models are described by Equations (1) and (2), respectively:

$$\log q \;=\; \frac{1}{n}\log C_e \;+\; \log k, \tag{1}$$

$$1/q = 1/(W_s a C_e) + 1/W_s, \tag{2}$$

where q is the quantity of Pb^{2+} adsorbed (mg g^{-1}), C_e is the equilibrium concentration (mg L^{-1}), and k and n are the adsorption capacity and intensity, respectively. Moreover, W_s is the maximum quantity of adsorbed Pb^{2+} (mg g^{-1}), and a is the coefficient reflecting the relative sorption and desorption rates at equilibrium (L mg^{-1}). The Freundlich and Langmuir constants for the adsorption of Pb^{2+} are summarized in Table 3. In this study, the isotherm data were fitted to both the Freundlich (correlation coefficient: ≥0.991) and Langmuir (correlation coefficient: ≥0.960) models. The maximum adsorption capacity (W_s) of Pb^{2+} increased with raising temperature, thereby indicating that the adsorption of Pb^{2+} by FA48 is an endothermic process (Figure 3). Additionally, when the value of $1/n$ is 0.1–0.5, adsorption readily occurs. However, when the value of $1/n$ exceeds 2, adsorption is difficult [42]. Herein, the value of $1/n$ was 0.30–0.32, and the adsorption of Pb^{2+} using FA48 in aqueous solutions were more favorable.

Table 2. Correlation coefficients between quantity adsorbed and physicochemical properties.

Adsorbents		FAs
Concentration of basic functional groups (mmol g^{-1})		0.677
Concentration of acidic functional groups (mmol g^{-1})		0.044
CEC (mmol g^{-1})	pH 5	0.986
	pH 10	0.999
pH_{pzc}		0.921
Specific surface area (m^2 g^{-1})		0.549
Pore volume (μL g^{-1})	$d \leq 20$ (Å)	0.980
	$20 < d \leq 500$ (Å)	0.201
	Total	0.227
Mean pore diameter (Å)		0.262

To evaluate the adsorption mechanism of Pb^{2+} using FA48, the relationships between the quantities of Pb^{2+} and K^+ adsorbed by and released from FA48 were explored, respectively (Figure 4A). The correlation coefficient was positive at 0.958 under our experimental conditions, suggesting that ion exchange was involved in the adsorption of Pb^{2+}. As mentioned above, the correlation coefficient of the relationship between the quantity of Pb^{2+} adsorbed and the CEC value was 0.986–0.999, demonstrating that ion exchange was involved in the removal capacity on Pb^{2+} from aqueous media. A similar result was achieved using Na-type zeolite in a previous study [26]. Additionally, the binding energies of lead before and after adsorption were measured (Figure 4B). New peaks of Pb(4f) were detected at 135 and 140 eV after adsorption, indicating that Pb^{2+} was adsorbed onto the surface of FA48 in this study. Thus, the surface properties of FA48 are vital in the removal ability on Pb^{2+} from aqueous media, and these results agree with those in Table 2.

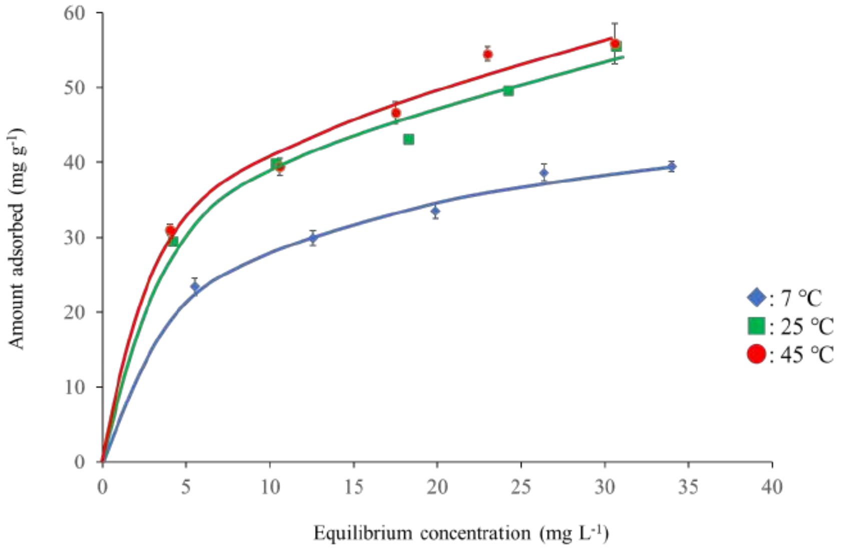

Figure 3. Adsorption isotherms of Pb^{2+} using FA48 at different temperatures. Initial concentration 10, 20, 30, 40, and 50 mg L^{-1}, solvent volume 50 mL, adsorbent 0.01 g, contact time 24 h.

Table 3. Langmuir and Freundlich constants for the adsorption of Pb^{2+}.

Adsorbent	**Temperatures (°C)**	**Langmuir Constants**			**Freundlich Constants**		
		W_s (mg g^{-1})	a (L mg^{-1})	r	log$k$	1/n	r
FA48	7	74.1	0.20	0.982	1.38	0.30	0.994
	25	98.0	0.24	0.987	1.51	0.30	0.997
	45	102.0	0.25	0.960	1.52	0.25	0.960

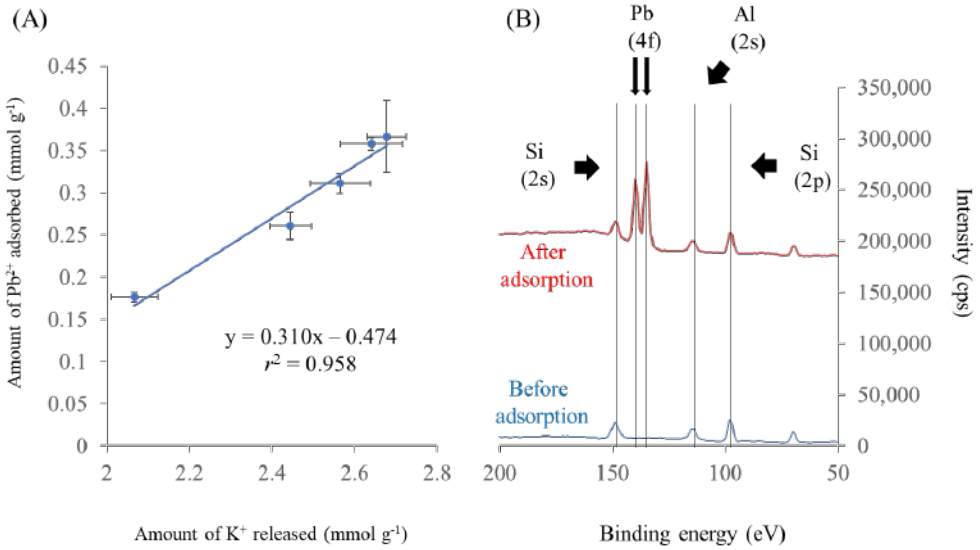

Figure 4. Correlation coefficient between quantity of Pb^{2+} adsorbed and quantity of K^+ released from FA48 (**A**) and binding energy of lead onto FA48 surface before and after adsorption (**B**).

3.4. Effect of pH on Pb^{2+} Adsorption

The solution pH is critical for determining the capacity of Pb^{2+} adsorption from aqueous media. Figure 5 exerts the effect of pH on the adsorption of Pb^{2+}. The quantity adsorbed increased as the pH raised from 2 to 5 under our experimental conditions. Above pH 5, the adsorption capacity decreased sharply. Under acidic conditions, the FA48's surface will be covered with protons (H^+), with which Pb^{2+} competes for adsorption sites. A previous study reported that zeolite could preferentially adsorb H^+ from aqueous media also containing heavy metal ions [43]. The edge groups with a positive charge ($Al\text{-}OH_2^+$ and $Si\text{-}OH_2^+$) on the FA48 surface are explained below [44].

$$\begin{aligned} &\text{-AlOH} + H_2O\ (H^+ + OH^-) \rightarrow \text{-AlOH}_2^+ + OH^- \\ &\text{-SiOH} + H_2O\ (H^+ + OH^-) \rightarrow \text{-SiOH}_2^+ + OH^- \end{aligned} \quad (3)$$

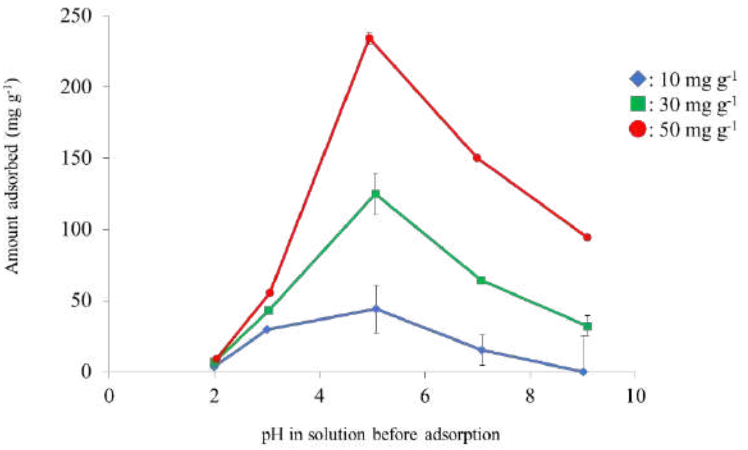

Figure 5. Effect of pH on the adsorption of Pb^{2+} onto FA48. Initial concentration 10, 30, and 50 mg L^{-1}, solvent volume 50 mL, adsorbent 0.01 g, pH 2, 3, 5, 7, and 9, contact time 24 h, temperature 25 °C, agitation speed 100 rpm.

Thus, electrostatic repulsion easily occurred between them, and it was also difficult for ion exchange to occur between Pb^{2+} and K^+ in aqueous media. As the pH increased, the deprotonation of hydroxyl groups increased, indicating that the number of anionic sites (adsorption sites) on FA48 increased, thereby contributing to the adsorption of Pb^{2+} [17]. However, this did not increase the removal percentage of Pb^{2+} beyond pH 6.0 in our experimental condition. The forms of Pb^{2+} in the solution are Pb^{2+}, $Pb(OH)^+$, $Pb(OH)_2$, $Pb(OH)_3^-$, $Pb(OH)_4^{2-}$, $Pb_2(OH)_3^+$, and $Pb_3(OH)_4^{2+}$ [45], and the predominant species of Pb^{2+} at $pH < 7$ are Pb^{2+} and $Pb(OH)^+$, whereas $Pb(OH)_2$, $Pb(OH)_3^-$, and $Pb(OH)_4^{2-}$ are the main forms of Pb^{2+} at $pH > 7$–8. Thereby the complexion between free Pb^{2+} available and FA48 surface was not occurred in our experimental condition. Similar trend was reported by a previous study [46]. Additionally, there is deprotonation as basicity increases beyond pH 6.0 [46], suggesting that electron repulsion occurred between the dissolved negatively charged Pb species and the negatively charged surface of FA48. Thus, the Pb^{2+} adsorption capacity decreased under basic conditions. However, further studies are necessary for elucidate the effect of pH on the adsorption of Pb^{2+} using FA48 from aqueous media in detail.

3.5. *Effect of Contact Time on Pb^{2+} Adsorption*

The effect of contact time on the adsorption capability of Pb^{2+} is shown in Figure 6. The adsorption equilibrium was attained within approximately 6 h under our experimental conditions. Kinetic experiments were conducted to indicate the rate of adsorption and the potential of the rate-limiting step [2]. The pseudo-first-order (Equation (4)) and pseudo-second-order (Equation (5)) models were employed to evaluate these factors and can be described as follows [47,48].

$$\ln(q_{e,exp} - q_t) = \ln q_{e,cal} - k_1 t, \quad (4)$$

$$\frac{t}{q_t} = \frac{t}{q_{e,cal}} + \frac{1}{k_2 \times q_{e,cal}{}^2}, \tag{5}$$

where $q_{e,exp}$ and $q_{e,cal}$ are the quantities of Pb^{2+} adsorbed in the experiment and calculation (mg g^{-1}), and k_1 and k_2 are the pseudo-first-order (h^{-1}) and pseudo-second-order (g mg^{-1} h^{-1}) rate constants, respectively. The rapid adsorption during the initial stage was due to the availability of adsorption sites on FA48. Afterwards, the adsorption equilibrium may have been reached due to the limited mass transfer of Pb^{2+} from the bulk liquid phase to the external surface of FA48 [24]. Similar trends were reported in previous studies [49,50]. Table 4 summarizes the kinetic constants of the pseudo-first-order and second-order models. The kinetic data fitted to the pseudo-second-order model (correlation coefficient: 0.998) better than the pseudo-first-order model (correlation coefficient: 0.602). Therefore, the adsorption mechanism of Pb^{2+} using FA48 in this study may be chemisorption. Additionally, the value of $q_{e,exp}$ (99.5 mg g^{-1}) was similar to that of $q_{e,cal}$ (98.0 mg g^{-1}) in the pseudo-second-order model. Thus, chemical adsorption, one of the adsorption mechanisms, could be the rate-limiting step in the adsorption of Pb^{2+} using FA48 [3].

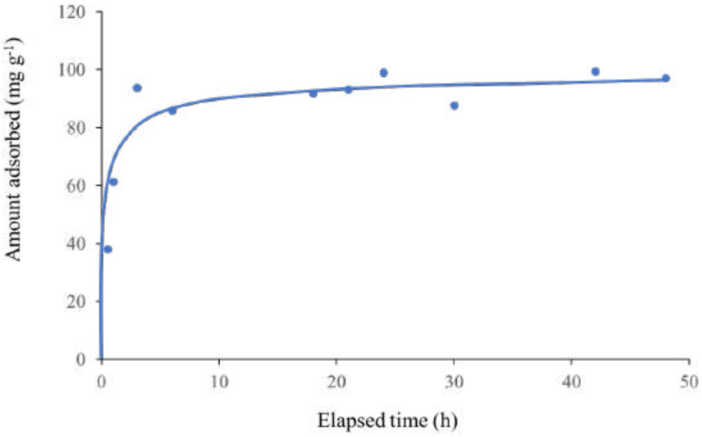

Figure 6. Effect of contact time on the adsorption of Pb^{2+} using FA48. Initial concentration 50 mg L^{-1}, solvent volume 50 mL, adsorbent 0.01 g, contact time 0.5, 1, 3, 6, 18, 21, 24, 30, 42, and 48 h, temperature 25 °C, agitation speed 100 rpm.

Table 4. Kinetic parameters for the adsorption of Pb^{2+}.

Adsorbent	$q_{e,exp}$	**Pseudo-First-Order Model**			**Pseudo-Second-Order Model**		
		k_1 (h^{-1})	$q_{e,cal}$ (mg g^{-1})	r	k_2 (g mg^{-1} h^{-1})	$q_{e,cal}$ (mg g^{-1})	r
FA48	99.5	0.057	19.7	0.602	0.010	98.0	0.998

3.6. Effect of Coexisting Ions on Pb^{2+} Adsorption

In this study, the effect of coexisting ions on the adsorption capability of Pb^{2+} using FA48 was demonstrated in Table 5. Na^+, Mg^{2+}, K^+, Ca^{2+}, Ni^+, Cu^{2+}, Zn^{2+}, Sr^{2+}, and Cd^{2+} were selected as the components of the binary solution system, which exist in aquatic environments or wastewater from factories (human activities) [38,51]. The adsorption percentage of Pb^{2+} using FA48 in a single solution system was 75.7%. The Pb^{2+} adsorption selectivity of FA48 in a binary solution system (adsorption percentage was approximately >60.7%) exceeded that of other cations under our experimental conditions. These results indicate that the adsorption capacity of FA48 was influenced by cationic factors, such as charge density and hydrate ion diameter, and the accessibility of the active sites of FA48 [51]. The radius of hydrated ions and electronegativity of Pb^{2+} exceed those of other cations, such as Ni^{2+}, Cu^{2+}, Cd^{2+}, and Zn^{2+}. Similar trends were reported in previous studies [38,51].

Additionally, the adsorption capacity of cations excluding Pb^{2+} was significantly lower than that of Pb^{2+} in this study. Thus, FA48 is useful for the selective removal of Pb^{2+} from aqueous media.

Table 5. Adsorption capacity of Pb^{2+} in binary solution system.

Components in Binary Solution	Removal Percentage of Pb^{2+} (%)	Removal of Other Cations (%)
Pb^{2+} + Na^{+}	60.7	0.2
Pb^{2+} + Mg^{2+}	69.4	0
Pb^{2+} + K^{+}	75.7	0
Pb^{2+} + Ca^{2+}	62.4	0
Pb^{2+} + Ni^{+}	73.2	0
Pb^{2+} + Cu^{2+}	62.7	3.7
Pb^{2+} + Zn^{2+}	63.7	0.9
Pb^{2+} + Sr^{2+}	70.0	0.7
Pb^{2+} + Cd^{2+}	64.4	4.1

4. Conclusions

In this study, K type-zeolite (FA48) was synthesized from coal fly ash. The CEC, pH_{pzc}, and pore volume ($d \leq 20$ (Å)) of FA48 were higher than those of other zeolites. Additionally, the quantity of Pb^{2+} adsorbed using FA48 (55.53 mg g^{-1}) exceeded that of other zeolites. The adsorption of Pb^{2+} was related to physicochemical properties, such as the CEC (0.986–0.999), pH_{pzc} (0.921), and pore volume ($d \leq 20$ (Å)) (0.980). The relationship between the amounts of Pb^{2+} and K^{+} adsorbed by and released from FA48 was 0.958, respectively. Thus, ion exchange with K^{+} in the interlayer of FA48 is strongly related to the adsorption capacity. Furthermore, the binding energy of lead at 135 and 140 eV could be detected after adsorption, indicating that the adsorbent's surface characteristics were critical for the removal of Pb^{2+} from aqueous media. The adsorption isotherms and kinetics data demonstrated that the adsorption of Pb^{2+} using FA48 was an endothermic process. Finally, FA48 exhibited selectivity for Pb^{2+} adsorption from a binary solution system containing cations. These results provide useful information for the recycling of coal fly ash and the removal of Pb^{2+} from aqueous media.

Author Contributions: Conceptualization, N.K. and F.O.; investigation, Y.K., C.S. and T.N.; writing—original draft preparation, Y.K. and F.O.; writing—review and editing, Y.K., F.O. and C.S.; project administration, N.K. All authors have read and agreed to the published version of the manuscript.

Funding: This research received no external funding.

Conflicts of Interest: The authors declare no conflict of interest.

References

1. About the Sustainable Development Goals. Available online: https://www.un.org/sustainabledevelopment/sustainable-development-goals/ (accessed on 19 May 2020).
2. Venkata Ramana, D.K.; Kumar Reddy, D.H.; Kumar, B.N.; Seshaiah, K.; Chandra Rao, G.P.; Lu, C. Adsorption of Pb(II) from aqueous solutions by chemically modified zeolite supported carbon nanotubes: Equilibrium, kinetic, and thermodynamic studies. *Sep. Sci. Technol.* **2013**, *48*, 403–412. [CrossRef]
3. Kragovic, M.; Dakovic, A.; Markovic, M.; Krstic, J.; Gatta, G.D.; Rotiroti, N. Characterization of lead sorption by the natural and Fe(III)-modified zeolite. *Appl. Surf. Sci.* **2013**, *283*, 764–774. [CrossRef]
4. Hamidpour, M.; Kalbasib, M.; Afyunib, M.; Shariatmadarib, H.; Holmic, P.E.; Hansenc, H.C.B. Sorption hysteresis of Cd(II) and Pb(II) on natural zeolite and bentonite. *J. Hazard. Mater.* **2010**, *181*, 686–691. [CrossRef] [PubMed]
5. Lead Poisoning and Health. Available online: https://www.who.int/news-room/fact-sheets/detail/lead-poisoning-and-health (accessed on 19 May 2020).
6. Sarma, P.R.; Chattopadhyay, A.; Zhan, C.; Sharma, S.K.; Geng, L.; Hsiao, B.S. Lead removal from water using carboxycellulose nanofibers prepared by nitro-oxidation method. *Nature* **2018**, *25*, 1961–1973.
7. Torrice, M. How lead ended up in flint's tap water. *Chem. Eng. News* **2016**, *94*, 26–29.

8. Edwards, M.; Triantafyllidou, S.; Best, D. Elevated blood lead in young children due to lead-contaminated drinking water: Washington, DC, 2001–2004. *Environ. Sci. Technol.* **2009**, *43*, 1618–1623. [CrossRef] [PubMed]
9. Mankikar, D.; Campbell, C.; Greenberg, R. Evaluation of a home-based environmental and educational intervention to improve health in vulnerable households: Southeastern Pennsylvania lead and healthy homes program. *Int. J. Environ. Res. Public Health* **2016**, *13*, 900. [CrossRef] [PubMed]
10. Pieper, K.J.; Krometis, L.A.; Gallagher, D.; Benham, B.; Edwards, M. Profiling private water system to identify patterns of waterborne lead exposure. *Environ. Sci. Technol.* **2015**, *49*, 12697–12704. [CrossRef] [PubMed]
11. Japan Coal Energy Center. Available online: http://www.jcoal.or.jp/ashdb/ashstatistics/upload/H30_ashstatistics.pdf (accessed on 19 May 2020).
12. Franus, W.; Wdowin, M.; Franus, M. Synthesis and characterization of zeolites prepared from industrial fly ash. *Environ. Monit. Assess.* **2014**, *186*, 5721–5729. [CrossRef]
13. Blissett, R.S.; Rowson, N.A. A review of the multi-component utilization of coal fly ash. *Fuel* **2012**, *97*, 1–23. [CrossRef]
14. Flores, C.G.; Schneider, H.; Marcillio, N.R.; Ferret, L.; Oliveira, J.C.P. Potassic zeolites from Brazilian coal ash for use as a fertilizer in agriculture. *Waste Manag.* **2017**, *70*, 263–271. [CrossRef] [PubMed]
15. Visa, M.; Isac, L.; Dute, A. Fly ash adsorbents for multi-cation wastewater treatment. *App. Surf. Sci.* **2012**, *258*, 6345–6352. [CrossRef]
16. Ahmaruzzaman, M. A review on the utilization of fly ash. *Prog. Energy Combust. Sci.* **2010**, *36*, 327–363. [CrossRef]
17. He, K.; Chen, Y.; Tang, Z.; Hu, Y. Removal of heavy metal ions from aqueous solution by zeolite synthesized from fly ash. *Environ. Sci. Pollut. Res.* **2016**, *23*, 2778–2788. [CrossRef]
18. Wdowin, M.; Franus, M.; Panek, R.; Badura, L.; Rranus, W. The conversation technology of fly ash into zeolites. *Clean Technol. Environ. Policy* **2014**, *16*, 1217–1223. [CrossRef]
19. Derkowski, A.; Franus, W.; Beran, E.; Czimerova, A. Properties and potential applications of zeolitic materials produced from fly ash using simple method of synthesis. *Powder Technol.* **2006**, *166*, 47–54. [CrossRef]
20. Derkowski, A.; Franus, W.; Waniak-Nowicka, H.; Czimerova, A. Textural properties vs. CEC and EGME retention of Na-X zeolite prepared from fly ash at room temperature. *Int. J. Miner. Process.* **2007**, *82*, 57–68. [CrossRef]
21. Shaheen, S.M.; Derbalah, A.S.; Moghanm, F.S. Removal of heavy metals from aqueous solution by zeolite in competitive sorption system. *Int. J. Environ. Sci. Dev.* **2012**, *3*, 362–367. [CrossRef]
22. Siddique, R. Performance characteristics of high-volume class F fly ash concrete. *Cem. Concr. Res.* **2004**, *34*, 487–493. [CrossRef]
23. Izidoro, J.C.; Fungaro, D.A.; Abbott, J.E.; Wang, S. Synthesis of zeolite X and A from fly ashes for cadmium and zinc removal from aqueous solutions in single and binary ion systems. *Fuel* **2013**, *103*, 827–834. [CrossRef]
24. Golbad, S.; Khoshnoud, P.; Abu-Zahra, N. Hydrothermal synthesis of hydroxyl sodalite from fly ash for the removal of lead ions from water. *Int. J. Environ. Sci. Technol.* **2017**, *14*, 135–142. [CrossRef]
25. Ogata, F.; Tominaga, H.; Yabutani, H.; Taga, A.; Kawasaki, N. Recovery of molybdenum from fly ash by gibbsite. *Toxicol. Environ. Chem.* **2011**, *93*, 635–642. [CrossRef]
26. Kobayashi, Y.; Ogata, F.; Nakamura, T.; Kawasaki, N. Synthesis of novel zeolites produced from fly ash hydrothermal treatment in alkaline solution and its evaluation as an adsorbent for heavy metal. *J. Environ. Chem. Eng.* **2020**, *8*, 103687. [CrossRef]
27. Ogata, F.; Tominaga, H.; Kangawa, M.; Inoue, K.; Kawasaki, N. Adsorption capacity of Cu(II) and Pb(II) onto carbon fiber produced from wool. *J. Oleo Sci.* **2012**, *3*, 149–154. [CrossRef] [PubMed]
28. Yu, B.; Zhang, Y.; Shukla, A.; Shukla, S.S.; Dorris, K.L. The removal of heavy metals from aqueous solutions by sawdust adsorption removal of lead and comparison of its adsorption with copper. *J. Hazard. Mater.* **2001**, *B84*, 83–94. [CrossRef]
29. Pehlivan, E.; Yamk, B.H.; Ahmetli, G.; Pehlivan, M. Equilibrium isotherm studies for the uptake of cadmium and lead ions onto sugar beet pulp. *Bioresour. Technol.* **2008**, *99*, 3520–3527. [CrossRef] [PubMed]
30. Battacharyya, K.G.; Sharma, A. Adsorption of Pb(II) from aqueous solution by Azadirachta indiea (Neem) leaf powder. *J. Hazard. Mater.* **2004**, *113*, 97–109. [CrossRef]
31. Slater, J.C. Atomic radii in crystals. *J. Chem. Phys.* **1964**, *41*, 3199–3204. [CrossRef]

32. Ogata, F.; Iwata, Y.; Kawasaki, N. Properties of novel adsorbent produced by hydrothermal treatment of waste fly ash in alkaline solution and its capability for adsorption of tungsten from aqueous solution. *J. Environ. Chem. Eng.* **2015**, *3*, 333–338. [CrossRef]
33. Faria, P.C.C.; Orfao, J.J.M.; Pereira, M.F.R. Adsorption of anionic and cationic dyes on activated carbons with different surface chemistries. *Water Res.* **2004**, *38*, 2043–2052. [CrossRef]
34. Boehm, H.P. Chemical identification of surface groups. *J. Adv. Catal. Sci. Technol.* **1966**, *16*, 179–274.
35. Nassar, N.N. Rapid removal and recovery of Pb(II) from wastewater by magnetic nanoadsorbents. *J. Hazard. Mater.* **2010**, *184*, 538–546. [CrossRef] [PubMed]
36. Kwon, Y.T.; Lee, C.W. Ecological risk assessment of sediment in wastewater discharging area by means of metal speciation. *Microchem. J.* **2001**, *70*, 255–264. [CrossRef]
37. Wang, C.; Hu, X.; Chen, M.L.; Wu, Y.H. Total concentrations and fractions of Cd, Cr, Pb, Cu, Ni and Zn in sewage sludge municipal and industrial wastewater treatment plants. *J. Hazard. Mater.* **2005**, *B119*, 245–249. [CrossRef] [PubMed]
38. Hernandez-Montoya, V.; Perez-Cruz, M.; Mendoza-Castillo, D.I.; Moreno-Virgen, M.R.; Bonilla-Petriciolet, A. Competitive adsorption of syes and heavy metals on zeolitic structures. *J. Environ. Manag.* **2013**, *116*, 213–221. [CrossRef]
39. Murayama, N.; Ymamamoto, H.; Shibata, J. Mechansim of zeolite synthesis from coal fly ash by alkali hydrothermal reaction. *Int. J. Miner. Process.* **2002**, *64*, 1–17. [CrossRef]
40. Freundlich, H.M.T. Over the adsorption in solution. *J. Phy. Chem.* **1906**, *57*, 385–471.
41. Langmuir, I. The constitution and fundamental properties of solids and liquids. *J. Am. Chem. Soc.* **1916**, *38*, 2221–2295. [CrossRef]
42. Abe, I.; Hayashi, K.; Kitagawa, M. Studies on the adsorption of surfactants on activated carbons. I. Adsorption of nonionic surfactants. *Yukagaku* **1976**, *25*, 145–150.
43. Myroslav, S.; Boguslaw, B.; Artur, T.P.; Jacek, N. Study of the selection mechanism of heavy metal (Pb^{2+}, Cu^{2+}, Ni^{2+}, and Cd^{2+}) adsorption on clinoptilolite. *J. Colloid Interface Sci.* **2006**, *304*, 21–28.
44. Sari, A.; Tuzen, M.; Citak, D.; Soylak, M. Equilibrium, kinetic and thermodynamic studies of adsorption of Pb(II) from aqueous solution onto Turkish kaolinite clay. *J. Hazard. Mater.* **2007**, *149*, 283–291. [CrossRef] [PubMed]
45. Yang, X.; Yang, S.; Yang, S.; Hu, J.; Tan, X.; Wang, X. Effect of pH, ionic strength and temperature on sorption of Pb(II) on NKF-6 zeolite studied by batch technique. *Chem. Eng. J.* **2011**, *168*, 86–93. [CrossRef]
46. Alswat, A.A.; Ahmad, M.B.; Saleh, T.A. Zeolite modified with copper oxide and iron oxide for lead and arsenic adsorption from aqueous solutions. *J. Water Supply Res. Technol. AQUA* **2016**, *65*, 465–479. [CrossRef]
47. Lagergren, S. Zur theorie der sogenannten adsorption geloster stoffie, *Kunglia Svenska Vetenskapsakademiens. Handlingar* **1898**, *24*, 1–39.
48. Ho, Y.S.; McKay, G. Pseudo-second order model for sorption process. *Process Biochem.* **1999**, *34*, 451–465. [CrossRef]
49. Xie, J.; Wang, Z.; Wu, D.; Zhang, Z.; Kong, H. Synthesis of zeolite/aluminum oxide hydrate from coal ash: A new type of adsorbent for simultaneous removal of cationic and anionic pollutants. *J. Ind. Eng. Chem.* **2013**, *52*, 14890–14897. [CrossRef]
50. Yadanaparthi, S.K.P.; Graybill, D.; Wandruszka, R.V. Adsorbents for the removal of arsenic, cadmium, and lead from contaminated waters. *J. Hazard. Mater.* **2009**, *171*, 1–15. [CrossRef]
51. Merrikhpour, H.; Jalali, M. Comparative and competitive adsorption of cadmium, copper, nickel, and lead ions by Iranian natural zeolite. *Clean Technol. Environ. Policy* **2013**, *15*, 303–316. [CrossRef]